Dynamics, Electromyography and Vibroarthrography as Non-Invasive Diagnostic Tools: Investigation of the Patellofemoral Joint

A Dissertation

Presented for the

Doctor of Philosophy

Degree

The University of Tennessee, Knoxville

Filip Leszko

August 2011

© by Filip Leszko, 2011
All Rights Reserved.

Abstract

The knee joint plays an essential role in the human musculoskeletal system. It has evolved to withstand extreme loading conditions, while providing almost frictionless joint movement. However, its performance may be disrupted by disease, anatomical deformities, soft tissue imbalance or injury. Knee disorders are often puzzling, and accurate diagnosis may be challenging. Current evaluation approach is usually limited to a detailed interview with the patient, careful physical examination and radiographic imaging. The X-ray screening may reveal bone degeneration, but does not carry sufficient information of the soft tissue conditions. More advanced imaging tools such as MRI or CT are available, but expensive, time consuming and can be used only under static conditions. Moreover, due to limited resolution the radiographic techniques cannot reveal early stage arthritis. The arthroscopy is often the only reliable option, however due to its semi-invasive nature, it cannot be considered as a practical diagnostic tool. Therefore, the motivation for this work was to combine three scientific methods to provide a comprehensive, non-invasive evaluation tool bringing insight into the in vivo, dynamic conditions of the knee joint and articular cartilage degeneration.

Electromyography and inverse dynamics were employed to independently determine the forces present in several muscles spanning the knee joint. Though both methods have certain limitations, the current work demonstrates how the use of these two methods concurrently enhances the biomechanical analysis of the knee joint conditions, especially the performance of the extensor mechanism. The kinetic analysis was performed for 12 TKA, 4 healthy individuals in advanced age and 4 young subjects. Several differences in the knee biomechanics were found between the three groups, identifying age-related and post-operative decrease in the extensor mechanism efficiency, explaining the increased effort of performing everyday activities experienced by the elderly and TKA subjects.

The concept of using accelerometers to assess the cartilage degeneration has been proven based on a group of 23 subjects with non-symptomatic knees and 52 patients suffering from knee arthritis. Very high success (96.2%) of pattern classification obtained in this work clearly demonstrates that vibroarthrography is a promising, non-invasive and low-cost technique offering screening capabilities.

Contents

List of Tables viii

List of Figures ix

Acronyms xxi

1 Introduction 1

1.1 Statement of the Problem 2

2 Review of Related Literature 5

2.1 Biomechanical functions of the patella 5

2.2 Patellofemoral kinematics, tracking and contact 6

2.2.1 Unambiguous description 6

2.2.2 Patella kinematics 8

2.2.3 Patellofemoral contact 15

2.3 Extensor mechanism forces and patellofemoral stresses 18

2.4 Vibroarthrography of the knee joint 27

2.4.1 Historical background 27

2.4.2 Current research 32

3 Originality and Contributions of the Presented Research 34

3.1 Originality of the Dissertation Topic 34

3.2 Fundamental Contributions 36

4 Biomechanical Analysis of the Extensor Mechanism Moment Arms 40

4.1 What is a moment arm? . . . 40

4.2 Literature data discrepancy . . . 42

4.3 Moment arms in the natural, patellectomy and TKA knees . . . 46

5 Materials and Methods 50

5.1 Research Study Design . . . 50

5.2 Determination of the In-Vivo Kinematics . . . 54

5.3 Musculoskeletal Model Development . . . 59

5.3.1 Inverse Dynamics Analysis . . . 60

5.3.2 Muscle Dynamics Analysis . . . 81

5.4 Pattern Classification of the Vibroarthrography Signals . . . 97

6 Results 105

6.1 Kinematic analysis . . . 105

6.1.1 Patellofemoral tracking . . . 105

6.1.2 Tibiofemoral rotations . . . 106

6.1.3 Patellofemoral rotations . . . 110

6.1.4 Patellofemoral contact . . . 112

6.2 Kinetic Analysis . . . 118

6.2.1 Muscle Properties . . . 118

6.2.2 Muscle Activation . . . 118

6.2.3 Muscle dynamics analysis . . . 123

6.2.4 Inverse dynamics analysis . . . 126

6.2.5 EMG vs Inverse Dynamics: Quadriceps forces . . . 127

6.2.6 EMG vs Inverse Dynamics: Quadriceps force distribution . . . 127

6.2.7 Knee Joint Reaction Forces . . . 133

6.3 Vibroarthrography . . . 136

7 Discussion **150**

7.1 Kinematics . . . 150

7.1.1 Patellofemoral and Tibiofemoral Kinematics . . . 150

7.1.2 Patellofemoral contact . . . 153

7.2 Biomechanics of the Extensor Mechanism . . . 155

7.2.1 Muscle Activation . . . 155

7.2.2 Muscle Forces . . . 157

7.3 Interactive Forces . . . 161

7.4 Vibroarthrography . . . 164

7.5 Summary . . . 167

8 Conclusions **169**

8.1 Clinical significance . . . 171

Bibliography **174**

A Detailed Patients' Analysis Results **206**

A.1 Patient 1T . . . 207

A.1.1 Kinematics analysis results . . . 207

A.1.2 Electromyography and Inverse Dynamics analyses results . . . 211

A.2 Patient 3T . . . 214

A.2.1 Kinematics analysis results . . . 214

A.2.2 Electromyography and Inverse Dynamics analyses results . . . 218

A.3 Patient 4T . . . 221

A.3.1 Kinematics analysis results . . . 221

A.3.2 Electromyography and Inverse Dynamics analyses results . . . 225

A.4 Patient 8T . . . 228

A.4.1 Kinematics analysis results . . . 228

A.4.2 Electromyography and Inverse Dynamics analyses results . . . 232

A.5 Patient 12T . . . 235

A.5.1 Kinematics analysis results . . . 235
A.5.2 Electromyography and Inverse Dynamics analyses results . . . 239
A.6 Patient 13T . . . 242
A.6.1 Kinematics analysis results . . . 242
A.6.2 Electromyography and Inverse Dynamics analyses results . . . 246
A.7 Patient 17T . . . 249
A.7.1 Kinematics analysis results . . . 249
A.7.2 Electromyography and Inverse Dynamics analyses results . . . 253
A.8 Patient 21T . . . 256
A.8.1 Kinematics analysis results . . . 256
A.8.2 Electromyography and Inverse Dynamics analyses results . . . 260
A.9 Patient 11T . . . 263
A.9.1 Kinematics analysis results . . . 263
A.9.2 Electromyography and Inverse Dynamics analyses results . . . 267
A.10 Patient 11N . . . 270
A.10.1 Kinematics analysis results . . . 270
A.10.2 Electromyography and Inverse Dynamics analyses results . . . 274
A.11 Patient 19T . . . 277
A.11.1 Kinematics analysis results . . . 277
A.11.2 Electromyography and Inverse Dynamics analyses results . . . 281
A.12 Patient 19N . . . 284
A.12.1 Kinematics analysis results . . . 284
A.12.2 Electromyography and Inverse Dynamics analyses results . . . 288
A.13 Patient 22T . . . 291
A.13.1 Kinematics analysis results . . . 291
A.13.2 Electromyography and Inverse Dynamics analyses results . . . 295
A.14 Patient 22N . . . 298
A.14.1 Kinematics analysis results . . . 298
A.14.2 Electromyography and Inverse Dynamics analyses results . . . 302

A.15 Patient 23T 305
A.15.1 Kinematics analysis results 305
A.15.2 Electromyography and Inverse Dynamics analyses results . . . 309
A.16 Patient 23N 312
A.16.1 Kinematics analysis results 312
A.16.2 Electromyography and Inverse Dynamics analyses results . . . 316
A.17 Patient 6N 319
A.17.1 Kinematics analysis results 319
A.17.2 Electromyography and Inverse Dynamics analyses results . . . 323
A.18 Patient 7N 326
A.18.1 Kinematics analysis results 326
A.18.2 Electromyography and Inverse Dynamics analyses results . . . 330
A.19 Patient 15N 333
A.19.1 Kinematics analysis results 333
A.19.2 Electromyography and Inverse Dynamics analyses results . . . 337
A.20 Patient 16N 340
A.20.1 Kinematics analysis results 340
A.20.2 Electromyography and Inverse Dynamics analyses results . . . 344

Vita **347**

List of Tables

5.1 Patient demographics 51

6.1 Tibiofemoral joint rotations. 109
6.2 Patellofemoral joint rotations. 113
6.3 Muscle properties of all the subjects 119
6.4 Comparison of peak muscle force time found using EMG and inverse dynamics. 128
6.5 Average values and significance of 33 signal features (DKB activity) . 145
6.6 Average values and significance of 33 signal features (all activities) . . 147

7.1 Comparison of current work results with telemetry data 163
7.2 Comparison of current work with previous VAG classification studies 166

List of Figures

2.1 Patellofemoral joint coordinate system. 9
2.2 Shift of the natural and TKA patella reported in the literature. . . . 11
2.3 Flexion of the natural and TKA patella reported in the literature . . 13
2.4 Rotation of the natural and TKA patella reported in the literature . 14
2.5 Tilt of the natural and TKA patella reported in the literature 16
2.6 Patellofemoral contact location reported in the literature 17
2.7 Patellofemoral contact area reported in the literature 19
2.8 Quadriceps muscle force reported in the literature 21
2.9 Patellar ligament force reported in the literature 22
2.10 Patellofemoral joint reaction force reported in the literature 23
2.11 Quadriceps muscle group pull directions 24
2.12 Patellofemoral joint reaction to the quadriceps force ratio reported in the literature 25
2.13 Patellofemoral joint reaction to the quadriceps force ratio reported in the literature 26
2.14 Pioneering study revealing the value of joint auscultation. 29
2.15 Early research approach to study joint auscultation. 30
2.16 Early work conserning the classification of the knee joint sounds. . . . 31

3.1 Top-level diagram of the methods employed in the dissertation 35
3.2 Patellofemoral joint kinematics correlated with vibroarthrography . . 38

4.1 Definition of the moment of force 41
4.2 Extensor mechanism free body diagram. 43
4.3 Patellar ligament moment arm calculated using different reference points 44
4.4 Differences between patellar ligament moment arm length calculated using different reference points 45
4.5 Patellar ligament moment arm length for healthy, elderly and TKA knees 47
4.6 Effects of patellectomy on the patellofemoral moment arm length . . 48

5.1 EMG electrodes and accelerometers placement 52
5.2 Segmentation of the natural bones 55
5.3 Example 3D CAD model of the knee joint. 56
5.4 Segmentation of the resurfaced patella 57
5.5 Example 3D CAD model of a resected patella. 58
5.6 Registration of the natural bones 58
5.7 Registration of the TKA CAD models and the resurfaced patella . . . 59
5.8 Conversion of the force plate data 61
5.9 Bone reconstruction for the healthy legs 63
5.10 Bone reconstruction for the TKA legs 64
5.11 Ankle joint kinematics estimation based on the video images 65
5.12 Ankle joint kinematics determined in-vivo for TAA subjects 66
5.13 Hip flexion compared to the knee flexion during stair climbing 67
5.14 Muscle and ligament attachment points modeled for the healthy leg . 68
5.15 Muscle and ligament attachment points modeled for the implanted leg 69
5.16 Test of the wrapping algorithm (1^{st} generation). 70
5.17 Test of the wrapping algorithm (2^{nd} generation). 71
5.18 Test of the final wrapping algorithm. 72
5.19 Muscle wrapping in the final dynamic model. 73
5.20 Tibiofemoral contact location tracking relative to tibia 74
5.21 Tibiofemoral contact location tracking relative to femur 74

5.22 Patellofemoral contact location tracking relative to patella 75
5.23 Patellofemoral contact location tracking relative to femur 76
5.24 Segmentation of the knee muscles based on the CT images 78
5.25 Muscle mass center offset calculation. 79
5.26 Patellar ligament and PFJR force calculations - healthy knee example. 82
5.27 Patellar ligament and PFJR force calculations - TKA example. 83
5.28 EMG signal recording and envelope detection 85
5.29 Comparison between different envelope detection algorithms. 86
5.30 Maximum voluntary contraction procedure for different muscle groups. 87
5.31 EMG signal to Neural Activation conversion 89
5.32 Muscle and neural activation for an example subject 91
5.33 Force-velocity relationship of the muscle contraction dynamics 93
5.34 Force-length relationship of the muscle contraction dynamics 94
5.35 Active muscle force as a function of muscle activation, length and shortening speed 95
5.36 Intrasurgical evaluation sheet used for joint condition assessment . . . 99
5.37 Vibration data collection and decomposition 101
5.38 An example of patellofemoral vibroarthrogram of a healthy knee correlated with fluoroscopy footage 102
5.39 An example of patellofemoral vibroarthrogram of an arthritic knee correlated with video footage 102
5.40 Example vibroarthrogram of a healthy and arthritic patellofemoral joint. 103

6.1 Patellar tracking. 106
6.2 Tibiofemoral joint rotations. 107
6.3 Tibiofemoral joint rotations arranged wrt activity increments. 108
6.4 Patellofemoral joint rotations. 111
6.5 Patellofemoral joint rotations arranged wrt activity increments. . . . 112
6.6 Patellofemoral contact maps on femur (at selected activity increments) 115

6.7 Patellofemoral contact maps on femur (animation). 116
6.8 Patellofemoral contact maps on patella (animation). 116
6.9 Patellofemoral contact maps on patella (at selected activity increments) 117
6.10 Muscle activation vs stair climb activity progress. 121
6.11 Average muscle activation arranged wrt activity increments. 122
6.12 Muscle force calculated based on EMG signals vs stair climb activity progress. 124
6.13 Average muscle force calculated based on EMG signals arranged wrt activity increments. 125
6.14 Muscle force calculated using inverse dynamics vs stair climb activity progress. 130
6.15 Average muscle force calculated using inverse dynamics arranged wrt activity increments. 131
6.16 Muscle force distribution - EMG vs Inv.Dyn. 132
6.17 Normalized muscle force distribution - EMG vs Inv.Dyn. 134
6.18 Knee joint reaction forces 135
6.19 Patellofemoral joint VAG signal feature comparison for healthy and arthritic knees. 137
6.20 The pattern classification algorithm performance test. 138
6.21 Distribution 33 signal features for healthy and arthritic subjects (DKB activity) 140
6.22 Distribution of 33 signal features for healthy and arthritic subjects (all activities) 146
6.23 Distribution of 33 signal features for healthy and arthritic subjects (all activities) 148
6.24 Best classification results 149

7.1 Total quadriceps force comparison - EMG vs Inv.Dyn. 159

A.1 Patient 1T patellofemoral joint kinematics. 207

A.2 Patient 1T tibiofemoral joint kinematics. 207
A.3 Patient 1T patellofemoral contact location 208
A.4 Patient 1T patella tracking 209
A.5 Patient 1T tibiofemoral contact location 210
A.6 Patient 1T knee joint reaction forces 211
A.7 Patient 1T muscle activation 212
A.8 Patient 1T muscle forces predicted from EMG and inverse dynamics 212
A.9 Patient 1T quadriceps muscle forces predicted from EMG and inverse dynamics 213
A.10 Patient 1T total knee joint reaction forces 213
A.11 Patient 3T patellofemoral joint kinematics. 214
A.12 Patient 3T tibiofemoral joint kinematics. 214
A.13 Patient 3T patellofemoral contact location 215
A.14 Patient 3T patella tracking 216
A.15 Patient 3T tibiofemoral contact location 217
A.16 Patient 3T knee joint reaction forces 218
A.17 Patient 3T muscle activation 219
A.18 Patient 3T muscle forces predicted from EMG and inverse dynamics 219
A.19 Patient 3T quadriceps muscle forces predicted from EMG and inverse dynamics 220
A.20 Patient 3T total knee joint reaction forces 220
A.21 Patient 4T patellofemoral joint kinematics. 221
A.22 Patient 4T tibiofemoral joint kinematics. 221
A.23 Patient 4T patellofemoral contact location 222
A.24 Patient 4T patella tracking 223
A.25 Patient 4T tibiofemoral contact location 224
A.26 Patient 4T knee joint reaction forces 225
A.27 Patient 4T muscle activation 226
A.28 Patient 4T muscle forces predicted from EMG and inverse dynamics 226

A.29 Patient 4T quadriceps muscle forces predicted from EMG and inverse dynamics . . . 227
A.30 Patient 4T total knee joint reaction forces . . . 227
A.31 Patient 8T patellofemoral joint kinematics. . . . 228
A.32 Patient 8T tibiofemoral joint kinematics. . . . 228
A.33 Patient 8T patellofemoral contact location . . . 229
A.34 Patient 8T patella tracking . . . 230
A.35 Patient 8T tibiofemoral contact location . . . 231
A.36 Patient 8T knee joint reaction forces . . . 232
A.37 Patient 8T muscle activation . . . 233
A.38 Patient 8T muscle forces predicted from EMG and inverse dynamics 233
A.39 Patient 8T quadriceps muscle forces predicted from EMG and inverse dynamics . . . 234
A.40 Patient 8T total knee joint reaction forces . . . 234
A.41 Patient 12T patellofemoral joint kinematics. . . . 235
A.42 Patient 12T tibiofemoral joint kinematics. . . . 235
A.43 Patient 12T patellofemoral contact location . . . 236
A.44 Patient 12T patella tracking . . . 237
A.45 Patient 12T tibiofemoral contact location . . . 238
A.46 Patient 12T knee joint reaction forces . . . 239
A.47 Patient 12T muscle activation . . . 240
A.48 Patient 12T muscle forces predicted from EMG and inverse dynamics 240
A.49 Patient 12T quadriceps muscle forces predicted from EMG and inverse dynamics . . . 241
A.50 Patient 12T total knee joint reaction forces . . . 241
A.51 Patient 13T patellofemoral joint kinematics. . . . 242
A.52 Patient 13T tibiofemoral joint kinematics. . . . 242
A.53 Patient 13T patellofemoral contact location . . . 243
A.54 Patient 13T patella tracking . . . 244

A.55 Patient 13T tibiofemoral contact location 245
A.56 Patient 13T knee joint reaction forces 246
A.57 Patient 13T muscle activation 247
A.58 Patient 13T muscle forces predicted from EMG and inverse dynamics 247
A.59 Patient 13T quadriceps muscle forces predicted from EMG and inverse dynamics 248
A.60 Patient 13T total knee joint reaction forces 248
A.61 Patient 17T patellofemoral joint kinematics. 249
A.62 Patient 17T tibiofemoral joint kinematics. 249
A.63 Patient 17T patellofemoral contact location 250
A.64 Patient 17T patella tracking 251
A.65 Patient 17T tibiofemoral contact location 252
A.66 Patient 17T knee joint reaction forces 253
A.67 Patient 17T muscle activation 254
A.68 Patient 17T muscle forces predicted from EMG and inverse dynamics 254
A.69 Patient 17T quadriceps muscle forces predicted from EMG and inverse dynamics 255
A.70 Patient 17T total knee joint reaction forces 255
A.71 Patient 21T patellofemoral joint kinematics. 256
A.72 Patient 21T tibiofemoral joint kinematics. 256
A.73 Patient 21T patellofemoral contact location 257
A.74 Patient 21T patella tracking 258
A.75 Patient 21T tibiofemoral contact location 259
A.76 Patient 21T knee joint reaction forces 260
A.77 Patient 21T muscle activation 261
A.78 Patient 21T muscle forces predicted from EMG and inverse dynamics 261
A.79 Patient 21T quadriceps muscle forces predicted from EMG and inverse dynamics 262
A.80 Patient 21T total knee joint reaction forces 262

A.81 Patient 11T patellofemoral joint kinematics. 263
A.82 Patient 11T tibiofemoral joint kinematics. 263
A.83 Patient 11T patellofemoral contact location 264
A.84 Patient 11T patella tracking 265
A.85 Patient 11T tibiofemoral contact location 266
A.86 Patient 11T knee joint reaction forces 267
A.87 Patient 11T muscle activation 268
A.88 Patient 11T muscle forces predicted from EMG and inverse dynamics 268
A.89 Patient 11T quadriceps muscle forces predicted from EMG and inverse dynamics 269
A.90 Patient 11T total knee joint reaction forces 269
A.91 Patient 11N patellofemoral joint kinematics. 270
A.92 Patient 11N tibiofemoral joint kinematics. 270
A.93 Patient 11N patellofemoral contact location 271
A.94 Patient 11N patella tracking 272
A.95 Patient 11N tibiofemoral contact location 273
A.96 Patient 11N knee joint reaction forces 274
A.97 Patient 11N muscle activation 275
A.98 Patient 11N muscle forces predicted from EMG and inverse dynamics 275
A.99 Patient 11N quadriceps muscle forces predicted from EMG and inverse dynamics 276
A.100 Patient 11N total knee joint reaction forces 276
A.101 Patient 19T patellofemoral joint kinematics. 277
A.102 Patient 19T tibiofemoral joint kinematics. 277
A.103 Patient 19T patellofemoral contact location 278
A.104 Patient 19T patella tracking 279
A.105 Patient 19T tibiofemoral contact location 280
A.106 Patient 19T knee joint reaction forces 281
A.107 Patient 19T muscle activation 282

A.108 Patient 19T muscle forces predicted from EMG and inverse dynamics 282
A.109 Patient 19T quadriceps muscle forces predicted from EMG and inverse dynamics . . . 283
A.110 Patient 19T total knee joint reaction forces . . . 283
A.111 Patient 19N patellofemoral joint kinematics. . . . 284
A.112 Patient 19N tibiofemoral joint kinematics. . . . 284
A.113 Patient 19N patellofemoral contact location . . . 285
A.114 Patient 19N patella tracking . . . 286
A.115 Patient 19N tibiofemoral contact location . . . 287
A.116 Patient 19N knee joint reaction forces . . . 288
A.117 Patient 19N muscle activation . . . 289
A.118 Patient 19N muscle forces predicted from EMG and inverse dynamics 289
A.119 Patient 19N quadriceps muscle forces predicted from EMG and inverse dynamics . . . 290
A.120 Patient 19N total knee joint reaction forces . . . 290
A.121 Patient 22T patellofemoral joint kinematics. . . . 291
A.122 Patient 22T tibiofemoral joint kinematics. . . . 291
A.123 Patient 22T patellofemoral contact location . . . 292
A.124 Patient 22T patella tracking . . . 293
A.125 Patient 22T tibiofemoral contact location . . . 294
A.126 Patient 22T knee joint reaction forces . . . 295
A.127 Patient 22T muscle activation . . . 296
A.128 Patient 22T muscle forces predicted from EMG and inverse dynamics 296
A.129 Patient 22T quadriceps muscle forces predicted from EMG and inverse dynamics . . . 297
A.130 Patient 22T total knee joint reaction forces . . . 297
A.131 Patient 22N patellofemoral joint kinematics. . . . 298
A.132 Patient 22N tibiofemoral joint kinematics. . . . 298
A.133 Patient 22N patellofemoral contact location . . . 299

A.134 Patient 22N patella tracking 300
A.135 Patient 22N tibiofemoral contact location 301
A.136 Patient 22N knee joint reaction forces 302
A.137 Patient 22N muscle activation 303
A.138 Patient 22N muscle forces predicted from EMG and inverse dynamics 303
A.139 Patient 22N quadriceps muscle forces predicted from EMG and inverse dynamics 304
A.140 Patient 22N total knee joint reaction forces 304
A.141 Patient 23T patellofemoral joint kinematics. 305
A.142 Patient 23T tibiofemoral joint kinematics. 305
A.143 Patient 23T patellofemoral contact location 306
A.144 Patient 23T patella tracking 307
A.145 Patient 23T tibiofemoral contact location 308
A.146 Patient 23T knee joint reaction forces 309
A.147 Patient 23T muscle activation 310
A.148 Patient 23T muscle forces predicted from EMG and inverse dynamics 310
A.149 Patient 23T quadriceps muscle forces predicted from EMG and inverse dynamics 311
A.150 Patient 23T total knee joint reaction forces 311
A.151 Patient 23N patellofemoral joint kinematics. 312
A.152 Patient 23N tibiofemoral joint kinematics. 312
A.153 Patient 23N patellofemoral contact location 313
A.154 Patient 23N patella tracking 314
A.155 Patient 23N tibiofemoral contact location 315
A.156 Patient 23N knee joint reaction forces 316
A.157 Patient 23N muscle activation 317
A.158 Patient 23N muscle forces predicted from EMG and inverse dynamics 317
A.159 Patient 23N quadriceps muscle forces predicted from EMG and inverse dynamics 318

A.160 Patient 23N total knee joint reaction forces 318
A.161 Patient 6N patellofemoral joint kinematics. 319
A.162 Patient 6N tibiofemoral joint kinematics. 319
A.163 Patient 6N patellofemoral contact location 320
A.164 Patient 6N patella tracking 321
A.165 Patient 6N tibiofemoral contact location 322
A.166 Patient 6N knee joint reaction forces 323
A.167 Patient 6N muscle activation 324
A.168 Patient 6N muscle forces predicted from EMG and inverse dynamics 324
A.169 Patient 6N quadriceps muscle forces predicted from EMG and inverse dynamics 325
A.170 Patient 6N total knee joint reaction forces 325
A.171 Patient 7N patellofemoral joint kinematics. 326
A.172 Patient 7N tibiofemoral joint kinematics. 326
A.173 Patient 7N patellofemoral contact location 327
A.174 Patient 7N patella tracking 328
A.175 Patient 7N tibiofemoral contact location 329
A.176 Patient 7N knee joint reaction forces 330
A.177 Patient 7N muscle activation 331
A.178 Patient 7N muscle forces predicted from EMG and inverse dynamics 331
A.179 Patient 7N quadriceps muscle forces predicted from EMG and inverse dynamics 332
A.180 Patient 7N total knee joint reaction forces 332
A.181 Patient 15N patellofemoral joint kinematics. 333
A.182 Patient 15N tibiofemoral joint kinematics. 333
A.183 Patient 15N patellofemoral contact location 334
A.184 Patient 15N patella tracking 335
A.185 Patient 15N tibiofemoral contact location 336
A.186 Patient 15N knee joint reaction forces 337

A.187 Patient 15N muscle activation 338
A.188 Patient 15N muscle forces predicted from EMG and inverse dynamics 338
A.189 Patient 15N quadriceps muscle forces predicted from EMG and inverse dynamics 339
A.190 Patient 15N total knee joint reaction forces 339
A.191 Patient 16N patellofemoral joint kinematics. 340
A.192 Patient 16N tibiofemoral joint kinematics. 340
A.193 Patient 16N patellofemoral contact location 341
A.194 Patient 16N patella tracking 342
A.195 Patient 16N tibiofemoral contact location 343
A.196 Patient 16N knee joint reaction forces 344
A.197 Patient 16N muscle activation 345
A.198 Patient 16N muscle forces predicted from EMG and inverse dynamics 345
A.199 Patient 16N quadriceps muscle forces predicted from EMG and inverse dynamics 346
A.200 Patient 16N total knee joint reaction forces 346

Acronyms

α-MN alpha motor neuron.

2D two-dimensional.

3D three-dimensional.

ACL Anterior Cruciate Ligament.

AMZ anteromedialization.

BF Biceps Femoris.

CAD Computer Aided Design.

CNS Central Nervous System.

CT Computed Tomography.

DKB deep knee bend.

ECG electrocardiography.

EEG Electroencephalography.

EMG electromyography.

FFT fast Fourier transform.

FIR finite impulse response.

GL Gastrocnemius Lateralis.

GM Gastrocnemius Medialis.

GRF ground reaction force.

ICR instantaneous center of rotation.

IIR infinite impulse response.

ISA instantaneous screw axis.

ISEK International Society of Electrophysiology and Kinesiology.

KOOS Knee injury and Osteoarthritis Outcome Score.

MRI Magnetic Resonance Imaging.

MVC maximum voluntary contraction.

PCL Posterior Cruciate Ligament.

PCSA physiological cross-sectional area.

PFJR patellofemoral joint reaction.

RF Rectus Femoris.

STFT short-time Fourier transform.

TFCP tibiofemoral contact point.

TKA Total Knee Arthroplasty.

TKR Total Knee Replacement.

TMJ temporomandibular joint.

UHMWPE Ultra-high-molecular-weight polyethylene.

VAG vibroarthrography.

VI Vastus Intermedius.

VL Vastus Lateralis.

VM Vastus Medialis.

WFT windowed Fourier transform.

xBW times body weight.

Chapter 1

Introduction

The patellofemoral joint is an integral part of the knee. It has evolved to withstand remarkable loading conditions and facilitate human locomotion. However, its performance may be disrupted by disease, anatomical deformities, soft tissue imbalance or injury. Patellofemoral disorders may be puzzling, and accurate diagnosis often proves challenging for the physicians.[78]

Most often the patient's complaints about their ailment are nonspecific and the correct diagnosis may be difficult. The affections may have a number of causes and their nature may be related to kinematics (e.g. maltracking of the patella, subluxation), kinetics (e.g. deficient extensor mechanism, excessive bearing loads) or soft tissue deficiency (e.g. meniscus tear, degeneration the the articular cartilage).

The diagnosis is often limited to a detailed interview with the patient, careful physical examination (palpitation) and x-ray imaging. Although the patella is located peripherally, the articulating surfaces are not easily accessible and the conditions of the cartilage cannot be examined directly by the physician. The X-ray screening may reveal bone degeneration, but does not carry sufficient information of the soft tissues' conditions. More advanced imaging tools such as Magnetic Resonance Imaging (MRI) or Computed Tomography (CT) are available, but expensive, time consuming and are suitable only for detection of advanced arthritis. The arthroscopy is often the only

reliable option, however due to its semi-invasive nature, it cannot be considered as a practical diagnostic tool.

Moreover, the patella bone accommodates substantial movements, which in addition to small dimensions and large forces acting on it, present a challenge for biomedical engineers designing partial patellofemoral or total knee replacement prostheses. In fact, complications concerning resurfaced patellofemoral joints have been widely reported as one of the major causes of revision surgery in TKA.[5, 16, 20, 29, 54, 71, 86, 90, 113, 153, 174, 48, 61, 204, 209] Considering that the demand for knee revisions is expected to double by 2015,[149] there is an immediate need to improve the current implant designs. The high-flexion implants, desired by Total Knee Arthroplasty (TKA) candidates, may be especially vulnerable to patellofemoral complications, due to significant loads acting at this joint and increasing with increasing flexion [186, 143, 213]. Therefore, understanding of the biomechanical function of the patella, the mechanisms of load transmission and stability may help with better diagnosis, treatment and rehabilitation. Recognizing the dynamical conditions that the patellofemoral implant components are exposed to, may also help to improve the design of the replacement prostheses.

1.1 Statement of the Problem

In order to better understand the biomechanics of the natural and replaced patellofemoral joint, this work represents an in-depth, in-vivo analysis of the natural and implanted knee joints focused on better understanding of the kinematics and kinetics of the patellofemoral joint.

To achieve this goal 12 total knee arthroplasty (TKA) patients had their implanted knee kinematics recorded under fluoroscopic surveillance while climbing up the stairs. In order to compare the TKA knees with their natural counterparts, four of these patients also had their contralateral knees evaluated. Since the kinematics of the contralateral leg may be affected by the performance of the TKA knee, four young

and healthy (non-symptomatic) subjects had been recruited to constitute the control group. All participants have underwent CT scanning procedure and the images have been used to reconstruct the Computer Aided Design (CAD) models of their bones. The study comprised recreating the three-dimensional (3D) kinematics utilizing the 3D-to-2D registration process[165], inverse dynamics modeling and electromyography-based muscle dynamics analysis.

The stair climbing activity has been chosen for analysis for two reasons. First, it is one of the most commonly performed everyday tasks, and therefore the results of the analysis will provide valuable information for the orthopedic companies striving to improve the existing TKA devices. Second, climbing up the stairs relies mostly on the extensor mechanism performance and the stance phase involves only one leg. This ensures that the lower extremity being analyzed is isolated, so that its biomechanics is not affected by the other leg. In other words, this activity will ensure that, in case a subject experiences some dysfunction related to the knee joint, she/he will not be able to compensate (i.e. alternate) their biomechanics by supporting on the other leg (often present during kneeling activity) and this dysfunction will be reflected in abnormal kinematics and/or kinetics of the patellofemoral joint.

Additionally, it is hypothesized that the magnitude of the vibration of the patellofemoral joint increases with articular cartilage degeneration (i.e. increasing roughness of the articulating surfaces). Although this hypothesis is plausible from the mechanical point of view, it is not clear whether the vibration recorded by the surface sensors can be successfully used for diagnostic purposes. Therefore, this work is also an attempt to assess the feasibility of using miniature accelerometers to study the vibration of the articulating surfaces of the patellofemoral joint.

To this end, additional subjects have been recruited to (1) increase the group of subjects having healthy knees (and intact articular cartilage) to a total of fifteen, and (2) to build an additional group of twenty patients suffering from knee arthritis. The arthritic group patients has been recruited from the primary total knee replacement candidates. This made it possible to record and compare the vibration signals

recorded for patients having intact cartilage with those whose cartilage has been considerably worn.

Chapter 2

Review of Related Literature

2.1 Biomechanical functions of the patella

The patella plays an integral role in transmitting the forces of the extensor mechanism. It also increases the moment arms of these forces and thus facilitates the task. John Shelton in 1789, identified this mechanical function felicitously explaining that "muscles extend the leg by pulling up the *Patella*, which plays in the groove between the two condyles of the *Os Femoris*, as a rope in a pulley, and therefore these muscles (...) act with great mechanical advantage; they not only extend the leg, but assist, likewise, in keeping the thigh-bone fixed upon the *Tibia* in the erect posture; in balancing the body; and in straightening the knee-joint".[214] However, this message was not accepted universally. In 1937, Brooke concluded that the function of the knee after patellectomy was better than before[31] and the excision as treatment gained many followers[94, 239] and supporting long-term clinical studies.[241, 84, 255] Tippett further insisted that "one must learn to accept the fact that the patella, like the appendix, is superfluous - a recessive structure."[231] More recent research proved that the knee extension is impaired[126] and the peak torque of the quadriceps is significantly reduced after patellectomy.[239] Therefore preservation of patella is recommended whenever possible.[124, 133] Moreover, if patellectomy is

necessary, tibial tuberoplasty or other reconstructive procedure should be taken into consideration.[133]

The patella not only links the quadriceps muscle with the tibial tuberosity, but thanks to its structure, it also allows for transmitting forces several times exceeding the body weight, in almost frictionless way.[183] The articulating portion of the patella is completely covered by hyaline cartilage 4-5mm thick in its central portion, making it the thickest articular cartilage in the human body.[78] The hyaline cartilage is aneural and therefore it is well suited for transmitting high compressive forces. The resulting patellofemoral contact stresses are distributed within the thick cartilage so that the pain threshold in subchondral and cancellous bone is not exceeded. The tendons and ligaments are not resistant to frictional forces therefore patella also helps to isolate the extensor mechanism soft tissues from direct interaction with the femoral trochlea. The extensor muscles are attached to the patella base through the quadriceps tendon, and patella helps to centralize these forces. The kneecap also protects the trochlea and femoral condyles from injuries, especially in deeper flexion.

Finally, the patella is an aesthetic element of the knee joint giving the lower extremity smooth and continuous appearance which can be contrasted with the squared look of the knee following patellectomy, especially in flexion.[78]

2.2 Patellofemoral kinematics, tracking and contact

2.2.1 Unambiguous description

In order to study the kinematics of the patellofemoral joint, its motion needs to be described in unambiguous terms that could be readily interpreted. Since the patella articulates only with the femur, most frequently (and appropriately) its motion is described relative to the femur. The patella can translate in three directions (anterior-posterior, medial-lateral and proximal-distal) and rotate in three planes (coronal,

sagittal and transverse). Unfortunately, due to the lack of a standard description convention of patellar motion many researchers used different coordinate systems and developed their own definitions of motion. As a result there is significant discrepancy in the data reported in the literature and often there is not enough information that would allow transforming the data from one description to another. For instance, the rotations can be defined using clinical (flexion, rotation and tilt) or engineering terms (such as Euler or Cardan angles). The discrepancy arises because the engineering terms do not always match the clinical rotations. It will also depend on whether one defines the rotations relative to the coordinate system fixed to the patella or femur (or possibly another, global reference system). It will also depend on how such a reference system is oriented relative to the bones. Finally, if Euler rotations are employed, their magnitudes will depend on the chosen sequence of rotations.

In 1983, Grood and Suntay proposed the convention for describing the kinematics of the human joints using a standardized joint coordinate system.[93] The novelty of this description was that they proposed to form a coordinate system by using one axis fixed to each of the two bodies and define the third axis as the cross product of the previous two (hence being mutually perpendicular to the previous two). As a result such a coordinate system is not orthogonal and the third axis changes its direction depending on the directions of the two fixed axes (therefore it is often called a floating axis). Application of this convention offers two main advantages:

(1) the rotations remain consistent with clinical terms throughout the range of motion, and

(2) the rotations are sequentially independent.

The authors presented their elegant mathematical derivations on an example of the knee joint, but the system can be readily applied to any other joint.

In 2002, the The Standardization and Terminology Committee of the International Society of Biomechanics (ISB) recommended using the joint coordinate system as the standard for reporting human joint kinematics.[250] The ISB described how

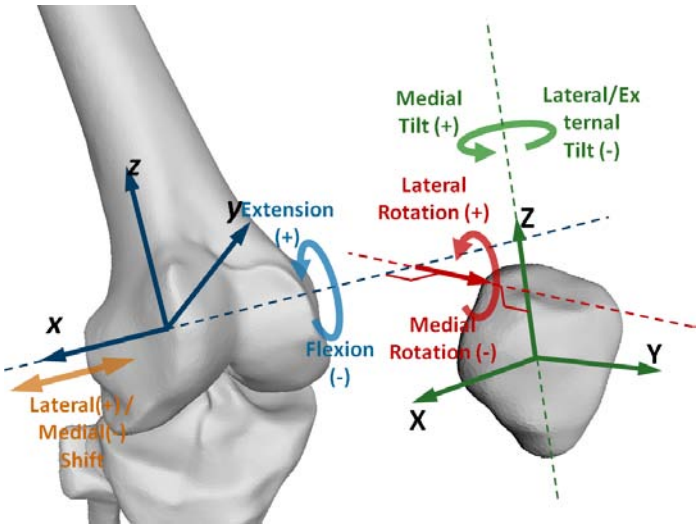
to apply this convention to the ankle, hip, spine,[250] shoulder, elbow, wrist and hand.[249] However, the ISB did not present the application of this system to the patellofemoral joint, perhaps because two months earlier, Bull et al. scrutinized the discrepancies between existing systems and recommended using the Grood and Suntay convention.[35] Bull et al. also noted that there are many various terms being used to describe the same motion, e.g. the rotation of the patella about its anterior-posterior axis is often referred to as medial/lateral rotation, internal/external rotation or varus/valgus rotation. Therefore, in order to avoid ambiguity, throughout this dissertation the standard and terminology proposed by Bull et al. will be used as shown in the Figure 2.1. Since it is the motion of the patella relative to the femur, that is being described, the femur will be considered a fixed and the patella a moving body.

It is also important to notice, that even after including all the recommendations, if one wants to report the data measured for left and right knees on a common graph, the signs have to be changed to match one of the knees terminology. For instance, the positive translation along the femoral x axis will be interpreted as the *medial* shift for the left knee (Fig. 2.1b), but as the *lateral* shift for the right knee (Fig. 2.1a). Therefore, all data in this manuscript was converted to match the signs of the right knee. In addition, although Grood and Suntay originally proposed the translations to be measured along the joint coordinate system axes, it is actually more appropriate to describe the translations relative to the coordinate system fixed to one of the bodies,[10] and this approach will be followed throughout this dissertation.

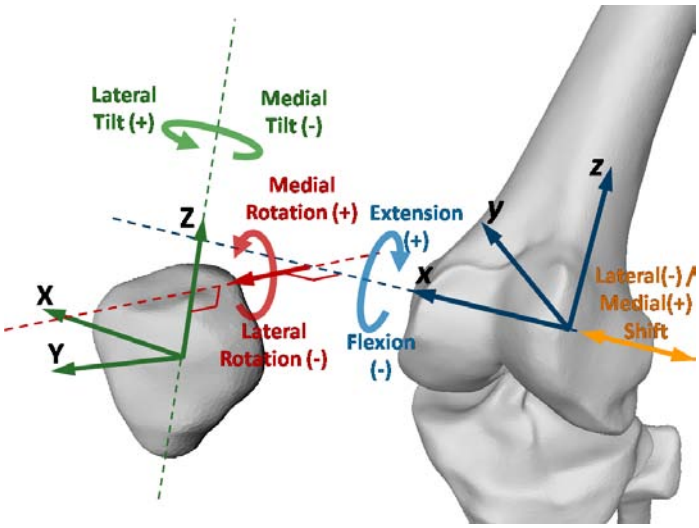
2.2.2 Patella kinematics

Patellar shift

At full extension the patella is located above the trochlear groove and may not be in contact with the femur, but it comes quickly into contact when the knee is being flexed. When patella enters the trochlea, it is located centrally with respect to the



(a) Right knee.



(b) Left knee.

Figure 2.1: Application of the joint coordinate system proposed by Grood and Suntay[93] to the patellofemoral joint of the right (2.1a) and left knee (2.1b).

groove (Figure 2.2a). Within the first 30° of knee flexion, the femur rotates externally and the patella either remains central or moves slightly medially.[114, 97, 163] With increasing flexion, it slides distally and into the femoral groove. At this point the quadriceps is contracting to help balance the knee and the forces exerted by the extensor mechanism, pull the patella against the femur. Therefore, the confines of the trochlear groove restrict the patellar medial/lateral translation and "'guide"' the

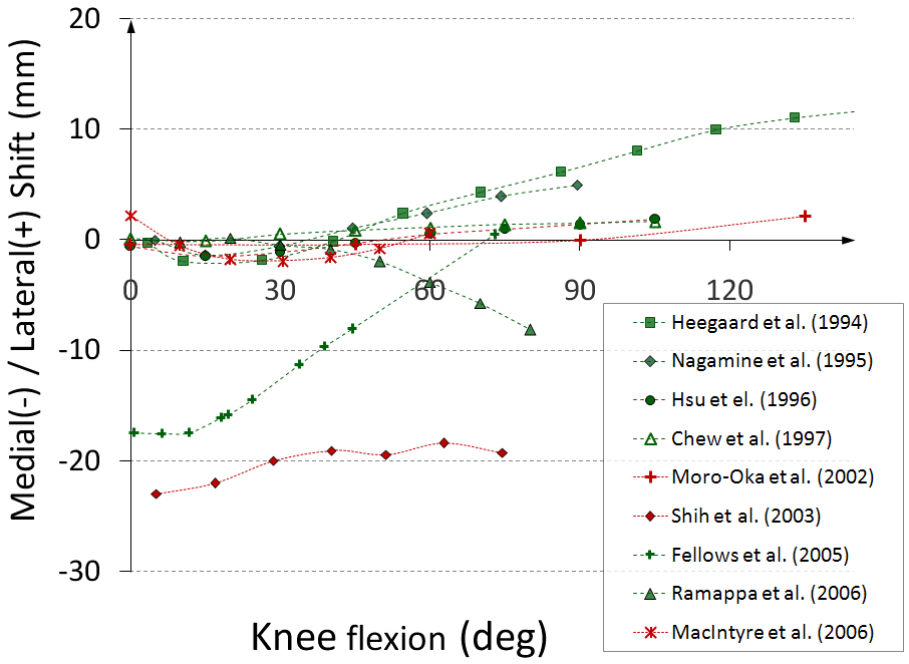
patella along the trochlea. In-vitro studies showed that after initially remaining centrally, the patella shifts lateraly with increasing flexion[97, 114, 41, 69, 185] which was confirmed in-vivo using MRI[181] and ultrasound measurements.[215] Some of these studies showed that from extension to flexion, this lateral translation may be as large as 17mm[69] or 12mm,[97] but others reported lower values of 5mm,[185] 3mm[215] and 2mm.[181, 41]

Chew et al.[41] studied the patellar kinematics of three total knee replacement designs. They found that after the arthroplasty, the patella also translated laterally with increasing flexion, but above 60° it started moving medially (Figure 2.2b). However, the range of this secondary medial shift in deeper flexion was small; 1.79mm for Genesis II, 1.55mm for NexGen and 2.28mm for PFC Total Knee Arthroplasty (TKA). Chew et al. used the onlay patella buttons for all three TKA designs, therefore the differences in kinematics may be attributed to the differences in geometry of the femoral components. However, the amount of the medial-lateral translation may be also influenced by the type of the patellar button. Ezzet et al.[66] also used PFC Sigma TKA with onset patellar button and found approximately 1mm of medial-lateral translation, similar to results showed by Chew et al., but when the inset patellar component was used, the patella translated 10mm laterally (Figure 2.2b).

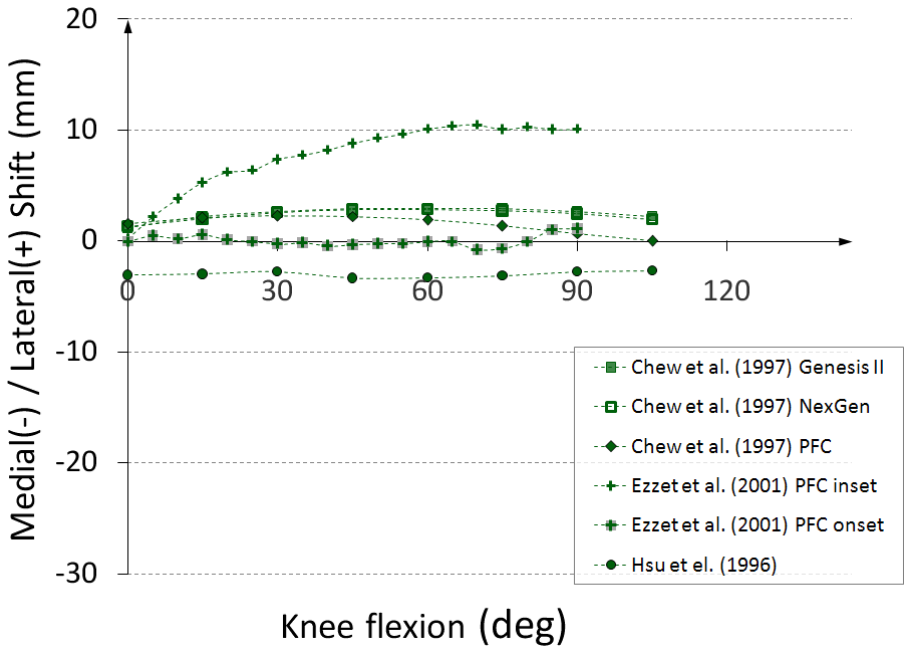
Patellar flexion

The patellar flexion increases with increasing knee flexion. This relatioship was consistently observed in-vitro[234, 97, 114, 154, 192, 3, 151, 69] as well as in-vivo.[223, 109, 163, 158] The patella flexes with lower rate than the femur relative to tibia (compare the gray solid line with the dashed line in Figure 2.3a). The relationship between patellar and tibiofemoral flexion seems to be linear, as the regression line fitted to the data shown in Figure 2.3a yields $r^2 = 0.96$ and the following equation:

$$PatellaFlexion = 0.68 \cdot (FemoralFlexion) + 0.74 \tag{2.1}$$



(a) Shift of the natural patella.



(b) Shift of the TKA patella.

Figure 2.2: Shift of the natural (top) and TKA (bottom) patella reported in the literature measured in-vitro (green) and in-vivo (red).

The flexion of the implanted patella also increases with knee flexion (Figure 2.3b) similarly to that observed for the natural patella and can also be approximated by a linear function ($r^2 = 0.97$):

$$TKAPatellaFlexion = 0.67 \cdot (TKAFemoralFlexion) + 0.86 \tag{2.2}$$

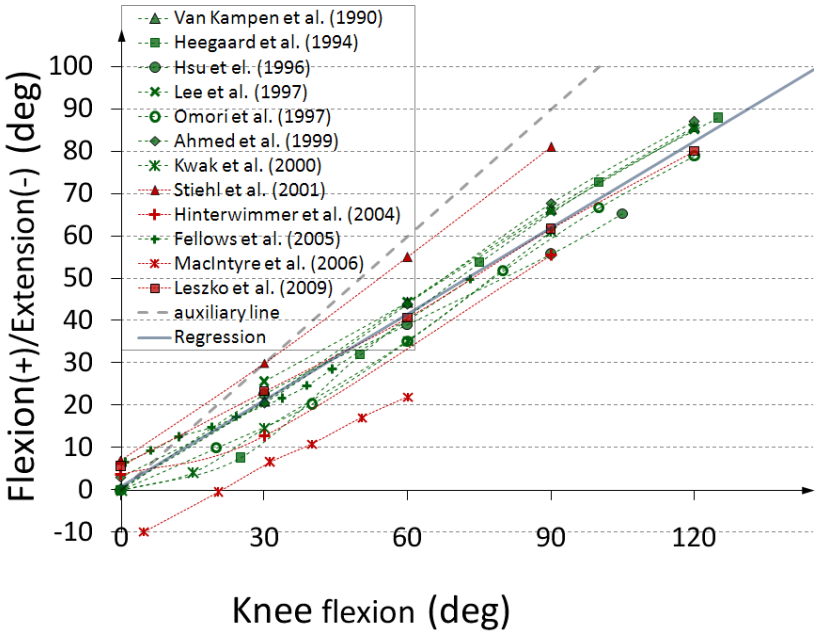
Patellar rotation

On average, the patella rotates medially with increasing flexion (Figure 2.4a).[75, 185, 114, 41, 69, 203, 163] Fellows et al.[69] observed almost linear increase of patella rotation of 8° from full extension to 50° of flexion. Ramappa et al.[203] reported also almost linear increase of 12° between 20° and 80° of knee flexion. Nagamine et al.[185] and Chew et al.[41] however, found nonlinear relationship of patellar rotation with femoral flexion and within considerably smaller ranges; 3° and 4°, respectively. MacIntyre et al.[163] also observed a general trend of patella rotating medially with increasing flexion but noted high inter-subject variability in the population of sixty patients that they evaluated in-vivo using MRI.

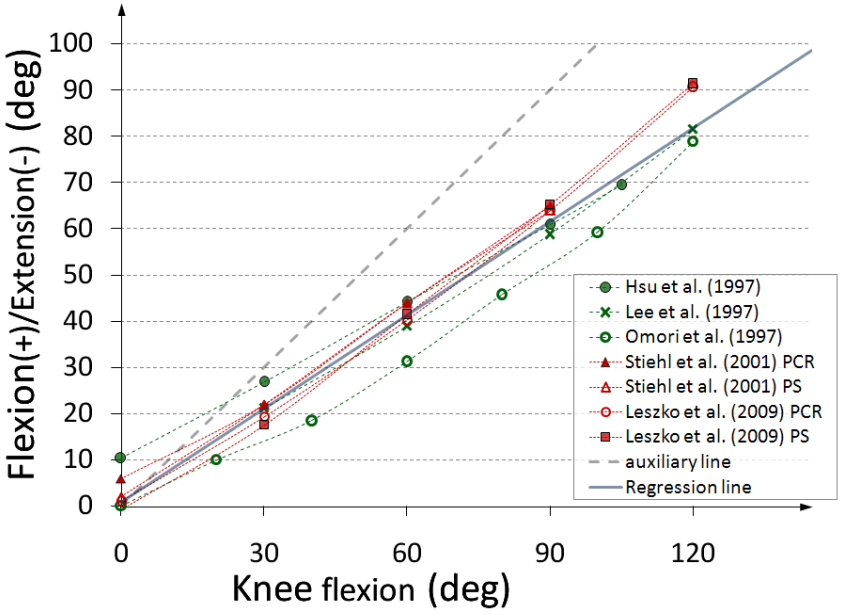
Chew et al. found almost linear change of patella rotation for all three TKA systems they investigated.[41] Their results show that the implanted patella was 2.5° laterally rotated af full extension and rotated 7° medially with increasing flexion (Figure 2.4b). Ezzet et al.[66] found even more medial rotation of TKA patella; 8° for the inset and 12° for the onset patella. Their results, however, show that the resurfaced patella rotates mostly after 30° of knee flexion.

Patellar tilt

The measurement of the patellar tilt reported in the literature vary considerably (Figure 2.5a). Chew et al.[41] found almost no chage in patellar tilt for the intact knee throughout the flexion range. Heegard et al.,[97] Nagamine et al.[185] and Fellows et al.[69] reported slight medial tilt of the patella in the first 30° of knee

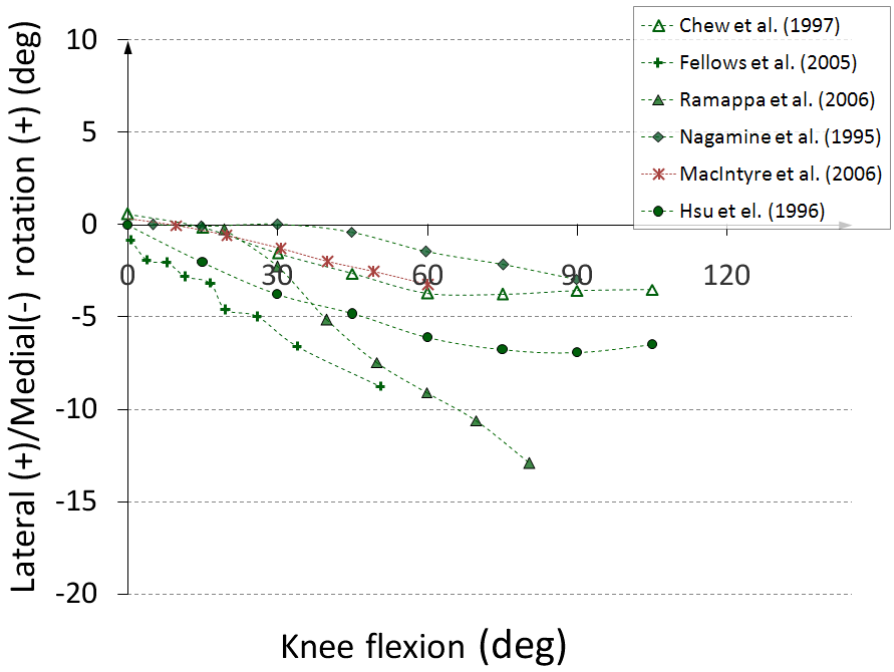


(a) Flexion of the natural patella.

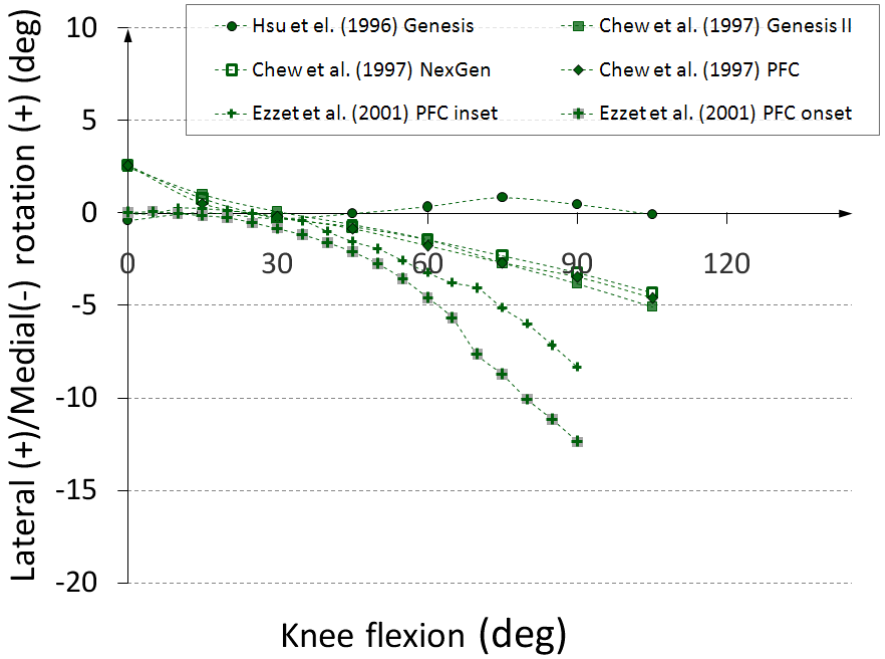


(b) Flexion of the TKA patella.

Figure 2.3: Flexion of the natural (top) and TKA (bottom) patella reported in the literature measured in-vitro (green) and in-vivo (red). Although, according to the chosen convention (Fig. 2.1), the flexion of the patella has negative sign, it has been plotted as positive to match the style used in past literature.



(a) Rotation of the natural patella.



(b) Rotation of the TKA patella.

Figure 2.4: Rotation of the natural (top) and TKA (bottom) patella reported in the literature measured in-vitro (green) and in-vivo (red).

flexion followed by lateral tilting in deeper flexion. MacIntyre et al.[163] reported a similar trend in-vivo, but stressed that patellar tilt had very large variability in the observed patterns. This may also explain differences in the magnitude of the lateral tilt reported by different authors and varying from 3° [185] to 16°.[69]

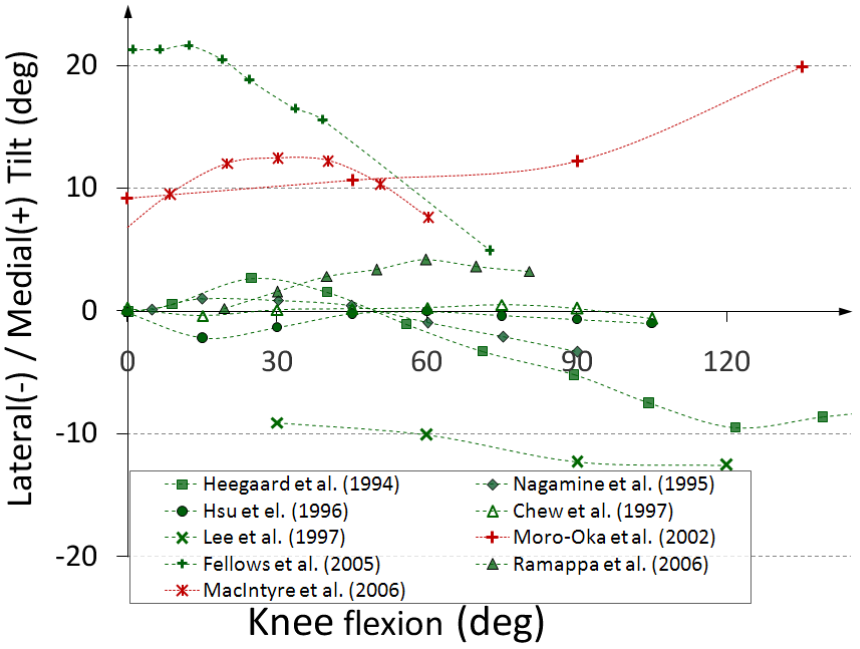
Large intersubject variability might be the reason why some authors observed an opposite trend. Ramappa et al.[203] reported that patella tilted about 4° medially with increasing flexion. Under in-vivo conditions, Moro-oka et al.[181] measured the "'patellar tilting angle formed between the line parallel to the tangent of the anterior condyle and the line drawn tangential to the lateral facet of the articular surface of the patella"'. An increase of this angle is equivalent to the increasing medial tilt of the patella (Figure 2.1). These authors, found that the medial tilt increases from 9° at full extension to 20° at 135° of knee flexion (Figure 2.5a).

Chew et al.[41] and Ezzet et al.[66] investigated the tilt of the replaced patella and found more consistent patterns (Figure 2.5b). Data reported by these groups show slight medial tilt in the first 30° of flexion, followed by lateral tilt in deeper flexion. Only the patella of the NexGen design lacked the initial medial tilt and was tilting laterally throughout the range of motion, similar to the results reported for Genesis TKA by Hsu et al.[114]

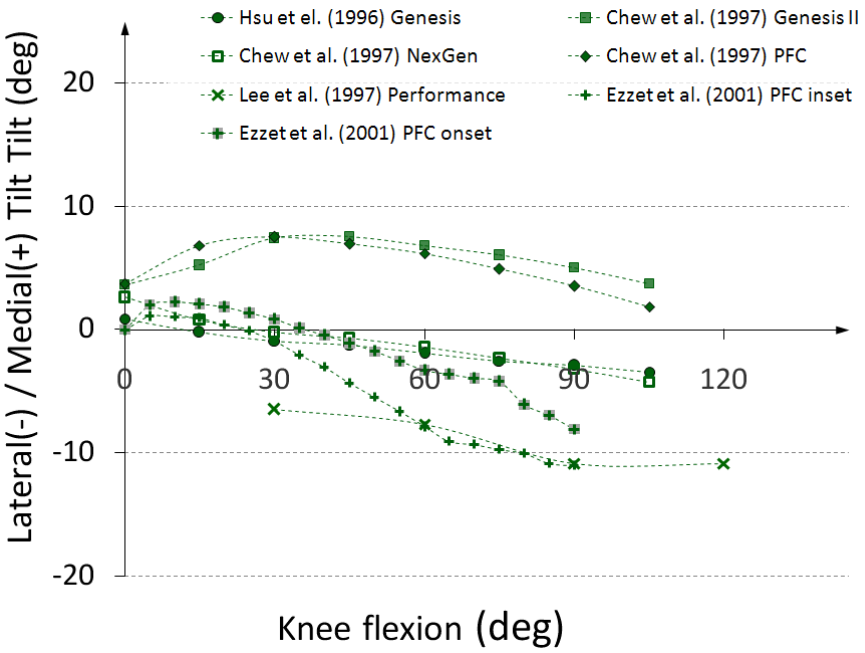
2.2.3 Patellofemoral contact

In healthy knee joint, at full extension the patella is located above the trochlea and is not always in contact with the femur bone (Figure 2.6). In-vivo and in-vitro studies, revealed that the patella becomes in contact with the femur within the first 30° of flexion and the contact location translates distally with increasing flexion.[99, 63]

The contact on the patella for natural knees, first occurs on the lower portion of the border of the articular surface and migrates proximally with increasing flexion (Figure 2.6).[87, 2, 99, 216, 192, 223, 158] For the replaced patella, the contact remains more centrally located throughout the range of motion.[223, 192, 158] This central location



(a) Tilt of the natural patella.



(b) Tilt of the TKA patella.

Figure 2.5: Tilt of the natural (top) and TKA (bottom) patella reported in the literature measured in-vitro (green) and in-vivo (red).

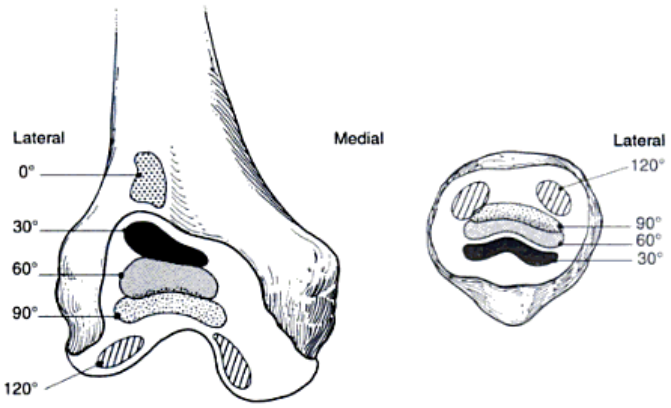


Figure 2.6: Patellofemoral contact location determined in-vitro. Source: [1]

of the contact area may be favorable because the center of the patellar component is thicker and may facilitate the distribution of the patellofemoral joint reaction force (PFJR).

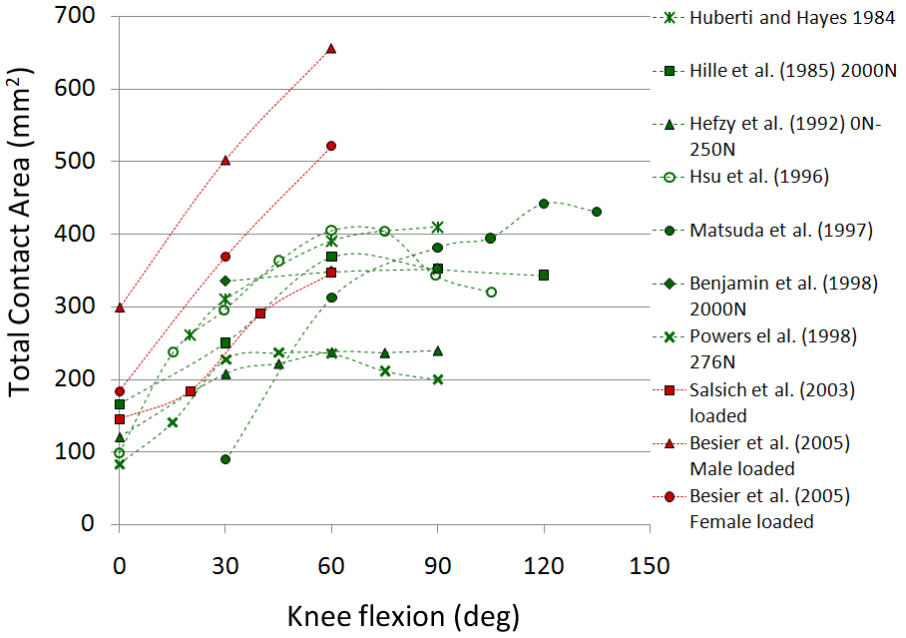
Under in-vitro conditions, the contact area is most frequently measured by means of a pressure sensitive film inserted between the articulating surfaces or by miniature pressure transducers implanted into the bone of a cadaver. The results, however, will inherently depend on the magnitude of loads applied during the experiment, and on the direction of that load. More recently the contact areas were determined in-vivo using MRI. However, due to long time required for image acquisition, this technique cannot be used for dynamic activities, such as squat. Therefore, a static load is usually applied to the lower extremity, and the subject contracts the quadriceps to balance the load simulating dynamic conditions.

Despite the differences in measurement techniques, the researchers found that for intact patella, the area of the contact tends to increase with flexion (Figure 2.7a).[108, 99, 114, 171, 18, 198, 212, 21] After TKA surgery, however, the patellofemoral contact area is considerably reduced. Matsuda et al.[171] found that the reduction was significant for both dome shaped (Profix, Smith & Nephew, Memphis, TN) and conforming (Low-Contact Stress, DePuy, Warsaw, IN) patellar components. Interestingly, they found that the total contact area was not significantly

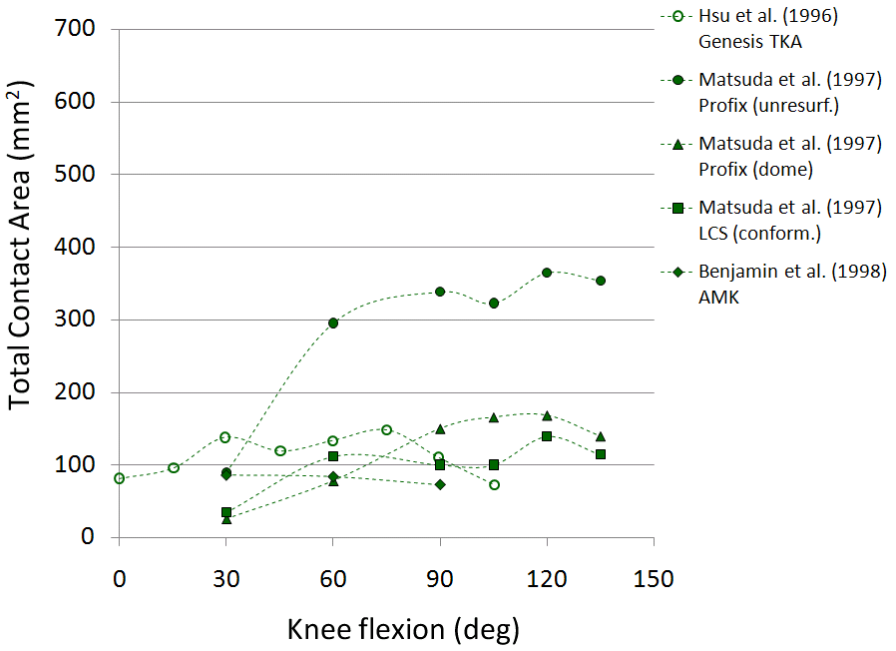
reduced after the replacement procedure when the patella was chosen to be not resurfaced. Similarly, Omori et al.[192] noticed that compared to intact knee, the contact area was significantly reduced after implanting the Genesis TKA (Smith & Nephew, Memphis, TN), but it was not significantly reduced when the patella was left unresurfaced with the same TKA system. Therefore, these authors suggested, that the patella might be left unresurfaced for selective patients depending on the cartilage condition. However, patellar resurfacing has been a controversial topic and was widely debated in the literature.[28, 37, 68, 238, 14] Although the long-term results are very similar for both options,[172] resurfacing is mandatory in patients with inflammatory arthritis and desirable for patients with severely worn or lateralized patella.[27]

2.3 Extensor mechanism forces and patellofemoral stresses

The knee joint provides support and stability for the upper body, and the patellofemoral joint plays an essential role in facilitating these functions. When a person stands upright with the knees fully extended (as shown in Figure 4.2c), all the major forces acting on the body act mainly in the vertical direction and therefore act on relatively small moment arms (see Sec. 4.1) relative to the tibiofemoral contact point. However, when the knee is being flexed, such as during squatting exercise, although the weight of the person does not change, the moment arms of the weight and reaction forces carried by the hip joint increase significantly (compare the d_W and d_{Hip} in Figures 4.2a and 4.2c). If the person attempts to maintain the balance with the knees flexed, the resultant moment $M_T FCP$ needs to be reduced to zero, so that the body could achieve static equilibrium. In this case, it follows from Eq. 4.3, that the resultant force generated by the quadriceps muscle F_{Quad} will be the only one counterbalancing the moment generated by the F_{Hip}, W and F_{PFJR} (note that $F_{Quad}d_{Quad}$ is the only



(a) Patellofemoral contact area in healthy knees.



(b) Patellofemoral contact area in TKA.

Figure 2.7: Patellofemoral contact area measured using in-vitro (green) and in-vivo (red) approach for non-implanted (top) and implanted (bottom) knees.

component with positive sign in the equation):

$$0 = F_{Quad}d_{Quad} - F_{PFJR}d_{PFJR} - Wd_W - F_{Hip}d_{Hip} \tag{2.3}$$

or simply:

$$F_{Quad}d_{Quad} = F_{PFJR}d_{PFJR} + Wd_W + F_{Hip}d_{Hip} \tag{2.4}$$

Since the moment arms of the d_W and d_{Hip} are much larger than the quadriceps moment arm d_{Quad}, the force generated by quadriceps muscle has to be significantly larger than the other forces to counterbalance them. Indeed, both theoretical and experimental studies showed that the quadriceps force increases with increasing flexion and its magnitude exceeds several times the body weight (Figure 2.8).[208, 50, 213] The magnitudes and patterns of the forces depend on the activity being investigated. They will also vary between subjects and depend on a number of physiological parameters such as height or weight. Gender also affects the muscle activation patterns employed in athletic tasks.[167]

It is not possible to measure the in-vivo forces acting in the extensor mechanism directly. Therefore, researchers attempted to estimate them. The methodologies can be grouped into to broad categories: (1) in-vitro measurements and (2) mathematical prediction. In-vitro approach usually involves constraining a cadaveric knee joint in a mounting device (such as Oxford rig) and simulating a physiological activity while measuring the forces by means of pressure or force transducers implemented into the cadaver. The mathematical modeling tries to estimate the forces by using either a forward or inverse dynamics theory. In a forward solution model, typically, an attempt is made to optimize the forces so that they produce a desired motion. The inverse models make use of measured in-vitro or in-vivo kinematics and attempt to calculate for the forces that have produced this motion. Both of these methodologies suffer from certain limitations. The results of in-vitro studies will depend on the loading[198] and boundary conditions being used in the simulation and therefore are difficult to extrapolate to in-vivo conditions. The mathematical models, on the other hand,

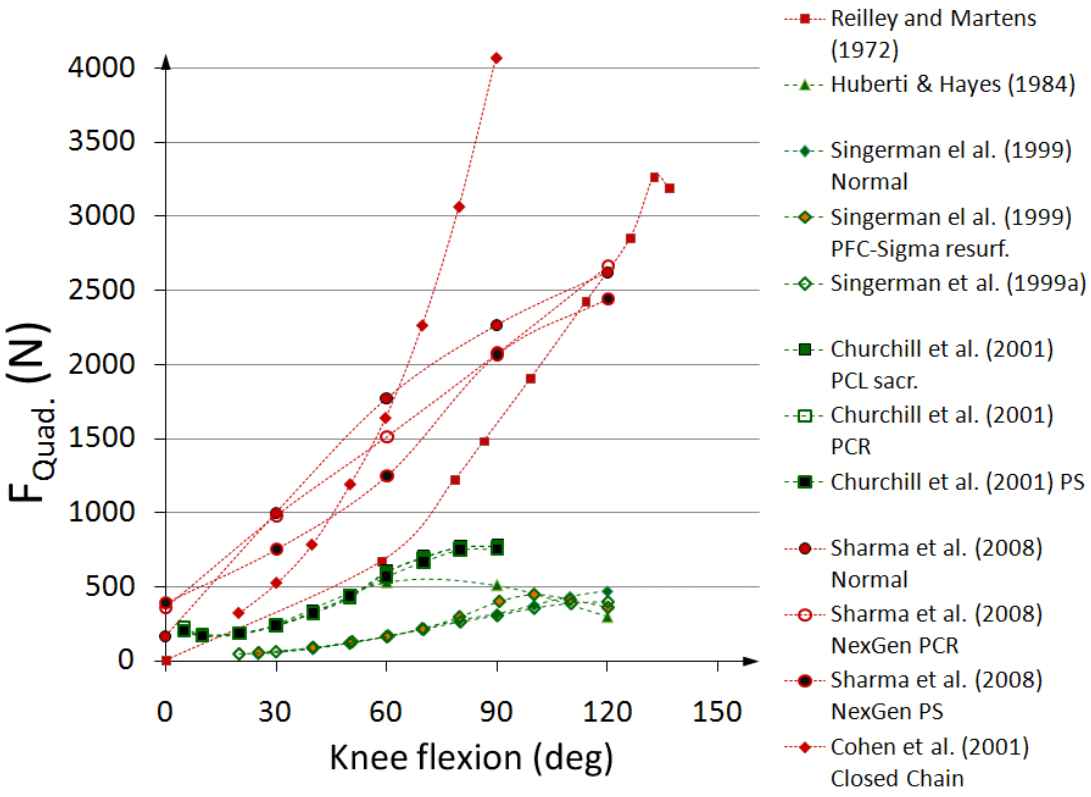


Figure 2.8: Quadriceps muscle force F_{Quad} determined in-vitro using cadaver experiments (green) and predicted using mathematical modeling with in-vivo input (red).

encounter a problem of indeterminacy as there are more unknowns than equations of motion available to solve for them. Therefore these models will depend on a chosen optimization criterion or on the reduction strategy. Nevertheless, both approaches contribute to better understanding of the mechanics of the extensor mechanism.

The results available in the literature reveal that the quadriceps (F_{Quad}), patellar ligament ($F_{Pat.Lig}$) and patellofemoral joint reaction (F_{PFJR}) forces increase with increasing flexion (Figures 2.8, 2.9, 2.10). At full extension, the normal knee is in valgus position and the quadriceps tendon is aligned at the Q angle with the patellar tendon (Figure 2.11). The patella, at this instance, is not confined by the trochlea and the contraction of the quadriceps produces a resultant force acting laterally, often referred to as *Valgus Vector*. This lateral pull may contribute to the occurrence of

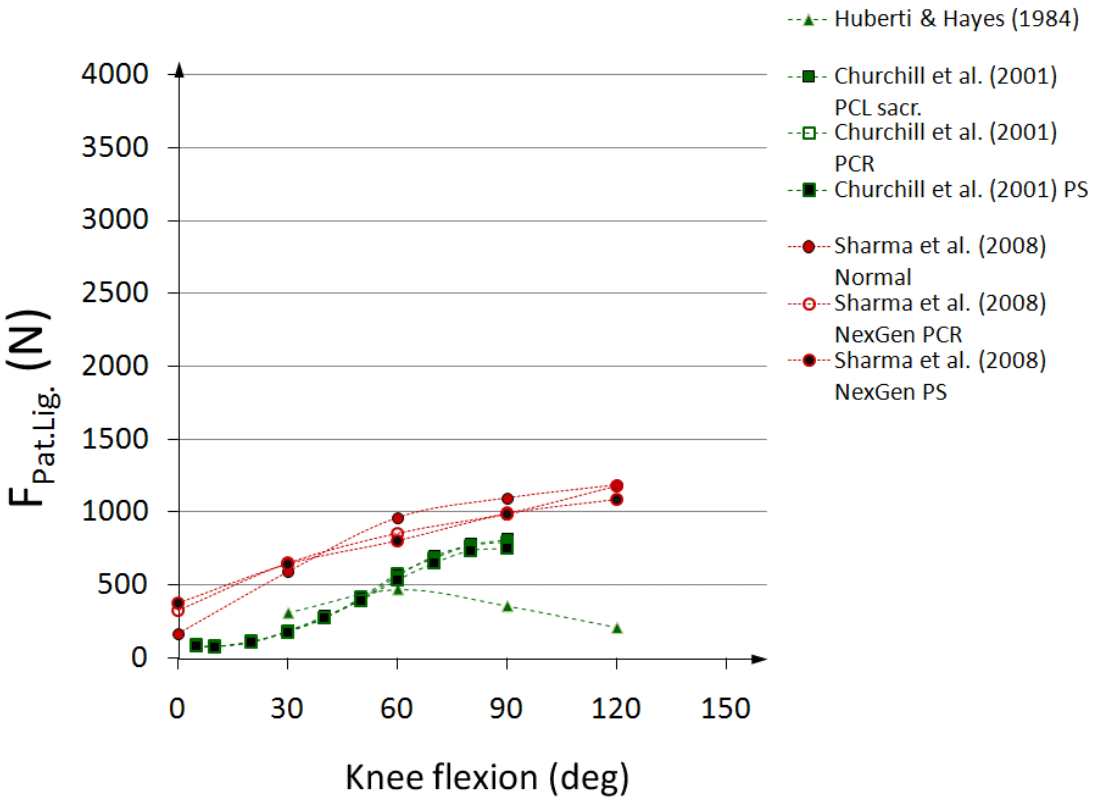


Figure 2.9: Patellar ligament force $F_{Pat.Lig.}$ determined in-vitro using cadaver experiments (green) and predicted using mathematical modeling with in-vivo input (red).

lateral subluxation of the patella in terminal extension, but Q angle is only one of a number of factors affecting patellar balance[78] The Valgus Vector is counterbalanced by the Vastus Medialis Obliquus and by the medial retinacular structures.

In the past, the patellofemoral joint was modeled as a frictionless pulley, but its function is much more sophisticated.[2, 118, 23, 34, 64, 168] The patella as a body has six degrees of freedom and its kinematics is far from trivial (Sec. 2.2.2). The patellofemoral contact location changes with flexion and so does the location of application of the patellofemoral joint reaction force. Most importantly, as demonstrated by Hehne,[100] the patella has its own lever arms and tendon insertions at different heights (Figures 4.2d and 4.2d). Therefore, unlike in a simple pulley, the forces on patellar and quadriceps tendons are not equal. Only at full extension, when

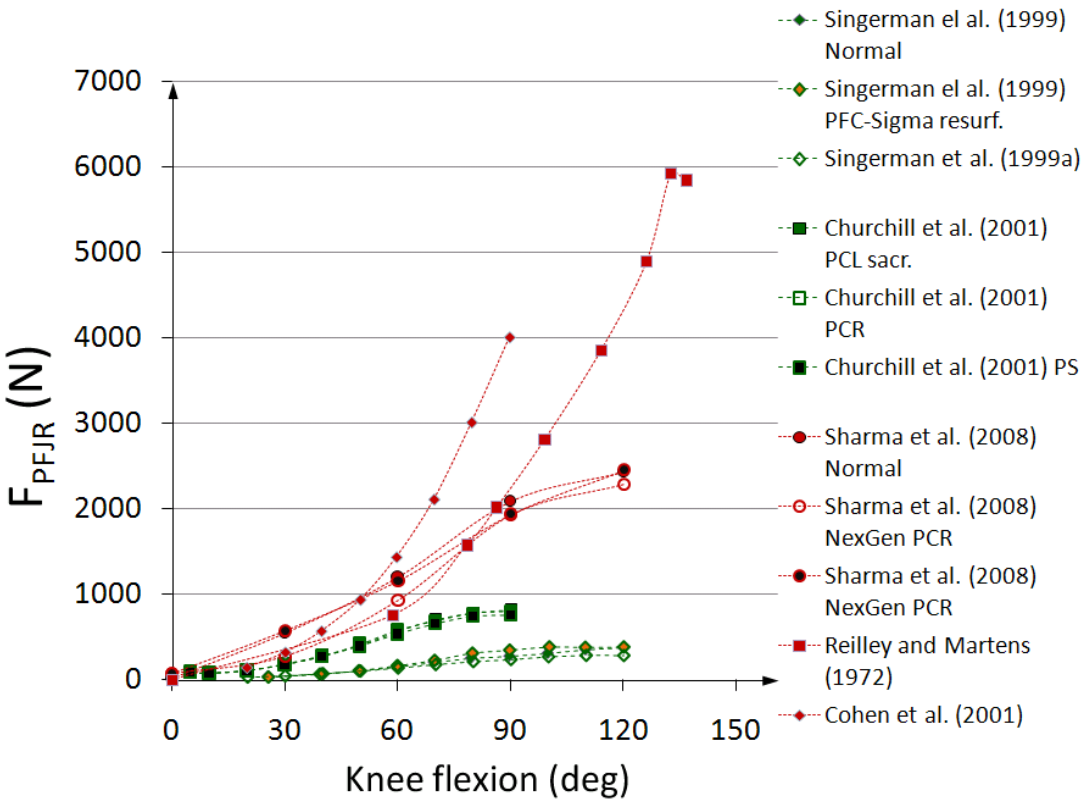


Figure 2.10: Patellofemoral joint reaction force F_{PFJR} determined in-vitro using cadaver experiments (green) and predicted using mathematical modeling with in-vivo input (red).

the opening angle between the quadriceps and patellar ligament forces is large (angle γ in Figure 4.2), the quadriceps pull is almost directly transfered to the patellar ligament, and therefore forces carried by these two structures are similar (note the ratio in Figure 2.13a is close to 1). Moreover, since the quadriceps force is almost directly transfered to the tibial tuberosity, the patellofemoral joint reaction force is small at terminal extension (Figure 2.10). However, as the knee flexes the opening angle decreases and the quadriceps and patellar ligament forces start pulling the patella. As a result, the patellofemoral joint reaction force increases from almost zero at full extension to approximately 3.1xBW at 120° (2430N for an 80kg person)[213] The ratio of the patellofemoral joint reaction (PFJR) to the quadriceps force also inccreases; from about 0.5 at full extension to almost 1 at 90° of flexion (Figure 2.12).

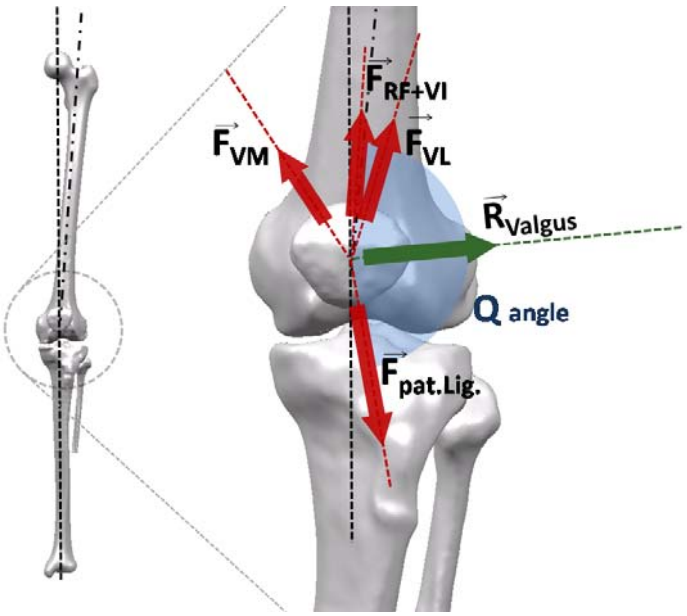
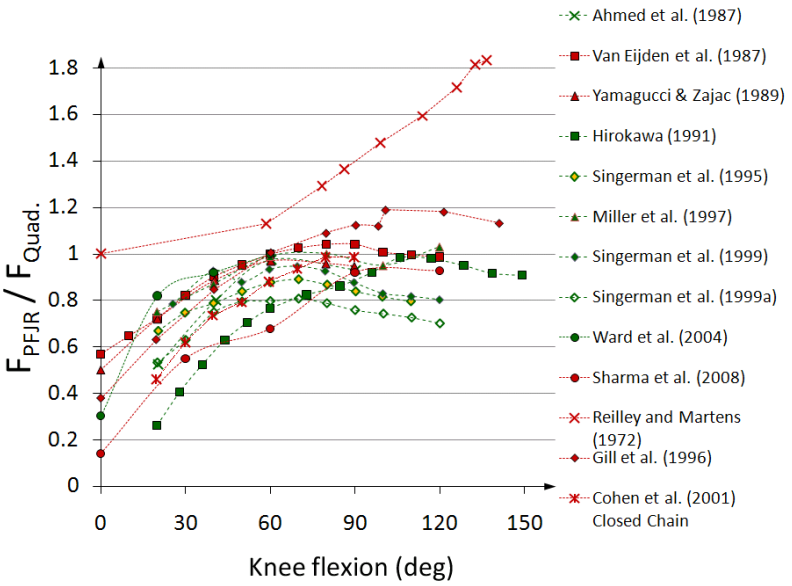


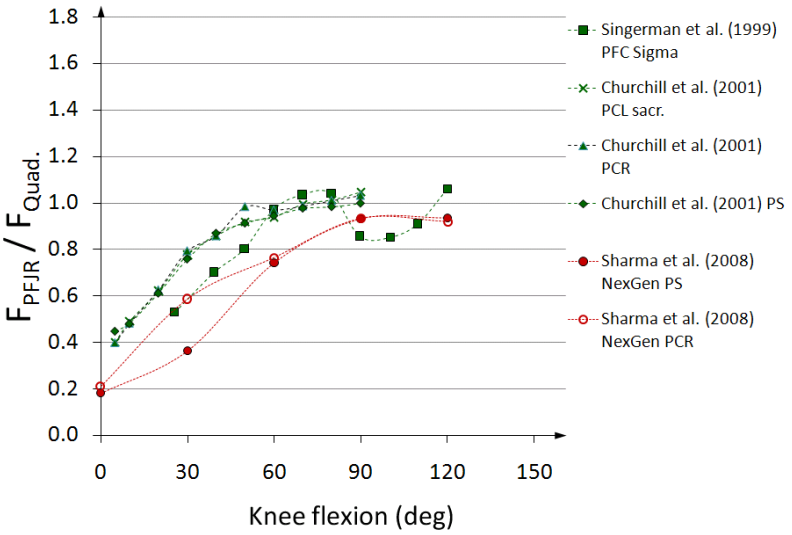
Figure 2.11: Schematic representation of the directions of the quadriceps muscle group pull.

Above 90° of flexion there is no further increase in this ratio, although both forces continue to increase with flexion. This may be explained by the fact that in deeper flexion the patella slides distally, the quadriceps tendon wraps about the trochlea and portion of the quadriceps force is transmitted directly to the femur. Huberti and Hayes found that this tendofemoral contact accounted for $\frac{1}{3}$ of the total contact force at 120°.[116] In deeper flexion the quadriceps pull is counterbalanced more by the PFJR rather than the patellar ligament, and therefore the proportion of the patellar ligament force to the quadriceps force decreases to about 0.6 at 120° (Figure 2.13a).

The total knee arthroplasty alters patellofemoral kinematics (Sec 2.2.2) and may influence the extensor mechanism kinetics. The tibiofemoral kinematics is also affected by the TKA surgery. The amount of posterior femoral translation is often decreased compared to healthy knees[39] Dennis et al.[56] suggested that this might decrease the patellar moment arm postoperatively and result in higher quadriceps muscle forces. Indeed, Ostermeier et al.[194] found a postoperative increase in the quadriceps force of 11.9% for Interax and 6.6% for LCS prostheses, needed to extend

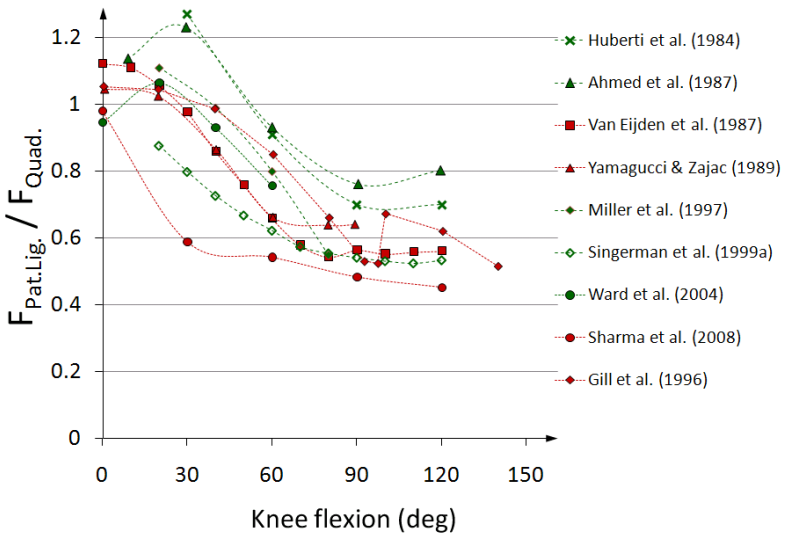


(a) Patellofemoral joint reaction force F_{PFJR} vs Quadriceps muscle force F_{Quad} for a normal knee.

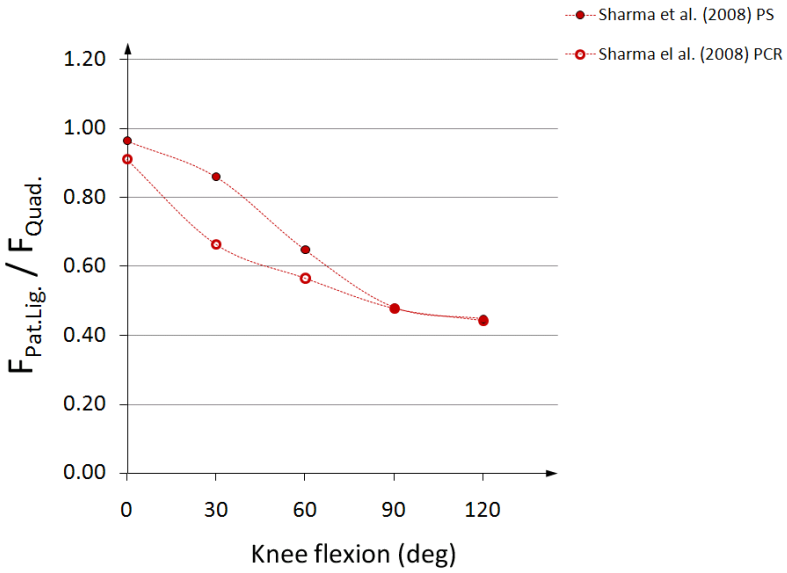


(b) Patellofemoral joint reaction force F_{PFJR} vs Quadriceps muscle force F_{Quad} for a TKA knee.

Figure 2.12: Relationship of the patellofemoral joint reaction force to the quadriceps force reported in the literature for normal and TKA knees determined in-vitro using cadaver experiments (green) or predicted using mathematical modeling with in-vivo input (red).



(a) Patellar ligament force $F_{Pat.Lig.}$ vs Quadriceps muscle force F_{Quad} for a normal knee.



(b) Patellar ligament force $F_{Pat.Lig.}$ vs Quadriceps muscle force F_{Quad} for a TKA knee.

Figure 2.13: Relationship of the patellar ligament force to the quadriceps force reported in the literature for normal and TKA knees determined in-vitro using cadaver experiments (green) or predicted using mathematical modeling with in-vivo input (red).

the knee. Sharma et al.[213] found that during deep knee bend, at maximum flexion, the quadriceps and PFJR forces are significantly higher for NexGen CR-Flex and NexGen LPS-Flex TKAs than for healthy knees. However, at lower flexion the forces were not significantly different and the patterns of the patellar ligament and PFJR forces relative to quadriceps were very similar to the non-implanted knees (Figures 2.12, 2.13).

Nevertheless, even if the PFJR force is similar in TKA and non-implanted knees, the decrease in the contact area (Figure 2.7) observed for resurfaced patella is significant and leads to higher stresses in the patellar component,[18, 171, 192] which may decrease the longevity of the prosthesis. The natural patella uniformly distributes contact pressures[116] over larger areas, which allows transferring high PFJR forces without exceeding the pain threshold of highly innervated subhondral bone. Benjamin et al.[18] found that after resurfacing the contact area amounted to only 8% of the patellar surface available for contact and 64% of the contact stresses exceeded the yield strength of Ultra-high-molecular-weight polyethylene (UHMWPE). The authors also found that non-resurfaced the patella in the TKA, maintained high contact area and the contact stresses were below the yield strength of the articular cartilage in 80% of total contact area.

2.4 Vibroarthrography of the knee joint

2.4.1 Historical background

Patellofemoral joint complaints are one of the most frequently reported musculoskeletal complaints in all age groups. Most often the patient's complains are nonspecific and the correct diagnosis may be difficult. The diagnosis is often limited to detailed interview with the patient, careful physical examination (palpitation) and x-ray imaging. Although the patella is located peripherally the articulating surfaces are not easily accessible and the conditions of the cartilage cannot be examined by the

physician. X-ray screening may reveal bone degeneration, but does not carry sufficient information of the soft tissues' conditions. More advanced imaging tools such as MRI or CT are available, but expensive, time consuming and are suitable only for detection of advanced arthritis. The arthroscopy is often the only reliable option, however due to its semi-invasive nature, it cannot be considered as a practical diagnostic tool. Therefore, an alternative screening methodology was needed to enhance the screening capabilities.

Early physicians have noticed that the knee joint often makes certain noises while being put into functional test, or even during everyday locomotion. This is because, when the bones are in motion the interaction between articulating surfaces induces vibrations of the bones, that may reach audible level. In a healthy joint the articulating surfaces are smooth and the vibration is minimal, but as the cartilage degenerates, the articular surfaces become rougher and vibrations increase, and may become audible. Therefore, the auscultation of the knee joint has been considered an interesting and promising diagnostic technique.

The first attempts to use auscultatory tools to the diagnosis of the pathological changes have been made in the XIX century. Heuter,[104] in 1885 was the first to use myo-dermato-ostetoscope to localize the joint bodies. In 1902, Blodgett[25] used a stethoscope to auscultate the knee joints and noted that the sound increased with the age of the subjects. He reported creaking, grating and cracking sounds present in chronic arthritic joints. In order to determine whether the auscultation offers any practical value in distinguishing between different forms of joint affections, in 1929, Walters examined nearly 1600 knee joints.[235] He categorized the joints into 5 groups: *smooth*, *rough*, *grating I*, *grating II* and *grating III*, and found, similar to Blodgett, that joints became more rough with age. The joints appeared smooth in the first decade of life but the rough and grating noise increased with increasing age and 81.5% of subjects in their 80s were audible (Figure 2.14). Later, joint sounds were studied to investigate the patella chondromalacia, different types of arthritis and meniscus lesions.[65, 220, 196]

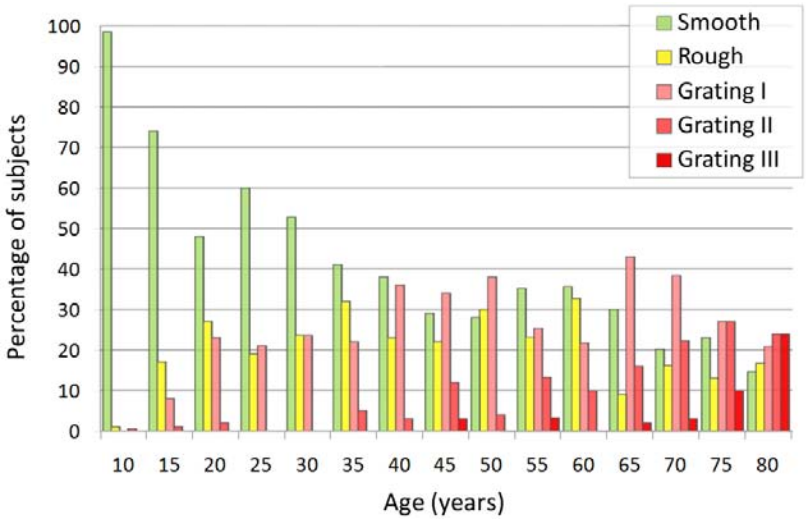
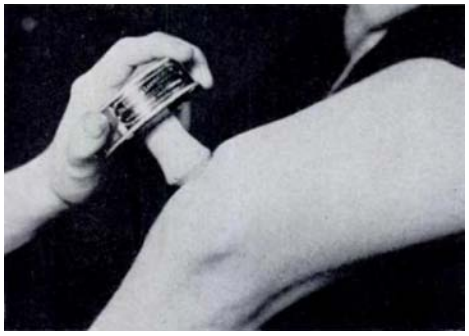


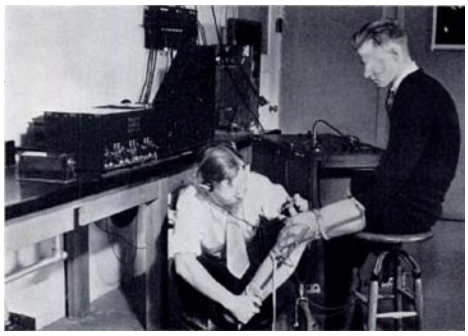
Figure 2.14: In 1929, Walters examined 1600 knee joints and found steadily ascending ratio of all forms of audibility with increasing age. Vertical axis presents percentage of subjects with rough, grating I, II or III noise. *Source: [235].*

These pioneering studies gave the basis for further research. The first graphical presentation of the joint sounds was presented by Erb in 1933.[65] The author investigated chondromalacia of the patella, arthritis and meniscal lesions, and reported low frequency of meniscus sounds. Later, Steindler [220] practiced auscultation of joints, particularly knee, and used a cardiophone (Figure 2.15) because its soft-rubber attachment helped to eliminate the noises caused by the friction between the skin and the stethoscope.

Peylan, in 1953, investigated 214 patients with different types of arthritis by the means of a regular and electronic stethoscopes.[196] He believed that he could distinguish between periarticular sounds, osteoarthrits and rehumatoid arthrits. Fisher and Johnson [72] found that the the rheumatoid arthritis could be recognized in the early stage, before the changes could be observed in x-ray images. However, these evaluations of the knee joint sounds were subjective and lacked the more precise, repetitive methodology. The first objective methods, based on statistical parameters of the signals were proposed by Chu et al. in late 1970s.[46, 45] The authors used a double-microphone differential-amplifier sound-retrieval setup to record the knee



(a) A cardiophone used to study of the auscultation of the knee joint.



(b) Experimantal set-up used by Steinler in 1933.

Figure 2.15: In 1937, Steinler used cardiophone (2.15a) to minimize the friction noises of the skin. *Source: [220].*

joint sounds. They found that the normal knees had very low acoustic power output (ranging from 0-0.02 W/cycle), while the pathological knees revealed significantly higher power outputs (Figure 2.16), and therefore were the first attempts for the objective classification between normal, rheumatoid and degenerative knees. They noted, that on average the acoustic power varies logarithmically with the surface roughness.

Further improvements were done by Mollan et al. who compared the joint vibration detected using microphones and accelerometers and concluded that the microphone was a poor transducer in terms of frequency and dynamic sensitivities for use with human joint emission.[179] Particularly limiting the use of microphones, were the skin friction noise and the ambient room noise. Therefore, many researchers replaced the microphone with three tiny accelerometers taped around the knee.[179, 137, 178, 136, 173]

The decision made by Molland et al. about replacing the microphones with accelerometers was later proven to be right, by scientists studying sounds emitted by temporomandibular joint (TMJ).[82, 81, 42, 43, 44, 125, 226] Christiansen et al. [42] reported that the condenser microphone is highly sensitive to 'irrelevant' sound fields leading to artifactual registration of any airborne wave. They recommended that in general microphones should not be used for recording TMJ sounds - only

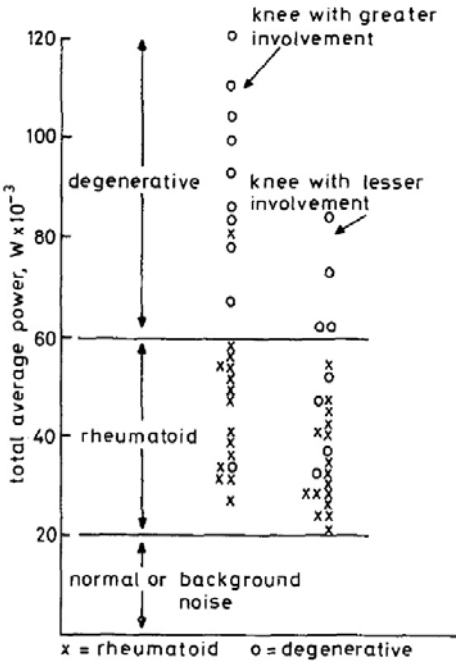


Figure 2.16: In 1978, Chu et al. attempted to classify the knee joint conditions based on the relative acoustic power. *Source: [45].*

accelerometers could be advocated for recording of solid borne TMJ vibrations. In another study, Christiansen further noted that errors were found in sound frequency measurements recorded with microphones, while comparable measurements made with skin-contact vibration transducers were accurate.[43] Similar conclusions were described by Kernohan et al. in an article reviewing the development of various techniques to evaluate sounds from human joints.[135] For these reasons, the accelerometers quickly replaced the microphones and therefore a new name of the research field, ***vibroarthrography*** came into popular use.

Parallel to the technological developments of the recording devices, the new mathematical methods were also proposed. Since the vibroarthrogaphic signals are inherently non-stationary, the fast Fourier transform (FFT) could not be accurately used to localize the frequency content in time and therefore inapplicable to correlate the abnormal signals with the joint kinematics. The windowed Fourier transform (WFT) (also called short-time Fourier transform (STFT)) offered some help in

localizing the frequency content in the time domain, but the breakthrough came with the introduction of the wavelet transform. Using the continuous wavelet transform, signals can be locally characterized in both the time and frequency domains simultaneously and self-adaptively. Therefore, it is termed multi-resolution analysis (MRA) and can be efficiently applied to analyze and process the non-stationary signals. For these reasons the wavelet theory found a wide application in the pattern recognition research field.[228]

The pattern recognition techniques have also undergone significant development and nowadays advanced signal classifiers are built as neural networks. The wavelet theory and pattern classification techniques have found countless applications and are among the fastest developing methods at present. The use of the new sensors and analytical tools accelerated the development of the vibroarthrography and resulted in a number of clinical trials, publications and patents [83, 211, 201, 202, 206] and has a great potential of becoming a reliable diagnostic tool for early diagnosis of patellofemoral disorders.

2.4.2 Current research

Currently, the vibration signals are most frequently collected by means of highly sensitive, miniature accelerometers attached externally to the skin by an adhesive or elastic wrapping tape. The vibrations are recorded while the subject is asked to perform various activities, such as flexion-extension of the knee, gait, squat etc. Since during these activities the entire knee is moving, the sensors record the changes in acceleration resulting from both, the motion and the vibration. Generally, the bones move less rapidly than they vibrate, therefore it is possible to decompose a raw vibroarthrogram into the motion and vibration components by using a low-pass filter. Next, the signal-to-noise ratio of the vibration signals can be increased by using adaptive TF decomposition methods.[147] Then statistical parameters of the signals are extracted and processed by pattern recognition algorithms. Usually a

database containing a larger number of training datasets is build so that the pattern of a new signal can be compared to datasets of known conditions and classified as indicating a pathology or a lack of it, similarly to the existing techniques employed in electrocardiography (ECG) or Electroencephalography (EEG).

Krishnan et al.[148] used an adaptive time-frequency distribution to calculate entropy, energy spread, frequency and frequency spread of the vibroarthrography (VAG) signals and was able to discriminate the normal vs. abnormal conditions with up to 77.5% accuracy. Umapathy and Krishnan[232] used wavelet packet decompositions and modified local discriminant bases algorithm and obtained accuracy as high as 80% on a set consisting of 51 normal and 38 abnormal samples. More, recently Rangayyan and Wu[205] used simpler statistical parameters, such as form factors, skewness, kurtosis and entropy and were able to obtain comparable accuracies to the aforementioned, more sophisticated methods. Application of simpler statistical features, however, required application of a more sophisticated algortihm based on radial basis functions network.

Jiang et al.[127] applied vibration arthrometry to study patients with total knee replacement. They found that VAG signals in rapid knee motion can be used to detect early stage of polyethylene wear of the patellar component. They were also able to detect prosthetic metal wear in the late stage, when the knee was being swing slowly, at $2^\circ/s$ speed.

Chapter 3

Originality and Contributions of the Presented Research

3.1 Originality of the Dissertation Topic

In this work, a number of different methodologies have been used to provide three sources of information; kinematics, kinetics and vibroarthrography, which may contribute to better understanding of the in vivo condition of the patellofemoral joint. The significance of this work is the potential of using the described approach in the future to develop a new, low-cost screening tool for improved, non-invasive diagnosis of the patellofemoral joint disorders (Figure 3.1). Simultaneous determination of in vivo kinematics, dynamics, electromyography and vibroarthrography is original, and to the best of the author's knowledge, has not been done before.

Kinematic analysis may reveal the pathologies related to the patellofemoral joint (such as patellar subluxation), and to the tibiofemoral joint (such as reduced posterior femoral rollback, or abnormal anterior-posterior translation of the femoral condyles typical of cruciate ligament dysfunction). Moreover, an abnormality present in one compartment of the knee may affect another one. For instance, reduced posterior femoral rollback, has a direct effect on the patellar ligament moment arms (see Section

4.3) and may lead to impaired extensor mechanism efficiency, therefore it is important to study both the tibiofemoral and patellofemoral joints simultaneously.

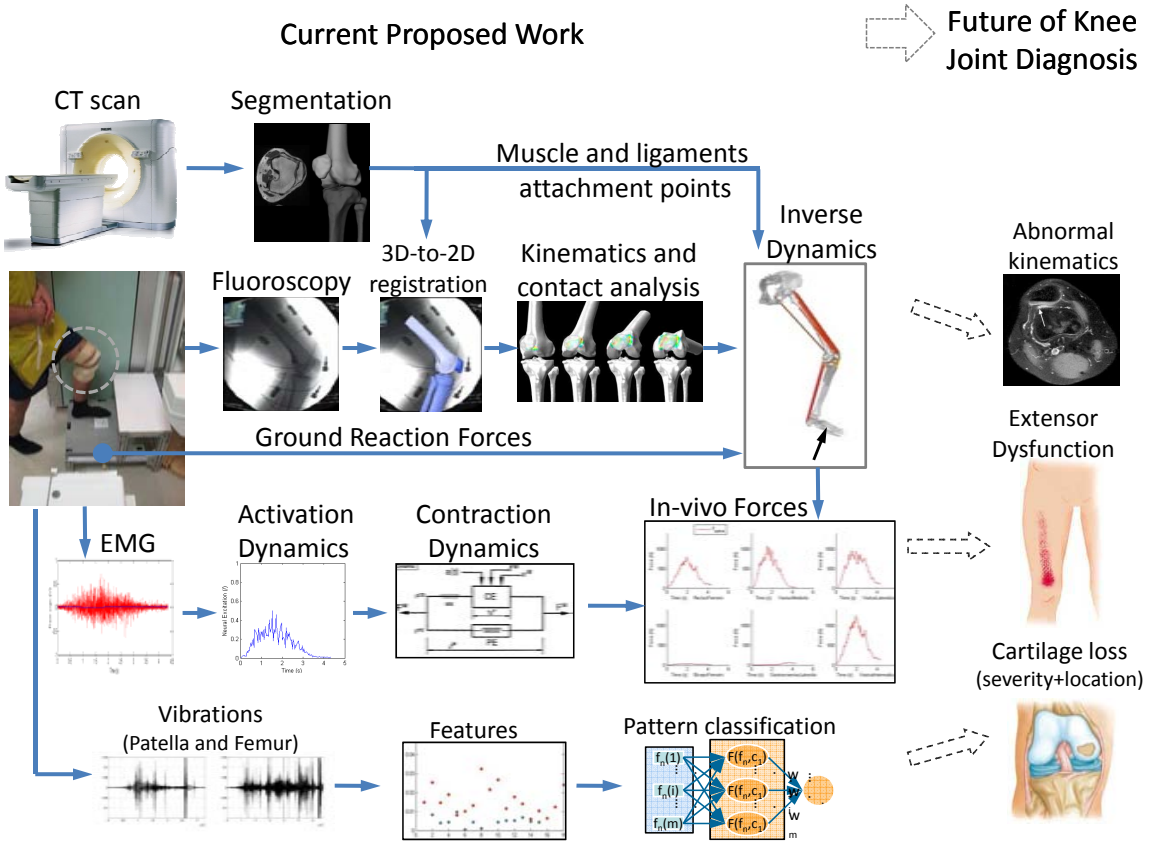


Figure 3.1: Top-level diagram of the methods employed in the dissertation, and their clinical significance.

Kinetic analysis may bring further insight by predicting whether the loading conditions are within the range observed for healthy individuals or if the abnormal kinematics causes excessive forces, which may exceed the articular cartilage strength limit and eventually damage it. Furthermore, even if the forces are within their natural range, the electromyography (EMG) data may reveal whether the forces are distributed optimally between the muscles, or if resultant force creates an abnormal pull towards one side (which may cause patellar subluxation). Abnormal kinematic and kinetic patterns may also be an indication of a defensive strategy employed by the central nervous system as a respond to the pain present in the knee joint. The

pain frequently appears if there is loss of articular cartilage, which can be reflected in the vibration emitted by the knee. Therefore the vibroartrography is proposed to be used as the third source of data that can be collected non-invasively under in vivo conditions, to enhance the diagnostic capabilities.

Simultaneous application of the aforementioned methodologies may bring a new insight in the patellofemoral joint disorders and help understand the interaction between the mechanical conditions that the knee joint is exposed to, and the neural control applied accordingly by the nervous system. Moreover, all methods that are proposed are non-invasive and can be used under dynamic, weight bearing, in vivo conditions, making it suitable for use as a future tool for more accurate and more comprehensive diagnosis of the patellofemoral joint disorders, which still remain puzzling even for experienced physicians.[78]

3.2 Fundamental Contributions

The current study contributes the scientific and clinical community with the comprehensive analysis of the patellofemoral joint mechanics with simultaneous determination of the kinematics, muscle forces, muscle activation and patellofemoral vibration patterns. All these data have been examined for a group of patients having implanted knees and a group of healthy individuals for comparisons. To achieve this goal a number of challenging problems had to be solved, which by itself provide further fundamental contributions, as listed below.

Most of the previous in vivo kinematic studies pertaining to the knee joint reported the data only for the tibia and femur, omitting the patella bone.[131, 67, 9, 222] However, patella plays a crucial role in human locomotion and its function cannot be overestimated (see Section 2.1). Therefore, determination of the three-dimensional (3D) patellofemoral kinematics under in vivo, weight bearing and dynamic conditions contributes to better understanding of the interaction conditions of this joint. Even more importantly the current study has determined the 3D kinematics of the

implanted patella, which to the best of the author's knowledge, has never been done under in vivo, dynamic, weight-beating conditions. The reason why the implanted patella motion has never been determined in vivo, is that the patellar button is made of polyethylene and hence is not visible in radiographic images (such as computed tomography or fluoroscopy). The magnetic resonance imaging cannot be applied to study the implanted knees either, because the femoral and tibial components are made of metal, which when exposed to presence of large magnetic field might break off the bones. The current work has overcome (although not without difficulties) these limitations by combining the fluoroscopy, computed tomography and 3D-to-2D registration technique (see Section 5.2).

The present work also provides important contribution to better understanding of biomechanics of the extensor mechanism. The methodology utilizes two fundamentally different approaches to determine the quadriceps muscle forces:

(1) using the inverse dynamics, and

(2) using the muscle activation signals detected for individual muscles by electromyography electrodes.

Both of these approaches have certain limitations. Mathematical modeling results depend on the underlying assumptions and yield optimal solution, which satisfies the mechanical conditions, but may not express the actual activation of the individual muscles. Application of electromyography is fraught with technical problems and cannot be used to accurately determine the force magnitudes,[53] but it reflects more accurately the actual muscle recruitment. Realizing that neither of these methods is perfect, the current study uses both approaches simultaneously, so that the boundaries of the actual muscle forces can be outlined.

Finally, the vibroarthrography has been evaluated for its potential application to determining the articular cartilage condition. Although this methodology has been proposed by a few other researchers, the current work will be the first to examine the vibration signals with the correlated 3D, in vivo kinematics. This may allow

to determine not only the severity but also the location of the articular cartilage degeneration (Figure 3.2). This information may be very helpful for surgeons planning TKA procedure and may eliminate the need for imaging modalities involving harmful radiation.

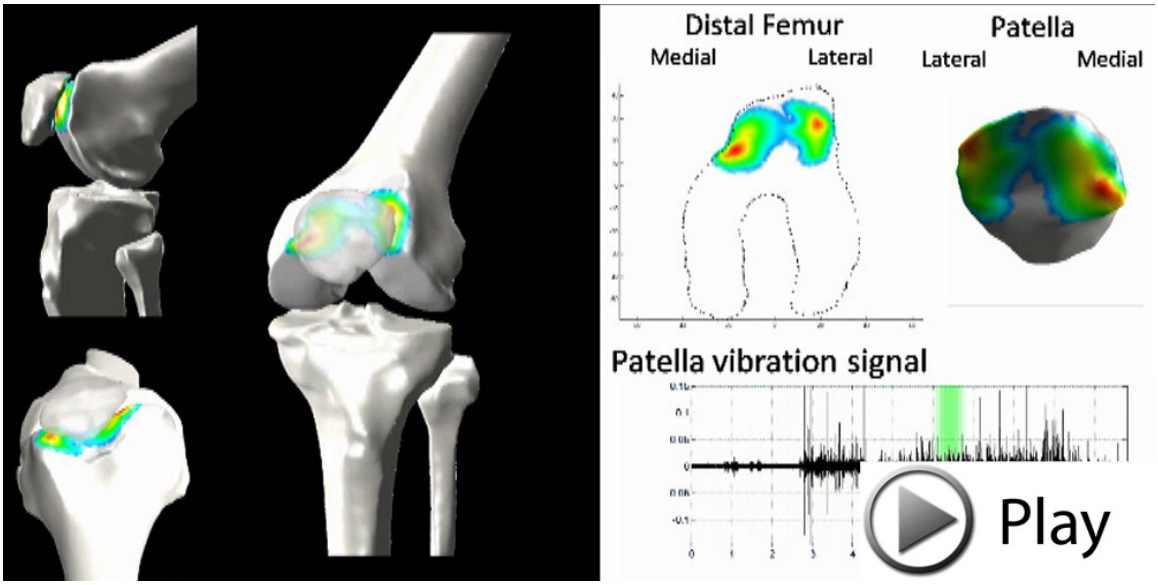


Figure 3.2: In vivo kinematics, predicted contact location map correlated with the vibration data may bring insight into not only the severity of the articular cartilage degeneration, but also the location of the affected compartment of the joint - information invaluable for treatment planning.

The methodologies investigated in the current dissertation may be combined in the future to develop a non-invasive screening tool for diagnosing patellofemoral joint disorders. Such application of the proposed work may significantly contribute to enhanced accuracy of patient screening, improved quality of treatment planning and more cost-effective health care system.

There are also several more direct contributions that have been made while developing the research tools required to complete this dissertation. The algorithms, which were developed to perform a number of analyses and calculations, have been written as graphical user interface (GUI) application and have been made available to the students working at the Center for Musculoskeletal Research at the University of Tennessee. The applications have been used by undergraduate and graduate research

assistants working on various research projects. Users' feedback was gathered, and the software has been constantly improved, resulting in a more intuitive and user-friendly program. All tools were developed keeping in mind that they should be applicable to any human joint, not only patellofemoral. In fact, they have already been successfully applied to research projects pertaining to ankle, knee, hip, spine and shoulder joints. The most significant software development contributions include:

- contact analysis and visualization module,
- muscle and ligament visualization (including wrapping),
- points and surfaces module,
- unfold surface tool,
- tracking points mode,
- moment arms calculation,
- cartilage damage mapping tool,
- helical axis calculation,
- Grood&Suntay rotations calculation,
- efficient handling and rendering of multiple objects.

Chapter 4

Biomechanical Analysis of the Extensor Mechanism Moment Arms

4.1 What is a moment arm?

Patella facilitates the extension of the knee by increasing the moment arms of the extensor mechanism forces. In order to correctly interpret this function, it is necessary to clarify the definition of a *moment arm*.

According to principles of engineering dynamics the *moment* of a force is the cross product of the *position vector* (from the reference point to any point on the line of action of this force) and this *force*.[130] The force $\vec{F}$ acting on a particle P shown in the Figure 4.1 creates moment $\vec{M_O}$ about the origin of the coordinate system O:

$$\vec{M_O} = \vec{r_{OP}} \times \vec{F} \tag{4.1}$$

where, $\vec{r_{OP}}$ is the position vector from the origin O to the particle P. The resulting moment $\vec{M_O}$ will be perpendicular to the plane created by the vectors $\vec{F}$ and $\vec{r_{OP}}$, or in other words, it will cause the particle P to rotate in that plane.

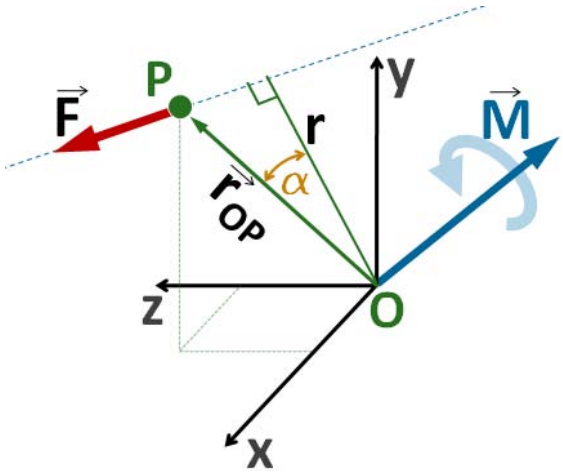


Figure 4.1: Definition of the moment of force.

The equation (4.1) can be rewritten in scalar form as:

$$M_O = \left|\vec{r_{OP}}\right| cos(\alpha)F = rF \tag{4.2}$$

where r is the ***moment arm*** (also called lever arm) of the force $\vec{F}$. This equation implies that the magnitude of the moment is equal to the magnitude of the force multiplied by the perpendicular distance between the reference point and the line of action of that force. Alternatively, we can reformulate this statement and make the following definition of the moment arm:

moment arm is the perpendicular (hence minimum) distance between the reference point and the line of action of the force creating the moment.

It is important to note that the moment arm will depend on the choice of the reference point about which the moment is defined. The choice of the reference point is arbitrary. Engineers use this fact to their advantage and often choose it to lay on a line of action of the force that is unknown or difficult to calculate. By doing this, the moment arm of this force equals zero and the moment of this force will be automatically eliminated from the equations of motion. Figure 4.2b shows the

schematic, two-dimensional representation of the forces acting on the femoral bone and their moment arms determined with respect to the tibiofemoral contact point (TFCP). The resulting moment equation (applying the convention that moments acting in the clockwise direction are positive, in the counterclockwise direction are negative) is:

$$M_{TFCP} = d_{Quad}F_{Quad} - d_{PFJR}F_{PFJR} - d_W W - d_{Hip}F_{Hip}. \tag{4.3}$$

Since the tibiofemoral reaction force passes through the TFCP, its moment arm is zero, and this force does not come into the equation.

If for the same system, the reference point is chosen to be at the instantaneous center of rotation (Figure 4.2c), the moment equations would be:

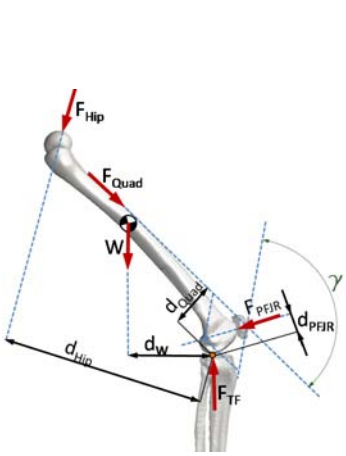
$$M_{TFCP} = d_{Quad}F_{Quad} + d_{TF}F_{TF} - d_{PFJR}F_{PFJR} - d_W W - d_{Hip}F_{Hip}. \tag{4.4}$$

(note: the distances d_{Quad}, d_{PFJR}, d_W, d_{Hip} used in eq. 4.3 and 4.4 are nor equal).

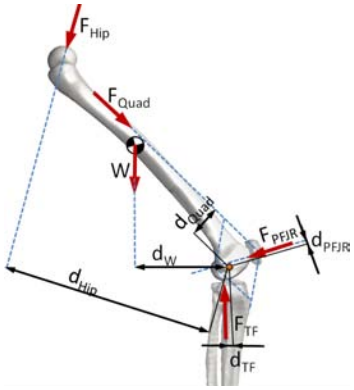
4.2 Literature data discrepancy

The above example shows how the fact, that moment arms can be defined with respect to any arbitrary point, may be used to simplify the equations of motion. However, this flexibility contributed to discrepancy in the data reported in the literature.

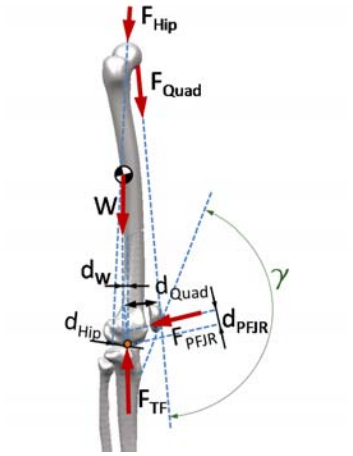
The moment arm of the patellar ligament force was calculated using a number of different reference points such as the tibiofemoral contact point (TFCP),[233, 221, 92, 11, 134, 190, 248, 103, 253] the instantaneous center of rotation,[133, 217, 237] intersection of the cruciate ligaments [85, 122] or with respect to the instantaneous screw (helical) axis.[146] As a consequence, although theoretically all measurements are correct, they differ considerably in magnitude and cannot be accurately compared. Figure 4.3 presents the patellar ligament moment arm calculated in vivo for the same subject using medial and lateral tibiofemoral contact points (4.3a) and the



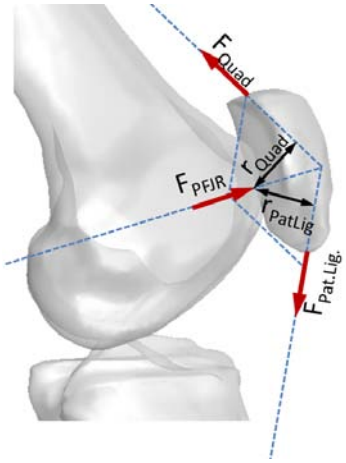
(a) Main forces acting on the femur bone and their moment arms defined with respect to the tibiofemoral contact point at 30° of flexion.



(b) Main forces acting on the femur bone and their moment arms defined with respect to the instantaneous center of rotation at 30° of flexion.



(c) Main forces acting on the femur bone and their moment arms defined with respect to the tibiofemoral contact point at full extension.



(d) Main forces acting on the patella bone.

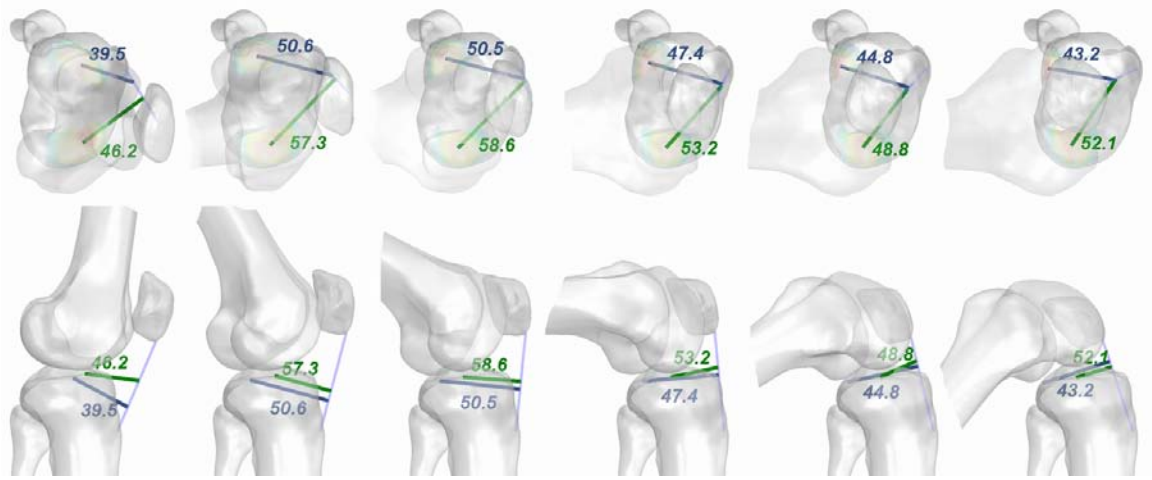


(e) Forces of the extensor mechanism.

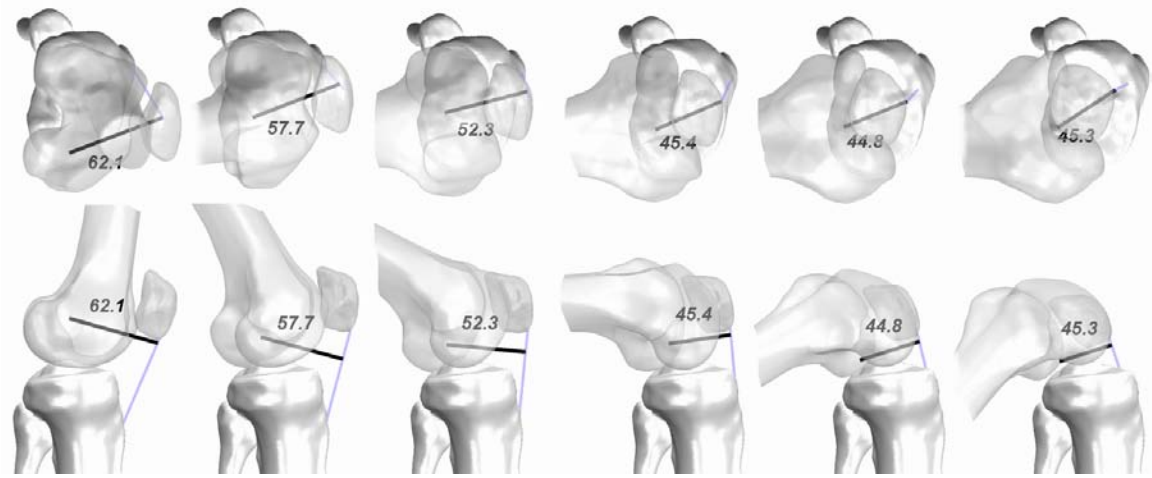
Figure 4.2: Free body diagrams aiding the analysis of the main forces acting on the femur (4.2a - 4.2c), patella (4.2d) and forces of the extensor mechanism (4.2e).

instantaneous center of rotation (4.3b) used as reference points. The differences in the moment arm length between the two measurements are shown in Fig. 4.4.

As mentioned above, using the tibiofemoral contact point as the reference point is advantageous from the analytical point of view. Another adventage is that this point can be easily estimated under in vivo conditions using x-rays, Computed Tomography



(a) Patellar ligament moment arm calculated with reference to tibiofemoral contact point (TFCP).



(b) Patellar ligament moment arm calculated with reference to instantaneous center of rotation (ICR).

Figure 4.3: Patellar ligament moment arm calculated in vivo for the same subject using two different reference points: tibiofemoral contact point (4.3a) and instantaneous center of rotation (4.3b).

(CT) or Magnetic Resonance Imaging (MRI) images. This point can be used as reference under static (e.g. during isometric tasks) and dynamic conditions.

The choice of the instantaneous center of rotation or the screw axis as the reference may be problematic. In order to find the instantaneous screw axis (ISA) or instantaneous center of rotation (ICR), it is necessary to obtain the relative orientation of the femur and tibia, at least at two consecutive instances. Therefore,

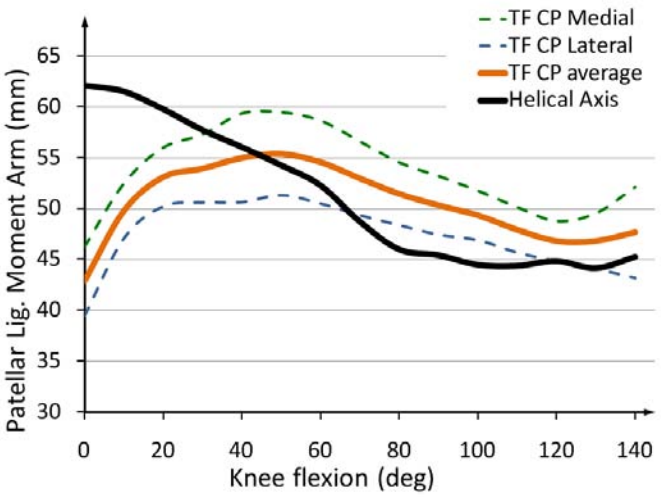


Figure 4.4: The difference between the patellar ligament moment arm length calculated using different reference points.

it cannot be applied to static scenarios. Theoretically, there may also be a situation when the femur only translates without rotation with respect to tibia. In this case, the center of rotation would be located in the infinity and could not be used as a reference. Finally, even in presence of tibiofemoral rotation the calculation of the location of the ICR is prone to error and the accuracy decreases with decreasing intervals between the measured instances.[180, 195, 247]

The rationale of using the intersection point of the Anterior Cruciate Ligament (ACL) and Posterior Cruciate Ligament (PCL) ligaments stems from the classic model of knee kinematics; the crossed four-bar link.[257] This model assumed that the cruciate ligaments act as ropes and are in tension at all times. Under these assumptions, the crossing point is the point of zero velocity and coincide with the center of rotation. The application of this method in vivo requires finding the two cruciate ligaments, which cannot be done using x-ray or CT scans. It may be done using MRI images, however, due to long time required for image acquisition, the measurement is limited to static conditions.

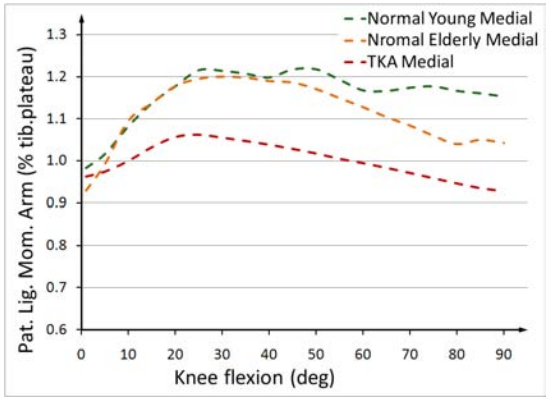
Therefore, the tibiofemoral contact point, seems to be the most readily applicable reference point for calculating the extensor mechanism moment arms. It can be

estimated under in vivo and in vitro, static and dynamic conditions using radiographs, CT or MRI scans.

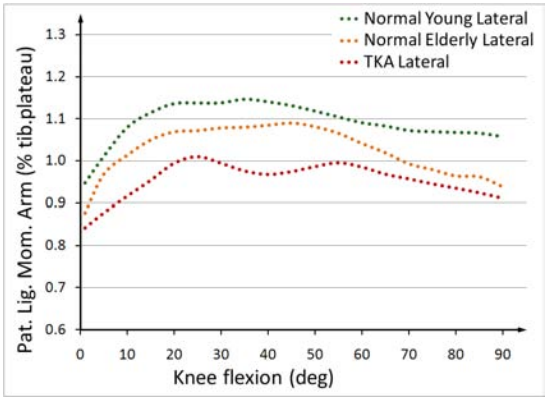
4.3 Moment arms in the natural, patellectomy and TKA knees

In the knee joint the patella acts as a spacer increasing the patellar ligament and quadriceps tendon moment arms. This mechanical advantage faciltates the process of balancing the moments acting on the knee joint, as according to Eq. 4.2 the increase of moment arm r allows decrease of the force F required to balance the moment M_O.

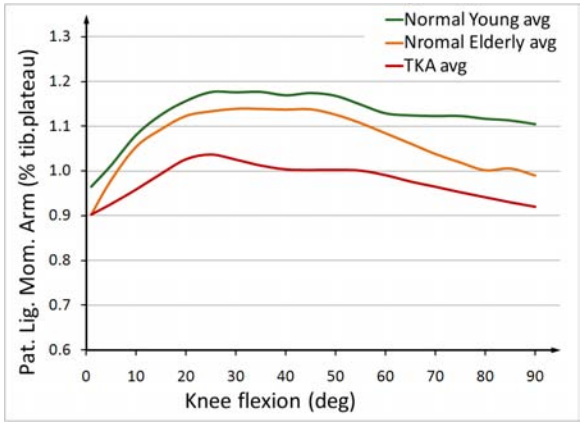
In the first 30° of knee flexion, the patella enters the trochlea and is located anterior to the femur, thus significantly increasing the patellar tendon moment arm (Fig. 4.5). At the same time, the femur rotates externally, the Q angle decreases and the extensor mechanism becomes aligned in a more straight line, thus reducing probability of lateral subluxation of the patella. Simultaneously, the tibiofemoral contact points move posteriorly due to changes in the geometry of distal portion of femoral condyles,[74] what significantly contributes to the increase of the patella ligament and quadriceps tendon moment arms. This prepares the patellofemoral joint to respond to the loading conditions required to balance, bend or extend the knee in a secure and controlled fashion. The moment arms remain near their maximum length till approximately 60°, after which the patella begins sinking into the intercondylar groove and its ability to offset the line of action of the extensor mechanism decreases. However, in the healthy joint, the tibiofemoral contact points continue translating posteriorly until the maximum flexion, and therefore the moment arm remains higher than at full extension (Fig. 4.5). This compensating effect of posterior translation of TFCPs may be diminished in elderly and Total Knee Arthroplasty (TKA) patients. Tibiofemoral contact points translate less posteriorly for TKA subjects,[55] which may explain the decrease in the patellar moment arm (Fig. 4.5).



(a) Medial



(b) Lateral

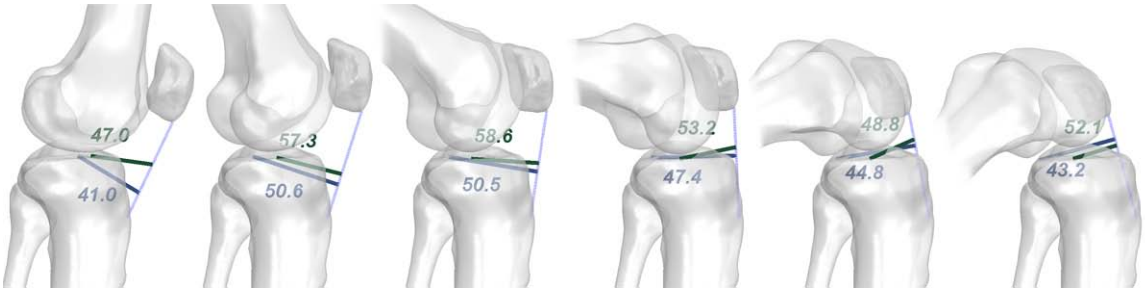


(c) Average

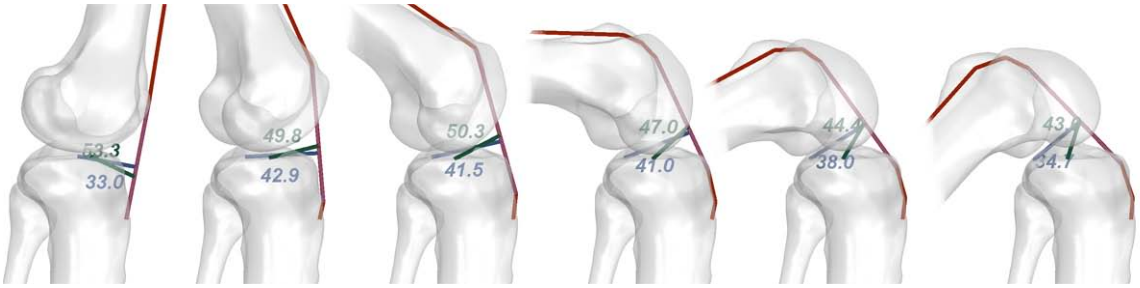
Figure 4.5: Comparison of the patellar ligament moment arm length (normalized with respect to tibial plateau length) calculated with reference to medial (4.5a) and lateral (4.5b) TFCP for 5 healthy, young (green), 5 healthy elderly (orange), and 5 TKA subjects (red).

The loss of mechanical advantage of the patella is especially severe for patients undergoing patellectomy. Figure 4.6 shows the patellar ligament moment arm determined for a healthy individual and the effects of a simulated removal of the patella for the same subject. After patellectomy the moment arm would be reduced to an average of 86% of the presurgical length (Fig. 4.6e), which would diminish the performance of the extensor mechanism. Kaufer [133] demonstrated that the extensor power is reduced by 15% after patellectomy and transverse closure and by 30% after

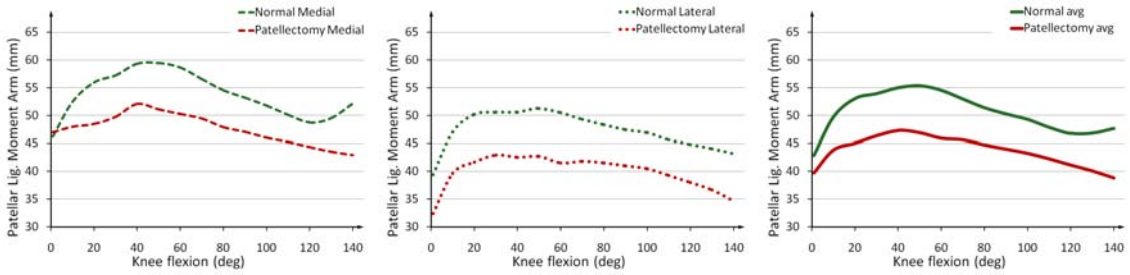
patellectomy and longitudinal closure. These adverse effects may explain the inability to fully extend the knee often observed for patients after patellectomy.



(a) Patellar ligament moment arm measured in vivo for a healthy knee joint.



(b) Patellar ligament moment arm predicted for the above subject after patellectomy.



(c) Medial. **(d)** Lateral. **(e)** Average.

Figure 4.6: Patellar ligament moment arm length determined in vivo for a healthy subject and the effects of patellectomy on moment arm length simulated for the same subject. The reference points at the medial (4.6c), and lateral (4.6d) tibiofemoral contact points were used to find the average (4.6e).

To increase the extensor mechanism efficiency, the anterior transfer of the tibial tubercle has been proposed.[12, 168] However, due to high complication rate associated with straight anterioriazation,[132, 161] Fulkerson developed anteromedialization (AMZ) as a refined procedure.[77] This procedure makes it possible to increase the patellar ligament moment arm, and to correct the patellar balance in the trochlea,

which is extremely helpful for patellofemoral disorders related to malalignment and recurrent subluxation of patella.[38, 207]

Chapter 5

Materials and Methods

5.1 Research Study Design

To study the biomechanics of the patellofemoral joint, twelve Total Knee Arthroplasty (TKA) patients and four healthy subjects were recruited and performed stair climb activity under fluoroscopic surveillance. All TKA knees have been replaced with the NexGen Mobile-Bearing Hi-Flex PS implant (Zimmer Inc., Warsaw, IN) by a single surgeon. The patients participated in the study at least 6 months post-operatively. All TKA subjects had the Knee injury and Osteoarthritis Outcome Score (KOOS) of 90 or higher. The healthy subjects had no history of knee injuries, pain, instability or ligament loosening. Additionally four of the TKA patients were also analyzed for their contralateral (non-implanted) knee, so that the biomechanics of a healthy but elderly knee could be assessed (Table 5.1).

In order to study the extensor mechanism muscle activation, five electromyography (EMG) surface electrodes were attached to the skin adjacent to the location of five muscles:

- Vastus Lateralis,
- Rectus Femoris,
- Vastus Medialis,

Table 5.1: Demographic data of the subjects recruited for the study.

Group	Sbjct Nr	Age *(years)*	Height *(m)*	Weight *(kg)*	BMI *(kg/m^2)*
TKA	1	75	1.49	57.0	25.7
	2	75	1.65	74.0	27.2
	3	62	1.57	79.0	32.0
	4	70	1.50	74.0	32.9
	5	83	1.73	70.0	23.4
	6	66	1.57	66.0	26.8
	7	68	1.59	68.0	26.9
	8	78	1.47	55.0	25.5
	9	80	1.68	72.0	25.5
	10	76	1.58	60.0	24.0
	11	66	1.44	58.0	28.0
	12	84	1.50	54.0	24.0
	average	**73.6**	**1.56**	**65.6**	**26.8**
	SD	7.1	0.09	8.5	3.0
	min	62.0	1.44	54.0	23.4
	max	84.0	1.73	79.0	32.9
Contralateral	1	75	1.65	74.0	27.2
	2	62	1.57	79.0	32.0
	3	70	1.50	74.0	32.9
	4	80	1.68	72.0	25.5
	average	**71.8**	**1.6**	**74.8**	**29.4**
	SD	7.7	0.1	3.0	3.6
	min	62.0	1.5	72.0	25.5
	max	80.0	1.7	79.0	32.9
Healthy	1	28	1.79	85.5	26.7
	2	35	1.84	81.4	24.0
	3	30	1.80	83.0	25.6
	4	30	1.84	98.0	28.9
	average	**30.8**	**1.8**	**87.0**	**26.3**
	SD	3.0	0.0	7.5	2.1
	min	28.0	1.8	81.4	24.0
	max	35.0	1.8	98.0	28.9

- Biceps Femoris, and
- Gastrocnemius Medialis.

The location for the electrode placement was selected by the physician's assistant, to make sure that the electrode was placed in the midline of the belly of the muscle between the nearest innervation zone and the myotendonous junction. This location

ensures that the electromyography (EMG) signal with the greatest amplitude is detected.[53] Prior to EMG electrode placement, the hair was shaved and the skin was cleaned with alcohol soaked cleaning swab to remove all natural oily residues and ensure good electrode adherence and constant resistance. To eliminate the movement of the electrodes relative to the skin, the EMG sensors were attached with hypoallergenic adhesive tape and elastic wrap. The EMG signals were recorded with the MA-300 system (Motion Lab Systems, Inc., Baton Rouge, LA). This system is noninvasive and uses surface EMG sensors.

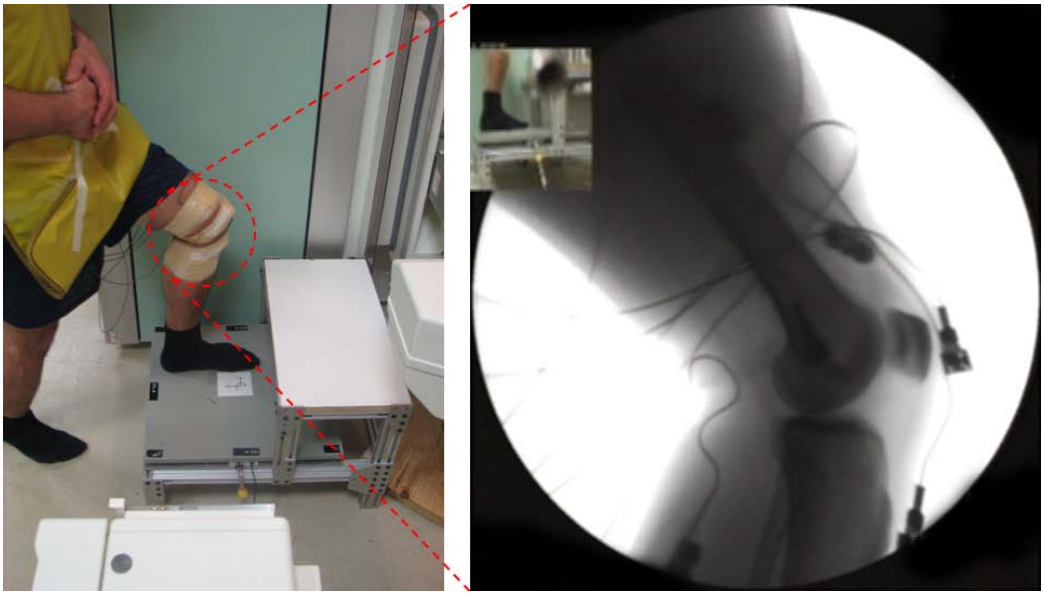


Figure 5.1: Five EMG surface electrodes and two miniature accelerometers were attached to the subjects knee. The electrodes recorded electrical manifestation of the *Vastus Lateralis*, *Rectus Femoris*, *Vastus Medialis*, *Biceps Femoris*, and *Gastrocnemius Medialis* muscles. The accelerometers were attached to the patella and medial femoral epicondyle to record the vibrations of the respective bones.

To detect the vibration of the patellofemoral joint, two miniature 3-axial accelerometers (356A12, PCB Piezoctronics, Inc., Depew, NY) were attached to the middle of the patella and medial femoral epicondyle by means of adhesive tape and elastic wrap (Figure 5.1). The vibration signals were magnified by the factor of 10 and low-pass filtered at 5 kHz using a signal conditioner (583A, PCB Piezoctronics, Inc., Depew, NY) prior to analog to digital conversion (using DI-720 Data Acquisition

System, DATAQ Instruments, Inc. Akron, OH). The data was recorded with the total of 250 kHz sample rate (10869 Hz/channel).

The subjects have also undergone Computed Tomography (CT) procedure to acquire images of their knee joints, which were later used to reconstruct the three-dimensional (3D) models of their bones (see Sec. 5.2). The leg was scanned 7 inches below and above the joint line using 0.3 mm thick slices.

All participants were asked to climb up the stairs in their natural, dynamic fashion without using any supporting devices. The stairs were custom designed to accommodate the AMTI (Advanced Mechanical Technology, Inc., Watertown, MA) force plate embedded in the first level stair. The ground reaction force, acceleration and EMG data were recorded synchronously with the fluoroscopy video.

The stair climbing activity has been chosen for two reasons. First, beside walking, it is one of the most commonly performed everyday tasks, and therefore the results of the analysis will provide valuable information for the orthopaedic community striving to improve the existing TKA devices. Second, climbing up the stairs relies on the performance of the extensor mechanism and the stance phase involves only one leg, hence isolates the lower extremity being analyzed and its biomechanics can be adequately studied. In other words, this activity ensures that, in case a subject experiences some dysfunction related to the knee joint, she/he will not be able to compensate (i.e. alternate) their biomechanics by supporting on the other leg (unlike during kneeling) and this dysfunction will be reflected in abnormal kinematics, kinetics and/or vibration of the patellofemoral joint.

In order to assess the suitability of the vibration signals for knee arthritis diagnosis, it was necessary to recruit an additional group of subjects with confirmed joint degeneration. To this end, 23 healthy subjects, and 52 candidates for the TKA surgery were recruited and the vibration signals were recorded for them prior to undergoing the replacement procedure. For these additional subjects the vibration data was recorded without fluoroscopic surveillance. Since, there was no harmful radiation involved, the data was collected for a few additional activities: non-weight

bearing flexion-extension at 0.5 Hz rate, deep knee bend, chair rise, and stair descent. Later, at the time of the surgery, when the joint was opened, the surgeon assessed the condition of the articular cartilage and filled out an intra-surgical evaluation sheet specifying the location and severity of the damage (Figure 5.36).

All study protocols were approved by the Internal Review Board at the University of Tennessee and the consent form was obtained from each participant prior to the data acquisition session.

5.2 Determination of the In-Vivo Kinematics

The stair climb activity was analyzed from the foot contact until the toe off at 33% increements, so that the entire weight-bearing phase could be studied.

The Computer Aided Design (CAD) models of the tibia, fibula, and femur bones were recreated in a segmentation process, based on computed tomography images obtained for each participant. The volumetric data were constructed at the interpolated slices in the transverse plane. Segmentation was semi-automatically performed by applying a thresholding filter to the slices using AMIRA software (TGS Inc., San Diego, CA), which isolated the bone from the soft tissues (Figure 5.2). The resulting data were used to create full three-dimensional polygonal surface models for the distal part of the femur and the proximal part of the tibia and fibula (Figure 5.3).

For the TKA knees, the implant CAD models were obtained from the manufacturer. However, the patellar insert made of polyethylene is not visible in the fluoroscopic video. Therefore, the resurfaced portion of the patella bone was reconstructed (Figure 5.4). The three holes drilled during the surgery to accommodate the patellar button pegs were identified in the CT images and recreated in the 3D models (Figure 5.5). This allowed the correct assembly of the polyethylene model with the resurfaced patella bone.

The 3D kinematics was recovered by overlaying the 3D CAD bone models onto their respective silhouettes in fluoroscopic images (Figure 5.6) using a previously

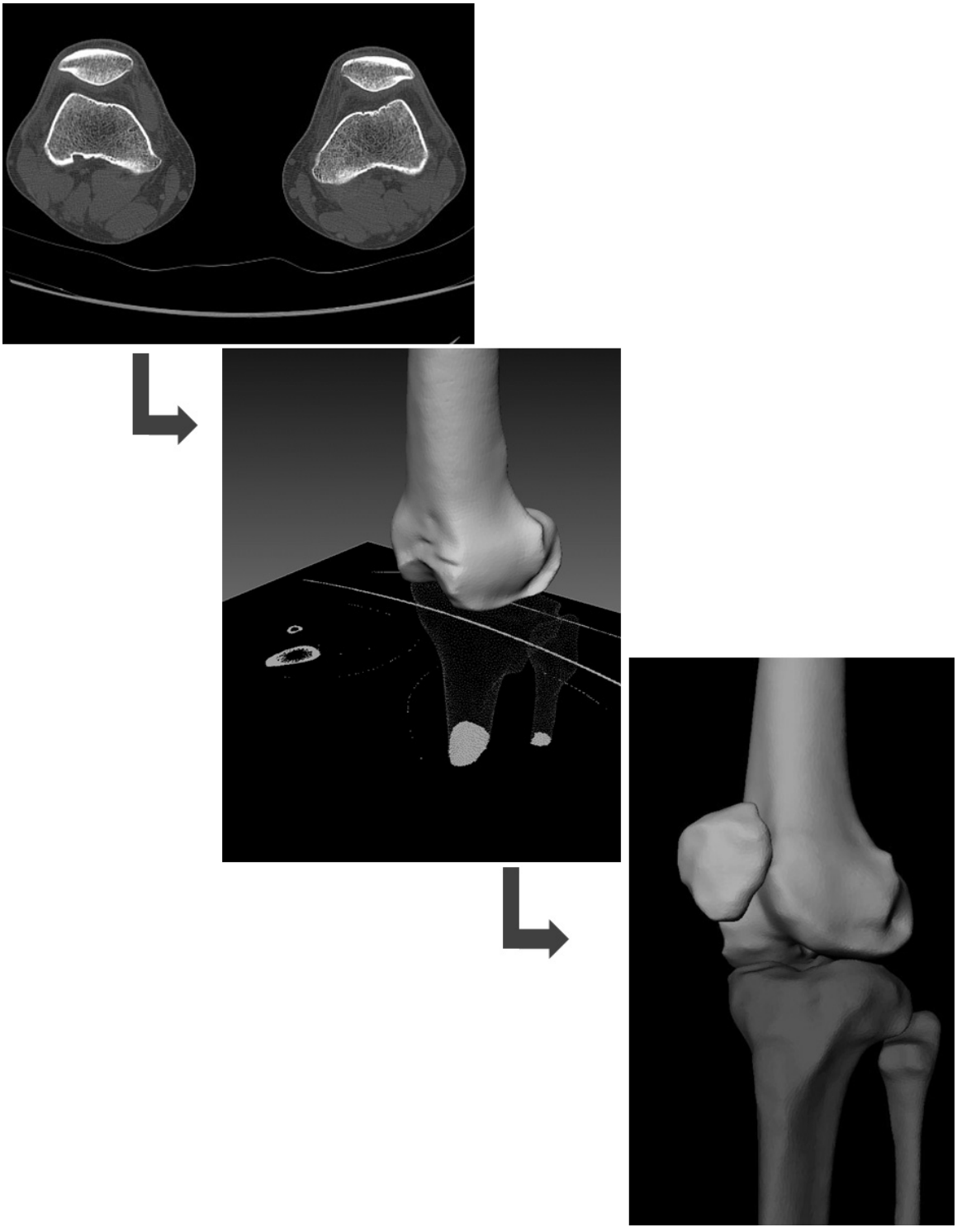


Figure 5.2: CT scan images were used to recreate the 3D, patient-specific bone models.

(kneeBones.u3d)

Figure 5.3: Example of a segmented 3D CAD model of the knee joint. *Use mouse to manipulate the 3D object (right button to zoom).*

described 3D-to-2D registration technique.[57, 56, 112, 165] Similarly for the TKA knees, the CAD implant models were overlaid onto their respective silhouettes. However, since the polyethylene is not visible in the fluoroscopic images, the model of the resected patella bone was matched with its silhouette first. Then the polyethylene patellar insert was assembled with the resected bone, and displayed in the fluoroscopic scene (Figure 5.7).

An error analysis of the 3D-to-2D registration process was previously performed for TKA components, documenting the translational error to be less than 0.5 mm and the rotational error less than 0.5°.[165] Unlike for metal objects, the fluoroscopic images of the bones contain visible internal details, rather than just a black silhouette. This allows prediction of the intensities inside the object silhouette, which can lead to even more accurate prediction and enhanced registration of 3D bone models to the fluoroscopic images.[165]

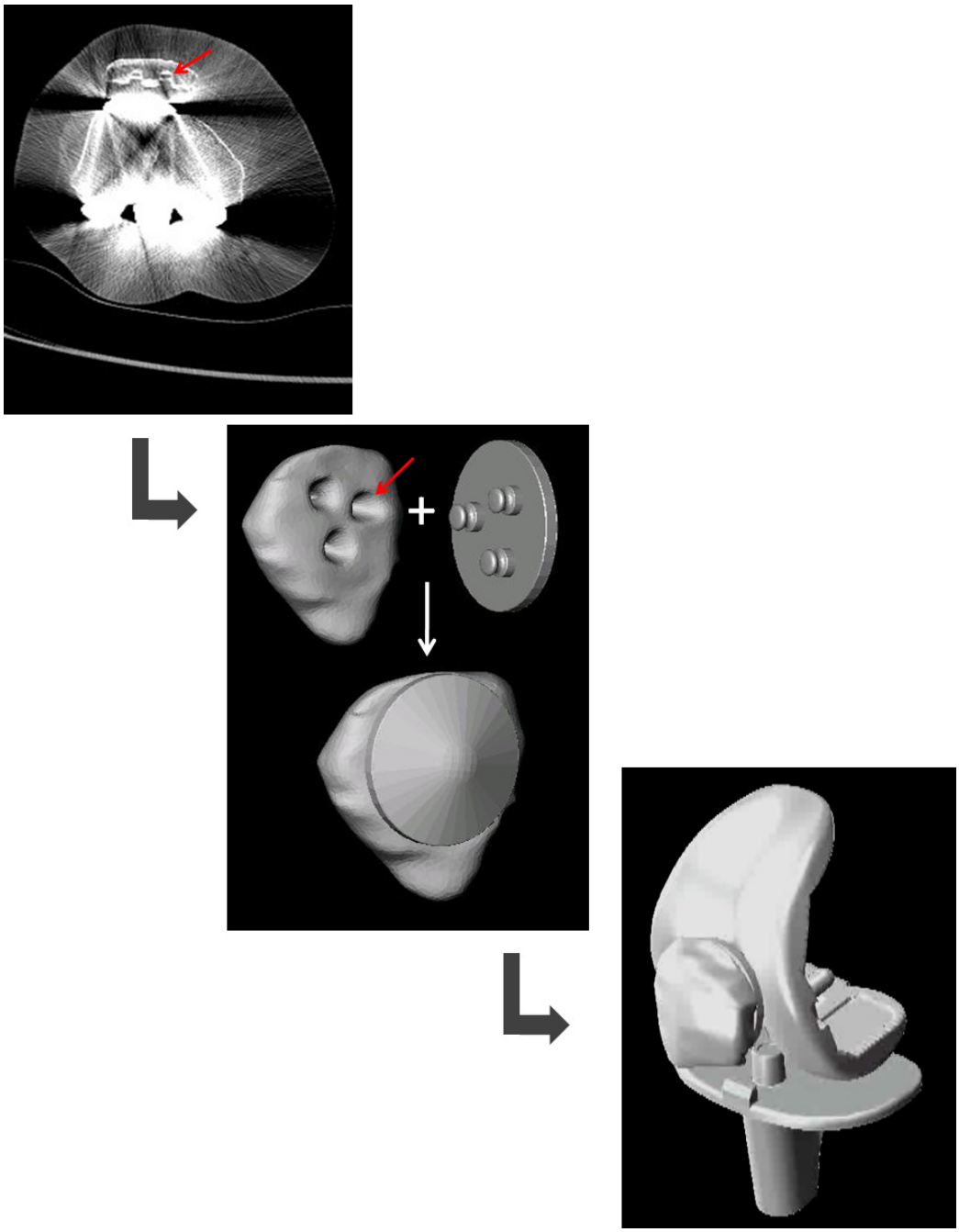


Figure 5.4: For the TKA knees, the resurfaced portion of the patella was reconstructed and assembled with the polyethylene model. The CAD models of the femoral and tibial implant components were obtained from the manufacturer. Note that the holes drilled to hold the three patellar button pegs were identified in the CT scans (red arrows), so that the location of the polyethylene could be correctly recreated.

(resectedPatella.u3d)

Figure 5.5: Example of a segmented 3D CAD model of resected patella. Note the 3 holes drilled to accommodate the patellar button pegs. *Use mouse to manipulate the 3D object (right button to zoom).*

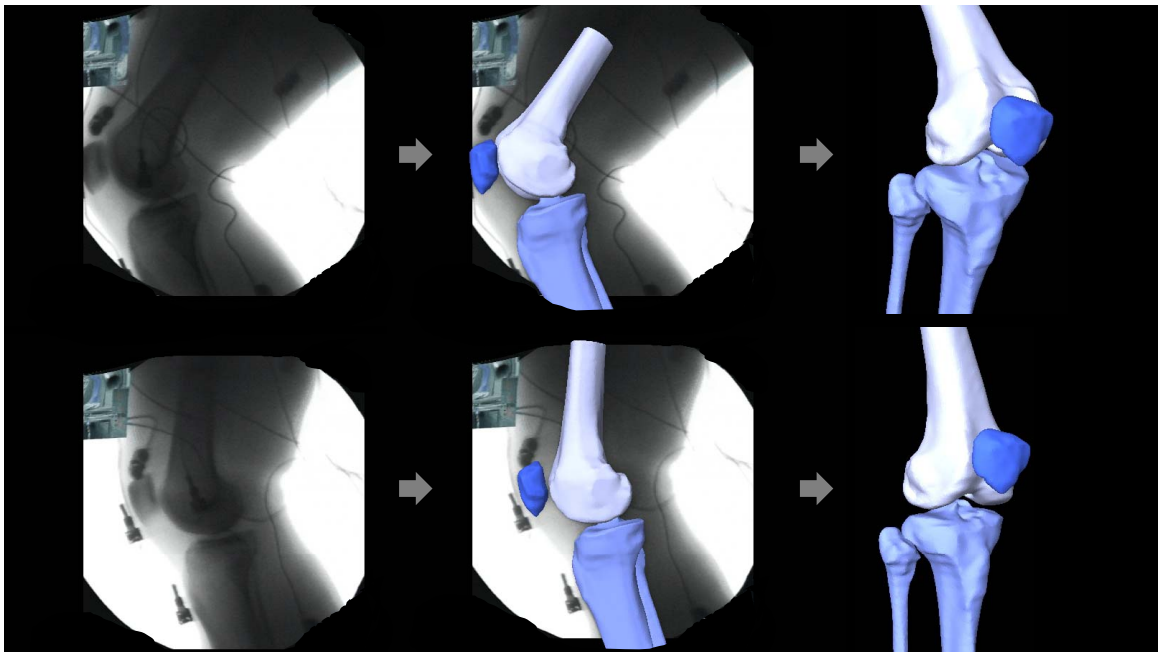


Figure 5.6: The patient-specific bone models were used during the 3D-to-2D registration process to recover the 3D kinematics of all the bones from the fluoroscopic images.

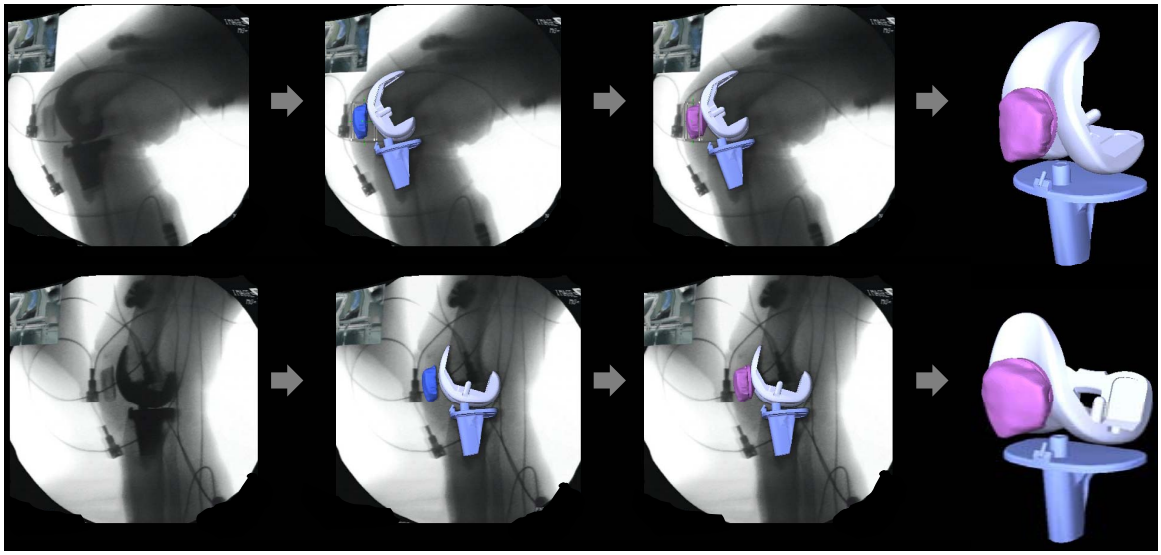


Figure 5.7: The implant CAD models and the model of the resurfaced patella were used during the 3D-to-2D registration process to recover the 3D kinematics of all the components from the fluoroscopic images.

Once the 3D kinematics was recreated, the flexion, rotation and tilt of the patella relative the the femur was calculated using the joint coordinate system (see Section 2.2.1).[93] The translations of the patella were measured in the femoral (local) coordinate system. An analogous approach was taken to describe the kinematics of the femur relative to the tibia bone.

5.3 Musculoskeletal Model Development

Muscle forces cannot be calculated directly under in-vivo conditions, therefore, in this research study, two different but non-invasive approaches have been chosen to study the biomechanics of the extensor mechanism. First an inverse dynamics model was developed to determine the in-vivo forces in seven muscles (12 bundles total) spanning the knee joint based on the joint kinematics and ground reaction forces. Next, the muscle electrical signals detected by the surface EMG electrodes were used to calculate the muscle forces by converting the muscles' electrical manifestation into neural excitation, muscle activation and finally muscle contraction dynamics.

5.3.1 Inverse Dynamics Analysis

The multi-body dynamics model was developed using Kane's dynamics approach.[130] The model consists of five rigid-body elements; (1) foot, (2) tibia and fibula, (3) femur, (4) patella and (5) pelvis and all of them have been modeled as full six degrees of freedom elements. The inputs to the model are the patient-specific ground reaction forces, joint kinematics and inertia properties, while the output are the joint reactions and the muscle forces of: (1) *Vastus Lateralis*, (2) *Vastus Intermedius*, (3) *Rectus Femoris*, (4) *Vastus Medialis*, (5) *Biceps Femoris*, (6) *Gastrocnemius Medialis* and (7) *Gastrocnemius Lateralis*.

Studying the upper body parts was out of the scope of this dissertation, therefore only the joint reactions of the ankle, knee and hip joints were calculated. In this case, the pelvis did not need to be included in the dynamic model, but it was taken into account and modeled as a rigid frame so that the location of the muscle attachment points could be tracked throughout the activity. Also, due to small dimensions, very small mass and insignificant accelerations of the patella, its inertia properties are negligible compared to the remaining parts of the body, and therefore it was simplified and modeled as a frame as well.

The entire model is a 30 degrees of freedom multibody system (5x6DOF elements). Since not all of the reactions are contributing forces, the Kane's dynamics approach[130] does not require to derive all 30 dynamic equations of motion. Therefore, only those 18 joint reactions that are of interest for the biomechanical analysis were brought into evidence. These included the reactions at the ankle, knee and the hip joint. The equations of motion were derived using the AutoLev software (OnLine Dynamics, Inc., Stanford, CA).

The ground reaction force was obtained from the AMTI force plate. The raw data was converted into three reaction forces and three reaction moments (Figure 5.8). Using all six reactions as the input to the model is not correct, because the load applied to the force plate away from its center will result in bending moments

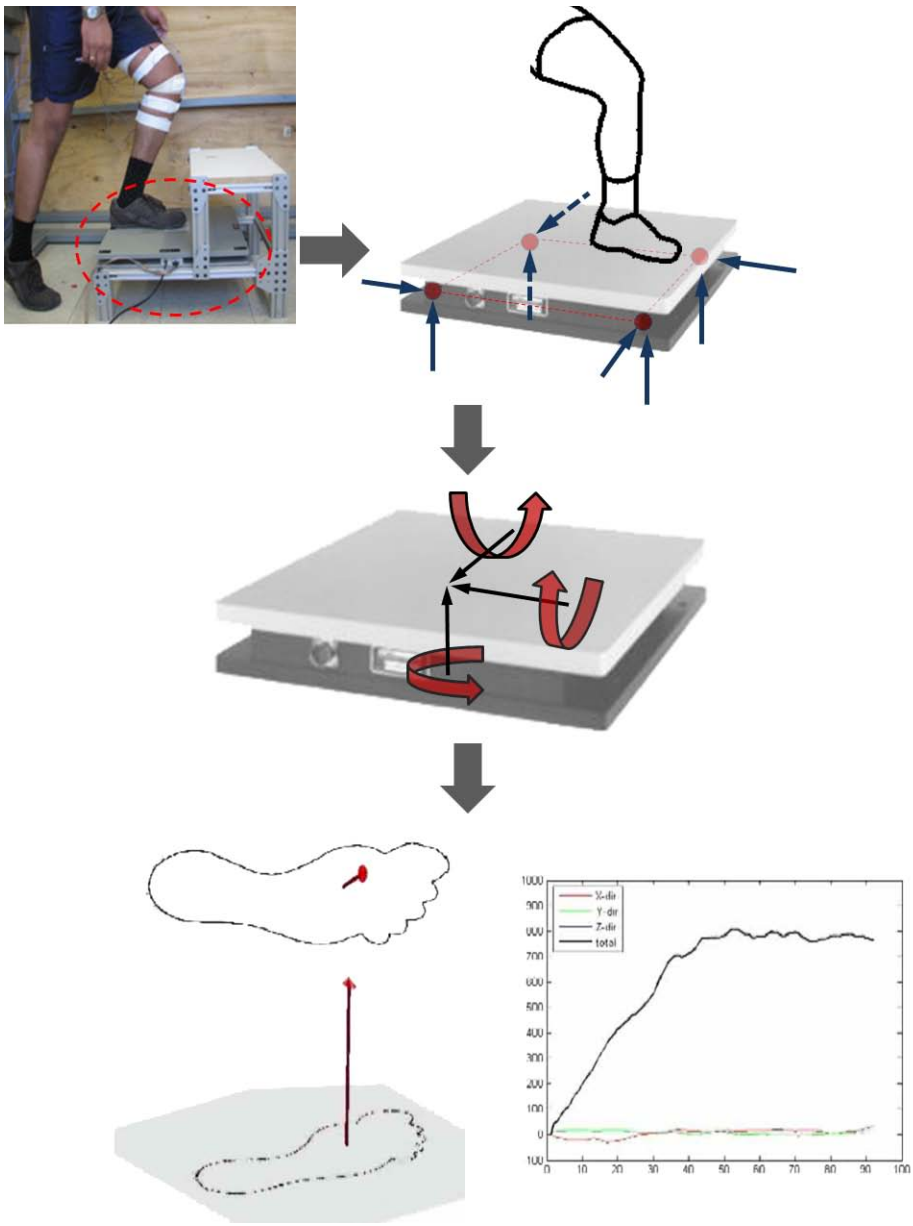


Figure 5.8: The ground reaction force was recorded using the AMTI force plate (top left). The 8 channel raw data (top right) was transformed into the reaction forces and moments. Knowing the 3 forces and 3 moments, the magnitude, direction and location (relative to the foot) of the resultant force was found.

and torsion reactions of the force plate, but this does not mean that the force plate applies opposite forces on the foot. For instance, the person standing still in one corner of the force plate will induce a vertical reaction and bending moments about the horizontal axes of the force plate. However, the only reaction experienced by this

person is the vertical reaction force, not the bending moments. The bending moment reactions would not arise in the force plate, if the person was standing directly above the center of the force plate. In other words, the location where the person stands on the force plate changes the output of the force plate, but does not change the reaction experienced by that person.

In real situation the weight is not applied as a point load, but rather as pressure, therefore it is important to calculate the magnitude, direction and location of the resultant reaction force responded to the foot by the force plate. The direction and magnitude of the reaction force was obtained directly from the force plate data (after conversion). Next the bending moments were divided by the respective reaction force components to calculate the location of that force component. Since the location of the foot on the force plate can be found from the live video camera, the location of the resulting force can also be found on the foot (Figure 5.8). Finally, the patient specific ground reaction force, its direction and location relative to the foot was used as the input to the dynamics model.

To correctly model the muscles, it was necessary to find their attachment points and their lines of action. This was done based on the CT images. However, in order to reduce the amount of harmful radiation that the participants were exposed to (both CT and fluoroscope emit X-rays), the CT scanning region was restricted to 7 inches below and above the joint line. Therefore, it was not possible to reconstruct the entire bones and muscles of the lower extremity. However, Dr. Mahfouz from the Center for Musculoskeletal Research has developed a gender specific bone atlas [164, 227] and algorithms capable of recreating the entire bones based on their distal or proximal parts (Figure 5.9). The average bone models of this atlas were used to reconstruct the entire bones of the femur and tibia. Since, no CT scans of the foot and pelvis were available, the average models of these bones were scaled according to subject's height and weight,[242] and used in the mathematical models.

For the implanted legs, this process involved one additional step. The TKA components are being oriented relative to the bones during the surgery. To determine

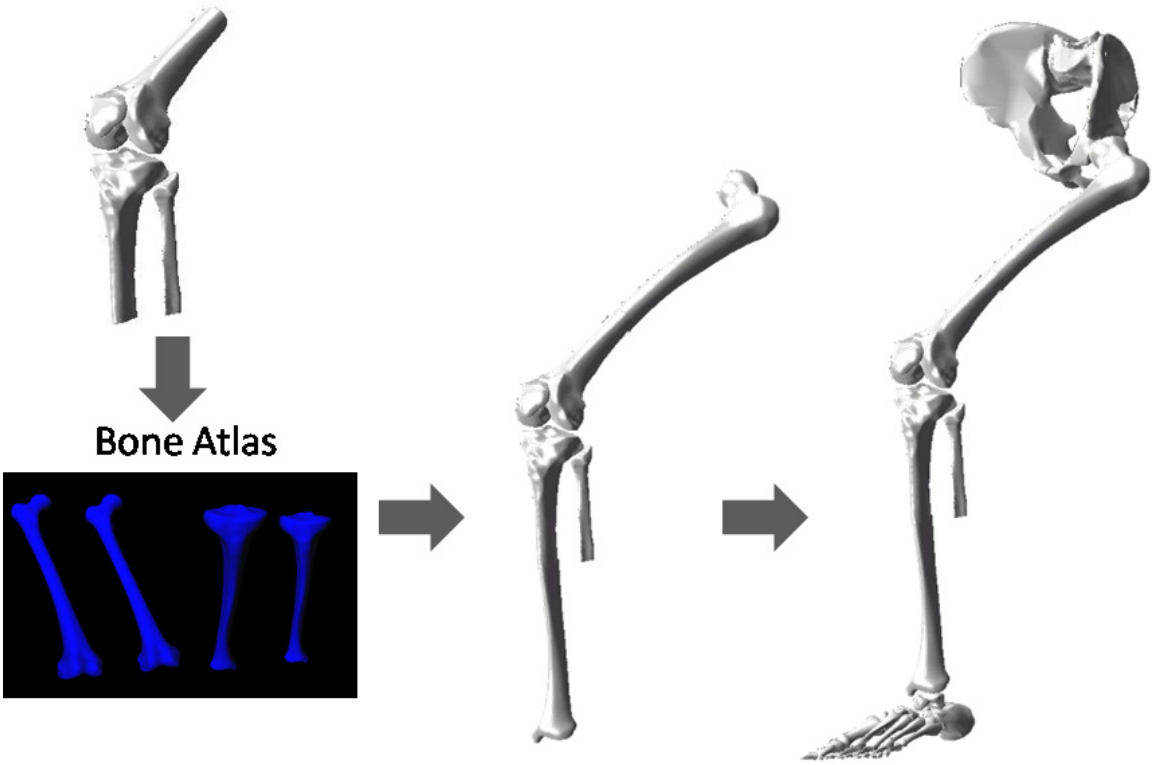


Figure 5.9: The bone atlas [164, 227] was used to reconstruct the entire bone models of the femur and tibia based on their distal and proximal portions reconstructed based on the CT images. The models of the foot and pelvis were uniformly scaled based on subject's height and weight.[242]

this relative orientation, the bone models of the contralateral leg were mirrored and fitted into the bone silhouettes in the fluoroscopic images using the aforementioned 3D-to-2D registration process. Once the entire bone models were oriented relative to their respective TKA components, the foot and pelvis models were added to the dynamics model using the same approach as for the healthy leg models (Figure 5.10).

The ankle joint was out of the scope of the fluoroscopic video and the kinematics of this joint could not be found using the 3D-to-2D registration. However, the lower portion of each subject's leg was captured by the live camera recording the foot interaction with the force plate. Therefore, the ankle joint kinematics in the sagittal plane could be found from the live video images (Figure 5.11).

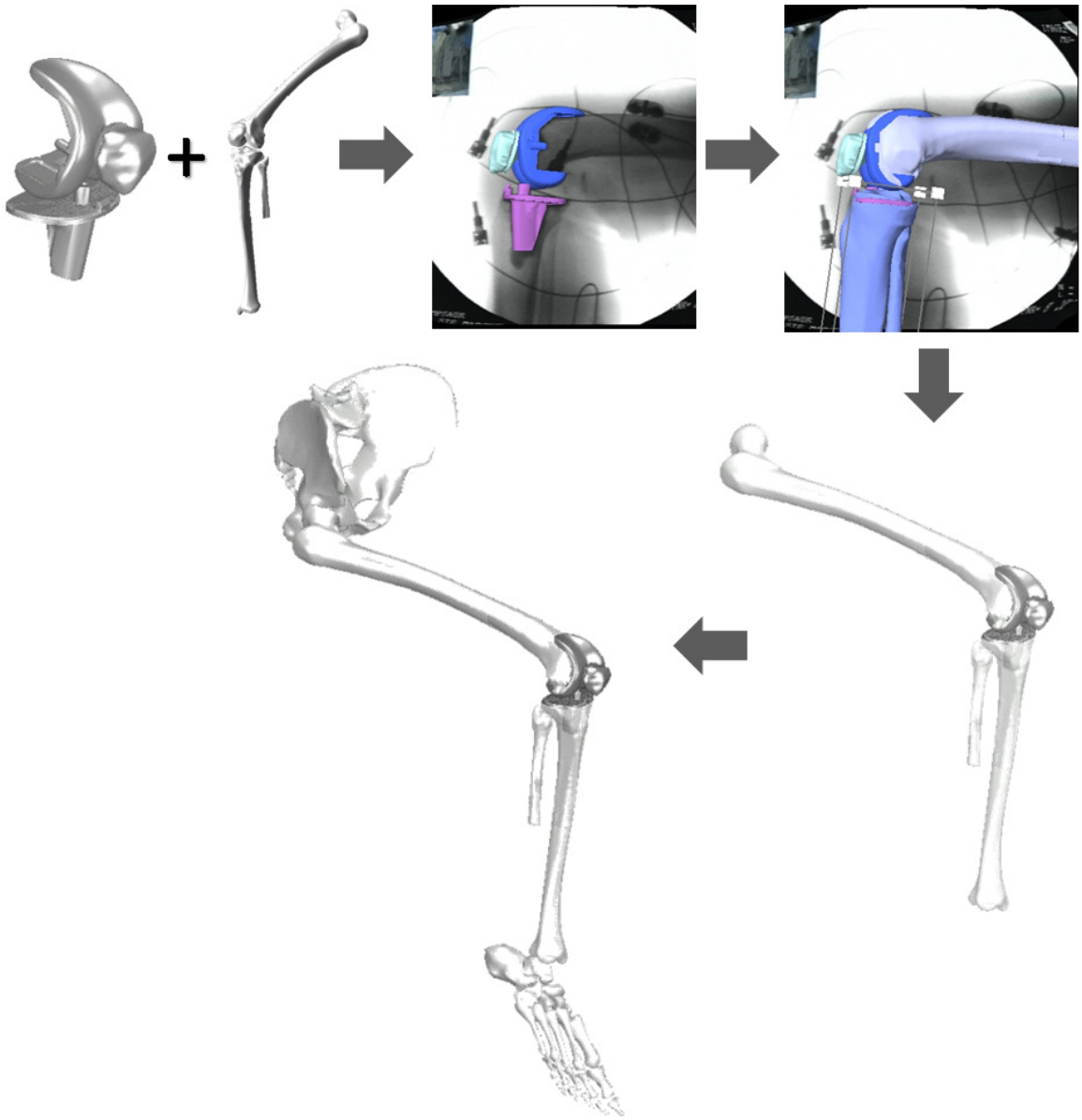


Figure 5.10: The entire bone models for the TKA leg were reconstructed analogously to the process applied for the healthy legs (Figure 5.9), with an additional step in which the orientations of the tibia and femur bones relative to the TKA components were determined by registering the bones onto the fluoroscopic images.

The out-of-plane rotations and translations of the ankle joint could not be measured based on the sagittal images. However, Leszko et al. studied the replaced ankle joint under in-vivo condition for twenty subjects and found, that for the stair climbing activity the plantar- and dorsiflexion were the most significant rotations.[157]

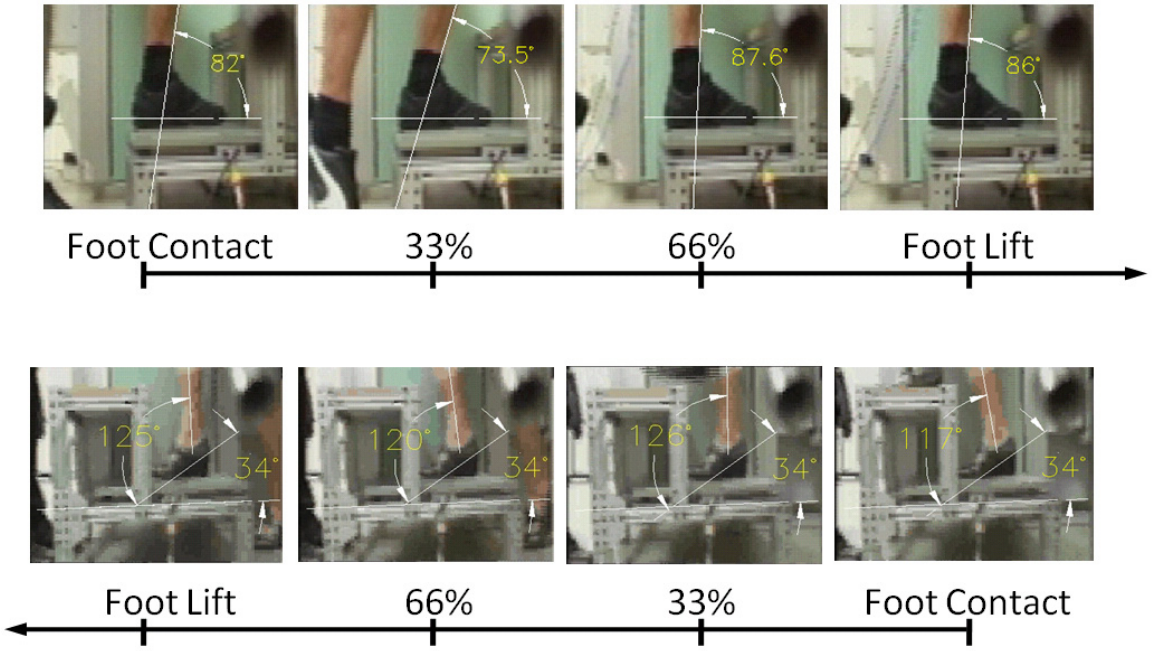


Figure 5.11: The sagittal plane kinematics of the ankle joint was estimated based on the video images available from the live camera footage.

The average internal/extarnal rotation changed only two degrees throughout the activity. There was also almost no inversion/eversion rotation observed for the subjects. The translations of the ankle joint were also very small and the anterior-posterior translation was limited to only 1 mm on average (Figure 5.12). Therefore, the sagittal plane rotations are the major components of the motion of the ankle joint, and have been assumed to appropriately represent the kinematics of this joint for the dynamic modeling purposes.

The motion of the foot relative to the force plate in the sagittal plane was also measured. This was especially important for subjects wearing heels, as the angle between the foot and ground may play an important role in the biomechanical conditions present in the lower extremity and needed to be adequately included in the dynamic model.

The hip joint was neither within the filed of view of the fluoroscope nor within the live camera view. Therefore the rotation of the pelvis relative to the femur could

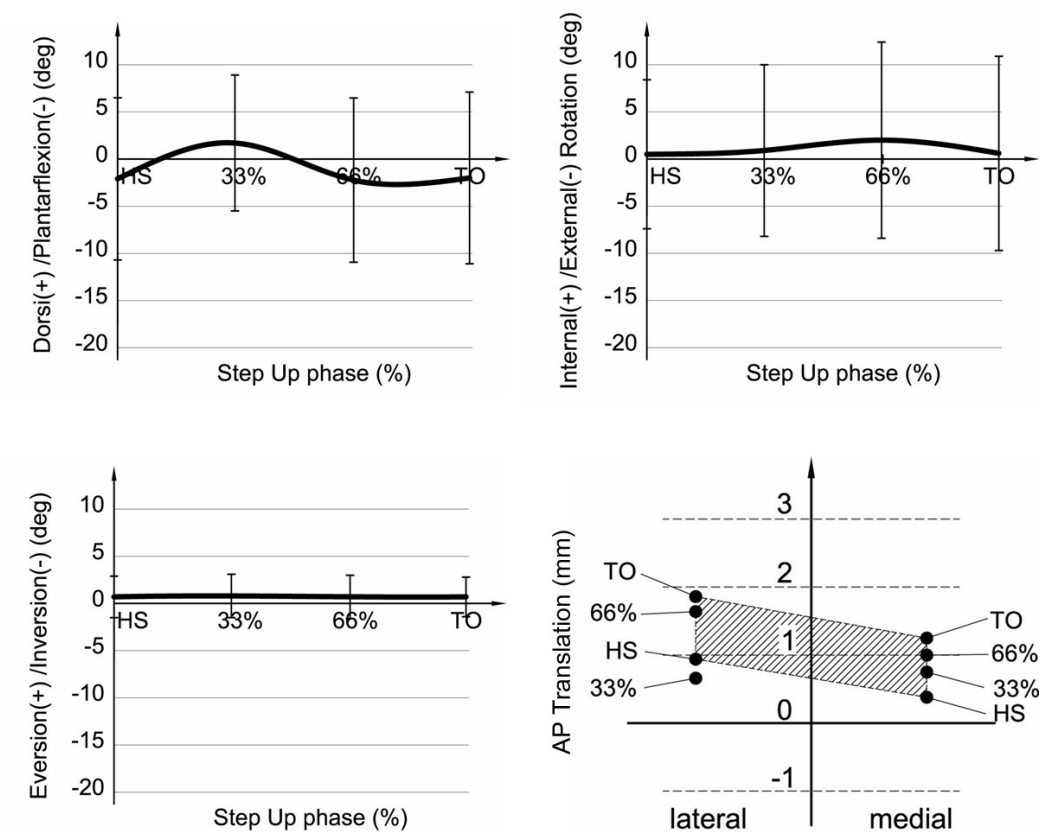


Figure 5.12: The in-vivo kinematics of the ankle joint was previously determined for 20 TAA subjects for the stair climbing activity. *Source: [157]*

not be measured directly. However, the hip joint is a ball and socket joint therefore the relative translations can be assumed to be negligible. It was also reported that the in-vivo rotation of the hip joint during the stance phase of the stair ascent has very similar pattern to the flexion of the knee joint (Figure 5.13).[199] In fact, the hip remains flexed approximately 8° more than the knee joint throughout this activity. Therefore, this relationship has been used to describe the rotation of the pelvis relative to the femur in the mathematical model.

The foot, shank and thigh mass, the location of their center of mass and inertia properties were calculated based on human body segment properties tabulated by Winter.[242] These properties are given as functions of subject's height and weight (refer to Figure 3.1 and Table 3.1 in [242] for details).

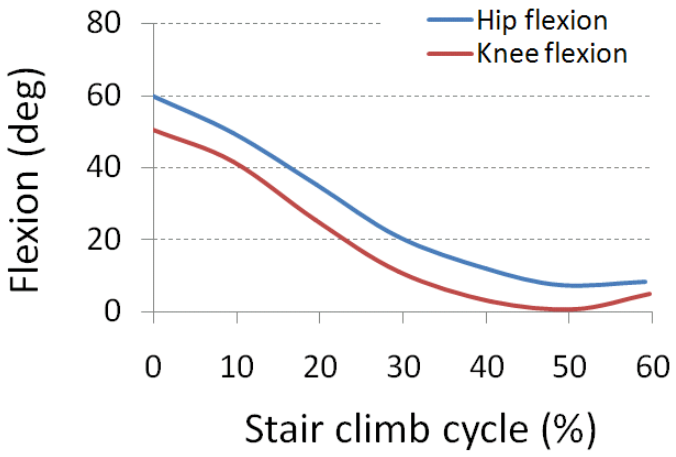


Figure 5.13: Previous gait study[199] reported that the hip flexion is about 8 degrees larger than the flexion of the knee joint throughout the weight-bearing portion of the stair climbing activity.

The direction of the force generated by the muscles depends on the location of the muscle attachment to the bones and the relative orientation of the bones that are spanned by the muscle. The location of the attachment sites for each muscle does not vary significantly between individuals and can be found in anatomy atlases (e.g. [229]). Some of the muscles of the knee joint have relatively small attachment sites (e.g. biceps femoris attachment at the fibula) and their lines of action can be modeled as single lines connecting the corresponding attachment points at the bone. However, some of the muscles, have wide attachment sites (e.g. vastus lateralis or vastus medialis attachment at the femur) and modeling them as single lines would be an oversimplification. Therefore, such large muscles were divided into several bundles, each bundle modeled as a line attached at single points. The number of bundles depends on the size and complexity of the attachment site, but most of the large muscles were satisfactorily modeled by two to three bundles (Figure 5.14).

Similarly the attachment points were identified for the patients having a knee replacement (Figure 5.15). As for healthy legs, the muscles having large attachment sites were divided into separate bundles. A significant difference between the biomechanical boundary conditions between the TKA and healthy knees is the lack

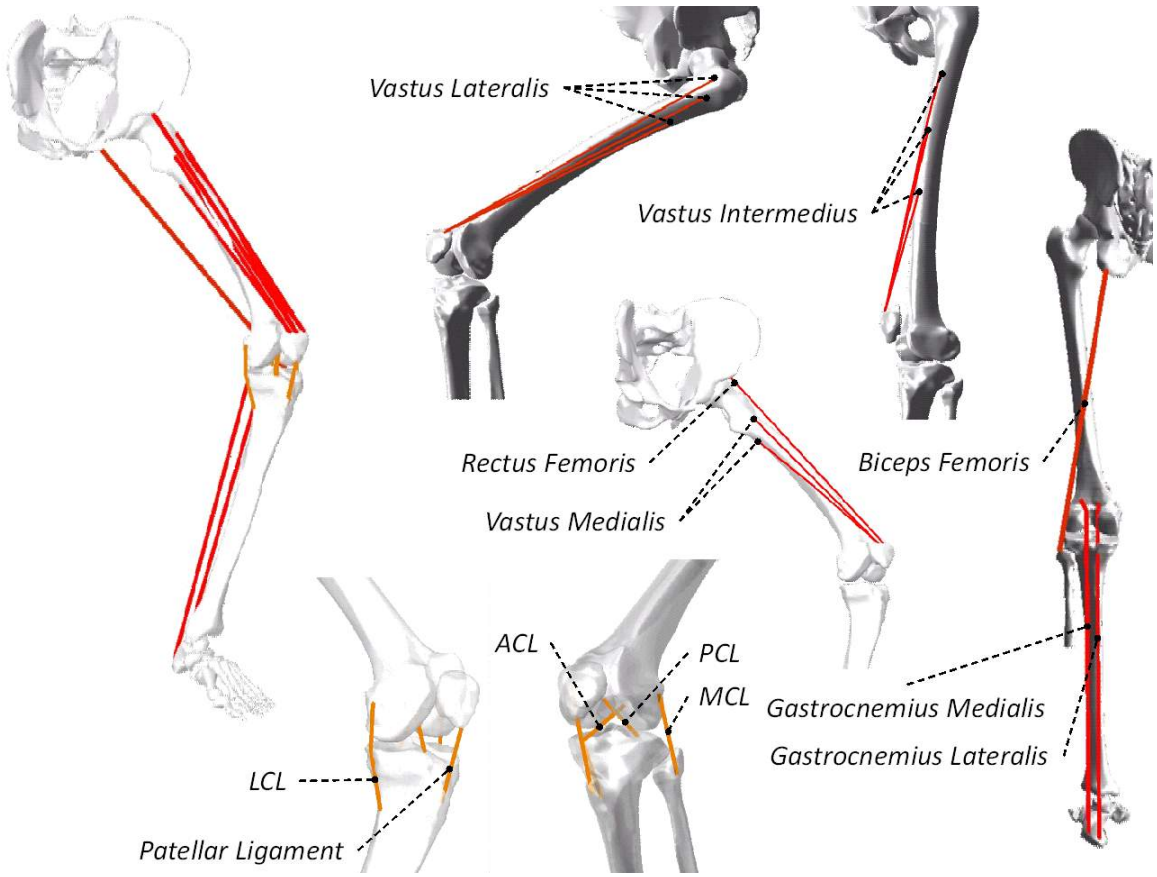


Figure 5.14: The muscles and ligaments of the healthy lower extremity were modeled as lines spanning the knee joint, attached at their respective tendon attachment sites. Depending on the size and complexity of the attachment sites, some muscles were divided into bundles (e.g. *Vastus Lateralis*). Legend: *ACL - Anterior Cruciate Ligament, PCL - Posterior Cruciate Ligament, MCL - Medial Collateral Ligament, LCL - Lateral Collateral Ligament.*

of anterior and posterior cruciate ligament present in the replaced joints, which are sacrificed during the TKA procedure. These ligaments, therefore were absent in the dynamic models created for the TKA subjects.

Finding the attachment points of the muscles is not sufficient to correctly determine the lines of action of the muscles and ligaments. Depending on the orientation of the bones, the soft tissues wrap around the bones changing the directions of the forces present in these structures. To model the interaction of the soft

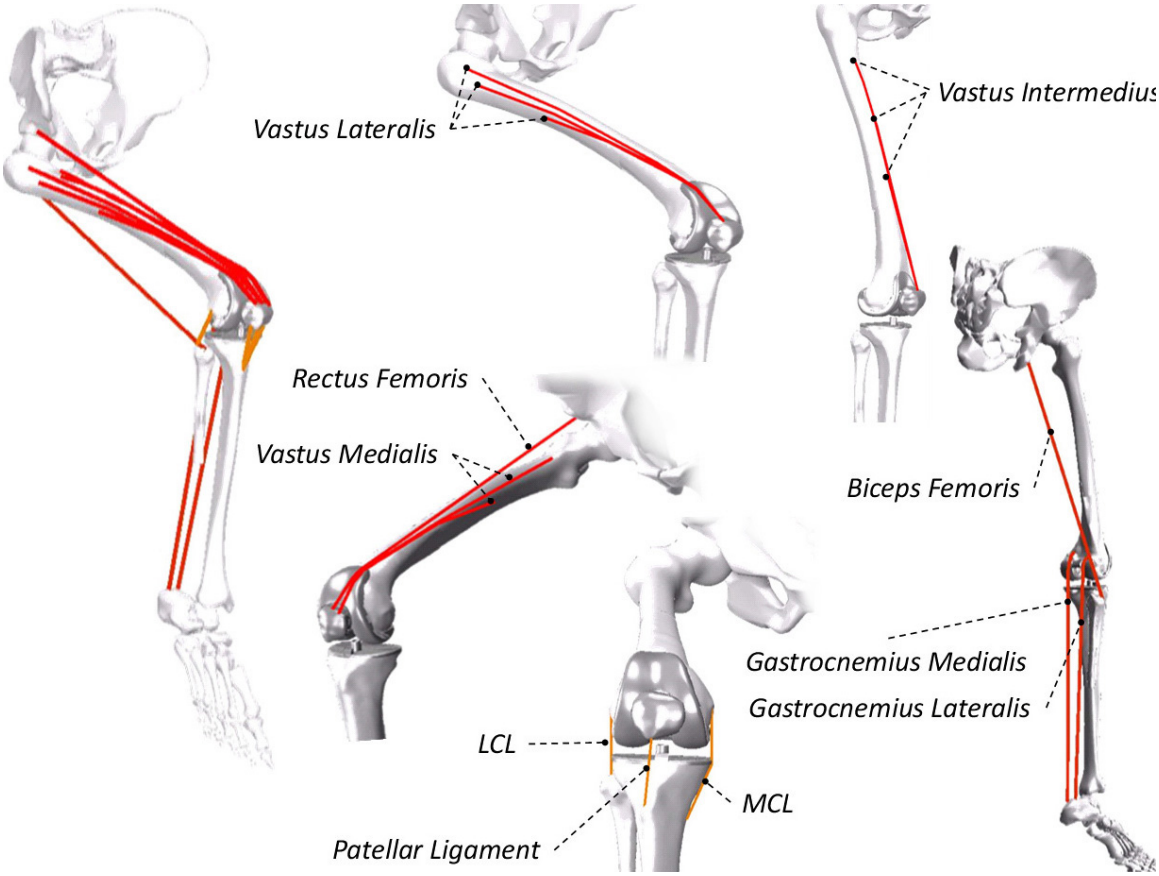


Figure 5.15: The muscles and ligaments of the TKA leg were modeled as lines spanning the knee joint, attached at their respective tendon attachment sites. Depending on the size and complexity of the attachment sites, some muscles were divided into bundles (e.g. *Vastus Lateralis*). Note that the *Anterior* and *Posterior Cruciate Ligaments* are not present for the TKA knees. Legend: *MCL - Medial Collateral Ligament, LCL - Lateral Collateral Ligament.*

tissues with the bones, a wrapping algorithm has been developed and programmed as a graphical user interface application in Matlab (MathWorks, Inc., Natick, MA).

The wrapping algorithm connects two selected points with a line and determines whether the line is colliding with any body of the model. If there is no collision, the line remains straight, connecting the attachment points directly. If the collision is detected, the algorithm calculates a number (controlled by the user) of possible lines joining the two points and wrapping about the surface of the colliding body (see the animation in the Figure 5.16). Since the muscle is an visco-elastic structure, according

the ***Minimum Total Potential Energy Principle***, it can be assumed that from a number of possible pathways, the muscle will assume the one which minimizes its length, and hence minimizes potential energy. Therefore, in its 1^{st} generation, at every flexion increment, the algorithm measured the length of all possible pathways connecting the two points and chose the shortest one as the actual path of the muscle.

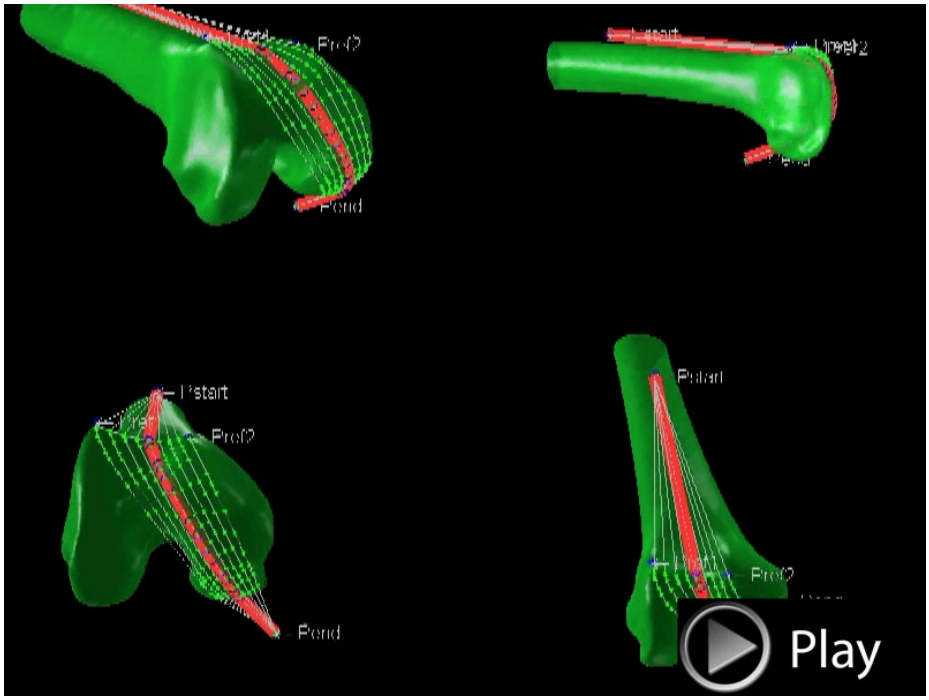


Figure 5.16: The robustness test of the soft tissue wrapping algorithm (1^{st} generation).

Choosing the shortest line from all the possible pathways, however, may result in abrupt jumps between local minima changing at different flexion increments (as seen in the animation in the Figure 5.16). Such abrupt changes are rather unlikely to be experienced by the soft tissues under in-vivo conditions. Therefore, the algorithm was modified to initially determine the wrapping location from all possible pathways, but once this location was established, the line was allowed to move only to the pathway immediately next to it. In other words, if the location of the shortest pathway changed during the motion of the bones, the muscle/ligament line was allowed to slide towards the local minimum searching for the shortest pathway, rather than jump to it, (see

the animation in the Figure 5.17). This resulted in a performance much more closely resembling a natural soft tissue behaviour.

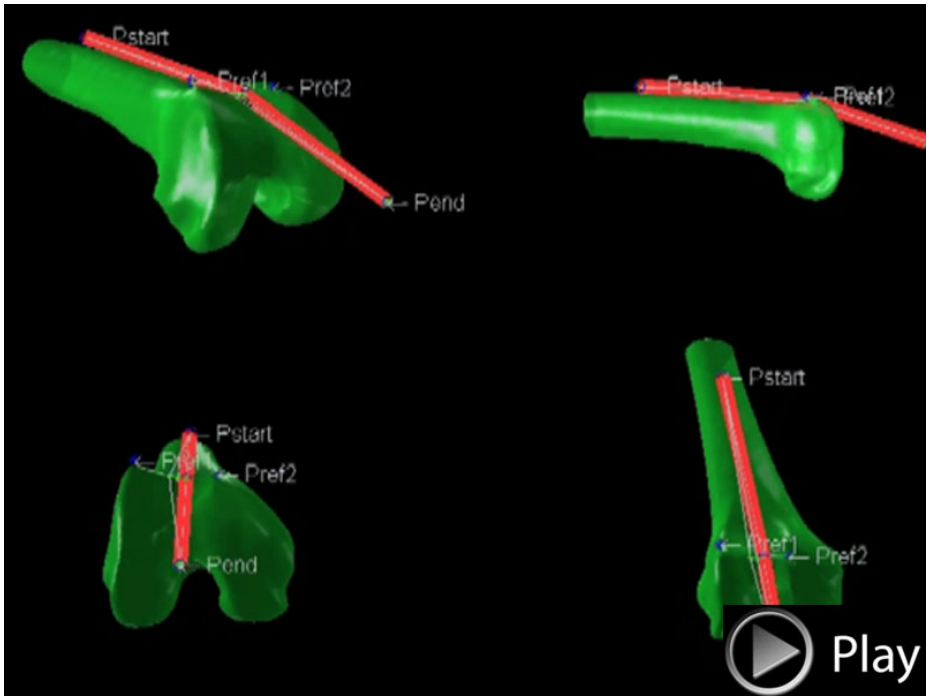


Figure 5.17: The robustness test of the soft tissue wrapping algorithm (2^{nd} generation).

Under the natural biomechanical conditions, the muscle once being in contact with the bone, does not have to remain in contact throughout the activity. For instance, during the gait the quadriceps muscle may be wrapping around the femoral trochlea during the swing phase (when the knee is flexed), but may not wrap during the stance phase (when the knee is in relatively low flexion). Therefore, in the final version, the wrapping algorithm also allowed the line to loose the contact with the colliding bone and come into contact again, at a different instance of motion and most likely at a different location. In fact, whenever the line is not colliding with any body, the algorithm will detect the new collision wherever and whenever it occurs (see the animation in the Figure 5.18).

The wrapping was taken into account for all the muscles and ligaments included in the dynamic model. The resulting model for an example TKA patient is shown in Figure 5.19.

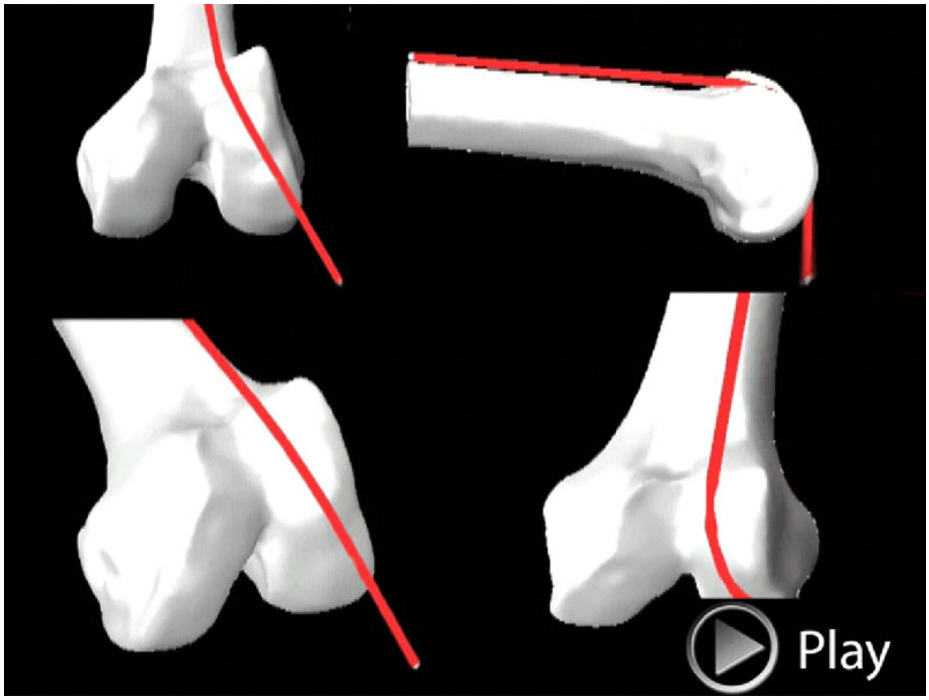


Figure 5.18: The robustness test of the final soft tissue wrapping algorithm.

The direction of the line of action of the muscle forces is one of the important factors influencing the biomechanics of the knee joint. Another crucial factor is the location of the reaction (interactive) forces acting on each bone. The location depends on the relative orientation, location and geometry of the articulating surfaces. In natural joints, the contact pressure is distributed within the layer of the articular cartilage and this distribution is difficult to study non-invasively under in-vivo condition. However, in multibody dynamics all the bodies are assumed to be rigid, and therefore the location of the application of the resultant interaction force, rather than the pressure distribution, is required. Additionally, assuming that the contact forces are uniformly distributed within the articular cartilage, the pressure distribution is related to the distance between the interacting bodies. Therefore, the location of the contact points was determined based on the distance between the articulating

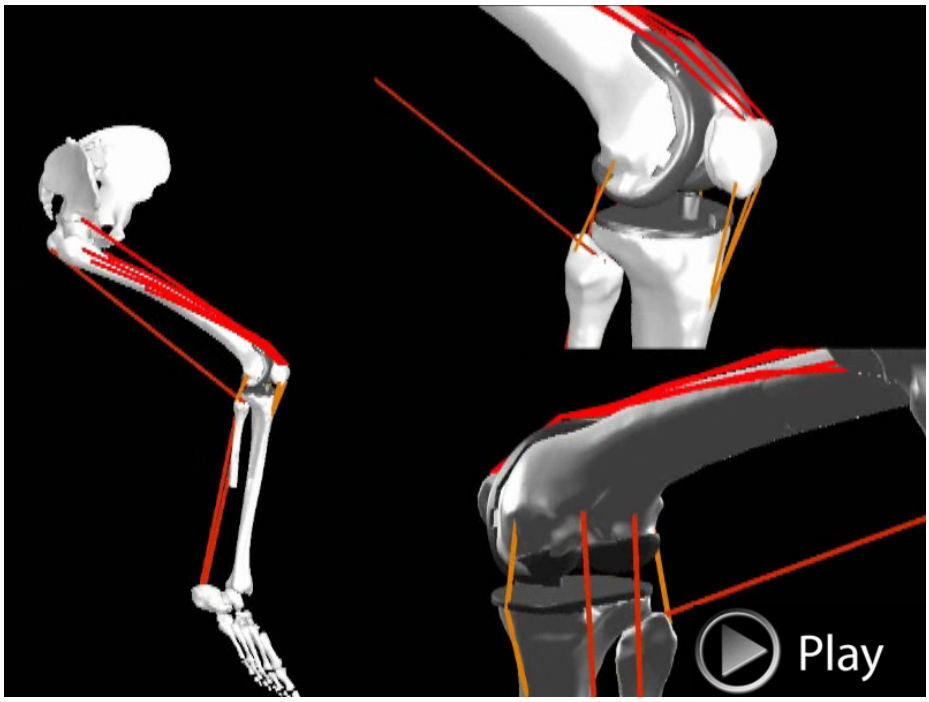


Figure 5.19: The muscle and ligaments wrapping was included in the dynamic model.

surfaces. Knowing the distance distribution, the location of the contact point was assumed to be at the centroid of the surface being within 1 mm from the closest point between the surfaces (Figures 5.20, 5.21, 5.22, 5.23). The contact points were tracked throughout the activity relative to the local coordinate systems fixed to the respective bodies and used as the application points of the reaction forces.

The muscles generate forces driving the musculoskeletal system and therefore may be considered active elements. The ligaments, however, apply tension only when stretched beyond the slack length and hence are passive elements. They have been included in the dynamic model as passive elements governed by non-linear force-strain relationship for low strains and linear in higher strain regions[246], written as the following a function of strain:

$$f = \tfrac{1}{4} k\epsilon^2/\epsilon_r, \text{ for } 0 \leq \epsilon \leq 2\epsilon_r$$
$$f = k(\epsilon - \epsilon_r), \text{ for } \epsilon \geq 2\epsilon_r$$
$$f = 0, \text{ for } \epsilon < 0$$

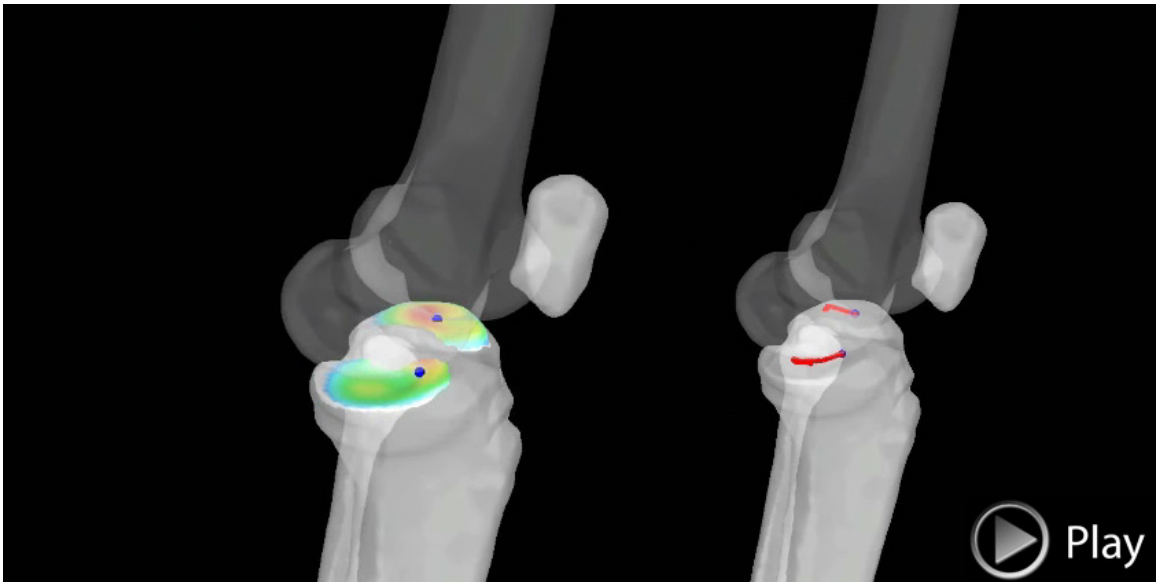


Figure 5.20: The tibiofemoral contact map on tibia (left) was used to predict and track the location of the tibiofemoral contact points relative to the tibia (right).

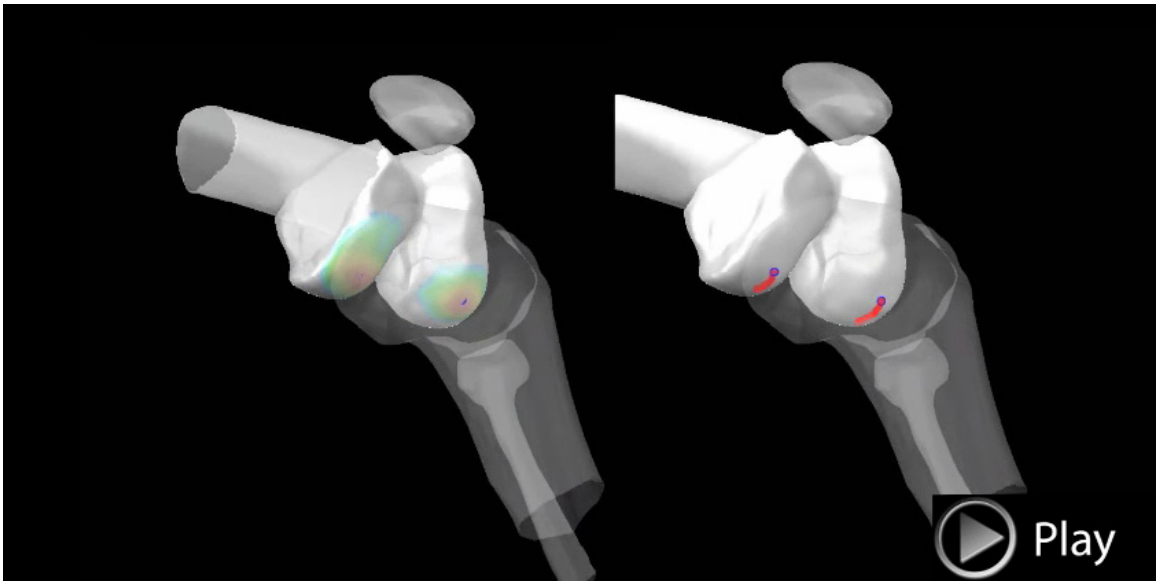


Figure 5.21: The tibiofemoral contact map on femur (left) was used to predict and track the location of the tibiofemoral contact points relative to the femur (right).

where, the f is the tensile force applied by the ligament element, k is the ligament linear stiffness, ϵ is the strain in the ligament, and the ϵ_r is the reference strain. The ligament stiffness and reference strain values were adopted from the data available in the literature.[24]

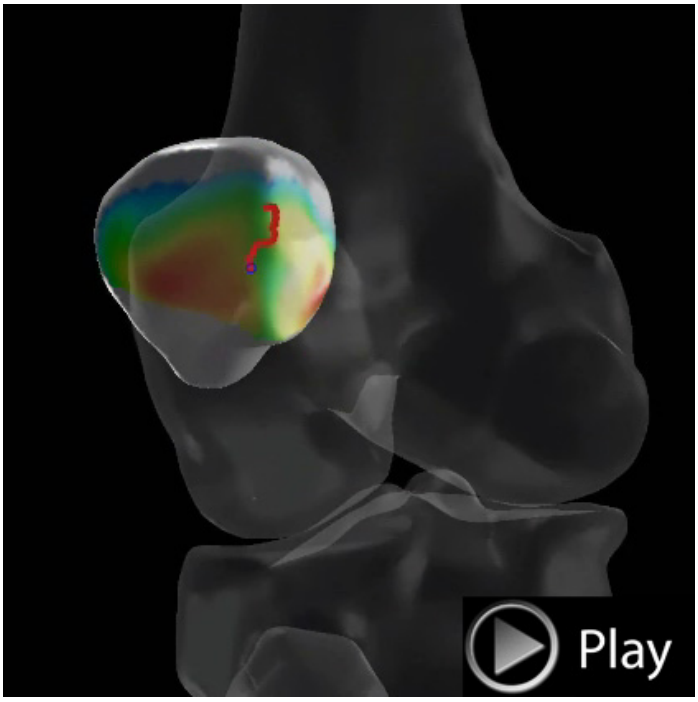


Figure 5.22: The patellofemoral contact map on patella was used to predict and track the location of the patellofemoral contact point relative to patella.

All of the above parameters were included as the input data to the complete patient-specific dynamic model. The model therefore reflected each subject's in-vivo, 3D kinematics, bone geometry, body segment properties, muscle lines of action, ligament force direction and force-strain relationship, contact point locations, ground reaction force (GRF) magnitude, direction and its application point location. Using these input data, the resulting joint reaction forces and torques were found using the inverse dynamics approach. However, the purpose of this work was to calculate not only the joint reactions, but also to determine the forces in the individual muscles. Therefore, the resultant torques had to be decomposed into the forces applied by the individual muscles. This, however cannot be solved directly because the number of unknown muscles forces is larger larger than the number of available equations of motion.

To find the solution to this redundant problem, the pseudoinverse method[251] was employed. This method is a very efficient way of performing dynamics optimization of

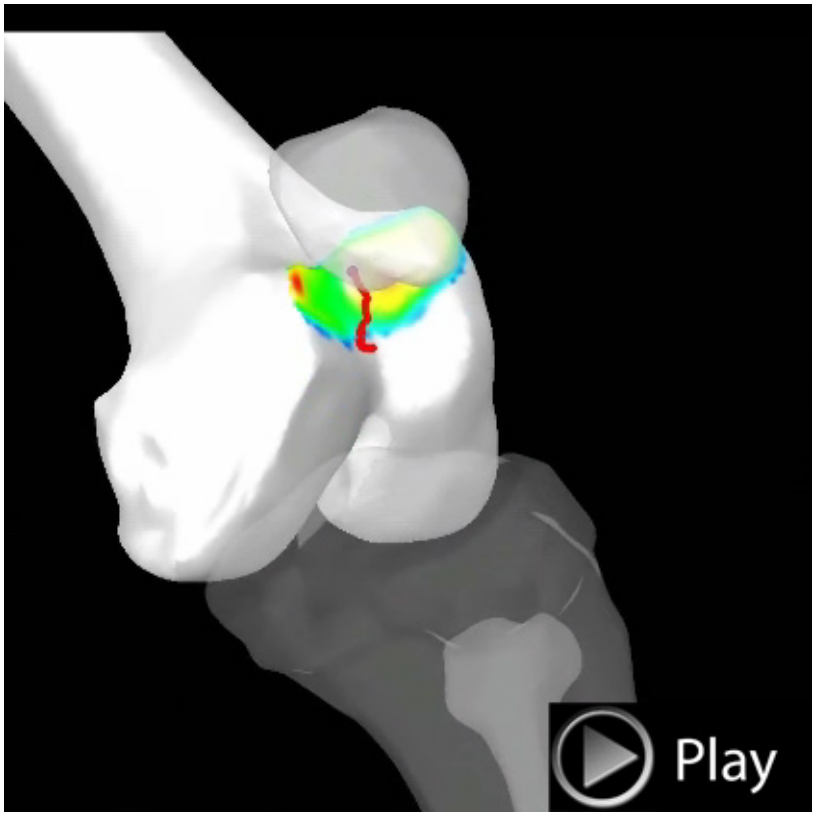


Figure 5.23: The patellofemoral contact map on femur was used to predict and track the location of the patellofemoral contact point relative to femur.

movement without many undesirable features of parameter optimization or gradient searching.[252] It neatly circumvents many of the problems associated with other methods of obtaining solutions to biomechanical force distribution problem. Typically the method requires that the desired motion trajectory be predefined. However, in this work it was used in a slightly modified way. Namely, since the resultant torques acting on the femur bone were calculated by the inverse dynamics model, it was decided to use the pseudoinverse method to directly decompose these desired torques into the muscle forces. In other words, instead of prescribing the desired motion trajectory, the resultant torques were used as the desired kinetic trajectory.

In the dynamic model, the redundancy occurs because there are 12 muscle forces to be found based on 3 torque equations. Since every muscle's line of action lies in three dimensional space, the contraction of each muscle will induce a torque acting in

all of the 3 degrees of freedom. Therefore, it is necessary to first calculate the torque resulting from an application of a unit force acting along the line of action for every muscle. These resulting torques are stored in an matrix A, which is referred to as the *Muscle Unit Response Matrix*. Note that in general case this will build an nxm matrix, where n is the number of degrees of freedom, and m is the number of muscles, and for musculoskeletal systems m is usually much larger than n.

The thickness and arrangement of the muscles surrounding the bones increases the offset at which the muscle resultant forces act. In order to include these effects, the 3D muscle CAD models were recreated based on the CT scan images (Figure 5.24). It has been assumed that the muscle fibers are uniformly activated and apply equal tension throughout the muscle belly. Under this assumption the resultant force passes through the mass center of the muscle belly, which has been calculated from the CAD models (using RapidForm 2006, INUS Technology, Inc., Seoul, Korea) assuming homogeneous density of the soft tissue (Figure 5.25). Next, the muscle's mass center offset was measured from the bone surface. For large and flat muscles surrounding the bones (e.g. vastus intermedius), the muscle belly was divided into smaller bundles and the average of the bundles' offsets was used as the offset of the muscle (Figure 5.25).

Once the muscles unit response matrix has been formed, the problem may be written as:

$$Ax = b, \tag{5.1}$$

where A is the *Muscle Unit Response Matrix*, x is the column vector of the n unknown muscle forces (to be solved for), and b is the column vector of the m desired torques (found from the inverse dynamics).

This equation cannot be solved by simply inverting the A matrix and pre-multiplying by b because A in not a square matrix. Therefore, the solution is achieved by using the right pseudoinverse A^+ of matrix A, because:

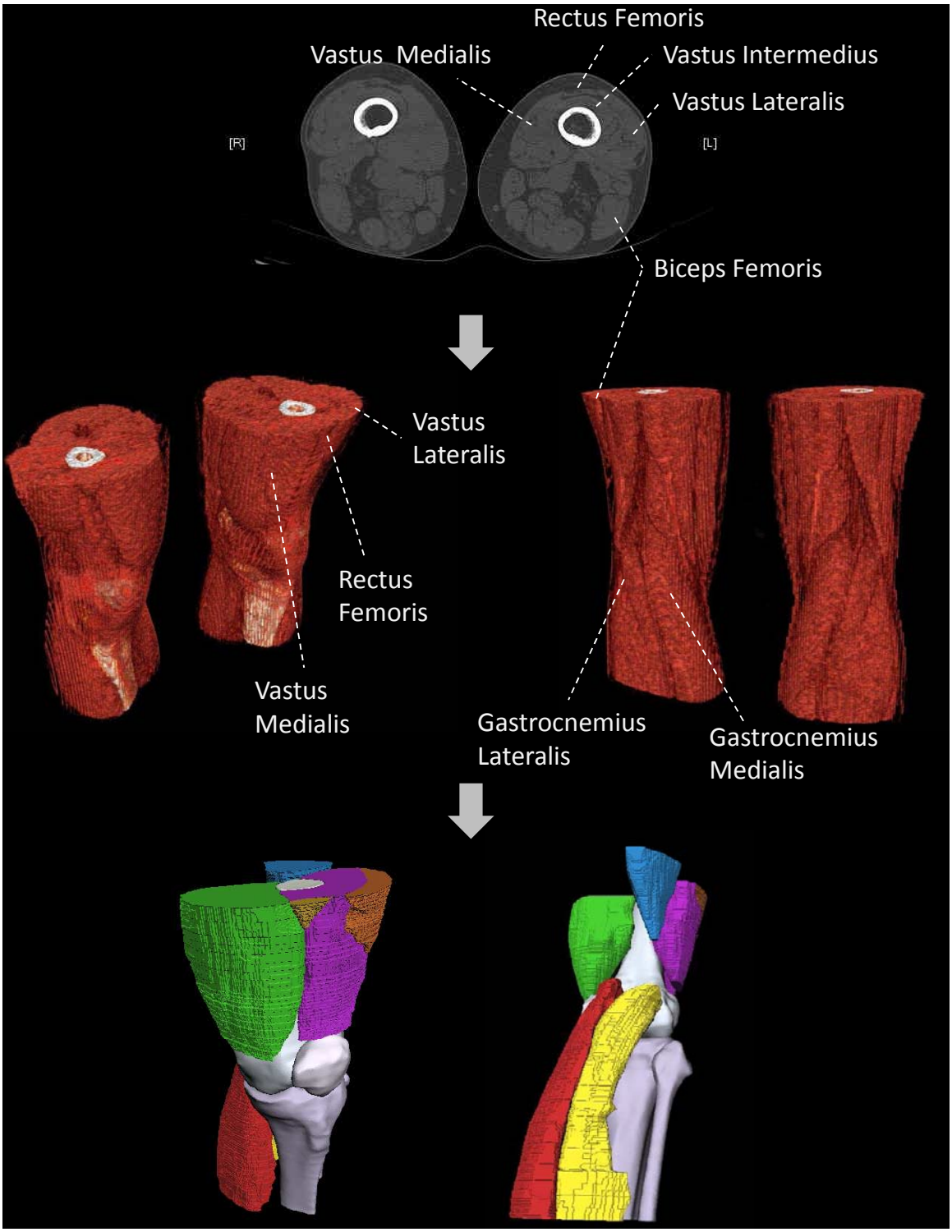


Figure 5.24: Muscle CAD models were segmented based on the CT images for every participant. The muscle volume data were used to calculate the physiological cross-sectional area of each muscle.

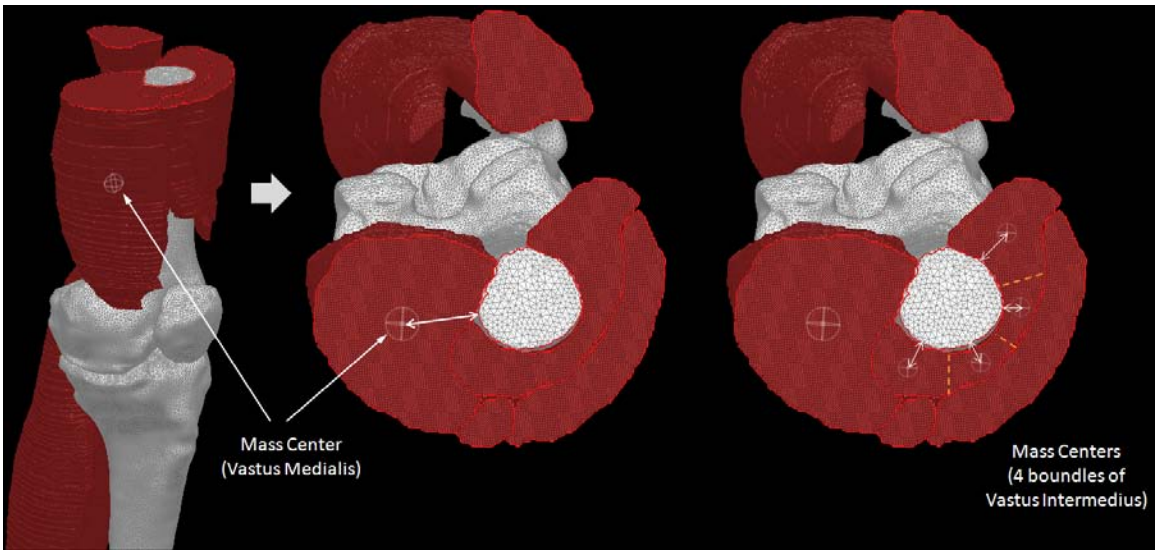


Figure 5.25: The muscle mass center has been calculated based on the 3D muscle models recreated based on the CT images (left). Next, the muscle's mass center offset from the bone surface was found (middle). For large and flat muscles surrounding the bones (e.g. vastus intermedius), the muscle belly was divided into smaller bundles to find the average muscle mass center offset (right).

$$Ax = (AA^{+})b = b, \tag{5.2}$$

and hence:

$$x = A^{+}b, \tag{5.3}$$

where A^{+} is given by:

$$A^{+} = A^{T}(AA^{T})^{-1}. \tag{5.4}$$

The solution x obtained by the pseudoinverse method yields the optimal solution having minimum error $|\epsilon| = |Ax - b|$, and minimum vector length.[225, 252] Therefore, the solution:

$$x = [F_1 F_2 F_3 ... F_m]^T, \tag{5.5}$$

will have minimum magnitude:

$$min(|x|) = \sqrt{F_1^2 + F_2^2 + F_3^2 + ... + F_m^2} = \sqrt{\sum_{j=1}^{m} F_j^2}. \tag{5.6}$$

Replacing the muscle unit force by the muscle unit stress, the solution of the problem would minimize the stress in the individual muscles:

$$min(|x|) = \sqrt{\sigma_1^2 + \sigma_2^2 + \sigma_3^2 + ... + \sigma_m^2} = \sqrt{\sum_{j=1}^{m} \sigma_j^2}. \tag{5.7}$$

This result is equivalent to minimizing the Crowninshield-Brand criterion (cost) function[52] for the exponent parameter $p = 2$:

$$C = \sqrt[p]{\sum_{j=1}^{m} \left(\frac{f_j}{PCSA_j} \right)^p}. \tag{5.8}$$

Thus, the pseudoinverse method yields the optimal solution without running any optimization algorithm. Although Crowninshield and Brand found that the $p = 3$ yields results that are the most consistent with other data available in the literature, they also reported that there was no difference in the number of active muscles and only slight differences in the muscle forces for $p = 2, 3, 4$.

Once the individual muscles forces of the quadriceps group were found, it was possible to calculate the patellofemoral joint reaction (PFJR) force, and the patellar ligament force. To this end it was assumed that the individual quadriceps muscle forces, PFJR and patellar ligament forces act in one plane and remain in equilibrium. This assumption is plausible because the patella does not experience substantial accelerations, and therefore the dynamic effects are can be assumed to play secondary effects, especially considering very small mass and inertia of this bone. Therefore the PFJR and patellar ligament force were directly solved for from two equilibrium equations formed in the plane created by the patellar ligament and each of the quadriceps muscle's line of action (Figures 5.26 and 5.27).

The patellar ligament force is applied at the tibial tubericle on the tibia, therefore contributing to the total tibiofemoral joint reaction force. Therefore after the total magnitude of the patellar ligament force was found, its component acting along the tibial long axis was found and added to its corresponding component of the tibiofemoral joint reaction force found using the inverse dynamics. This way, the total in-vivo tibiofemoral joint reaction force including the effects of the action of the quadriceps muscle forces was calculated. This is the same force that has recently been determined for the TKA subjects under in-vivo conditions by direct measurements using the instrumented tibial components.[60, 102] The telemetry technology, however, cannot be used to determine forces in the natural (non-implanted) knees due to its invasive nature.

5.3.2 Muscle Dynamics Analysis

The EMG signals represent the electrical manifestation of contracting muscles.[15] This electrical activity stems from the action potentials reaching the alpha motor neurons (α-MNs) innervating the skeletal muscle and causing it to contract. The result of contraction of the skeletal muscle is tension in the muscle. A close relationship was found between the integrated electromyogram and tension in human muscle contracting *isometrically*.[123] However, during dynamic tasks such as stair ascending, the muscles contract anisometrically. When the muscle is allowed to change its length, various mechanical, physiological, anatomical and electrical modifications occur throughout the contraction and substantially affect the relationship between the signal amplitude and the muscle force.[53] Therefore, the application of surface EMG to study the muscle contraction is fraught with problems. Apart from technical limitations of the surface EMG, the relationship between the raw EMG and muscle force is far from trivial and involves a number of mathematical transformation that can be summarized as (1) neural excitation, (2) muscle activation dynamics and (3)

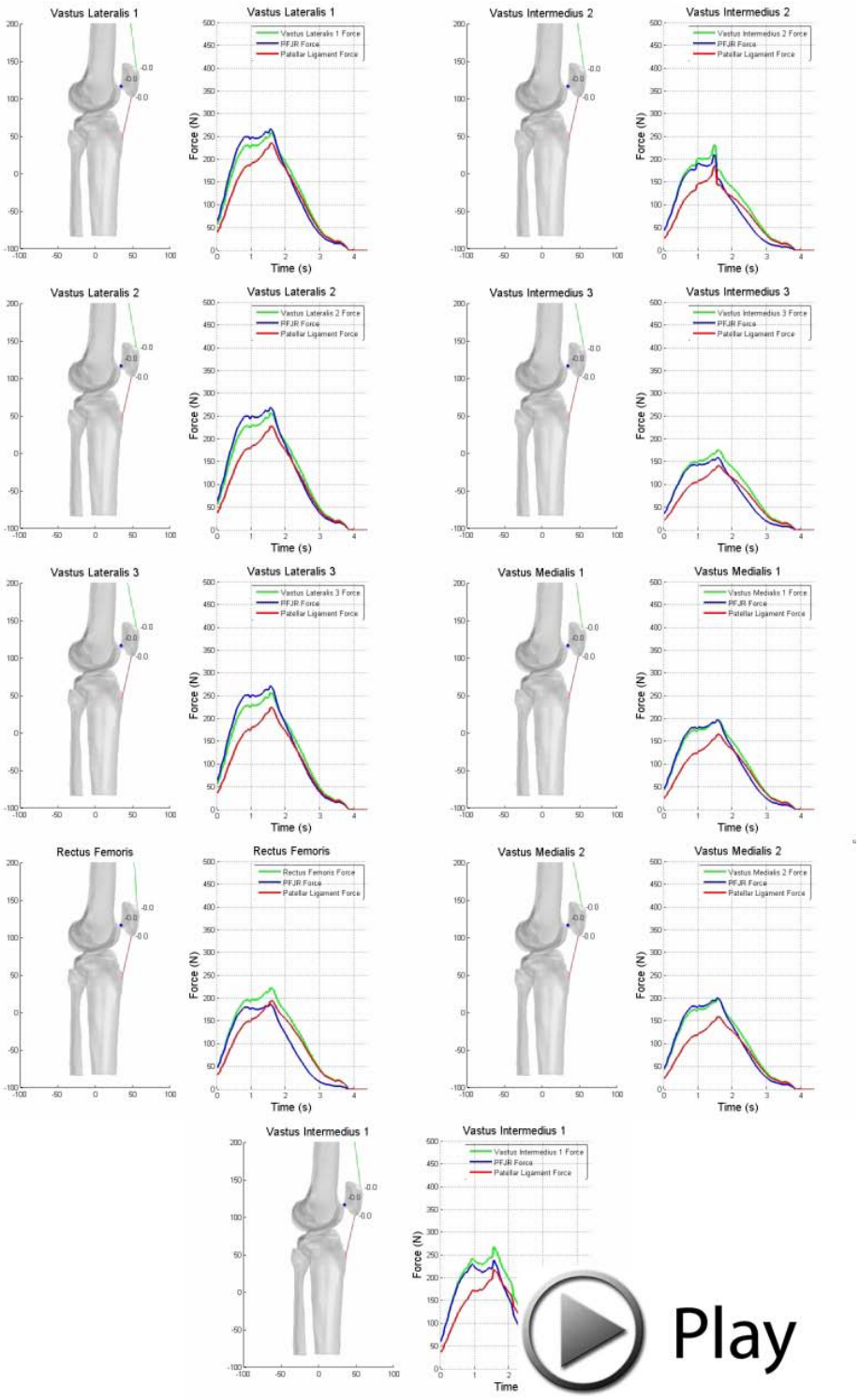


Figure 5.26: Example of the patellofemoral joint reaction and patellar ligament force calculation for a healthy subject.

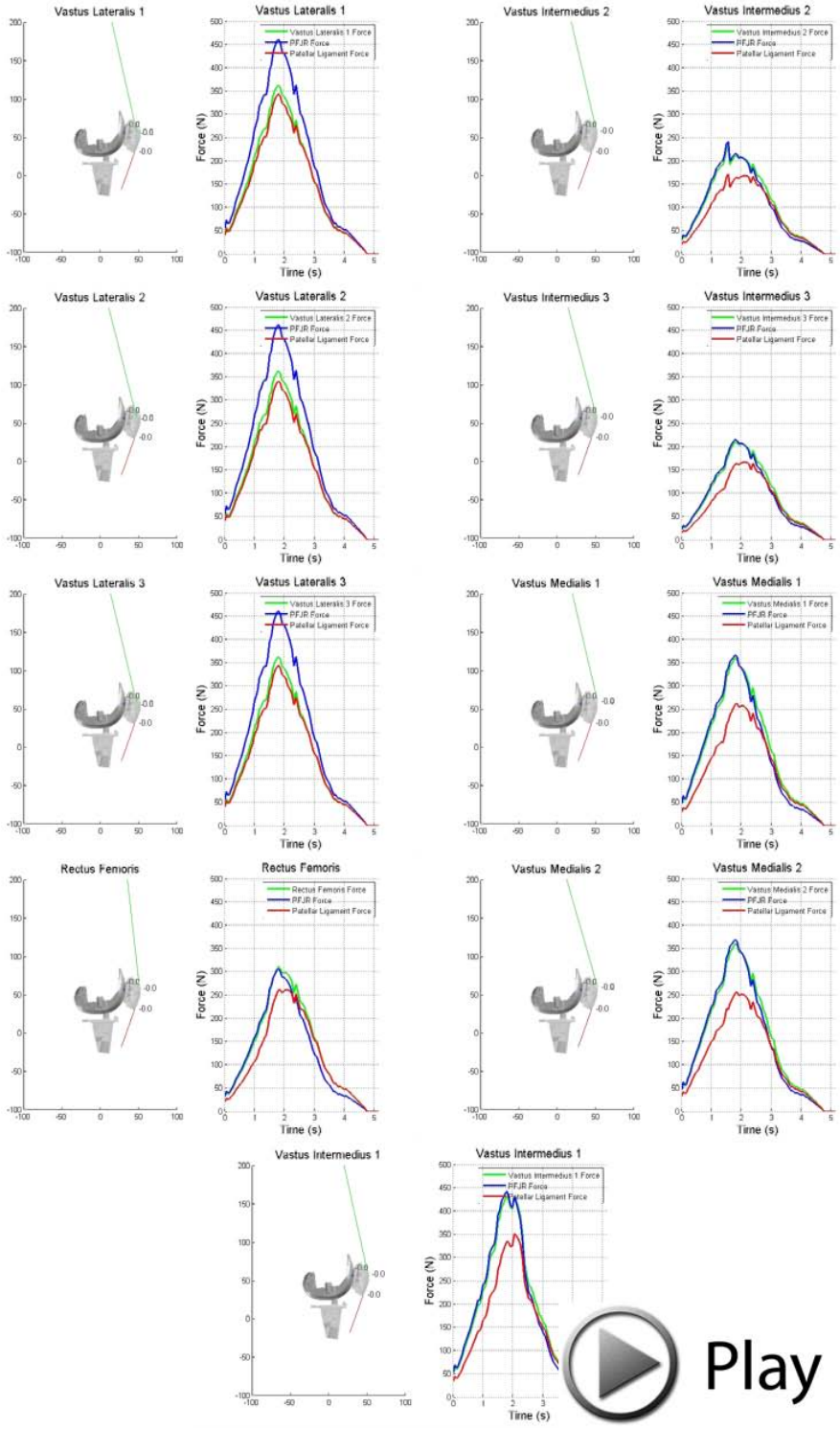


Figure 5.27: Example of the patellofemoral joint reaction and patellar ligament force calculation for a TKA subject.

muscle contraction dynamics. These relationships have been described by Zajac[256] and have been used in this dissertation.

The EMG signals were acquired using the MA-300 EMG system (Motion Lab Systems, Inc., Baton Rouge, LA), as shown in Figure 5.28. The electrical activity was recorded by the MA-411 active electrodes, which preamplified the raw signal by the factor of 20. The system also has built-in selectable hardware filters making it possible to bandpass filter the signal before it is converted to digital form. The cutoff frequencies used in this study were set at 10Hz and 500Hz, as recommended by the International Society of Electrophysiology and Kinesiology (ISEK).[175] This range is sufficient because the signal spectrum for surface EMG, typically extends from 10 to 400Hz.[219] The data was sampled at 10869 Hz/channel, well above the Nyquist theorem requirement.

To find the neural activation level for each muscle, the preamplified and prefiltered EMG signals were first rectified, because the neural activation is a positive parameter varying between 0 and 1. Next the envelopes of the signals were found by squaring the input signal and sending it through a low-pass filter. Squaring the signal demodulates the input by using the input as its own carrier wave. As a result, half of the energy of the signal is pushed up to higher frequencies and half is shifted down toward DC. To maintain the correct scale, the signal had to be also amplified by the factor of two. Next, the signal was decimated (by factor of 16) to reduce sampling frequency, and low-pass filtered to eliminate the higher frequencies (using 20-order finite impulse response (FIR) band-pass filter with normalized cutoff frequencies set at 0.03-0.1). Finally the square root of the signal was taken, to reverse the scaling distortion that resulted from squaring the signal.

Two alternative algorithms were considered as the envelope detectors; one using the Hilbert transform and one using digital image processing. The method using Hilbert transform recreated the actual signal's envelope well, but the magnitude did not match the actual signal (Figure 5.29b). The image processing approach, did match the magnitude well, but it was difficult to find the optimal number of the

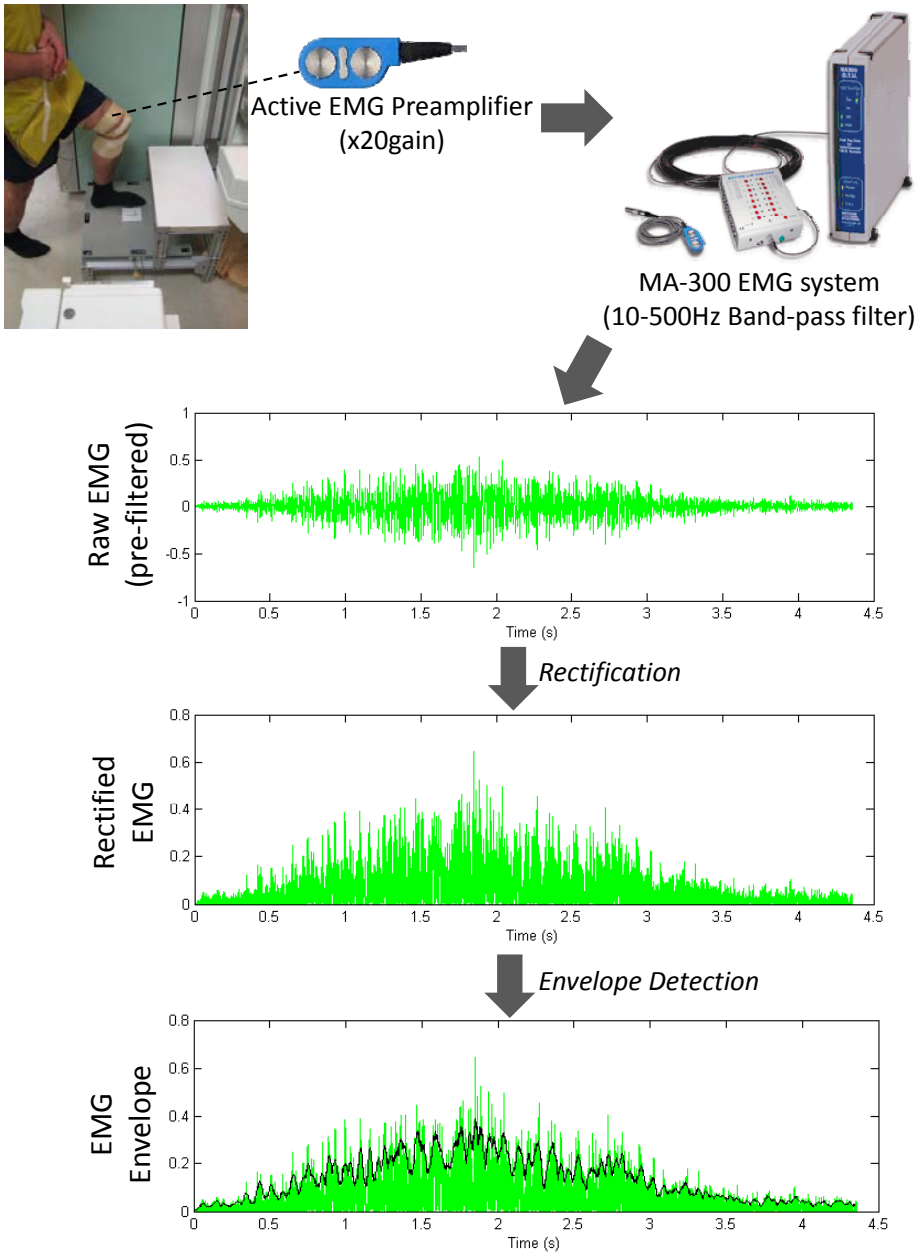
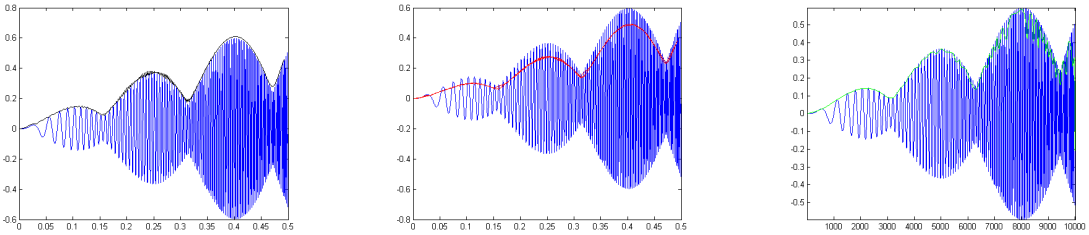


Figure 5.28: The EMG signals were recorded using the MA-300 surface EMG system. The signals were pre-amplified and band-pass filtered prior to the analog to digital conversion. The raw EMG was rectified to detect the envelope of the signal.



(a) Envelope detection by squaring and LP-filtering.

(b) Envelope detection using Hilbert transform.

(c) Envelope detection using image processing.

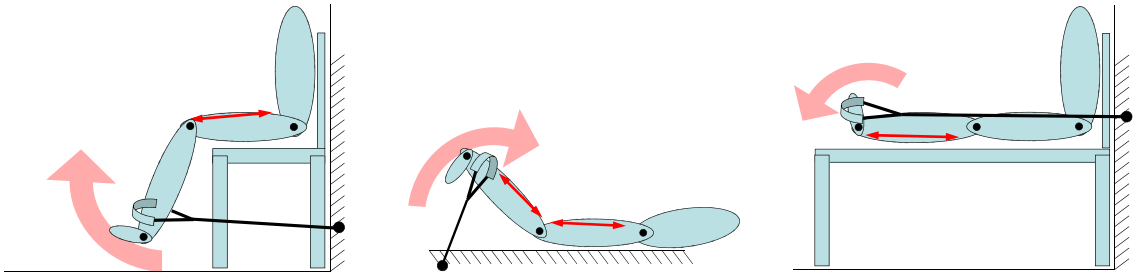
Figure 5.29: Three different approaches were tested to find the optimal envelope detection algorithm.

image regional maxima to be used in the calculation and resulted in more erratic envelope in higher frequency regions (Figure 5.29c). Therefore, the method using squaring and low-pass filtering was chosen as the final envelope detection algorithm. This method also uses a low-order filter, which minimizes the lag of the output.

The neural activation of the muscle is a parameter varying from 0 (no activation) to 1 (muscle fully activated). To find it, the EMG envelope needs to be normalized. Normalization has a significant effect on the inter- and intra-subject variability and different normalization techniques such as isometric maximum voluntary contraction (MVC), isokinetic MVC, submaximal voluntary contraction, mean dynamic EMG, peak dynamic EMG activity have been proposed and widely discussed in the literature.[19, 26, 36, 129, 140, 139, 156, 169, 177, 244, 243, 254] The early studies recommended using the peak[140, 254, 129] or mean[254, 244] EMG value obtained during dynamic activity. However, recent studies reported that the these methods did not yield consistent and reliable results, and have widely recommended the maximum voluntary contraction as the preferred method providing the highest measurement reliability and minimum inter- and intra-subject variability.[26, 19, 36, 139] In fact, this method has been recommended as the standard by ISEK[175] and by other guidelines for the use of surface EMG.[218]

The MVC is the most reliable method for normalizing the EMG data, but the maximum force that the muscle can generate depends on the length and velocity

of the muscle,[256] therefore the MVC depends on the position and kinematics of the musculoskeletal system. To eliminate the velocity variable, the limb is usually restricted from motion, and isometric MVC is performed. Mirka studied the trunk muscles and found that the normalization with respect to MVC yields widely different results depending at which trunk flexion angle the MVC was recorded.[177] Nieminen et al. studied the influence of the position of the arm on the neck muscles EMG normalization by MVC and recommended the middle of the range of motion as the preferred position for the MVC.[189] Therefore, in the current study a custom made setup was developed to record the isometric MVC of the knee flexor and extensor muscle groups at the middle of the range of motion (Figure 5.30).



(a) Quadriceps group MVC. **(b)** Hammstring group MVC. **(c)** Gastrocnemii MVC.

Figure 5.30: Three different position and constraints were used to find the ***isometric maximum voluntary contraction*** of every muscle group. Every maximum contraction was sustained for three seconds and repeated three times allowing the subjects rest for at least two minutes between trials.

To ensure that the true MVC was recorded, the subjects repeated the procedure three times for every muscle group, resting for minimum of 2 minutes between the trials. The maximum of the peak EMG envelopes of the three trials was used for normalization (Figure 5.31). The normalized EMG envelope represents the neural activation ($u(t)$) of the muscle.[256] Due to limited number of the channels available for the EMG signal recording, the activity of the gastrocnemius lateralis and vastus intermedius could not be collected. However, the gastrocnemius lateralis is located next to the gastrocnemius medialis, and both perform very similar biomechanical

function, therefore it has been assumed that these two muscles had the same activation pattern. The vastus intermedius is located under the rectus femoris and its activity cannot be measured using the surface EMG. However, since the bellies of both of these muscles are located below the EMG electrode, and since they have very similar function and line of action, it was assumed that the signal collected for the rectus femoris is also representative of the activation of the vastus intermedius.

A number of experimental studies examined the relationship between the EMG signals, neural activation and muscle activation.[88, 89, 111, 245] Based on these studies a differential equation relating the neural activation $u(t)$ to muscle activation $a(t)$ has been established:[256]

$$\frac{da(t)}{dt} + \left[\frac{1}{\tau_{act}} \cdot (\beta + [1-\beta]\, u(t))\right] \cdot a(t) = \left(\frac{1}{\tau_{act}}\right) \cdot u(t), \tag{5.9}$$

where, τ_{act} is the time constant for buildup in fully activated muscle (i.e. when $u(t) = 1$), β is the parameter relating the time constant for buildup (τ_{act}) to the time constant for relaxation (τ_{deact}), when the muscle is fully deactivated (i.e. when $u(t) = 0$) and $0 < \beta = const. < 1$.

This equation, models the response of the muscle to the neural activation that it receives, depending on the level of excitation. This response can be explained more simply, when two extreme cases are considered. First, if there is no neural activation ($u(t) = 0$), the equation 5.9 becomes:

$$\frac{da(t)}{dt} = -\frac{\beta}{\tau_{act}} a(t) \tag{5.10}$$

which has a simple solution of:

$$a(t) = e^{\frac{-\beta}{\tau_{act}} t}. \tag{5.11}$$

In the second case, when the muscle is fully activated ($u(t) = 1$), the equation 5.9 becomes:

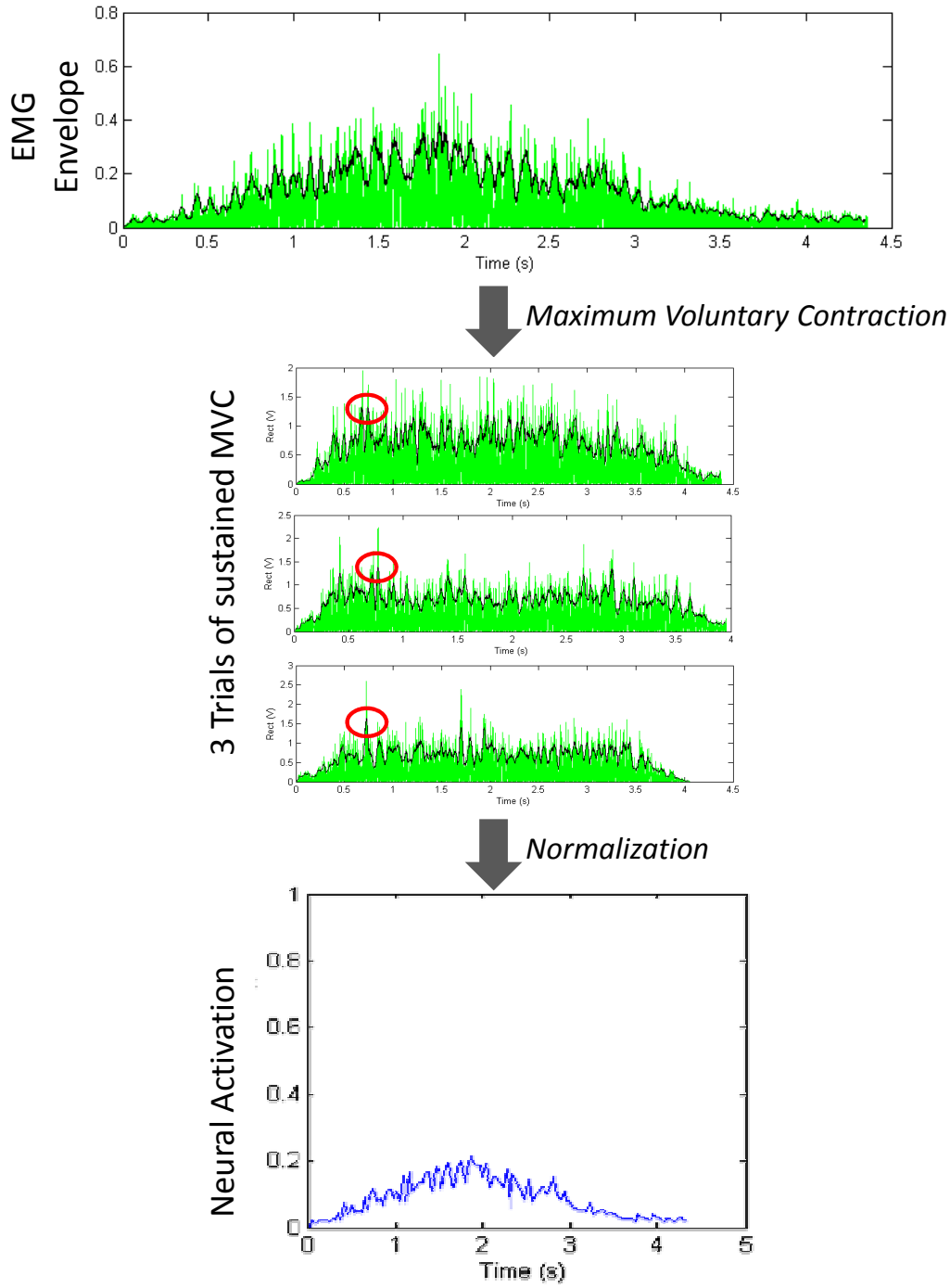


Figure 5.31: The MVC peak value was used to normalize the envelope of the processed EMG signal. The normalized EMG signal varying from 0 to 1 represents the *Neural Activation*[256] of the muscle.

$$\frac{da(t)}{dt} = -\frac{1}{\tau_{act}}a(t) + \frac{1}{\tau_{act}} \tag{5.12}$$

which can be rewritten as ($a(t) = y$):

$$\begin{gathered}
\frac{dy}{dt} = -\frac{1}{\tau_{act}}y + \frac{1}{\tau_{act}} \\
\frac{dy}{-\frac{1}{\tau_{act}}y + \frac{1}{\tau_{act}}} = dt \\
\int \frac{dy}{-\frac{1}{\tau_{act}}y + \frac{1}{\tau_{act}}} = \int dt
\end{gathered}$$

and noting that: $\int \frac{c}{ay+b}dy = \frac{c}{a}\ln|ax+b|$, we find that:

$$\begin{gathered}
-\tau_{act}\ln\left(-\frac{1}{\tau_{act}}y + \frac{1}{\tau_{act}}\right) = t + C \\
\ln\left(-\frac{1}{\tau_{act}}y + \frac{1}{\tau_{act}}\right) = -\frac{1}{\tau_{act}}(t + C) \\
-\frac{1}{\tau_{act}}y + \frac{1}{\tau_{act}} = e^{-\frac{1}{\tau_{act}}t - \frac{1}{\tau_{act}}C}
\end{gathered}$$

considering $y(0) = 0$, the constant $c = -\tau_{act}\ln(\frac{1}{\tau_{act}})$, we finally get:

$$y = a(t) = -\tau_{act}e^{-\frac{1}{\tau_{act}}t - \ln\frac{1}{\tau_{act}}} + 1. \tag{5.13}$$

Both equations 5.11 and 5.13, represent exponential functions (reflected about the y-axis), the first decreasing to its horizontal asymptote of $x = 0$, and the second increasing to the asymptote $x = 1$. Apart from the constants, the functions differ only by their time constants, which are related by the parameter β. Now, the relationship between τ_{deact} and τ_{act} is easy to note:

$$\frac{1}{\tau_{deact}} = \frac{\beta}{\tau_{act}}, \tag{5.14}$$

and since $\beta = const. \in (0, 1)$

$$\frac{1}{\tau_{deact}} < \frac{1}{\tau_{act}}, \tag{5.15}$$

which means that the force builds up faster during activation, than it falls during relaxation, what is a well documented phenomenon.[89, 107]

The time constant depends on the electromechanical delay between receiving the action potential by the muscle fibers and their response to begin the contraction. Experimental studies determined that this delay depends on the type of contraction, muscle fiber length, shortening velocity and stimulus frequency,[32] whether the contraction is concentric or eccentric.[191] This delay for human skeletal muscles typically varies between 30-100 ms. Cavanagh and Komi studied human skeletal muscles and found the average electromechanical delay to be 49.5 ms for eccentric and 55.5 ms for concentric contraction.[40] Brown and Loeb found that both the muscle force rise and fall offsets depend on fascicle length and stimulus frequency, and vary between 20-30 ms for rise and 20-50 ms for fall.[32] Their data confirms that the force rises faster than it falls, and the parameter β can be estimated to be in the range of 0.6-1. The muscle activation as the response to the neural activation for an example subject climbing up the stairs is shown in Figure 5.32.

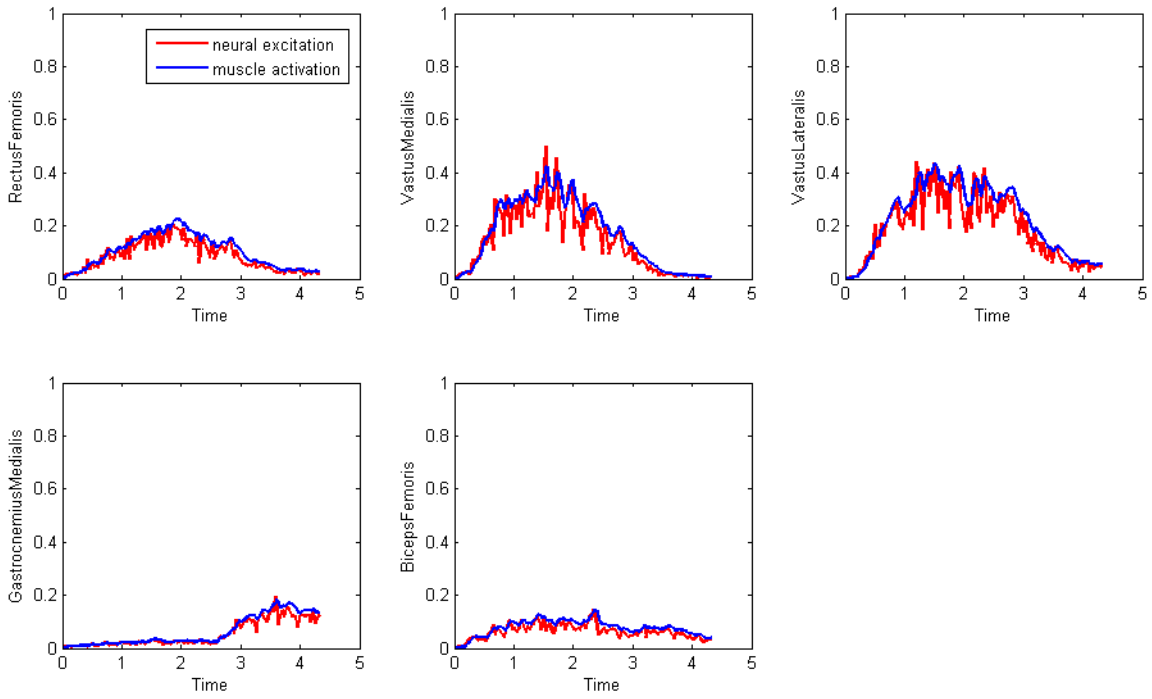


Figure 5.32: The relationship between the muscle and neural activation is governed by the *muscle activation dynamics* equation[256] derived based on experimental work done by Hill.[106, 107]

Once the muscle is excited, the biochemical processes (cross-bridge cycle) begin during which actin interacts with myosin and adenosine triphosphate (ATP) to produce force, adenosine diphosphate (ADP) and inorganic phosphate.[120, 121, 105, 30, 240] The magnitude of the contraction force depends on the level of muscle activation ($a(t)$), length of the muscle fibers ($l^M(t)$), velocity of muscle stretch or contraction ($v^M(t)$) and of the maximum isometric active muscle force (F_0^M):

$$F^M(t) = a(t)f(l^M)f(v^M)F_0^M \tag{5.16}$$

The pioneering experiments performed by Hill[106] revealed the effects of shortening speed on the muscle force. He studied the energy dissipation, by heat expenditure of muscle fibers during contraction under tetanic stimulus. The results revealed that the isotonic muscle tension (P) is inversely proportional to shortening speed(v) and Hill described it as:

$$(P + a)v = b(P_0 - P), \tag{5.17}$$

where a is a constant having the same dimension as the force (in grams weight), b is a constant defining the absolute rate of energy liberation, P_0 is the isometric tetanic muscle tension. This relationship may be rewritten as:

$$(P + a)(v + b) = (Po + a)b = const., \tag{5.18}$$

which shows that this relationship is constant at a given temperature and is modeled by a rectangular hyperbola having the asymptotes at $P = -a$ and $v = -b$.

Bigland and Lippold[22] further explored the relationship between shortening speed on muscle force at different activation levels. Hill also studied the differences between concentric and eccentric contraction, which were further scrutinized by Komi.[141]. These and many other experimental research studies brought a tremendous insight into the understanding of the muscle contraction dynamics, which

was summarized by Zajac,[256] and the force-velocity relationship described in his review was adopted in this work (Figure 5.33).

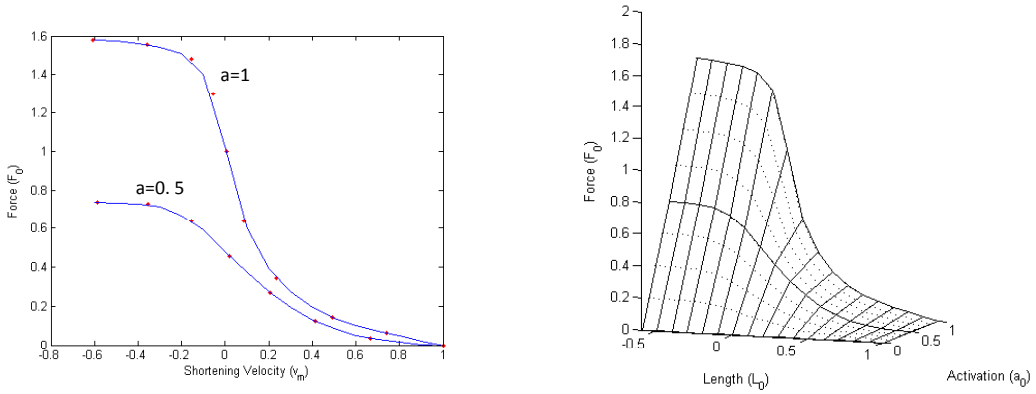


Figure 5.33: Muscle contraction force depends on the shortening ($v > 0$) or stretching ($v < 0$) velocity of the muscle fibers. If the muscle shortens faster than its maximum contraction velocity (v_m), the crossbridge interactions do not have enough time to form and the muscle cannot develop tension. On the other hand if the muscle contracts eccentrically, it can develop forces larger than the peak isometric active muscle force (F_0^M). Abrupt stretch exceeding $v_m < -0.6$ may result in muscle injury.

Experimental research also revealed that the muscle tension depends on the length of the muscle fibers.[200] The largest force can be generated when the muscle is at its optimal length, but it drops whenever the muscle fibers are shortened or extended beyond their optimal length.[256] Recent studies found that the optimal muscle fiber length is not constant, but increases with decreasing activation level.[95, 119] Apart from the active force, there is also a passive force component resulting from the myofibrillar elasticity of the muscles. This force develops when the muscle fibers are stretched above their optimal length. These coupled effects result in the force-length relationship as shown in Figure 5.34, adapted from Lloyd and Besier.[160]

Combining the force-length and the force-velocity relationships, the rise of the active muscle force can be described as a function of increasing muscle activation (Figure 5.35). It is worth noting that even if the muscle is maximally excited, the muscle will be unable to develop any tension if the fibers are shorter than 0.4 of their optimal length, or are contracting faster than the maximal shortening

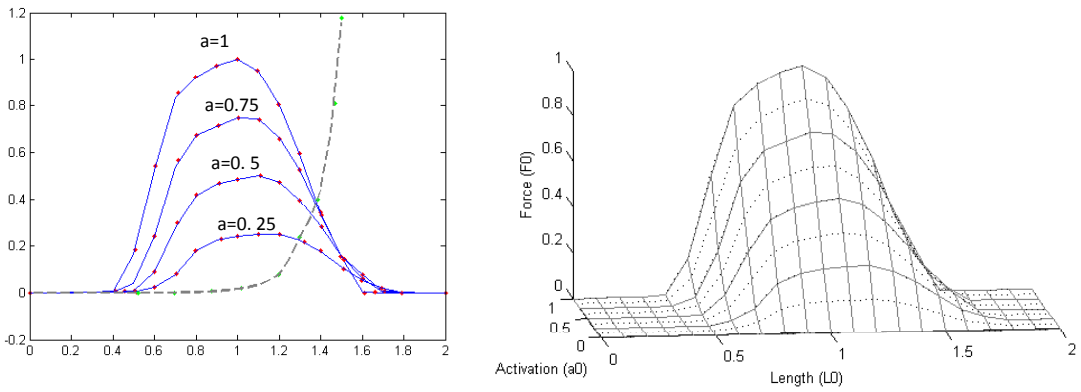


Figure 5.34: Muscle contraction force depends on the length of the muscle fibers. The maximum force can be developed by the muscle at its optimal length, but there are also critical muscle lengths below and above which the crossbridge interactions cannot be formed and the muscle is unable to produce any force.

speed. In the current work, the muscle lengths were calculated based on the in-vivo kinematics, patient-specific muscle attachment point locations, and taking into account the wrapping around the rigid bones (see Sec. 5.3.1). The muscle shortening speed was calculated by taking the discrete derivative of the muscle length.

The last parameter, that is left to calculate the muscle force is the peak isometric muscle force (F_0^M). This maximum force can be calculated as:

$$F_0^M = \sigma^M A^M, \tag{5.19}$$

where σ^M is the maximum muscle fiber stress, and A^M is the physiological cross-sectional area (PCSA). The maximum muscle stress varies between fast- and slow-twitching muscle fibers,[49, 197] but for mixed type muscles (as those investigated in the current study) the value of $35N/cm^2$ ($350kPa$) has been recommended as a good approximation.[256] The PCSA, can be calculated based on the muscle volume:

$$PCSA = \frac{V^M}{l_f} cos(\alpha), \tag{5.20}$$

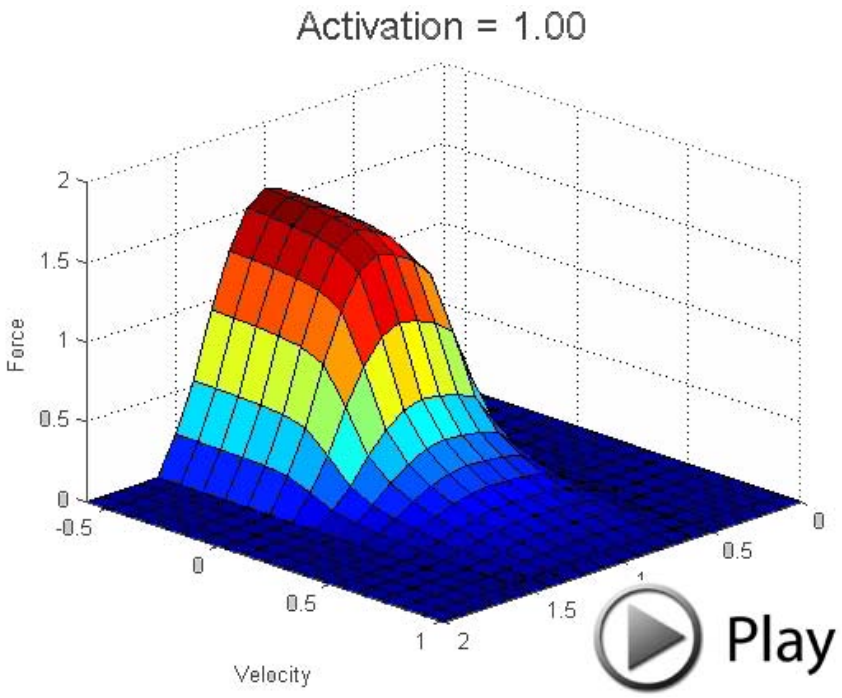


Figure 5.35: The active muscle force increases with increasing activation ($a(t)$), but this relationship is complex and depends also on the muscle fiber length ($l(t)$) and muscle fiber shortening speed ($v(t)$).

where V^M is the volume of a muscle, l_f is the muscle fiber length, and α is the pennation angle. The muscle volume varies significantly between muscles as well as individuals. To account for these differences the muscle CAD models were recreated based on the CT scan images (Figure 5.24) and their volume was measured. Since the CT images were taken only for the section of the knee joint 7 inches below and above the joint line, the entire muscle models could not be reconstructed. However, the distribution of the muscle tissue was studied experimentally and is available in the literature.[170, 188, 187] Fukunaga et al.[76] used Magnetic Resonance Imaging (MRI) to measure the volume of the calf muscles for 12 healthy individuals. The muscle volume distribution reported by them was used to extrapolate the entire volume of the gastrocnemius medialis and lateralis based on the proximal part of these muscles available in the current study. Similar approach was used by Narici et al.[187] to reconstruct the volume of the quadriceps muscle group and the cross sectional area

distribution reported by them was used to find the volume of the vastus lateralis, vastus intermedius, vastus medialis and rectus femoris. The MRI was also used by Mathur et al.[170] to find the cross sectional area and volume of thigh muscles. However, their measurements were taken only at three levels of the thigh, offering less detailed distribution information than the data presented by Narici et al. Therefore their data was used to extrapolate only the volume of the biceps femoris, which was not included in the study performed by Narici et al.

The muscle fiber length and pennation angle vary among the muscles, but do not vary significantly among individuals. Recent study by Ward et al.[236] investigated the lower extremity muscle architecture of 27 muscles dissected from 21 cadavers. The average values of muscle length and pennation angle reported by them were used in the current work.

To sum up briefly, the muscle force is a function of a number of parameters. It is different for every muscle and varies with time, depending on neural activation, muscle activation dynamics, muscle contraction dynamics, muscle length, muscle shortening speed, physiological cross-sectional area, maximum muscle fiber stress, ratio between fast and slow twitching fibers, pennation angle and a number of other processes dictated by the central nervous system, which await better understanding. Detecting the EMG signals itself is a process fraught with problems, and calculating muscle force during dynamic exercises is not possible to do with precision.[53] The EMG to force relationship is far from being trivial and the muscle force magnitude can be only approximated with current technology. The up-to-date knowledge and the widely accepted mathematical models were applied in the current work to estimate the forces based on the in-vivo EMG signals, taking into account as many patient-specific parameters as possible. The raw EMG signals were filtered and rectified to find the envelope of the signals. Next, the neural activation was found by normalizing the processed EMG data by the peak values obtained during the MVC. The muscle activation dynamics was employed to convert the neural activation to the muscle activation. The time constants for each muscle were found in the literature. Then,

muscle contraction dynamics model made it possible to calculate the muscle forces. The magnitudes of both active and passive muscle force depend on the muscle length, which was calculated based on in-vivo kinematics, taking into account the wrapping of the soft tissues around the bones (see Sec 5.3.1). The active muscle force development also depends on the shortening velocity, which was also calculated for every participant. Also, the PCSA was determined for each muscle for every subject. Therefore, although the resulting muscle force magnitude is still an estimate, it is the best patient-specific estimate that could be found based on the current knowledge and data available in the current study.

5.4 Pattern Classification of the Vibroarthrography Signals

The current study is an attempt to find new tools for improved diagnosis of the patellofemoral disorders. The kinematics analysis may reveal the pathologies related to abnormal motion of the patella, such as subluxation, and also abnormal motion of the tibiofemoral joint, which may have an impact on the quadriceps mechanism moment arm lengths (see Sec. 4). Kinetics analysis may give further insight by predicting whether the forces are within the range observed in healthy individuals or if the abnormal kinematics results in excessive loading conditions which may exceed the articular cartilage strength. Furthermore, even if the forces are within their natural range, the EMG data may reveal whether the forces are distributed optimally between the muscles, or if there is present an abnormal pull towards one side. An abnormal kinetic profile may indicate a defensive strategy employed by the central nervous system as a respond to the pain present in the knee joint. The pain frequently appears if there is loss of articular cartilage, and therefore the vibroartrography has been evaluated in this work for its potential use as another source of data that can be

collected non-invasively, under in-vivo conditions and used to possibly enhance the accuracy of the diagnosis of patellofemoral disorders.

During a dynamic activity, the interaction between the moving articulating surfaces induces vibrations of the bones. In a healthy joint the articulating surfaces are smooth and the vibration is minimal, but as the cartilage degenerates, the articular surfaces become more rough and vibrations increase, and may become audible in extreme cases. Loss of cartilage is a natural process of aging[25] but may not necessarily be severe enough to cause pain. However, if the cartilage deteriorates due to arthritis, its loss is accelerated and most often causes unbearable pain limiting the patient's mobility. In case of a complete loss of articular cartilage, the raw bone surfaces rub against each other and it has been hypothesized that they will produce a distinct vibration pattern. In this dissertation, it has been proposed to use accelerometers and perform a feasibility study to determine if vibrations can be detected by surface sensor under in-vivo conditions and whether the signal quality is sufficient for pattern classification purposes that may be used as future diagnostic tools.

The vibration data was collected for total of 23 subjects having healthy knees (and intact articular cartilage), and additional 52 patients suffering from knee arthritis. These patients were recruited from a group of candidates for the primary Total Knee Replacement (TKR) procedure. During the TKA surgery, after opening the joint capsule, the surgeon examined the condition of the articular cartilage and filled out an intrasurgical evaluation sheet (Figure 5.36). This assessment provided an insight into the exact condition of the cartilage and the amount of damage at every compartment of the knee joint, as well as any other factors possibly altering the vibration pattern, such as any ligament deficiency or meniscal injuries. This information was crucial for the assessment of the actual condition of the knee joint.

The vibration of the patellofemoral articulation were detected using two miniature, 3-axial accelerometers (Model 356A12, 100 mV/g, 50 g, 0.5 to 5k Hz, PCB Piezotronics Inc., Depew, NY) attached to the surface of the skin at the middle of the

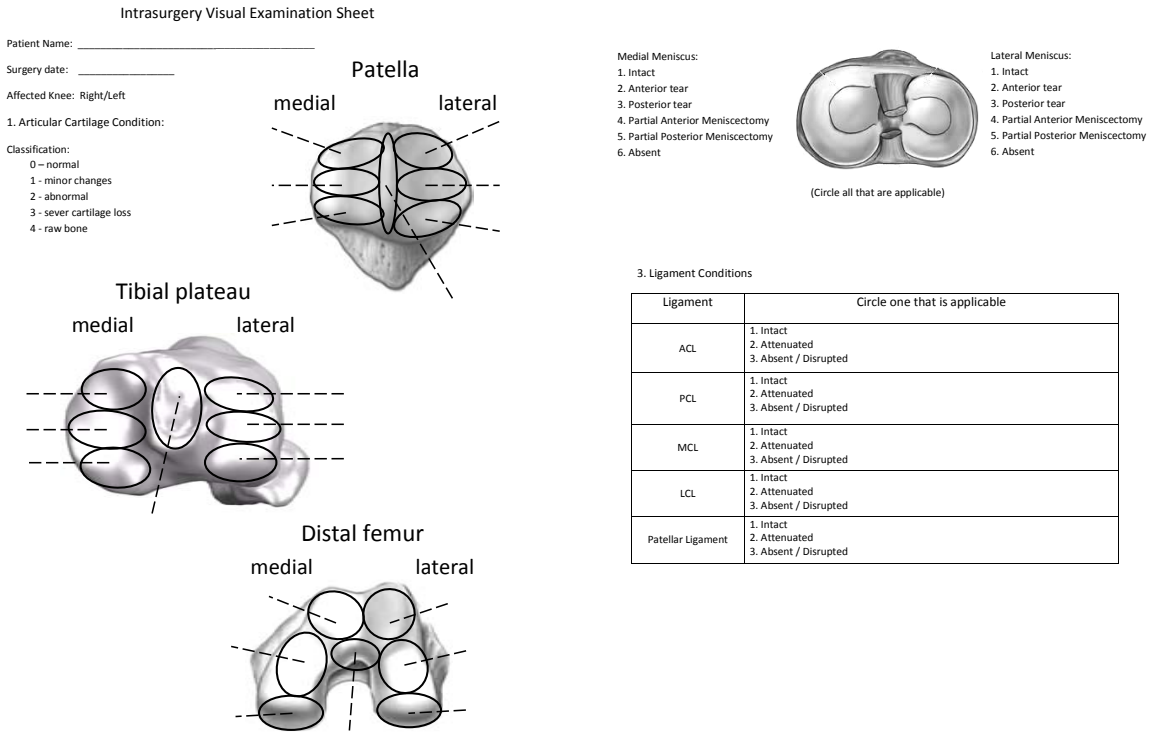


Figure 5.36: The intrasurgical evaluation sheet was filled out by the surgeon during the TKA procedure to provide the information about the location and severity of the articular cartilage damage. Other factors that might affect the vibration outcome, such as ligament deficiency or meniscus injuries were also examined and described.

patella and medial femoral epicondyle by means of elastic wrap and hypoallergenic adhesive tape (Figure 5.37). The signal conditioner (Model 583A, PCB Piezotronics Inc., Depew, NY) was used to increase the magnitude of the vibration signal by the factor of ten and to low-pass filter the data at cut-off frequency of 4700Hz prior to analog-to-digital conversion (Model DI-720, DATAQ Instruments Inc., Akron, OH).

The accelerometers record the change in acceleration resulting from both the movement of the joint as well as from the vibration of the bones. Therefore the raw accelerometer signals had to be decomposed into the motion and vibration component. This was achieved by high-pass filtering the acceleration signal using Butterworth infinite impulse response (IIR) filter attenuating the signal by 80 dB at the cut-off frequency of 20 Hz. This eliminated the low frequency, motion components of

the signals and yielded a vibroarthrogram suitable for further analysis (Figure 5.37, bottom).

The filtered vibroarthrogram can be also converted into audible form and synchronized with the fluoroscopy or regular video footage. An example of the patellofemoral vibration pattern and sound correlated with the knee kinematics video for a healthy subject is shown in the Figure 5.38, and for an arthritic patient in the Figure 5.39. Comparison of these two example vibroarthrograms confirms the early observations made by Blodgett[25] and Walters,[235] who could hear more grating and cracking knee joint sounds being emitted by older subjects, most probably resulting from the deterioration of their articular cartilage. Similarly in the current study the sounds emitted by the knee joint with confirmed arthritis is much louder than the sound of the healthy subject's knee.

The early investigators used stethoscope to auscultate the knee joint, but listening to the sounds emitted by the articulation is subjective. Therefore, in the current work more objective, numerical methods based on the digital signature of the vibration, such as pattern recognition were used.[62, 230] The vibroarthrograms shown in the Figure 5.40, clearly demonstrate differences between healthy and arthritic knee joints. However, during the data collection for the present study, it became evident that the vibration signal pattern can be affected by a number of factors including:

1. severity of degeneration,
2. thickness of the subcutaneous tissue present between the articulating bone and the accelerometer (the soft tissue has a damping effect),
3. location of the accelerometer relative to the underlying bones,
4. type of activity,
5. speed of the activity (faster movements result in higher accelerations),
6. direction in which the acceleration is being measured.

Some of these parameters can be controlled to some extend (e.g. the speed of the activity), some can be optimized (direction and location of the accelerometer's placement). However, the anatomical diversity and various stages of arthritis, which

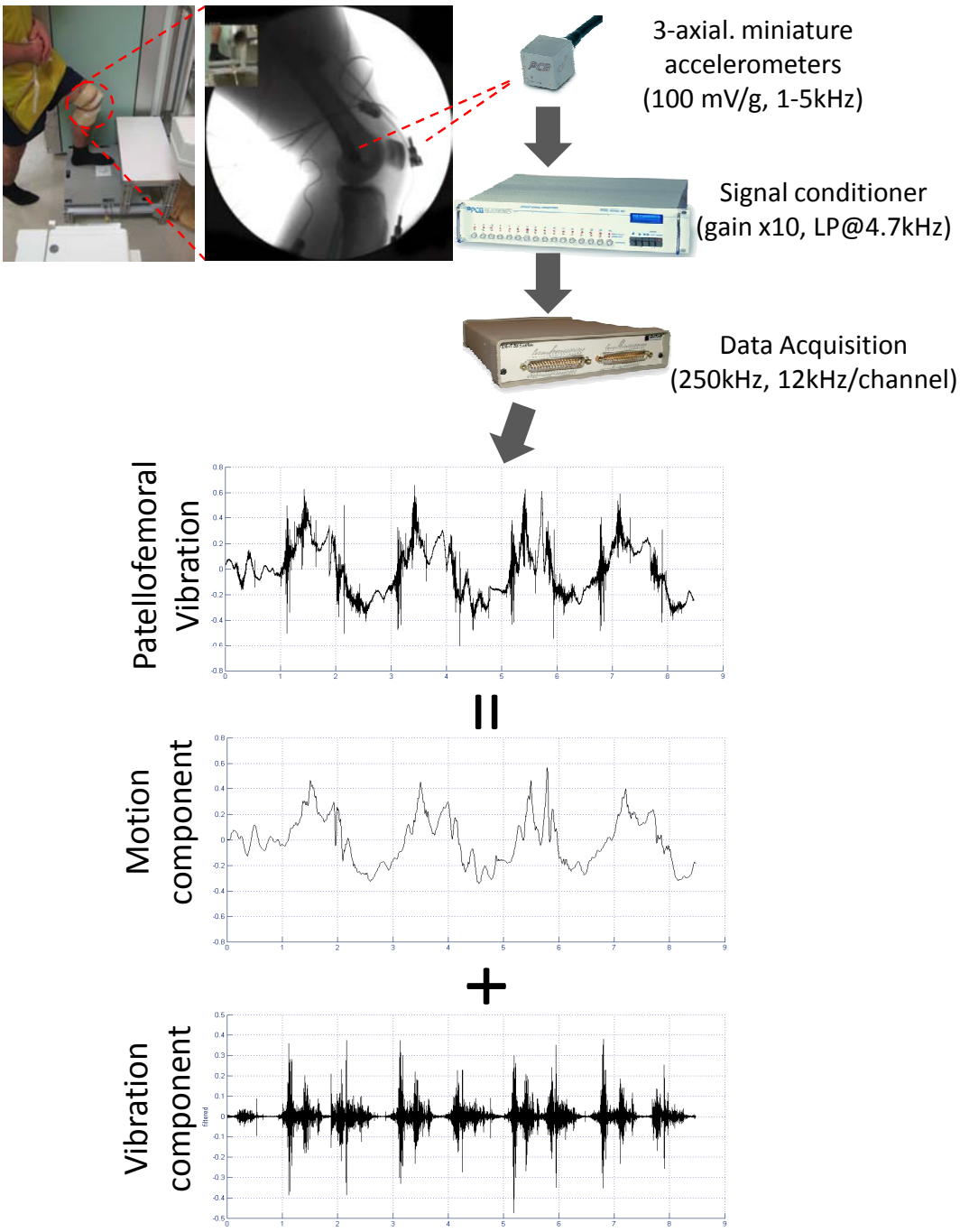


Figure 5.37: Miniature, highly sensitive 3-axial accelerometrs were attached firmly to the skin above the patella and medial femoral condyle to detect the patellofemoral joint vibration. The signals were magnified and low-pass pre-filtered prior to analog-to-digital conversion. Next the raw vibroarthrogram was decomposed into motion and vibration components for further analysis.

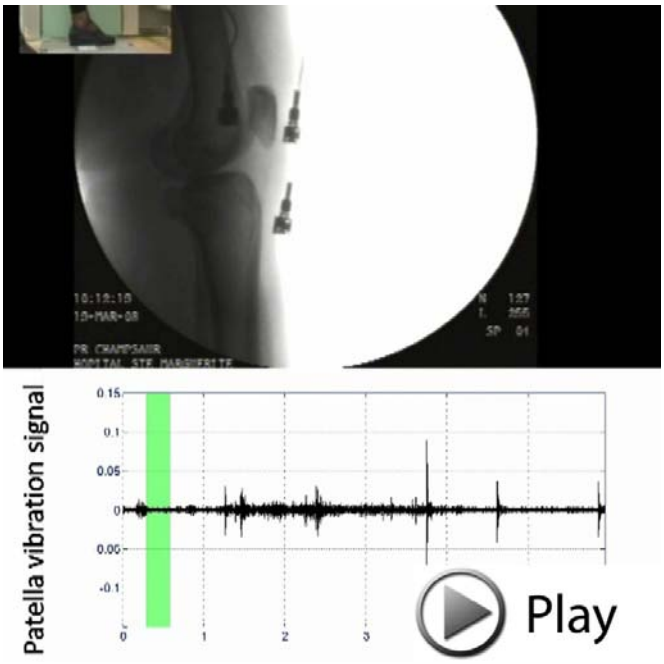


Figure 5.38: An example of patellofemoral vibroarthrogram typically revealed by a healthy knee joint correlated with fluoroscopic video.

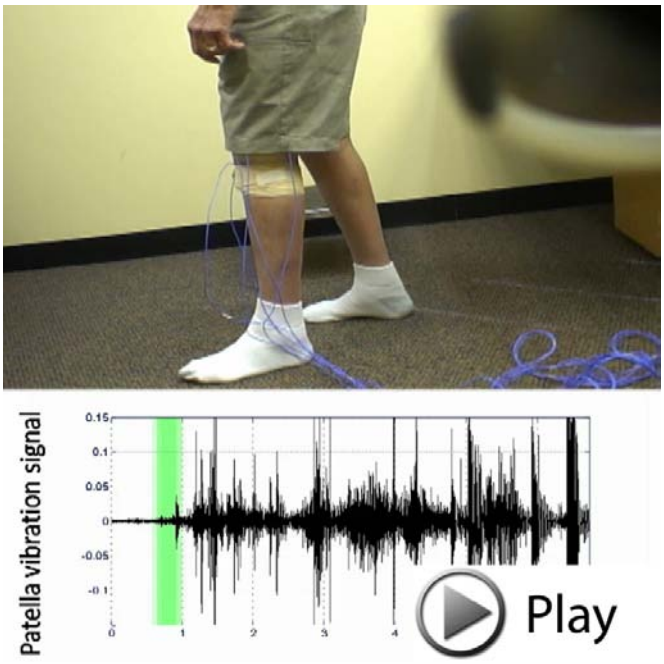
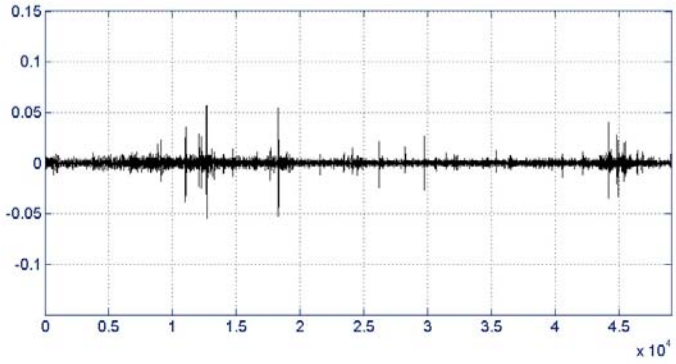
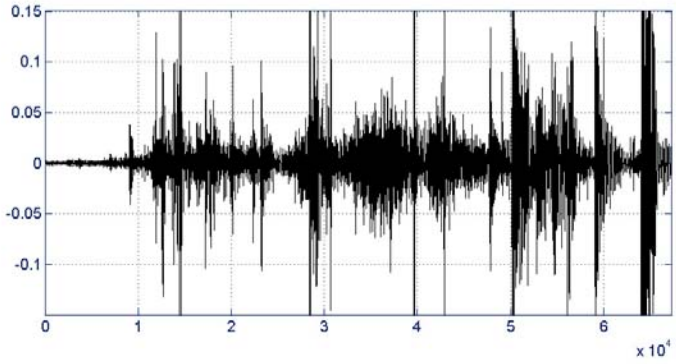


Figure 5.39: An example of patellofemoral vibroarthrogram typically revealed by an arthritic knee joint correlated with regular video.

contribute greatly to the variability observed between the vibration patterns, remain beyond the investigator's influence. Moreover, the magnitude of the vibration emitted by the articulating surfaces is often low, and so is the signal to noise ratio, which make development of a robust pattern classification algorithm a challenging task.



(a) Example vibroathrogram of a healthy patellofemoral joint.



(b) Example vibroathrogram of an arthritic patellofemoral joint.

Figure 5.40: Comparison between a vibroarthrogram obtained for a healthy subject and patient diagnosed with patellofemoral joint arthritis.

Several statistical parameters of the original and rectified vibroarthrograms were calculated to examine features that could be used to form the feature vector of the signals (Figure 6.19). Based on the observations reported by Blodgett[25] and Walters[235] the magnitude of the vibration can be expected to be higher for the degenerated knees. Therefore, the mean of the rectified vibroarthrograms and standard deviation were selected as good candidate features for building a classifier.

Other desirable features are these, which provide the greatest separation between the samples of the two classes (healthy from arthritic), as these will yield the highest success rate of the classification. Other statistical selected for analysis included:

- Skewness,
- Kurtosis,
- Median,
- 90^{th} quantile,
- 95^{th} quantile,
- 97.5^{th} quantile,
- 99^{th} quantile,
- Signal Envelope integral,
- Product of Signal Envelope integral and activity duration.

Chapter 6

Results

6.1 Kinematic analysis

6.1.1 Patellofemoral tracking

The center of the patella tracked with respect to the femur was mapped on the unfolded articulating surface (Figure 6.1). In order to make inter-subject comparisons the unfolded surfaces were normalized with respect to the articulating portion height and width (note that the dimensions vary between -1 and 1 for both dimensions).

The results revealed that the center of the patella tracked in a very uniform fashion for the Total Knee Arthroplasty (TKA) group, starting close to the anterior edge of the intercondylar fossa of the femoral component (near the $(0, 0)$ coordinate in Figure 6.1). As the knee extended during the stair climbing activity, the patella center tracked in the superior direction approximately a quarter of height of the unfolded surface and shifted slightly in the lateral direction. These results were noticeably consistent among the TKA subjects and the patella tracked nearly in a straight line.

The center of the natural patella also tracked from inferior to superior, and slightly in the lateral direction with the extension of the knee. However, the motion occurred about quarter of the height of the unfolded surface more superiorly, compared to the

TKA subjects. Also the results in both contralateral and healthy groups were more variable than in the TKA group.

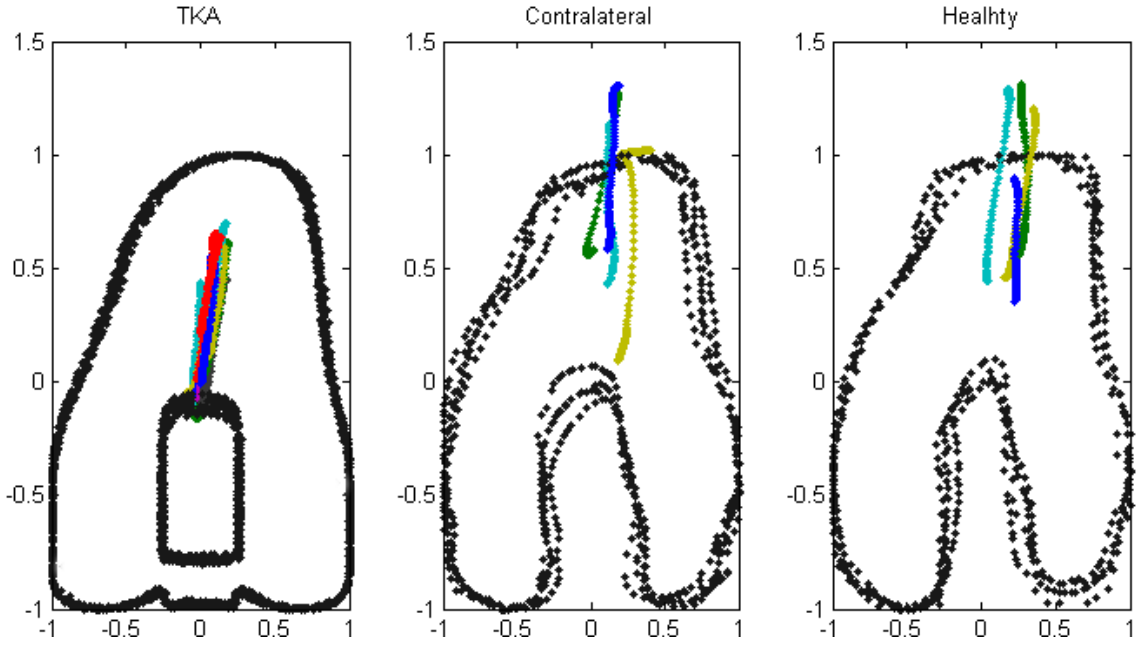


Figure 6.1: Tracking of the center of the patella with respect to femur mapped on the unfolded articulating surface of the femoral component (for replaced knees) or distal femur (for natural knees).

6.1.2 Tibiofemoral rotations

The tibiofemoral flexion pattern was very consistent among the healthy subjects with the majority of the extension occurring in the middle of the activity (Figure 6.2). A similar pattern, but more variable, was observed in both the contralateral and the TKA groups. This variability was due to different strategies employed by different individuals to perform the task. Some of the subjects took more time at the beginning of the activity to place the foot securely on the stair, while some started the extension immediately after foot contact and took more time to lift the foot after they already climbed the stair (compare Patients #15T vs 12T in the Attachment A).

The differences in the stair climbing fashion (mainly in the knee extension) revealed that the average patterns cannot be calculated while the data is calculated

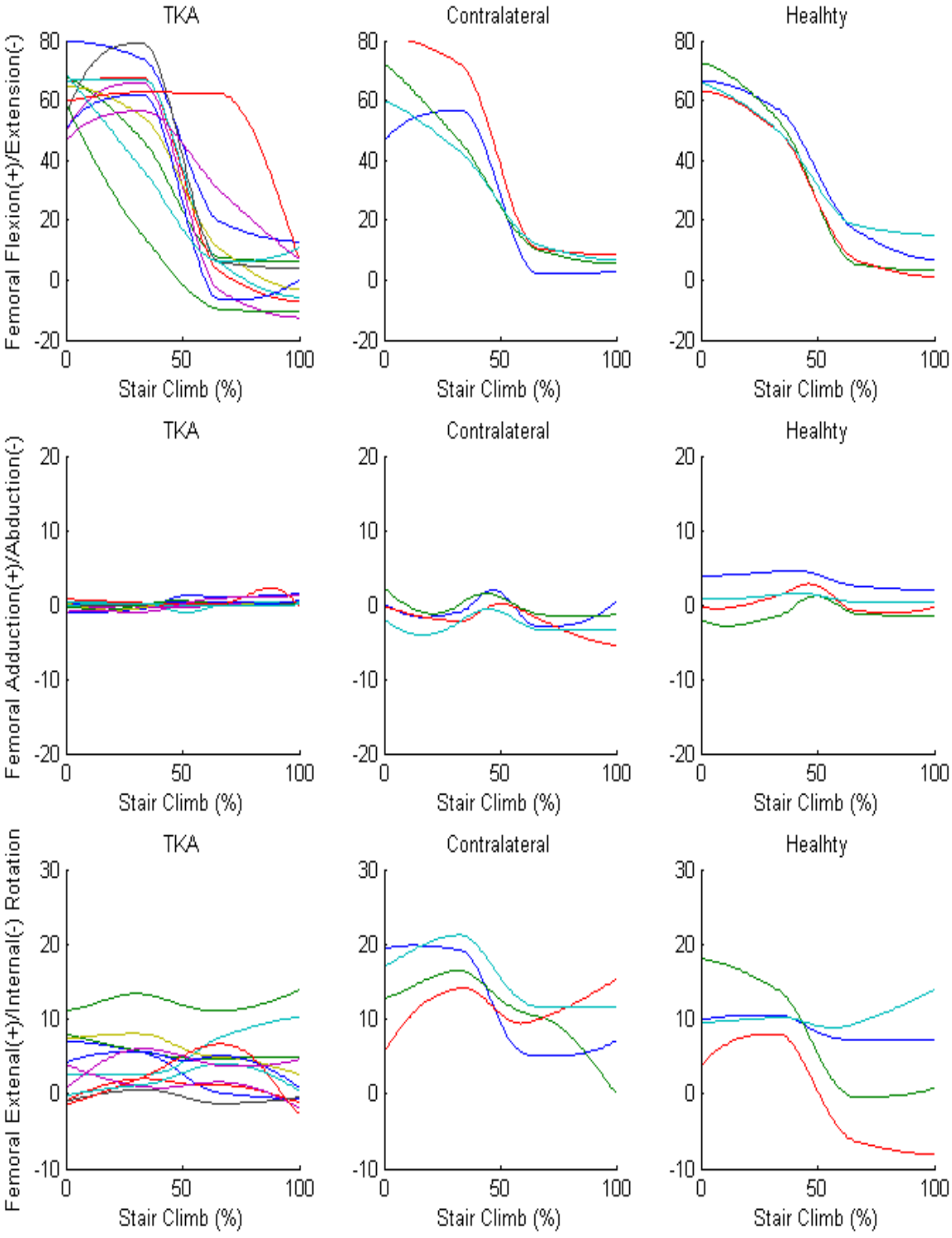


Figure 6.2: Tibiofemoral joint rotations plotted against the percentage of the stair climbing for all subjects from the three groups.

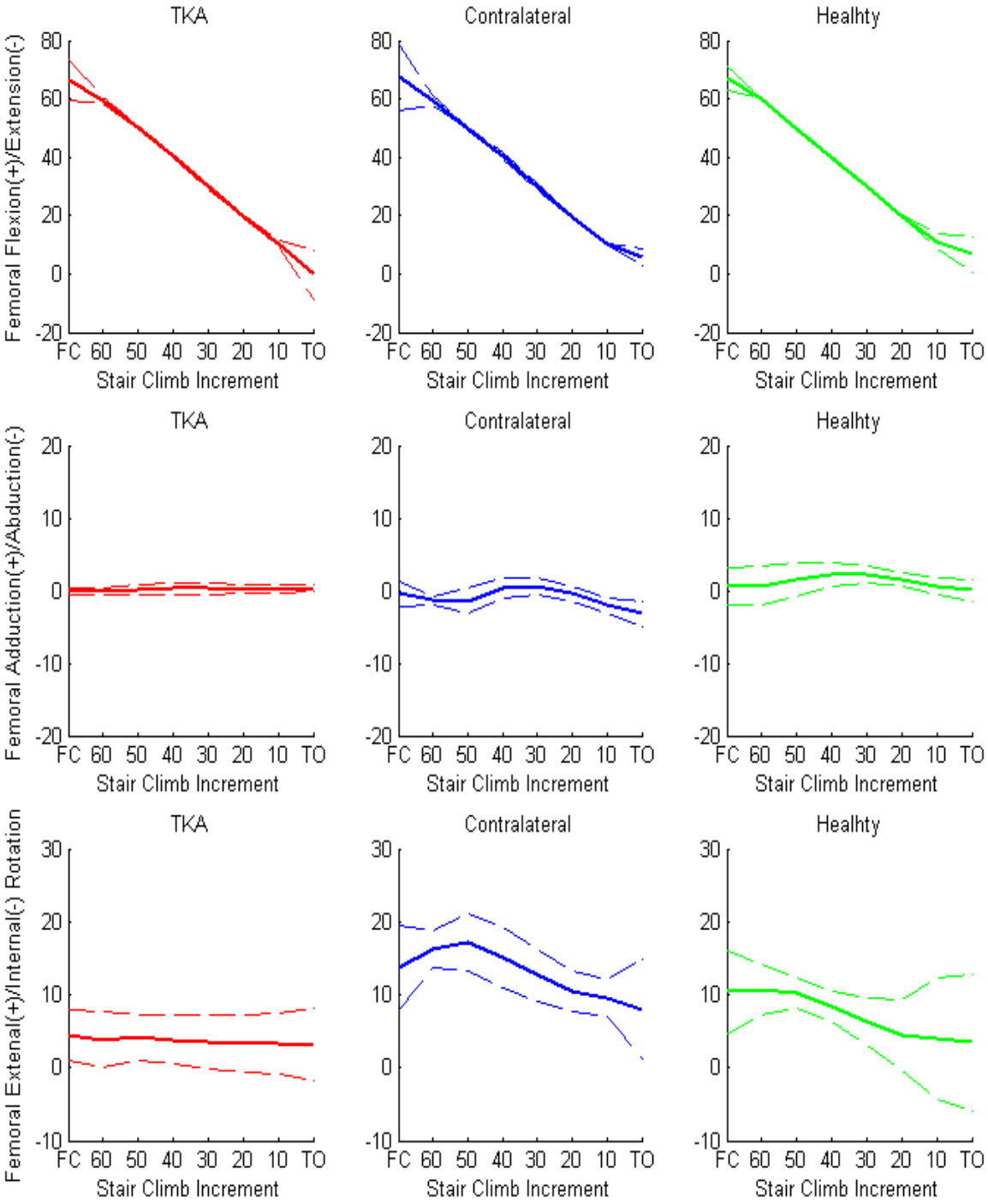


Figure 6.3: Tibiofemoral joint rotations arranged with respect to standardized activity increments/knee flexion for all three groups of subjects (dashed lines mark ±SD). **FC**-*Foot Contact*, **TO**-*Toe Off*.

Table 6.1: Tibiofemoral joint rotations for all three groups of subjects.

		TKA		Contralateral		Healthy	
		avg (deg)	*SD (deg)*	**avg** (deg)	*SD (deg)*	**avg** (deg)	*SD (deg)*
Femoral Flexion(+) / Extension(-)	FC	**61.4**	*9.2*	**65.0**	*14.7*	**66.8**	*4.0*
	60	**59.6**	*1.3*	**59.3**	*1.8*	**60.1**	*0.1*
	40	**40.4**	*0.7*	**40.4**	*0.9*	**40.0**	*0.5*
	20	**19.8**	*0.4*	**19.5**	*0.4*	**19.8**	*0.3*
	TO	**-0.2**	*8.3*	**5.7**	*2.7*	**6.6**	*6.1*
	min	**-0.2**	*8.3*	**5.7**	*2.7*	**6.6**	*6.1*
	max	**66.5**	*7.1*	**67.4**	*11.2*	**66.8**	*4.0*
	abs. range	**66.7**	*8.3*	**61.6**	*9.5*	**60.2**	*7.8*
Femoral Adduction(+) / Abduction(-)	FC	**-0.11**	*0.51*	**-0.14**	*1.69*	**0.55**	*2.50*
	60	**-0.06**	*0.50*	**-1.33**	*0.58*	**0.68**	*2.70*
	40	**0.28**	*0.85*	**0.41**	*1.42*	**2.19**	*1.62*
	20	**0.23**	*0.63*	**-0.36**	*1.05*	**1.48**	*1.00*
	TO	**0.31**	*0.54*	**-3.25**	*1.71*	**0.11**	*1.51*
	min	**-0.53**	*0.38*	**-3.51**	*1.64*	**-0.43**	*2.05*
	max	**0.69**	*0.64*	**0.84**	*1.30*	**2.52**	*1.54*
	abs. range	**1.22**	*0.84*	**4.34**	*1.03*	**2.96**	*1.29*
Femoral Extenal(+) / Internal(-) Rotation	FC	**3.5**	*4.2*	**13.8**	*5.9*	**10.4**	*5.7*
	60	**3.8**	*3.7*	**16.2**	*2.6*	**10.7**	*3.4*
	40	**3.8**	*3.3*	**15.2**	*4.2*	**8.4**	*2.1*
	20	**3.4**	*3.9*	**10.5**	*2.8*	**4.4**	*4.9*
	TO	**3.2**	*5.0*	**8.0**	*6.8*	**3.5**	*9.4*
	min	**1.2**	*3.8*	**5.7**	*4.8*	**1.9**	*7.7*
	max	**6.3**	*3.6*	**18.2**	*2.8*	**12.6**	*4.3*
	abs. range	**5.1**	*2.3*	**12.5**	*3.7*	**10.7**	*7.6*

with respect to the percentage of the activity. In the extreme cases seen in the the Figure 6.2, taking the average at 60% of the activity would mean taking data at over 60° of flexion for one subject (red line) and at the knee fully extended for a second subject (green line). Therefore, several common instances of the activity have been chosen in order to normalize the data. These instances are: Foot Contact (FC), 60°, 50°, 40°, 30°, 20°, 10° of knee flexion and Toe Off (TO). The data plotted with respect to these instances identified for each individual, revealed that it has been adequately normalized (Figure 6.3).

The average, normalized data demonstrated a similar pattern of femoral rotations for both contralateral and healthy knee groups. The average range of natural knee abduction/adduction was 4.2° and 2.5° for contralateral and healthy knees respectively. Interestingly, for the TKA group this range was very small averaging only 1.1°.

The femoral axial rotation also revealed similarities between the contralateral and healthy knees. As expected for natural knee joint, for both of these groups, the femur rotated internally with decreasing flexion. However, the TKA group experienced significantly reduced pattern, with almost no change in the axial rotation compared to the natural counterparts (Figure 6.3, bottom). The range of axial rotation was 4.5° for the TKA group, compared to the average of 12.3° and 10.5° found for Contralateral and Healthy subjects, respectively (Table 6.1).

6.1.3 Patellofemoral rotations

The patellofemoral kinematics also varied among the subjects (Figure 6.4) and had to be normalized using the same method described for the tibiofemoral joint (see Sec. 6.1.2). Once the data was normalized, it became evident that the patellar flexion was closely related to tibiofemoral flexion (Figure 6.5), which is consistent with previously reported data for both implanted and non-implanted knees (see Equations (2.1) and (2.2) and Figure 2.3 in Section 2.2.2).

Patellar rotation was similar among the subjects and ranged within 5.7°, 7.4° and 6.7° for TKA, Contralateral and Healthy groups, respectively (Table 6.2). The rotation pattern was more distinct for the Healthy subjects, revealing that the patella was rotated laterally at foot contact and turned medially with the extension of the knee. There was no unique pattern for either Contralateral or TKA groups, but it is worth noting that there was significantly more variability among the implanted patients (Figure 6.5, middle row).

The patellar tilt varied quite significantly among the natural patella subjects, as a distinct pattern could be not determined for either of the three groups (Figure 6.5, bottom row). The absolute range of patellar tilt was 2.6° for both TKA and Healhty groups and 4.4° for Contralateral (Table 6.2). Interestingly the variability was lowest for the TKA group, most probably due to the kinematic boundary conditions of the articulating surfaces of the implant components.

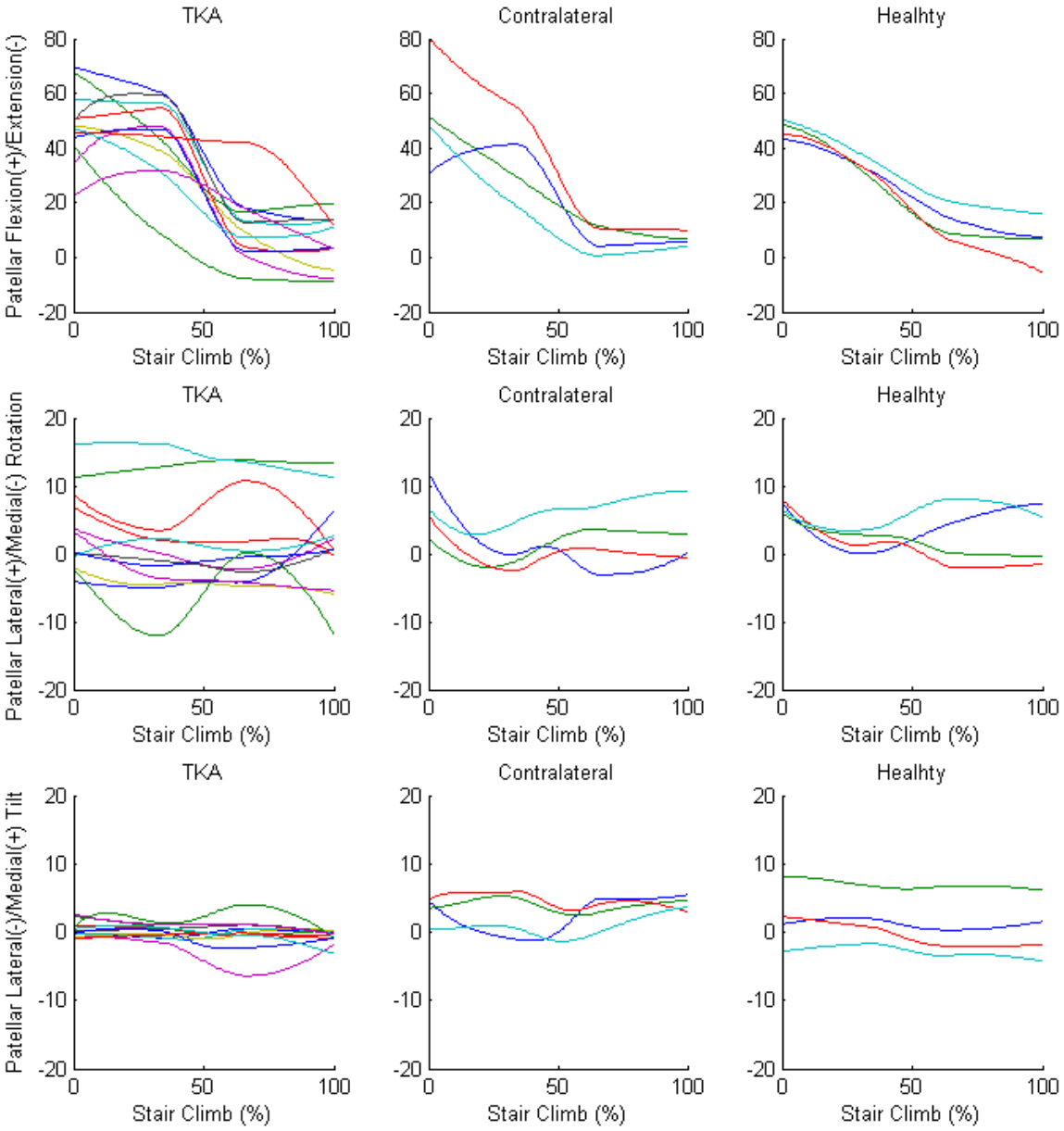


Figure 6.4: Patellofemoral joint rotations for all three groups of subjects.

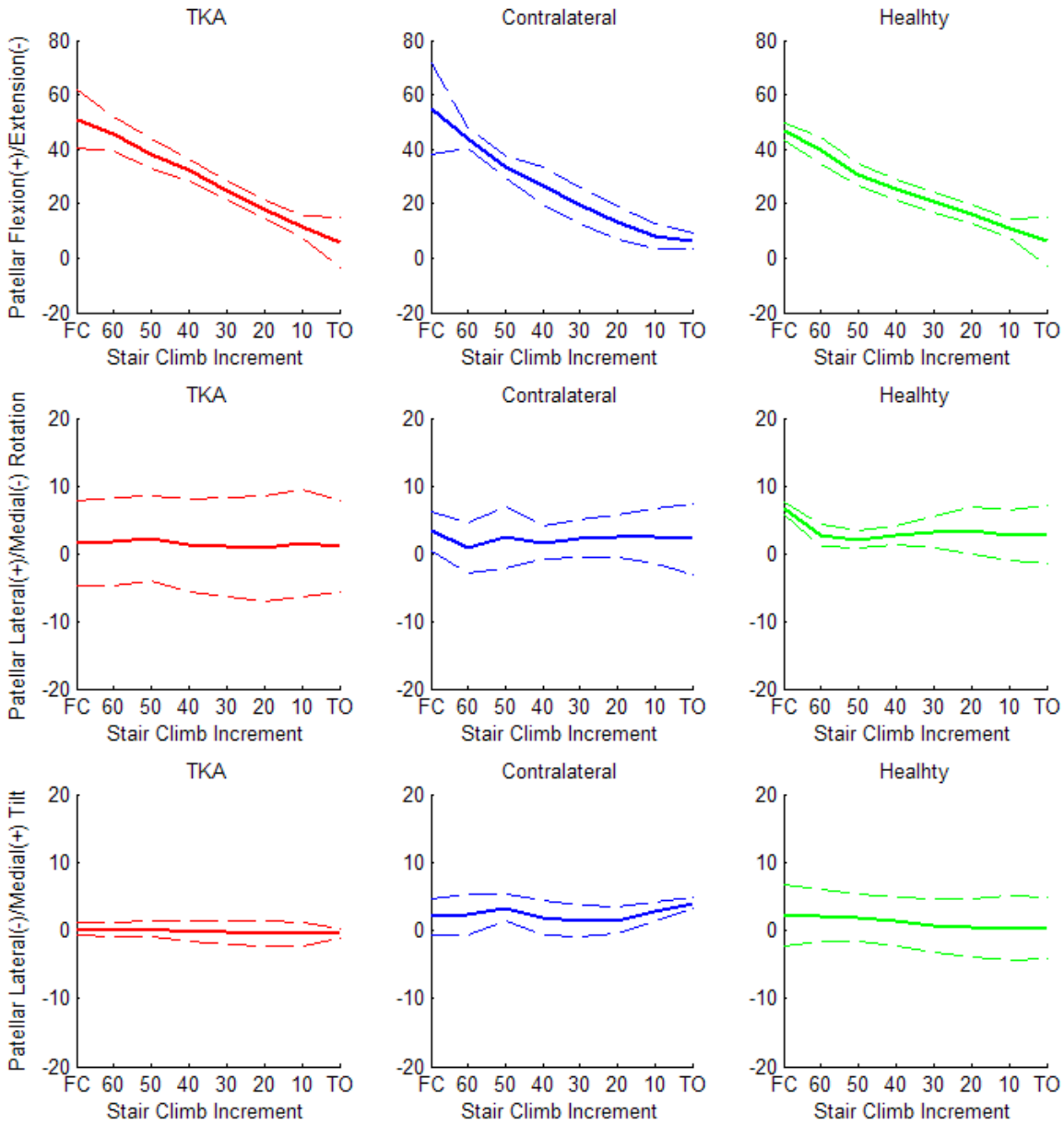


Figure 6.5: Patellofemoral joint rotations arranged with respect to standardized activity increments/knee flexion for all three groups of subjects (dashed lines mark ±SD). **FC**-*Foot Contact*, **TO**-*Toe Off*.

6.1.4 Patellofemoral contact

The patellofemoral contact location normalized with respect to height and width of the unfolded articulating surface was very similar for both groups having intact

Table 6.2: Patellofemoral joint rotations for all three groups of subjects.

		TKA		Contralateral		Healthy	
		avg (deg)	*SD (deg)*	**avg** (deg)	*SD (deg)*	**avg** (deg)	*SD (deg)*
Patellar Flexion(+) / Extension(-)	FC	**48.2**	*12.9*	**52.2**	*19.9*	**46.7**	*3.1*
	60	**45.9**	*6.4*	**44.0**	*3.7*	**39.6**	*4.8*
	40	**32.1**	*4.1*	**26.4**	*7.0*	**25.2**	*3.7*
	20	**17.9**	*3.5*	**13.1**	*6.2*	**15.9**	*3.5*
	TO	**5.6**	*9.3*	**6.3**	*2.8*	**6.2**	*8.9*
	min	**5.0**	*8.7*	**5.4**	*3.9*	**6.2**	*8.9*
	max	**51.4**	*10.9*	**54.7**	*16.8*	**46.7**	*3.1*
	abs. range	**46.4**	*8.4*	**49.3**	*13.9*	**40.5**	*7.5*
Patellar Lateral(+) / Medial(-) Rotation	FC	**3.3**	*6.2*	**6.1**	*3.9*	**6.6**	*0.9*
	60	**1.8**	*6.6*	**0.8**	*3.7*	**2.6**	*1.6*
	40	**1.2**	*6.9*	**1.6**	*2.5*	**2.6**	*1.5*
	20	**0.7**	*7.8*	**2.5**	*3.1*	**3.4**	*3.5*
	TO	**1.1**	*6.7*	**2.1**	*5.3*	**2.7**	*4.3*
	min	**-1.1**	*6.7*	**-1.2**	*2.7*	**0.3**	*2.3*
	max	**5.2**	*5.8*	**7.3**	*3.5*	**7.2**	*1.1*
	abs. range	**6.3**	*3.5*	**8.5**	*4.0*	**6.9**	*2.1*
Patellar Lateral(-) / Medial(+) Tilt	FC	**0.4**	*1.1*	**3.3**	*2.0*	**2.2**	*4.5*
	60	**0.1**	*1.1*	**2.3**	*3.1*	**2.2**	*3.8*
	40	**-0.1**	*1.6*	**1.8**	*2.6*	**1.3**	*3.7*
	20	**-0.5**	*1.7*	**1.4**	*2.0*	**0.4**	*4.3*
	TO	**-0.5**	*0.8*	**4.0**	*0.9*	**0.4**	*4.5*
	min	**-1.6**	*1.7*	**0.7**	*2.3*	**0.0**	*4.4*
	max	**1.1**	*1.3*	**5.1**	*1.0*	**2.7**	*4.0*
	abs. range	**2.6**	*1.6*	**4.4**	*1.8*	**2.6**	*1.1*

knees (Figure 6.6). For both groups the patella contacted the femoral trochlea in the upper quarter of within the upper quarter of the unfolded surface. At foot contact the interaction occured approximately in the middle of the femoral trochlea and translated superiorly as the knee extended during stair climbing (see animation in Figure 6.7). Interestingly, at Toe Off the most probable contact area was located at the very edge of the articulating surface, and the patella might no be contacting the femur at this stage.

In the TKA group the contact location also translated superiorly with decreasing knee flexion. However, the interaction occurred more distally on the articulating

portion of the femoral component (Figure 6.6). The contact was observed near the middle of the unfolded surface of the femur at the Foot Contact and moved approximately a quarter of the height of the unfolded surface as the stair was being climbed. It is worth noting that the resurfaced patella remained in contact for all subjects at all instances.

The patellofemoral interaction on the natural patella was located in the superior portion of the patella and translated distally with decreasing flexion (see animation in Figure 6.8). This pattern was very similar in comparison to both the Healthy and Contralateral groups, although the most probable location in the younger population occupied mostly medial facet and the ridge of patella, while in the elderly group the contact was spread between the medial and lateral facets of the patella (Figure 6.9).

In the TKA group, the patellofemoral contact location on the patella remained near the middle of the patellar button throughout the entire activity (see animation in Figure 6.8). A slight distal shift can be noticed, but within much smaller range than in either of the natural knee groups. More noticeable movement appeared in the medial/lateral distribution of the contact region - initially the contact appeared at the medial portion of the patellar button, then shifted laterally at mid-flexion and settled in the middle of the patellar button at Toe Off (Figure 6.9).

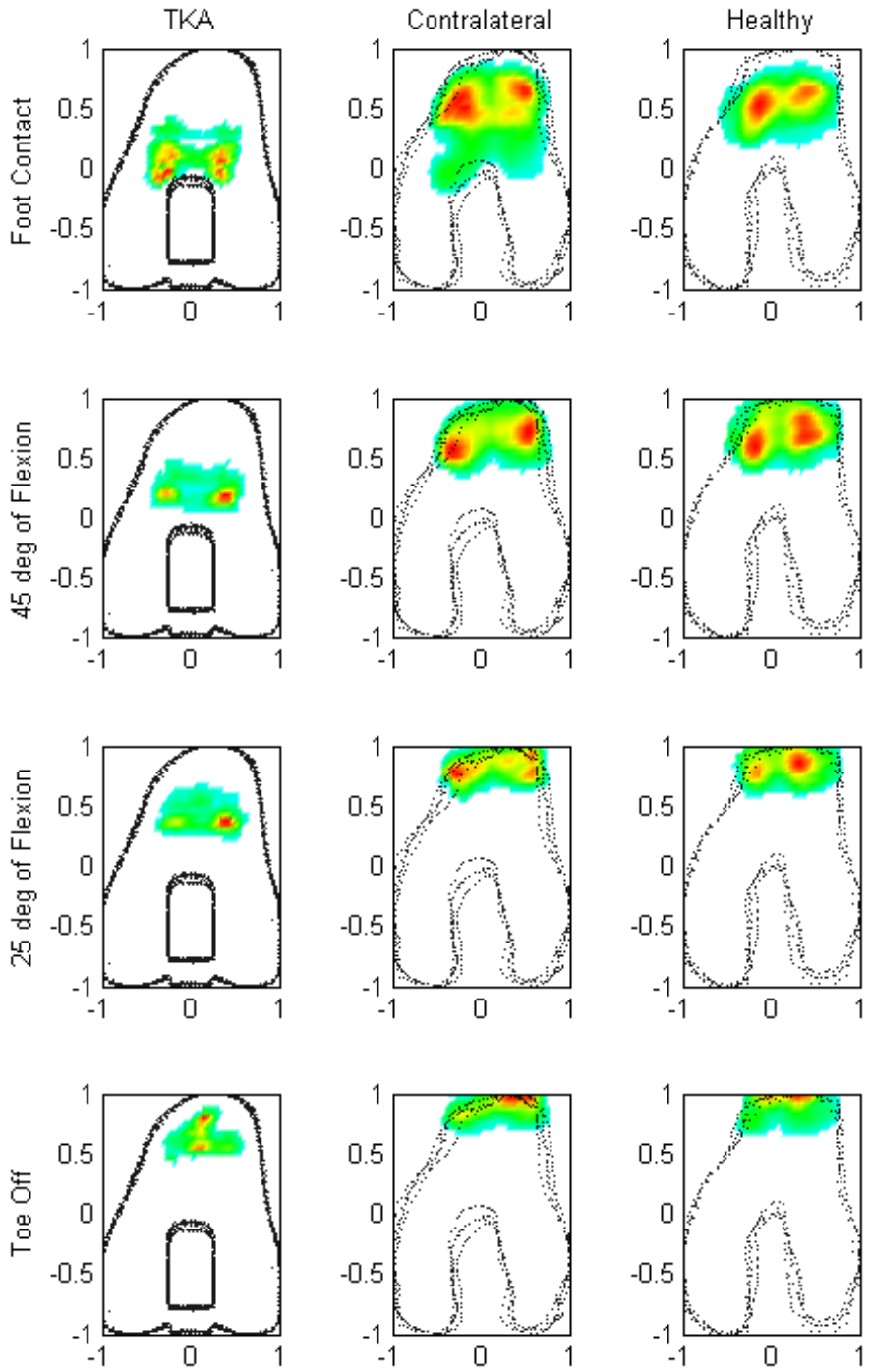


Figure 6.6: Patellofemoral contact location mapped on the unfolded articulating surface of the femoral component (for replaced knees) or distal femur (for natural knees) for all three groups of subjects at selected stair climbing increments. Red color indicates the most probable location of the contact between the articulating surfaces.

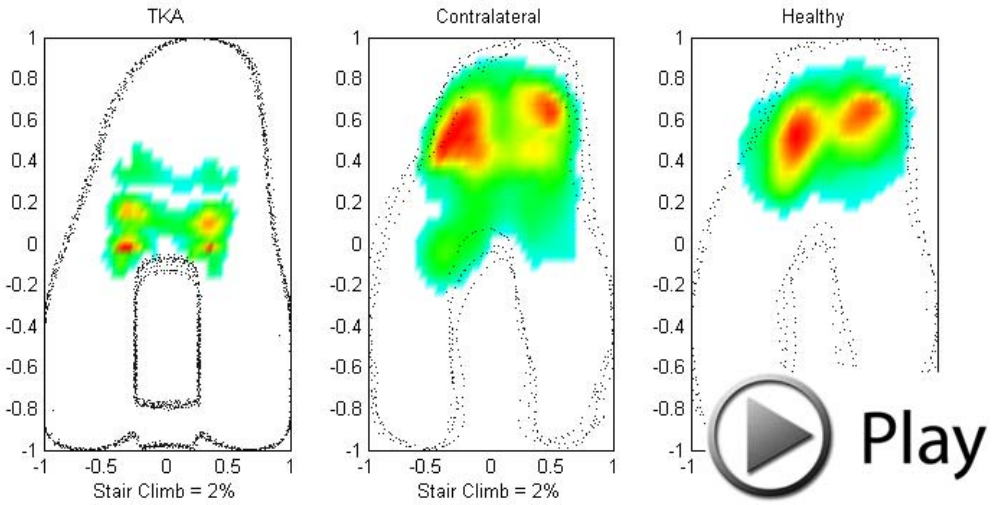


Figure 6.7: Patellofemoral contact location mapped on the unfolded articulating surface of the femoral component (for replaced knees) or distal femur (for natural knees) for all three groups of subjects (click to play animation). Red color indicates the most probable location of the contact between the articulating surfaces.

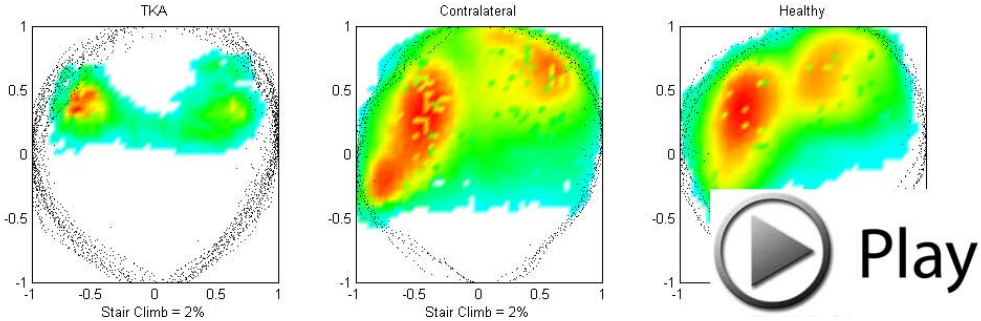


Figure 6.8: Patellofemoral contact location maps on patella for all three groups of subjects (click to play animation). Red color indicates the most probable location of the contact between the articulating surfaces.

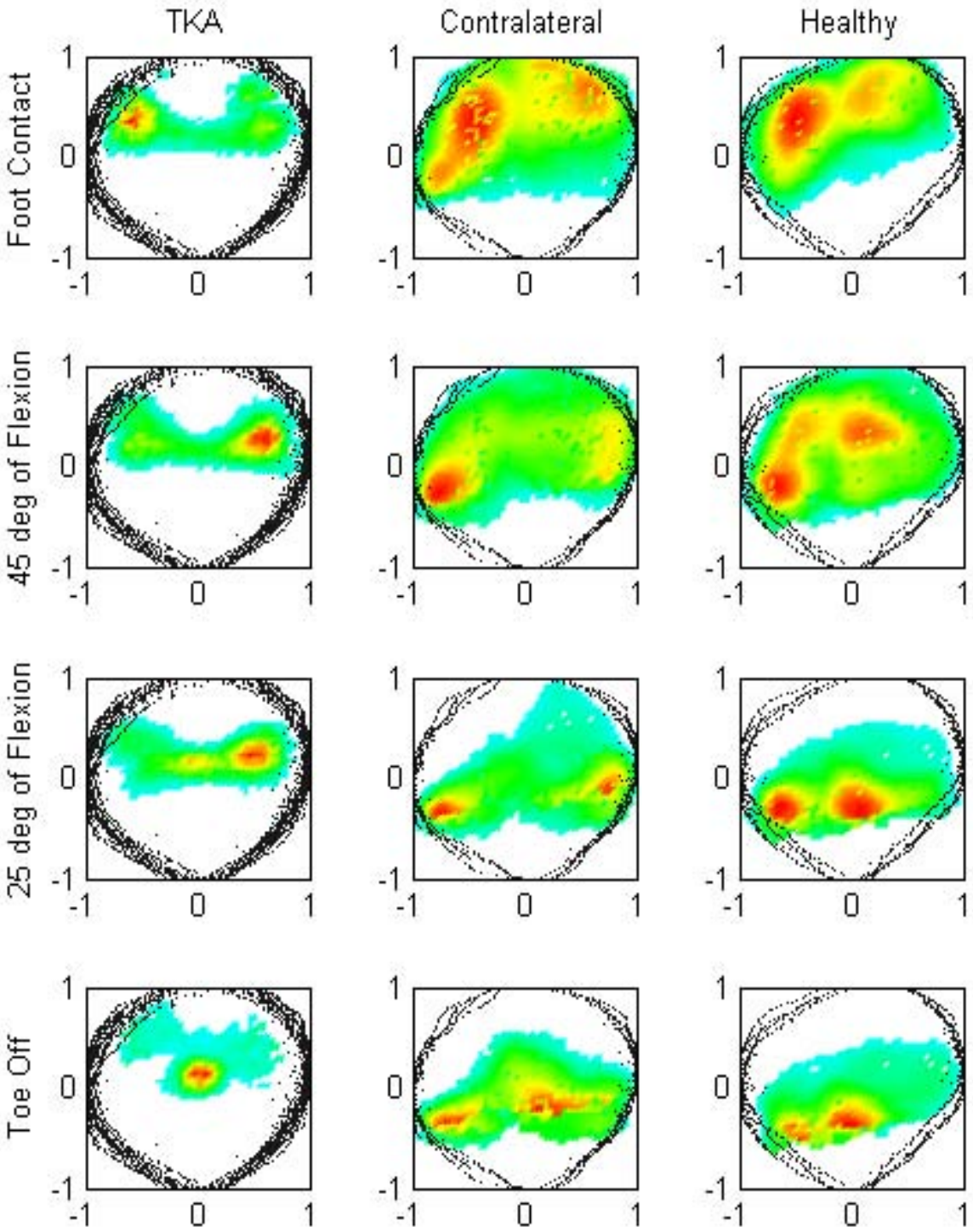


Figure 6.9: Patellofemoral contact location maps on patella for all three groups of subjects at selected stair climbing increments. Red color indicates the most probable location of the contact between the articulating surfaces.

6.2 Kinetic Analysis

6.2.1 Muscle Properties

The musculoskeletal model built in the course of this study included a number of in-vivo input data (kinematics, ground reaction force etc.) but also a number of muscle parameters. Though not all of these parameters could be determined directly for each participant non-invasively, the effort was made to gather or estimate as many patient specific parameters as possible (see Section 5.3).

The patients' muscle parameters used in the model are presented in the Table 6.3. These parameters mostly reflect the physiological differences between the subjects. The muscle slack length for all muscles was larger for the Healthy subjects, than for either TKA or Contralateral group. This finding can be explained by the simple fact that the Healthy subjects were significantly taller (1.80 m) than the elderly subjects in the two other groups (1.56 m and 1.60 m, see Table 5.1 for details). The taller the person, the higher the muscle length and hence the slack length.

Similarly, the physiological cross-sectional area (PCSA) was seen to by higher in the Healthy group than in the two others (Table 6.3). Depending on the muscle the healthy subjects had was 50% to 129% larger PCSA than the elderly subjects. This is also coherent, cosidering that the healthy group consisted of four young males with athletic build and much lower body fat percentage then the two other groups.

The maximum muscle force depends on the maximum muscle fiber stress, but is also directly proportional to the PCSA. Consequently, the maximum muscle forces were also found to by much higher for healthy than for elderly subjects.

6.2.2 Muscle Activation

In general the muscle activation patterns were fairly consistent among the subjects (Figure 6.10), but in order to improve the analysis of the average activation patterns the data had to be normalized as it was the case for the kinematics data (see discussion

Table 6.3: Properties of the muscles of subjects from all three groups. **VL** - *Vastus Lateralis*, **VI** - *Vastus Intermedius*, **RF** - *Rectus Femoris*, **VM** - *Vastus Medialis*, **GM** - *Gastrocnemius Medialis*, **GL** - *Gastrocnemius Lateralis*, **BF** - *Biceps Femoris*.

Group	Sbjct Nr	Muscle Slack Length (mm)							Muscle PCSA (cm^3)							Muscle Fmax (N)						
		VL	VI	RF	VM	GM	GL	BF	VL	VI	RF	VM	GM	GL	BF	VL	VI	RF	VM	GM	GL	BF
TKA	1	332	262	420	309	389	378	433	39	58	36	27	41	21	17	1365	2030	1260	945	1435	735	595
	2	362	247	447	316	441	362	444	50	73	46	39	36	14	9	1750	2555	1610	1365	1260	490	315
	3	337	249	402	301	393	402	412	52	75	47	48	64	18	26	1820	2625	1645	1680	2240	630	910
	4	349	233	408	303	413	407	417	39	74	47	47	41	13	19	1365	2590	1645	1645	1435	455	665
	5	348	243	414	303	448	445	440	32	78	49	37	35	12	10	1120	2730	1715	1295	1225	420	350
	6	329	222	403	291	396	398	417	38	67	42	37	50	17	12	1330	2345	1470	1295	1750	595	420
	7	341	252	406	309	401	401	420	41	68	43	38	51	15	19	1435	2380	1505	1330	1785	525	665
	8	333	233	398	289	409	405	413	33	59	37	25	41	14	15	1155	2065	1295	875	1435	490	525
	9	332	222	436	286	483	475	429	43	75	47	37	42	14	11	1505	2625	1645	1295	1470	490	385
	10	356	412	412	306	419	419	421	36	55	35	42	34	16	9	1260	1925	1225	1470	1190	560	315
	11	311	212	383	275	395	388	393	35	59	37	31	27	10	11	1225	2065	1295	1085	945	350	385
	12	326	231	391	240	411	409	409	47	45	28	31	50	23	11	1645	1575	980	1085	1750	805	385
	average	**338**	**252**	**410**	**294**	**416**	**408**	**421**	**40**	**66**	**41**	**37**	**43**	**16**	**14**	**1415**	**2293**	**1441**	**1280**	**1493**	**545**	**493**
	SD	*14*	*52*	*18*	*21*	*28*	*30*	*14*	*6*	*10*	*6*	*7*	*10*	*4*	*5*	*227*	*357*	*227*	*251*	*344*	*130*	*183*
	min	311	212	383	240	389	362	393	32	45	28	25	27	10	9	1120	1575	980	875	945	350	315
	max	362	412	447	316	483	475	444	52	78	49	48	64	23	26	1820	2730	1715	1680	2240	805	910
Contralateral	1	341	247	428	312	428	423	449	50	73	46	39	36	14	9	1750	2555	1610	1365	1260	490	315
	2	308	229	391	276	417	420	406	52	75	47	48	64	18	26	1820	2625	1645	1680	2240	630	910
	3	334	234	395	295	408	403	416	39	74	47	47	41	13	19	1365	2590	1645	1645	1435	455	665
	4	347	230	430	287	457	455	449	43	75	47	37	42	14	11	1505	2625	1645	1295	1470	490	385
	average	**332**	**235**	**411**	**292**	**428**	**425**	**430**	**46**	**74**	**47**	**43**	**46**	**15**	**16**	**1610**	**2599**	**1636**	**1496**	**1601**	**516**	**569**
	SD	*17*	*8*	*21*	*15*	*21*	*22*	*22*	*6*	*1*	*1*	*6*	*12*	*2*	*8*	*212*	*34*	*18*	*195*	*436*	*78*	*273*
	min	308	229	391	276	408	403	406	39	73	46	37	36	13	9	1365	2555	1610	1295	1260	455	315
	max	347	247	430	312	457	455	449	52	75	47	48	64	18	26	1820	2625	1645	1680	2240	630	910
Healthy	1	342	218	417	306	451	454	458	78	137	86	58	53	19	17	2730	4795	3010	2030	1855	665	595
	2	353	253	422	326	485	478	444	55	138	87	63	43	10	8	1925	4830	3045	2205	1505	350	280
	3	336	427	427	287	461	461	461	63	136	85	66	43	10	12	2205	4760	2975	2310	1505	350	420
	4	380	280	478	343	527	529	500	46	186	117	65	51	14	13	1610	6510	4095	2275	1785	490	455
	average	**353**	**294**	**436**	**315**	**481**	**480**	**466**	**61**	**149**	**94**	**63**	**48**	**13**	**13**	**2118**	**5224**	**3281**	**2205**	**1663**	**464**	**438**
	SD	*19*	*92*	*28*	*24*	*34*	*34*	*24*	*14*	*25*	*16*	*4*	*5*	*4*	*4*	*475*	*858*	*543*	*125*	*184*	*150*	*129*
	min	336	218	417	287	451	454	444	46	136	85	58	43	10	8	1610	4760	2975	2030	1505	350	280
	max	380	427	478	343	527	529	500	78	186	117	66	53	19	17	2730	6510	4095	2310	1855	665	595

in Section 6.1.2). Therefore, the muscle activation was arranged with respect to common instances of the activity: Foot Contact (FC), 60°, 50°, 40°, 30°, 20°, 10° of knee flexion and Toe Off (TO) (Figure 6.11).

The average activation patterns were similar in both implanted and non-implanted groups, however substantial activation level differences were evident. The quadriceps muscles revealed the highest activation in comparison to all the analyzed muscles. Interestingly, all four muscles of the quadriceps group reached the maximum average values at 40° of knee flexion, in all three groups of subjects (Figure 6.11). For all subjects, involving all the quadriceps muscles, the Vastus Lateralis revealed the highest activation, followed by Vastus Medialis, Rectus Femoris and Vastus Intermedius. Biceps Femoris exhibited similar activation pattern to the quadriceps muscles, but at lower levels. The Gastrocnemii, on the other hand, were mostly active at the Toe Off increment for all three groups.

Very interesting differences were observed in the activation values. Both the groups of elderly subjects experienced significantly higher muscle activation than the younger subjects. The average quadriceps group activation was 0.50, 0.44 and only 0.28 for TKA, contralateral and healthy subjects, respectively. In general the highest activations were seen for the TKA subjects, and only the Biceps Femoris and Gastrocnemii muscles were slightly more active for the Contralateral subjects than for TKA. It is important to note that even these antagonist muscles were two to three time less active in the Healthy subjects group 6.11.

These differences were also evident when compared the maximum muscle activation levels. The maximum quadriceps muscles activation ranged between 79% and 86% in the TKA, between 73% and 80% in the Contralateral and between only 33% and 38% in the Healthy groups. Among all the muscles, the highest absolute activation was revealed by the Vastus Medialis on both the TKA (83%) and Contralateral (80%) groups, while in the Healthy group, the Vastus Lateralis achieved the highest absolute activation (38%).

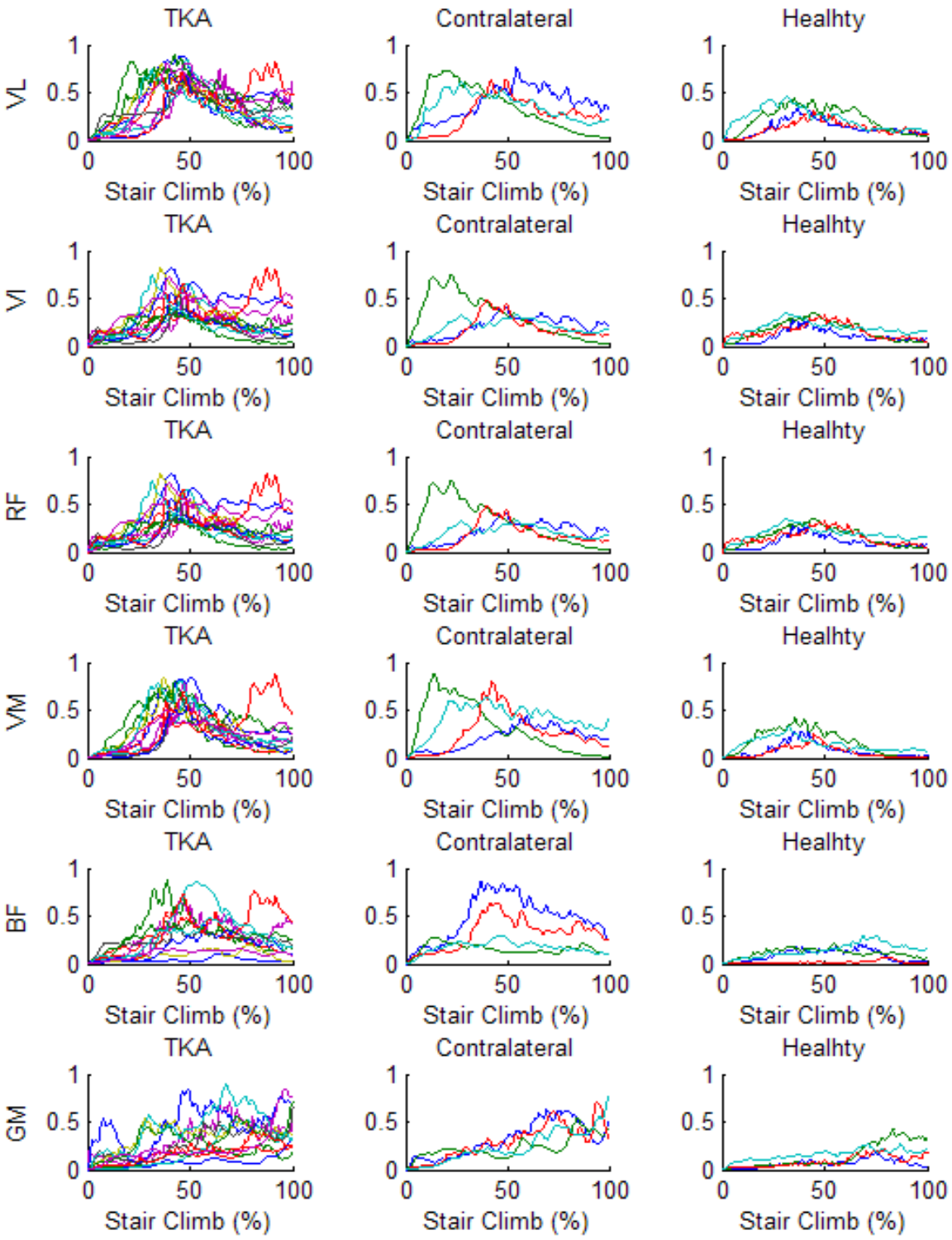


Figure 6.10: Quadriceps muscle activation plotted against the stair climbing progress for all subjects.

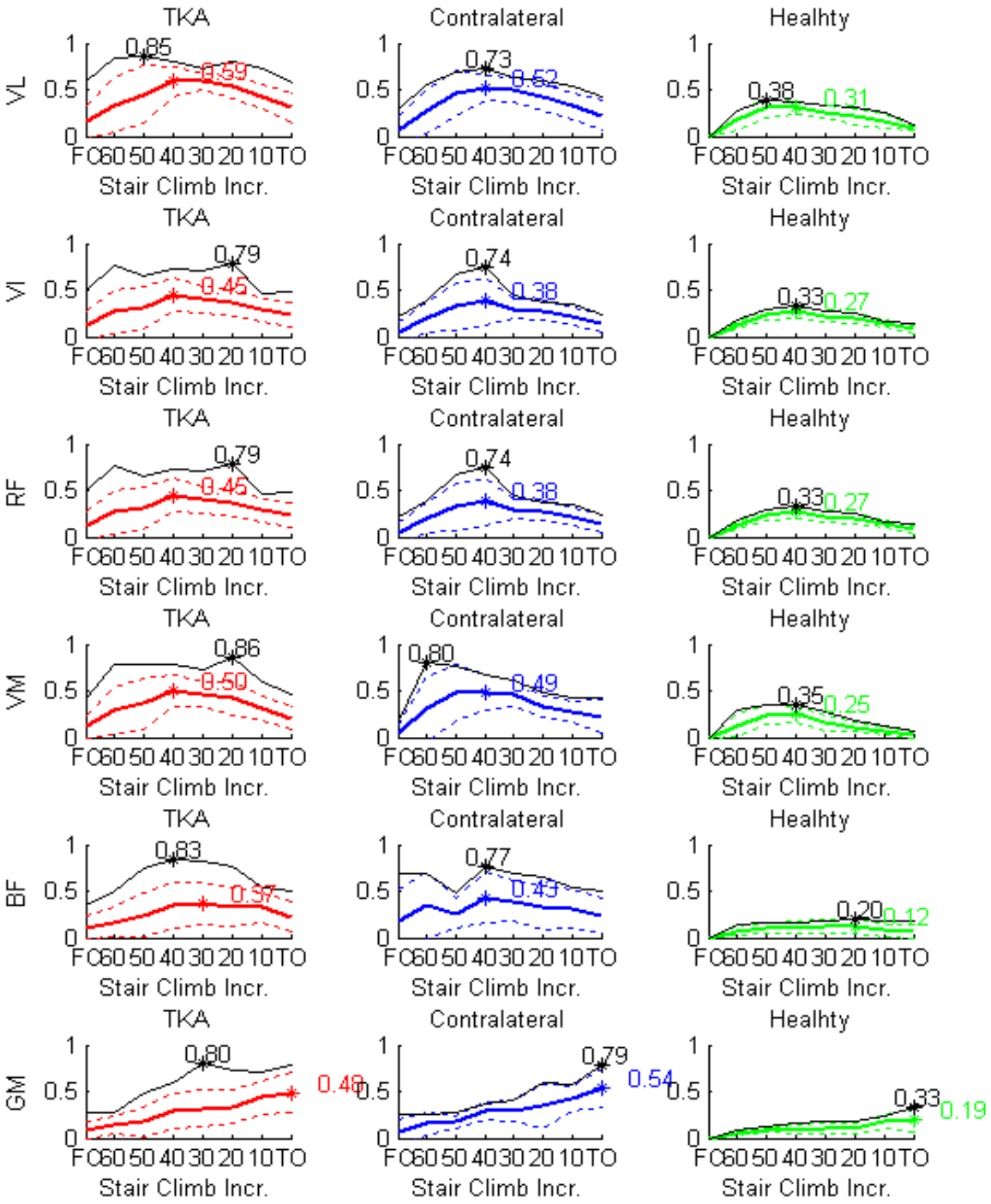


Figure 6.11: Average quadriceps muscle activation arranged with respect to standardized activity increments/knee flexion. (Color solid lines mark the average values, dashed lines mark ±SD, solid black lines mark the envelope of the maximum forces. **FC**-*Foot Contact*, **TO**-*Toe Off*.)

6.2.3 Muscle dynamics analysis

The surface electromyography (EMG) signals revealed the actual in-vivo activation patterns of the muscles selected for analysis. To a certain extent the EMG signals are related to the magnitude of the tensile force generated by the contracting muscles. However, this relationship between the muscle electrical manifestation detected by the surface electrodes and the muscle contraction force is complex and due to technical limitations the force magnitudes cannot be determined precisely (as discussed in Section 5.3.2). Nonetheless, since the procedures employed for the analysis of the EMG signals were exactly the same for every subject, it can be expected that the uncertainty is the same for all subjects, and hence intra-subjects comparisons should be valid. Therefore, the muscle dynamics analysis based on EMG signals provides valuable insight into the actual muscle activation timing, and in-vivo distribution of the muscle forces.

The EMG data analysis revealed significant differences in the muscle dynamics among the three groups (Figure 6.12). After normalizing with respect to the common activity increments, the data also revealed differences in the average muscle force patterns (Figure 6.13).

For all groups the highest average quadriceps forces occurred at either 40° or 50° of knee flexion. The highest forces in all of the quadriceps muscles were found for the TKA subjects. In order to climb up the stair, the TKA subjects had to generate the maximum forces ranging between 0.54times body weight (xBW) to 0.86xBW. The forces were smaller in the Contralateral group, ranging between 0.44xBW and 0.69xBW, while the Healthy subjects experienced lowest forces varying between only 0.21xBW and 0.53xBW, on average.

Comparing the muscle force envelopes (i.e. maximum muscle forces found for any subject at given flexion increment, see Figure 6.13), it was found that the highest maximum forces were present in the Vastus Intermedius in all three groups. The TKA subjects experienced the greatest requirement, needing to generate as much as

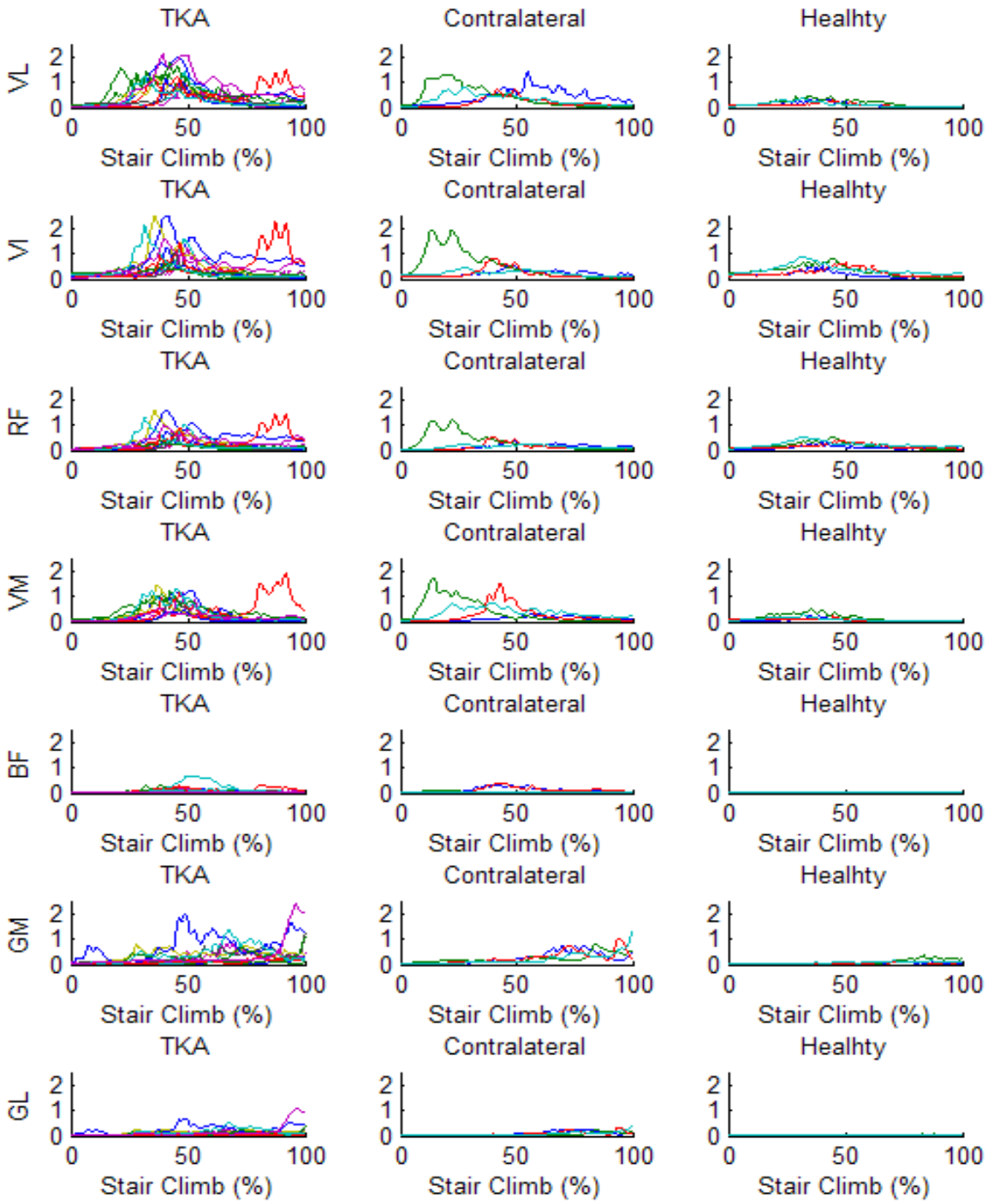


Figure 6.12: Quadriceps muscle force calculated based on EMG signals plotted against the stair climbing progress for all subjects.

2.22xBW in this muscle, while for their Contralateral counterparts this force did not exceed 1.93xBW, and 0.71xBW was found to be sufficient in the Healthy group.

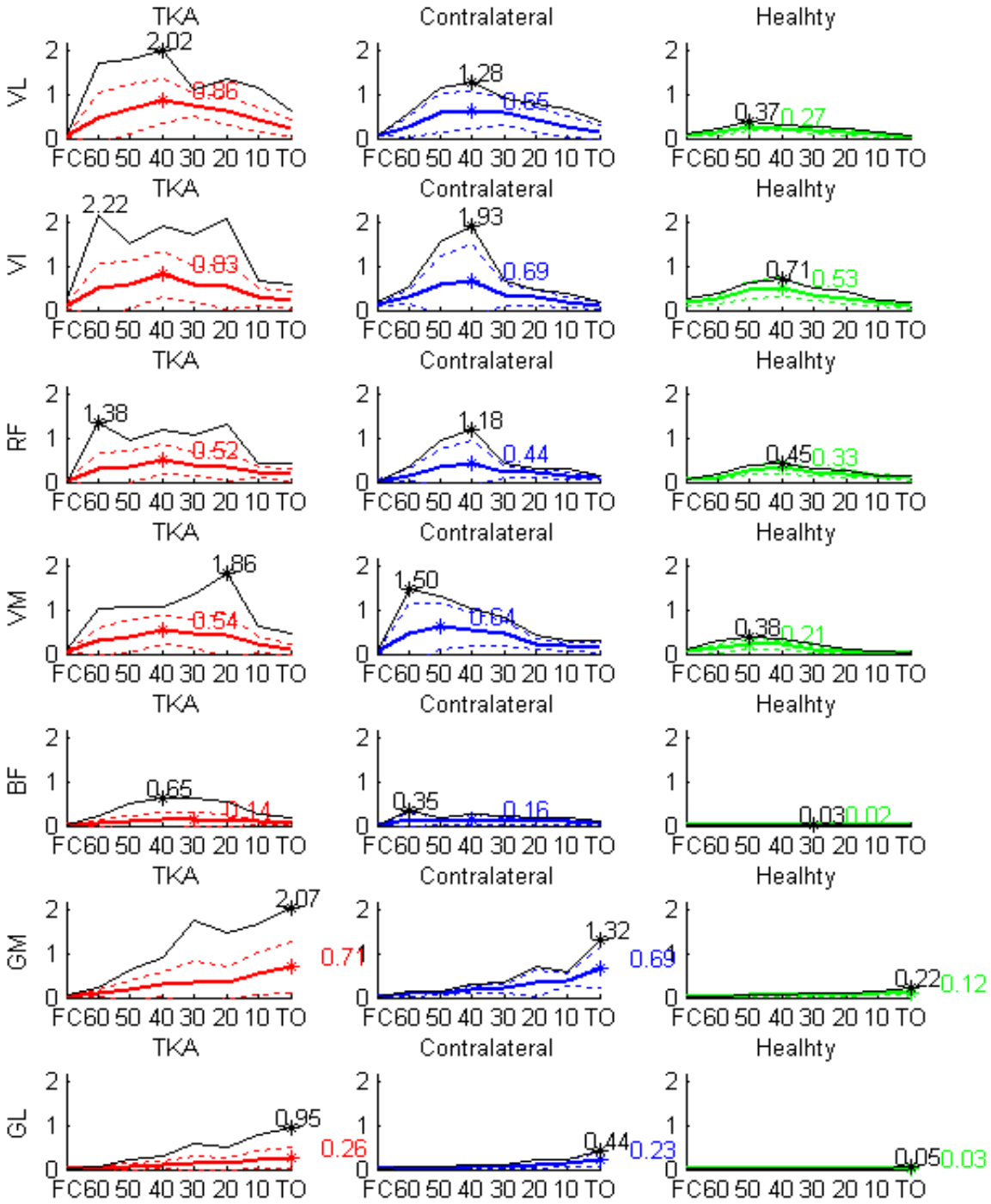


Figure 6.13: Average quadriceps muscle force calculated based on EMG signals arranged with respect to standardized activity increments/knee flexion. (Color solid lines mark the average values, dashed lines mark ±SD, solid black lines mark the envelope of the maximum forces. **FC**-*Foot Contact*, **TO**-*Toe Off*.)

The forces present in the antagonist muscles were also highest in the TKA group, followed by the Contralateral group and again significantly lower magnitudes were found for the Healthy subjects.

6.2.4 Inverse dynamics analysis

The muscle force profiles calculated using the musculoskeletal models use the patients' motion data as input and hence the kinetic results reflect the differences present in the kinematic data and therefore had to be normalized with respect to the common motion instances (see Section 6.1.2). All patients muscle force profiles are shown in the Figure 6.14 (and Attachment A), while the average patterns obtained after normalization are presented in the Figure 6.15.

Similarly to the EMG-based muscle dynamics analysis, the inverse dynamics evaluation revealed that the quadriceps forces were higher for the TKA and Contralateral subjects than those experienced by the Healthy subjects. In each group of subjects the highest forces were present in the Vastus Lateralis; 1.32xBW, 1.17xBW and 1.13xBW for TKA, Contralateral and Healhty groups, respectively. The lowest forces in the quadriceps group were present in the Rectus Femoris and its peak values were close to 0.4xBW in all three groups.

In the TKA group the peak average quadriceps forces occurred at 40° of flexion, which is the same as indicated by the EMG-based results. In the Contralateral group the peak force arose in deeper flexion - between 40° and 60° of flexion, while in Healthy group at 50°.

The muscle force envelopes were also highest for the TKA subjects for all quadriceps muscles. The envelopes also indicated that the muscle generating the highest contraction in every group was the Vastus Lateralis.

Interestingly, the antagonistic muscles (Biceps Femoris (BF), Gastrocnemius Medialis (GM) and Gastrocnemius Lateralis (GL)) did not generate any forces

throughout the activity for all three groups of subjects (Figure 6.15. All three muscles generated tension only near the end of the activity; between 10° and Toe Off.

6.2.5 EMG vs Inverse Dynamics: Quadriceps forces

The patterns of the quadriceps forces determined using both EMG signals and inverse dynamics were very similar (Figure 6.16). Both methods indicated that while climbing the stairs, the quadriceps generates highest forces at 40° - 50° of flexion.

The results revealed good agreement of the peak force occurrence predicted using both methods. When the difference in the occurrence of the peak force was determined in the time domain for every subject, it was found that the average offset between the peak EMG and inverse dynamics quadriceps forces was 0.09% activity duration in both TKA and Contralateral groups, and only 0.06% in the Healthy group (Table 6.4). Considering that the average activity duration for TKA subjects was only 3.3s, it means that the average offset between the two methods was only 0.3s for this gruop (0.22s for Contralateral and 0.34s for Healthy).

As discussed in the Section 5.3.2, the EMG signal analysis is fraught with error and the muscle force magnitude cannot be estimated precisely. The differences in the magnitude were highest in the Healthy group, where EMG prediction of the average total quadriceps force was only 1.31xBW compared to 3.13xBW predicted by inverse dynamics. For the TKA group, which included the most subjects, both methods actually yielded comparable results the average total quadriceps force equal 2.75xBW and 3.63xBW, obtained based on EMG and inverse dynamics, respectively (Figure 6.16).

6.2.6 EMG vs Inverse Dynamics: Quadriceps force distribution

The distribution of the muscle force within the quadriceps group can be obtained by normalizing each of the individual muscles force with respect to the total quadriceps

Table 6.4: Time of peak muscle forces calculated based on the EMG signals and using inverse dynamics. **VL** - *Vastus Lateralis*, **VI** - *Vastus Intermedius*, **RF** - *Rectus Femoris*, **VM** - *Vastus Medialis*, **GM** - *Gastrocnemius Medialis*, **GL** - *Gastrocnemius Lateralis*, **BF** - *Biceps Femoris*.

EMG vs Inverse Dynamics: Time of Peak muscle force (sec)

Group	Sbjct Nr	Stair Climb Duration (sec)	EMG							Inverse Dynamics							Absolute difference (% activity duration)							
			VL	VI	RF	VM	GM	GL	BF	VL	VI	RF	VM	GM	GL	BF	VL	VI	RF	VM	Quad peak	GM	GL	BF
TKA	1	1.6	0.7	0.7	0.7	0.8	1.6	1.6	1.0	0.3	0.3	0.3	0.3	1.5	1.5	1.5	0.3	0.2	0.2	0.3	0.3	0.1	0.1	0.3
	2	5.1	1.6	2.0	2.0	2.0	4.3	4.3	2.0	1.8	1.8	1.8	1.8	5.1	5.1	5.1	0.0	0.0	0.0	0.0	0.0	0.1	0.1	0.6
	3	2.3	1.1	0.8	0.8	0.9	2.3	2.3	1.1	0.9	0.9	0.9	0.9	0.9	0.9	1.7	0.1	0.0	0.0	0.0	0.0	0.6	0.6	0.2
	4	2.2	1.1	1.1	1.1	1.1	1.7	1.7	1.2	0.9	1.0	1.1	1.1	2.1	1.4	1.7	0.1	0.0	0.0	0.0	0.0	0.2	0.1	0.2
	5	7.6	3.5	3.8	3.8	3.6	5.3	5.3	3.4	3.7	3.7	3.7	3.7	6.7	5.9	6.7	0.0	0.0	0.0	0.0	0.0	0.2	0.1	0.4
	6	3.3	1.2	1.2	1.2	1.2	0.9	0.9	2.6	1.2	1.2	1.3	1.2	3.2	3.2	3.2	0.0	0.0	0.0	0.0	0.0	0.7	0.7	0.2
	7	3.7	1.8	1.7	1.7	1.6	3.7	3.7	1.6	1.9	1.9	2.1	2.0	3.7	3.7	3.7	0.0	0.1	0.1	0.1	0.1	0.0	0.0	0.5
	8	3.3	1.3	1.3	1.3	1.6	1.6	1.6	1.9	1.4	1.4	1.4	1.4	2.0	2.0	2.0	0.0	0.0	0.0	0.1	0.0	0.1	0.1	0.0
	9	3.1	1.3	1.3	1.3	1.3	3.1	3.1	1.5	0.7	0.7	0.7	0.7	3.0	3.0	3.0	0.2	0.2	0.2	0.2	0.2	0.0	0.0	0.5
	10	3.4	3.1	3.0	3.0	3.1	2.8	2.8	2.8	2.2	2.3	2.4	2.4	3.4	3.4	3.4	0.3	0.2	0.2	0.2	0.2	0.2	0.2	0.2
	11	2.3	0.7	0.7	0.7	1.1	1.6	1.6	1.6	0.9	0.8	0.9	0.9	2.3	2.1	2.3	0.0	0.0	0.0	0.1	0.1	0.3	0.2	0.3
	12	1.6	0.6	0.6	0.6	0.6	1.6	1.6	0.6	0.8	0.8	0.8	0.8	1.6	1.6	1.6	0.1	0.1	0.1	0.1	0.1	0.0	0.0	0.7
	average	**3.3**	**1.52**	**1.52**	**1.52**	**1.58**	**2.54**	**2.54**	**1.77**	**1.39**	**1.40**	**1.43**	**1.42**	**2.95**	**2.82**	**2.99**	**0.10**	**0.08**	**0.08**	**0.10**	**0.09**	**0.21**	**0.20**	**0.35**
	SD	*1.7*	*0.92*	*0.98*	*0.98*	*0.92*	*1.32*	*1.32*	*0.82*	*0.93*	*0.93*	*0.95*	*0.94*	*1.65*	*1.54*	*1.59*	*0.10*	*0.08*	*0.08*	*0.10*	*0.09*	*0.22*	*0.22*	*0.19*
	min	1.6	0.63	0.64	0.64	0.62	0.93	0.93	0.55	0.28	0.27	0.27	0.27	0.89	0.89	1.47	0.02	0.01	0.01	0.00	0.01	0.02	0.02	0.05
	max	7.6	3.55	3.80	3.80	3.62	5.25	5.25	3.43	3.73	3.73	3.73	3.73	6.72	5.91	6.72	0.28	0.24	0.24	0.34	0.28	0.68	0.68	0.66
Contralateral	1	3.0	1.6	1.5	1.5	1.8	2.1	2.1	1.1	1.2	1.3	1.3	1.2	3.0	3.0	3.0	0.1	0.0	0.0	0.2	0.1	0.3	0.3	0.6
	2	2.0	0.4	0.4	0.4	0.3	1.7	1.7	0.3	0.2	0.1	0.1	0.1	2.0	2.0	2.0	0.1	0.2	0.1	0.1	0.1	0.2	0.2	0.9
	3	2.9	1.4	1.2	1.2	1.3	2.8	2.8	1.2	1.2	1.1	1.2	1.2	3.0	3.0	3.0	0.1	0.0	0.0	0.0	0.0	0.1	0.1	0.6
	4	1.9	0.5	0.5	1.0	0.8	1.9	1.9	0.9	0.5	0.5	0.5	0.5	1.9	1.9	1.9	0.0	0.0	0.3	0.1	0.1	0.0	0.0	0.5
	average	**2.5**	**1.01**	**0.90**	**1.04**	**1.02**	**2.11**	**2.11**	**0.88**	**0.77**	**0.76**	**0.81**	**0.77**	**2.48**	**2.48**	**2.48**	**0.09**	**0.06**	**0.12**	**0.10**	**0.09**	**0.14**	**0.14**	**0.66**
	SD	*0.6*	*0.61*	*0.50*	*0.43*	*0.64*	*0.46*	*0.46*	*0.42*	*0.51*	*0.58*	*0.57*	*0.54*	*0.58*	*0.58*	*0.58*	*0.06*	*0.09*	*0.12*	*0.07*	*0.05*	*0.13*	*0.13*	*0.15*
	min	1.9	0.43	0.45	0.45	0.29	1.69	1.69	0.29	0.16	0.07	0.15	0.11	1.92	1.92	1.92	0.01	0.00	0.01	0.01	0.03	0.01	0.01	0.53
	max	3.0	1.63	1.47	1.47	1.77	2.76	2.76	1.22	1.22	1.33	1.33	1.22	3.00	3.00	3.00	0.14	0.19	0.27	0.19	0.14	0.31	0.31	0.87
Healthy	1	7.4	2.7	2.7	2.7	2.6	5.6	5.6	5.0	2.9	2.9	2.9	2.9	7.4	7.4	7.4	0.0	0.0	0.0	0.0	0.0	0.2	0.2	0.3
	2	4.3	1.5	1.9	1.9	1.5	3.6	3.6	1.4	1.5	1.5	1.5	1.5	4.4	4.4	4.4	0.0	0.1	0.1	0.0	0.0	0.2	0.2	0.7
	3	6.3	2.8	3.2	3.2	2.8	5.0	5.0	1.2	2.6	2.1	2.6	2.4	6.4	6.0	6.4	0.0	0.2	0.1	0.1	0.1	0.2	0.2	0.8
	4	3.1	1.0	1.0	1.0	1.0	2.7	2.7	2.1	0.7	0.7	0.7	0.7	3.1	3.1	3.1	0.1	0.1	0.1	0.1	0.1	0.1	0.1	0.3
	average	**5.3**	**2.01**	**2.18**	**2.19**	**1.99**	**4.23**	**4.23**	**2.43**	**1.93**	**1.79**	**1.93**	**1.89**	**5.31**	**5.22**	**5.31**	**0.04**	**0.10**	**0.07**	**0.05**	**0.06**	**0.19**	**0.18**	**0.53**
	SD	*1.9*	*0.90*	*0.96*	*0.96*	*0.86*	*1.31*	*1.31*	*1.76*	*0.99*	*0.93*	*0.99*	*0.96*	*1.92*	*1.86*	*1.92*	*0.04*	*0.06*	*0.03*	*0.04*	*0.03*	*0.05*	*0.05*	*0.26*
	min	3.1	1.00	0.96	0.97	1.02	2.71	2.71	1.18	0.71	0.68	0.71	0.71	3.13	3.13	3.13	0.00	0.03	0.03	0.00	0.03	0.13	0.13	0.32
	max	7.4	2.83	3.17	3.17	2.84	5.59	5.59	5.00	2.87	2.87	2.87	2.87	7.37	7.37	7.37	0.09	0.17	0.09	0.10	0.09	0.24	0.24	0.82

force. These normalized forces obtained using both EMG and inverse dynamics analyses are shown in Figure 6.17. The average total quadriceps force is not equal to 1, because not for all subjects did the maximum quadriceps force occur at the same increment.

The quadriceps force distribution revealed by the EMG data was the same for TKA and Contralateral groups of subjects. The highest forces were seen in Vastus Lateralis (VL), followed by Vastus Intermedius (VI), Vastus Medialis (VM) and Rectus Femoris (RF) in both elderly groups. The Healthy subjects, however, experienced highest contraction in the VI, followed by RF, VL and VM, as summarized in the table below:

EMG-based

Quadriceps force distribution (x max F_{Quad})

TKA	Contr.	Healthy
VL (0.24)	**VL** (0.26)	**VI** (0.36)
VI (0.21)	**VI** (0.20)	**RF** (0.22)
VM (0.14)	**VM** (0.20)	**VL** (0.19)
RF (0.13)	**RF** (0.13)	**VM** (0.15)

The distribution of quadriceps forces revealed by the inverse dynamics analysis was the same for all three groups of subjects with the VL generating most of the force, followed by VI, VM and RF. The average values of the proportions between the individual muscles were slightly different for each group, but remained within very similar range, as summarized in the following table:

Inverse Dynamics-based

Quadriceps force distribution (x max F_{Quad})

TKA	Contr.	Healthy
VL (0.32)	**VL** (0.27)	**VL** (0.36)
VI (0.27)	**VI** (0.23)	**VI** (0.28)
VM (0.20)	**VM** (0.20)	**VM** (0.23)
RF (0.09)	**RF** (0.09)	**RF** (0.12)

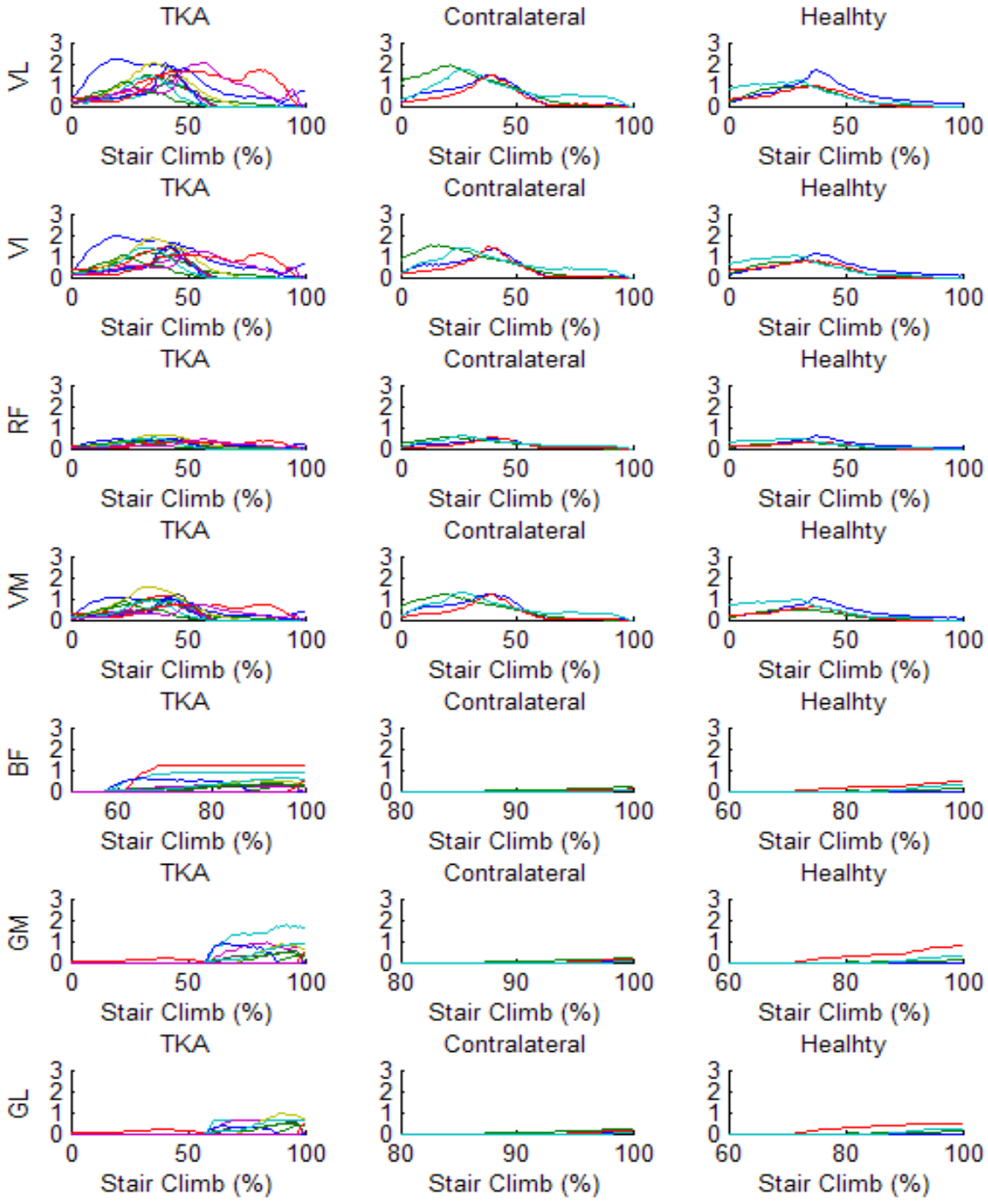


Figure 6.14: Quadriceps muscle force calculated using inverse dynamics plotted against the stair climbing progress for all subjects.

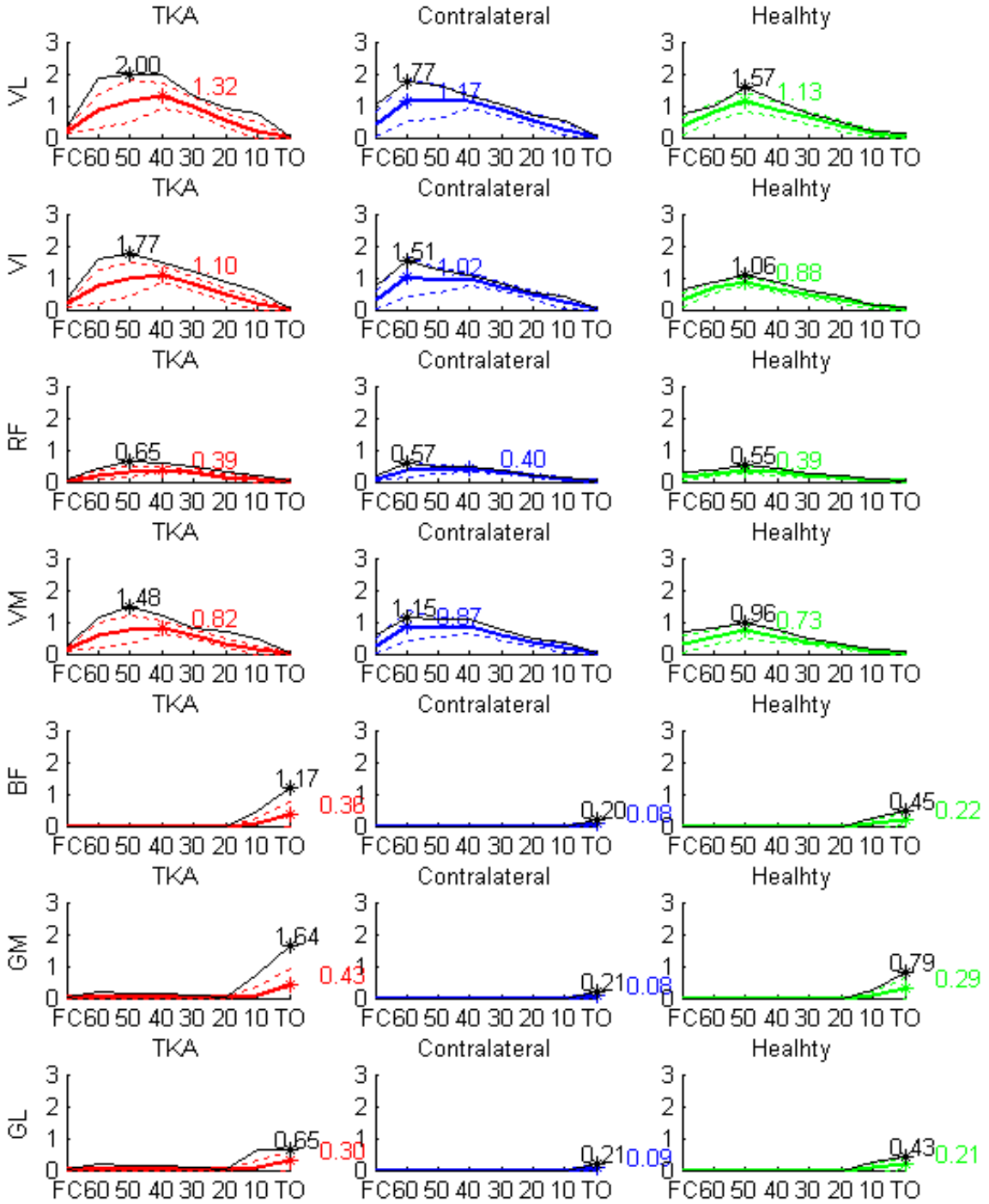


Figure 6.15: Average quadriceps muscle force calculated using inverse dynamics arranged with respect to standardized activity increments/knee flexion. (Color solid lines mark the average values, dashed lines mark ±SD, solid black lines mark the envelope of the maximum forces. **FC**-*Foot Contact*, **TO**-*Toe Off*.)

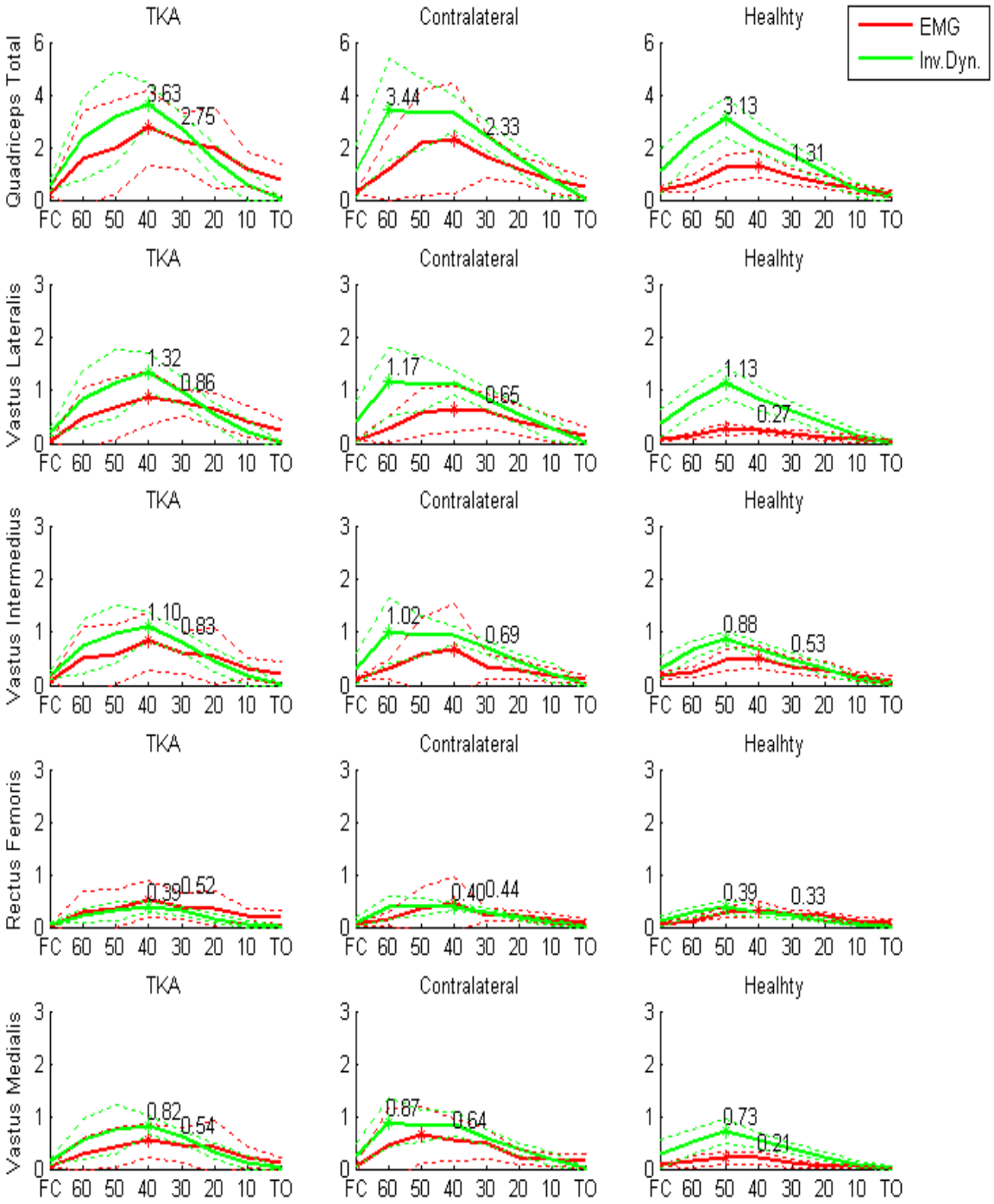


Figure 6.16: Muscle forces distribution calculated based on the EMG signals (red) and using inverse dynamics (green). (Solid lines mark the average values, dashed lines mark ±SD. **FC**-*Foot Contact*, **TO**-*Toe Off*.)

Interestingly, the quadriceps force distribution obtained from the EMG and musculoskeletal model analyses were the same for both TKA and Contralateral groups. However, in the healthy group the EMG analysis indicated that the RF is the muscle generating the second largest force within the quadriceps group, while the musculoskeletal model predicted it to be the muscle having lowest contribution.

6.2.7 Knee Joint Reaction Forces

Among the patellofemoral joint reaction (PFJR), Tibiofemoral joint reaction and Patellar Ligament forces, the PFJR was found to be the highest force, when a comparison was conducted for all three groups of subjects. Similar to other forces, all the joint reactions were highest in the TKA group, followed by the Contralateral and lowest in the Healthy group (Figure 6.18). The maximum PFJR averaged 3.67xBW, 3.68xBW and 3.19xBW for TKA, Contralateral and Healthy subjects, respectively. The patellar ligament force was similar for all groups; 2.68xBW, 2.54xBW and 2.40xBW for TKA, Contralateral and Healthy subjects, respectively.

The tibiofemoral force is the total joint reaction force resulting from the dynamic interaction between the body segments, as well as the compression resulting from the muscle contraction (see Sec. 5.3.1). The maximum of this interaction force averaged 3.32xBW, 3.25xBW and 3.09xBW in TKA, Contralateral and Healthy subjects, respectively.

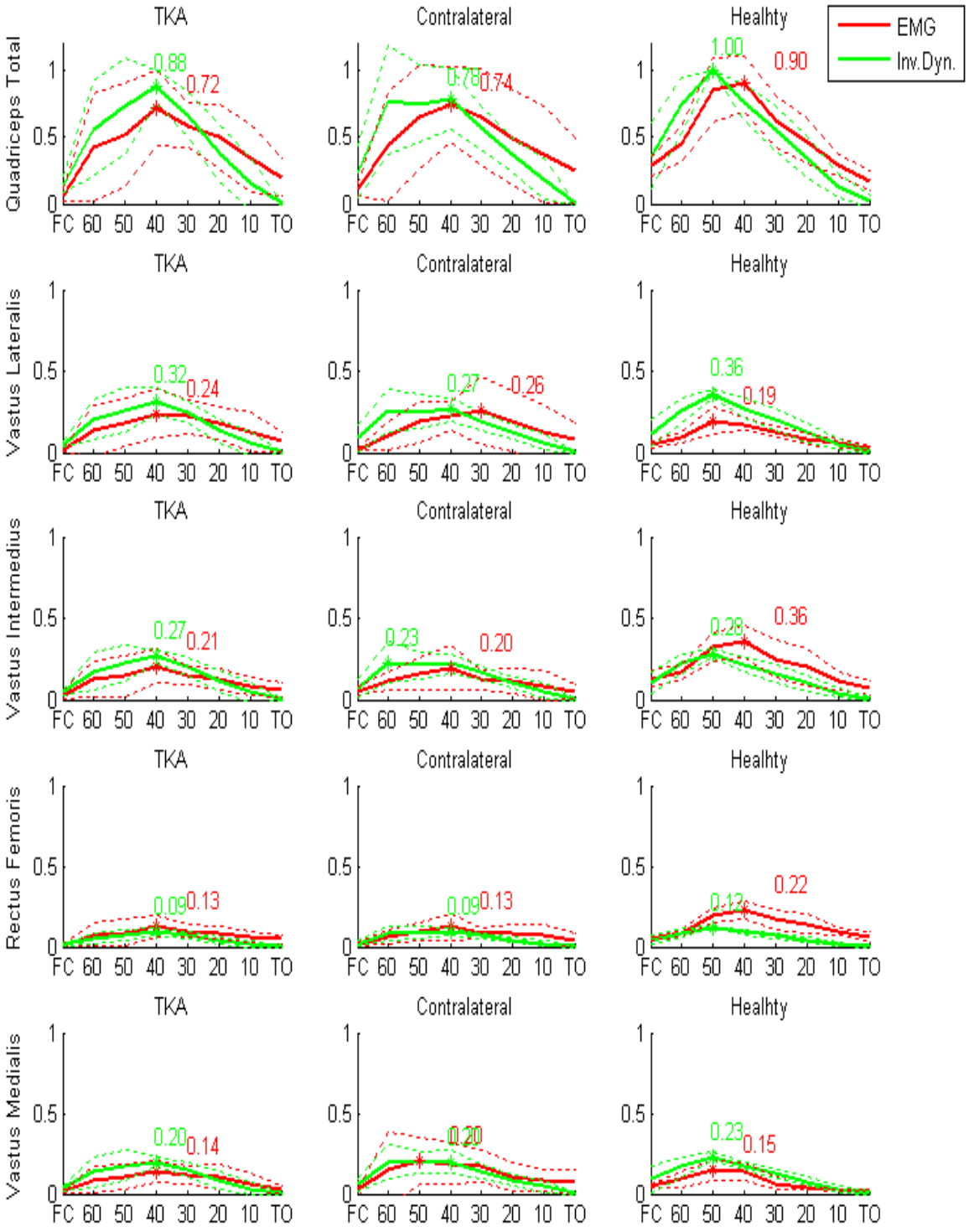


Figure 6.17: Muscle forces distribution normalized with respect to maximum total quadriceps force calculated based on the EMG signals (red) and using inverse dynamics (green). (Solid lines mark the average values, dashed lines mark ±SD. **FC**-*Foot Contact*, **TO**-*Toe Off*.)

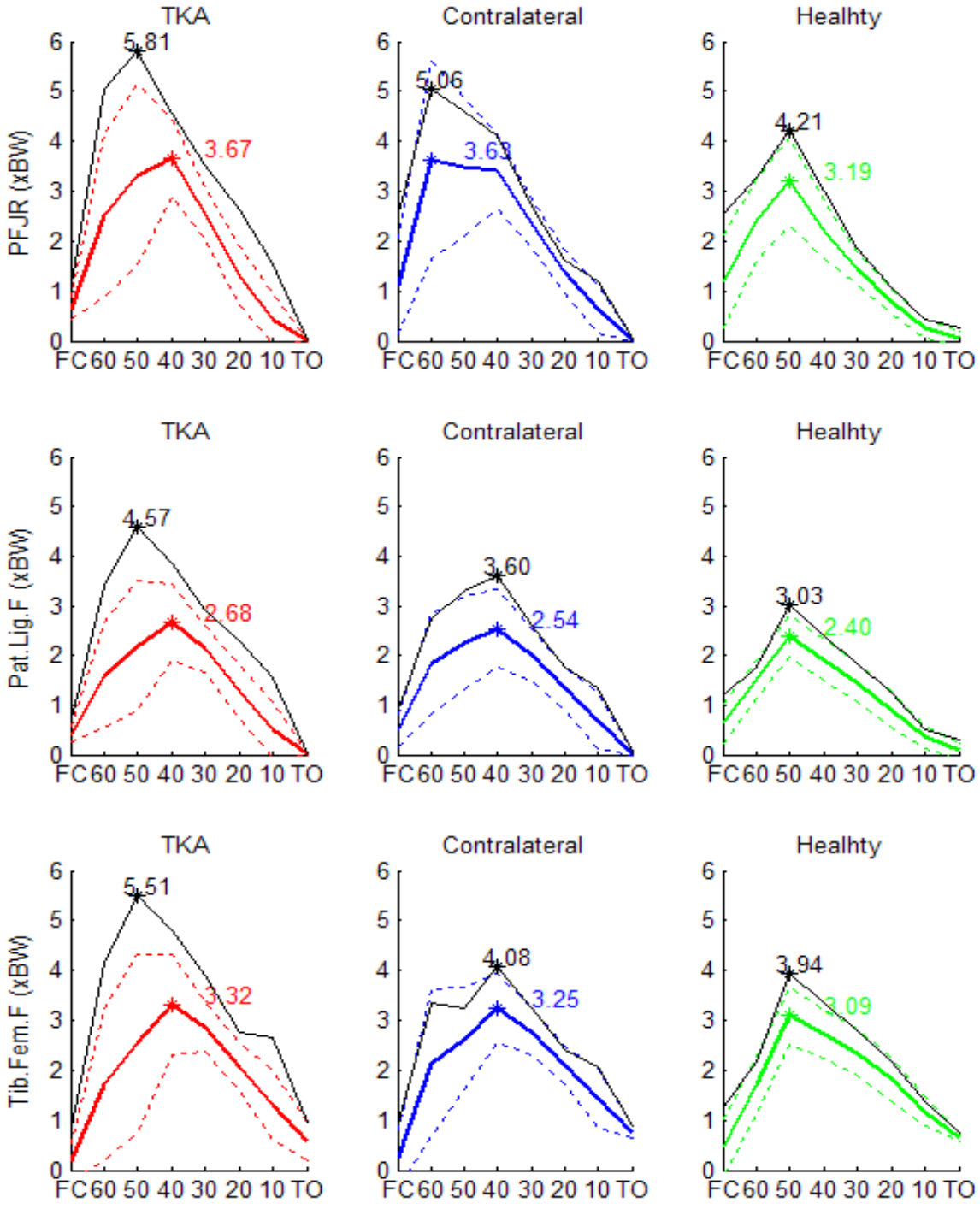


Figure 6.18: Patellofemoral Joint Reaction, Patellar Ligament and the total Tibiofemoral interaction force determined using inverse dynamics. (Color solid lines mark the average values, dashed lines mark ±SD, solid black lines mark the envelope of the maximum forces. **FC**-*Foot Contact*, **TO**-*Toe Off*.)

6.3 Vibroarthrography

In the preliminary phase of the presented research work, the vibroarthrography (VAG) signals were collected for 13 healthy and 13 arthritic subjects. Though limited in subjects number, this preliminary research yielded important information. It has been found that, as hypothesized (see Sec. 1.1), both the mean and standard deviation is typically higher for arthritic than for non-symptomatic joints (Figure 6.19). The 99^{th} quantile has also revealed promising separation between the groups. Therefore these three statistical parameters have been selected as good signal features for classification purposes.

After selecting the candidate features of the signals, a pattern classifier was designed. The objective of the classifier was to classify the given pattern of the patellofemoral VAG signal to one of the two groups: healhty or arthritic. The minimum-error-rate classification[62] was chosen for the first attempt to design the classifier. This classification can be achieved by the use of the discriminant functions:

$$g_i(x) = \ln p(x|\omega_i) + \ln P(\omega_i) \tag{6.1}$$

and assuming that the densities $p(x|\omega_i)$ are multivariate normal, the Eq. 6.1 becomes:

$$g_i(x) = -\frac{1}{2}(x-\mu_i)^t E_i^{-1}(x-\mu_i) - \frac{d}{2}\ln 2\pi - \frac{1}{2}\ln|E_i| + \ln P(\omega_i), \tag{6.2}$$

Since at the current stage of analysis there is no premise to classify the patient as either arthritic or healthy, the prior probabilities for both categories were assumed to be equal ($P(\omega_1) = P(\omega_2) = \frac{1}{2}$).

First, only one feature, the mean of the signal was used to design the dichotomizer. The success rate obtained with this classifier was 73% and the results are graphically represented in the Figure 6.20a. Next, the second feature; standard deviation, was included in the discriminant function, and the success rate increased to 81% (Figure

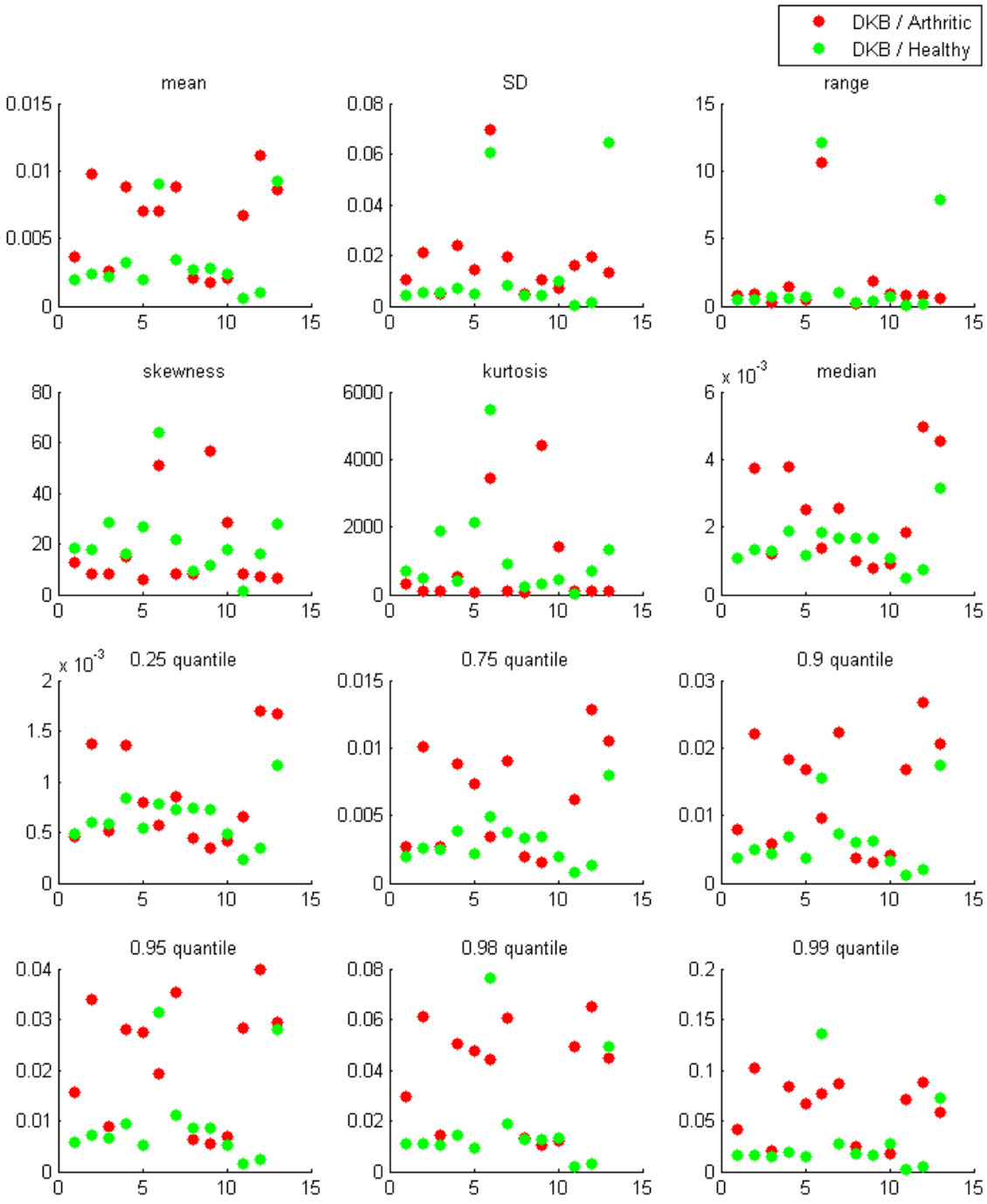
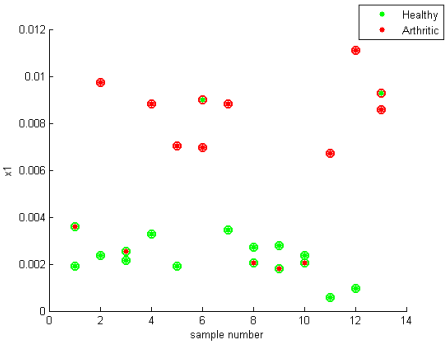
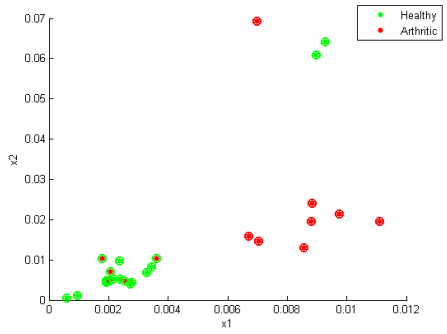


Figure 6.19: Comparison of several statistical parameters of the patellofemoral vibroarthrograms obtained for healthy (green) and arthritic (red) knee joints.

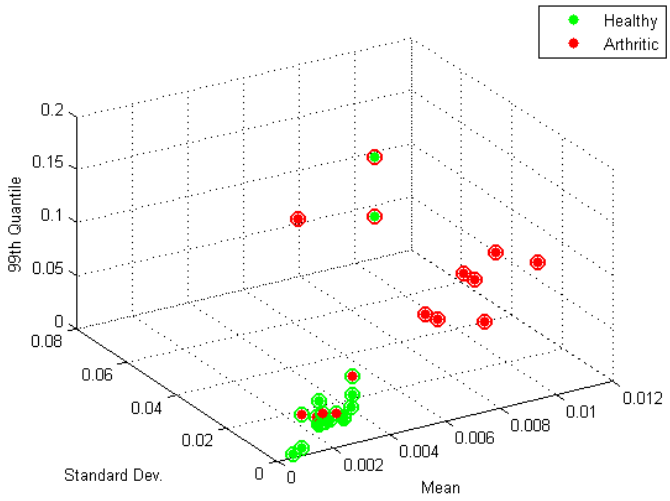
6.20b). Adding the third feature, the 99^{th} quantile, did not improve the classification and the success rate actually dropped back to 73% (Figure 6.20c).



(a) Features: x1=Mean. Success rate=73%.



(b) Features: x1=Mean, x2=Standard Deviation. Success rate=81%.



(c) Features: x1=Mean, x2=Standard Deviation, x3=99^{th} quantile. Success rate=73%.

Figure 6.20: The results of the classification using the minimum-error-rate classification (Eq. 6.2) using different sets of features. The color coded bullets (● and ●) show the members of the respective class, while the circles ○ and ○ show the classes assigned by the dichotomizer.

This initial phase of research has proven that the vibration data can be successfully collected from the knee joint and potentially used for classification. These encouraging results, prompted the decision to recruit more subjects for further

analysis. Ultimately, the database of 23 healthy and 52 arthritic knee joint VAG signals was created.

The early analysis also revealed that the signal range, 25 and 75^{th} quantiles did not provide any significant discrimination improvement compared to the other parameters, and have been excluded. Instead, the integral of the signal's envelope has been calculated for evaluation. Also, the VAG signal's envelope seemed to be higher for those subjects who performed the activity faster, therefore the product of the integral of the envelope and activity duration has been selected as the last (11^{th}) signal feature.

Similar to the initial phase, the deep knee bend (DKB) activity were selected for investigation using all the 75 datasets. However, it was noticed that the vibration patterns did differ between the trials even for the same subject. Therefore, a decision was then made to analyze all the trials of DKB performed by each subject rather than a single one. Once the statistical parameters (i.e. mean, SD, skewness, kurtosis, quantiles, etc.) were calculated for VAG signals from each trial, the mean, the absolute minimum, and the absolute maximum from all trials were calculated. That provided the total of 33 signal features selected for the assessment of their classification effectiveness (Figure 6.21).

The results obtained for the 23 healthy and 52 arthritic subjects, confirmed that the mean of rectified signal is higher for the arthritic ($4.6e^{-3}$) than for the healthy subjects ($3.1e^{-3}$). However, surprisingly the variance was lower for the damaged knee than for the intact knees. The skewness and kurtosis were also lower for the affected knees, but in general all the other parameters were higher for this group.

In order to better study the discrimination effectiveness of these statistical parameters, the two-sample t-test without assuming that the variances are equal. The null hypothesis (H_0) was that the data in both groups are independent random samples from normal distributions with equal means, against the alternative that the means are not equal. The $H = 1$ indicated the rejection of the null hypothesis at

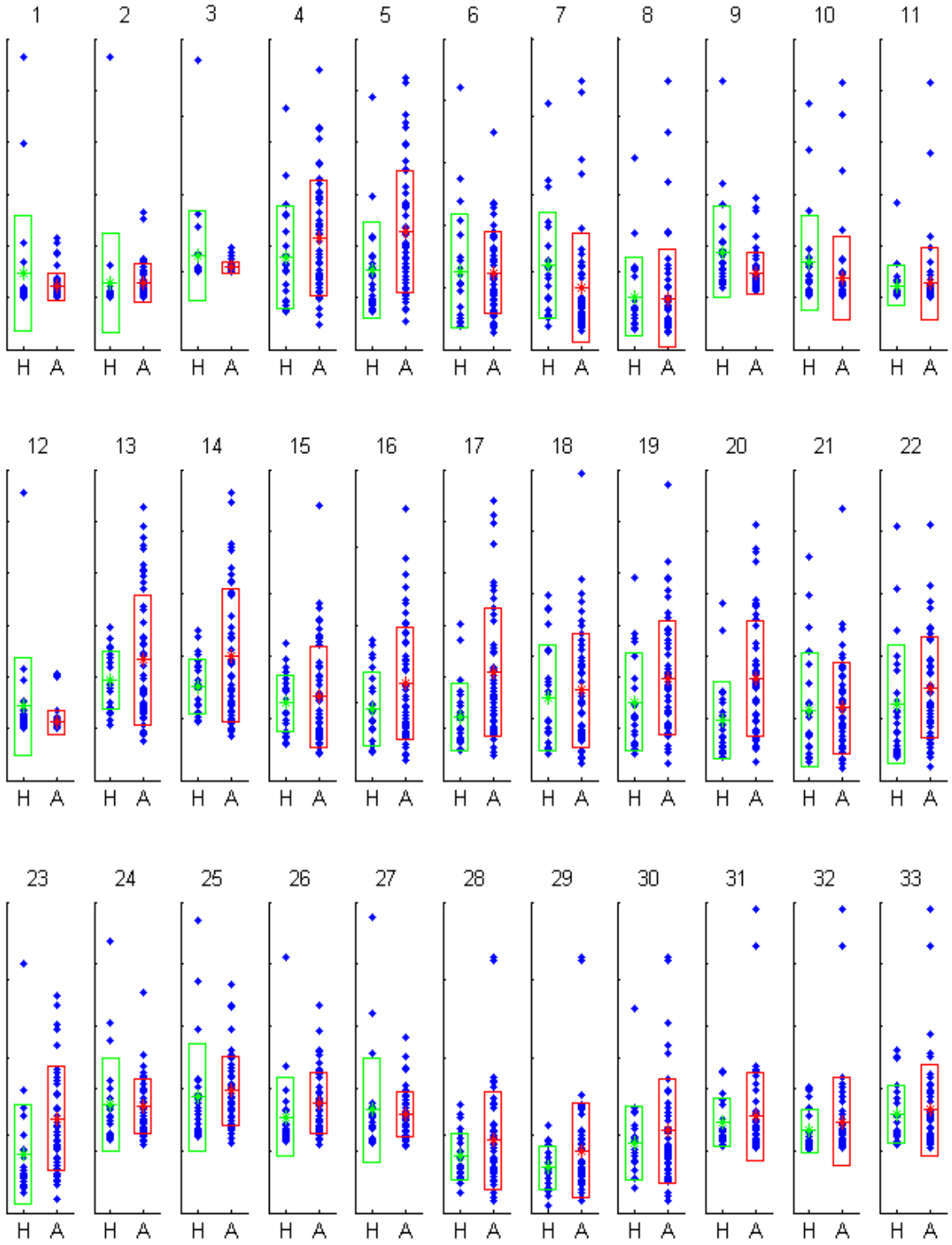


Figure 6.21: Distribution of selected 33 signal features for all 23 healthy (H), and 52 arthritic (A) subjects determined for all trials of the deep knee bend activity.

the 5% significance level. The signal features, which means are not equal ($p < 0.05$) could be considered good candidates for the pattern classification.

This approach identified 6 signal features, which means were significantly different for both groups (Table 6.5):

- minimum of the signal means from all trials,
- minimum of the signal median from all trials,
- mean of the signal 90^{th} quantiles from all trials,
- minimum of the signal 90^{th} quantiles from all trials,
- minimum of the signal 95^{th} quantiles from all trials,
- minimum of the integrals of signal envelope from all trials.

If the hypothesis, that the signals are different between the two knee conditions, is true, it should be valid for all activities, and including more activities could potentially enhance the classification rate. Therefore, it was decided to expand the analysis on all the activities collected for each subject; Deep Knee Bend, Chair Rise, Stair Climb, Stair Descent, Gait and Flexion-Extension. Then the feature means, absolute minimum and maximum were calculated for all trials of all activities (Figure 6.22).

Taking into account all activities, has more strongly confirmed the initial hypothesis that the signal mean and variance are higher for arthritic than healthy knees (Table 6.6). As a matter of fact, all signal features except skewness and kurtosis were higher for the affected knee joints. Also it was found that including all activities has yielded significantly better separation of the data than analyzing the DKB only. Surprisingly, the means of 26 out of 33 signal features were significantly different for the two groups (Table 6.6). Many of the parameters indicated extremely significant differences between the groups, e.g.:

- feature 15: maximum of the signals' median from all trials ($p = 5.4e^{-17}$),
- feature 4: mean of the signals' mean from all trials ($p = 3.7e^{-14}$),
- feature 13: mean of the signals' median from all trials ($p = 1.4e^{-15}$),
- feature 16: mean of the signals' 90^{th} quantile from all trials ($p = 2.4e^{-15}$),
- feature 19: mean of the signals' 95^{th} quantile from all trials ($p = 2.1e^{-13}$),

- feature 22: mean of the signals' 97.5^{th} quantile from all trials ($p = 5.9e^{-11}$),
- feature 28: mean of the signals' envelope integrals from all trials ($p = 5.8e^{-9}$).

From all of the examined features, the maximum of the signal medians of all the trials (feature 15) was most significantly different between the two groups ($p = 5.4e^{-17}$) and therefore has been selected as the main signal feature. Figure 6.23 shows the two-dimensional (2D) distribution of the six other features listed above plotted against the feature 15. These distributions reveal very good separation of the signal parameters between the two groups.

In order to derive the set of features that provide the best classification, all 528 possible combinations of 2, 5456 combinations of 3 and 40920 possible combinations of 4 signal features taken from all 33 parameters have been evaluated. The highest success rate obtained using two signal features was 92.21%, as summarized in the table below:

Features		Success Rate (%)
2	16	92.21
13	14	92.21
15	29	92.21
5	16	90.91
15	26	90.91
16	23	90.91
16	26	90.91
16	29	90.91
4	22	89.61
5	13	89.61

Using a set of three features has increased the classification rate up to 94.81% using a combinations of features nr 13, 14, 15, 29, 31 and 32. The ten best performing sets of 3 features are summarized below:

Features			Success Rate (%)
15	29	32	94.81
13	14	31	94.81
13	14	32	94.81
2	16	29	93.51
7	13	14	93.51
13	14	15	93.51
13	14	28	93.51
13	14	29	93.51
13	29	32	93.51
14	15	31	93.51

The best classification utilizing a set of three features was achieved using the following set:

- feature 15: maximum of the signals' median from all trials,

- feature 29: minimum of the signal envelope integral from all trials,

- feature 32: min. of the signal envelope integral times activity duration from all trials.

Figure 6.24 shows the distribution and the results of the classification obtained using this set of features.

Adding the 4^{th} parameter to pattern classification increased the success rate up to 96.1%, as summarized in following table:

Features				Success Rate (%)
4	25	29	32	96.10
7	13	29	32	96.10
8	16	29	32	96.10
9	13	29	32	96.10
9	16	23	29	96.10
10	13	29	32	96.10
13	14	31	33	96.10
15	16	26	29	96.10
15	16	26	33	96.10
2	16	29	32	94.81

Table 6.5: Statistical parameter average and standard deviation found for 23 healthy and 52 arthritic subjects for all trials of the DKB activity. The $H_0 = 1$ indicates a rejection of the null hypothesis (that samples are from population with equal means) at the 5% significance level.

Feature		Healthy		Arthritic		Ho	p
Nr	Name	avg	*SD*	avg	*SD*		
1	Variance (mean of all trials)	4.7E-04	*1.1E-03*	2.1E-04	*2.6E-04*	0	2.8E-01
2	Variance (min of all trials)	1.5E-04	*4.8E-04*	1.4E-04	*1.9E-04*	0	9.6E-01
3	Variance (max of all trials)	1.0E-03	*2.9E-03*	2.8E-04	*3.6E-04*	0	2.3E-01
4	Signal mean (mean of all trials)	4.4E-03	*2.5E-03*	5.4E-03	*2.7E-03*	0	1.4E-01
5	**Signal mean (min of all trials)**	**3.1E-03**	***1.9E-03***	**4.6E-03**	***2.4E-03***	**1**	**4.9E-03**
6	Signal mean (max of all trials)	6.3E-03	*4.6E-03*	6.2E-03	*3.3E-03*	0	9.2E-01
7	Skewness (mean of all trials)	1.1E+01	*6.9E+00*	7.9E+00	*7.0E+00*	0	9.4E-02
8	Skewness (min of all trials)	6.8E+00	*5.1E+00*	6.6E+00	*6.3E+00*	0	9.0E-01
9	Skewness (max of all trials)	1.8E+01	*1.8E+01*	9.3E+00	*8.0E+00*	1	3.9E-02
10	Kurtosis (mean of all trials)	3.4E+02	*4.6E+02*	1.9E+02	*4.0E+02*	0	1.9E-01
11	Kurtosis (min of all trials)	1.1E+02	*1.9E+02*	1.4E+02	*3.5E+02*	0	7.0E-01
12	Kurtosis (max of all trials)	8.5E+02	*1.9E+03*	2.4E+02	*4.8E+02*	0	1.4E-01
13	Median (mean of all trials)	1.9E-03	*5.6E-04*	2.3E-03	*1.2E-03*	0	6.1E-02
14	**Median (min of all trials)**	**1.5E-03**	***4.5E-04***	**2.0E-03**	***1.1E-03***	**1**	**6.2E-03**
15	Median (max of all trials)	2.5E-03	*9.1E-04*	2.7E-03	*1.6E-03*	0	5.0E-01
16	**90th quantile (mean of all trials)**	**9.2E-03**	***4.7E-03***	**1.2E-02**	***7.3E-03***	**1**	**2.4E-02**
17	**90th quantile (min of all trials)**	**6.1E-03**	***3.3E-03***	**1.0E-02**	***6.2E-03***	**1**	**1.6E-04**
18	90th quantile (max of all trials)	1.3E-02	*8.4E-03*	1.4E-02	*9.2E-03*	0	5.8E-01
19	95th quantile (mean of all trials)	1.5E-02	*9.4E-03*	2.0E-02	*1.1E-02*	0	7.1E-02
20	**95th quantile (min of all trials)**	**9.6E-03**	***6.2E-03***	**1.6E-02**	***9.2E-03***	**1**	**4.8E-04**
21	95th quantile (max of all trials)	2.3E-02	*1.8E-02*	2.3E-02	*1.5E-02*	0	9.0E-01
22	97.5 quantile (mean of all trials)	2.4E-02	*1.9E-02*	3.0E-02	*1.6E-02*	0	2.3E-01
23	97.5 quantile (min of all trials)	**1.5E-02**	***1.3E-02***	**2.4E-02**	***1.3E-02***	**1**	**8.3E-03**
24	97.5 quantile (max of all trials)	3.7E-02	*3.8E-02*	3.6E-02	*2.2E-02*	0	8.9E-01
25	99th quantile (mean of all trials)	4.3E-02	*4.3E-02*	4.8E-02	*2.8E-02*	0	5.9E-01
26	99th quantile (min of all trials)	2.7E-02	*3.2E-02*	3.9E-02	*2.4E-02*	0	1.2E-01
27	99th quantile (max of all trials)	6.6E-02	*8.3E-02*	5.8E-02	*3.7E-02*	0	6.8E-01
28	Envelope integral (mean of all trials)	3.6E+01	*1.5E+01*	4.6E+01	*3.1E+01*	0	6.5E-02
29	**Envelope integral (min of all trials)**	**2.9E+01**	***1.4E+01***	**4.0E+01**	***3.1E+01***	**1**	**3.9E-02**
30	Envelope integral (max of all trials)	4.4E+01	*2.4E+01*	5.3E+01	*3.3E+01*	0	2.2E-01
31	Env. integral*duration (mean of all trials)	2.3E+02	*2.0E+02*	2.8E+02	*3.5E+02*	0	4.2E-01
32	Env. integral*duration (min of all trials)	1.6E+02	*1.7E+02*	2.3E+02	*3.5E+02*	0	2.2E-01
33	Env. integral*duration (max of all trials)	2.9E+02	*2.3E+02*	3.3E+02	*3.7E+02*	0	6.1E-01

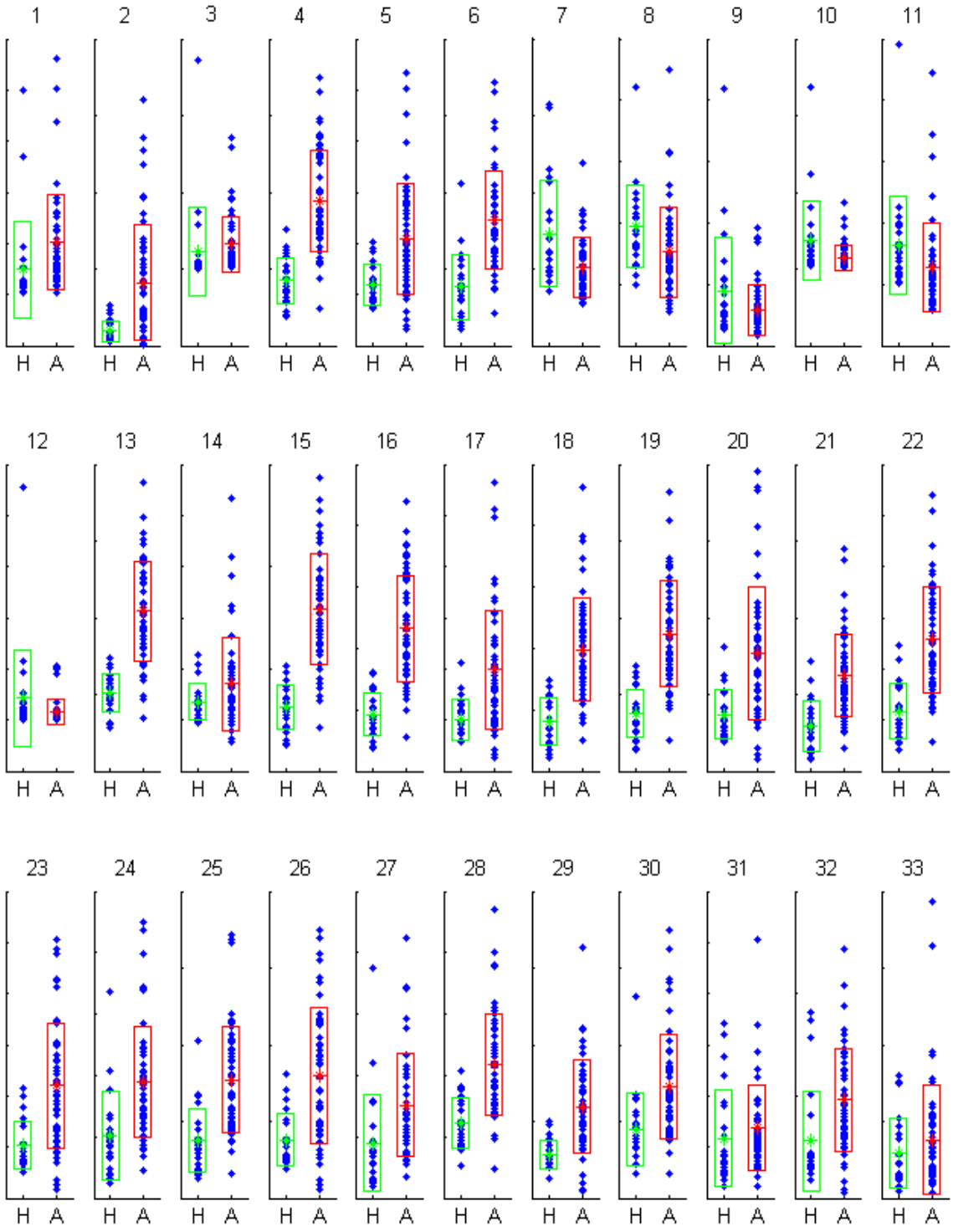


Figure 6.22: Distribution of selected 33 signal features for all 23 healthy (H), and 52 arthritic (A) subjects determined for all trials of all activities performed by the subjects.

Table 6.6: Statistical parameter average and standard deviation found for 23 healthy and 52 arthritic subjects for all trials of all activities performed by the subjects. The $H_0 = 1$ indicates a rejection of the null hypothesis (that samples are from population with equal means) at the 5% significance level.

Feature		Healthy		Arthritic		Ho	p
Nr	Name	avg	SD	avg	SD		
1	**Variance (mean of all trials)**	**2.5E-04**	***4.7E-04***	**5.2E-04**	***4.6E-04***	**1**	**2.6E-02**
2	**Variance (min of all trials)**	**1.9E-05**	***1.4E-05***	**8.2E-05**	***7.6E-05***	**1**	**2.8E-07**
3	Variance (max of all trials)	1.1E-03	*2.9E-03*	1.6E-03	*1.8E-03*	0	4.6E-01
4	**Signal mean (mean of all trials)**	**4.2E-03**	***1.5E-03***	**9.5E-03**	***3.3E-03***	**1**	**3.7E-14**
5	**Signal mean (min of all trials)**	**2.4E-03**	***8.0E-04***	**4.2E-03**	***2.2E-03***	**1**	**1.4E-06**
6	**Signal mean (max of all trials)**	**7.7E-03**	***4.2E-03***	**1.6E-02**	***6.4E-03***	**1**	**2.5E-09**
7	**Skewness (mean of all trials)**	**7.3E+00**	***3.5E+00***	**5.1E+00**	***2.0E+00***	**1**	**9.7E-03**
8	**Skewness (min of all trials)**	**2.9E+00**	***6.7E-01***	**2.5E+00**	***7.3E-01***	**1**	**1.8E-02**
9	Skewness (max of all trials)	1.8E+01	*1.7E+01*	1.2E+01	*8.3E+00*	0	1.0E-01
10	Kurtosis (mean of all trials)	1.8E+02	*2.6E+02*	7.3E+01	*8.1E+01*	0	5.8E-02
11	Kurtosis (min of all trials)	1.6E+01	*8.1E+00*	1.3E+01	*7.2E+00*	0	7.0E-02
12	Kurtosis (max of all trials)	8.6E+02	*1.9E+03*	3.2E+02	*5.2E+02*	0	1.9E-01
13	**Median (mean of all trials)**	**2.0E-03**	***4.9E-04***	**4.2E-03**	***1.3E-03***	**1**	**1.4E-15**
14	**Median (min of all trials)**	**1.4E-03**	***3.6E-04***	**1.7E-03**	***9.1E-04***	**1**	**2.0E-02**
15	**Median (max of all trials)**	**3.1E-03**	***1.1E-03***	**7.9E-03**	***2.7E-03***	**1**	**5.4E-17**
16	**90th quantile (mean of all trials)**	**9.2E-03**	***3.5E-03***	**2.3E-02**	***8.6E-03***	**1**	**2.4E-15**
17	**90th quantile (min of all trials)**	**5.0E-03**	***2.0E-03***	**9.9E-03**	***5.8E-03***	**1**	**1.1E-06**
18	**90th quantile (max of all trials)**	**1.6E-02**	***7.6E-03***	**4.0E-02**	***1.7E-02***	**1**	**3.1E-12**
19	**95th quantile (mean of all trials)**	**1.5E-02**	***6.3E-03***	**3.6E-02**	***1.4E-02***	**1**	**2.1E-13**
20	**95th quantile (min of all trials)**	**7.4E-03**	***3.2E-03***	**1.5E-02**	***8.7E-03***	**1**	**1.7E-07**
21	**95th quantile (max of all trials)**	**2.9E-02**	***1.7E-02***	**6.2E-02**	***2.7E-02***	**1**	**1.6E-08**
22	**97.5 quantile (mean of all trials)**	**2.3E-02**	***1.1E-02***	**5.1E-02**	***2.1E-02***	**1**	**5.9E-11**
23	**97.5 quantile (min of all trials)**	**1.0E-02**	***4.7E-03***	**2.2E-02**	***1.2E-02***	**1**	**7.7E-08**
24	**97.5 quantile (max of all trials)**	**5.1E-02**	***3.6E-02***	**9.5E-02**	***4.5E-02***	**1**	**3.6E-05**
25	**99th quantile (mean of all trials)**	**3.8E-02**	***2.1E-02***	**7.7E-02**	***3.5E-02***	**1**	**7.0E-08**
26	**99th quantile (min of all trials)**	**1.5E-02**	***6.8E-03***	**3.2E-02**	***1.8E-02***	**1**	**8.7E-08**
27	**99th quantile (max of all trials)**	**8.9E-02**	***7.9E-02***	**1.5E-01**	***8.4E-02***	**1**	**3.7E-03**
28	**Envelope integral (mean of all trials)**	**2.4E+01**	***8.1E+00***	**4.3E+01**	***1.7E+01***	**1**	**5.8E-09**
29	**Envelope integral (min of all trials)**	**1.2E+01**	***3.7E+00***	**2.4E+01**	***1.2E+01***	**1**	**5.4E-09**
30	**Envelope integral (max of all trials)**	**4.4E+01**	***2.4E+01***	**7.3E+01**	***3.4E+01***	**1**	**9.9E-05**
31	Env. integral*duration (mean of all trials)	1.2E+02	*9.5E+01*	1.4E+02	*8.3E+01*	0	3.9E-01
32	**Env. integral*duration (min of all trials)**	**2.8E+01**	***2.5E+01***	**4.8E+01**	***2.5E+01***	**1**	**2.2E-03**
33	Env. integral*duration (max of all trials)	2.9E+02	*2.3E+02*	3.8E+02	*3.6E+02*	0	2.1E-01

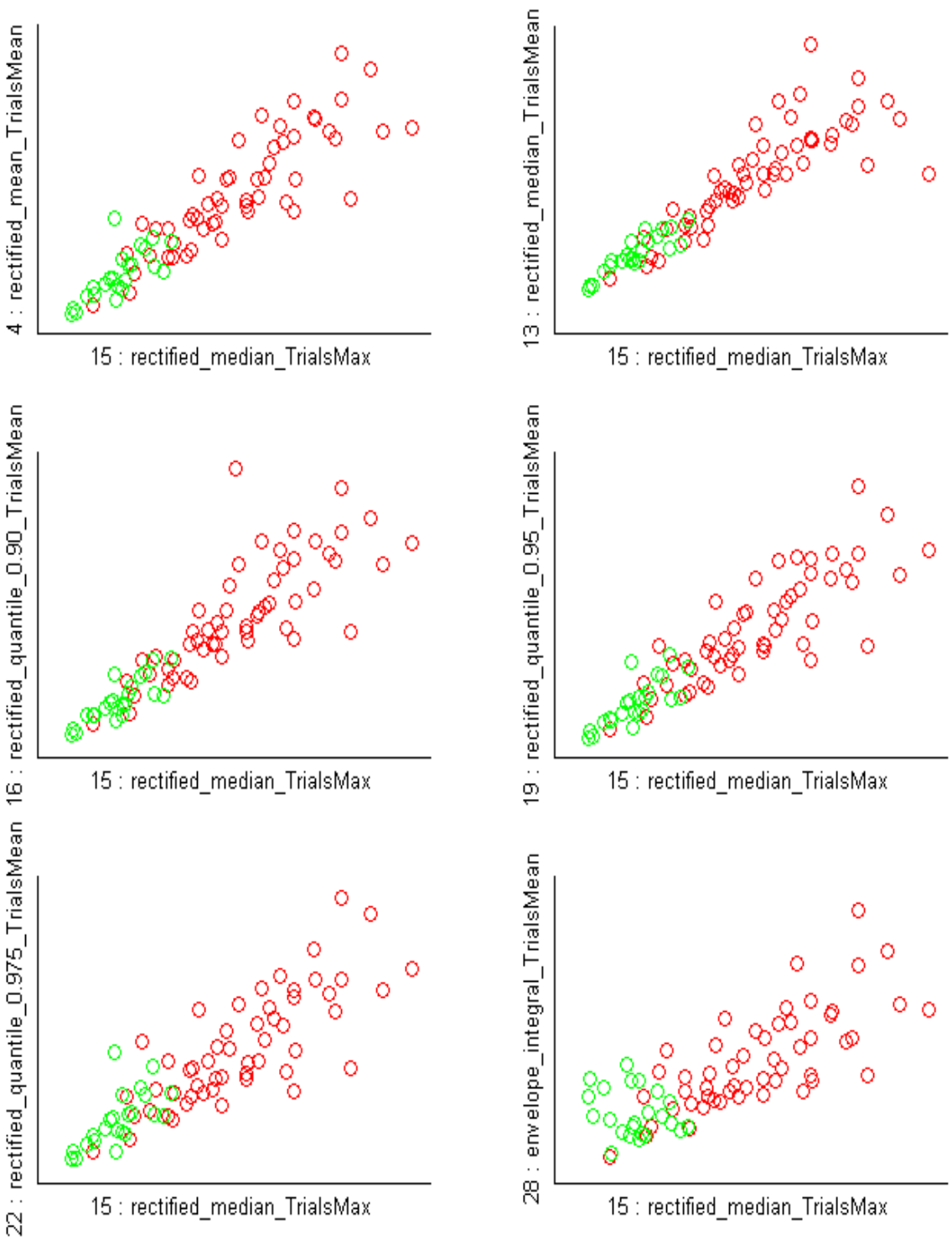
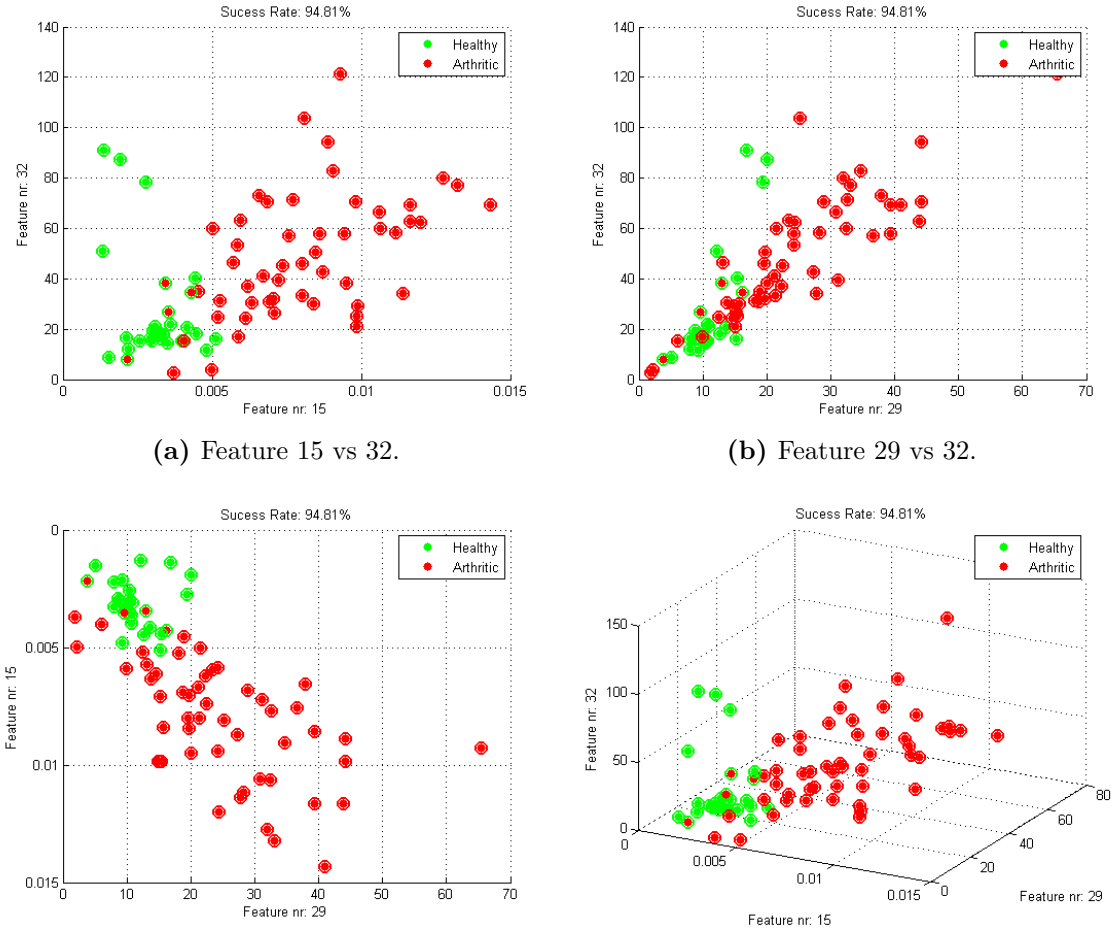


Figure 6.23: Distribution of selected 33 signal features for all 23 healthy (H), and 52 arthritic (A) subjects determined for all trials of all activities performed by the subjects.



(a) Feature 15 vs 32.

(b) Feature 29 vs 32.

(c) Feature 29 vs 15.

(d) 3D view.

Figure 6.24: Using features nr 15, 29 and 32 yielded the best classification rate of 94.81%. The color coded bullets (● and ●) show the members of the respective class, while the circles ○ and ○ show the classes assigned by the dichotomizer.

Chapter 7

Discussion

7.1 Kinematics

7.1.1 Patellofemoral and Tibiofemoral Kinematics

The trajectory of the center of the patella bone was considerably more consistent in the Total Knee Arthroplasty (TKA) group than in the two natural joint groups. When plotted on the unfolded articulating surface, the path resembled a straight line for resurfaced patella, while the natural bones revealed more variable medial and lateral translations during stair climbing (Figure 6.1). The variability seen for the normal knees hypothetically reflects the natural differences in the subjects' anatomy. In the TKA knees, the patella was sliding along the trochlear groove following the geometry of the components. This finding confirms that under in-vivo conditions the patella component does move as it was designed to. However, since the TKA designs have limited number component sizes, it is disputable how well they reproduce the patients' anatomy and to what extent the trajectory is altered post-operatively. Although the medial-lateral translation was not seen to be substantial in the healthy knees, it is difficult to estimate the effects of a more constrained pathway.

Andriacchi et al. investigated functional differences at the patellofemoral joint between two TKA designs, which differed primarily in the shape and curvature of the

femoral flange.[7] They found that during stair climbing, a group of subjects having the non-anatomic tracking of the patella had a higher than normal net quadriceps moment tending to flex the knee during late stance phase. The abnormal function occurred when the patella was tracking over the non-anatomic portion of the trochlea. These adverse effects were absent in the group of TKA subjects having more anatomic design of the trochlea. This is consistent with the findings of the current research work, as the quadriceps forces were higher in the TKA compared to the natural knees.

Another concerning fact was that the trajectory was located much more distally on the unfolded articulating surface in the TKA then in natural knees. This difference might partially be explained by the fact that the articulating surface of the TKA components, by itself, is different than the surface of the natural articular surface and hence the unfolded surfaces are inherently different. However, these differences should not be expected to be significant because the TKA component sizes are chosen to match the distal femur as closely as possible during the surgery. The difference quite possibly could be explained by the joint line elevation often resulting from the Total Knee Replacement (TKR) procedure. Elevation of the joint line, shifts the location of the patellofemoral interaction distally on the femur. This alteration may have an impact on the biomechanical boundary conditions and explain higher interactive forces experienced by the TKA subjects (see Section 6.2.7). König et al. recently reported that a 10 mm joint line elevation in revision TKA, affected primarily the patellofemoral joint and increased the contact forces by as much as 60% of the patients's body weight.[145]

For most of the subjects, the knee extension occurred in the middle of the stance phase, preceded and followed by a more stationary orientation the knee joint (Figure 6.2). This pattern can be explained by the subjects taking some time to assume a secure position after the initial contact with the stair. Once the foot was firmly supported on the stair, they quickly extended the knee to reach to the next stair. Once the other leg was placed on the next stair, the supporting knee remained in

extension, while the upper body leaned forward to shift the mass center onto the other leg. This explains the stationary knee flexion following the rapid extension.

Many TKA subjects experienced a small increase in knee flexion just before the rapid extension occurred (Figure 6.2). Andriacchi et al. noticed the same phenomenon in implanted knees during stair climbing.[7] This initial increase in flexion may helping the patients to accept the transfer of load to the supporting limb[7] and achieve better stability before the extension phase.

For both natural knee groups, the femur rotated internally with decreasing flexion (Figure 6.3), which is consistent with data previously reported in the literature.[9, 58, 73, 74, 128, 144, 158, 166] This pattern is commonly seen for well-functioning knees and may be attributed to the screw-home mechanism being engaged at the arc of terminal extension.[13, 73, 79, 96]

In the TKA group, however, the femoral axial rotation was more variable and no distinct pattern could be identified. The analyzed TKA was a mobile bearing design, which was designed to have a less constrained axial rotation pattern compared to fixed bearing implants. However, the femoral axial rotation data revealed that both contralateral and healthy knees experienced an average range of axial rotation of 12.3° and 10.5° respectively, while the TKA group achieved only 4.5° (Table 6.1). This difference cannot be explained only by the age of the TKA subjects, because the contralateral knee was studied within the same group of subjects.

The TKA knees also experienced reduced range of femoral abduction/adduction and much smaller variability then natural knees (Figure 6.3). Small standard deviation observed in the replaced knees could be related to the more uniform geometry of the TKA components compared to the natural knee joint. Similar to the patellar tracking, this data suggests that the tibiofemoral kinematics is driven by the geometrical features of the implant design, which is more uniform than the natural bone anatomy.

A similar relationship was observed in the patellar tilt - the TKA group revealed suprisingly consistent patterns (SD varied between 0.8-1.7° at different flexion

increments, compared to 0.9-4.5° seen for natural joints, see Table 6.2). It is assumed that this finding can be explained by the kinematic boundary conditions of the articulating surfaces of the implant components, which again drive the patella along the anterior femoral flange. The natural patella tilts according to patients shape of the trochlear groove, which varies between subjects, depending on height, weight and especially gender.

Patellar rotation, on the other hand, was the most variable among the TKA subjects (SD varied between 6.2-7.8° at different flexion increments, compared to 0.9-5.3 seen for natural joints, see Table 6.2). More variable results may be related to the dome shape of the patellar component allowing free patellar rotation. The articulating surface of natural patella consists of two concave facets divided by a vertical ridge oriented along the longitudinal axis.[78] The patellar facets are congruent with the femoral trochlea, which to some extent may limit patellar rotation.

The close relationship between the patellar and femoral flexion found in the current study is very consistent with previously reported data for deep knee bend.[4, 70, 98, 110, 115, 152, 155, 158, 163, 193, 224, 234] Once the data was normalized, it became evident that the patellar flexion increases nearly linearly with increasing knee flexion (Figure 6.5).

7.1.2 Patellofemoral contact

The patellofemoral contact location shifted proximally on the femur and distally on the patella, similar to previous in vivo[110, 158, 63] and in vitro[2, 50, 99, 108, 114, 176, 192, 216, 223] studies (see Section 2.2.3). At Toe Off the most probable contact area was located at the very edge of the articulating surface and the patella might conceivably be loosing contact with femur at this stage. This finding is possible because at Toe Off the knee is almost fully extended, and some authors suggested that patellofemoral interaction may be even entirely above the femoral trochlea.[1] This might be also explained by the fact that the weight of the upper body has already

been shifted to the opposite leg, the quadriceps relaxes as the leg transitions from stance to swing phase and the patella might naturally move away from the femur.

On the other hand, the resurfaced patella remained in contact for all subjects throughout the full motion cycle. This phenomenon might occur due to the contracture of the patellar ligament, or overall knee stiffness often following the surgery. However, it might actually be beneficial for the TKA components, reducing the risk of impact forces occurring when the two surfaces would engage abruptly. Komistek et al. have evaluated linear impulse forces associated with the patella separation occurring post-operatively and found impact forces of 78 to 213 N acting at the patellofemoral joint.[142] Since these forces occur rapidly they may induce fatigue of the polyethylene and contribute to the patellar component failure.

With respect to the surface of the patella, the contact distribution, remained more centrally located throughout the range of motion for TKA than for the natural knees, which is similar to data provided in the literature.[223, 192, 158] This central location of the contact area may be favourable because the center of the patellar component is thicker and distribution of the patellofemoral joint reaction (PFJR) at the thickest portion of the polyethylene may increase its longevity.

The size of the contact area is difficult to determine precisely because in natural joints, the contact pressure is distributed within the layer of the articular cartilage and depends on the relative orientation of the articulating surfaces, their cartilage thickness, and loading conditions within the knee. Under in-vitro conditions, the contact area is most frequently measured by means of a pressure sensitive film inserted between the articulating surfaces or by miniature pressure transducers implanted into the bone of a cadaver.[108, 117] The results, however, will inherently depend on the magnitude of loads applied during the experiment, and on the direction of that load, which applied under in vitro conditions may not reproduce the in vivo conditions accurately. More recently the contact areas were estimated in vivo using Magnetic Resonance Imaging (MRI).[109, 63] However, due to the length of time required for image acquisition, this technique cannot be used for dynamic activities, such as

stair climbing. Therefore, a static load is usually applied to the lower extremity, so that the subject contracts the quadriceps muscle to balance the load simulating dynamic conditions. The quality of recreating the dynamic conditions using this technique might also be debated. Therefore none of the currently available methods can determine the size of patellofemoral contact with precision, in vivo for dynamic activities.

Although this study cannot determine distribution of the patellofemoral contact precisely either, the contact location estimated based on the distance between the articulating surfaces does provide an approximation of the contact area (Figures 6.6 through 6.9). For the natural knee the contact area was larger at higher flexion (Foot Contact and 45° in Figure 6.6), at which time the interactive forces are also larger. These results were consistent with observations made by other researchers.[108, 99, 114, 171, 18, 198, 212, 21]

The results obtained for the resurfaced patella, indicate that the contact area is significantly reduced post operatively, at all flexion increments. Matsuda et al.[171] found that the reduction was significant for both dome shaped (Profix, Smith & Nephew, Memphis, TN) and conforming (Low-Contact Stress, DePuy, Warsaw, IN) patellar components. Similarly, Omori et al.[192] noticed that compared to intact knee, the contact area was significantly reduced after implanting the Genesis TKA (Smith & Nephew, Memphis, TN). Due to the reduced contact area, the stresses present at the polyethylene significantly increase and may impair the longevity of the patellar components.

7.2 Biomechanics of the Extensor Mechanism

7.2.1 Muscle Activation

For all groups, the activation of all of the quadriceps muscles was near zero at Foot Contact, but it increased quickly to achieve the maximum activation level just before

the midpoint of the activity and decreased thereafter (Figure 6.10). This pattern was expected because most of the extension of the knee joint occurred in the middle of the stance phase as well (Figure 6.2). The quadriceps muscles are the active elements of the extensor mechanism and therefore they were presumed to be the most active muscle group during stair climbing. Very similar electromyography (EMG) patterns were reported by Lin et al. for 10 normal young subjects ascending stairs.[159] They found that Vastus Medialis and Vastus Lateralis were the two most active muscles in the quadriceps group, which is consistent with the current study (Figure 6.11).

The gastrocnemii and biceps femoris play antagonistic role, and therefore it was not surprising to see significantly lower activation levels for these muscles. The contraction of one set of muscles accompanied by the relaxation of the antagonist muscles is called **reciprocal inhibition** and is controlled by the inhibitory interneurons of the spinal cord.[17] The interneurons are essential for proper execution of even simplest reflexes. The antagonistic muscles were not completely inactive, however, because their contraction is needed to stabilize the knee joint during extension.

In all three groups, the Gastrocnemii were activated at very low levels through most of the activity, but became more pronounced near Toe Off. Lin et al., found the exact same pattern in their study.[159] This can be explained by the fact that at Toe Off the body center of mass is already shifted to the contralateral foot and the ankle plantarflexors activate extensively to propel the body and to initiate the next stair climbing cycle.

Both elderly groups of subjects experienced significantly higher muscle activation levels than the group of young subjects; 1.6 to 2.0 times larger in the quadriceps muscles, and up to 3.6 times larger in the Biceps Femoris and Gastrocnemius Medialis (Figure 6.11). It can be inferred that climbing up the stairs required much more effort from the older subjects, especially while climbing on their leg having the replaced knee joint.

Substantially higher activation levels in the antagonistic muscle group also suggest that these subjects might have had difficulties with maintaining the stability. Recruitment of all muscles across the knee joint might reflect a cautious strategy employed to prevent falling from the stairs. This finding might be especially true for the TKA group, because both of their cruciate ligaments and menisci had been sacrificed during the surgery. The cruciate ligaments contain mechanosensitive axons, which provide the Central Nervous System (CNS) with the information about the angle, direction and velocity of movement of the knee joint.[17] Without this feedback, the proprioception may be impaired, which could explain more precautionary muscle recruitment seen in the TKA subjects.

These differences were also evident when compared the maximum muscle activation levels. The Quadriceps muscles were activated up to 86% of their total capacity in the TKA, up to 80% in the Contralateral but not more than 38% in the Healthy group (Figure 6.11), clearly demonstrating that climbing up the stairs was much more strenuous for the elderly population.

7.2.2 Muscle Forces

The muscle force patterns obtained based on the EMG signals confirmed that the highest forces were produced by the quadriceps muscle group. This finding was expected because the quadriceps muscle is the active element of the extensor mechanism delivering the contraction force needed for the extension of the knee. The force magnitudes were significantly higher in both of the elderly groups, especially the TKA group, than in the group of younger subjects. This confirms the observations made based on the activation levels (see Section 7.2.1), suggesting that climbing stairs was more difficult for elderly subjects.

The forces patterns in the antagonist muscles, in all groups, were at much lower levels than the quadriceps force. These results confirm the reciprocal inhibition mechanism controling the contraction and relaxation of muscles across the same joints.

However, as discussed in Section 5.3.2, the EMG signals provided qualitative data regarding muscle recruitment timing, but the force magnitudes could not be determined with precision. This limitation is especially apparent in the healthy group in the current study. The EMG-based quadriceps force magnitudes are rather underestimated. This underestimation was most likely due to very high activation achieved by these subjects during the maximum voluntary contraction (MVC), which has been used for normalization. Though MVC is currently the most reliable method recommended for normalization of the EMG signals (see discussion in Section 5.3.2), it worked well for the elderly subjects, but rather underestimated activation values for the younger subjects. For this reason, the inverse dynamics modeling, which does not rely on the EMG signals, was utilized in this study to provide more accurate prediction of the force magnitudes.

The muscle force profiles determined using the inverse dynamics analysis were very similar to those predicted using the EMG signals (Figure 6.16). This is a significant finding, confirming that the muscle recruitment timing predicted by the inverse dynamics modeling was nearly identical with that observed in vivo, revealed by the EMG data. The difference in the occurrence of the peak force predicted by the two methods was only 0.3 seconds on average.

As discussed above, the muscle force magnitudes determined by the inverse dynamics, are more accurate than those predicted from the EMG signals because they are obtained by the pseudoinverse algorithm based on the resultant joint torque (see Section 5.3.1). All muscle forces were highest in the TKA, folowed by the Contralateral and lowest in the healthy group. The TKA subjects experienced total quadriceps force of 3.63 times body weight (xBW), Contralateral 3.44xBW, while Healhty group 3.13xBW (Figure 7.1).

Due to the difficulty of determining the quadriceps force during dynamic activities, the relevant findings in the literature data seemed to be very limited. The joint reaction forces and torques were predicted more easily and were reported more often in the literature,[6, 8, 51, 159, 186, 210] but the forces in the individual muscles, or at

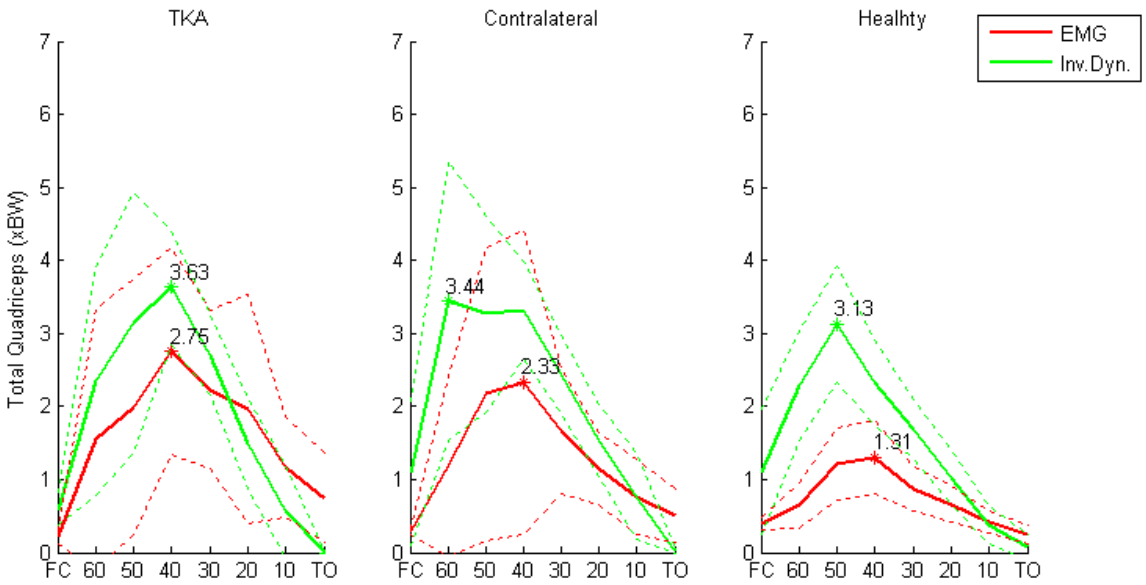


Figure 7.1: Total quadriceps force calculated based on the EMG signals (red) and using inverse dynamics (green). (Solid lines mark the average values, dashed lines mark ±SD. **FC**-*Foot Contact*, **TO**-*Toe Off.*)

least the total quadriceps force is very limited, especially for stair climbing activity. Reilly and Martens used mathematical modeling to predict the forces based on in vivo motion input for three healthy subjects climbing 20cm high stairs.[208] They reported total quadriceps force varying between 3.43xBW to 3.57xBW, which are only slightly larger than the total quadriceps force found in the current work. Some researchers attempted to simulate deep knee bend activity to study the quadriceps force under in vitro conditions, but their results vary cosiderably ranging from 0.98xBW[47] to 5.2xBW.[50]

The force profiles in the antagonistic muscles determined by the inverse dynamics were mostly zero throughout the activity for all three groups of subjects (Figure 6.15). This finding is not surprising, because from the theoretical point of view, only contraction of the agonistic muscles is necessary to provide the extension torque. The contraction of the antagonistic muscles created a flexion moment, which would cause the opposite action to what is required. This on one hand confirms that the mathematical model works correctly, but on the other hand it reveals the limitation

of using mathematical modeling to study musculoskeletal systems. As revealed by the EMG signals, under in vivo conditions there is a synergistic action of both knee extensor and flexor muscles. As discussed earlier this co-contraction is required to provide stability to the lower extremity and prevent falling. The EMG data revealed that these forces were not large (0.07-0.27xBW) and were probably kept at the minimum level, just enough to maintain balance. It can be concluded that neither of the two methods is perfect, but used concurrently they do provide better insight into the actual mechanics of the extensor mechanism.

Higher forces magnitudes were identified in the elderly groups and are certainly related to the higher stability required by older subjects. As discussed earlier this is especially true while supporting on the replaced joint, as the artificial knee is devoid of some of the natural mechanoreceptors affecting the patient's proprioception. This finding particularly explains the higher forces in the antagonistic muscles. The increase in the quadriceps muscle forces can be explained by the reduced moment arms of the extensor mechanism, found for both of the elderly groups (Figure 4.5). As discussed in Section 4.3, the decrease of the moment arm has to be compensated by the increase in the forces to create the same moment. Since the extensor mechanism moment arms were found to be the lowest in TKA group, the quadriceps forces were highest in this group. The effects of the extensor moment arm on the quadriceps and PFJR force were recently measured directly in vitro during dynamic closed chain activity simulating deep knee bend.[33] The authors compared a traditional TKA design with a long extensor moment arm (LMA) Scorpio TKA device, which had approximately 1cm longer extensor moment arm. The results confirmed that the quadriceps tension was lower in the design with higher moment arm. The patellofemoral compressive forces were also significantly reduced in the LMA design (8-18% lower at flexion greater than 50°).

Interestingly, the mathematical model indicated an increased activation of the gastrocnemii and biceps femoris muscles at the end of the stance phase, which has been also revealed by the EMG signals. This confirms that just before the Toe Off,

the ankle plantarflexors have to be activated to provide the initial propulsion of the body to initiate the next climbing cycle.

In summary, the muscle force analysis usign both EMG and inverse dynamics provided very important information about the in vivo performance of the extensor mechanism. The EMG data revealed the activation relationships between individual quadriceps muscles and their activation timing. EMG also indicated that the antagonistic muscles remain active, even though their action is not required to extend the knee. This increased activation was most likely due to impaired balancing of the knee often experienced by elderly subjects. This synergistic action was not revealed by the theoretical model based on inverse dynamics. On the other hand, the mathematical model provided more precise estimation of the individual muscle force magnitudes, and confirmed that the forces were indeed higher in the TKA and the Contralateral groups. The mechanical analysis also indicated relationship between the increased quadriceps forces and reduced moment arms of the extensor mechanism seen for these two groups compared with younger population.

7.3 Interactive Forces

From the implant design perspective, the most important information about knee biomechanics pertains to the joint interactive forces, as these are the forces that act directly on the prosthesis components. The load magnitude and direction is necessary to analyze the stress distribution within the components and to perform the failure mode and effects analysis. Therefore the goal of the current work was to also determine the tibiofemoral and patellofemoral joint interaction forces.

All of the interactive forces were highest in the TKA, followed by the Contralateral and lowest in the Healthy group (Figrure 6.2.7). The peak of the PFJR force was 15% and 14% higher in the TKA (3.67xBW) and Contralateral (3.63xBW) groups than in the Healthy group (3.19xBW). Tibiofemoral joint reaction was 7% and 5% higher in those two groups than in the control group. Similar increased forces were

seen in the patellar ligament force; 12% for the TKA and 6% for Contralateral groups compared with the Healthy subjects. All of these results confirm that the increased tension in the quadriceps muscles resulted in the increased joint reaction forces and patellar ligament tension. Consequently the performance of the entire extensor mechanism in the elderly and TKA subjects was impaired and climbing the stairs required more effort. The increase in the PFJR force may increase patellar complications such component loosening, increased wear, or cause anterior knee pain postoperatively. Similarly, high tibiofemoral forces may have similar adverse effects on the tibial components and impair the longevity of the prosthesis.

Recent technological advancements have led to the development of telemetric knee implants which provide the invaluable insight into the actual in vivo loads present at the tibiofemoral joint following TKA.[182, 91] Though there are only few subjects who have been implanted with these devices, the measurements obtained directly from these instrumented implants can be considered to be the most accurate data currently available.

D'Lima et al. reported results for one of the first telemetric implanted knees, generating results pertaining to knee loads during stair climbing.[60] They found that the tibiofemoral force was 1.9xBW on the sixth day after the surgery, and increased to 2.5xBW at 6 weeks post-operatively. Another TKA patient was evaluated by the same group 18 months postoperatively, and the force acting on the tibia was determined to be 3.59($\pm$0.20)xBW while climbing up the stairs.[184]

Later these same authors developed an improved telemetric TKA device capable of measuring all six components of tibial forces, which was received by an 83-year-old male individual.[59] Using this second generation device they determined that 3 months after the surgery, the peak total tibiofemoral force was 3.0($\pm$0.44)xBW during stair climbing.

A similar telemetric device was developed in Germany[101] and implanted into two male subjects; 63 and 71 years-old.[102] The results using this device revealed that the vertical components of the tibiofemoral force were 2.92($\pm$12)xBW and

Table 7.1: Comparison of the current results with the previous data reported in the literature for stair climbing activity.

Author	Publ. year	Method	Condition	Cohort	Age (years)		Post-Op time (months)	Tibiofemoral force (xBW)			
					avg	SD		avg	SD	min	max
Taylor et al.	2006	inv.dynamics	TKA	4	61.0		17.0	**5.38**	*0.35*	4.7	6.2
D'Lima et al.	2006	telemetry	TKA	1	80.0		1.5	**2.50**	*na*		
D'Lima et al.	2007	telemetry	TKA	1	83.0		3.0	**3.00**	*0.44*		
Muendermann et al.	2008	telemetry	TKA	1	81.0		18.0	**3.59**	*0.20*		
Heinlein et al.	2009	telemetry	TKA	1	63.0		10.0	**3.06**	*0.20*		
		telemetry	TKA	1	71.0		6.0	**2.92**	*0.12*		
Kutzner et al.	2010	telemetry	TKA	5	65.4	4.8	13.2	**3.16**	*0.30*	2.71	6.69
Current work	2011	inv.dyn.+EMG	TKA	12	73.6	7.1	17	**3.32**	*1.01*		5.51
		inv.dyn.+EMG	Healthy Elderly	4	71.8	7.7	na	**3.25**	*0.70*		4.08
		inv.dyn.+EMG	Healthy Young	4	30.8	3.0	na	**3.09**	*0.59*		3.94

3.06(±20)xBW for the two subjects, 6 and 10 months after surgery, respectively. Most recently the same group has published the in-vivo data obtained for 5 subjects (4 males, 1 female, 60-71 year-old), evaluated 7 to 22 months post-operatively.[150] This comprehensive study determined that during stair climbing the tibiofemoral forces averaged 3.16xBW.

Interestingly, the telemetry-based data reveals that the in-vivo forces increase during the first months after the surgery. The previous studies reported forces averaging 2.5xBW 6 weeks post-operatively,[60], 2.92xBW and 3.06 after 6 and 10 months, respectively[102], 3.16xBW after 13.2 months,[150] and 3.59xBW for a subject 18 months after surgery. The TKA subjects in the current study were evaluated on average 17 months post-operatively and therefore the average force of 3.32xBW agrees very well with the direct in vivo measurements (Table 7.1). Apart from the post-operative time, the force magnitudes may be affected by the differences in the shape of the articulating surface of the implant devices being investigated.

Another influencing factor may be the age of the subjects, because the average age of the cohort in the current study was 73.6 year old, while the subjects having telemetric knee (in Table 7.1) were 69.1 year old on average.

The instrumented TKA implants are currently the only devices offering access to experimentally derived in vivo loading conditions and have provided invaluable information about the tibiofemoral forces present during various daily activities. However, due to their invasive nature, these devices are only suitable to study the replaced knee joints. They cannot be used to evaluate patients suffering from other conditions, which do not qualify for TKA procedure. Additionally, the telemetry devices are capable of detecting only the tibiofemoral forces and there exists no implantable device that could measure the patellofemoral joint interaction forces in vivo.

The goal of the current work was to develop an non-invasive tools which could assist with the diagnosis of the knee joint. The methodology described in the current work has yielded results which concur with the telemtery-based data, but unlike telemetry, can be applied to both natural as well as TKA joints. Moreover, the described methods provided insight into the conditions of the biomechanics of the entire extensor mechanism. Current work offers better understanding of the forces in the individual muscles, and how they are transmitted by the patella to the patellar ligament and tibia. Also, the information about the loading conditions acting on the patella may contribute to designing improved patellar implant components. Lastly, the presented methods are cost effective and relay on commercially available technologies.

7.4 Vibroarthrography

The vibration signals have been collected to evaluate their potential application to diagnose the articular cartilage condition. According to the hypothesis stated in Section 1.1, the vibrations should increase as the cartilage degenerates. To prove this

concept, the signals have been collected from a group of subjects with osteoarthritis and a control group of healthy individuals (see Section 5.4).

Initially the vibration data was collected for 13 healthy and 13 arthritic knee joints. The best results for this set of subjects was achieved using two signal features; mean and standard deviation (Figure 6.19). The initial pattern classification yielded encouraging results and 81% of the signals were classified correctly (Figure 6.20). This initial analysis confirmed the hypothesis, because in general the vibrations had higher variation in the arthritic group (Figure 5.40). Recently Rangayyan et al. also reported that larger variability was observed in abnormal knee joints.[205]

The differences can be also heard when the signals are converted to audible forms (compare the sound in Figures 5.38 and 5.39). These distinct sound differences may confirm the early observations made by Blodgett[25] and Walters,[235] who could hear more grating and cracking knee joint sounds being emitted by older subjects, whos articular cartilage most probably deteriorated with age.

In the course of this study, more subjects were recruited and eventually a signals were collected for 23 healthy and 52 arthritic subjects performing 5 different activities. Initially only signals from the squatting exercise were analyzed, but further analysis revealed that the more activities are included in the feature extraction, the better discrimination could be achieved (compare Tables 6.5 and 6.6). Analysis of all the 75 samples confirmed that the variance is indeed significantly higher in the arthritic group, but other signal features yielded even better discrimination. A number of signal parameter combinations has been evaluated and eventually sets of features yielding accuracy up to **96.1%** have been identified. Such high success rate is very promissing and confirms that the vibration data could be potentially used for diagnostic purposes.

Krishnan and Rangayyan also studied knee vibroarthrographic signals for screening purposes.[147] They used one accelerometer attached at the middle of the patella and collected signals for 19 healthy and 18 pathologic knee joints during flexion-extension exercise. They decomposed the signals using wavelet packets and matching pursuit methods and computed the signal features based on energy and frequency

Table 7.2: Comparison of the current vibration classification results with the data reported in the literature.

Author	Publ. year	Transducer	Cohort		Activity	Classification method	Accuracy
			Normal	Abnormal			
Krishnan and Rangayyan	2000	accelerometer	19	18	flexion-extension	stepwise logistic regression analysis	83.8%
Rangayyan and Wu	2008	accelerometer	51	38	flexion-extension	Fisher's linear discriminant analysis	85.9%
Kim et al.	2009	electro-stetoscope	20	11	flexion-extension	back-propagation neural network	91.4%
Gajre et al.	2006	tetra-polar impedance plethysmography	8	10	flexion-extension	feed forward neural network	85.2%
Current work	2011	accelerometer	23	52	DKB, Chair Rise, Stair Climb, Stair Descent, Gait, Flexion-Extension	Bayesian minimum-error-rate classifier	96.1%

parameters. The analysis allowed them to classify the signals with 83.8% accuracy (Table 7.2).

Recently Rangayyan and Wu presented more extensive work evaluating vibroarthrography (VAG) samples collected for 51 healthy and 38 abnormal knee joints.[205] The abnormal conditions included various pathologies; patella chondromalacia of different grades, meniscal tears, tibial chondromalacia and ACL injuries. They normalized the VAG signals so that the amplitude ranged between 0 and 1, and then calculated a number of statistical parameters; mean, SD, skewness, kurtosis, entropy, as well as the "'form factor"' representing the variability of the signal. In the current study, the skewness and kurtosis were found to be the parameters providing the lowest discrimination (Table 7.2). Using the Fisher's linear discriminant analysis, they were able to classify normal vs abnormal cases with 75.6% accuracy. They achieved better classification of 85.9% when the conditions were narrowed down to discrimiate only between normal and the 20 patella chondromalacia cases.

Kim et al. studied knee joint sounds by means of an electro-stetoscope.[138] They gathered data for 20 non-symptomatic subjects and 11 patients with diagnosed

degenerative arthritis performing flexion-extension activity. The authors obtained features from the time-frequency distribution of VAG signals using segmentation by dynamic time warping. Next, they used back-propagation neural network for classification and reported 91.4% accuracy. Such high classification accuracy is very impressive, considering that samples from only 11 degenerative patients were available for analysis.

Gajre et al. proposed using electrical impedance signals for non-invasive diagnosis of osteoarthritic knees.[80] They collected the data around the knee by tetra-polar impedance plethysmography for 8 normal and 10 osteoarthritic subjects. They used variance and root mean square values as temporal features and energy band of 0-5Hz as frequency domain feature. A trained artificial multilayer feed forward neural network provided accuracy of 85.19% based on the knee-swing data.

Though methods using transducers other than accelerometers have been proposed and reported encouraging results,[80, 138] these findings were based on rather limited number of cases and await further investigation. There are no studies comparing the quality of the signals obtained using various transducers for the same subjects, therefore it is difficult to state with confidence which method is more reliable. Past research has unambiguously demonstrated the superiority of using accelerometers compared to microphones.[42, 43, 82, 125, 135, 179, 226] The results in the current work have been obtained using accelerometers and to the best of the author's knowledge, have yielded higher success rate than any other study reported in the literature to date. Current study also evaluated more arthritic subjects than the previous studies.

7.5 Summary

This is the first study to incorporate multiple facets of mechanics, under in vivo conditions to assess the mechanics of implanted and non implanted knees. Also, the non implanted knees pertained to both the normal and contralateral, arthritically

diseased group. This study revealed that an overall mechanics analysis, such as the one discussed in this study, may lead to a possible diagnostic methodology that could assist the surgeon in diagnosing specific clinical findings. The results from these multiple facets of mechanics correlated quite well and often supported findings derived specifically from one of the methodologies. The results from this study revealed important in vivo data that could also be used for future implant design and mechanical and theoretical testing of existing and future knee implant designs.

Chapter 8

Conclusions

The presented study has investigated and evaluated the three-dimensional (3D) mechanics, most specifically kinematics and kinetics of the knee joint, as well as the extensor mechanism biomechanics under in-vivo, dynamic, weight bearing conditions for 12 Total Knee Arthroplasty (TKA), 4 elderly and 4 young healthy subjects. The analysis revealed a number of differences between the TKA and natural, as well as between the elderly and young knee joints. To the best of the author's knowledge it is the first study to reveal biomechanical differences between young, elderly and replaced knees.

The analyses revealed that the extensor mechanism moment arms are decreased in elderly population, which is most likely the effect of aging and reduced posterior femoral rollback. More specifically, this study revealed that the moment arms are even more adversely affected after Total Knee Replacement (TKR). Reduced moment arms directly leads to higher muscle and interactive forces, leading to the patient to induce a greater effort to perform given tasks.

Indeed, as further analyses unfolded, it became evident that the extensor mechanism efficiency was impaired in elderly and especially TKA subjects. Higher forces experienced by the quadriceps muscle in these two groups led to higher forces present at the patellofemoral and tibiofemoral joints. These findings imply that

ascending the stairs not only required more effort from these subjects, but may potentially cause pain, problems with balance, and in case of replaced knees could accelerate the wear of the implant components.

The electromyography (EMG) data provided insight into the in vivo force patterns of individual muscles and demonstrated the synergistic action of agonist and antagonist muscles. This phenomenon could not be revealed by the inverse dynamics. On the other hand, using inverse dynamics it was possible to determine the muscle force magnitudes more precisely than based solely on the EMG signals. These observations confirm the hypothesis of this work that simultaneous application of these two methods provides better insight into the biomechanical conditions of the knee joint. The presented methodology may be used in the future as non-invasive evaluation tools leading to enhanced diagnosis of the knee disorders.

It should also be emphasized that the current work demonstrated a complete evaluation of the 3D biomechanics of both TKA and natural joints under in vivo, dynamic and weight-bearing conditions, which has not been previously derived. All of the presented methods are non-invasive, and could be used routinely during clinical evaluations, as they relay on commercially available technologies. Having such comprehensive information on a routine basis may also reveal certain musculoskeletal disorders at an earlier stage, when they can still be addressed by less invasive treatment.

Additionally, the presented work has investigated the vibrations emitted by the healthy and arthritic knee joints for their potential application for non-invasive assessment of the articular cartilage condition. A number of vibration signal features have been evaluated for their effectiveness in pattern recognition. The classification algorithm based on Bayesian decision theorem has yielded very satisfactory results with 96.1% success rate. These results ecourage farther research, which could be focused on determining earlier stages of arthritis, before they become symptomatic.

Though further research is certainly required, it is the author's hope that the proposed methods will in the future become available as screening tools benefiting

both patients and physicians, enabling them to diagnose and treat the causes, rather than the effects of musculoskeletal disorders.

8.1 Clinical significance

The methodology presented and applied in the current work carries a number of potential clinical applications. Comprehensive information about 3D kinematics, kinetics and articular cartilage conditions would certainly enhance the current musculoskeletal diagnostic capabilities.

The importance of having access to both kinematic and kinetic conditions of the knee was demonstrated in the current work. It was found that both elderly and TKA subjects put more effort then young participants to perform the same task. The information about increased muscle forces was provided by the kinetic analysis based on the EMG and inverse dynamics. However, this information by itself did not explain *why* the muscles experienced increased forces. It was the 3D kinematic evaluation that provided the answers, as it was found that due to the reduced posterior femoral rollback, the extensor mechanism moment arms were smaller in both of the elderly groups, which caused the increased extensor mechanism forces.

The analysis also revealed that the interactive forces were increased which might cause pain if the stresses exceeded the pain threshold. In the current work, only subjects with well functioning knee joints were recruited, but it can be hypothesized that a patient suffering from anterior knee pain might be seeking medical treatment. The anterior knee pain syndrome is often very non-specific and accurate diagnosis may be challenging. The methodology presented in this work could help evaluate the condition of such hypothetical patient, and indicate more precise treatment options.

The significance of the presented work pertaining to assessment of articular cartilage condition using accelerometers is multi-factorial. First, since the articular cartilage is devoid of nerve cells, therefore early stages of arthritis are asymptomatic and often remain undiagnosed until severe degeneration is present. However, the early

changes in the structure of the cartilage seem to affect the vibration characteristics and, therefore, may be detected at an earlier stage, permitting undertaking of a relevant non-invasive treatment. Also, as a low-cost technique, the vibroarthrography could be used routinely during visits in a clinic.

Secondly, a significant number of patients selected for arthroscopy due to symptoms in the patellofemoral joint is found to be free of any abnormality in the cartilage condition.[162] Arthroscopy, therefore may impose unnecessary risks on the patient and high costs to the healthcare system. A non-invasive screening tool utilizing vibroarthrography could assist the physician in selecting candidates for arthroscopy more accurately.

Finally, other preliminary studies revealed that the vibration patterns observed for the implanted knees may indicate the wear of the components.[127] It is also hypothesized that the vibration response changes with increasing osteointegration of the implant components. Therefore, it may be possible to monitor the process of bone ingrowth or to detect occurrence of implant loosening. Although, most research is currently focused on the knee joint, the findings can be also applicable to other joints, such as hip, shoulder or ankle.

The methodology described in the current work might assist with the evaluation of some of the following abnormal conditions:

1. kinematic evaluation:
    (a) patellar subluxation,
    (b) the patellofemoral malalignment and dynamic tracking problems,
    (c) the effects of the corrective procedure for tracking problems (such as a lateral retinacular release),
    (d) patellar clunk syndrome ('smoothness' of the entering of the patella into the trochlear groove)
    (e) occurrence of patellar subluxation,
    (f) occurrence of patellofemoral separation,

2. kinetic and EMG evaluation:
    (a) muscle atrophy,
    (b) abnormal muscle force distribution (excessive pull to one side),
    (c) increased muscle or interactive force,
    (d) neuromuscular abnormalities (muscle spasms, hyperreflexia, etc.)
    (e) the efficacy of certain drugs (such as skeletal muscle relaxants),
    (f) monitoring the effectiveness of physical therapy,
3. vibroarthrographic evaluation:
    (a) natural joints:
        i. patellar chondromalacia,
        ii. osteoarthritis at early stage,
        iii. meniscus tear,
        iv. ligament tear,
    (b) artificial joints:
        i. the loosening of the implant components,
        ii. implant component wear,
        iii. patellar clunk syndrome,
        iv. the level of osteointegration of the implant components postoperatievely,
        v. presence of loose particles (e.g. from the bone cement).

Bibliography

Bibliography

[1] Aglietti P, Insall J, Walker P, Trent P, A new patella prosthesis, in: *Clin Orthop*, 1975;107:175–187. 17, 153

[2] Ahmed A, Burke D, Hyder A, Force analysis of the patellar mechanism, in: *Journal of Orthopaedic Research*, 1987;5:69–85. 15, 22, 153

[3] Ahmed A, Duncan N, Tanzer M, In vitro measurement of the tracking pattern of the human patella, in: *Journal of biomechanical engineering*, 1999;121:222. 10

[4] Ahmed AM, Duncan NA, Tanzer M, In Vitro Measurement of the Tracking Pattern of the Human Patella, in: *Journal of Biomechanical Engineering*, 1999; 121:222. 153

[5] Anderson M, Becker D, Kieckbusch T, Patellofemoral complications after posterior-stabilized total knee arthroplasty: A comparison of 2 different implant designs, in: *The Journal of Arthroplasty*, 2002;17:422–426. 2

[6] Andriacchi T, Andersson G, Fermier R, Stern D, Galante J, A study of lower-limb mechanics during stair-climbing, in: *The Journal of Bone and Joint Surgery*, 1980;62:749. 158

[7] Andriacchi T, Yoder D, Conley A, Rosenberg A, Sum J, Galante J, Patellofemoral design influences function following total knee arthroplasty* 1, in: *The Journal of arthroplasty*, 1997;12:243–249, ISSN 0883-5403. 151, 152

[8] Andriacchi TP, Galante JO, Fermier RW, The influence of total knee-replacement design on walking and stair-climbing, in: *J Bone Joint Surg Am*, 1982;64:1328–1335, URL `http://www.ejbjs.org`. 158

[9] Asano T, Akagi M, Tanaka K, Tamura J, Nakamura T, In vivo three-dimensional knee kinematics using a biplanar image-matching technique, in: *Clinical Orthopaedics and Related Research*, 2001;388:157–166. 36, 152

[10] Baker R, ISB recommendation on definition of joint coordinate systems for the reporting of human joint motionpart I: ankle, hip and spine, in: *Journal of Biomechanics*, 2003;36:300–302. 8

[11] Baltzopoulos V, A videofluoroscopy method for optical distortion correction and measurement of knee-joint kinematics, in: *Clinical Biomechanics*, 1995; 10:85–92. 42

[12] Bandi W, Brennwald J, The significance of femoro-patellar pressure in the pathogenesis and treatment of chondromalacia patellae and femoro-patellar arthrosis, in: *The knee joint New York: American Elesevier Publishing*, 1974; :63–68. 48

[13] Barnett C, Locking at the knee joint, in: *Journal of Anatomy*, 1953;87:91–95. 152

[14] Barrack R, Wolfe M, Patellar resurfacing in total knee arthroplasty, in: *Journal of the American Academy of Orthopaedic Surgeons*, 2000;8:75. 18

[15] Basmajian J, De Luca C, *Muscles Alive: Their Functions Revealed by Electromyography*, Williams & Wilkins, 5th ed., 1985, ISBN 9780683004144. 81

[16] Bayley J, Scott R, Further observations on metal-backed patellar component failure, in: *Clinical Orthopaedics and Related Research*, 1988;236:82–87. 2

[17] Bear M, Connors B, Paradiso M, *Neuroscience: exploring the brain*, Lippincott Williams & Wilkins, 2001, ISBN 0683305964. 156, 157

[18] Benjamin J, Szivek J, Hammond A, Kubchandhani Z, Matthews Jr A, Anderson P, Contact areas and pressures between native patellas and prosthetic femoral components., in: *The Journal of arthroplasty*, 1998;13:693. 17, 27, 155

[19] Benoit D, Lamontagne M, Cerulli G, Liti A, The clinical significance of electromyography normalisation techniques in subjects with anterior cruciate ligament injury during treadmill walking, in: *Gait & posture*, 2003;18:56–63. 86

[20] Berger R, Crossett L, Jacobs J, Rubash H, Malrotation Causing Patellofemoral Complications After Total Knee Arthroplasty., in: *Clinical Orthopaedics and Related Research*, 1998;356:144. 2

[21] Besier T, Draper C, Gold G, Beaupré G, Delp S, Patellofemoral joint contact area increases with knee flexion and weight-bearing, in: *Journal of Orthopaedic Research*, 2005;23:345–350. 17, 155

[22] Bigland B, Lippold O, Relationship between force, velocity and integrated electrical activity in human muscle, in: *J Physiol (Lond)*, 1954;123:214–224. 92

[23] Bishop R, Denham R, A note on the ratio between tensions in the quadriceps tendon and infrapatellar ligament, in: *Eng Med*, 1977;6:53–54. 22

[24] Blankevoort L, Huiskes R, Ligament-bone interaction in a three-dimensional model of the knee, in: *J Biomech Eng*, 1991;113:263–9. 74

[25] Blodgett W, Auscultation of the knee joint, in: *Boston Med Surg J*, 1902; 146:63–66. 28, 98, 100, 103, 165

[26] Bolgla L, Uhl T, Reliability of electromyographic normalization methods for evaluating the hip musculature., in: *Journal of electromyography and*

kinesiology: official journal of the International Society of Electrophysiological Kinesiology, 2007;17:102. 86

[27] Bonnin M, *Osteoarthrisis of the Knee*, Springer France Editions, 2008. 18

[28] Bourne R, Rorabeck C, Vaz M, Kramer J, Hardie R, Robertson D, Resurfacing versus not resurfacing the patella during total knee replacement, in: *Clinical orthopaedics and related research*, 1995;321:156. 18

[29] Boyd A, Ewald F, Thomas W, Poss R, Sledge C, Long-term complications after total knee arthroplasty with or without resurfacing of the patella, in: *J Bone Joint Surg Am*, 1993;75:674–681, URL `http://www.ejbjs.org/cgi/content/abstract/75/5/674`. 2

[30] Brenner B, Eisenberg E, Rate of force generation in muscle: correlation with actomyosin ATPase activity in solution, in: *Proceedings of the National Academy of Sciences of the United States of America*, 1986;83:3542. 92

[31] Brooke R, The treatment of fractured patella by excision. A study of morphology and function, in: *Br J Surg*, 1937;24:733–747. 5

[32] Brown I, Loeb G, Measured and modeled properties of mammalian skeletal muscle: IV. Dynamics of activation and deactivation, in: *Journal of muscle research and cell motility*, 2000;21:33–47. 91

[33] Browne C, Hermida J, Bergula A, Colwell C, et al., Patellofemoral forces after total knee arthroplasty: effect of extensor moment arm, in: *The Knee*, 2005; 12:81–88, ISSN 0968-0160. 160

[34] Buff H, Jones L, Hungerford D, Experimental determination of forces transmitted through the patello-femoral joint., in: *Journal of biomechanics*, 1988;21:17. 22

[35] Bull A, Katchburian M, Shih Y, Amis A, Standardisation of the description of patellofemoral motion and comparison between different techniques, in: *Knee Surgery, Sports Traumatology, Arthroscopy*, 2002;10:184–193. 8

[36] Burden A, Bartlett R, Normalisation of EMG amplitude: an evaluation and comparison of old and new methods, in: *Medical engineering & physics*, 1999; 21:247–257. 86

[37] Burnett R, Bourne R, Indications for patellar resurfacing in total knee arthroplasty, in: *The Journal of Bone and Joint Surgery*, 2003;85:728. 18

[38] Cameron H, Huffer B, Cameron G, Anteromedial displacement of the tibial tubercle for patellofemoral arthralgia., in: *Canadian journal of surgery Journal canadien de chirurgie*, 1986;29:456. 49

[39] Cates H, Komistek R, Mahfouz M, Schmidt M, Anderle M, In vivo comparison of knee kinematics for subjects having either a posterior stabilized or cruciate retaining high-flexion total knee arthroplasty, in: *The Journal of Arthroplasty*, 2008;23:1057–1067. 24

[40] Cavanagh P, Komi P, Electromechanical delay in human skeletal muscle under concentric and eccentric contractions, in: *European journal of applied physiology and occupational physiology*, 1979;42:159–163. 91

[41] Chew J, Stewart N, Hanssen A, Luo Z, Rand J, An K, Differences in patellar tracking and knee kinematics among three different total knee designs, in: *Clinical orthopaedics and related research*, 1997;345:87. 10, 12, 15

[42] Christensen L, Physics and the sounds produced by the temporomandibular joints. Part I., in: *J Oral Rehabil*, 1992;19:471–83. 30, 167

[43] Christensen L, Physics and the sounds produced by the temporomandibular joints. Part II., in: *J Oral Rehabil*, 1992;19:615–617. 30, 31, 167

[44] Christensen L, Donegan S, McKay D, Temporomandibular joint vibration analysis in a sample of non-patients., in: *Cranio*, 1992;10:35–41. 30

[45] Chu M, Gradisar I, Mostardi R, A noninvasive electroacoustical evaluation technique of cartilage damage in pathological knee joints, in: *Medical and Biological Engineering and Computing*, 1978;16:437–442. 29, 31

[46] Chu M, Gradisar I, Railey M, Bowling G, Detection of knee joint diseases using acoustical pattern recognition technique., in: *J Biomech*, 1976;9:111–4. 29

[47] Churchill D, Incavo S, Johnson C, Beynnon B, The influence of femoral rollback on patellofemoral contact loads in total knee arthroplasty* 1, in: *The Journal of Arthroplasty*, 2001;16:909–918, ISSN 0883-5403. 159

[48] Clayton ML, Thirupathi R, Patellar complications after total condylar arthroplasty, in: *Clinical Orthopaedics and Related Research*, 1982;170:152–155. 2

[49] Close R, Dynamic properties of mammalian skeletal muscles, in: *Physiological Reviews*, 1972;52:129. 94

[50] Cohen Z, Roglic H, Grelsamer R, Henry J, Levine W, Mow V, Ateshian G, Patellofemoral stresses during open and closed kinetic chain exercises, in: *The American Journal of Sports Medicine*, 2001;29:480. 20, 153, 159

[51] Costigan P, Deluzio K, Wyss U, Knee and hip kinetics during normal stair climbing, in: *Gait & posture*, 2002;16:31–37, ISSN 0966-6362. 158

[52] Crowninshield R, Brand R, A physiologically based criterion of muscle force prediction in locomotion, in: *Journal of Biomechanics*, 1981;14:793–801. 80

[53] De Luca C, The use of surface electromyography in biomechanics, in: *Journal of Applied Biomechanics*, 1997;13:135–163. 37, 52, 81, 96

[54] Dennis D, Patellofemoral complications in total knee arthroplasty, in: *Am J Knee Surg*, 1992;5:156–166. 2

[55] Dennis D, Komistek R, Mahfouz M, Haas B, Stiehl J, Conventry Award Paper: Multicenter Determination of In Vivo Kinematics After Total Knee Arthroplasty, in: *Clinical orthopaedics and related research*, 2003;416:37. 46

[56] Dennis DA, Komistek RD, Colwell Jr CE, Ranawat CS, Scott RD, Thornhill TS, Lapp MAB, In vivo anteroposterior femorotibial translation of total knee arthroplasty: a multicenter analysis, in: *Clinical Orthopaedics and Related Research*, 1998;356:47–57. 24, 56

[57] Dennis DA, Komistek RD, Hoff WA, Gabriel SM, In vivo knee kinematics derived using an inverse perspective technique, in: *Clinical Orthopaedics and Related Research*, 1996;331:107–117. 56

[58] Dennis DA, Mahfouz MR, Komistek RD, Hoff W, In vivo determination of normal and anterior cruciate ligament-deficient knee kinematics, in: *Journal of Biomechanics*, 2005;38:241–253. 152

[59] D'Lima D, Patil S, Steklov N, Chien S, Colwell Jr C, In vivo knee moments and shear after total knee arthroplasty, in: *Journal of biomechanics*, 2007;40:S11–S17, ISSN 0021-9290. 162

[60] D'Lima D, Patil S, Steklov N, Slamin J, Colwell C, et al., Tibial forces measured in vivo after total knee arthroplasty, in: *The Journal of arthroplasty*, 2006; 21:255–262, ISSN 0883-5403. 81, 162, 163

[61] Doolittle KH, Turner RH, Patellofemoral problems following total knee arthroplasty, in: *Orthopaedic review*, 1988;17:696–702. 2

[62] Duda R, Hart P, Stork D, Pattern classification 2nd, in: *2nd Edition New York*, 2001;. 100, 136

[63] von Eisenhart-Rothe R, Siebert M, Bringmann C, Vogl T, Englmeier K, Graichen H, A new in vivo technique for determination of 3D kinematics and contact areas of the patello-femoral and tibio-femoral joint, in: *Journal of biomechanics*, 2004;37:927–934. 15, 153, 154

[64] Ellis M, Seedhom B, Wright V, Dowson D, An evaluation of the ratio between the tensions along the quadriceps tendon and the patellar ligament, in: *Eng Med*, 1980;9:189–194. 22

[65] Erb K, Über die Möglichkeit der Registrierung von Gelenkgeräuschen, in: *Langenbeck's Archives of Surgery*, 1933;241:237–245. 28, 29

[66] Ezzet K, Hershey A, D'Lima D, Irby S, Kaufman K, Colwell C, Patellar tracking in total knee arthroplasty Inset versus onset design, in: *The Journal of arthroplasty*, 2001;16:838–843. 10, 12, 15

[67] Fantozzi S, Leardini A, Banks S, Marcacci M, Giannini S, Catani F, Dynamic in-vivo tibio-femoral and bearing motions in mobile bearing knee arthroplasty, in: *Knee Surgery, Sports Traumatology, Arthroscopy*, 2004;12:144–151. 36

[68] Feller J, Bartlett R, Lang D, Patellar resurfacing versus retention in total knee arthroplasty, in: *The Journal of Bone and Joint Surgery-British Volume*, 1996; 78:226–228. 18

[69] Fellows R, Hill N, Gill H, MacIntyre N, Harrison M, Ellis R, Wilson D, Magnetic resonance imaging for in vivo assessment of three-dimensional patellar tracking, in: *Journal of biomechanics*, 2005;38:1643–1652. 10, 12, 15

[70] Fellows RA, Hill NA, Gill HS, MacIntyre NJ, Harrison MM, Ellis RE, Wilson DR, Magnetic resonance imaging for in vivo assessment of three-dimensional patellar tracking, in: *Journal of Biomechanics*, 2005;38:1643–1652. 153

[71] Figgie HE, Goldberg VM, Heiple KG, Moller HS, Gordon NH, The influence of tibial-patellofemoral location on function of the knee in patients with the

posterior stabilized condylar knee prosthesis, in: *J Bone Joint Surg Am*, 1986; 68:1035–1040, URL http://www.ejbjs.org/cgi/content/abstract/68/7/1035. 2

[72] Fischer H, Johnson E, Analysis of sounds from normal and pathologic knee joints., in: *Arch Phys Med Rehabil*, 1961;42:233–40. 29

[73] Freeman MAR, Pinskerova V, The movement of the knee studied by magnetic resonance imaging, in: *Clinical Orthopaedics and Related Research*, 2003; 410:35–43. 152

[74] Freeman MAR, Pinskerova V, The movement of the normal tibio-femoral joint, in: *Journal of Biomechanics*, 2005;38:197–208. 46, 152

[75] Fujikawa K, Seedhom B, Wright V, Biomechanics of the patello-femoral joint. Part I: A study of the contact and the congruity of the patello-femoral compartment and movement of the patella., in: *Engineering in medicine*, 1983; 12:3. 12

[76] Fukunaga T, Roy R, Shellock F, Hodgson J, Day M, Lee P, Kwong-Fu H, Edgerton V, Physiological cross-sectional area of human leg muscles based on mri, in: *Journal of Orthopaedic Research*, 1992;10:926–934. 95

[77] Fulkerson J, Anteromedialization of the tibial tuberosity for patellofemoral malalignment, in: *Clinical Orthopaedics and Related Research*, 1983;177:176. 48

[78] Fulkerson J, Hungerford D, *Disorders of the patellofemoral joint*, 2nd ed., 1990. 1, 6, 22, 36, 153

[79] Fuss F, Principles and mechanisms of automatic rotation during terminal extension in the human knee joint, in: *Acta Anatomica*, 1992;180:297–304. 152

[80] Gajre S, Anand S, Singh U, Saxena R, Novel Method of Using Dynamic Electrical Impedance Signals for Noninvasive Diagnosis of Knee Osteoarthritis, in: *Engineering in Medicine and Biology Society, 2006. EMBS'06. 28th Annual International Conference of the IEEE*, IEEE, ISBN 1424400325, ISSN 1557-170X, 2207–2210. 167

[81] Gay T, The acoustical characteristics of the normal temporomandibular joint, in: *Journal of Dental Research*, 1988;67:56–60. 30

[82] Gay T, Bertolami C, Bruce Donoff R, Keuth D, Kelly J, The acoustical characteristics of the normal and abnormal temporomandibular joint, in: *Journal of oral and maxillofacial surgery*, 1987;45:397–407. 30, 167

[83] Gay T, Bertolami CN, Solonche DJ, Method and apparatus for the acoustic detection and analysis of joint disorders, 1989, united States Patent number: 4836218. 32

[84] Geckler E, Quaranta A, Patellectomy for degenerative arthritis of the knee. Late results, in: *J Bone Joint Surg*, 1962;44-A:1109–1114. 5

[85] Gill H, O'Connor J, Biarticulating two-dimensional computer model of the human patellofemoral joint, in: *Clinical Biomechanics*, 1996;11:81–89. 42

[86] Goldberg V, Figgie H, Inglis A, Patellar fracture type and prognosis in condylar total knee arthroplasty, in: *Clinical Orthopaedics and Related Research*, 1988; 236:115–122. 2

[87] Goodfellow J, Hungerford D, Zindel. M.(1976): Patellofemoral joint mechanics and pathology: 1. Functional anatomy of the patello-femoral joint, in: *J Bone joint Surg[Br]*, 1976;58:287–290. 15

[88] Gottlieb G, Agarwal G, Filtering of electromyographic signals., in: *American journal of physical medicine*, 1970;49:142. 88

[89] Gottlieb G, Agarwal G, Dynamic relationship between isometric muscle tension and the electromyogram in man, in: *Journal of Applied Physiology*, 1971;30:345. 88, 90

[90] Gracem JN, Sim FH, Fracture of the patella after total knee arthroplasty, in: *Clinical Orthopaedics and Related Research*, 1988;230:168–175. 2

[91] Graichen F, Arnold R, Rohlmann A, Bergmann G, Implantable 9-channel telemetry system for in vivo load measurements with orthopedic implants, in: *Biomedical Engineering, IEEE Transactions on*, 2007;54:253–261, ISSN 0018-9294. 162

[92] Grood E, Suntay W, Noyes F, Butler D, Biomechanics of the knee-extension exercise. Effect of cutting the anterior cruciate ligament, in: *The Journal of Bone and Joint Surgery*, 1984;66:725. 42

[93] Grood ES, Suntay WJ, A joint coordinate system for the clinical description of three-dimensional motions: application to the knee, in: *Journal of biomechanical engineering*, 1983;105:136–144. 7, 9, 59

[94] Groves E, A note on the extension apparatus of the knee-joint, in: *British Journal of Surgery*, 1937;24. 5

[95] Guimaraes A, Herzog W, Hulliger M, Zhang Y, Day S, Effects of muscle length on the EMG-force relationship of the cat soleus muscle studied using non-periodic stimulation of ventral root filaments, in: *Journal of Experimental Biology*, 1994;193:49. 93

[96] Hallen L, Lindahl O, The "screw-home" movement in the knee joint, in: *Acta Orthopaedica Scandinavica*, 1966;37:97–106. 152

[97] Heegaard J, Leyvraz P, Kampen A, Rakotomanana L, Rubin P, Blankevoort L, Influence of soft structures on patellar three-dimensional tracking, in: *Clinical Orthopaedics and related research*, 1994;299:235. 9, 10, 12

[98] Heegaard J, Leyvraz P, Van Kampen A, Rakotomanana L, Rubin P, Blankevoort L, Influence of Soft Structures on Patellar Three-Dimensional Tracking., in: *Clinical Orthopaedics and Related Research*, 1994;299:235. 153

[99] Hefzy M, Jackson W, Saddemi S, Hsieh Y, Effects of tibial rotations on patellar tracking and patello-femoral contact areas., in: *Journal of biomedical engineering*, 1992;14:329. 15, 17, 153, 155

[100] Hehne H, Biomechanics of the patellofemoral joint and its clinical relevance, in: *Clinical orthopaedics and related research*, 1990;258:73. 22

[101] Heinlein B, Graichen F, Bender A, Rohlmann A, Bergmann G, Design, calibration and pre-clinical testing of an instrumented tibial tray, in: *Journal of biomechanics*, 2007;40:S4–S10, ISSN 0021-9290. 162

[102] Heinlein B, Kutzner I, Graichen F, Bender A, Rohlmann A, Halder A, Beier A, Bergmann G, ESB Clinical Biomechanics Award 2008: Complete data of total knee replacement loading for level walking and stair climbing measured in vivo with a follow-up of 6-10 Months, in: *Clinical Biomechanics*, 2009;24:315–326, ISSN 0268-0033. 81, 162, 163

[103] Herzog W, Read L, Lines of action and moment arms of the major force-carrying structures crossing the human knee joint., in: *Journal of anatomy*, 1993;182:213. 42

[104] Heuter C, *Grundriss der chirurgie*, FCW Vogel, 3rd ed., 1885, ISBN 9783540202424. 28

[105] Hibberd M, Dantzig J, Trentham D, Goldman Y, Phosphate release and force generation in skeletal muscle fibers, in: *Science*, 1985;228:1317. 92

[106] Hill A, The heat of shortening and the dynamic constants of muscle, in: *Proceedings of the Royal Society of London Series B, Biological Sciences*, 1938; 126:136–195. 91, 92

[107] Hill A, The abrupt transition from rest to activity in muscle, in: *Proceedings of the Royal Society of London Series B-Biological Sciences*, 1949;136:399. 90, 91

[108] Hille E, Schulitz K, Henrichs C, Schneider T, Pressure and contact-surface measurements within the femoropatellar joint and their variations following lateral release, in: *Archives of Orthopaedic and Trauma Surgery*, 1985;104:275–282. 17, 153, 154, 155

[109] Hinterwimmer S, von Eisenhart-Rothe R, Siebert M, Welsch F, Vogl T, Graichen H, Patella kinematics and patello-femoral contact areas in patients with genu varum and mild osteoarthritis, in: *Clinical Biomechanics*, 2004; 19:704–710. 10, 154

[110] Hinterwimmer S, von Eisenhart-Rothe R, Siebert M, Welsch F, Vogl T, Graichen H, Patella kinematics and patello-femoral contact areas in patients with genu varum and mild osteoarthritis, in: *Clinical Biomechanics*, 2004; 19:704–710. 153

[111] Hof A, Van Den Berg J, EMG to force processing I: an electrical analogue of the Hill muscle model, in: *Journal of Biomechanics*, 1981;14:747–753. 88

[112] Hoff WA, Komistek RD, Dennis DA, Gabrietl SM, Walker SA, Three-dimensional determination of femoral-tibial contact positions under in vivo conditions using fluoroscopy, in: *Clinical Biomechanics*, 1998;13:455–472. 56

[113] Hozack WJ, Goll SR, Lotke PA, Rothman RH, Booth RE, The treatment of patellar fractures after total knee arthroplast, in: *Clinical Orthopaedics and Related Research*, 1988;236:123–127. 2

[114] Hsu H, Luo Z, Rand J, An K, Influence of patellar thickness on patellar tracking and patellofemoral contact characteristics after total knee arthroplasty, in: *The Journal of arthroplasty*, 1996;11:69–80. 9, 10, 12, 15, 17, 153, 155

[115] Hsu H, Luo Z, Rand J, An K, Influence of patellar thickness on patellar tracking and patellofemoral contact characteristics after total knee arthroplasty., in: *J Arthroplasty*, 1996;11:69–80. 153

[116] Huberti H, Hayes W, Patellofemoral contact pressures. The influence of q-angle and tendofemoral contact, in: *The Journal of Bone and Joint Surgery*, 1984; 66:715. 24, 27

[117] Huberti H, Hayes W, Contact pressures in chondromalacia patellae and the effects of capsular reconstructive procedures, in: *Journal of orthopaedic research*, 1988;6:499–508, ISSN 1554-527X. 154

[118] Huberti H, Hayes W, Stone J, Shybut G, Force ratios in the quadriceps tendon and ligamentum patellae, in: *Journal of Orthopaedic Research*, 1984;2:49–54. 22

[119] Huijing P, Important experimental factors for skeletal muscle modelling: non-linear changes of muscle length force characteristics as a function of degree of activity, in: *European journal of morphology*, 1996;34:47–54. 93

[120] Huxley A, Muscle structure and theories of contraction., in: *Progress in biophysics and biophysical chemistry*, 1957;7:255. 92

[121] Huxley A, Muscular contraction., in: *The Journal of Physiology*, 1974;243:1. 92

[122] Imran A, Huss R, Holstein H, O'Connor J, The variation in the orientations and moment arms of the knee extensor and flexor muscle tendons with increasing muscle force: a mathematical analysis, in: *Proceedings of the Institution of Mechanical Engineers, Part H: Journal of Engineering in Medicine*, 2000; 214:277–286. 42

[123] Inman V, Ralston H, De CM S, Bertram Feinstein M, Wright Jr E, Relation of human electromyogram to muscular tension, in: *Electroencephalography and Clinical Neurophysiology*, 1952;4:187–194. 81

[124] Insall J, Intra-articular surgery for degenerative arthritis of the knee, in: *Journal of Bone and Joint Surgery (British Volume)*, 1967;:211–228. 5

[125] Ishigaki S, Bessette R, Maruyama T, Vibration of the temporomandibular joints with normal radiographic imagings: comparison between asymptomatic volunteers and symptomatic patients., in: *Cranio*, 1993;11:88–94. 30, 167

[126] Jensenius H, On the result of excision of the fractured patella., in: *Acta Chirurgica Scandinavica*, 1951;102:274. 5

[127] Jiang C, Lee J, Yuan T, Vibration arthrometry in the patients with failed total kneereplacement, in: *Biomedical Engineering, IEEE Transactions on*, 2000; 47:219–227. 33, 172

[128] Johal P, Williams A, Wragg P, Hunt D, Gedroyc W, Tibio-femoral movement in the living knee. a study of weight bearing and non-weight bearing knee kinematics using interventional mri, in: *Journal of biomechanics*, 2005;38:269–276. 152

[129] Kadaba M, Ramakrishnan H, Wootten M, Gainey J, Gorton G, Cochran G, Repeatability of kinematic, kinetic, and electromyographic data in normal adult gait, in: *Journal of Orthopaedic Research*, 1989;7:849–860. 86

[130] Kane T, Levinson D, *Dynamics, theory and applications*, McGraw Hill, 1985. 40, 60

[131] Kanekasu K, Banks S, Honjo S, Nakata O, Kato H, Fluoroscopic analysis of knee arthroplasty kinematics during deep flexion kneeling, in: *The Journal of arthroplasty*, 2004;19:998–1003. 36

[132] Karlsson, J and Bunketorp, O and Lansinger, O and Romanus, B and Swärd, L, Lowering of the patella secondary to anterior advancement of the tibial tubercle for the patellofemoral pain syndrome, in: *Archives of Orthopaedic and Trauma Surgery*, 1986;105:40–45. 48

[133] Kaufer H, Mechanical function of the patella, in: *The Journal of Bone and Joint Surgery*, 1971;53:1551. 5, 6, 42, 47

[134] Kellis E, Baltzopoulos V, In vivo determination of the patella tendon and hamstrings moment arms in adult males using videofluoroscopy during submaximal knee extension and flexion, in: *Clinical Biomechanics*, 1999;14:118–124. 42

[135] Kernohan W, Beverland D, McCoy G, Hamilton A, Watson P, Mollan R, Vibration arthrometry, in: *Acta Orthopaedica*, 1990;61:70–79. 31, 167

[136] Kernohan W, Beverland D, McCoy G, Shaw S, Wallace R, McCullagh G, Mollan R, The diagnostic potential of vibration arthrography., in: *Clin Orthop Relat Res*, 1986;210:106–12. 30

[137] Kernohan W, Mollan R, Microcomputer analysis of joint vibration, in: *Journal of Microcomputer Applications*, 1982;5:287–296. 30

[138] Kim K, Seo J, Kang J, Song C, An enhanced algorithm for knee joint sound classification using feature extraction based on time-frequency analysis, in: *Computer methods and programs in biomedicine*, 2009;94:198–206, ISSN 0169-2607. 166, 167

[139] Knutson L, Soderberg G, Ballantyne B, Clarke W, A study of various normalization procedures for within day electromyographic data, in: *Journal of electromyography and kinesiology*, 1994;4:47–59. 86

[140] Knutsson E, Richards C, Different types of disturbed motor control in gait of hemiparetic patients, in: *Brain*, 1979;102:405. 86

[141] Komi P, Relationship between muscle tension, EMG and velocity of contraction under concentric and eccentric work, in: *New developments in electromyography and clinical neurophysiology*, 1973;1:596–606. 92

[142] Komistek R, Dennis D, Mabe J, In-Vivo determination of patellofemoral separation and linear impulse forces, in: *Der Orthopäde*, 1998;27:612–618. 154

[143] Komistek R, Kane T, Mahfouz M, Ochoa J, Dennis D, Knee mechanics: a review of past and present techniques to determine in vivo loads, in: *Journal of Biomechanics*, 2005;38:215–228. 2

[144] Komistek RD, Dennis DA, Mahfouz MR, In vivo fluoroscopic analysis of the normal human knee, in: *Clinical Orthopaedics and Related Research*, 2003; 410:69–81. 152

[145] König, C and Sharenkov, A and Matziolis, G and Taylor, WR and Perka, C and Duda, GN and Heller, MO, Joint line elevation in revision TKA leads to increased patellofemoral contact forces, in: *Journal of Orthopaedic Research*, 2010;28:1–5, ISSN 1554-527X. 151

[146] Krevolin J, Pandy M, Pearce J, Moment arm of the patellar tendon in the human knee, in: *Journal of biomechanics*, 2004;37:785–788. 42

[147] Krishnan S, Rangayyan R, Automatic de-noising of knee-joint vibration signals using adaptive time-frequency representations, in: *Medical and Biological Engineering and Computing*, 2000;38:2–8. 32, 165

[148] Krishnan S, Rangayyan R, Bell G, Frank C, Adaptive time-frequency analysis of knee joint vibroarthrographic signals for noninvasive screening of articular cartilage pathology, in: *IEEE Transactions on Biomedical Engineering*, 2000; 47:773–783. 33

[149] Kurtz S, Ong K, Lau E, Mowat F, Halpern M, Projections of Primary and Revision Hip and Knee Arthroplasty in the United States from 2005 to 2030, in: *The Journal of Bone and Joint Surgery*, 2007;89:780. 2

[150] Kutzner I, Heinlein B, Graichen F, Bender A, Rohlmann A, Halder A, Beier A, Bergmann G, Loading of the knee joint during activities of daily living measured

in vivo in five subjects, in: *Journal of biomechanics*, 2010;43:2164–2173, ISSN 0021-9290. 163

[151] Kwak S, Ahmad C, Gardner T, Grelsamer R, Henry J, Blankevoort L, Ateshian G, Mow V, Hamstrings and iliotibial band forces affect knee kinematics and contact pattern, in: *Journal of Orthopaedic Research*, 2000;18:101–108. 10

[152] Kwak S, Ahmad C, Gardner T, Grelsamer R, Henry J, Blankevoort L, Ateshian G, Mow V, Hamstrings and iliotibial band forces affect knee kinematics and contact pattern., in: *J Orthop Res*, 2000;18:101–8. 153

[153] Leblanc JM, Patellar complications in total knee arthroplasty. a literature review, in: *Orthopaedic review*, 1989;18:296–304. 2

[154] Lee T, Gerken A, Glaser F, Kim W, Anzel S, Patellofemoral joint kinematics and contact pressures in total knee arthroplasty, in: *Clinical orthopaedics and related research*, 1997;340:257. 10

[155] Lee T, Gerken A, Glaser F, Kim W, Anzel S, Patellofemoral Joint Kinematics and Contact Pressures in Total Knee Arthroplasty., in: *Clinical Orthopaedics and Related Research*, 1997;340:257. 153

[156] Lehman G, McGill S, The importance of normalization in the interpretation of surface electromyography: a proof of principle, in: *Journal of manipulative and physiological therapeutics*, 1999;22:444–446. 86

[157] Leszko F, Komistek R, Mahfouz M, Ratron Y, Judet T, Bonnin M, Colombier J, Lin S, In Vivo Kinematics of the Salto Total Ankle Prosthesis, in: *Foot & ankle international*, 2008;29:1117–1125. 64, 66

[158] Leszko F, Sharma A, Komistek R, Mahfouz M, Cates H, Scuderi G, Comparison of In Vivo Patellofemoral Kinematics for Subjects Having High-Flexion Total Knee Arthroplasty Implant With Patients Having Normal Knees, in: *The Journal of Arthroplasty*, 2009;. 10, 15, 152, 153, 154

[159] Lin H, Lu T, Hsu H, Three-Dimensional Analysis of Kinematic and Kinetic Coordination of the Lower Limb Joints during Stair Ascent and Descent, in: *Biomedical Engineering Applications Basis Communications*, 2004;16:101–108, ISSN 1016-2356. 156, 158

[160] Lloyd D, Besier T, An EMG-driven musculoskeletal model to estimate muscle forces and knee joint moments in vivo, in: *Journal of biomechanics*, 2003; 36:765–776. 93

[161] Lund F, Nilsson B, Anterior displacement of the tibial tuberosity in chondromalacia patellae, in: *Acta Orthopaedica*, 1980;51:679–688. 48

[162] Lund F, Nilsson B, Arthroscopy of the Patello-Femoral Joint, in: *Acta Orthopaedica*, 1980;51:297–302. 172

[163] MacIntyre N, Hill N, Fellows R, Ellis R, Wilson D, Patellofemoral joint kinematics in individuals with and without patellofemoral pain syndrome, in: *The Journal of Bone and Joint Surgery*, 2006;88:2596. 9, 10, 12, 15, 153

[164] Mahfouz M, Badawi A, Fatah E, Kuhn M, Merkl B, Reconstruction of 3D patient-specific bone models from biplanar x-ray images utilizing morphometric measurements, in: *Proc. Int. Conf. on Image Processing, Computer Vision & Pattern Recognition, IPCV*, vol. 2, Citeseer, 345–349. 62, 63

[165] Mahfouz MR, Hoff WA, Komistek RD, Dennis DA, A robust method for registration of three-dimensional knee implant models to two-dimensional fluoroscopy images, in: *Medical Imaging, IEEE Transactions on*, 2003;22:1561–1574, ISSN 0278-0062, doi:10.1109/TMI.2003.820027. 3, 56

[166] Mahfouz MR, Komistek RD, Dennis DA, Hoff WA, In vivo assessment of the kinematics in normal and anterior cruciate ligament-deficient knees, in: *J Bone Joint Surg Am*, 2004;86:56–61. 152

[167] Malinzak R, Colby S, Kirkendall D, Yu B, Garrett W, A comparison of knee joint motion patterns between men and women in selected athletic tasks, in: *Clinical biomechanics*, 2001;16:438–445. 20

[168] Maquet P, Advancement of the tibial tuberosity, in: *Clinical Orthopaedics and Related Research*, 1976;115:225. 22, 48

[169] Mathur S, Eng J, MacIntyre D, Reliability of surface EMG during sustained contractions of the quadriceps., in: *Journal of electromyography and kinesiology: official journal of the International Society of Electrophysiological Kinesiology*, 2005;15:102. 86

[170] Mathur S, Takai K, MacIntyre D, Reid D, Estimation of thigh muscle mass with magnetic resonance imaging in older adults and people with chronic obstructive pulmonary disease, in: *Physical Therapy*, 2008;88:219. 95, 96

[171] Matsuda S, Ishinishi T, White S, Whiteside L, Patellofemoral joint after total knee arthroplasty:: Effect on contact area and contact stress, in: *The Journal of arthroplasty*, 1997;12:790–797. 17, 27, 155

[172] Mayman D, Bourne R, Rorabeck C, Vaz M, Kramer J, Resurfacing versus not resurfacing the patella in total knee arthroplasty 8-to 10-year results, in: *The Journal of arthroplasty*, 2003;18:541–545. 18

[173] McCoy G, McCrea J, Beverland D, Kernohan W, Mollan R, Vibration arthrography as a diagnostic aid in diseases of the knee. A preliminary report, in: *Journal of Bone & Joint Surgery, British Volume*, 1987;69:288–293. 30

[174] Merkow RL, Soudry M, Insall JN, Patellar dislocation following total knee replacement, in: *J Bone Joint Surg Am*, 1985;67:1321–1327, URL `http://www.ejbjs.org/cgi/content/abstract/67/9/1321`. 2

[175] Merletti R, Standards for reporting EMG data, in: *J Electromyogr Kinesiol*, 1999;9:3–4. 84, 86

[176] Miller R, Murray D, Gill H, O'Connor J, Goodfellow J, In vitro patellofemoral joint force determined by a non-invasive technique, in: *Clinical Biomechanics*, 1997;12:1–7, ISSN 0268-0033. 153

[177] Mirka G, The quantification of EMG normalization error, in: *Ergonomics*, 1991; 34:343–352. 86, 87

[178] Mollan R, Kernohan G, Watters P, Artefact encountered by the vibration detection system., in: *J Biomech*, 1983;16:193–9. 30

[179] Mollan R, McCullagh G, Wilson R, A critical appraisal of auscultation of human joints., in: *Clin Orthop Relat Res*, 1982;170:231–7. 30, 167

[180] Moorehead J, Montgomery S, Harvey D, Instant center of rotation estimation using the Reuleaux technique and a Lateral Extrapolation technique, in: *Journal of biomechanics*, 2003;36:1301–1307. 45

[181] Moro-oka T, Matsuda S, Miura H, Nagamine R, Urabe K, Kawano T, Higaki H, Iwamoto Y, Patellar tracking and patellofemoral geometry in deep knee flexion, in: *Clinical orthopaedics and related research*, 2002;394:161. 10, 15

[182] Morris B, D'Lima D, Slamin J, Kovacevic N, Arms S, Townsend C, Colwell Jr C, e-Knee: Evolution of the electronic knee prosthesis: Telemetry technology development, in: *The Journal of Bone and Joint Surgery*, 2001;83:S62. 162

[183] Mow V, Holmes M, Lai W, Fluid transport and mechanical properties of articular cartilage: a review., in: *Journal of biomechanics*, 1984;17:377. 6

[184] Mündermann A, Dyrby C, D'Lima D, Colwell Jr C, Andriacchi T, In vivo knee loading characteristics during activities of daily living as measured by an instrumented total knee replacement, in: *Journal of Orthopaedic Research*, 2008;26:1167–1172, ISSN 1554-527X. 162

[185] Nagamine R, Otani T, White S, McCarthy D, Whiteside L, Patellar tracking measurement in the normal knee, in: *Journal of Orthopaedic Research*, 1995; 13:115–122. 10, 12, 15

[186] Nagura T, Dyrby CO, Alexander EJ, Andriacchi TP, Mechanical loads at the knee joint during deep flexion, in: *Journal of Orthopaedic Research*, 2002; 20:881–886. 2, 158

[187] Narici M, Landoni L, Minetti A, Assessment of human knee extensor muscles stress from in vivo physiological cross-sectional area and strength measurements, in: *European journal of applied physiology and occupational physiology*, 1992;65:438–444. 95

[188] Narici M, Roi G, Landoni L, Minetti A, Cerretelli P, Changes in force, cross-sectional area and neural activation during strength training and detraining of the human quadriceps, in: *European journal of applied physiology and occupational physiology*, 1989;59:310–319. 95

[189] Nieminen H, Takala E, Viikari-Juntura E, Normalization of electromyogram in the neck-shoulder region, in: *European journal of applied physiology and occupational physiology*, 1993;67:199–207. 87

[190] Nisell R, Ericson M, Nemeth G, Ekholm J, Tibiofemoral joint forces during isokinetic knee extension, in: *The American Journal of Sports Medicine*, 1989; 17:49. 42

[191] Norman R, Komi P, Electromechanical delay in skeletal muscle under normal movement conditions, in: *Acta Physiologica Scandinavica*, 1979;106:241–248. 91

[192] Omori G, Koga Y, Bechtold J, Gustilo R, Nakabe N, Sasagawa K, Hara T, Takahashi H, Contact pressure and three-dimensional tracking of unresurfaced

patella in total knee arthroplasty, in: *The Knee*, 1997;4:15–21. 10, 15, 18, 27, 153, 154, 155

[193] Omori G, Koga Y, Bechtold J, Gustilo R, Nakabe N, Sasagawa K, Hara T, Takahashi H, Contact pressure and three-dimensional tracking of unresurfaced patella in total knee arthroplasty, in: *The Knee*, 1997;4:15–21. 153

[194] Ostermeier S, Hurschler C, Stukenborg-Colsman C, Quadriceps function after TKA—-an in vitro study in a knee kinematic simulator, in: *Clinical Biomechanics*, 2004;19:270–276. 24

[195] Panjabi M, Centers and angles of rotation of body joints: a study of errors and optimization., in: *Journal of biomechanics*, 1979;12:911. 45

[196] Peylan A, Direct auscultation of the joints; preliminary clinical observations., in: *Rheumatism*, 1953;9:77–81. 28, 29

[197] Powell P, Roy R, Kanim P, Bello M, Edgerton V, Predictability of skeletal muscle tension from architectural determinations in guinea pig hindlimbs, in: *Journal of Applied Physiology*, 1984;57:1715. 94

[198] Powers C, Lilley J, Lee T, The effects of axial and multi-plane loading of the extensor mechanism on the patellofemoral joint, in: *Clinical Biomechanics*, 1998;13:616–624. 17, 20, 155

[199] Protopapadaki A, Drechsler W, Cramp M, Coutts F, Scott O, Hip, knee, ankle kinematics and kinetics during stair ascent and descent in healthy young individuals, in: *Clinical Biomechanics*, 2007;22:203–210. 66, 67

[200] Rack P, Westbury D, The effects of length and stimulus rate on tension in the isometric cat soleus muscle, in: *The Journal of physiology*, 1969;204:443. 93

[201] Radke JC, Ryan GJ, Hershberger TW, Method and apparatus for diagnosing joints, 1995, united States Patent number: 5413116. 32

[202] Radke JC, Ryan GJ, Hershberger TW, Method and apparatus for diagnosing joints, 1996, united States Patent number: 5533519. 32

[203] Ramappa A, Apreleva M, Harrold F, Fitzgibbons P, Wilson D, Gill T, The effects of medialization and anteromedialization of the tibial tubercle on patellofemoral mechanics and kinematics, in: *The American Journal of Sports Medicine*, 2006;34:749. 12, 15

[204] Rand JA, Gustilo RB, Technique of patellar resurfacing in total knee arthroplasty, in: *Tech Orthop*, 1988;133:57–66. 2

[205] Rangayyan R, Wu Y, Screening of knee-joint vibroarthrographic signals using statistical parameters and radial basis functions, in: *Medical and Biological Engineering and Computing*, 2008;46:223–232. 33, 165, 166

[206] Rangayyan RM, Krishnan S, Bell DB, Frank CB, Auscultation of Joints, 2003, united States Patent number: 6537233. 32

[207] Rauschning W, Amici Jr F, Surgical treatment of recurrent subluxation of the patella in athletes., in: *Italian journal of orthopaedics and traumatology*, 1982; 8:167. 49

[208] Reilly D, Martens M, Experimental analysis of the quadriceps muscle force and patello-femoral joint reaction force for various activities, in: *Acta Orthopaedica*, 1972;43:126–137. 20, 159

[209] Reuben JD, McDonald L, Woodard PL, Hennington LJ, The effect of patella thickness on patella strain following total knee replacement, in: *Journal of Arthroplasty*, 1991;6:251. 2

[210] Riener R, Rabuffetti M, Frigo C, Stair ascent and descent at different inclinations, in: *Gait & posture*, 2002;15:32–44, ISSN 0966-6362. 158

[211] Russell J, Carlson TC, Vipraio GA, Device for non-invasive diagnosis and monitoring of articular and periarticular pathology, 1989, united States Patent number: 4823807. 32

[212] Salsich G, Ward S, Terk M, Powers C, In vivo assessment of patellofemoral joint contact area in individuals who are pain free, in: *Clinical orthopaedics and related research*, 2003;417:277. 17, 155

[213] Sharma A, Leszko F, Komistek RD, Scuderi GR, Jr HEC, Liu F, In vivo patellofemoral forces in high flexion total knee arthroplasty, in: *Journal of Biomechanics*, 2008;41:642–648. 2, 20, 23, 27

[214] Sheldon J, *An essay on the fracture of the patella or kneepan. With observations on the fracture of the olecranon.*, London: printed for the author, and sold by J. Johnson; P. Elmsley and T. Cadell; E. and C. Dilly; G. G. J. and J. Robinson; and J. Robson, 1789. 5

[215] Shih Y, Bull A, McGregor A, Humphries K, Amis A, A technique for the measurement of patellar tracking during weight-bearing activities using ultrasound, in: *Proceedings of the Institution of Mechanical Engineers, Part H: Journal of Engineering in Medicine*, 2003;217:449–457. 10

[216] Singerman R, Davy D, Goldberg V, Effects of patella alta and patella infera on patellofemoral contact forces., in: *Journal of biomechanics*, 1994;27:1059. 15, 153

[217] Smidt G, Biomechanical analysis of knee flexion and extension., in: *Journal of biomechanics*, 1973;6:79. 42

[218] Soderberg G, Knutson L, A guide for use and interpretation of kinesiologic electromyographic data, in: *Physical Therapy*, 2000;80:485. 86

[219] Soderberg G, et al., Selected topics in surface electromyography for use in the occupational setting: expert perspectives, in: *DHHS (NIOSH) publ*, 1992;. 84

[220] Steindler A, Auscultation of Joints, in: *The Journal of Bone and Joint Surgery*, 1937;19:121. 28, 29, 30

[221] Steinkamp L, Dillingham M, Markel M, Hill J, Kaufman K, Biomechanical considerations in patellofemoral joint rehabilitation, in: *The American Journal of Sports Medicine*, 1993;21:438. 42

[222] Stiehl J, Dennis D, Komistek R, Crane H, In vivo determination of condylar lift-off and screw-home in a mobile-bearing total knee arthroplasty, in: *The Journal of arthroplasty*, 1999;14:293–299. 36

[223] Stiehl J, Komistek R, Dennis D, Keblish P, Kinematics of the patellofemoral joint in total knee arthroplasty, in: *The Journal of Arthroplasty*, 2001;16:706–714. 10, 15, 153, 154

[224] Stiehl J, Komistek R, Dennis D, Keblish P, Kinematics of the patellofemoral joint in total knee arthroplasty, in: *The Journal of Arthroplasty*, 2001;16:706–714. 153

[225] Strang G, *Linear Algebra and its Applications*, Academic Press Inc, 1976, ISBN 9780126736502. 79

[226] Sutton D, Sadowsky P, Bernreuter W, McCutcheon M, Lakshminarayanan A, Temporomandibular joint sounds and condyle/disk relations on magnetic resonance images., in: *Am J Orthod Dentofacial Orthop*, 1992;101:70–8. 30, 167

[227] Sylvester A, Mahfouz M, Quantifying relative shape variation in modern human femora and humeri, in: *The FASEB Journal*, 2009;23:648–4. 62, 63

[228] Tang Y, *Wavelet Theory and Its Application to Pattern Recognition*, World Scientific, 2000. 32

[229] Tank P, Gest T, Burkel W, *Atlas of Anatomy*, Wolters Kluwer/Lippincott Williams & Wilkins, 1st ed., 2008, ISBN 9780781785051. 67

[230] Theodoridis S, Koutroumbas K, *Pattern Recognition. 2006*, Elsevier, Academic Press, Amsterdam, New York, 2006. 100

[231] Tippett G, Excision of the Patella, in: *British Medical Journal*, 1938;1:1284. 5

[232] Umapathy K, Krishnan S, Modified local discriminant bases algorithm and its application in analysis of human knee joint vibration signals, in: *IEEE Transactions on Biomedical Engineering*, 2006;53:517–523. 33

[233] Van Eijden T, Kouwenhoven E, Weijs W, Mechanics of the patellar articulation Effects of patellar ligament length studied with a mathematical model, in: *Acta Orthopaedica*, 1987;58:560–566. 42

[234] Van Kampen A, Huiskes R, The three-dimensional tracking pattern of the human patella, in: *Journal of Orthopaedic Research*, 1990;8:372–382. 10, 153

[235] Walters C, The value of joint auscultation, in: *Lancet*, 1929;1:920–921. 28, 29, 100, 103, 165

[236] Ward S, Eng C, Smallwood L, Lieber R, Are current measurements of lower extremity muscle architecture accurate?, in: *Clinical Orthopaedics and Related Research®*, 2009;467:1074–1082. 96

[237] Ward S, Powers C, The influence of patella alta on patellofemoral joint stress during normal and fast walking, in: *Clinical Biomechanics*, 2004;19:1040–1047. 42

[238] Waters T, Bentley G, Patellar resurfacing in total knee arthroplasty: a prospective, randomized study, in: *The Journal of Bone and Joint Surgery*, 2003;85:212. 18

[239] Watson-Jones R, Excision of patella, in: *British Medical Journal*, 1945;2:195. 5

[240] Webb M, Hibberd M, Goldman Y, Trentham D, Oxygen exchange between Pi in the medium and water during ATP hydrolysis mediated by skinned fibers from rabbit skeletal muscle. Evidence for Pi binding to a force-generating state., in: *Journal of Biological Chemistry*, 1986;261:15557. 92

[241] West F, End results of patellectomy, in: *The Journal of Bone and Joint Surgery*, 1962;44:1089. 5

[242] Winter D, *Biomechanics and Motor Control of Human Movement*, Wiley-Interscience, 2nd ed., 1990, ISBN 9783540202424. 62, 63, 66

[243] Winter D, Electromyogram recording, processing, and normalization: procedures and considerations, in: *Journal of Human Muscle Performance*, 1991; 1:5–15. 86

[244] Winter D, Yack H, EMG profiles during normal human walking: stride-to-stride and inter-subject variability, in: *Electroencephalography and clinical Neurophysiology*, 1987;67:402–411. 86

[245] Winters J, Stark L, Muscle models: what is gained and what is lost by varying model complexity, in: *Biological Cybernetics*, 1987;55:403–420. 88

[246] Wismans J, Veldpaus F, Janssen J, Huson A, Struben P, A three-dimensional mathematical model of the knee-joint, in: *Journal of Biomechanics*, 1980; 13:677–679, ISSN 0021-9290. 73

[247] Woltring H, Huiskes R, De Lange A, Veldpaus F, Finite centroid and helical axis estimation from noisy landmark measurements in the study of human joint kinematics., in: *Journal of Biomechanics*, 1985;18:379. 45

[248] Wretenberg P, Nemeth G, Lamontagne M, Lundin B, Passive knee muscle moment arms measured in vivo with MRI, in: *Clinical Biomechanics*, 1996; 11:439–446. 42

[249] Wu G, van der Helm F, Veeger H, Makhsous M, Van Roy P, Anglin C, Nagels J, Karduna A, McQuade K, Wang X, et al., ISB recommendation on definitions of joint coordinate systems of various joints for the reporting of human joint motionPart II: shoulder, elbow, wrist and hand, in: *Journal of biomechanics*, 2005;38:981–992. 8

[250] Wu G, Siegler S, Allard P, Kirtley C, Leardini A, Rosenbaum D, Whittle M, D'Lima DD, Cristofolini L, Witte H, Schmid O, Stokes I, A joint coordinate system for the clinical description of three-dimensional motions: application to the knee, in: *Journal of biomechanics*, 2002;35:543–548. 7, 8

[251] Yamaguchi G, *Dynamic modeling of musculoskeletal motion: a vectorized approach for biomechanical analysis in three dimensions*, Springer Verlag, 2005. 75

[252] Yamaguchi G, Moran D, Si J, A computationally efficient method for solving the redundant problem in biomechanics, in: *Journal of Biomechanics*, 1995; 28:999–1005. 76, 79

[253] Yamaguchi G, Zajac F, A planar model of the knee joint to characterize the knee extensor mechanism., in: *Journal of biomechanics*, 1989;22:1. 42

[254] Yang J, Winter D, Electromyographic amplitude normalization methods: improving their sensitivity as diagnostic tools in gait analysis., in: *Archives of physical medicine and rehabilitation*, 1984;65:517. 86

[255] Young H, Regan J, Total Excision of the Patella for Arthritis of the Knee, in: *Minnesota Med*, 1945;28:909–914. 5

[256] Zajac F, Muscle and tendon: properties, models, scaling, and application to biomechanics and motor control., in: *Critical reviews in biomedical engineering*, 1989;17:359. 84, 87, 88, 89, 91, 93, 94, 212, 219, 226, 233, 240, 247, 254, 261, 268, 275, 282, 289, 296, 303, 310, 317, 324, 331, 338, 345

[257] Zuppinger H, Die aktive Flexion im unbelasteten Kniegelenk, in: *Anatomy and Embryology*, 1904;25:701–764. 45

Appendix

Appendix A

Detailed Patients' Analysis Results

A.1 Patient 1T

Patient demographic details:

ID# 1T

age: 76 yrs

height: 1.58 m

mass: 60 kg

leg side: Left

condition: TKA

A.1.1 Kinematics analysis results

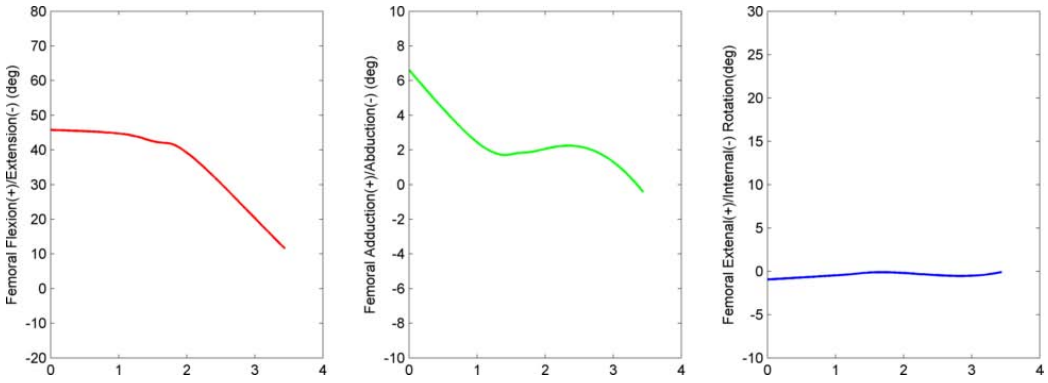


Figure A.1: Patient 1T patellofemoral joint kinematics.

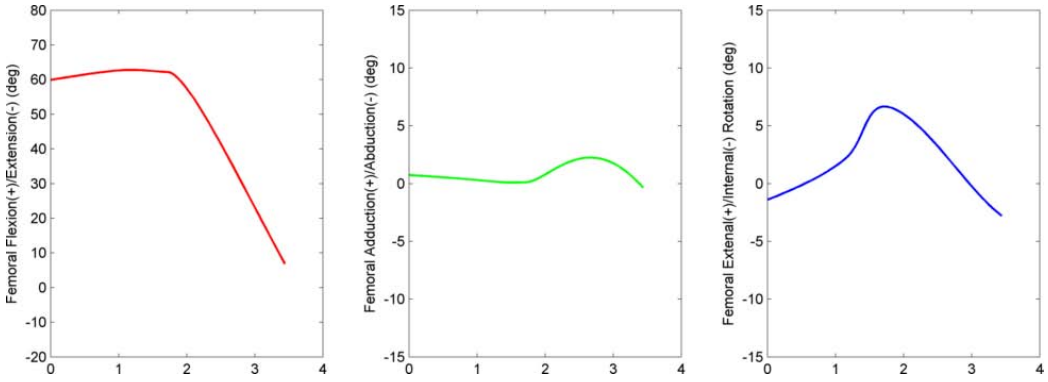


Figure A.2: Patient 1T tibiofemoral joint kinematics.

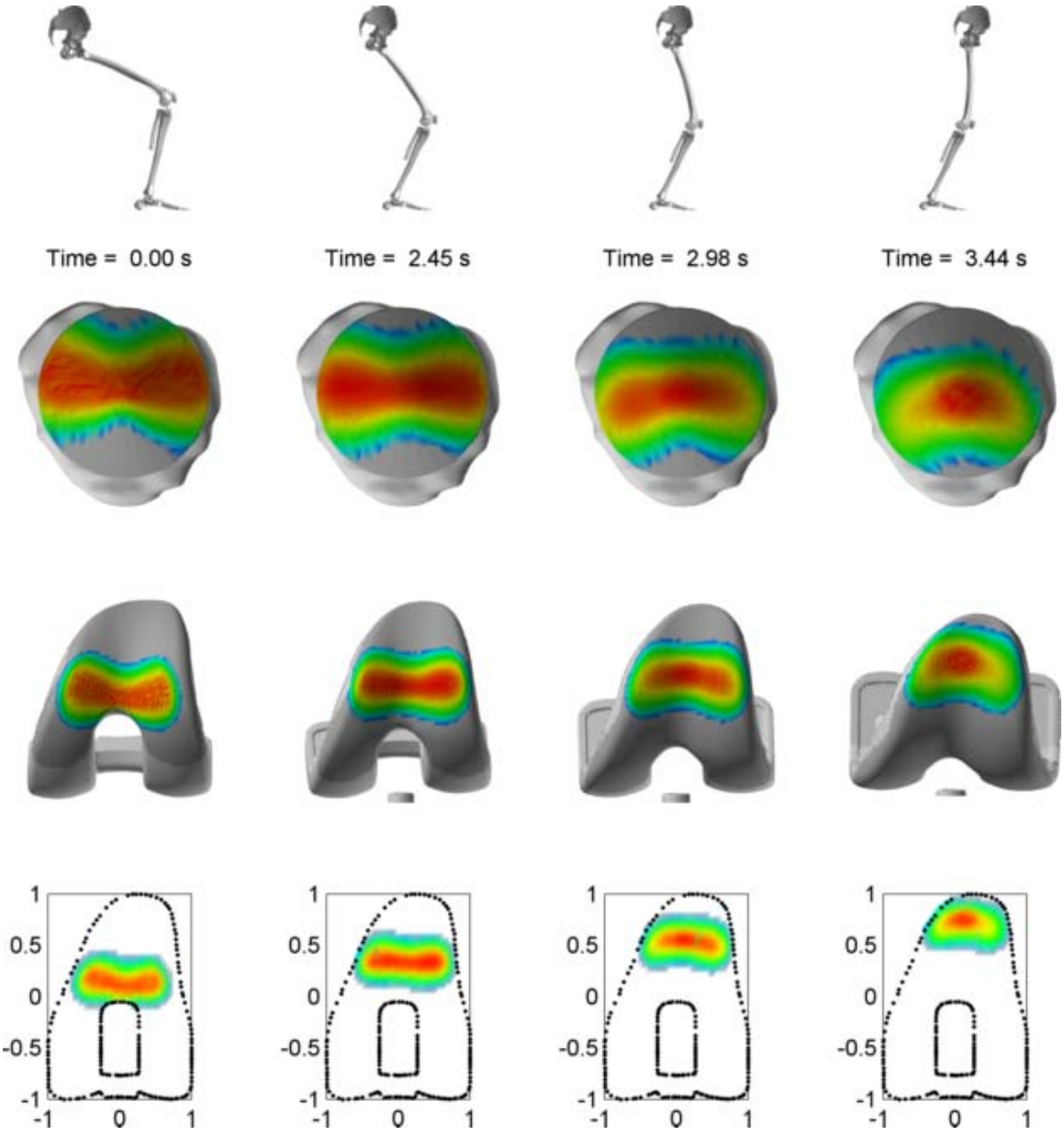


Figure A.3: Patient 1T dynamics model (top), patellofemoral contact location mapped on the patient's specific patella (2^{nd} from top) and femur (2^{nd} from bottom) bone models, as well as the normalized contact location mapped on the unfolded femoral trochlea surface (bottom).

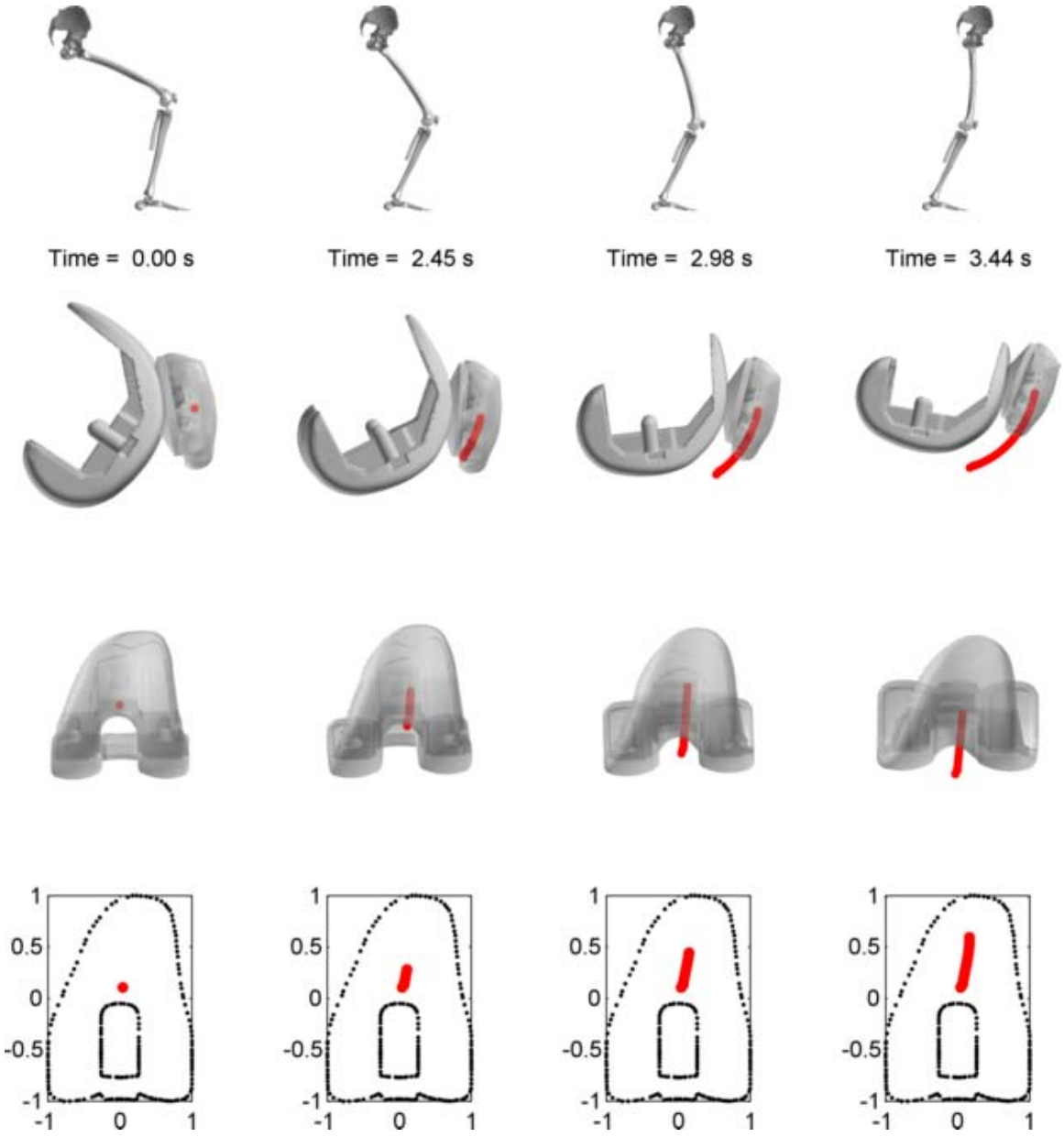


Figure A.4: Patient 1T dynamics model (top), patella center tracking in the sagittal (2^{nd} from top) and coronal (2^{nd} from bottom) planes, as well as the normalized patella tracking mapped on the unfolded femoral trochlea surface (bottom).

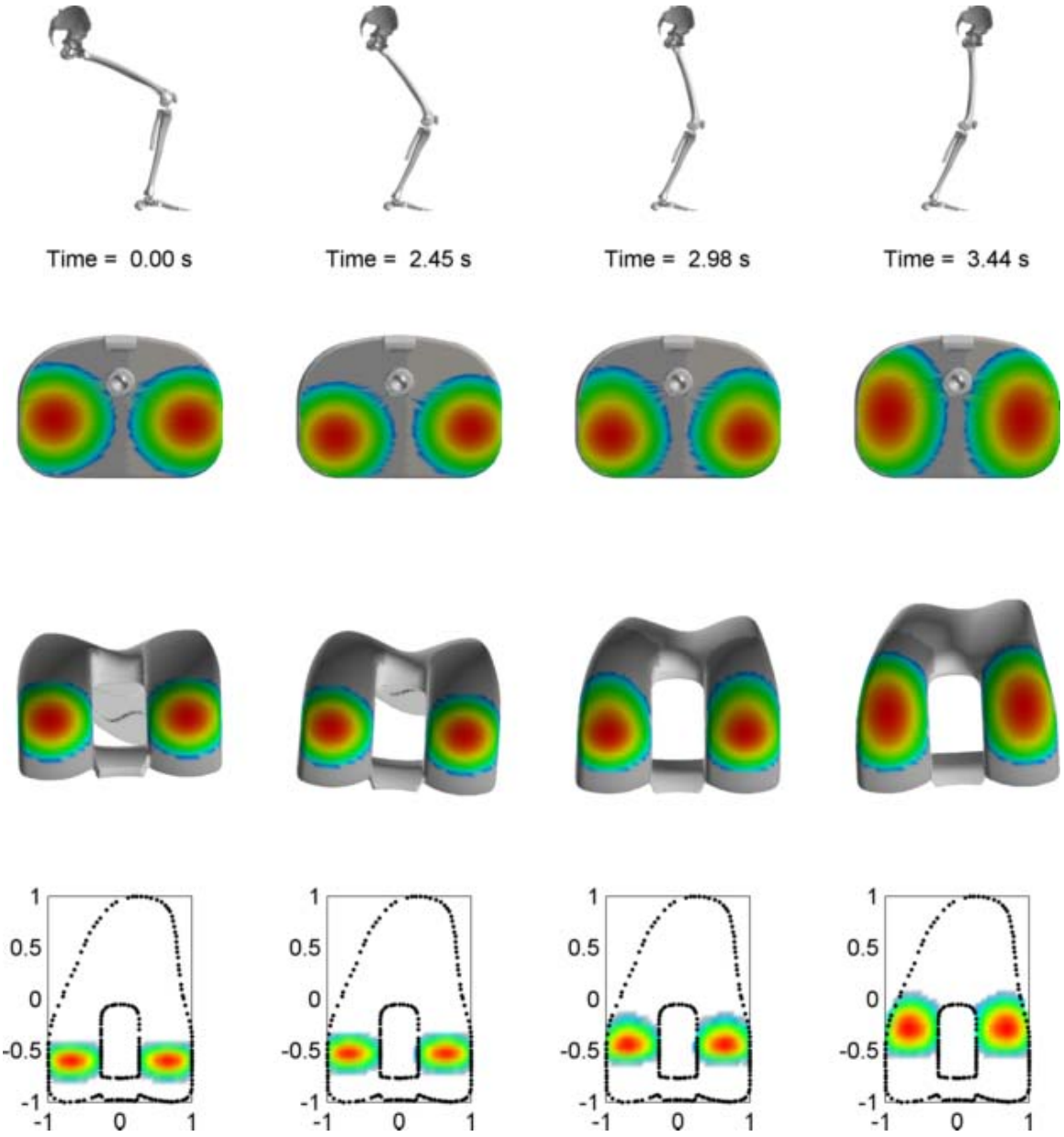


Figure A.5: Patient 1T dynamics model (top), tibiofemoral contact location mapped on the patient's specific patella (2^{nd} from top) and femur (2^{nd} from bottom) bone models, as well as the normalized contact location mapped on the unfolded femoral trochlea surface (bottom).

A.1.2 Electromyography and Inverse Dynamics analyses results

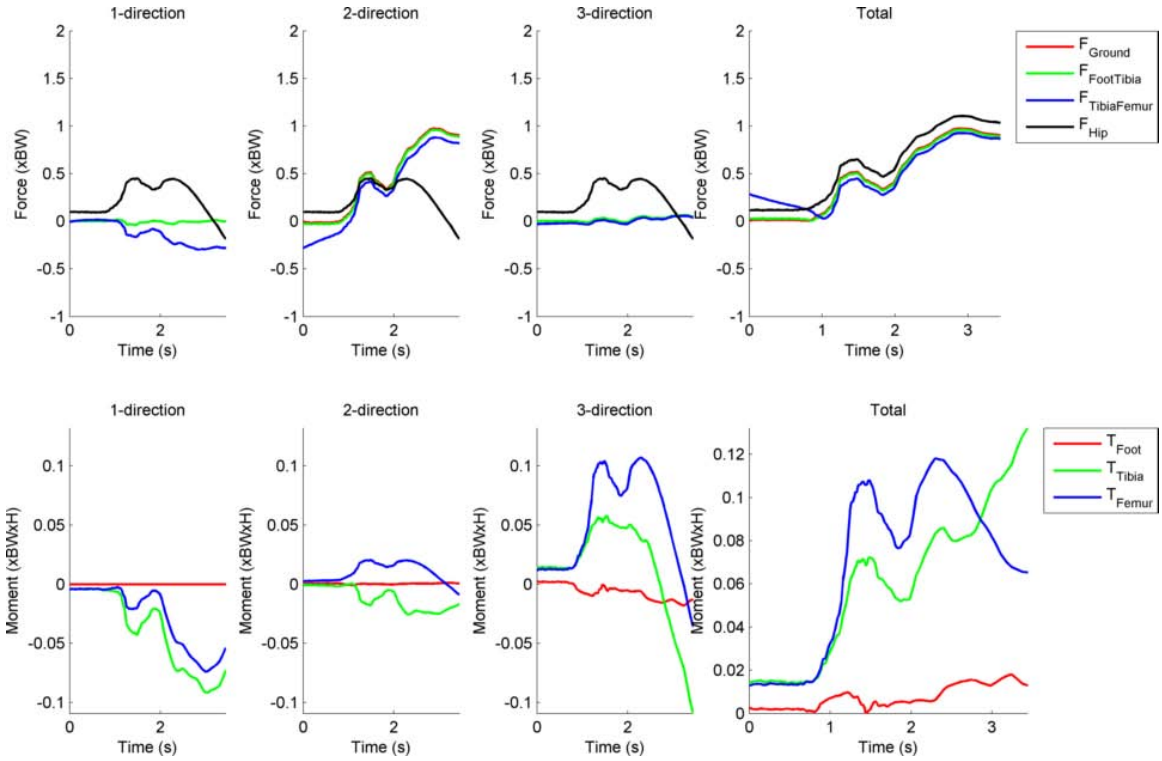


Figure A.6: Patient 1T knee joint reaction forces (top) and moments (bottom) normalized with respect to patient's body weight (BW). 1-direction = Anterior(+)/Posterior(-), 2-direction = Superior(+)/Inferior(-), 3-direction = Medial(+)/Lateral(-).

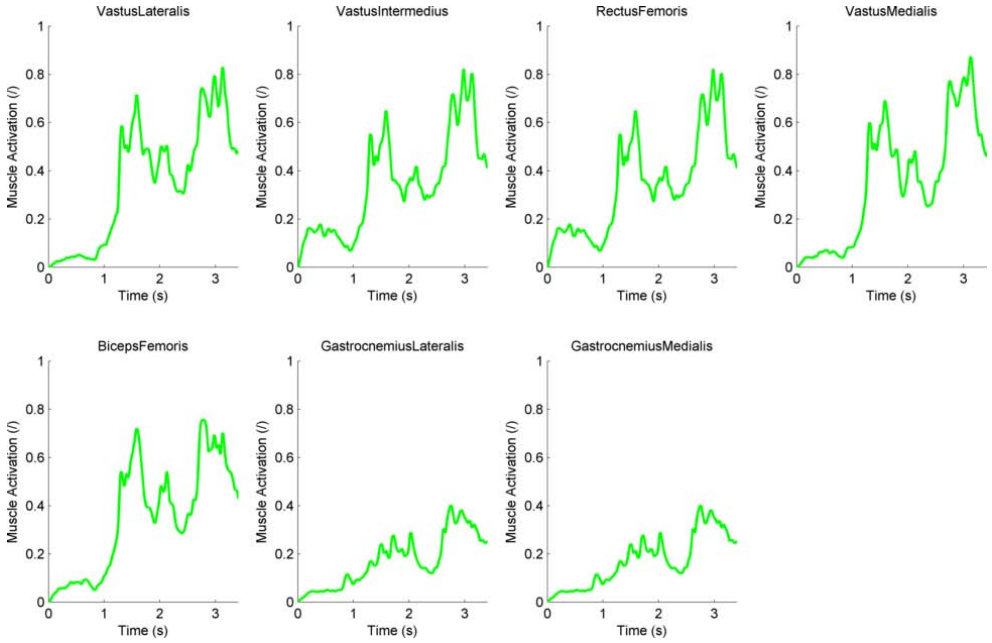


Figure A.7: Patient 1T muscle activation values obtained using the muscle activation dynamics[256].

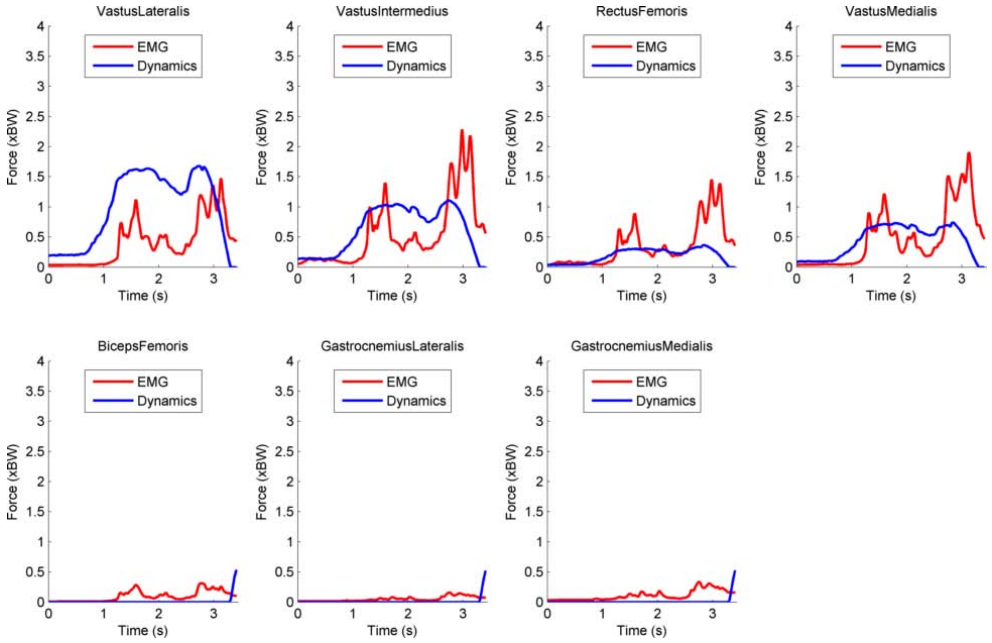


Figure A.8: Patient 1T muscle forces obtained using the EMG signal analysis (red) and pseudoinverse dynamics approach (green) normalized by patient's body weight (BW).

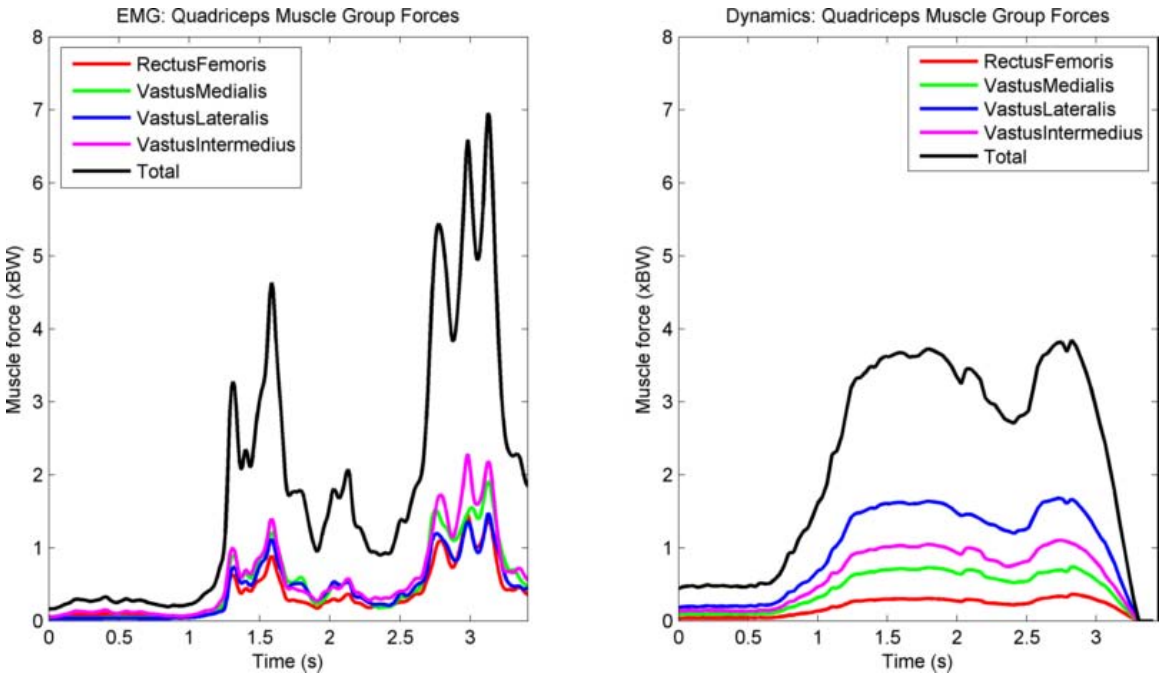


Figure A.9: Patient 1T quadriceps muscle group forces calculated from the EMG signals (left) and from the inverse dynamics (right) normalized by patient's body weight (BW).

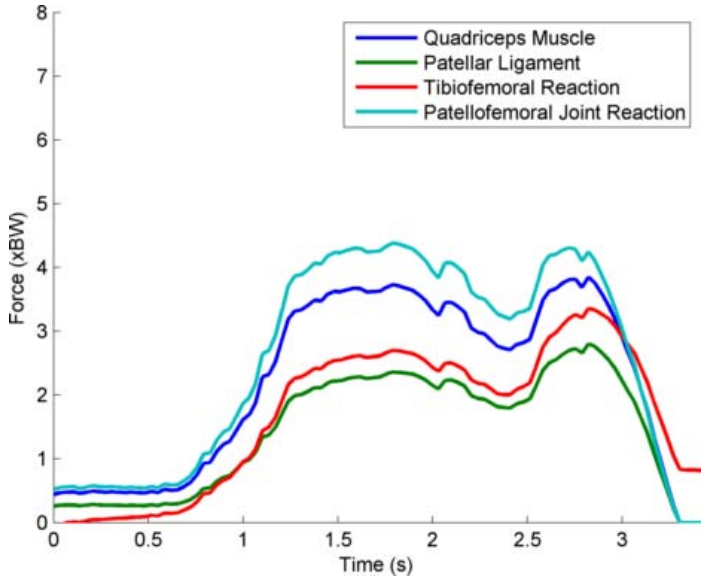


Figure A.10: Patient 1T total knee joint reaction forces incuding the action of the muscles, as well as the forces in the patellofemoral ligament, collateral and cruciate ligaments (if present) normalized by patient's body weight (BW).

A.2 Patient 3T

Patient demographic details:

ID# 3T

age: 75 yrs

height: 1.49 m

mass: 57 kg

leg side: Right

condition: TKA

A.2.1 Kinematics analysis results

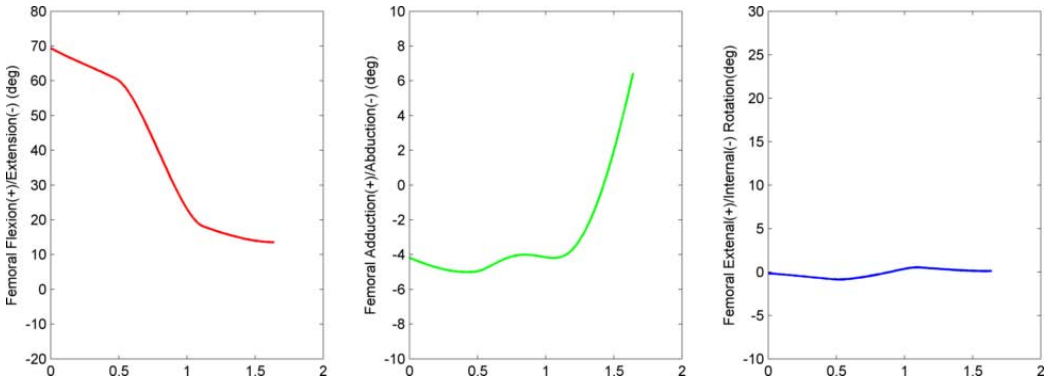


Figure A.11: Patient 3T patellofemoral joint kinematics.

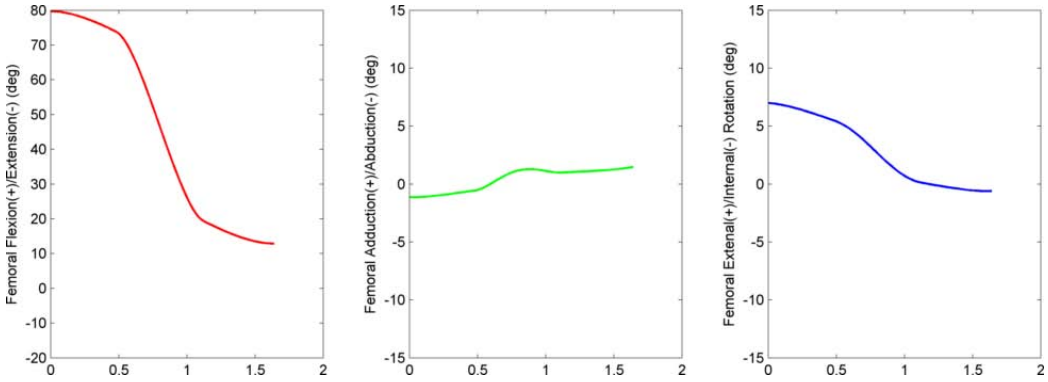


Figure A.12: Patient 3T tibiofemoral joint kinematics.

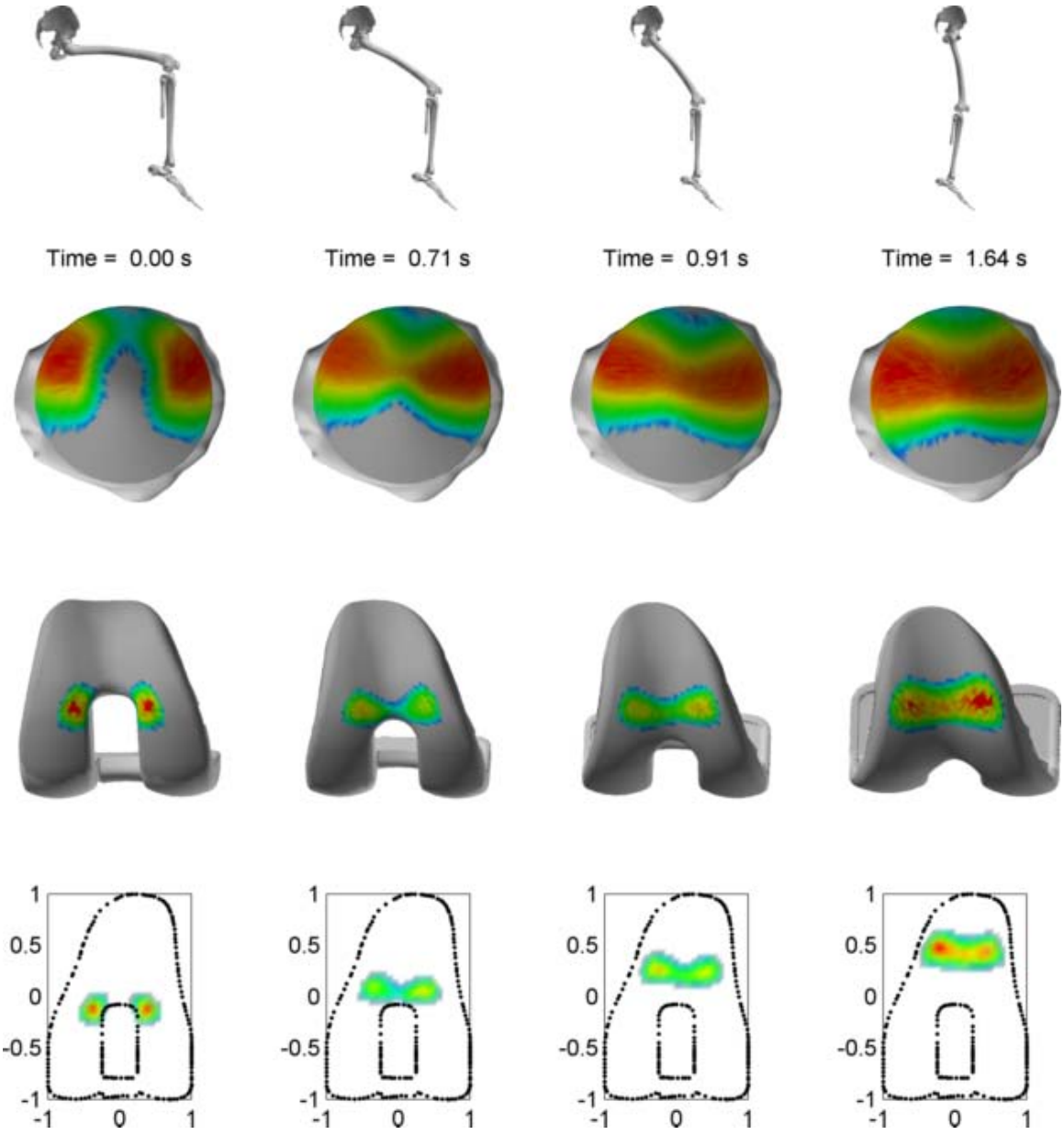


Figure A.13: Patient 3T dynamics model (top), patellofemoral contact location mapped on the patient's specific patella (2^{nd} from top) and femur (2^{nd} from bottom) bone models, as well as the normalized contact location mapped on the unfolded femoral trochlea surface (bottom).

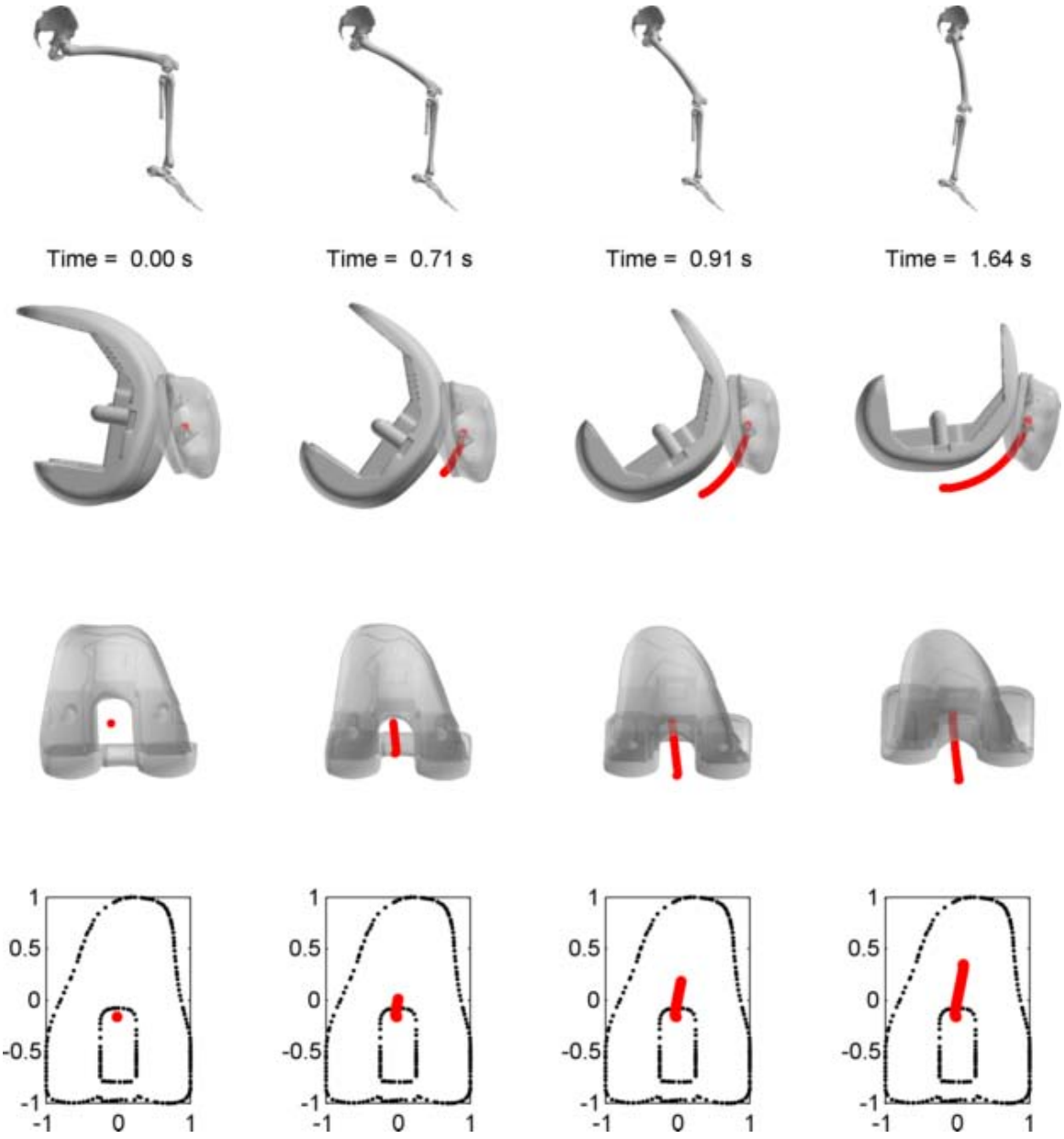


Figure A.14: Patient 3T dynamics model (top), patella center tracking in the sagittal (2^{nd} from top) and coronal (2^{nd} from bottom) planes, as well as the normalized patella tracking mapped on the unfolded femoral trochlea surface (bottom).

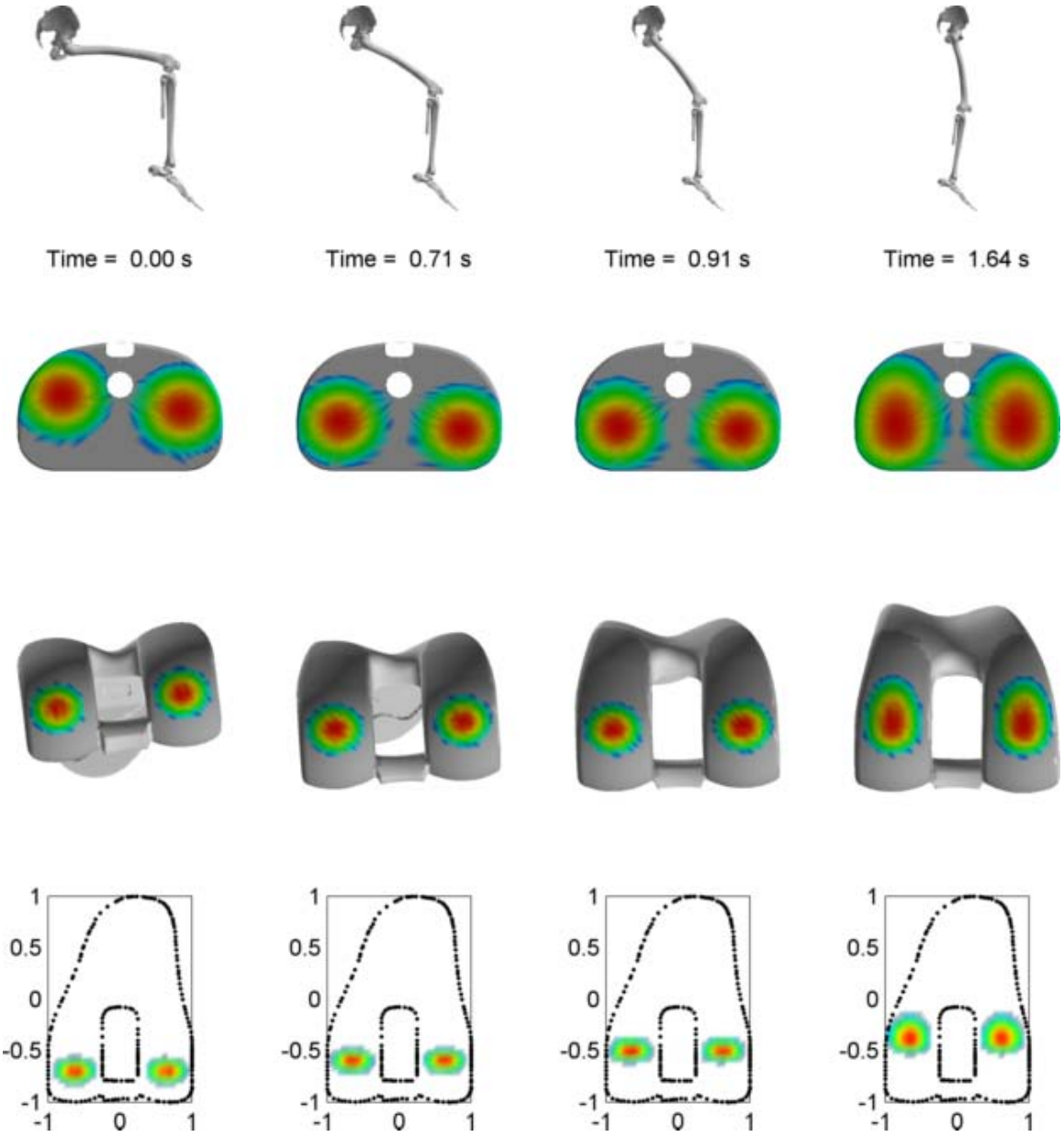


Figure A.15: Patient 3T dynamics model (top), tibiofemoral contact location mapped on the patient's specific patella (2^{nd} from top) and femur (2^{nd} from bottom) bone models, as well as the normalized contact location mapped on the unfolded femoral trochlea surface (bottom).

A.2.2 Electromyography and Inverse Dynamics analyses results

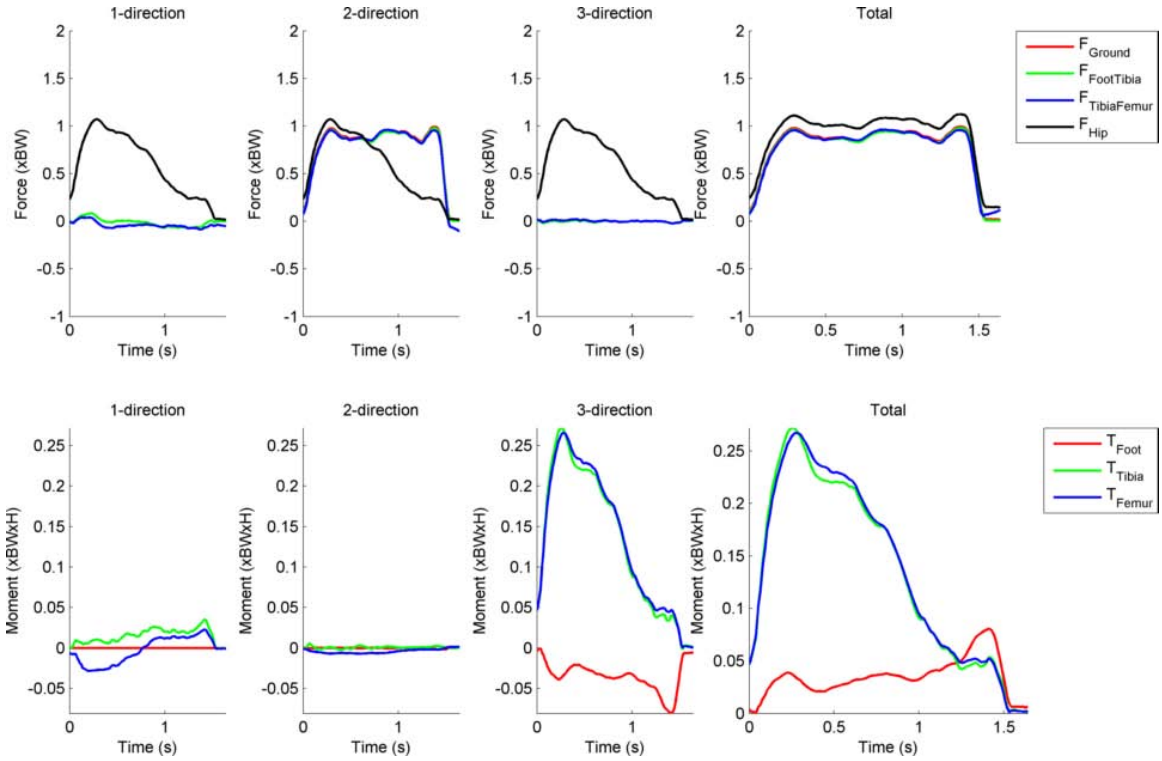


Figure A.16: Patient 3T knee joint reaction forces (top) and moments (bottom) normalized with respect to patient's body weight (BW). 1-direction = Anterior(+)/Posterior(-), 2-direction = Superior(+)/Inferior(-), 3-direction = Medial(+)/Lateral(-).

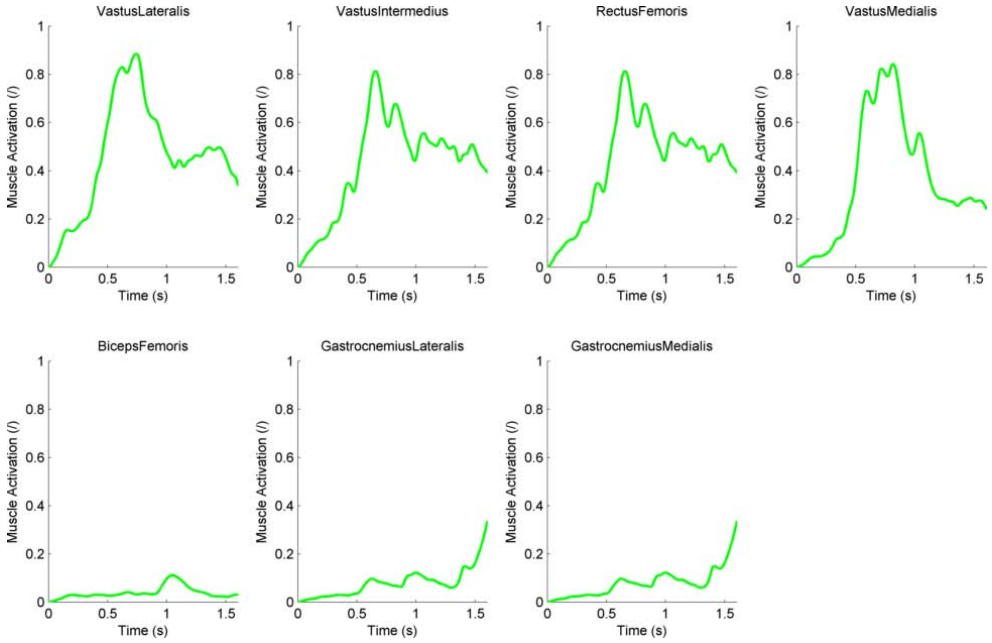


Figure A.17: Patient 3T muscle activation values obtained using the muscle activation dynamics[256].

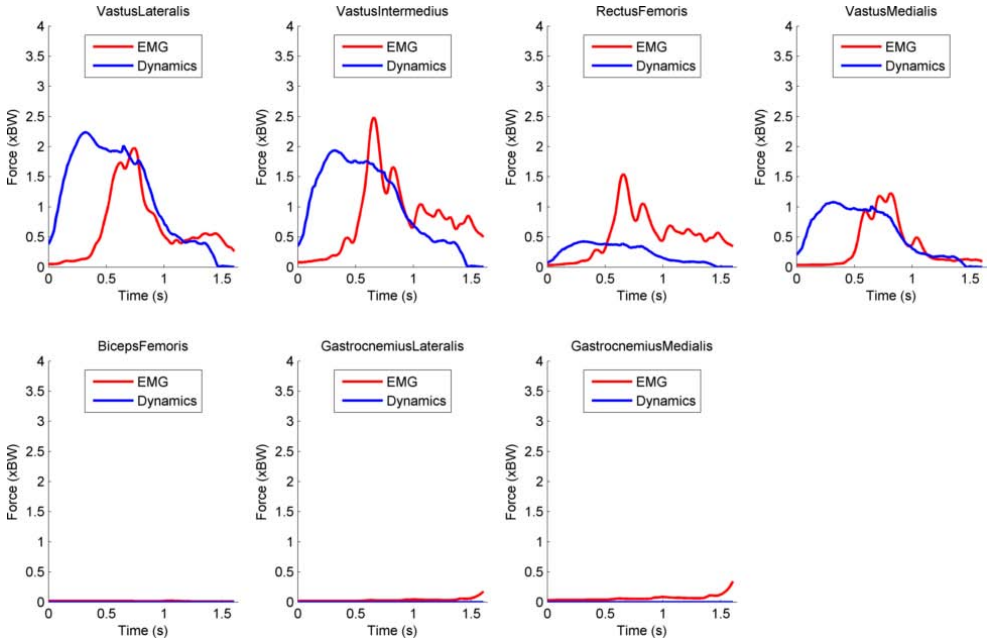


Figure A.18: Patient 3T muscle forces obtained using the EMG signal analysis (red) and pseudoinverse dynamics approach (green) normalized by patient's body weight (BW).

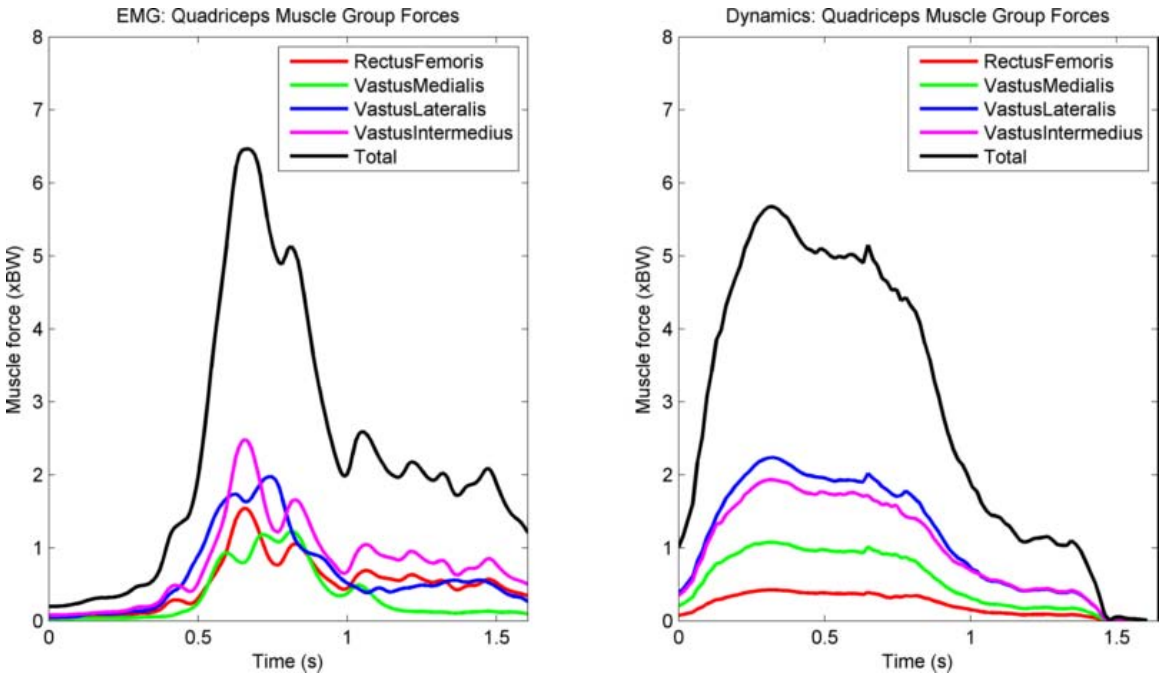


Figure A.19: Patient 3T quadriceps muscle group forces calculated from the EMG signals (left) and from the inverse dynamics (right) normalized by patient's body weight (BW).

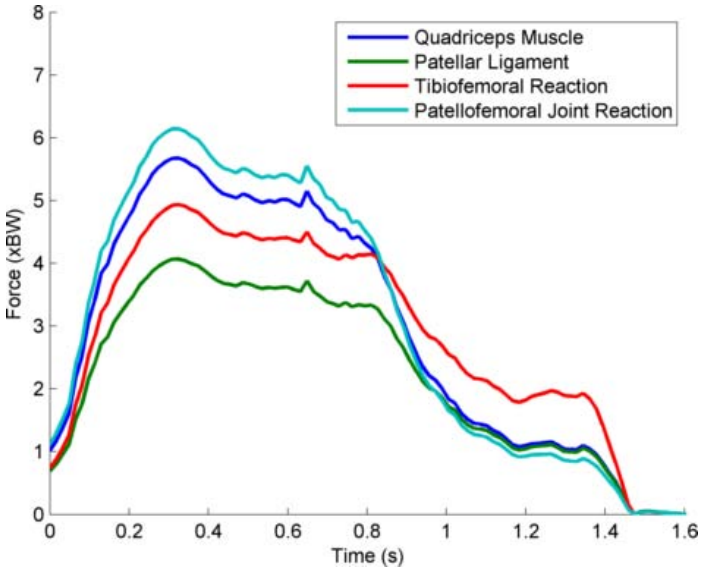


Figure A.20: Patient 3T total knee joint reaction forces incuding the action of the muscles, as well as the forces in the patellofemoral ligament, collateral and cruciate ligaments (if present) normalized by patient's body weight (BW).

A.3 Patient 4T

Patient demographic details:

ID# 4T

age: 84 yrs

height: 1.5 m

mass: 54 kg

leg side: Right

condition: TKA

A.3.1 Kinematics analysis results

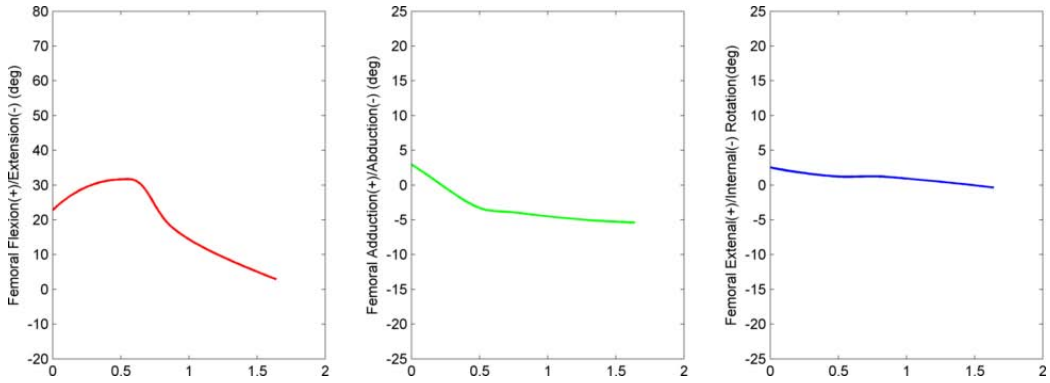


Figure A.21: Patient 4T patellofemoral joint kinematics.

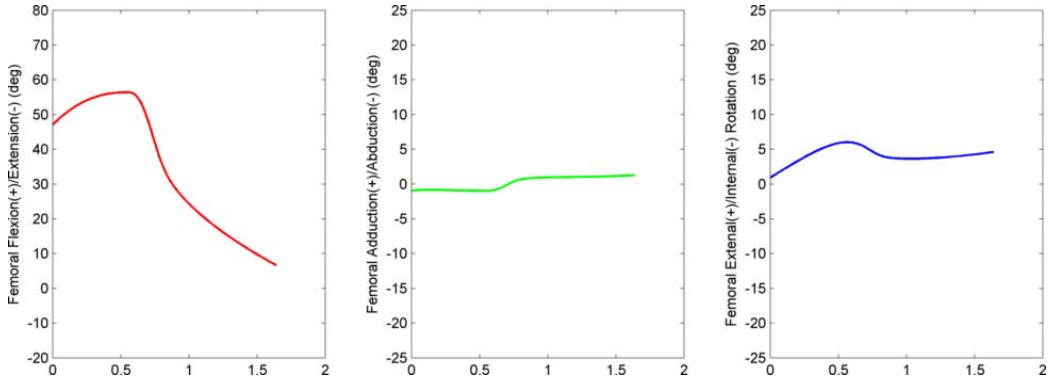


Figure A.22: Patient 4T tibiofemoral joint kinematics.

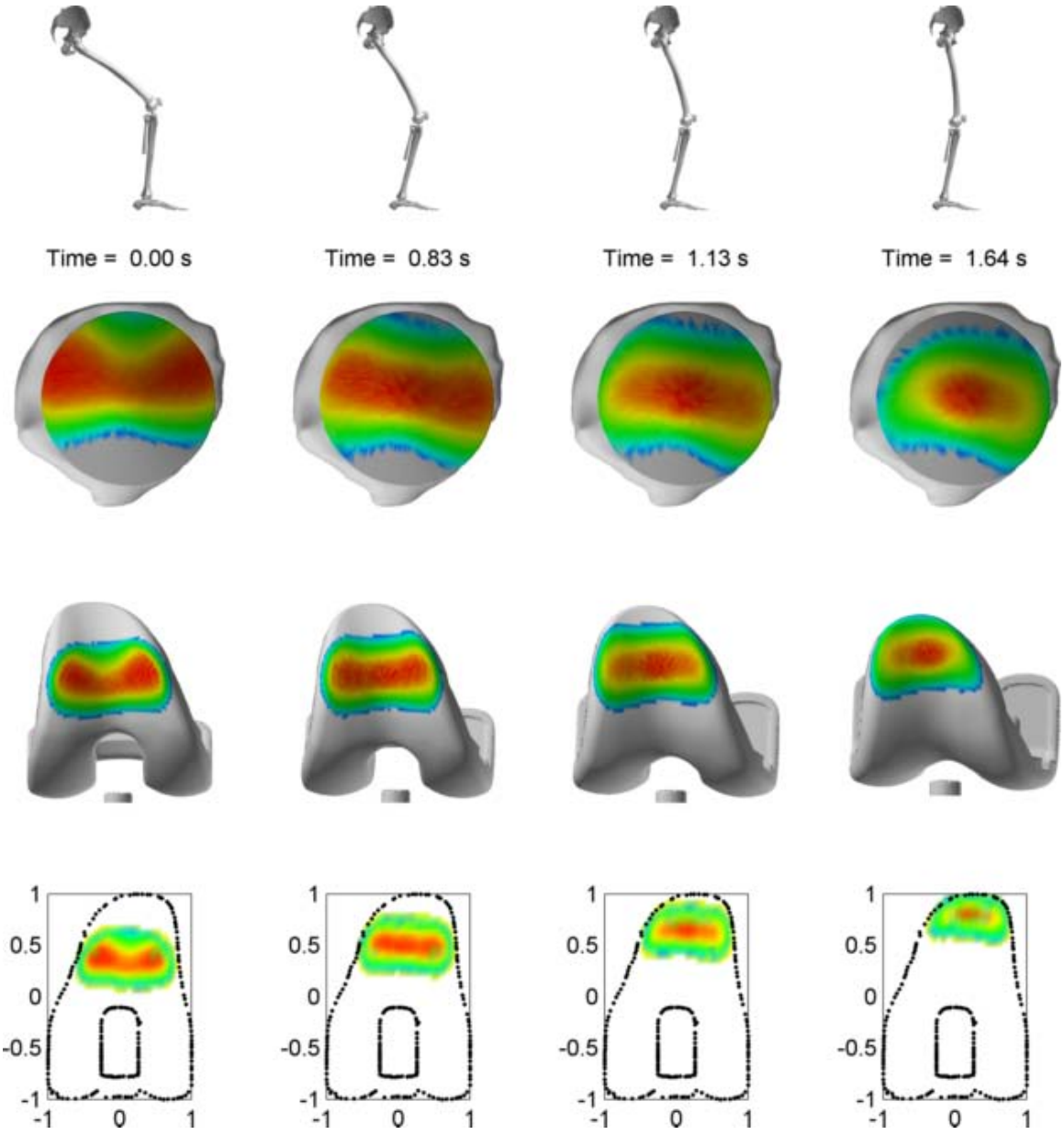


Figure A.23: Patient 4T dynamics model (top), patellofemoral contact location mapped on the patient's specific patella (2^{nd} from top) and femur (2^{nd} from bottom) bone models, as well as the normalized contact location mapped on the unfolded femoral trochlea surface (bottom).

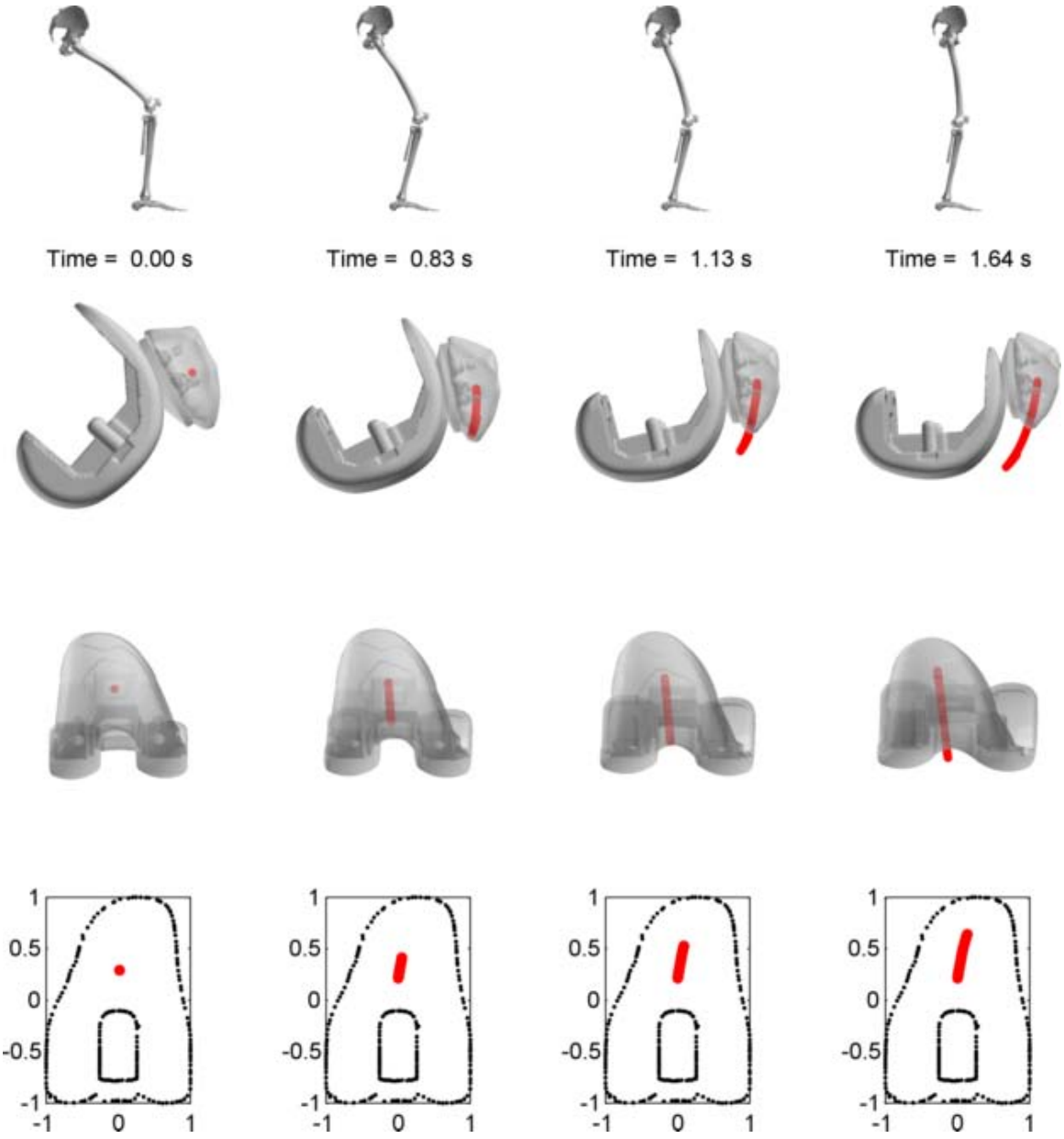


Figure A.24: Patient 4T dynamics model (top), patella center tracking in the sagittal (2^{nd} from top) and coronal (2^{nd} from bottom) planes, as well as the normalized patella tracking mapped on the unfolded femoral trochlea surface (bottom).

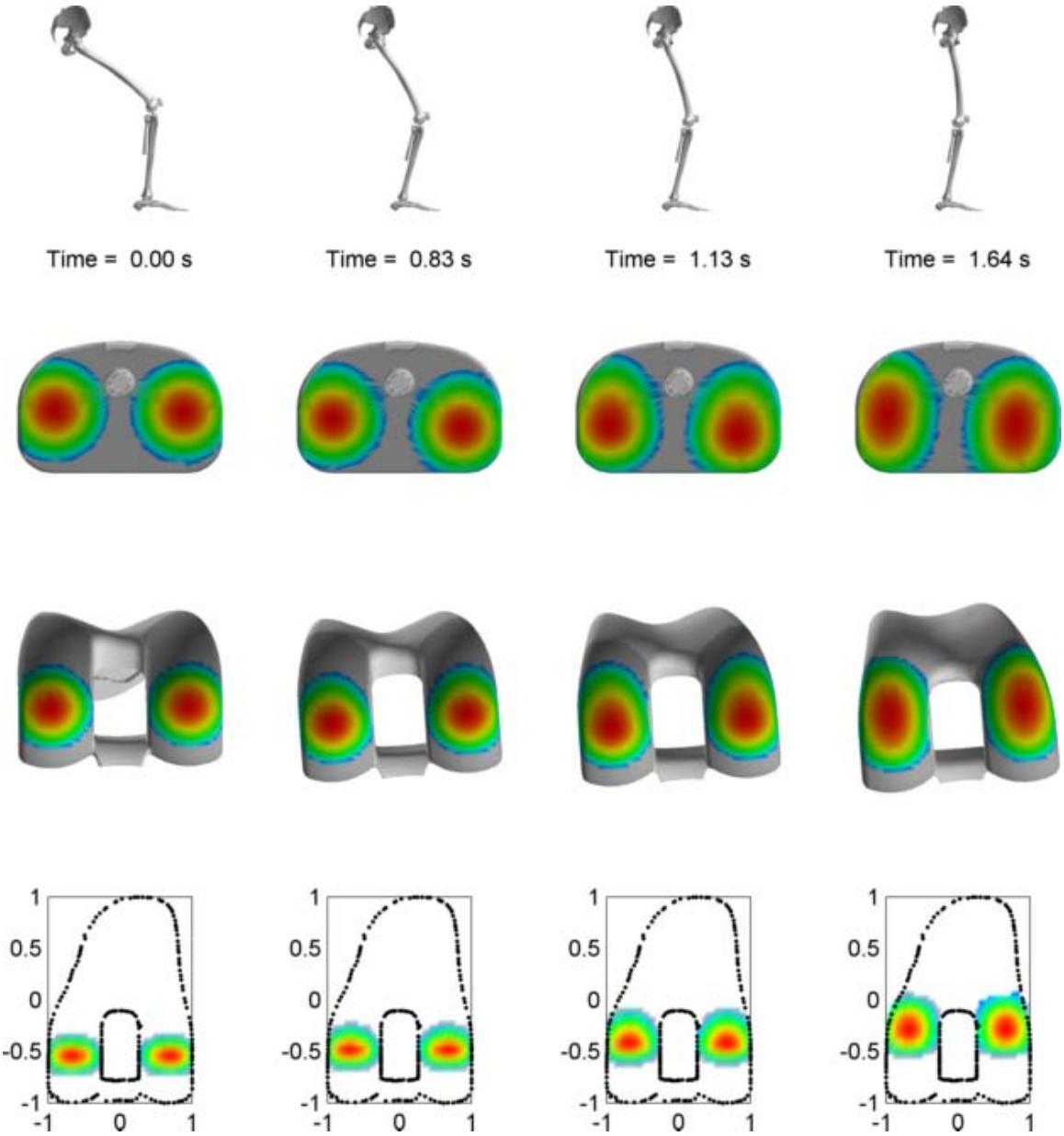


Figure A.25: Patient 4T dynamics model (top), tibiofemoral contact location mapped on the patient's specific patella (2^{nd} from top) and femur (2^{nd} from bottom) bone models, as well as the normalized contact location mapped on the unfolded femoral trochlea surface (bottom).

A.3.2 Electromyography and Inverse Dynamics analyses results

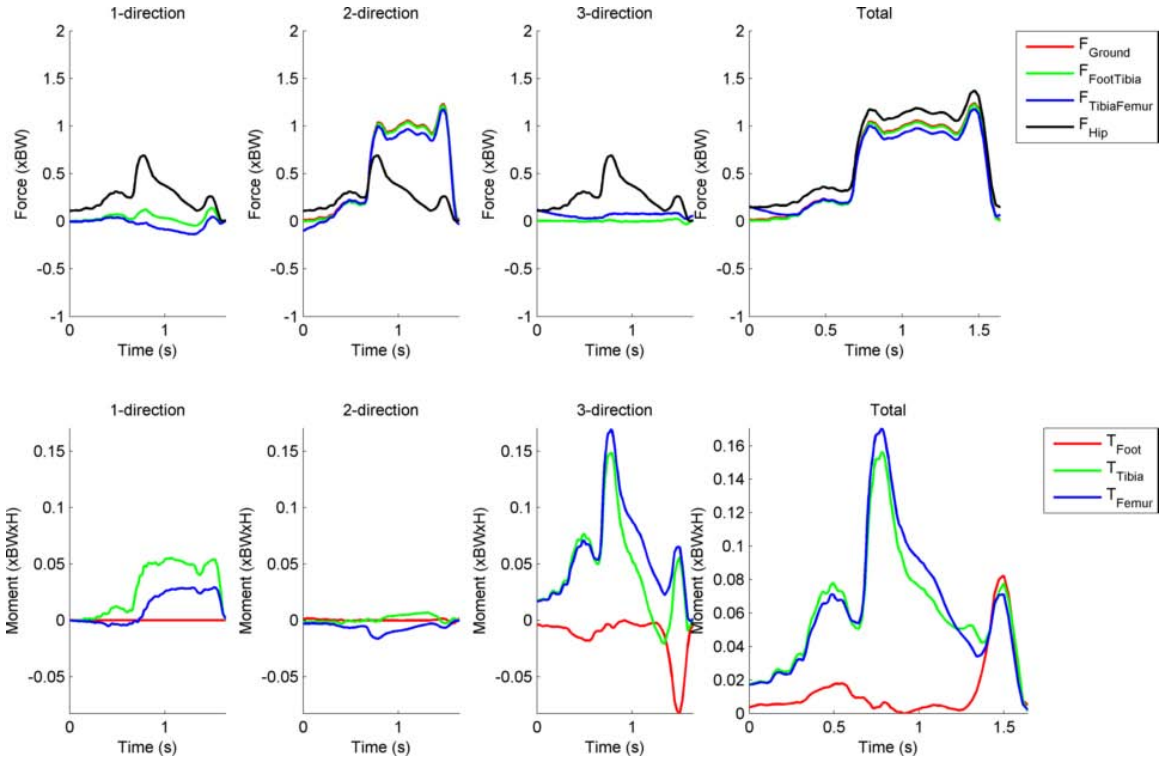


Figure A.26: Patient 4T knee joint reaction forces (top) and moments (bottom) normalized with respect to patient's body weight (BW). 1-direction = Anterior(+)/Posterior(-), 2-direction = Superior(+)/Inferior(-), 3-direction = Medial(+)/Lateral(-).

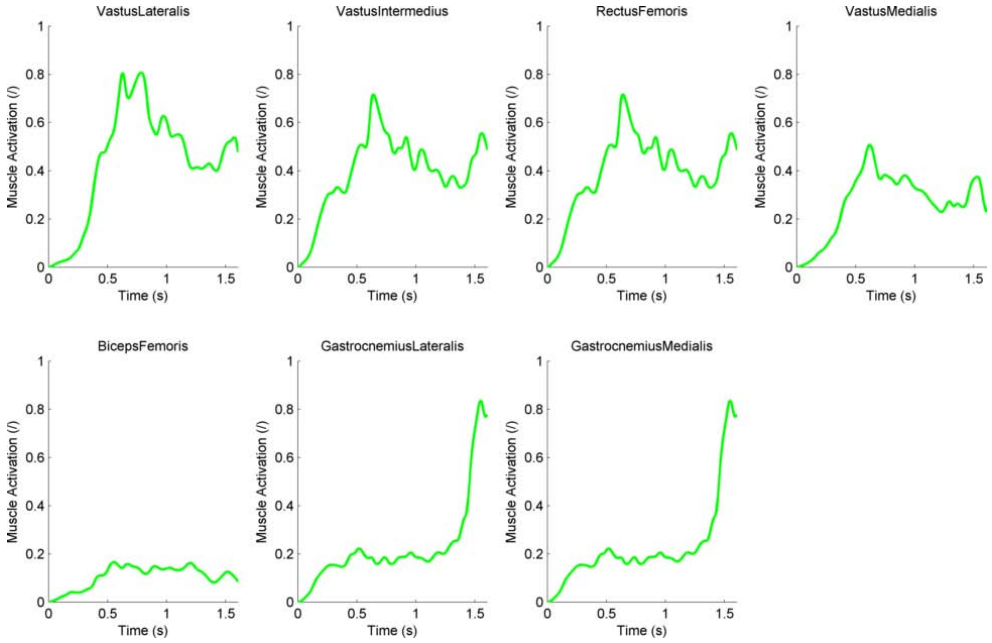


Figure A.27: Patient 4T muscle activation values obtained using the muscle activation dynamics[256].

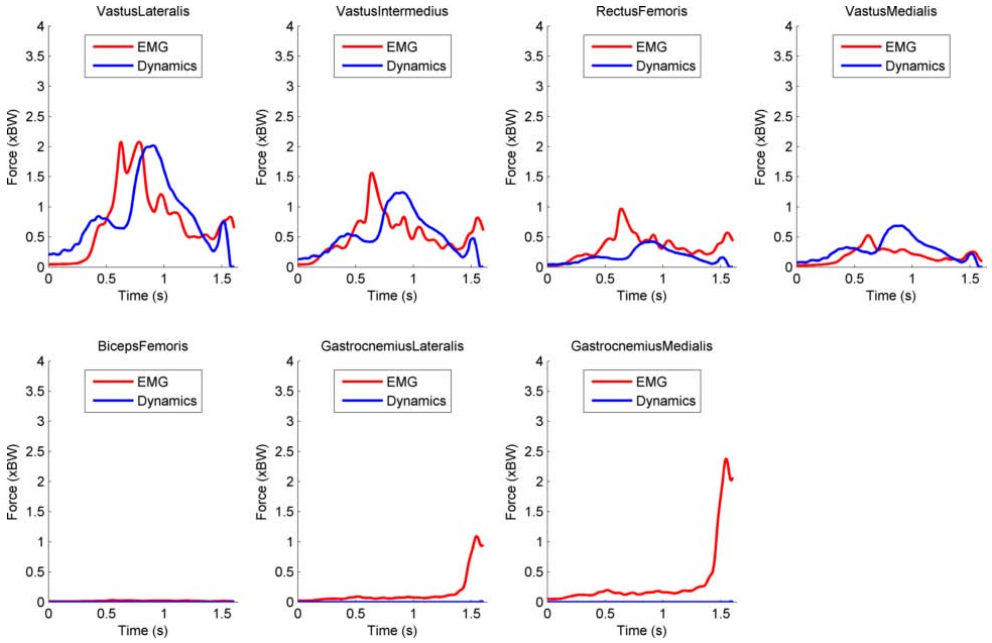


Figure A.28: Patient 4T muscle forces obtained using the EMG signal analysis (red) and pseudoinverse dynamics approach (green) normalized by patient's body weight (BW).

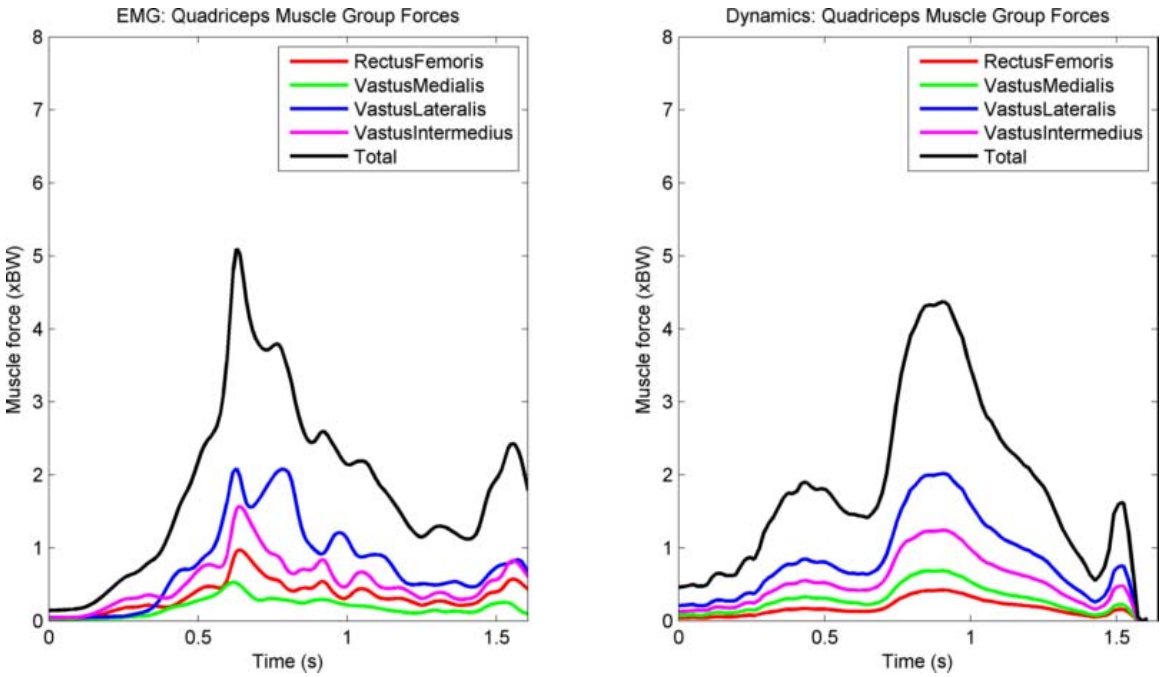


Figure A.29: Patient 4T quadriceps muscle group forces calculated from the EMG signals (left) and from the inverse dynamics (right) normalized by patient's body weight (BW).

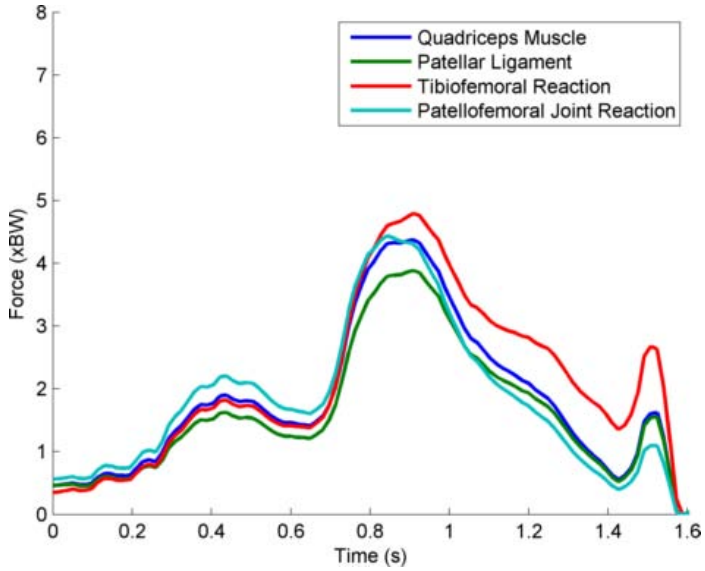


Figure A.30: Patient 4T total knee joint reaction forces incuding the action of the muscles, as well as the forces in the patellofemoral ligament, collateral and cruciate ligaments (if present) normalized by patient's body weight (BW).

A.4 Patient 8T

Patient demographic details:

ID# 8T

age: 66 yrs

height: 1.57 m

mass: 66 kg

leg side: Right

condition: TKA

A.4.1 Kinematics analysis results

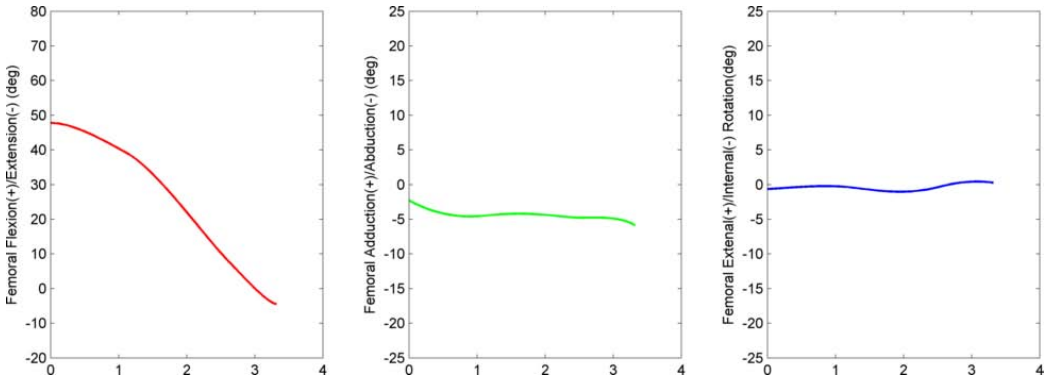


Figure A.31: Patient 8T patellofemoral joint kinematics.

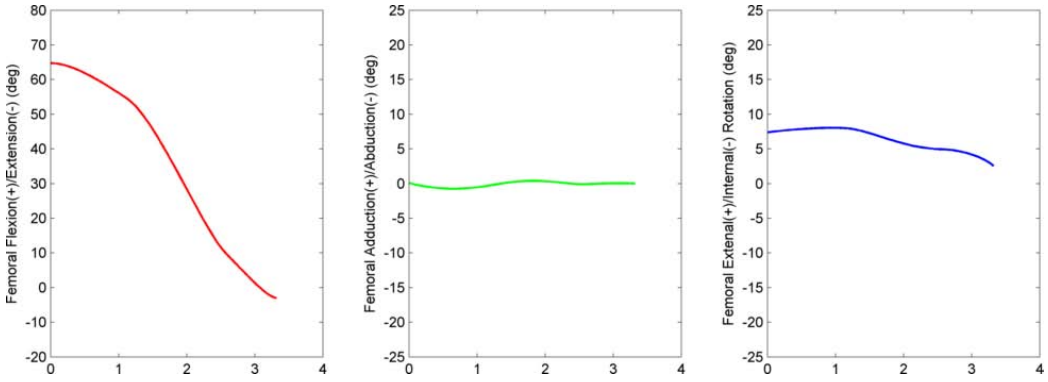


Figure A.32: Patient 8T tibiofemoral joint kinematics.

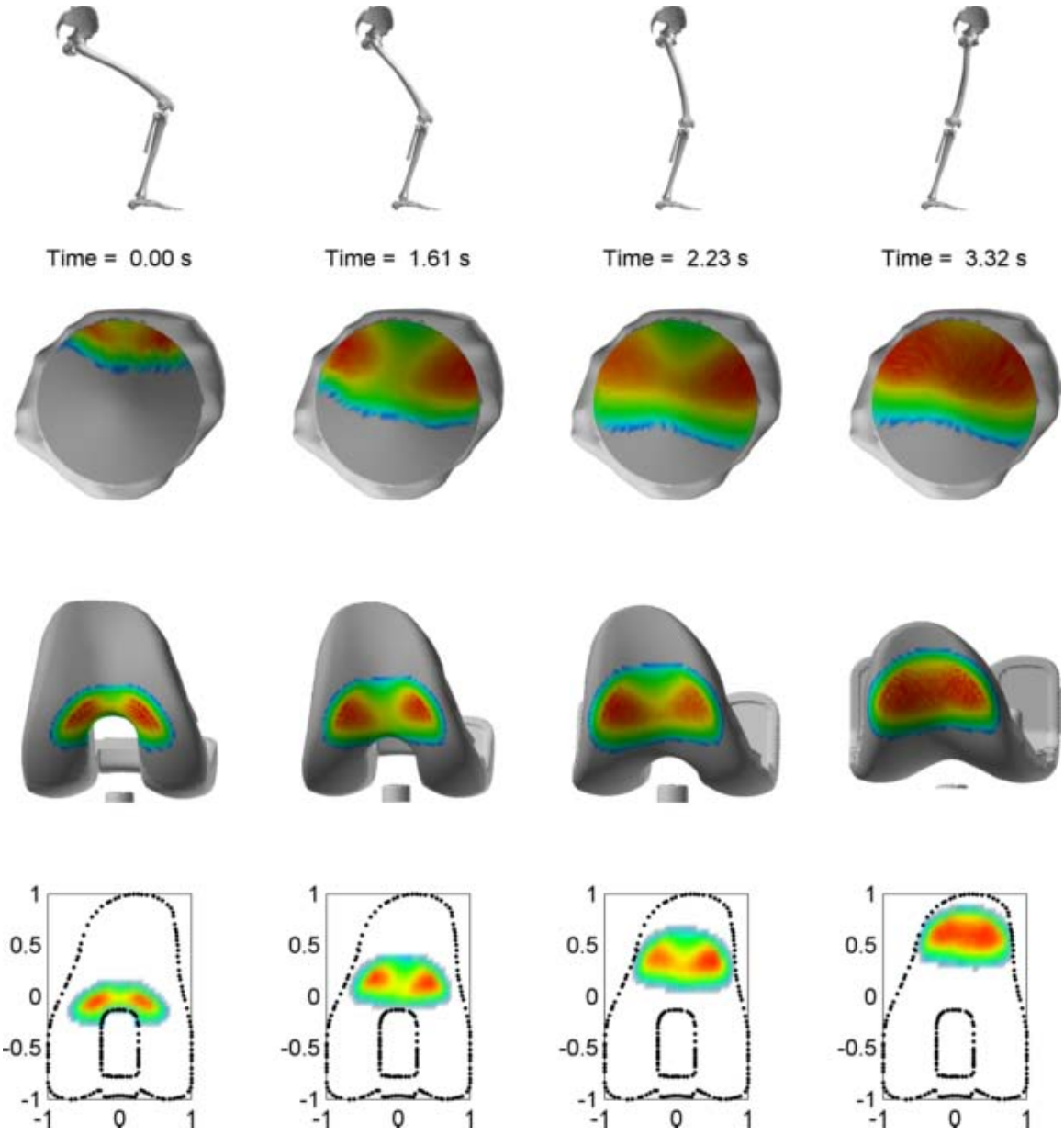


Figure A.33: Patient 8T dynamics model (top), patellofemoral contact location mapped on the patient's specific patella (2^{nd} from top) and femur (2^{nd} from bottom) bone models, as well as the normalized contact location mapped on the unfolded femoral trochlea surface (bottom).

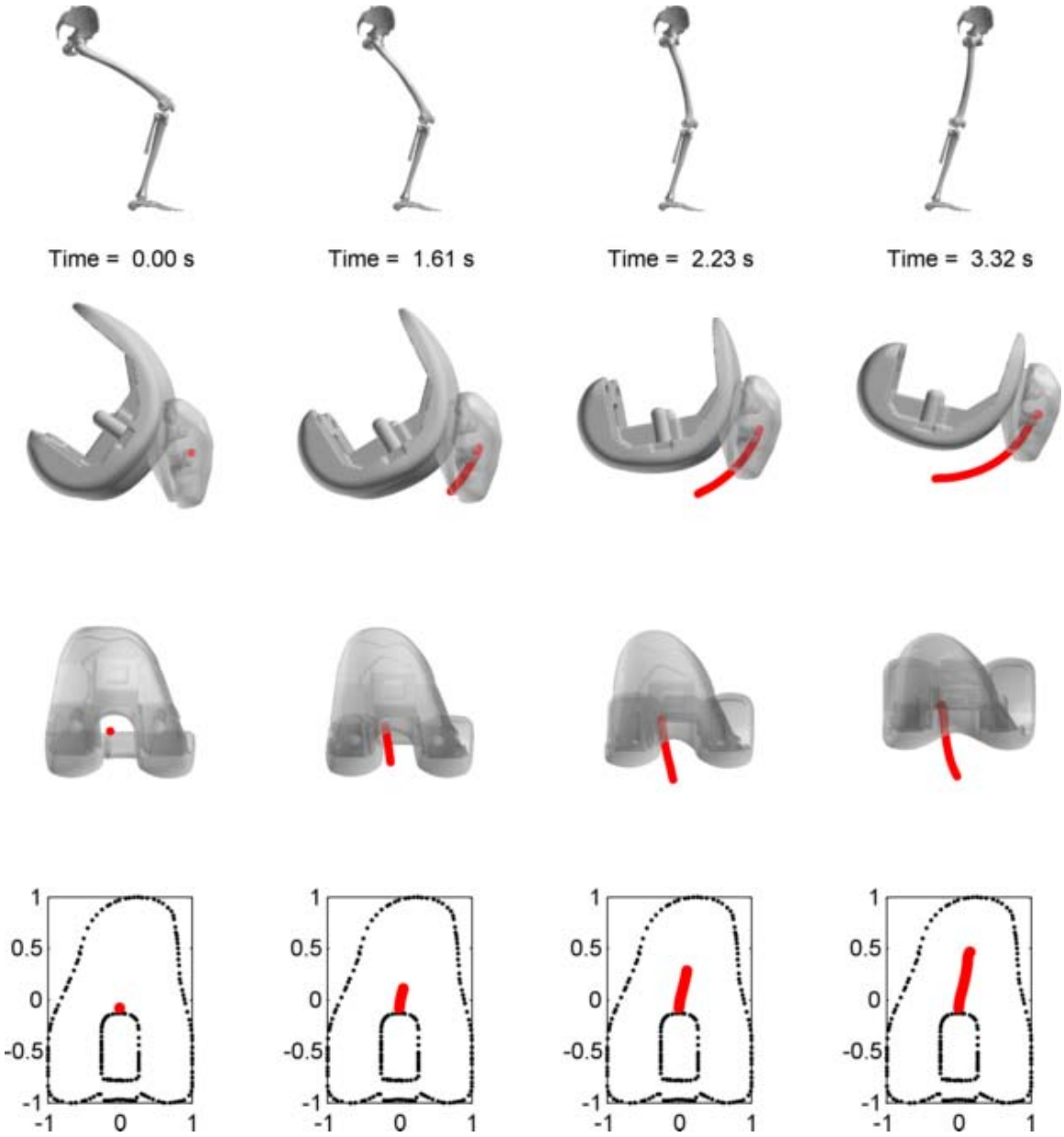


Figure A.34: Patient 8T dynamics model (top), patella center tracking in the sagittal (2^{nd} from top) and coronal (2^{nd} from bottom) planes, as well as the normalized patella tracking mapped on the unfolded femoral trochlea surface (bottom).

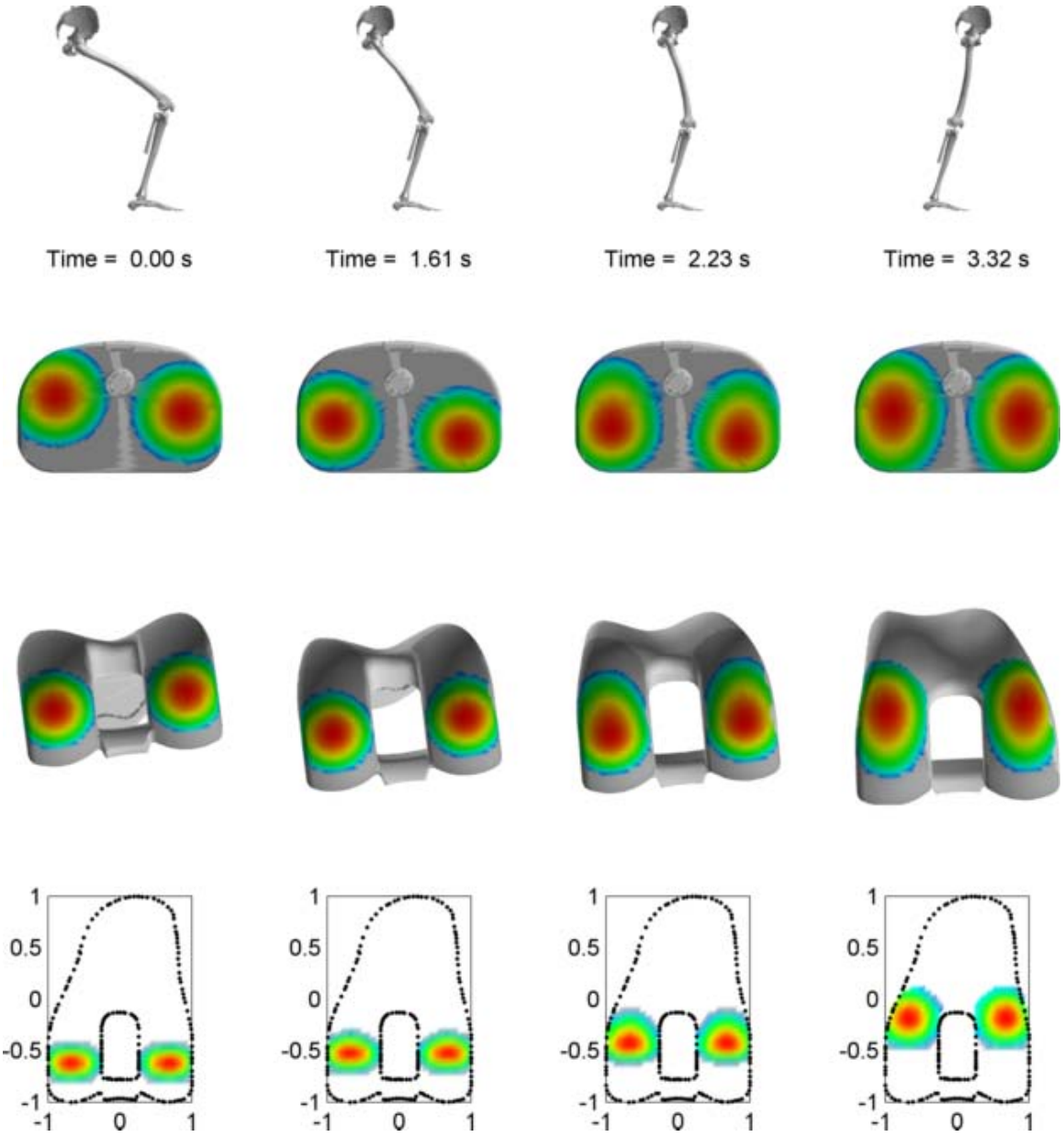


Figure A.35: Patient 8T dynamics model (top), tibiofemoral contact location mapped on the patient's specific patella (2^{nd} from top) and femur (2^{nd} from bottom) bone models, as well as the normalized contact location mapped on the unfolded femoral trochlea surface (bottom).

A.4.2 Electromyography and Inverse Dynamics analyses results

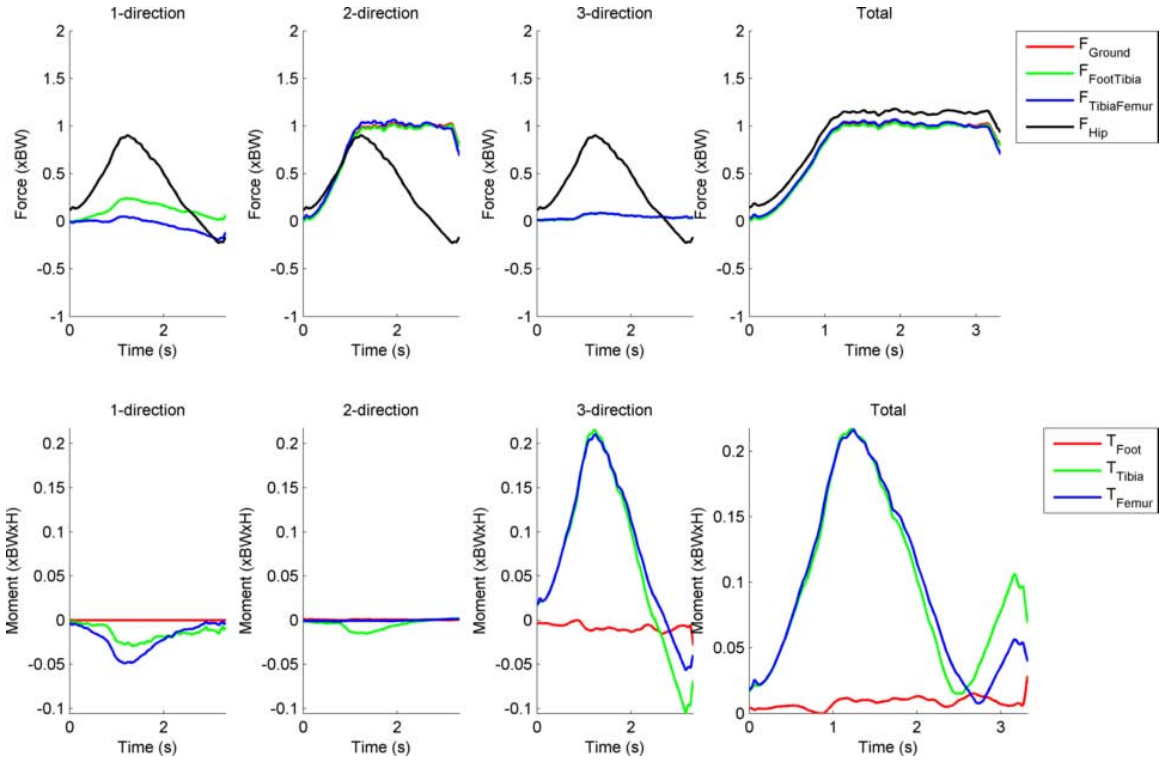


Figure A.36: Patient 8T knee joint reaction forces (top) and moments (bottom) normalized with respect to patient's body weight (BW). 1-direction = Anterior(+)/Posterior(-), 2-direction = Superior(+)/Inferior(-), 3-direction = Medial(+)/Lateral(-).

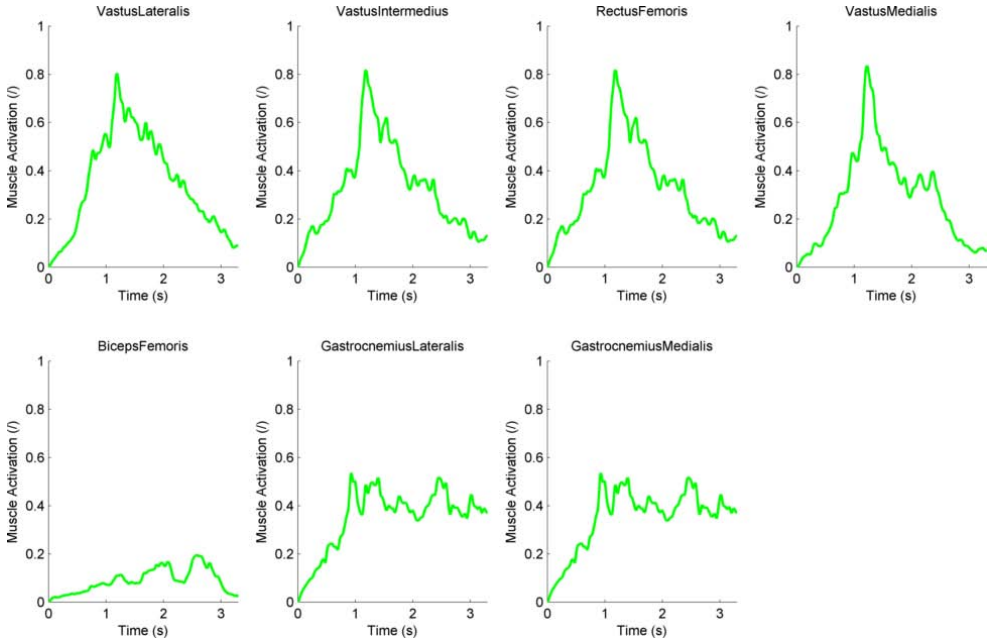


Figure A.37: Patient 8T muscle activation values obtained using the muscle activation dynamics[256].

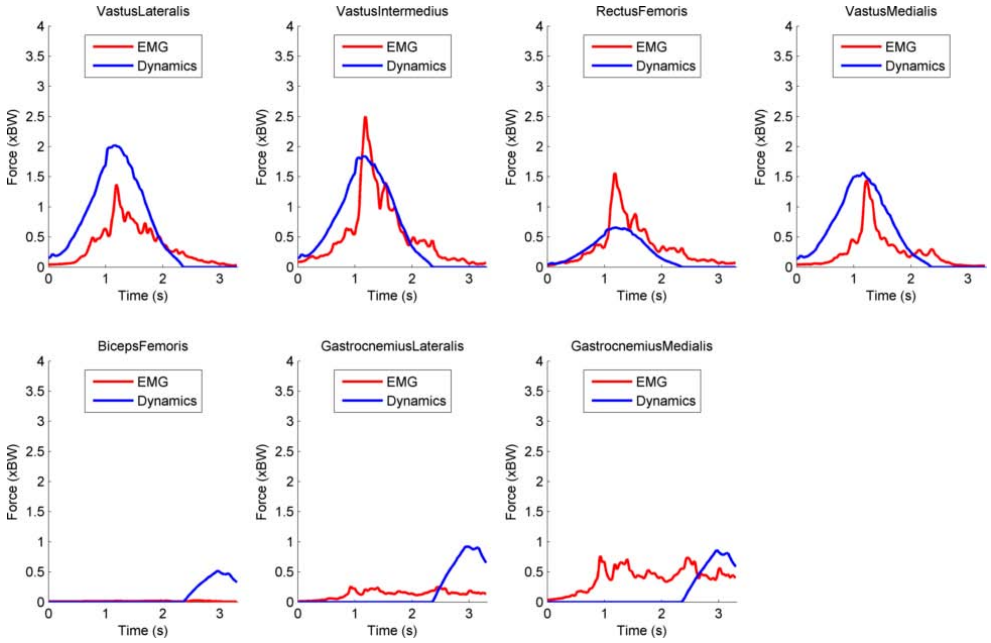


Figure A.38: Patient 8T muscle forces obtained using the EMG signal analysis (red) and pseudoinverse dynamics approach (green) normalized by patient's body weight (BW).

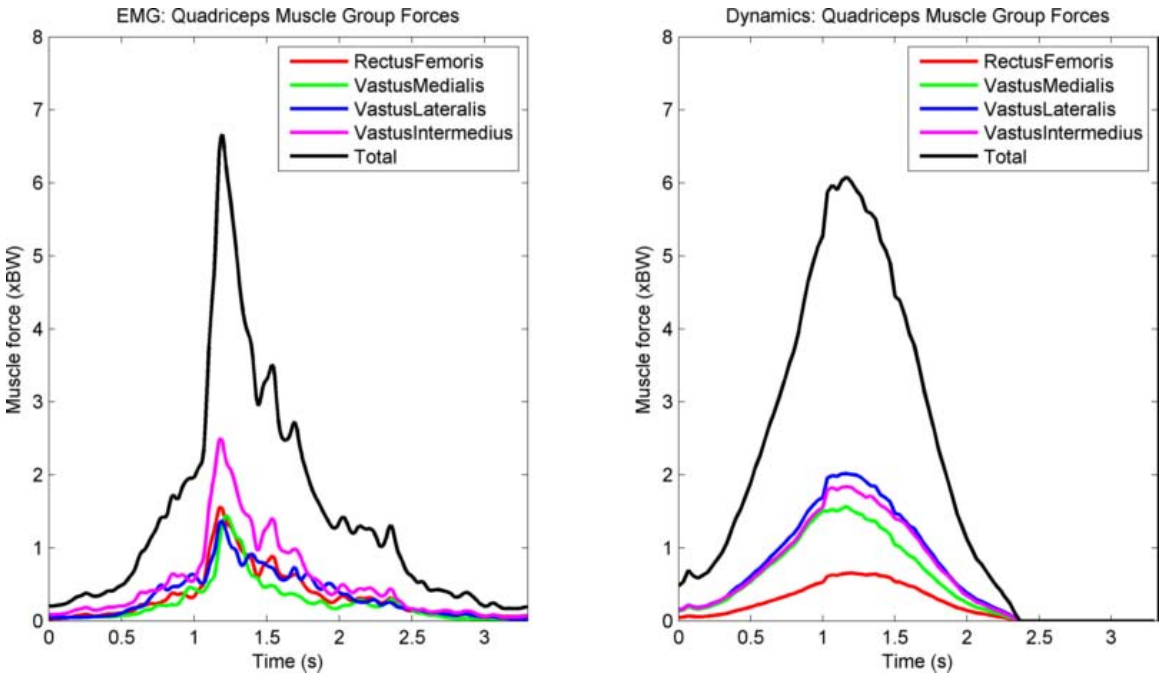


Figure A.39: Patient 8T quadriceps muscle group forces calculated from the EMG signals (left) and from the inverse dynamics (right) normalized by patient's body weight (BW).

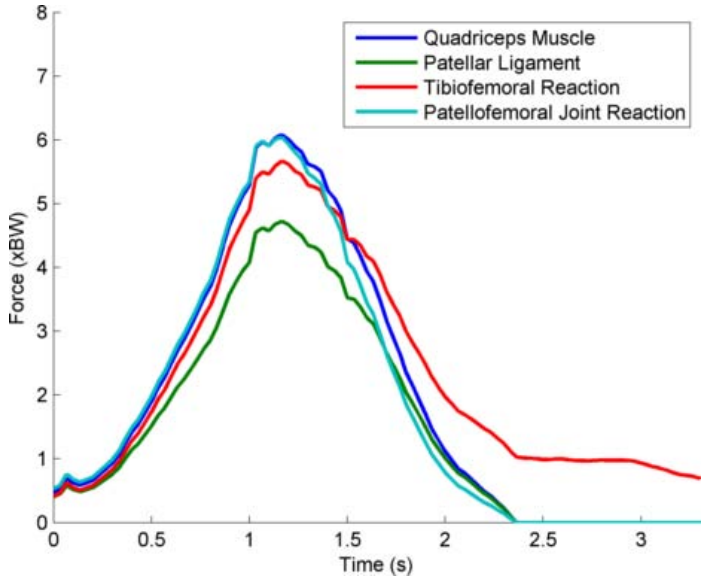


Figure A.40: Patient 8T total knee joint reaction forces incuding the action of the muscles, as well as the forces in the patellofemoral ligament, collateral and cruciate ligaments (if present) normalized by patient's body weight (BW).

A.5 Patient 12T

Patient demographic details:

ID# 12T

age: 66 yrs

height: 1.44 m

mass: 58 kg

leg side: Right

condition: TKA

A.5.1 Kinematics analysis results

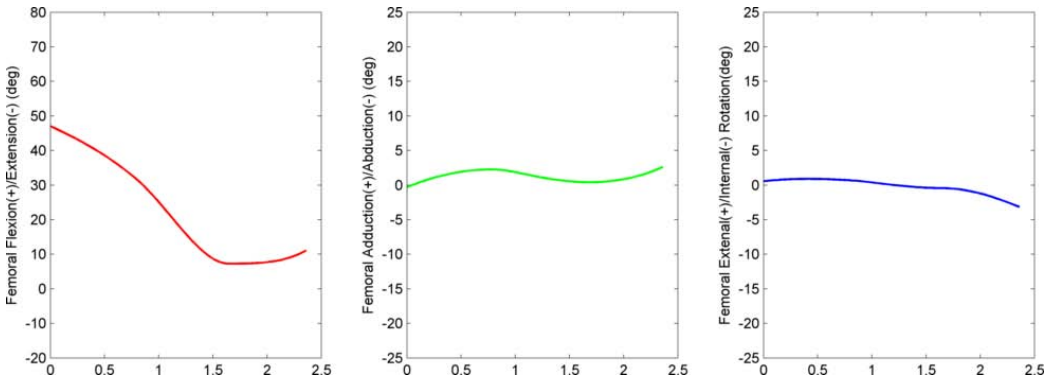


Figure A.41: Patient 12T patellofemoral joint kinematics.

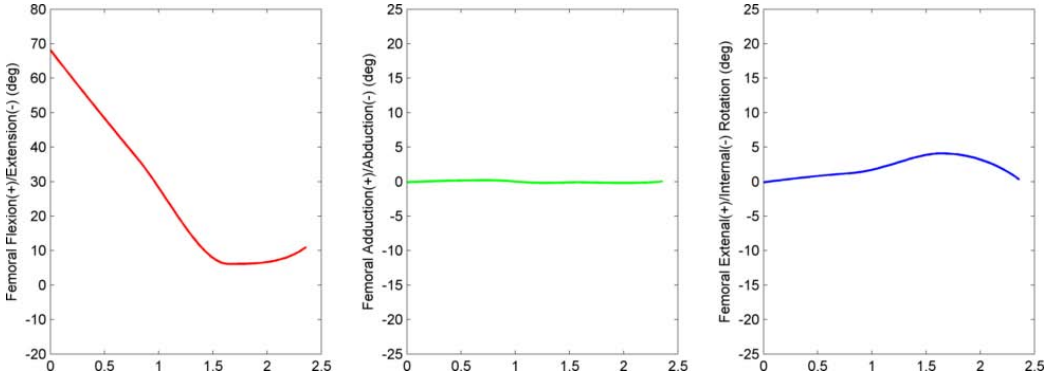


Figure A.42: Patient 12T tibiofemoral joint kinematics.

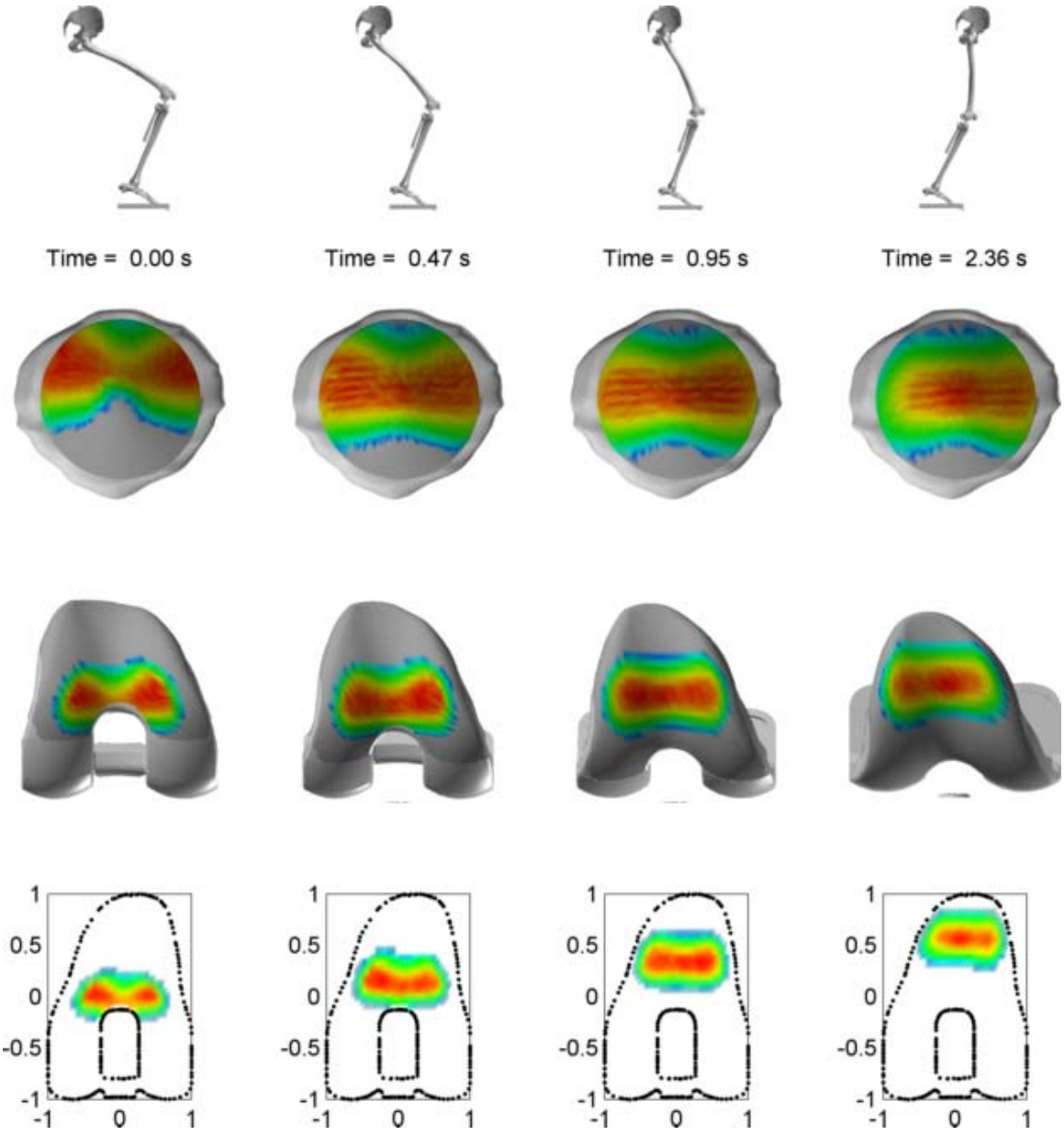


Figure A.43: Patient 12T dynamics model (top), patellofemoral contact location mapped on the patient's specific patella (2^{nd} from top) and femur (2^{nd} from bottom) bone models, as well as the normalized contact location mapped on the unfolded femoral trochlea surface (bottom).

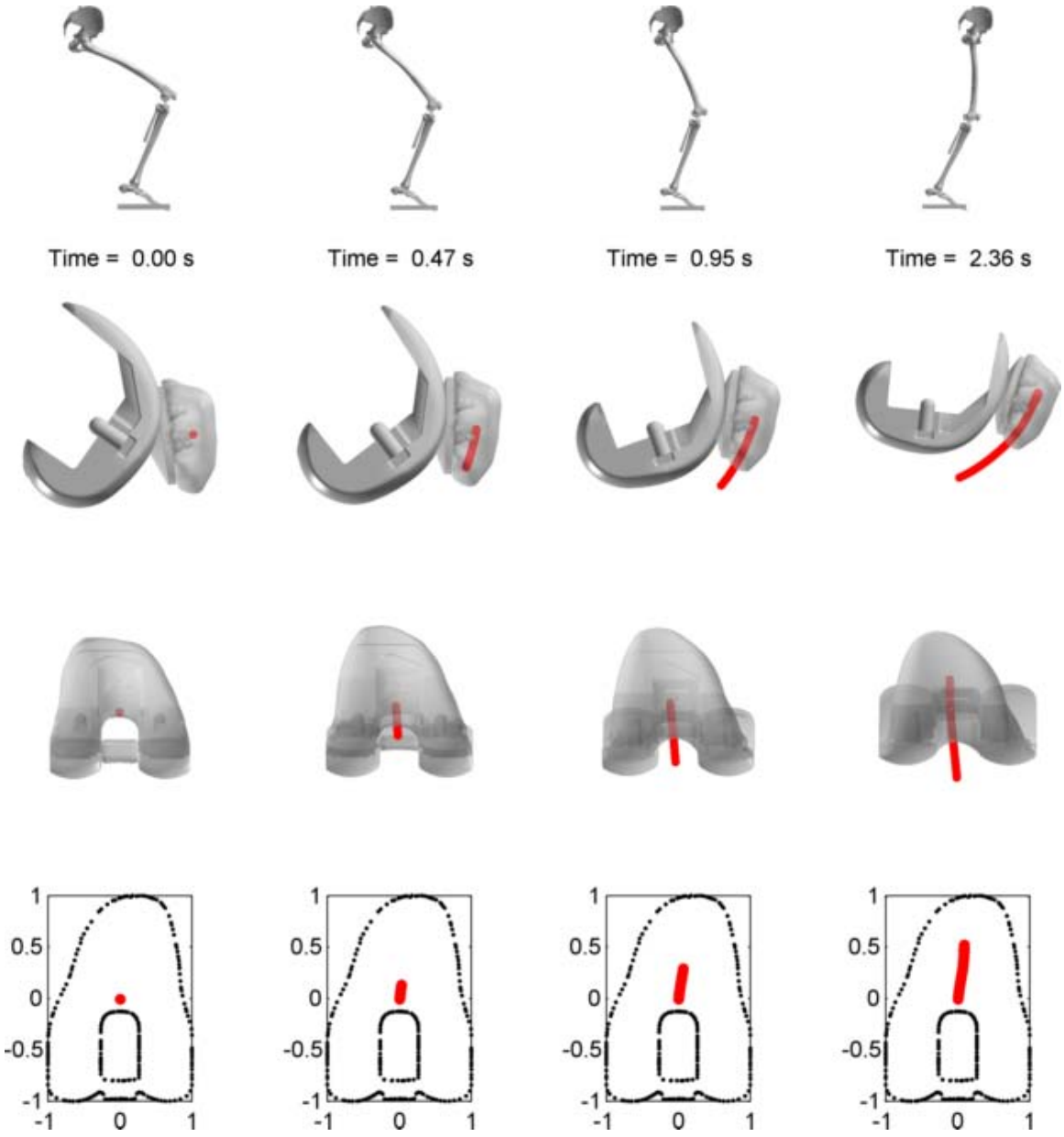


Figure A.44: Patient 12T dynamics model (top), patella center tracking in the sagittal (2^{nd} from top) and coronal (2^{nd} from bottom) planes, as well as the normalized patella tracking mapped on the unfolded femoral trochlea surface (bottom).

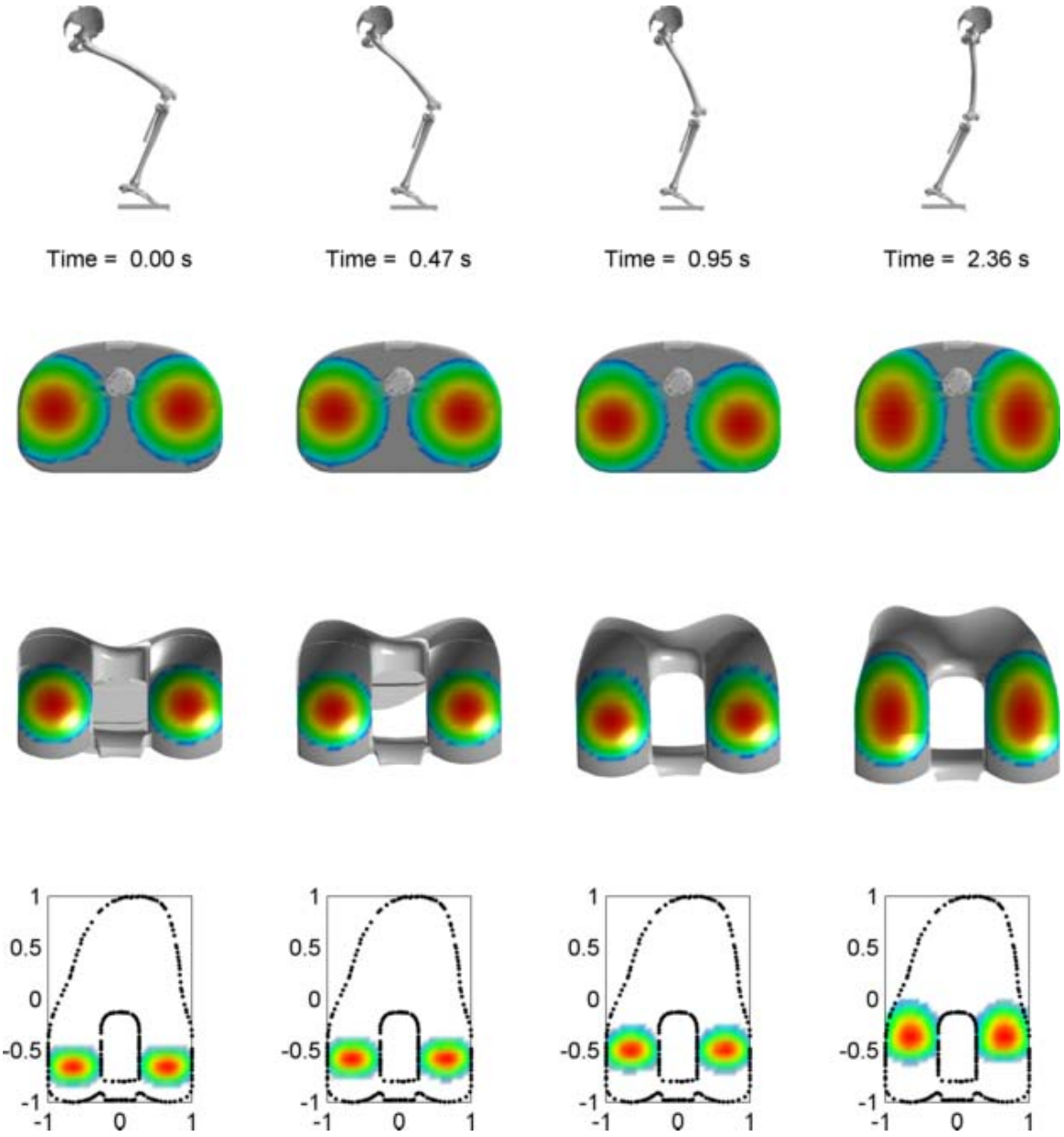


Figure A.45: Patient 12T dynamics model (top), tibiofemoral contact location mapped on the patient's specific patella (2^{nd} from top) and femur (2^{nd} from bottom) bone models, as well as the normalized contact location mapped on the unfolded femoral trochlea surface (bottom).

A.5.2 Electromyography and Inverse Dynamics analyses results

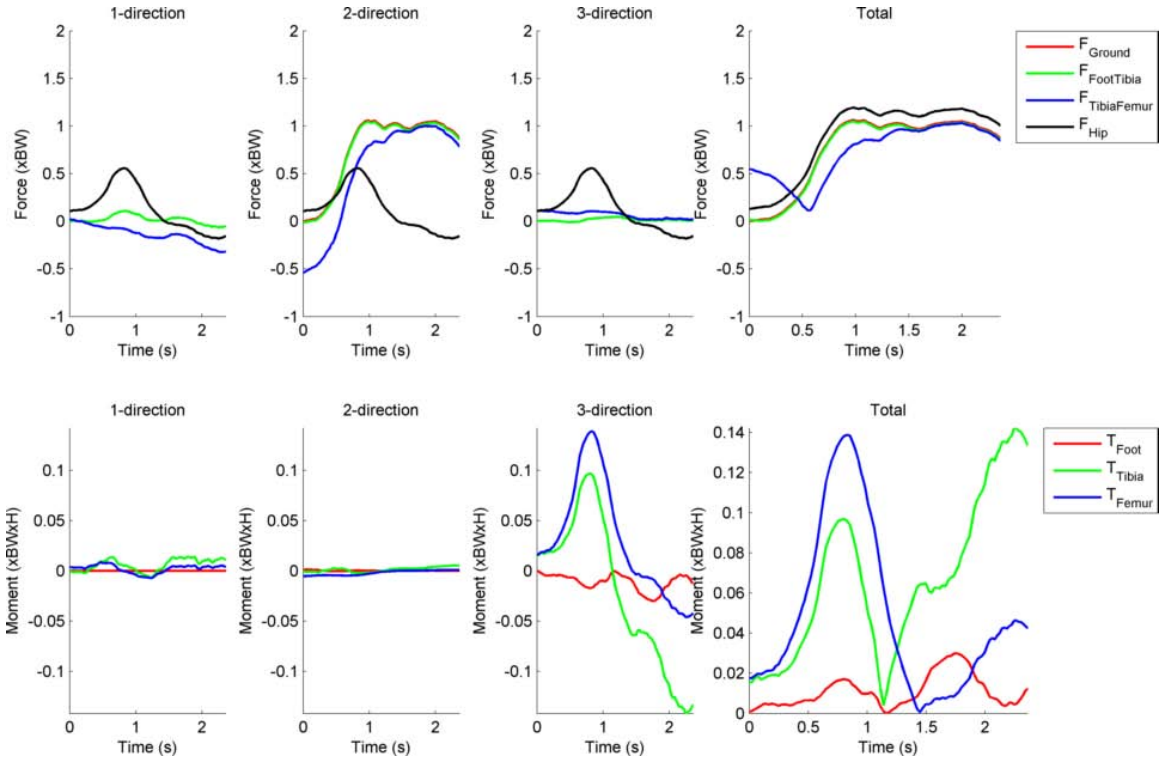


Figure A.46: Patient 12T knee joint reaction forces (top) and moments (bottom) normalized with respect to patient's body weight (BW). 1-direction = Anterior(+)/Posterior(-), 2-direction = Superior(+)/Inferior(-), 3-direction = Medial(+)/Lateral(-).

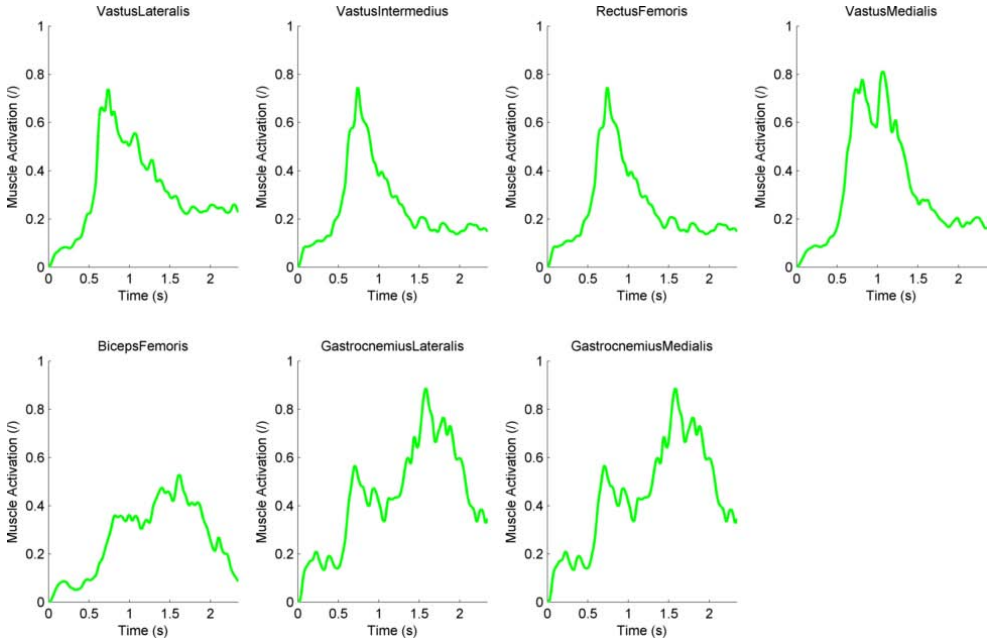


Figure A.47: Patient 12T muscle activation values obtained using the muscle activation dynamics[256].

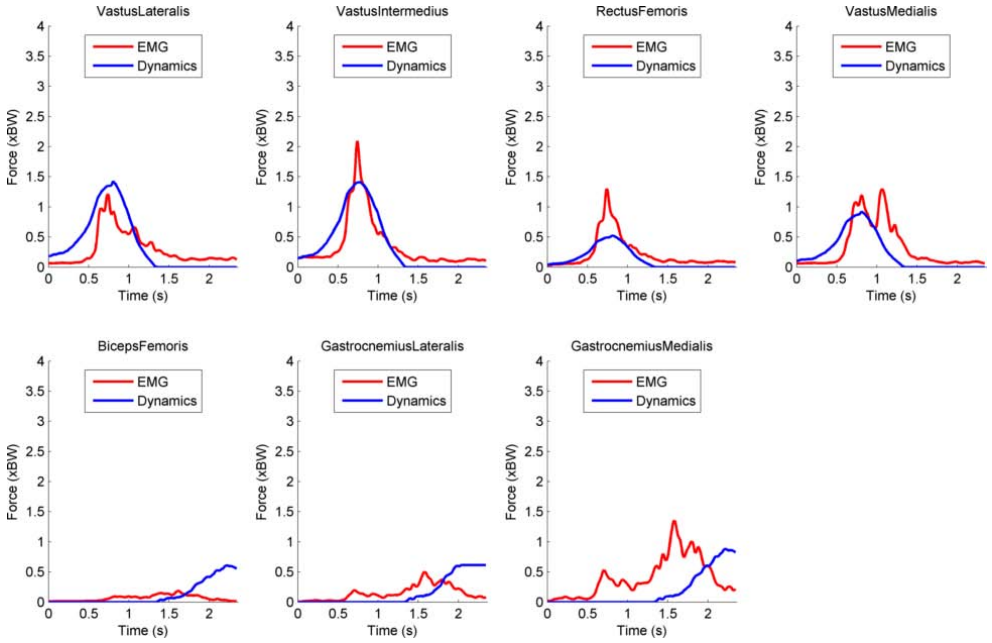


Figure A.48: Patient 12T muscle forces obtained using the EMG signal analysis (red) and pseudoinverse dynamics approach (green) normalized by patient's body weight (BW).

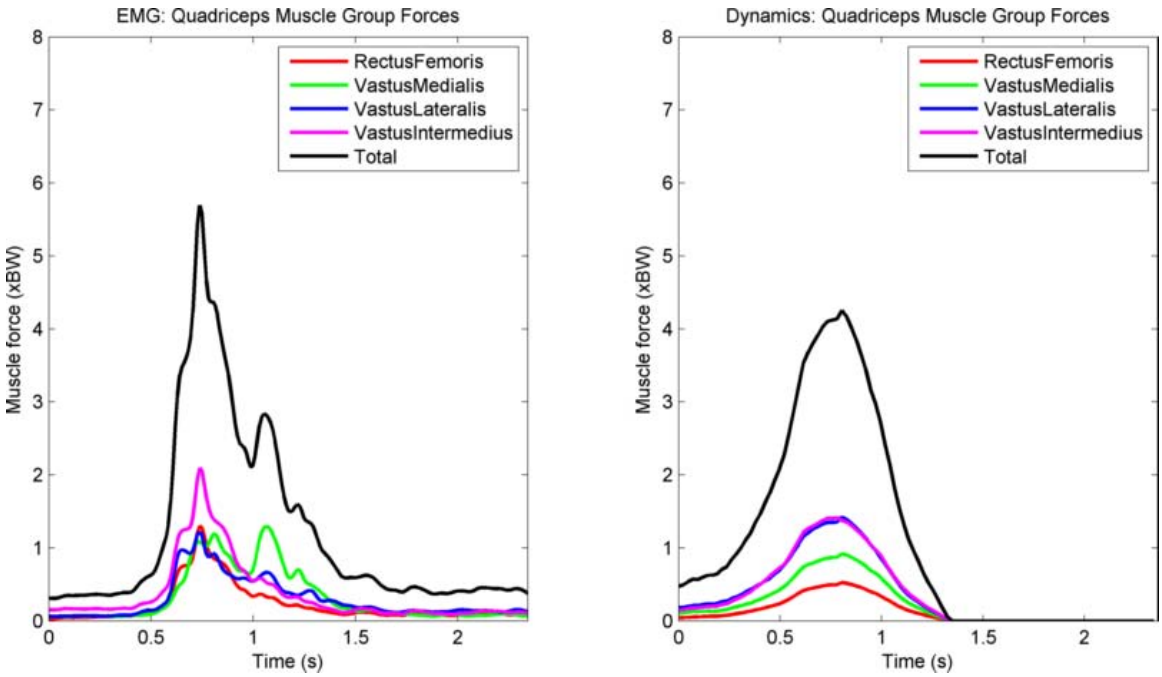


Figure A.49: Patient 12T quadriceps muscle group forces calculated from the EMG signals (left) and from the inverse dynamics (right) normalized by patient's body weight (BW).

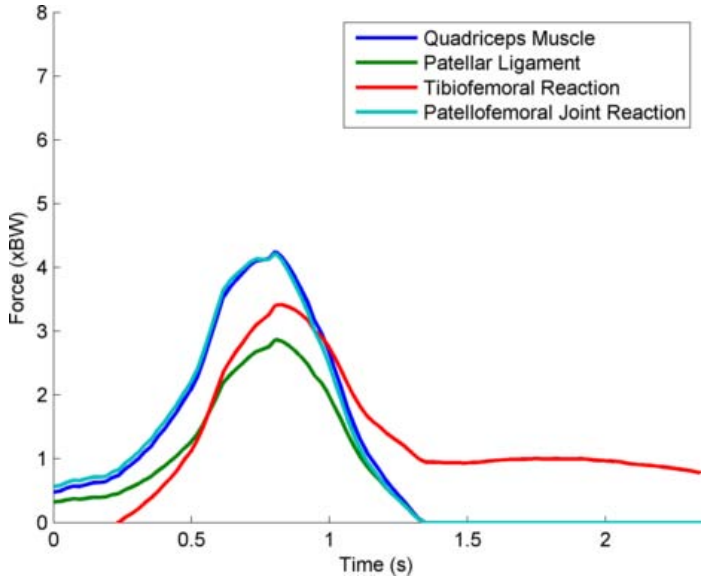


Figure A.50: Patient 12T total knee joint reaction forces incuding the action of the muscles, as well as the forces in the patellofemoral ligament, collateral and cruciate ligaments (if present) normalized by patient's body weight (BW).

A.6 Patient 13T

Patient demographic details:

ID# 13T

age: 83 yrs

height: 1.73 m

mass: 70 kg

leg side: Left

condition: TKA

A.6.1 Kinematics analysis results

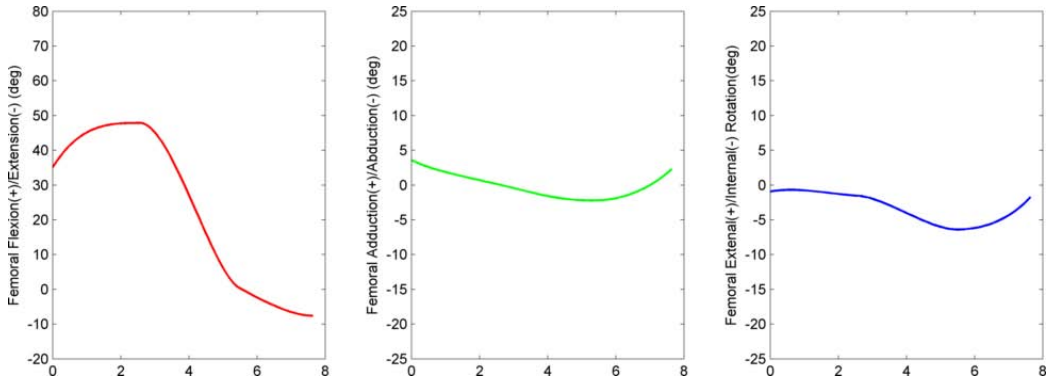


Figure A.51: Patient 13T patellofemoral joint kinematics.

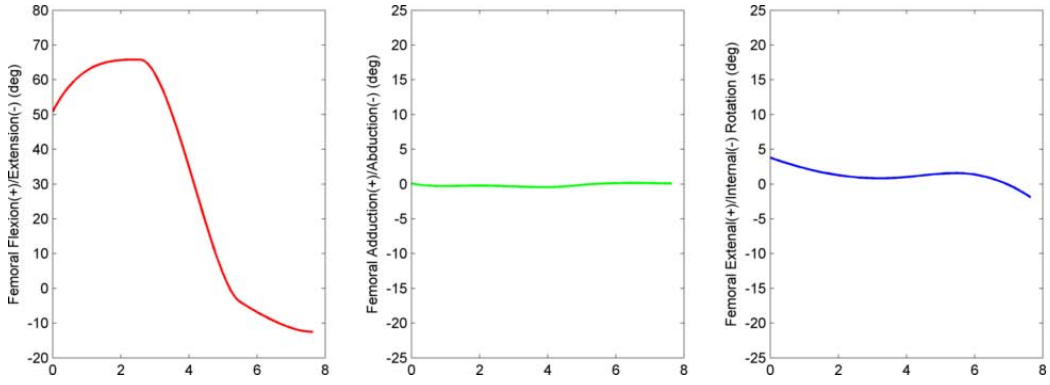


Figure A.52: Patient 13T tibiofemoral joint kinematics.

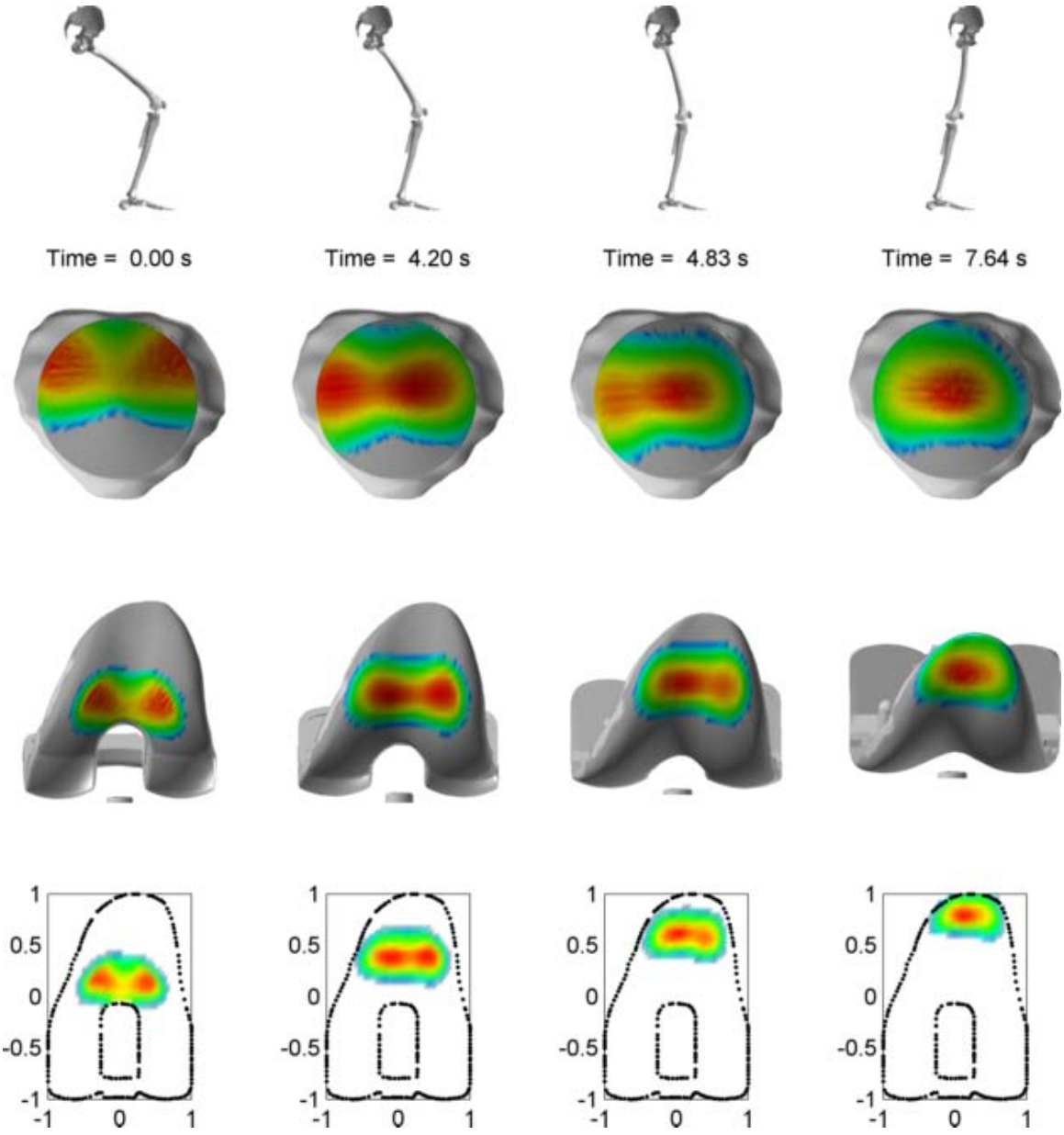


Figure A.53: Patient 13T dynamics model (top), patellofemoral contact location mapped on the patient's specific patella (2^{nd} from top) and femur (2^{nd} from bottom) bone models, as well as the normalized contact location mapped on the unfolded femoral trochlea surface (bottom).

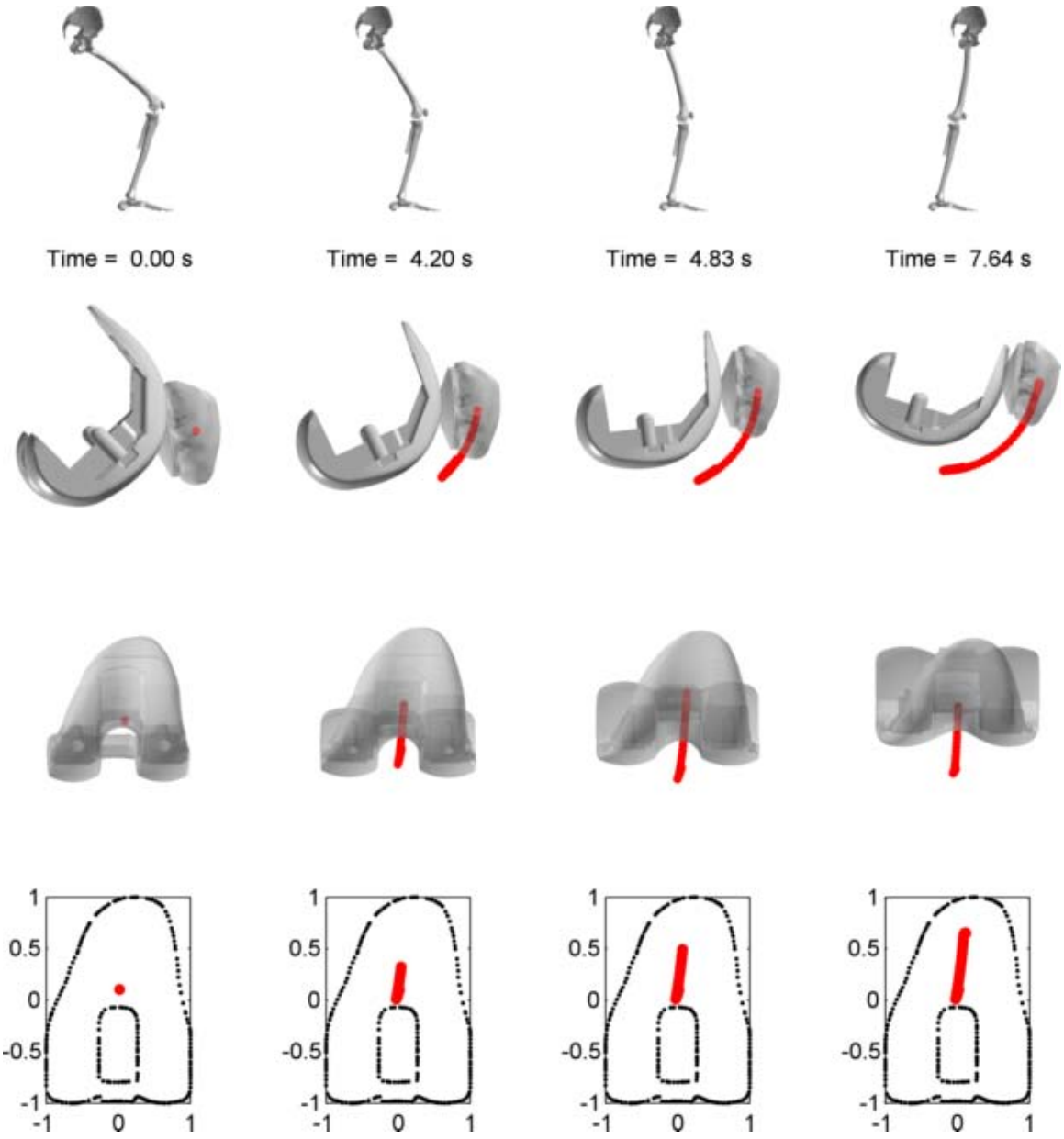


Figure A.54: Patient 13T dynamics model (top), patella center tracking in the sagittal (2^{nd} from top) and coronal (2^{nd} from bottom) planes, as well as the normalized patella tracking mapped on the unfolded femoral trochlea surface (bottom).

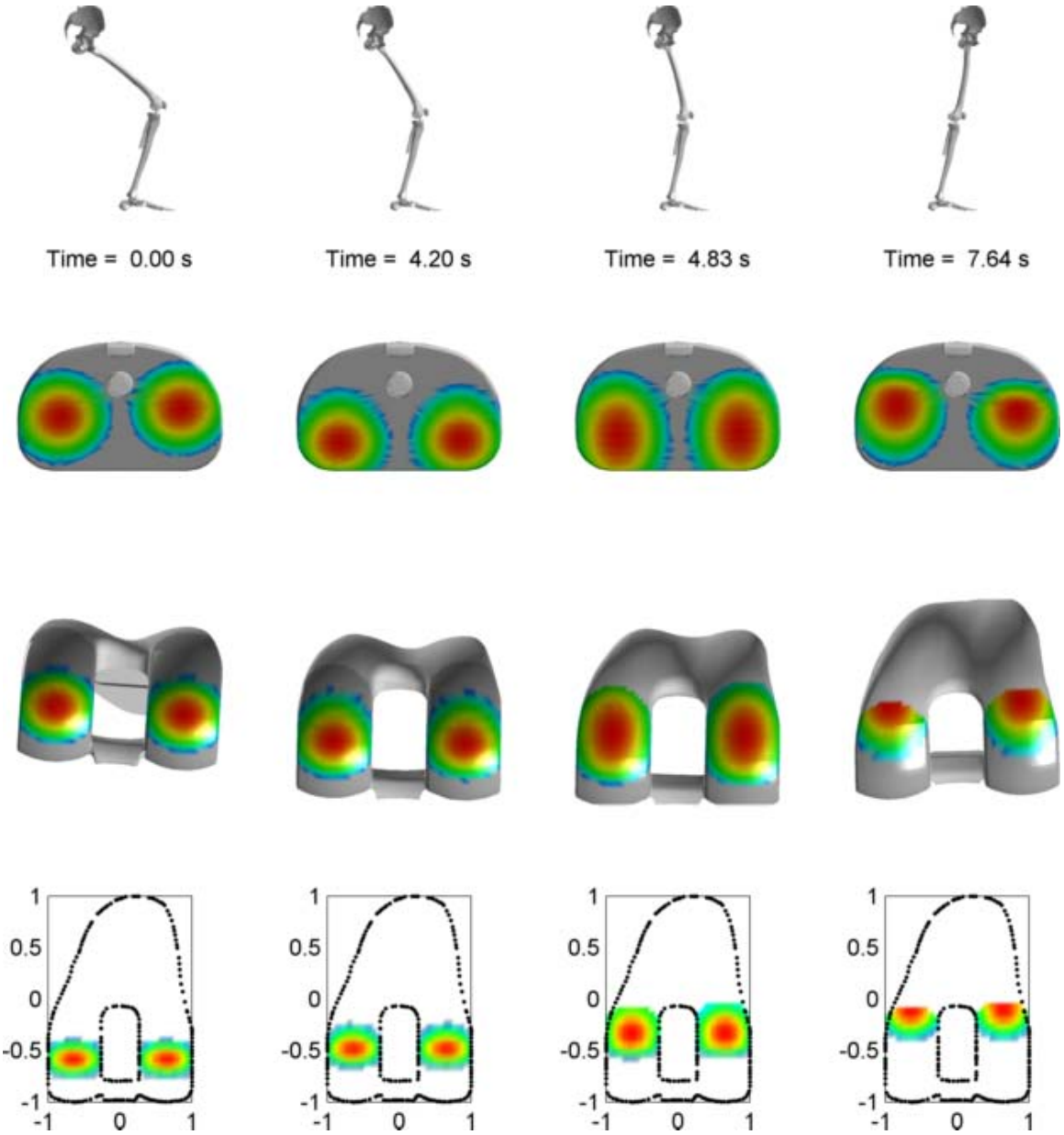


Figure A.55: Patient 13T dynamics model (top), tibiofemoral contact location mapped on the patient's specific patella (2^{nd} from top) and femur (2^{nd} from bottom) bone models, as well as the normalized contact location mapped on the unfolded femoral trochlea surface (bottom).

A.6.2 Electromyography and Inverse Dynamics analyses results

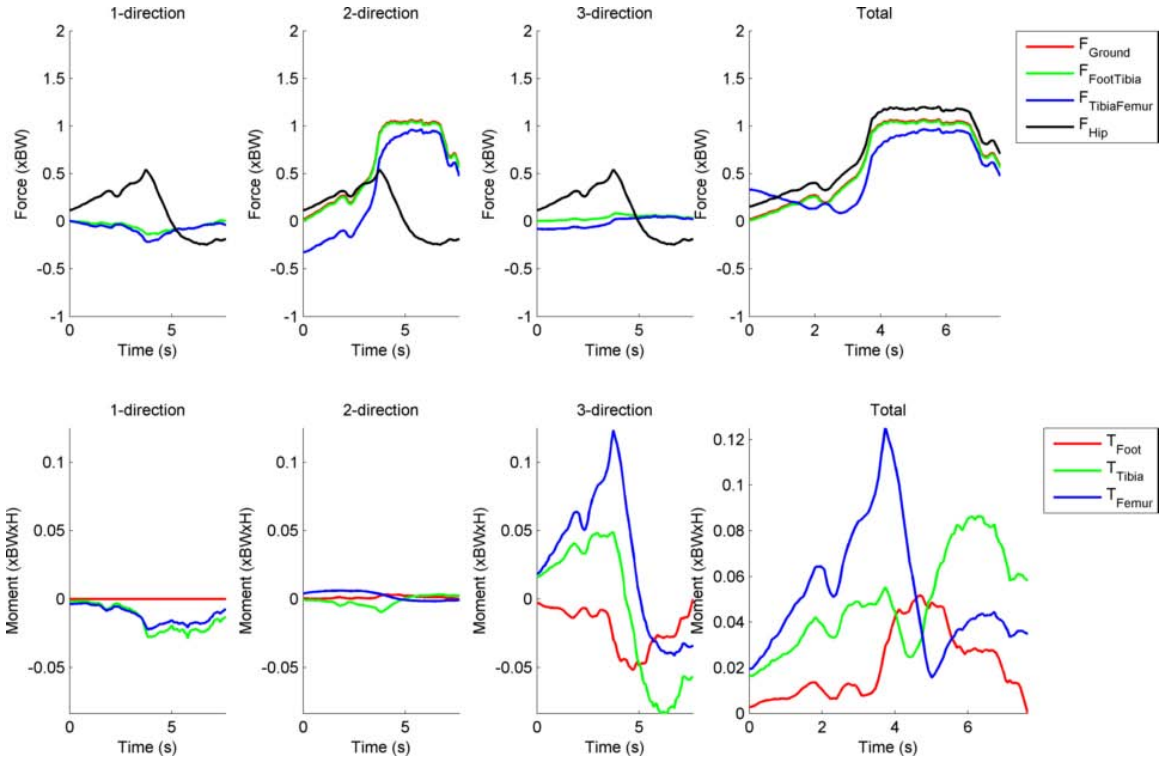


Figure A.56: Patient 13T knee joint reaction forces (top) and moments (bottom) normalized with respect to patient's body weight (BW). 1-direction = Anterior(+)/Posterior(-), 2-direction = Superior(+)/Inferior(-), 3-direction = Medial(+)/Lateral(-).

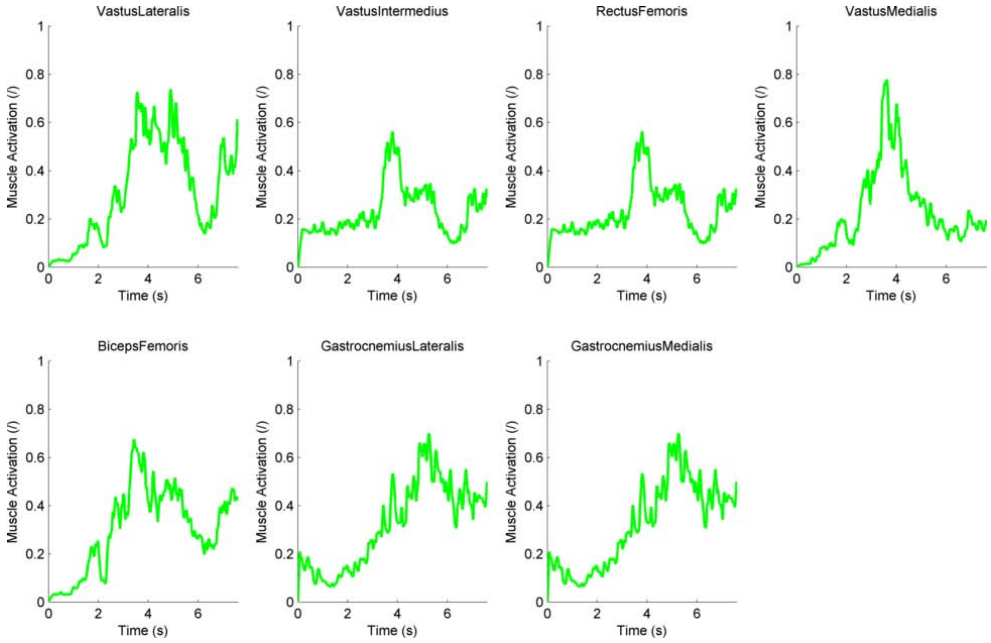


Figure A.57: Patient 13T muscle activation values obtained using the muscle activation dynamics[256].

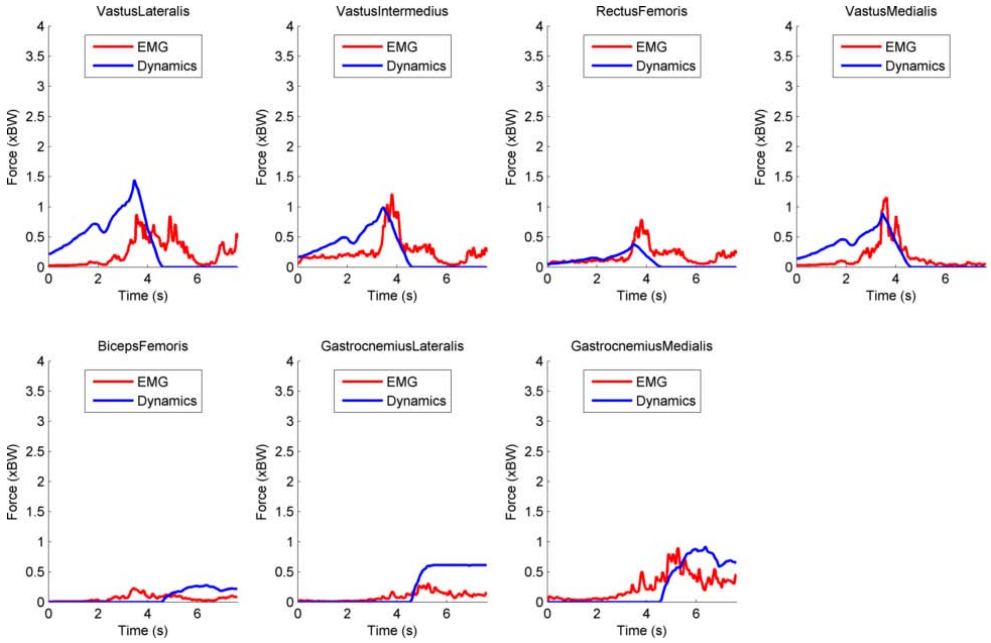


Figure A.58: Patient 13T muscle forces obtained using the EMG signal analysis (red) and pseudoinverse dynamics approach (green) normalized by patient's body weight (BW).

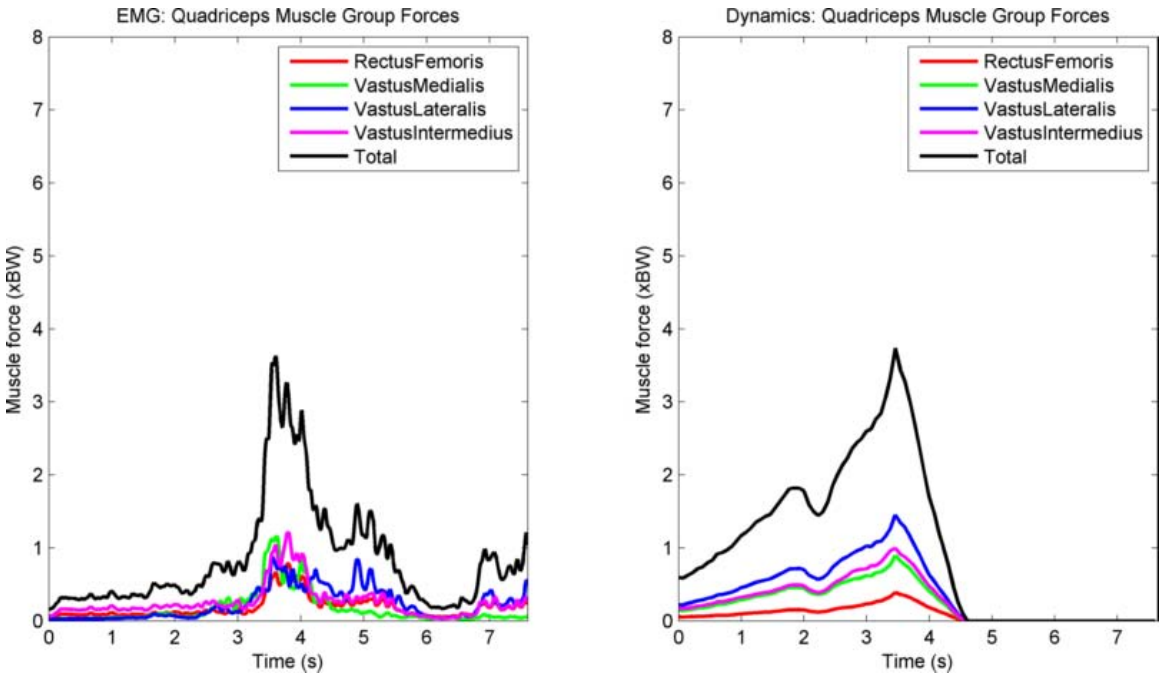


Figure A.59: Patient 13T quadriceps muscle group forces calculated from the EMG signals (left) and from the inverse dynamics (right) normalized by patient's body weight (BW).

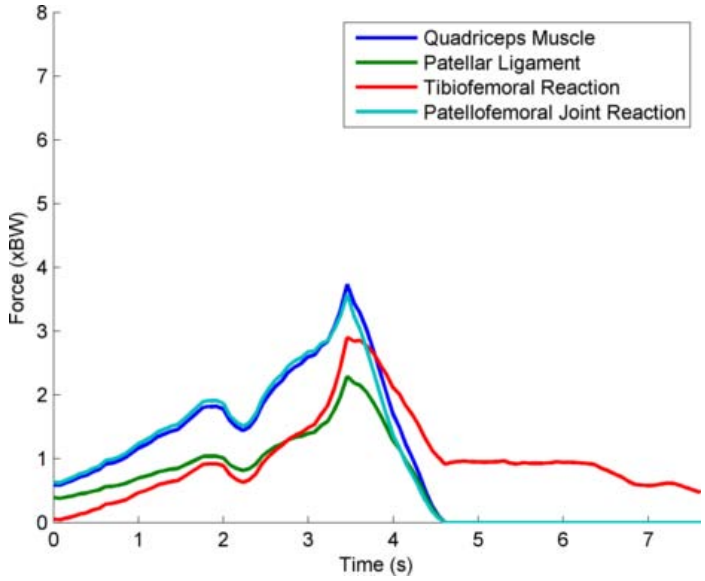


Figure A.60: Patient 13T total knee joint reaction forces incuding the action of the muscles, as well as the forces in the patellofemoral ligament, collateral and cruciate ligaments (if present) normalized by patient's body weight (BW).

A.7 Patient 17T

Patient demographic details:

ID# 17T

age: 78 yrs

height: 1.47 m

mass: 55 kg

leg side: Right

condition: TKA

A.7.1 Kinematics analysis results

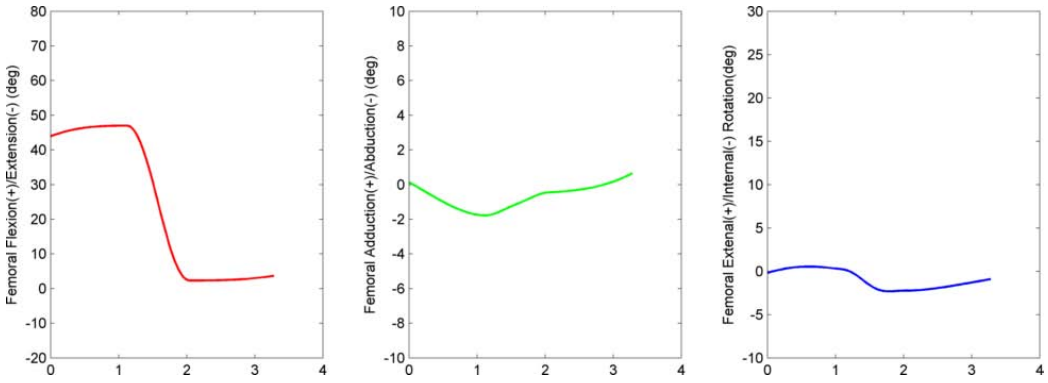


Figure A.61: Patient 17T patellofemoral joint kinematics.

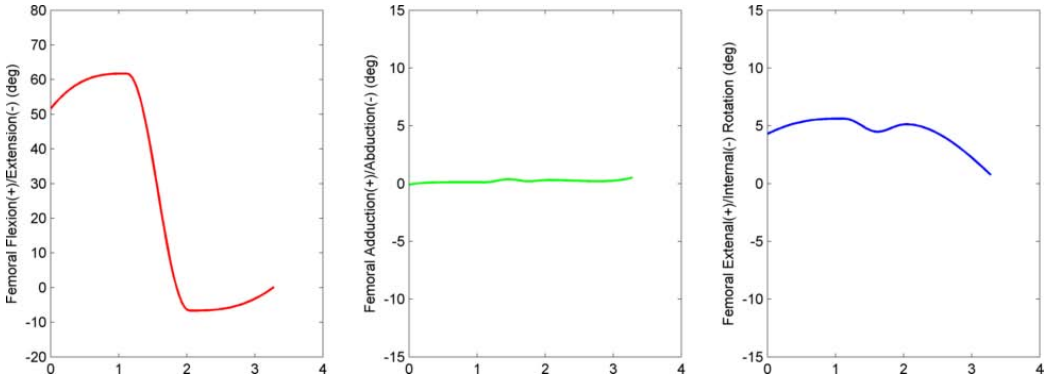


Figure A.62: Patient 17T tibiofemoral joint kinematics.

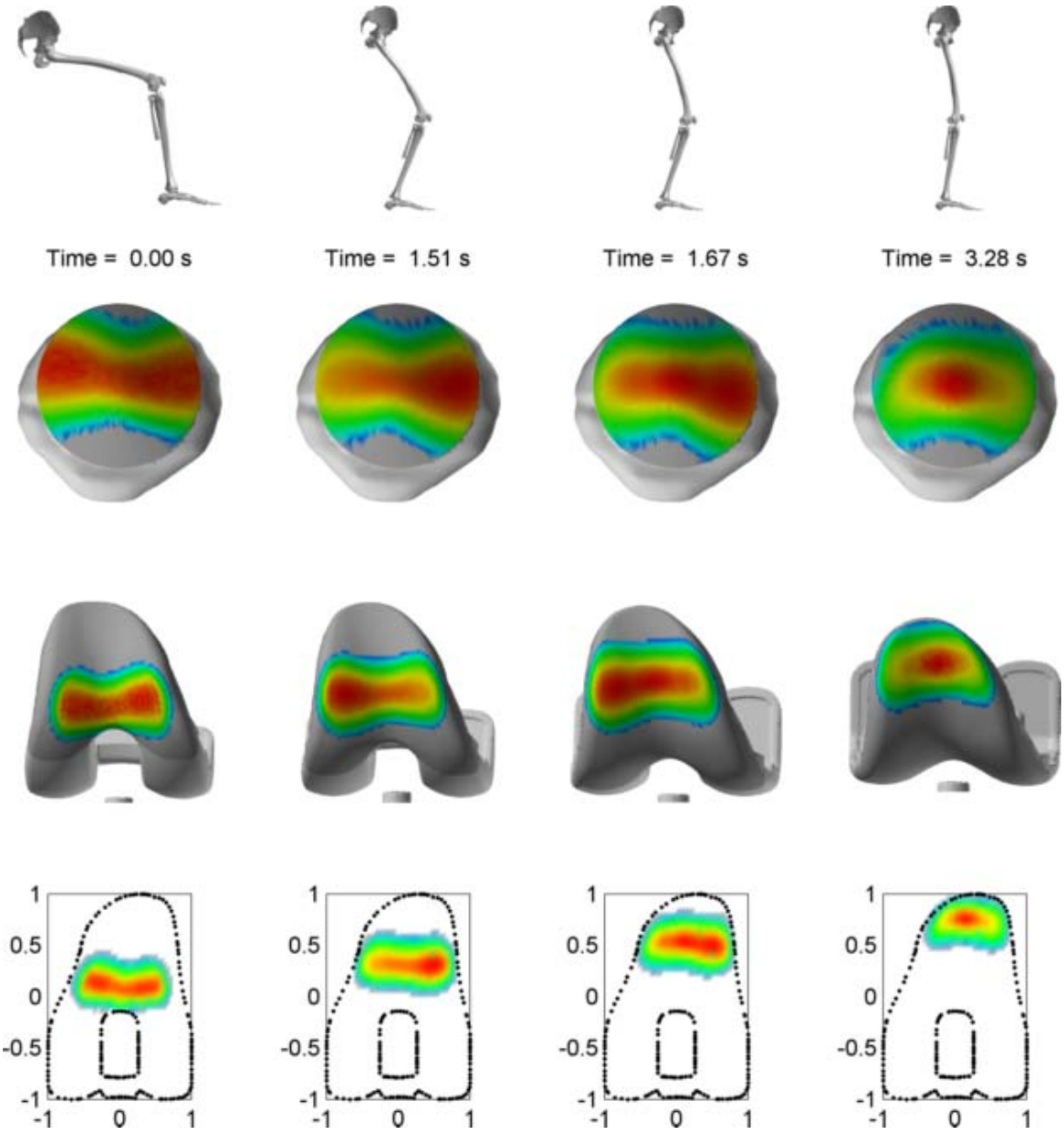


Figure A.63: Patient 17T dynamics model (top), patellofemoral contact location mapped on the patient's specific patella (2^{nd} from top) and femur (2^{nd} from bottom) bone models, as well as the normalized contact location mapped on the unfolded femoral trochlea surface (bottom).

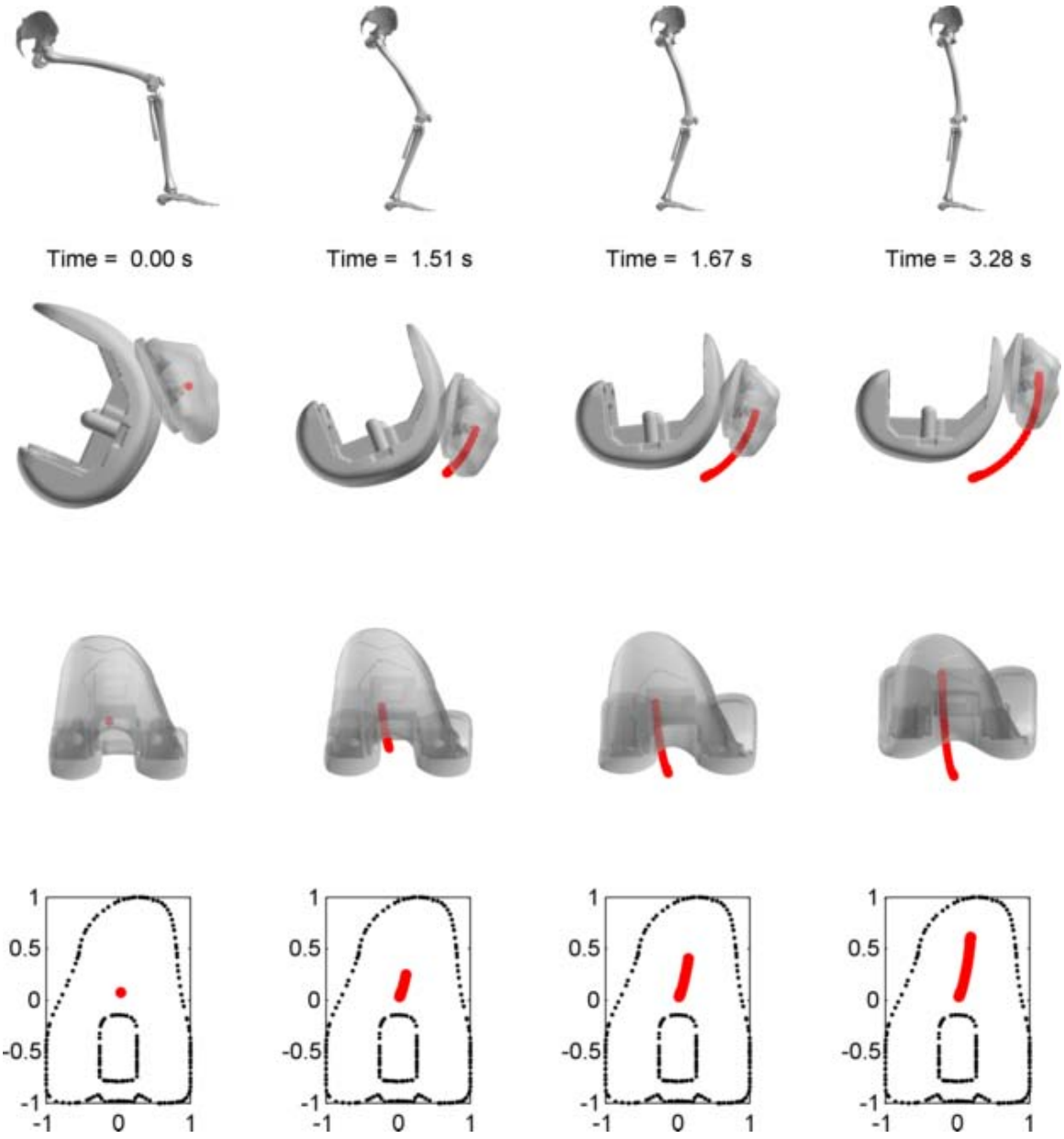


Figure A.64: Patient 17T dynamics model (top), patella center tracking in the sagittal (2^{nd} from top) and coronal (2^{nd} from bottom) planes, as well as the normalized patella tracking mapped on the unfolded femoral trochlea surface (bottom).

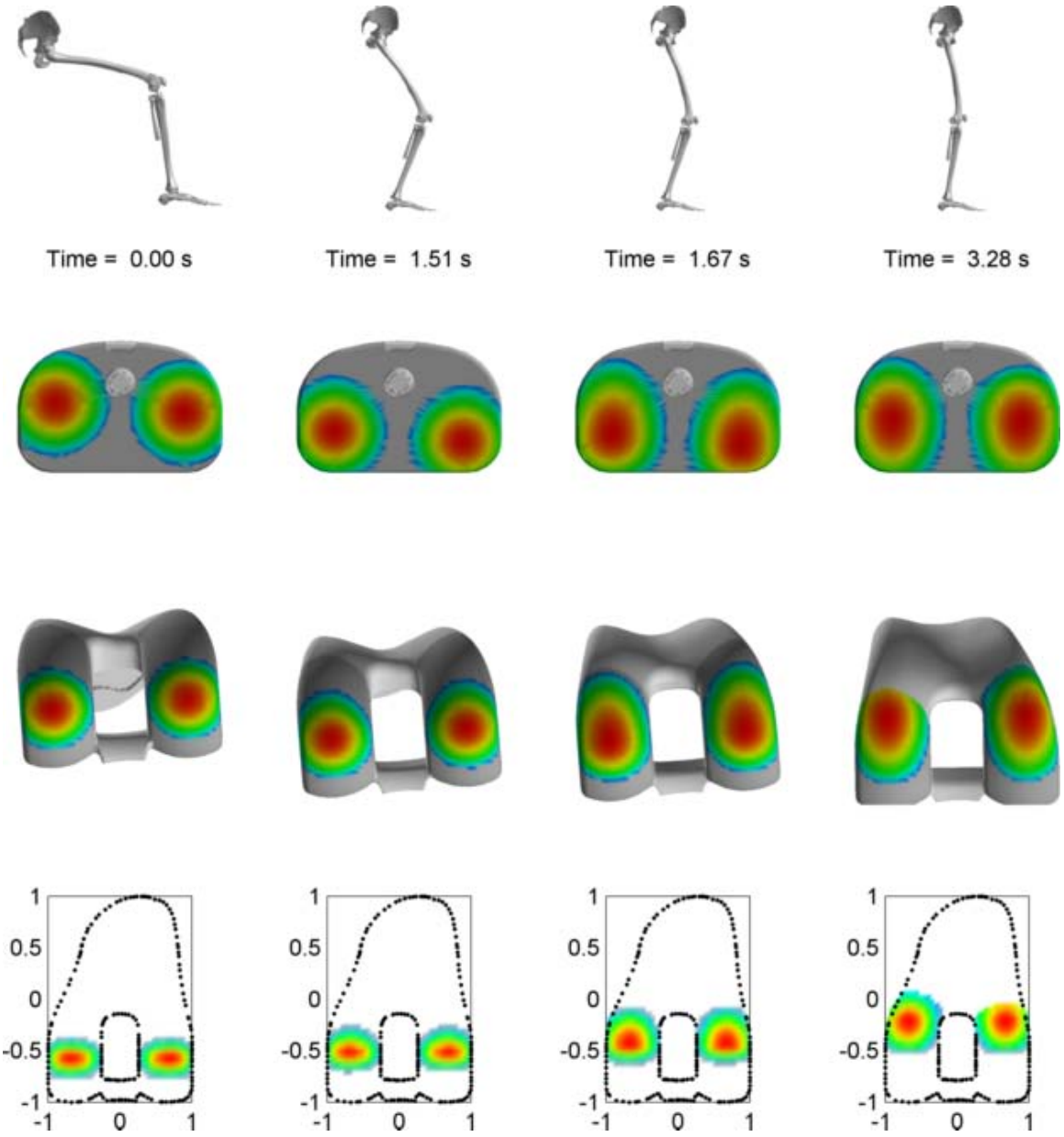


Figure A.65: Patient 17T dynamics model (top), tibiofemoral contact location mapped on the patient's specific patella (2^{nd} from top) and femur (2^{nd} from bottom) bone models, as well as the normalized contact location mapped on the unfolded femoral trochlea surface (bottom).

A.7.2 Electromyography and Inverse Dynamics analyses results

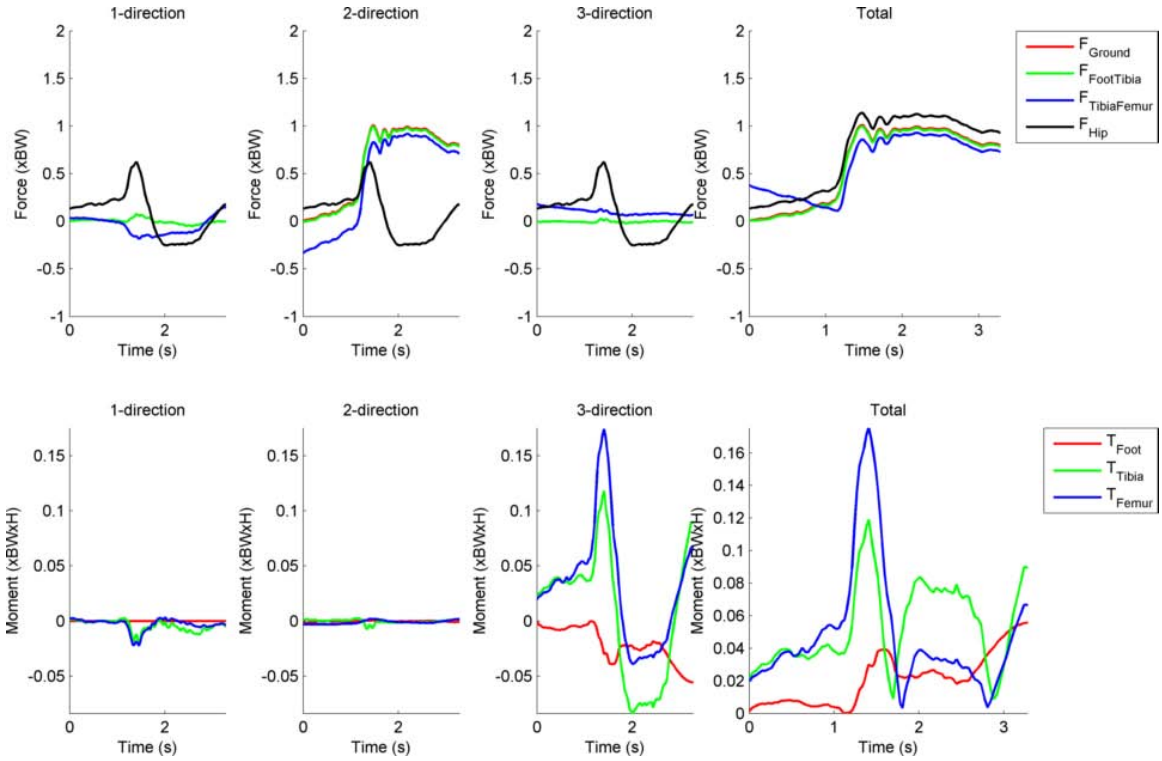


Figure A.66: Patient 17T knee joint reaction forces (top) and moments (bottom) normalized with respect to patient's body weight (BW). 1-direction = Anterior(+)/Posterior(-), 2-direction = Superior(+)/Inferior(-), 3-direction = Medial(+)/Lateral(-).

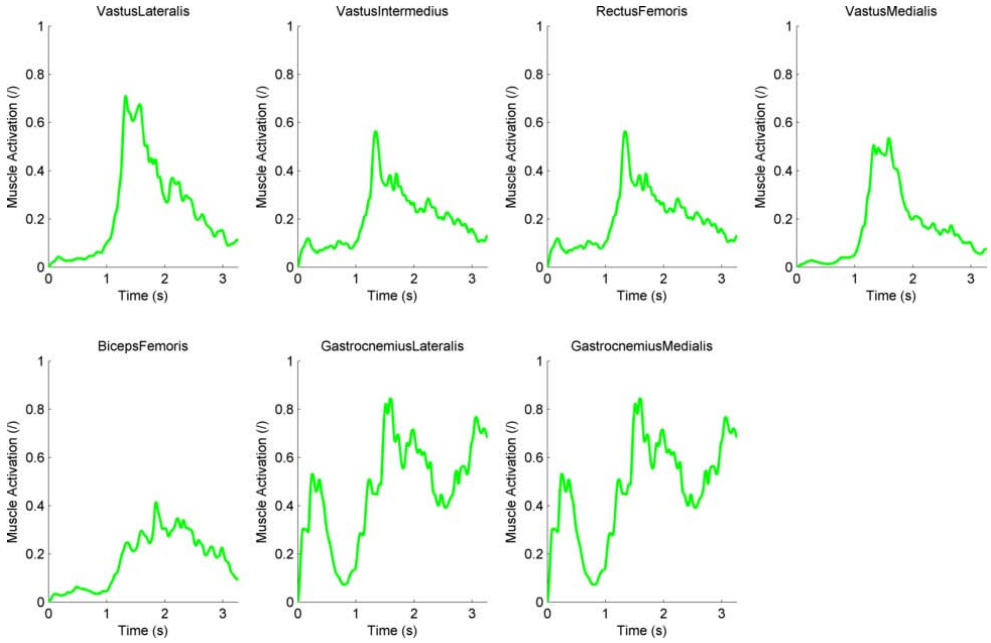


Figure A.67: Patient 17T muscle activation values obtained using the muscle activation dynamics[256].

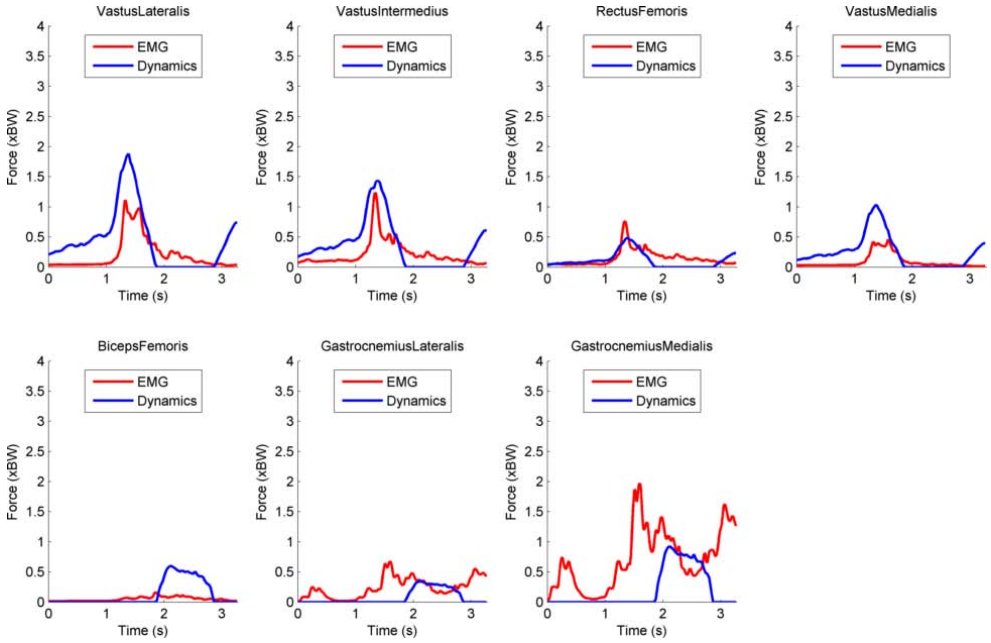


Figure A.68: Patient 17T muscle forces obtained using the EMG signal analysis (red) and pseudoinverse dynamics approach (green) normalized by patient's body weight (BW).

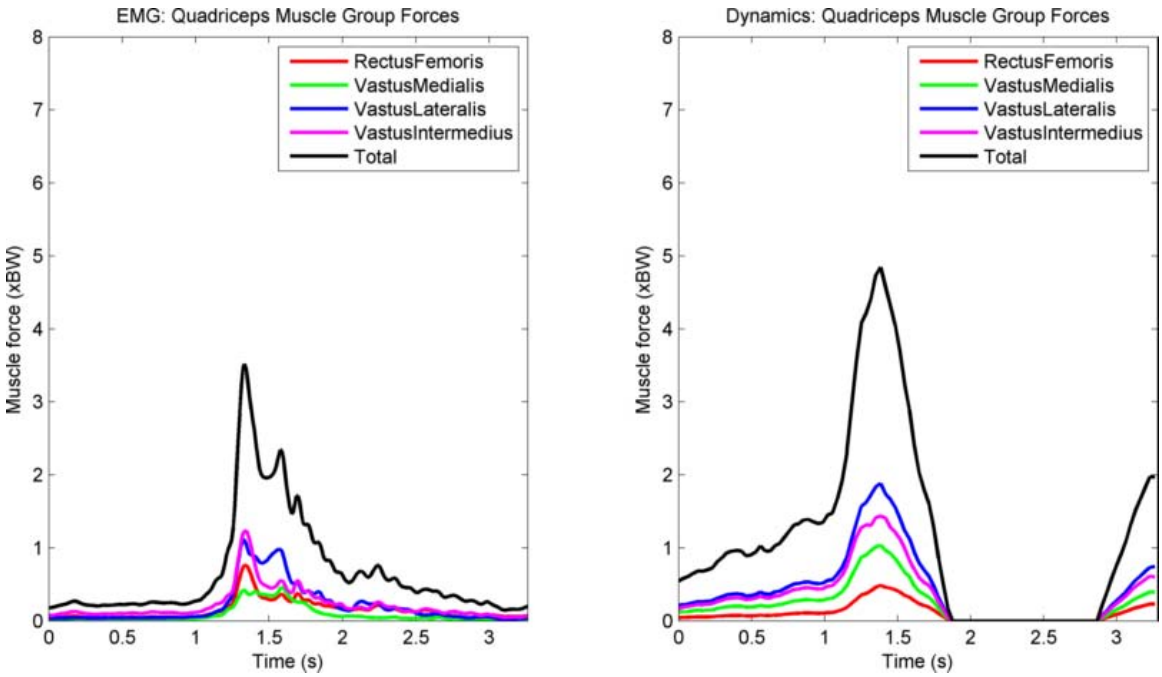


Figure A.69: Patient 17T quadriceps muscle group forces calculated from the EMG signals (left) and from the inverse dynamics (right) normalized by patient's body weight (BW).

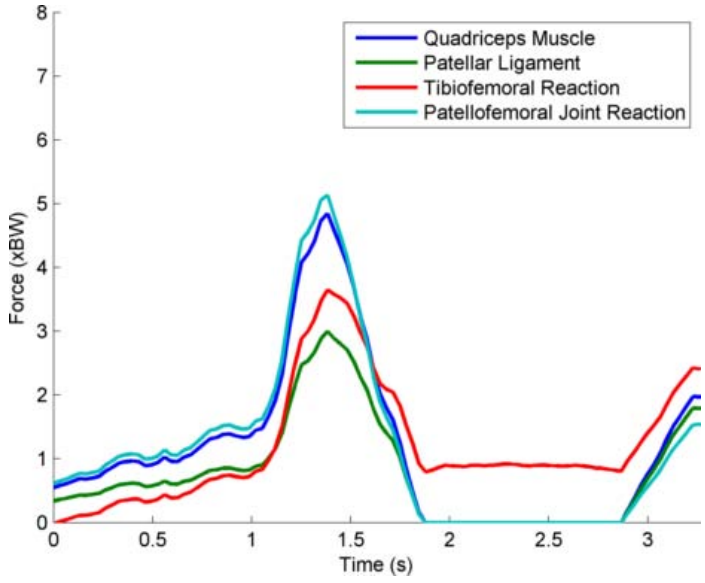


Figure A.70: Patient 17T total knee joint reaction forces incuding the action of the muscles, as well as the forces in the patellofemoral ligament, collateral and cruciate ligaments (if present) normalized by patient's body weight (BW).

A.8 Patient 21T

Patient demographic details:

ID# 21T

age: 68 yrs

height: 1.59 m

mass: 68 kg

leg side: Right

condition: TKA

A.8.1 Kinematics analysis results

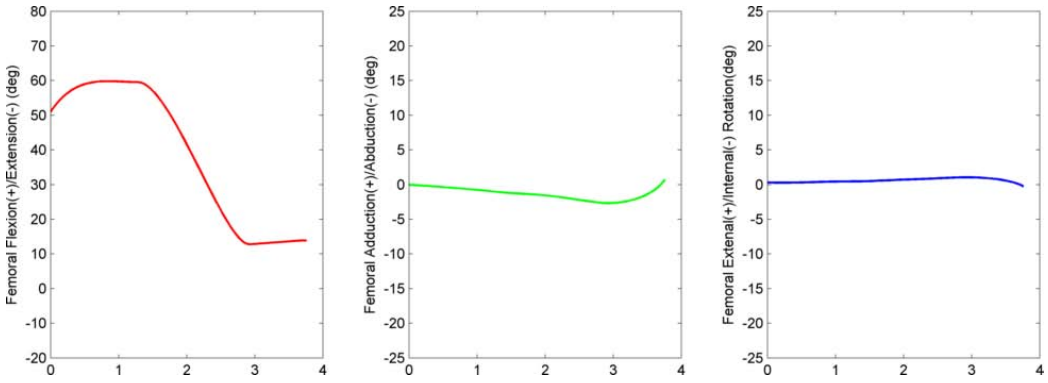


Figure A.71: Patient 21T patellofemoral joint kinematics.

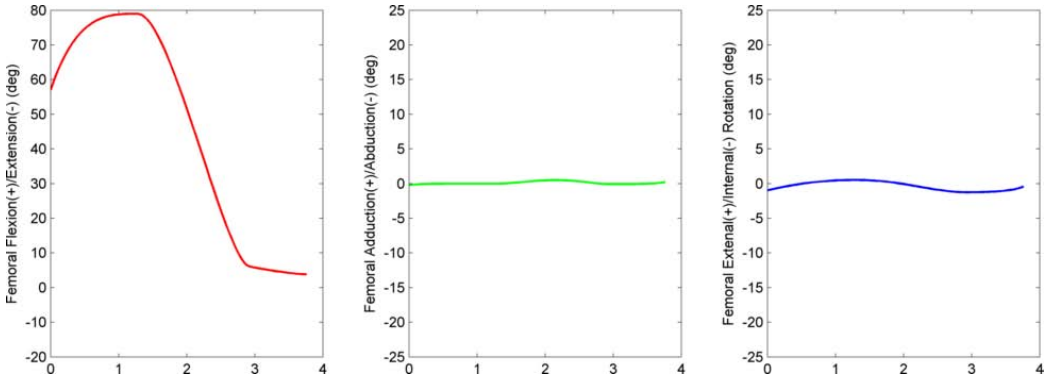


Figure A.72: Patient 21T tibiofemoral joint kinematics.

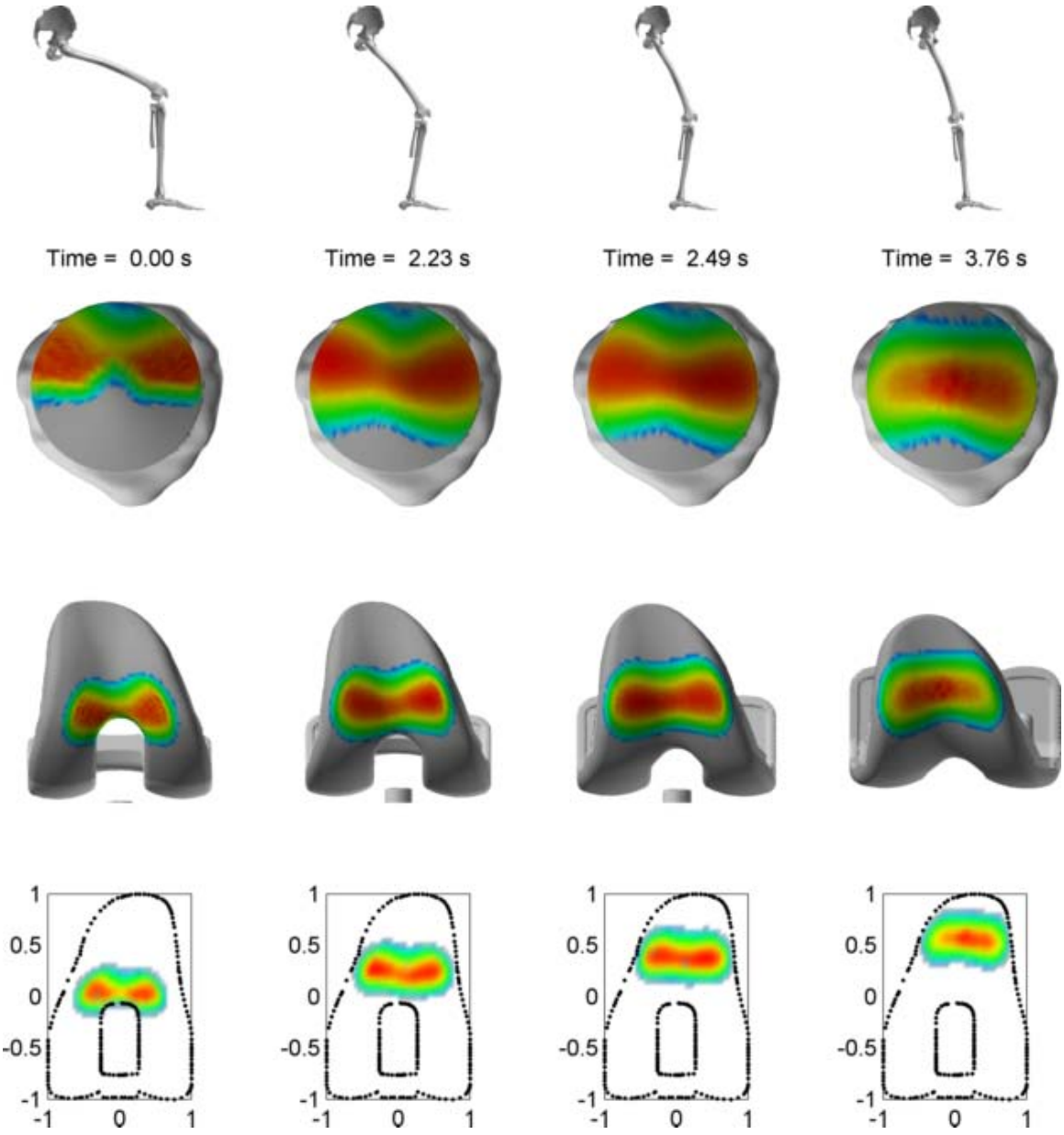


Figure A.73: Patient 21T dynamics model (top), patellofemoral contact location mapped on the patient's specific patella (2^{nd} from top) and femur (2^{nd} from bottom) bone models, as well as the normalized contact location mapped on the unfolded femoral trochlea surface (bottom).

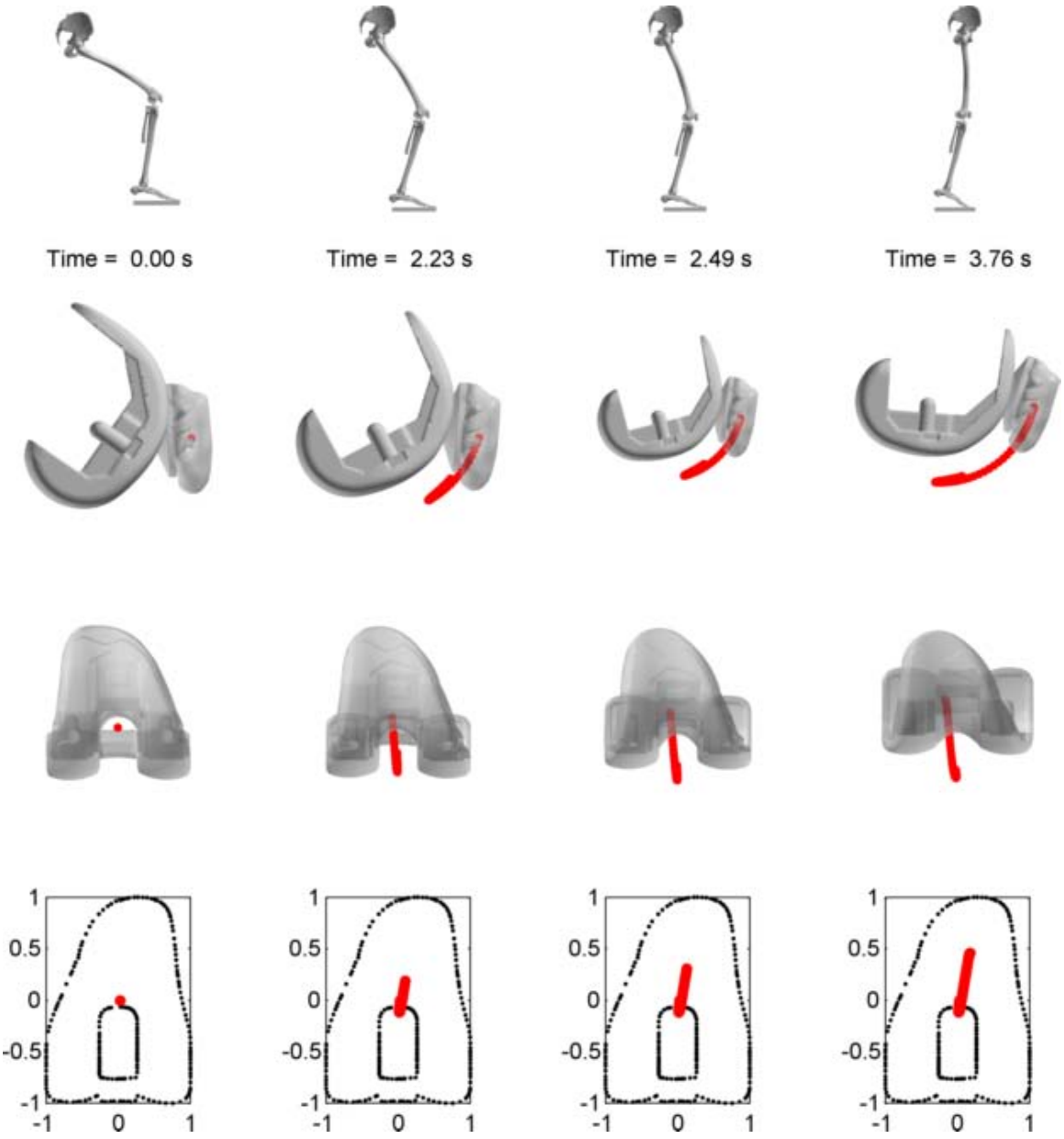


Figure A.74: Patient 21T dynamics model (top), patella center tracking in the sagittal (2^{nd} from top) and coronal (2^{nd} from bottom) planes, as well as the normalized patella tracking mapped on the unfolded femoral trochlea surface (bottom).

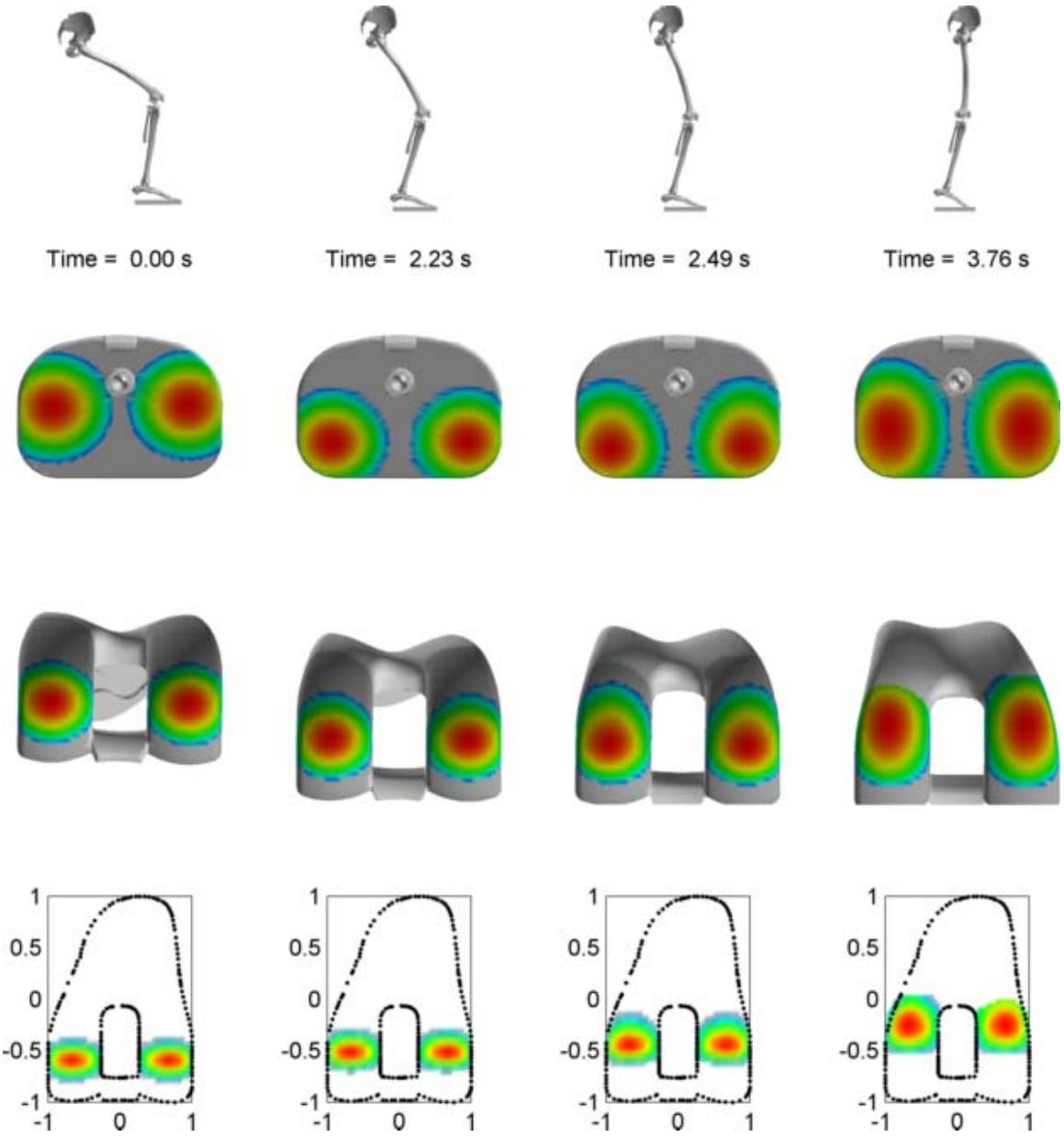


Figure A.75: Patient 21T dynamics model (top), tibiofemoral contact location mapped on the patient's specific patella (2^{nd} from top) and femur (2^{nd} from bottom) bone models, as well as the normalized contact location mapped on the unfolded femoral trochlea surface (bottom).

A.8.2 Electromyography and Inverse Dynamics analyses results

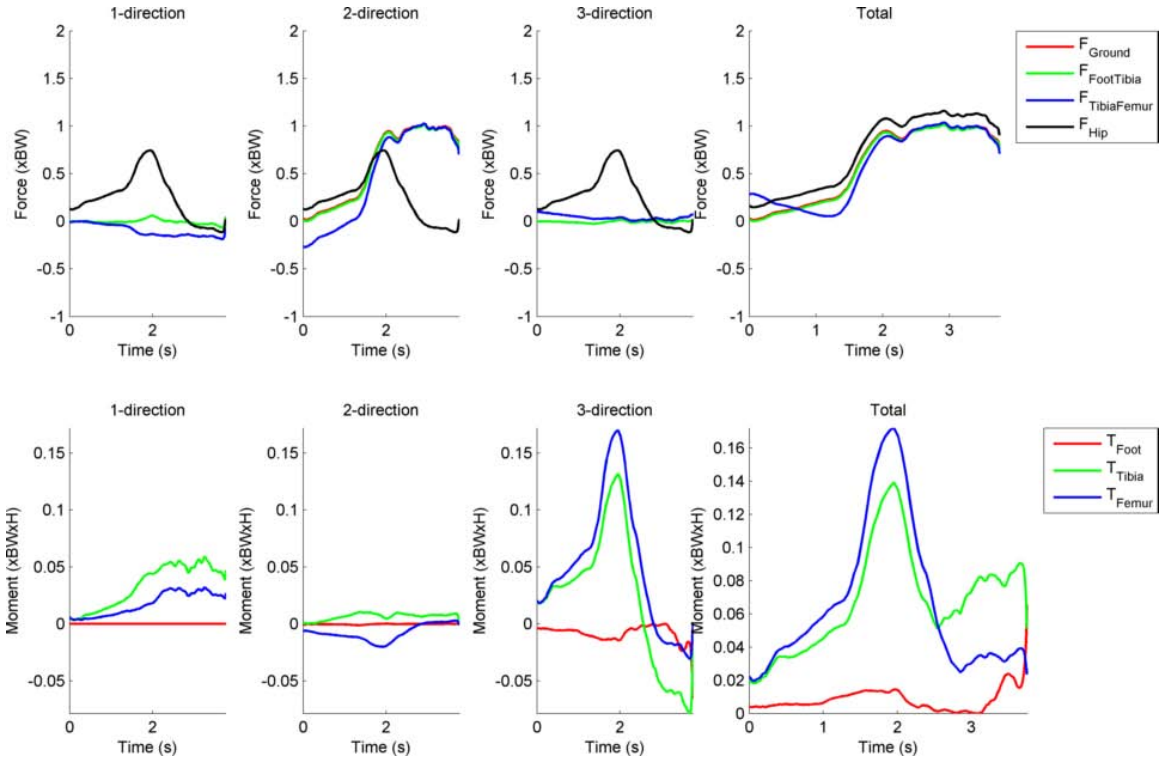


Figure A.76: Patient 21T knee joint reaction forces (top) and moments (bottom) normalized with respect to patient's body weight (BW). 1-direction = Anterior(+)/Posterior(-), 2-direction = Superior(+)/Inferior(-), 3-direction = Medial(+)/Lateral(-).

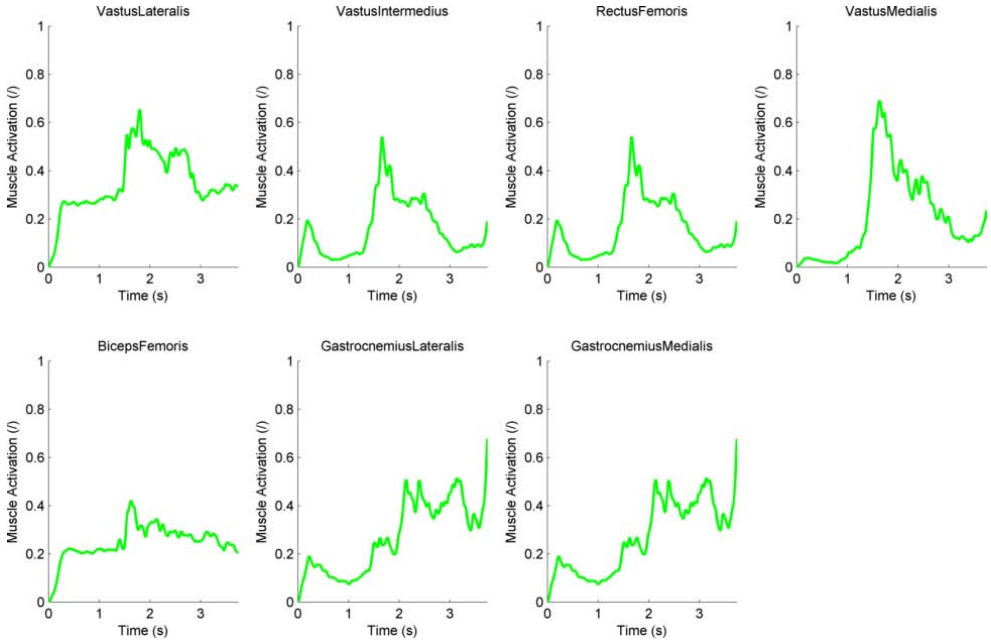


Figure A.77: Patient 21T muscle activation values obtained using the muscle activation dynamics[256].

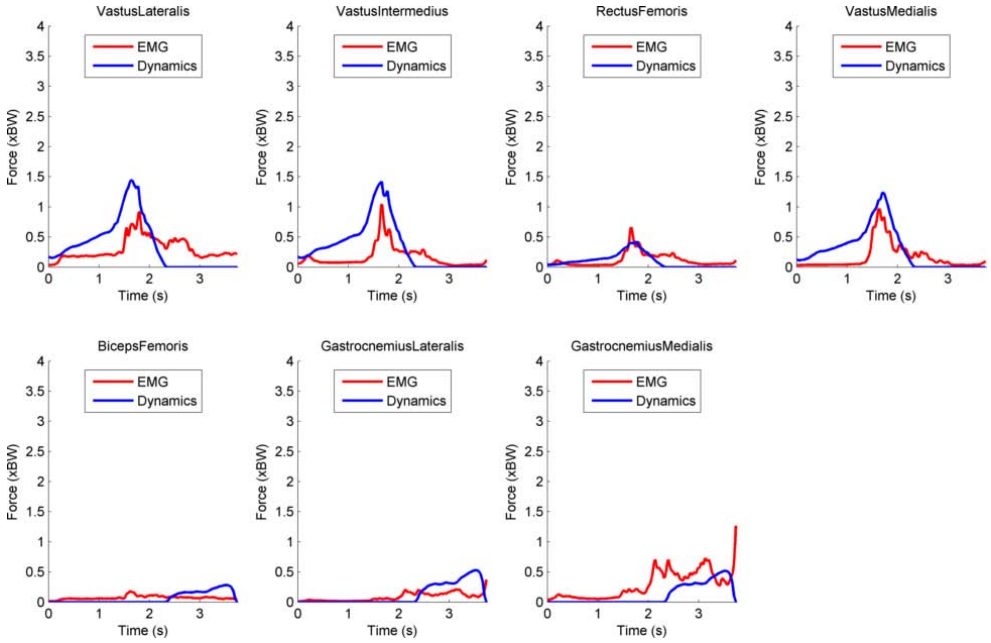


Figure A.78: Patient 21T muscle forces obtained using the EMG signal analysis (red) and pseudoinverse dynamics approach (green) normalized by patient's body weight (BW).

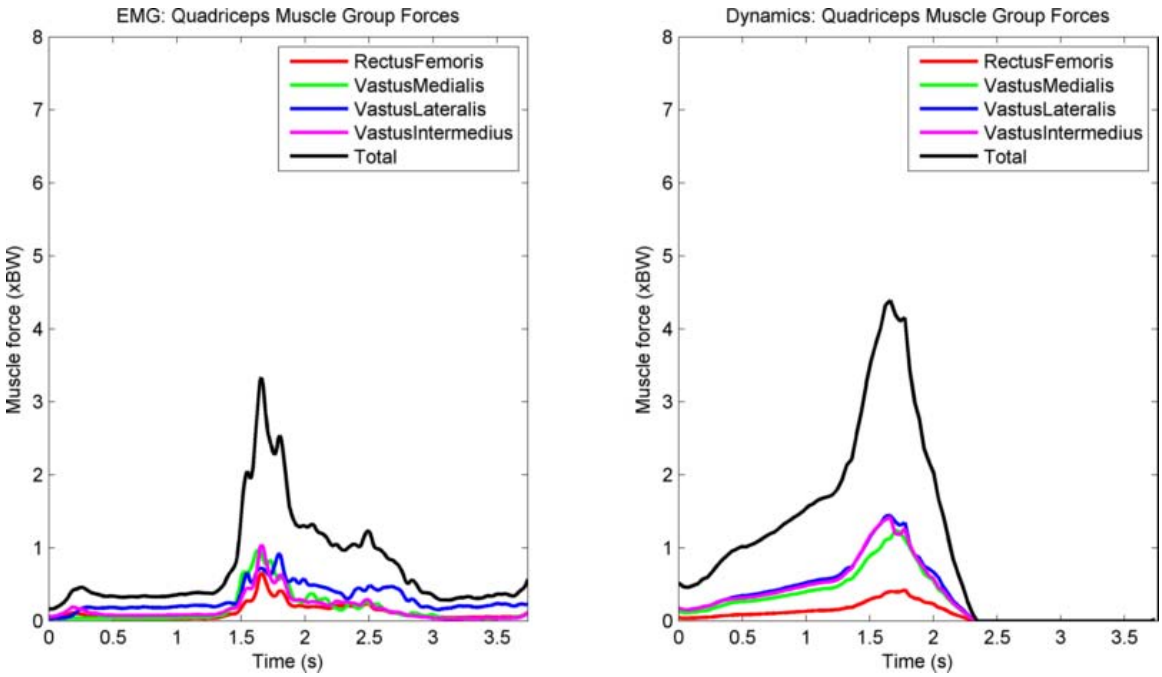


Figure A.79: Patient 21T quadriceps muscle group forces calculated from the EMG signals (left) and from the inverse dynamics (right) normalized by patient's body weight (BW).

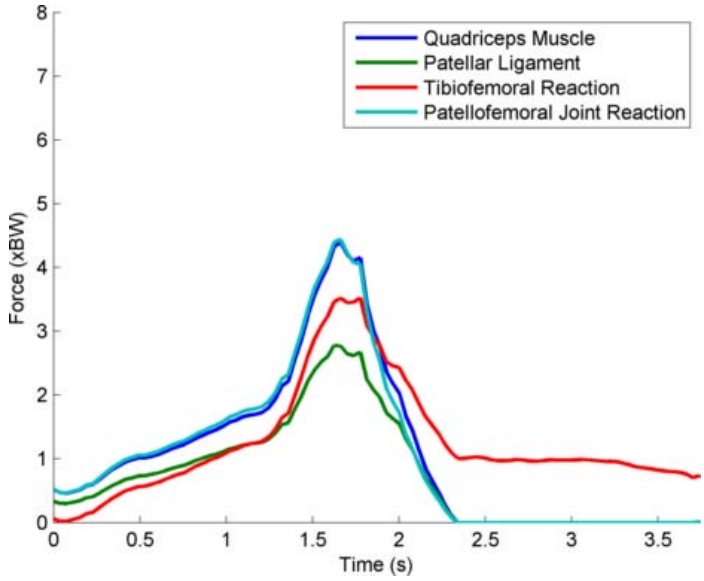


Figure A.80: Patient 21T total knee joint reaction forces incuding the action of the muscles, as well as the forces in the patellofemoral ligament, collateral and cruciate ligaments (if present) normalized by patient's body weight (BW).

A.9 Patient 11T

Patient demographic details:

ID# 11T

age: 80 yrs

height: 1.68 m

mass: 72 kg

leg side: Right

condition: TKA

A.9.1 Kinematics analysis results

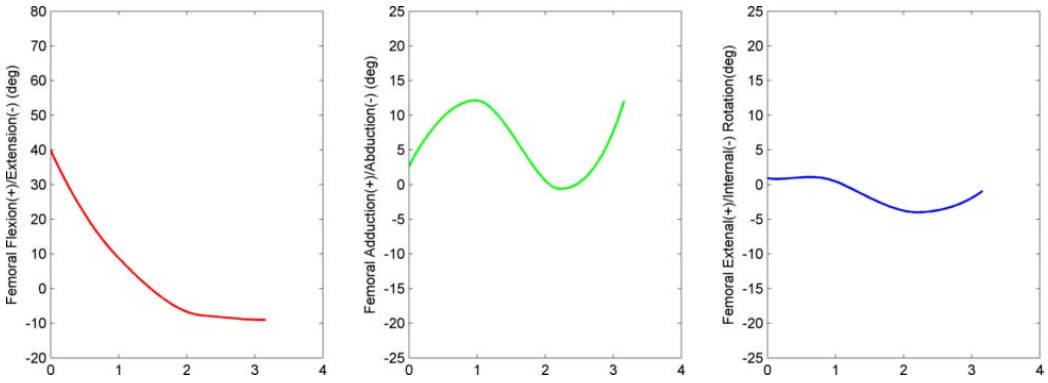


Figure A.81: Patient 11T patellofemoral joint kinematics.

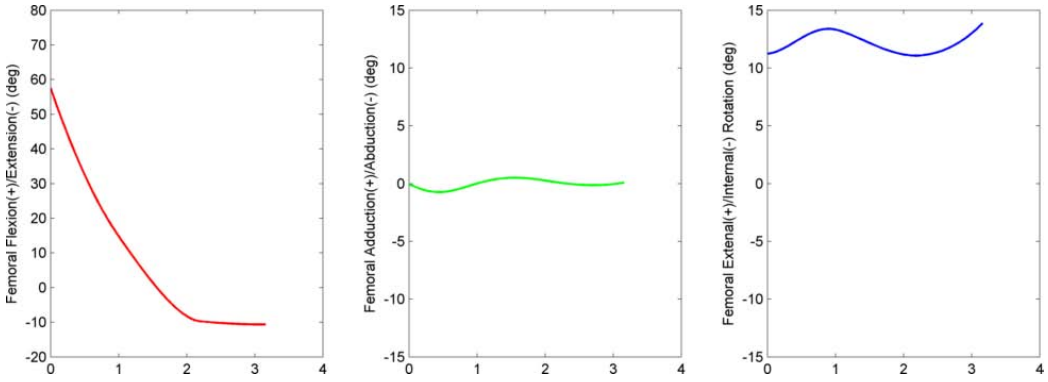


Figure A.82: Patient 11T tibiofemoral joint kinematics.

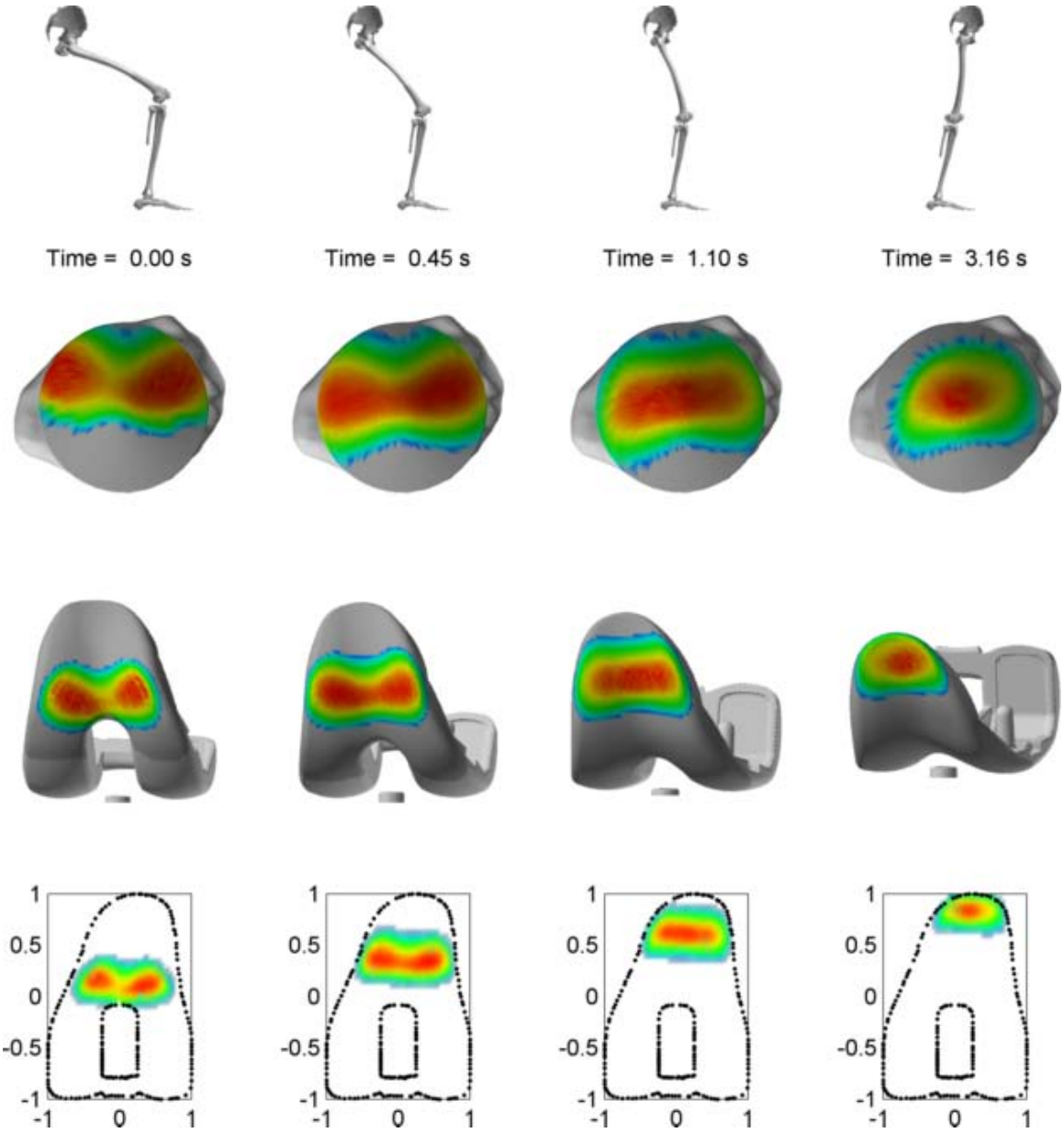


Figure A.83: Patient 11T dynamics model (top), patellofemoral contact location mapped on the patient's specific patella (2^{nd} from top) and femur (2^{nd} from bottom) bone models, as well as the normalized contact location mapped on the unfolded femoral trochlea surface (bottom).

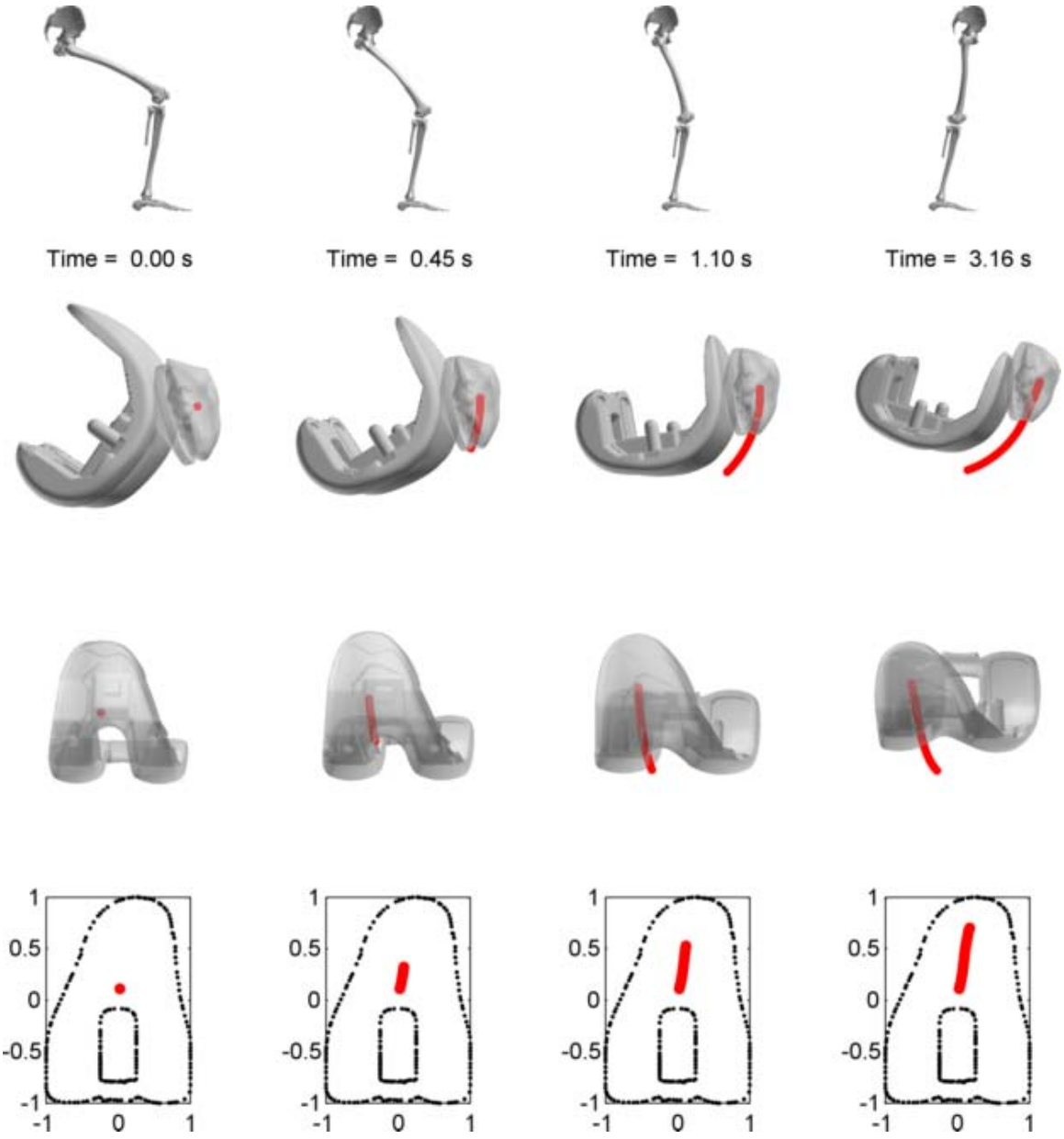


Figure A.84: Patient 11T dynamics model (top), patella center tracking in the sagittal (2^{nd} from top) and coronal (2^{nd} from bottom) planes, as well as the normalized patella tracking mapped on the unfolded femoral trochlea surface (bottom).

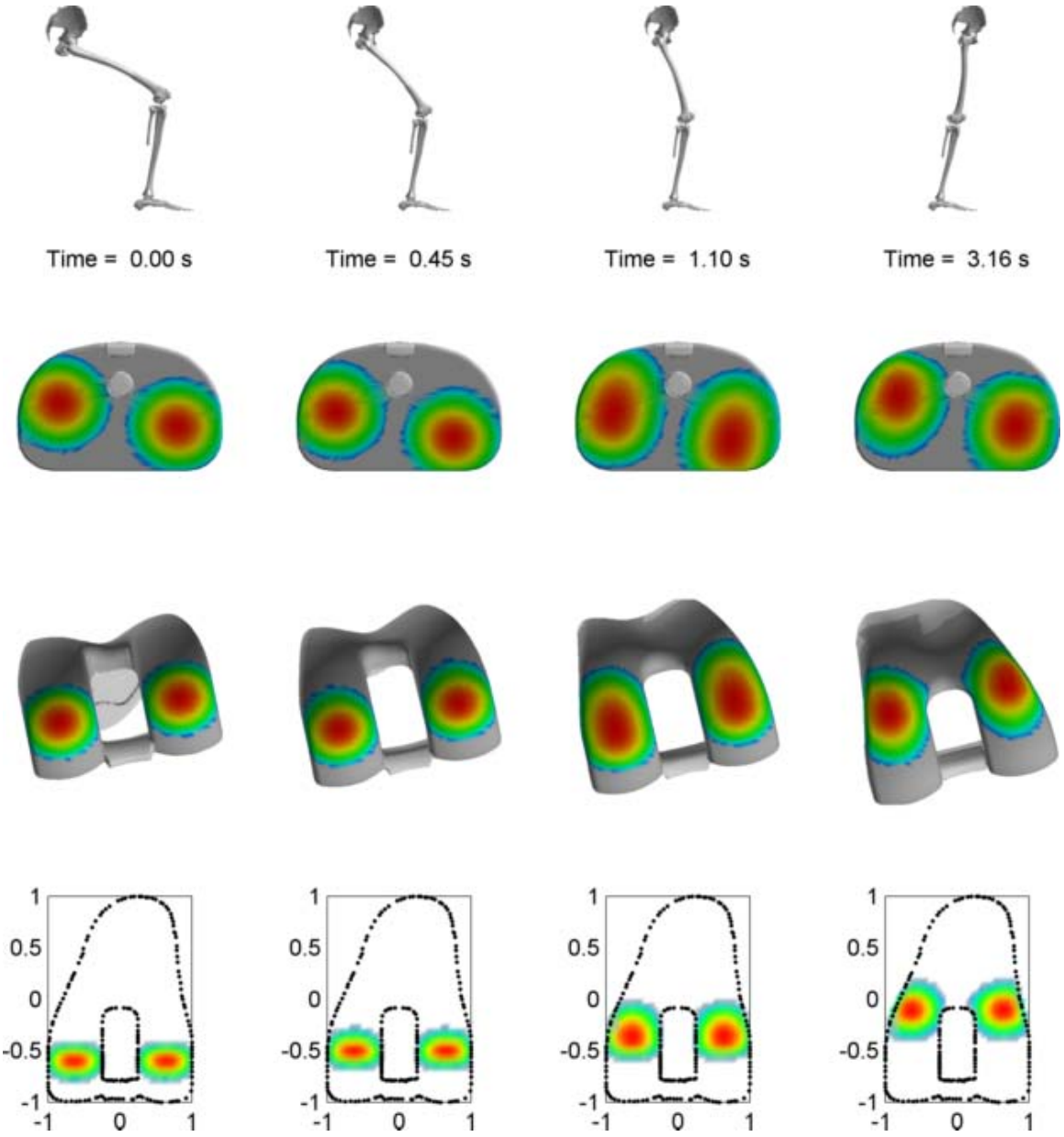


Figure A.85: Patient 11T dynamics model (top), tibiofemoral contact location mapped on the patient's specific patella (2^{nd} from top) and femur (2^{nd} from bottom) bone models, as well as the normalized contact location mapped on the unfolded femoral trochlea surface (bottom).

A.9.2 Electromyography and Inverse Dynamics analyses results

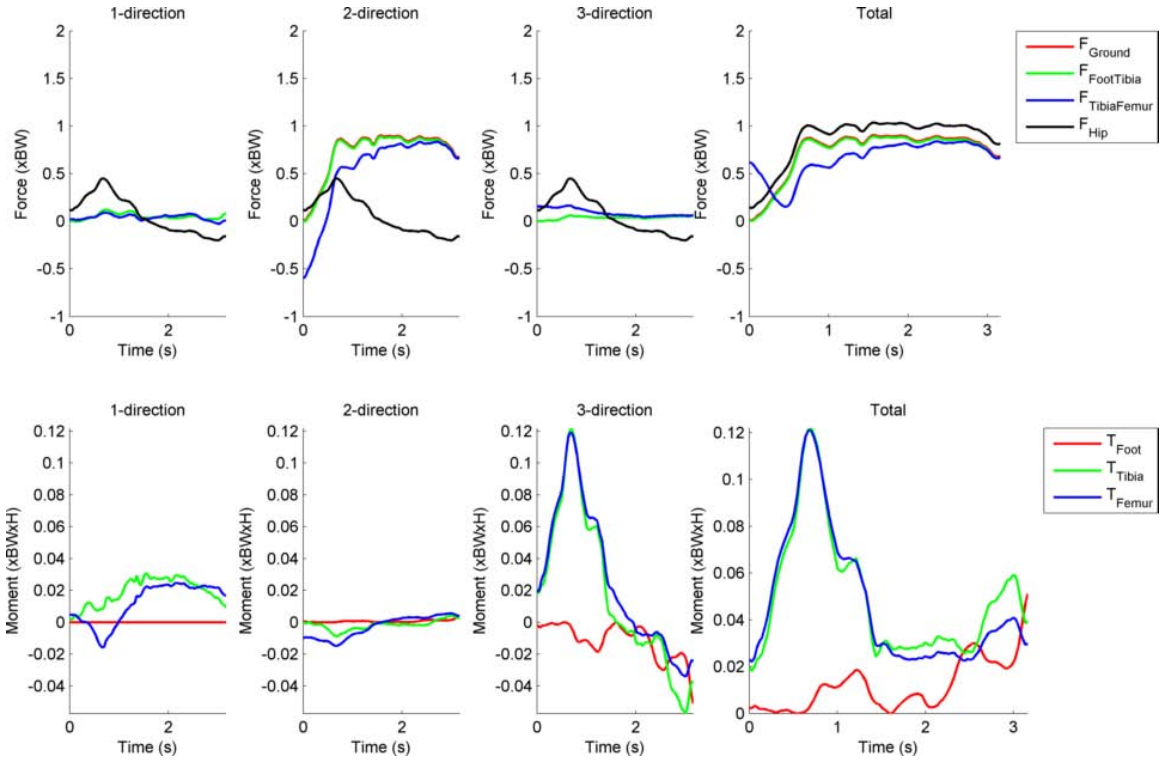


Figure A.86: Patient 11T knee joint reaction forces (top) and moments (bottom) normalized with respect to patient's body weight (BW). 1-direction = Anterior(+)/Posterior(-), 2-direction = Superior(+)/Inferior(-), 3-direction = Medial(+)/Lateral(-).

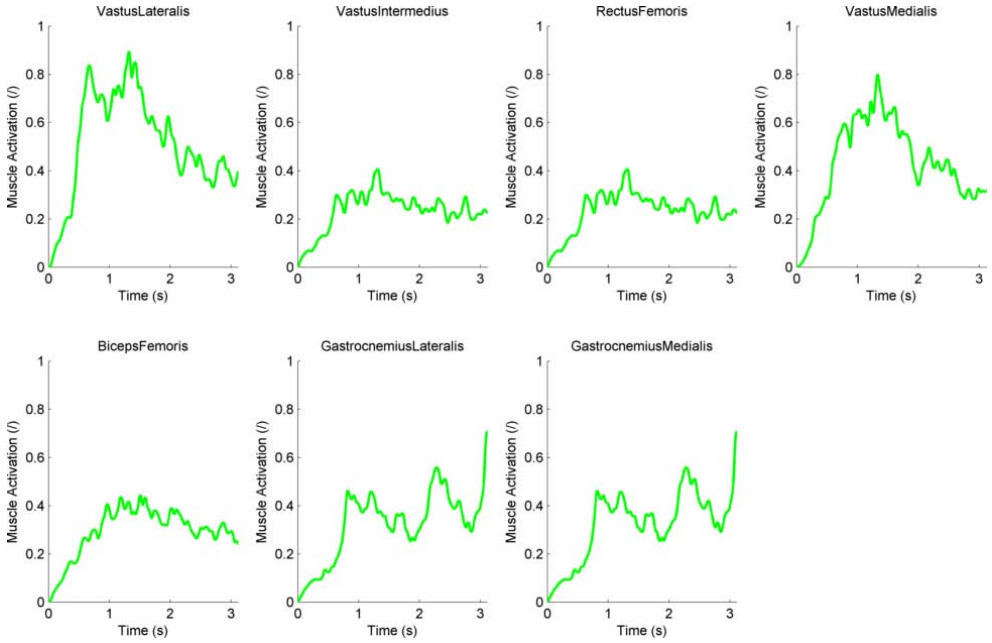


Figure A.87: Patient 11T muscle activation values obtained using the muscle activation dynamics[256].

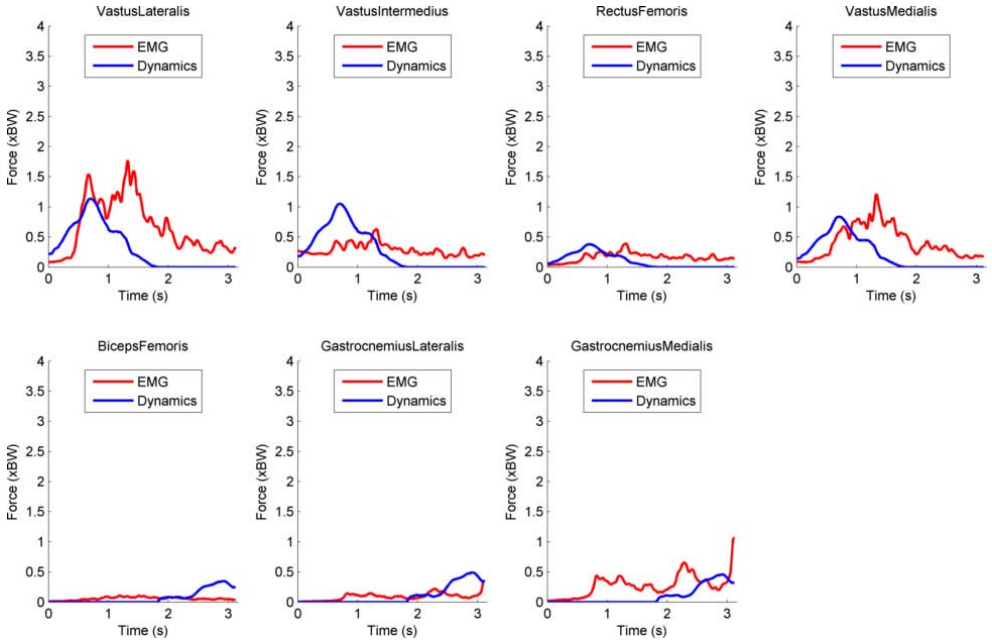


Figure A.88: Patient 11T muscle forces obtained using the EMG signal analysis (red) and pseudoinverse dynamics approach (green) normalized by patient's body weight (BW).

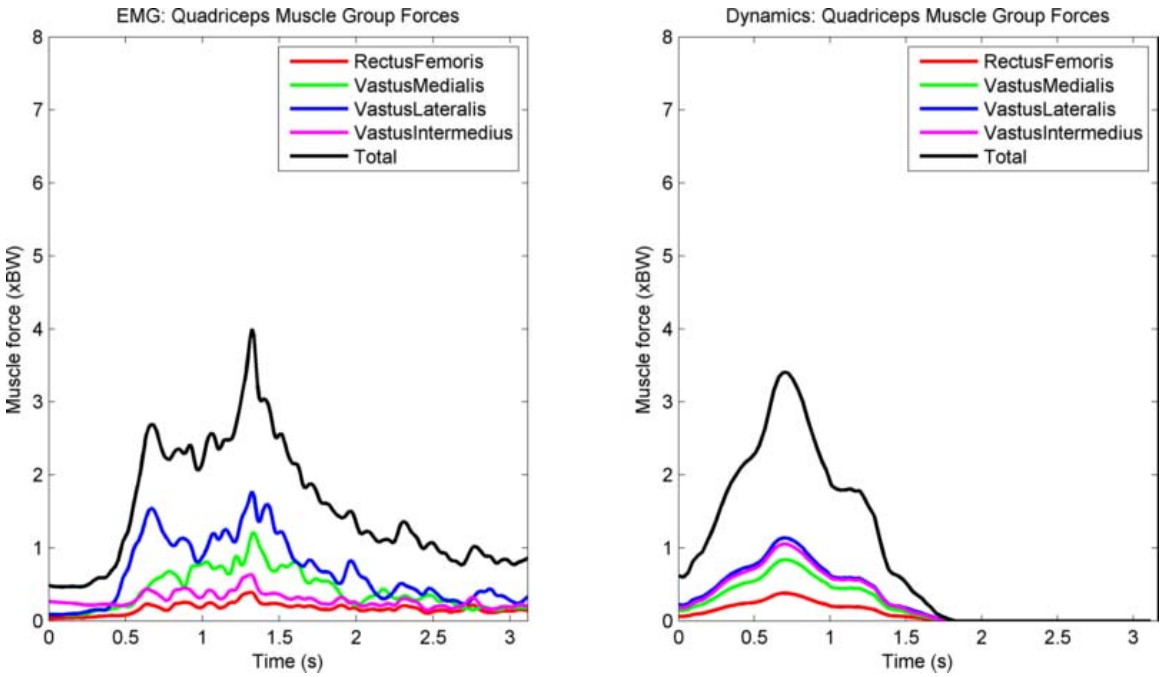


Figure A.89: Patient 11T quadriceps muscle group forces calculated from the EMG signals (left) and from the inverse dynamics (right) normalized by patient's body weight (BW).

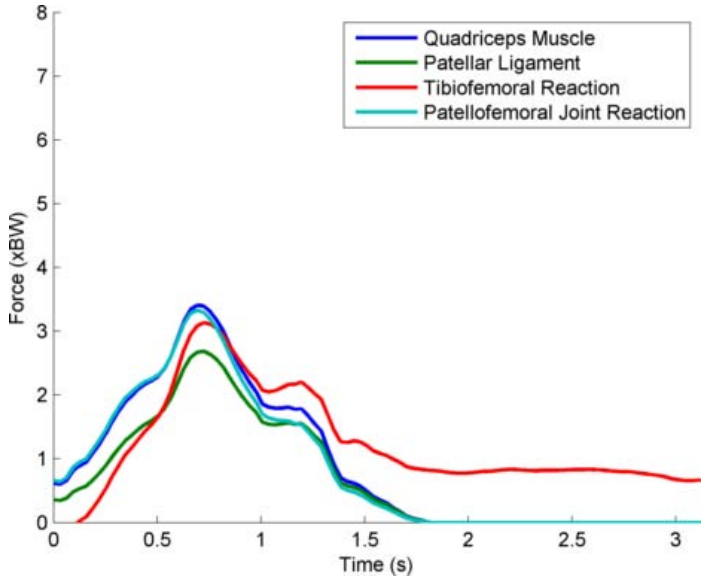


Figure A.90: Patient 11T total knee joint reaction forces incuding the action of the muscles, as well as the forces in the patellofemoral ligament, collateral and cruciate ligaments (if present) normalized by patient's body weight (BW).

A.10 Patient 11N

Patient demographic details:

ID# 11N

age: 80 yrs

height: 1.68 m

mass: 72 kg

leg side: Left

condition: Healthy

A.10.1 Kinematics analysis results

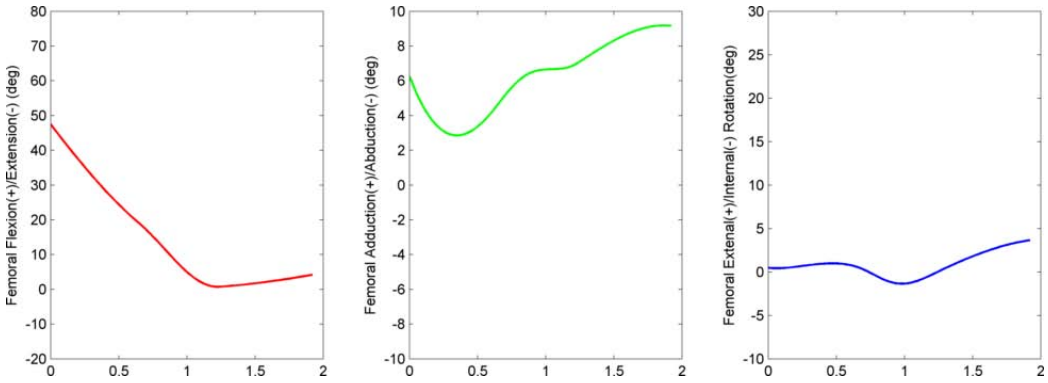


Figure A.91: Patient 11N patellofemoral joint kinematics.

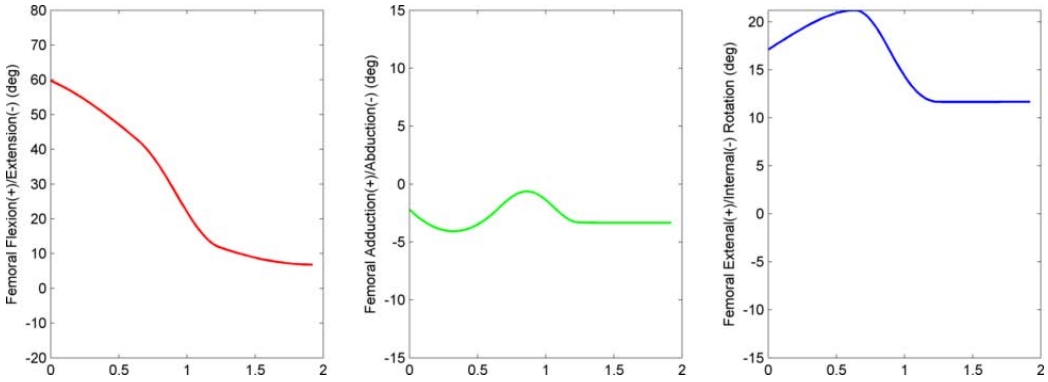


Figure A.92: Patient 11N tibiofemoral joint kinematics.

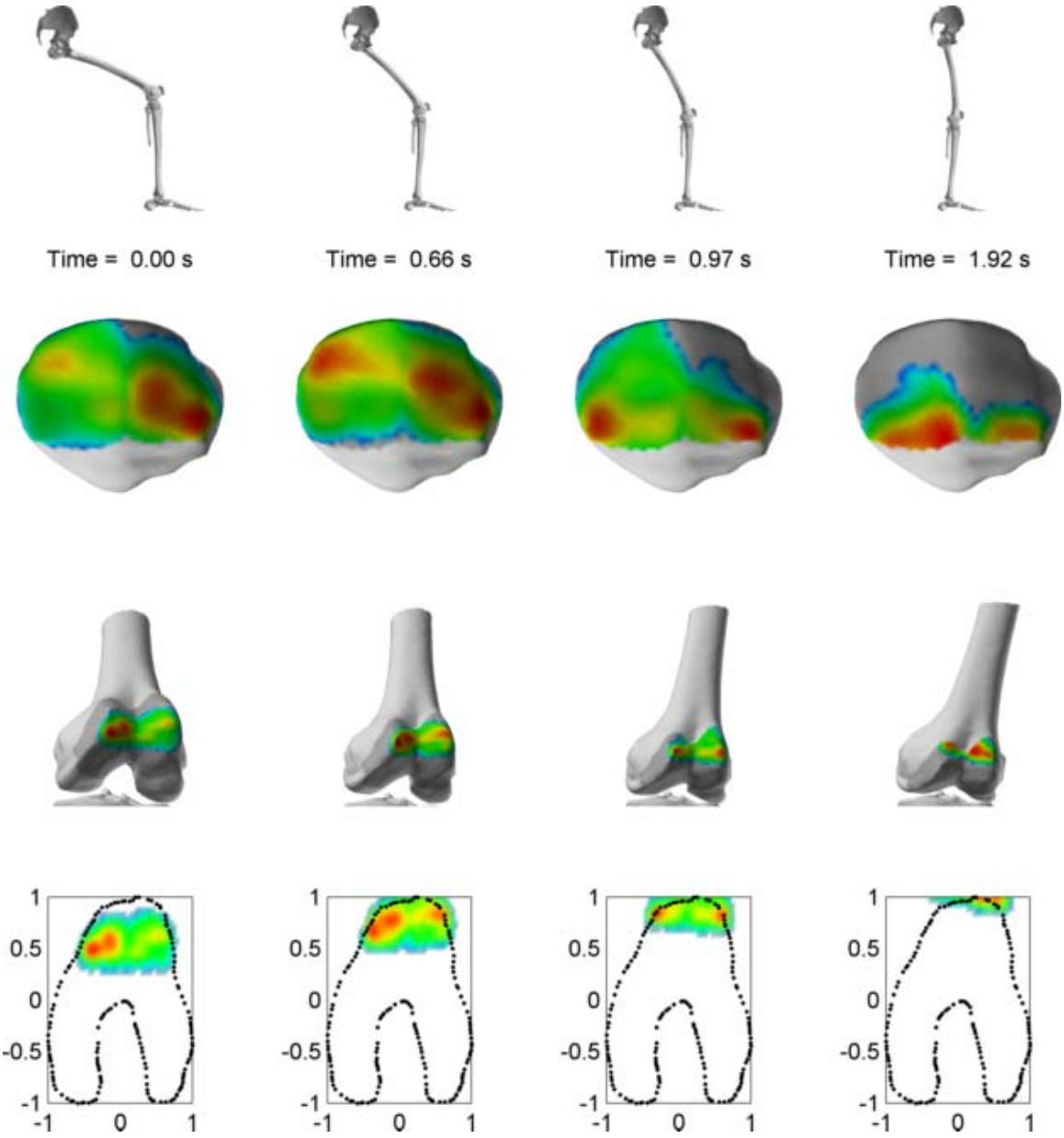


Figure A.93: Patient 11N dynamics model (top), patellofemoral contact location mapped on the patient's specific patella (2^{nd} from top) and femur (2^{nd} from bottom) bone models, as well as the normalized contact location mapped on the unfolded femoral trochlea surface (bottom).

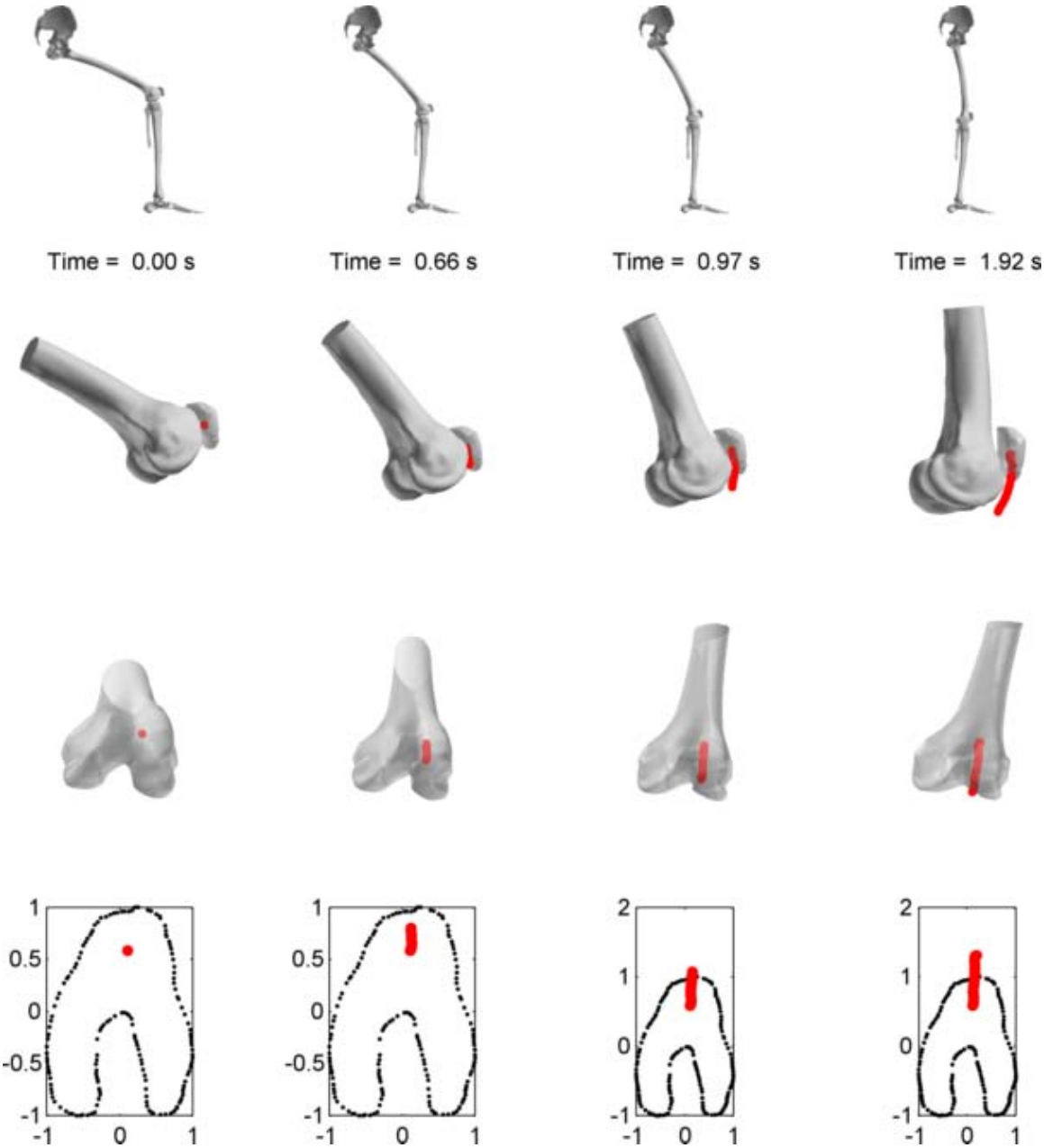


Figure A.94: Patient 11N dynamics model (top), patella center tracking in the sagittal (2^{nd} from top) and coronal (2^{nd} from bottom) planes, as well as the normalized patella tracking mapped on the unfolded femoral trochlea surface (bottom).

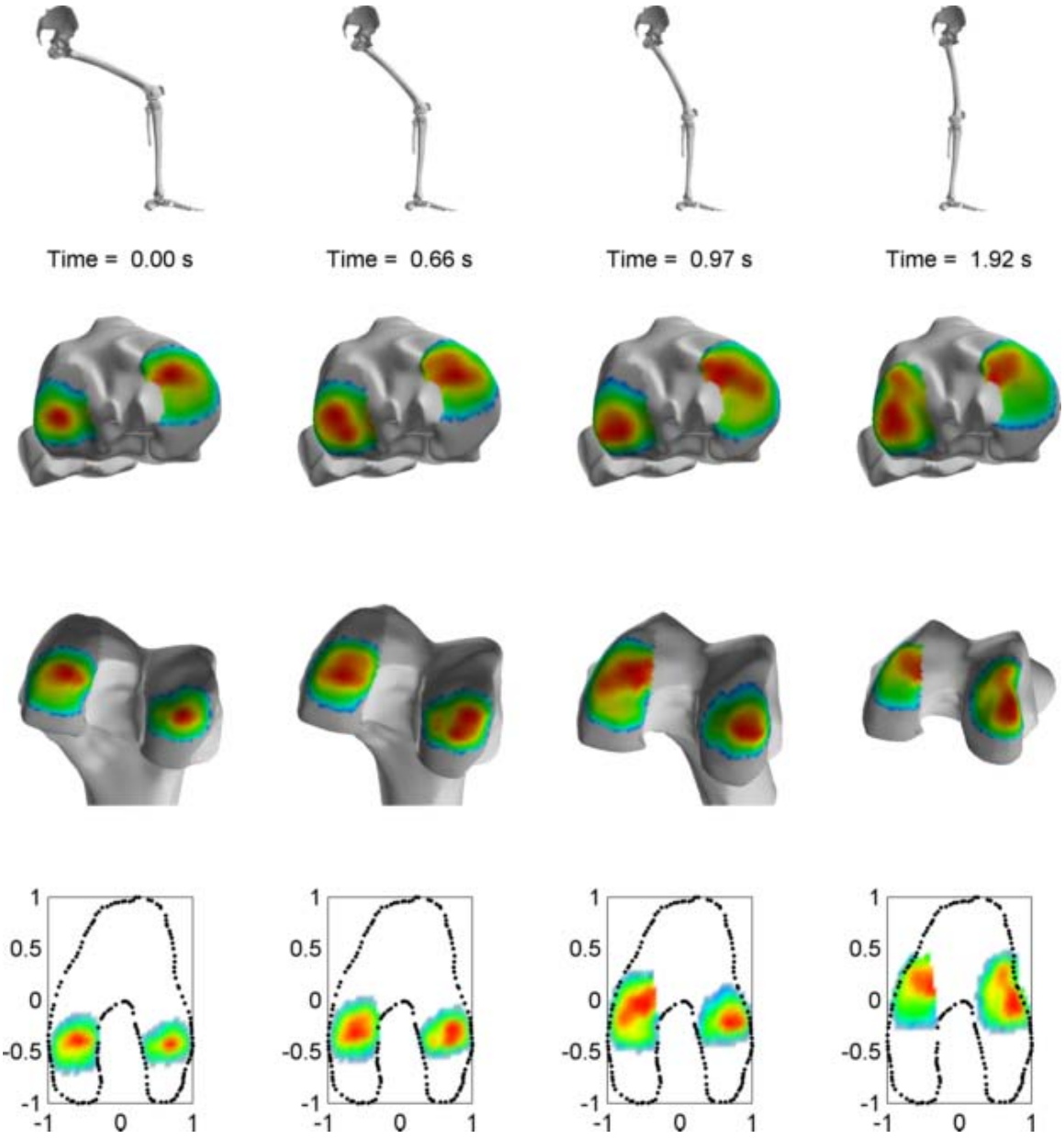


Figure A.95: Patient 11N dynamics model (top), tibiofemoral contact location mapped on the patient's specific patella (2^{nd} from top) and femur (2^{nd} from bottom) bone models, as well as the normalized contact location mapped on the unfolded femoral trochlea surface (bottom).

A.10.2 Electromyography and Inverse Dynamics analyses results

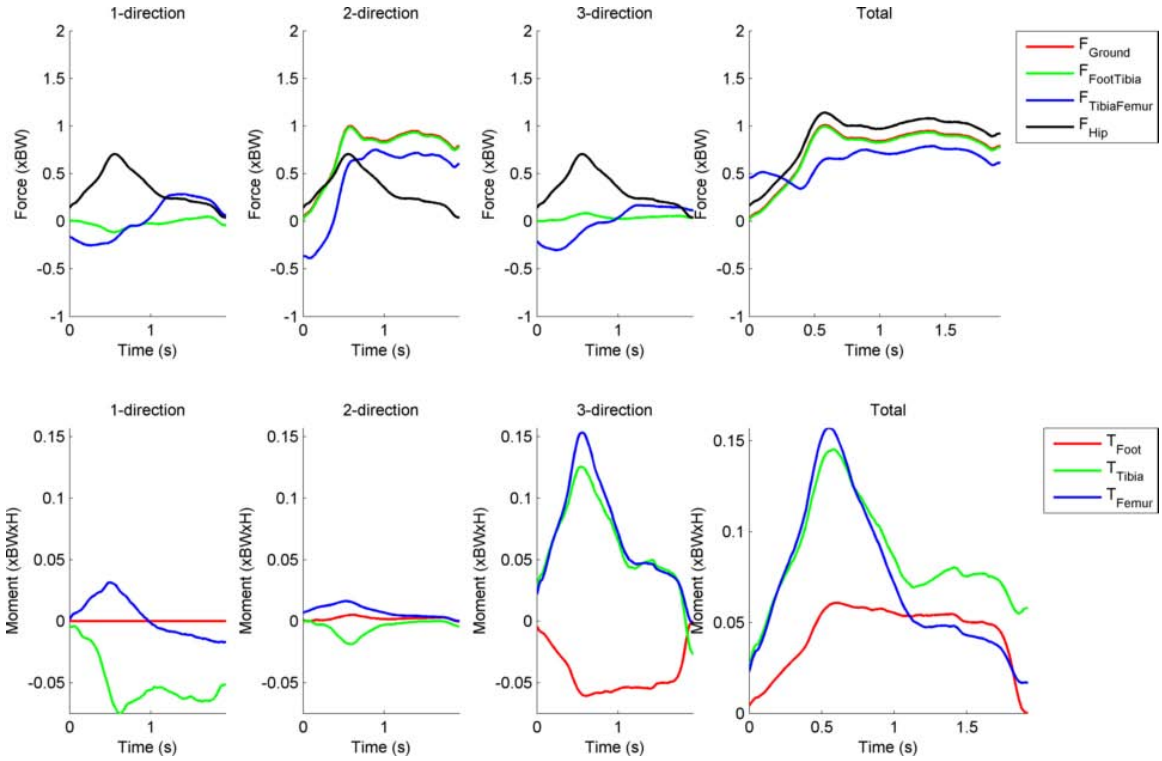


Figure A.96: Patient 11N knee joint reaction forces (top) and moments (bottom) normalized with respect to patient's body weight (BW). 1-direction = Anterior(+)/Posterior(-), 2-direction = Superior(+)/Inferior(-), 3-direction = Medial(+)/Lateral(-).

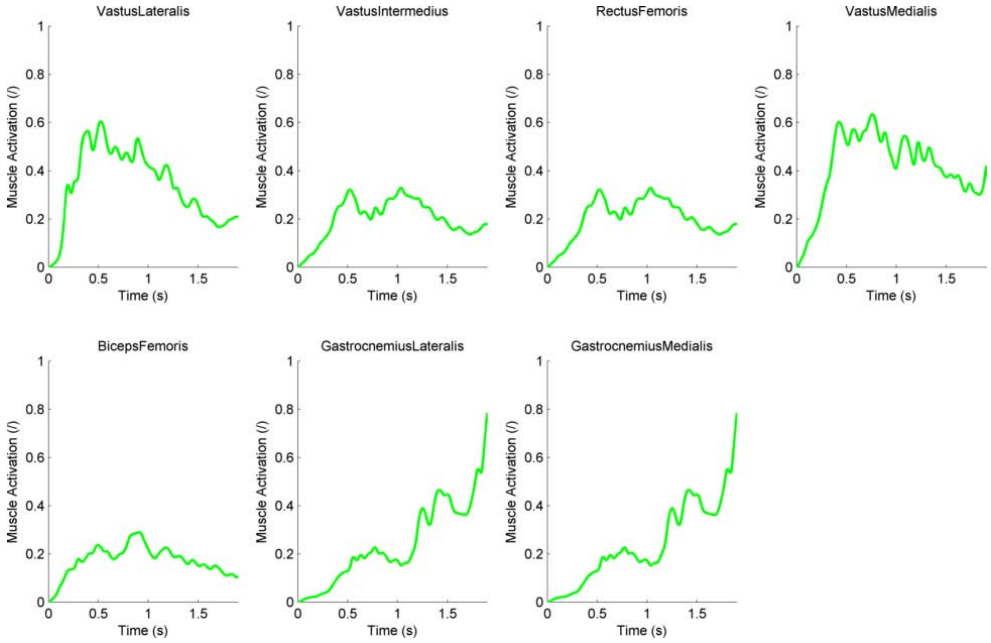


Figure A.97: Patient 11N muscle activation values obtained using the muscle activation dynamics[256].

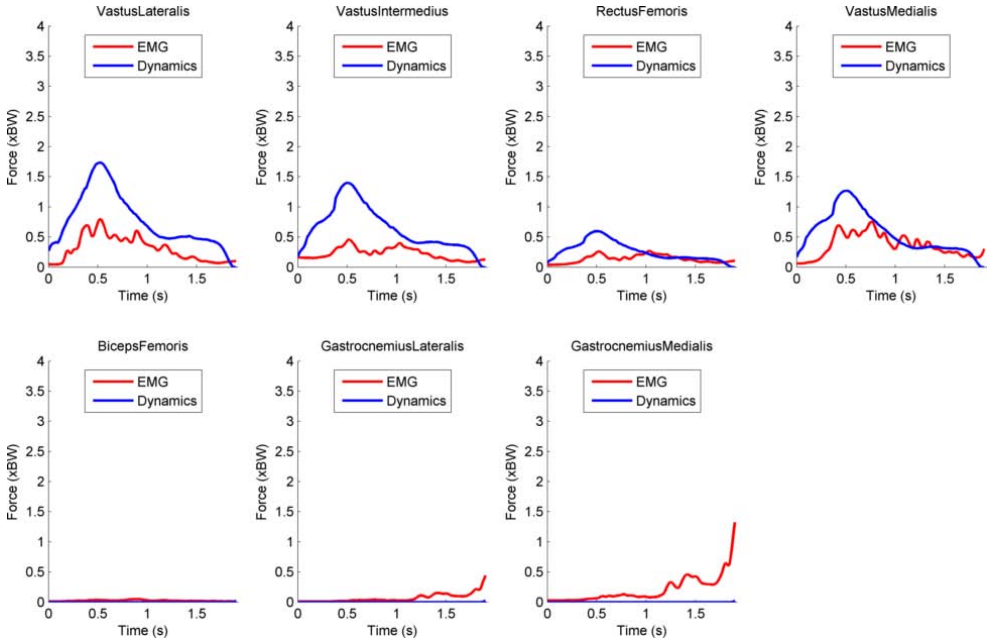


Figure A.98: Patient 11N muscle forces obtained using the EMG signal analysis (red) and pseudoinverse dynamics approach (green) normalized by patient's body weight (BW).

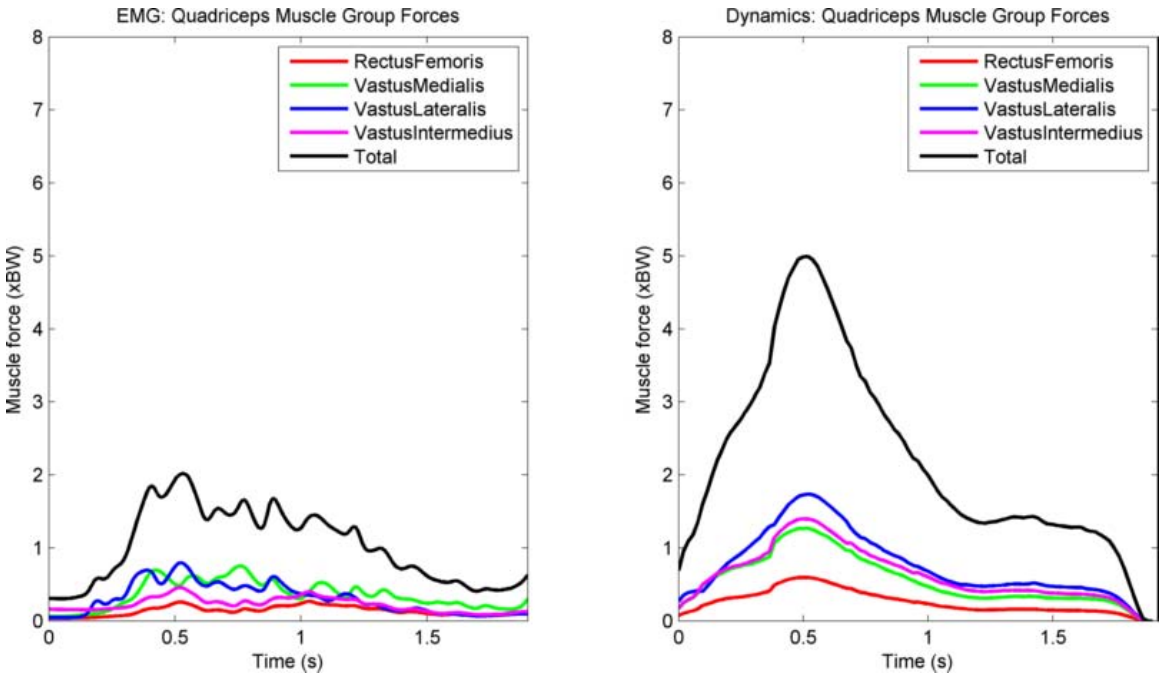


Figure A.99: Patient 11N quadriceps muscle group forces calculated from the EMG signals (left) and from the inverse dynamics (right) normalized by patient's body weight (BW).

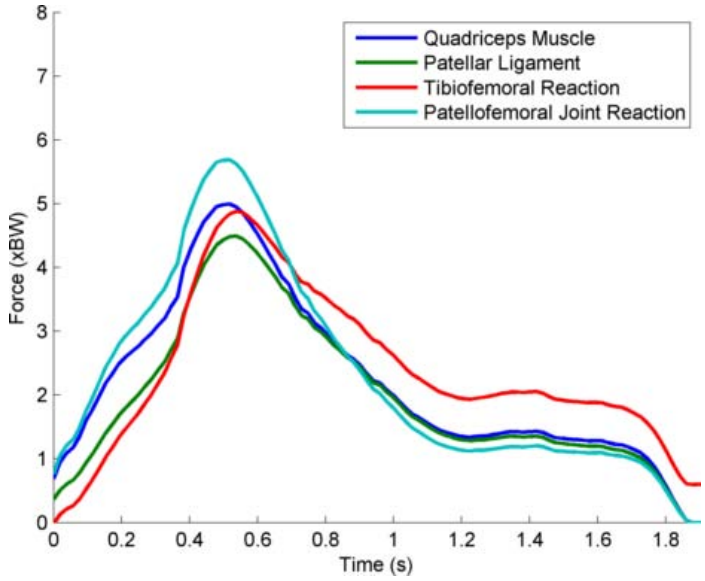


Figure A.100: Patient 11N total knee joint reaction forces incuding the action of the muscles, as well as the forces in the patellofemoral ligament, collateral and cruciate ligaments (if present) normalized by patient's body weight (BW).

A.11 Patient 19T

Patient demographic details:

ID# 19T

age: 62 yrs

height: 1.57 m

mass: 79 kg

leg side: Right

condition: TKA

A.11.1 Kinematics analysis results

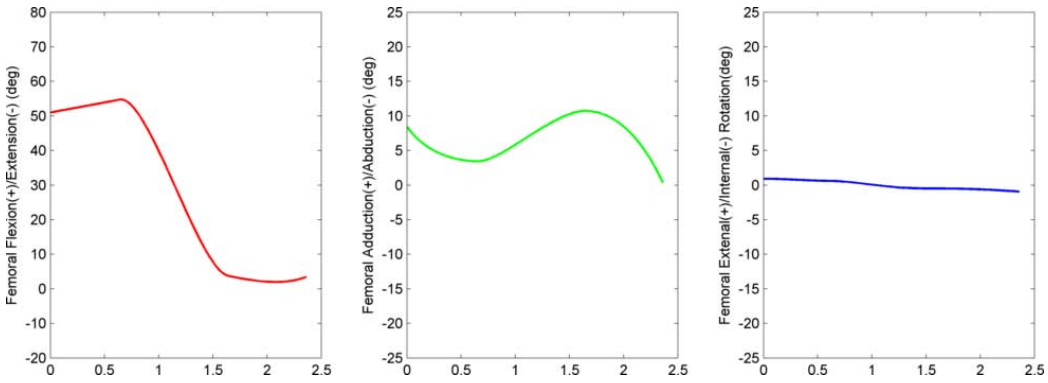


Figure A.101: Patient 19T patellofemoral joint kinematics.

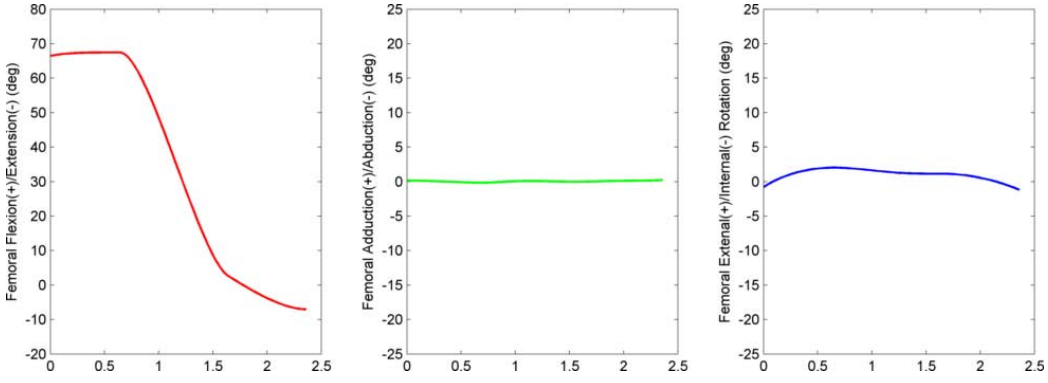


Figure A.102: Patient 19T tibiofemoral joint kinematics.

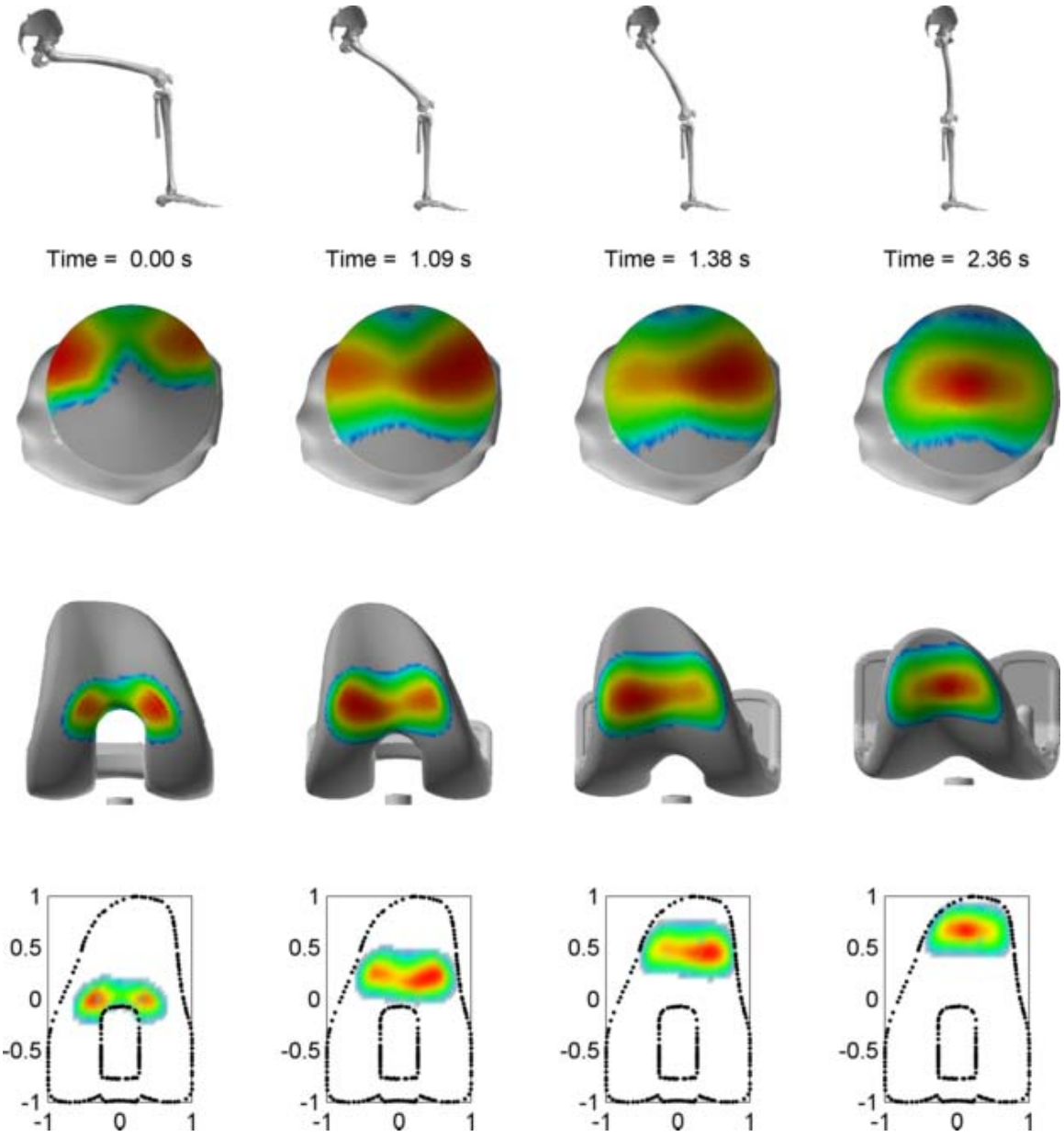


Figure A.103: Patient 19T dynamics model (top), patellofemoral contact location mapped on the patient's specific patella (2^{nd} from top) and femur (2^{nd} from bottom) bone models, as well as the normalized contact location mapped on the unfolded femoral trochlea surface (bottom).

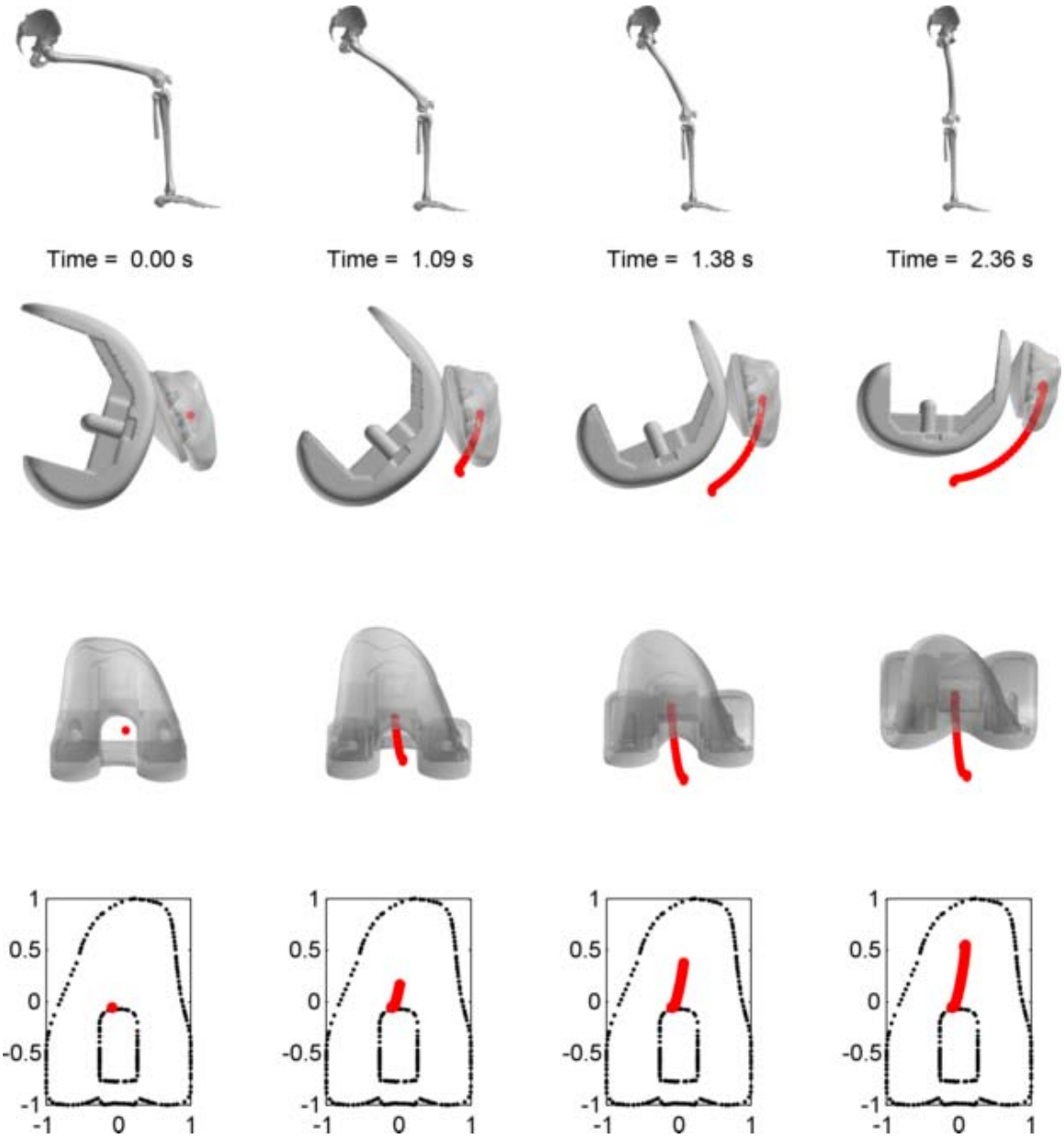


Figure A.104: Patient 19T dynamics model (top), patella center tracking in the sagittal (2^{nd} from top) and coronal (2^{nd} from bottom) planes, as well as the normalized patella tracking mapped on the unfolded femoral trochlea surface (bottom).

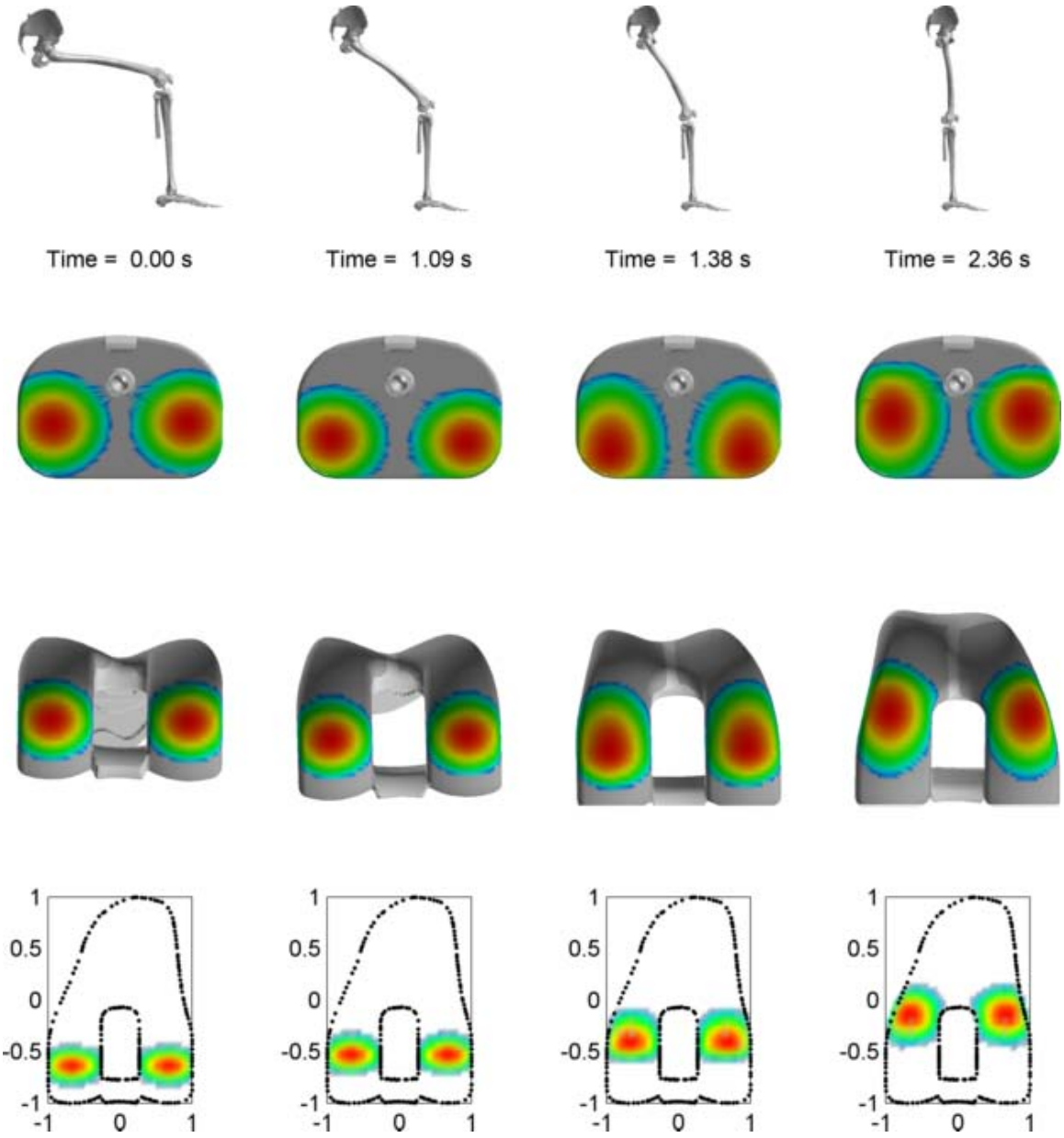


Figure A.105: Patient 19T dynamics model (top), tibiofemoral contact location mapped on the patient's specific patella (2^{nd} from top) and femur (2^{nd} from bottom) bone models, as well as the normalized contact location mapped on the unfolded femoral trochlea surface (bottom).

A.11.2 Electromyography and Inverse Dynamics analyses results

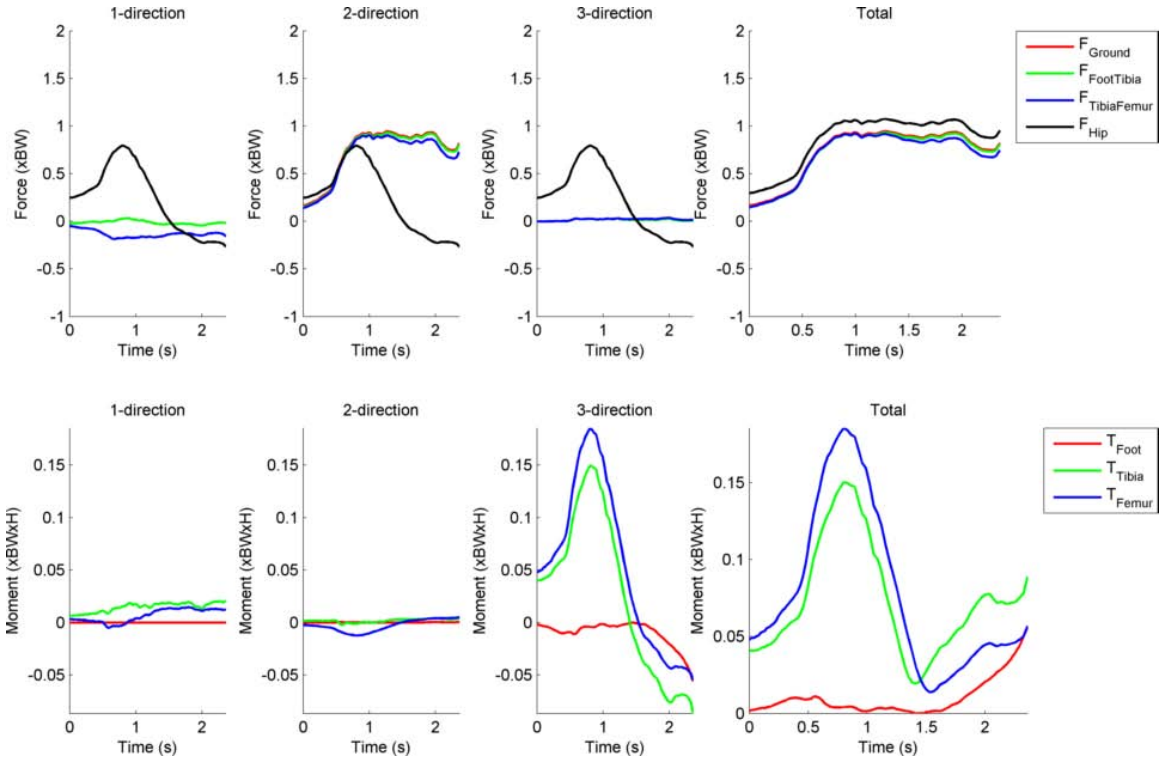


Figure A.106: Patient 19T knee joint reaction forces (top) and moments (bottom) normalized with respect to patient's body weight (BW). 1-direction = Anterior(+)/Posterior(-), 2-direction = Superior(+)/Inferior(-), 3-direction = Medial(+)/Lateral(-).

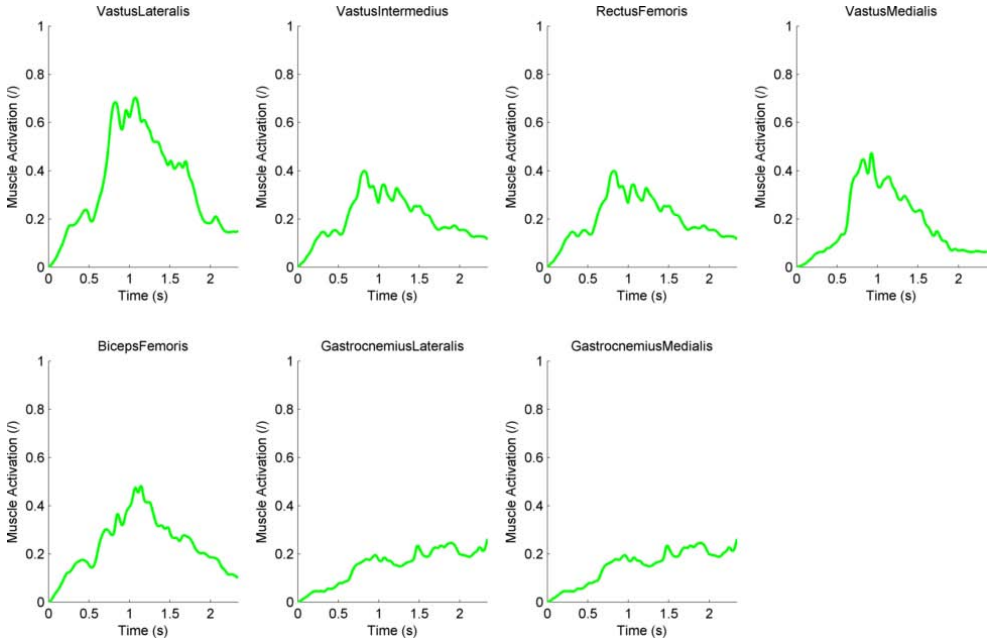


Figure A.107: Patient 19T muscle activation values obtained using the muscle activation dynamics[256].

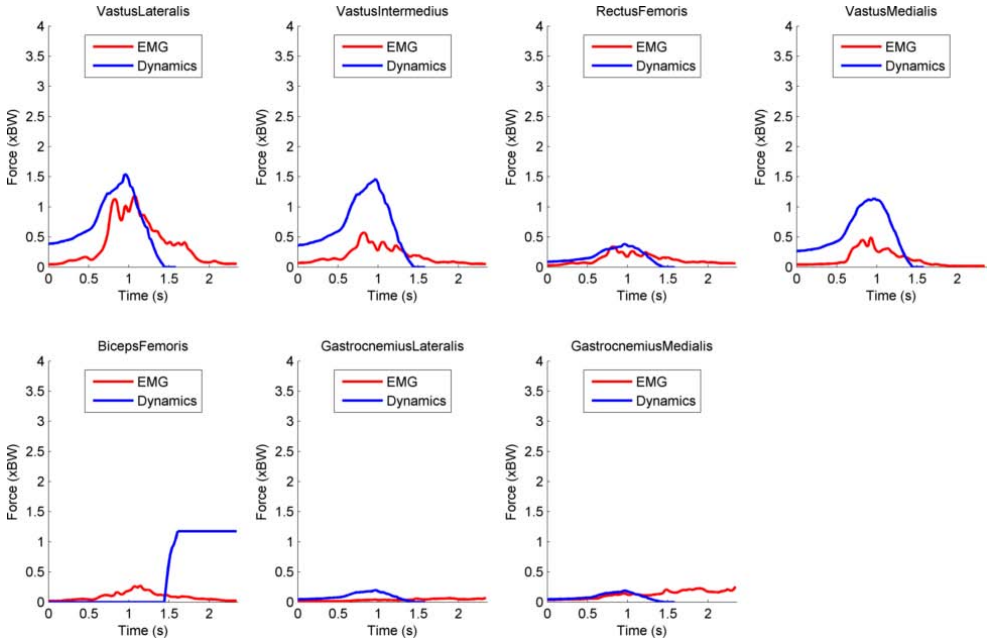


Figure A.108: Patient 19T muscle forces obtained using the EMG signal analysis (red) and pseudoinverse dynamics approach (green) normalized by patient's body weight (BW).

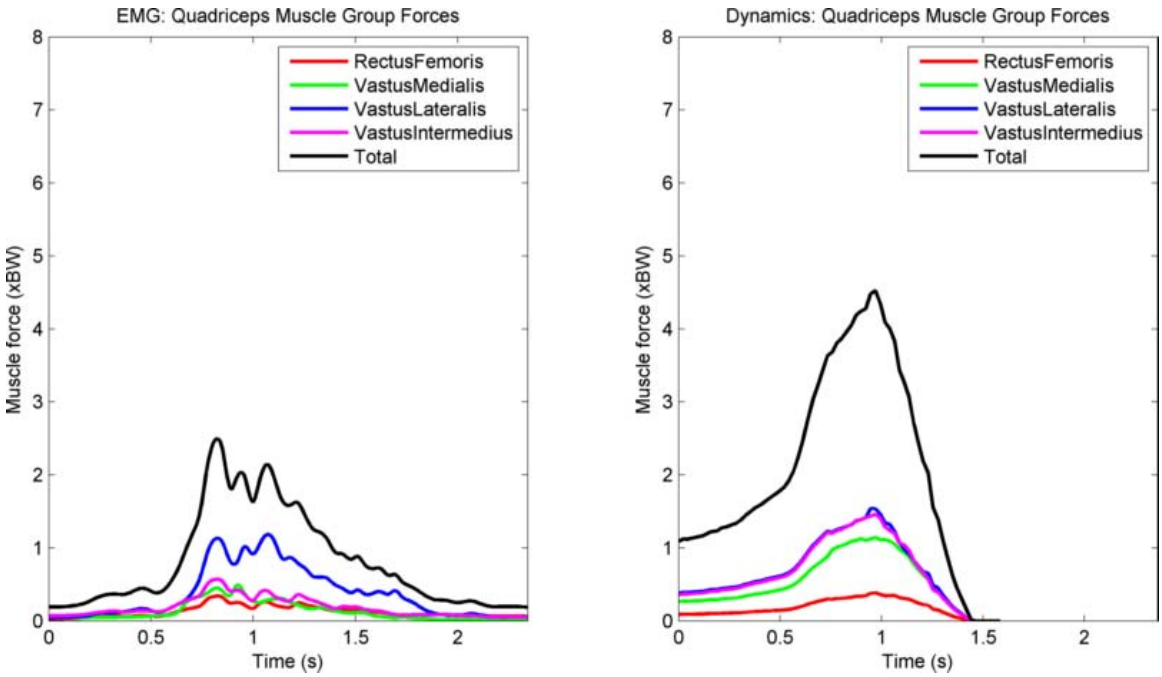


Figure A.109: Patient 19T quadriceps muscle group forces calculated from the EMG signals (left) and from the inverse dynamics (right) normalized by patient's body weight (BW).

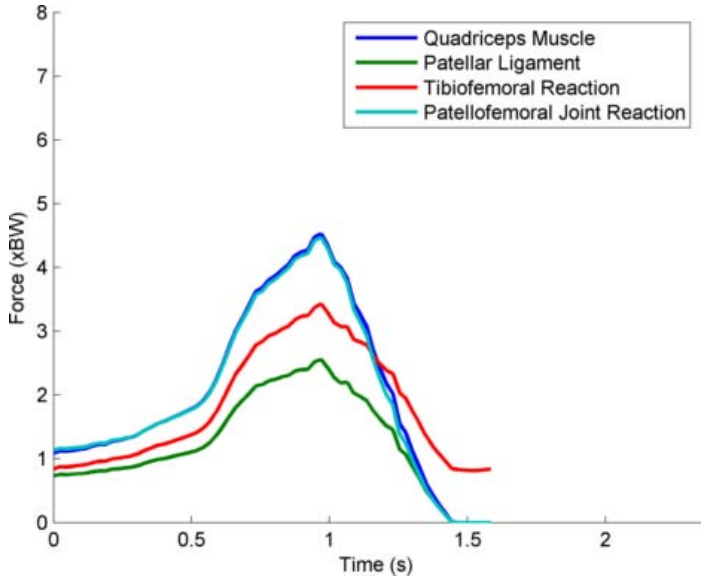


Figure A.110: Patient 19T total knee joint reaction forces incuding the action of the muscles, as well as the forces in the patellofemoral ligament, collateral and cruciate ligaments (if present) normalized by patient's body weight (BW).

A.12 Patient 19N

Patient demographic details:

ID# 19N

age: 62 yrs

height: 1.57 m

mass: 79 kg

leg side: Left

condition: Healthy

A.12.1 Kinematics analysis results

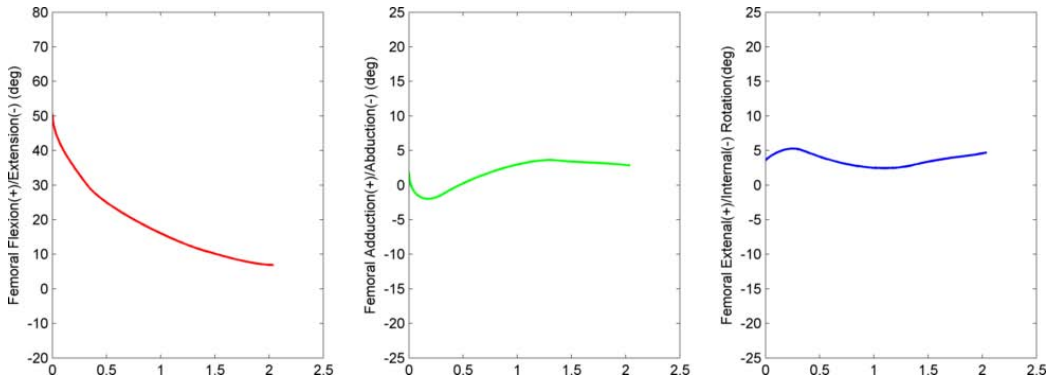


Figure A.111: Patient 19N patellofemoral joint kinematics.

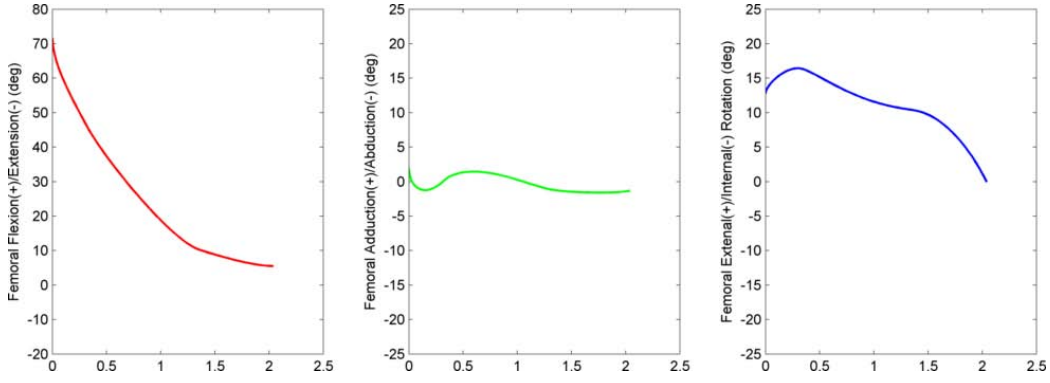


Figure A.112: Patient 19N tibiofemoral joint kinematics.

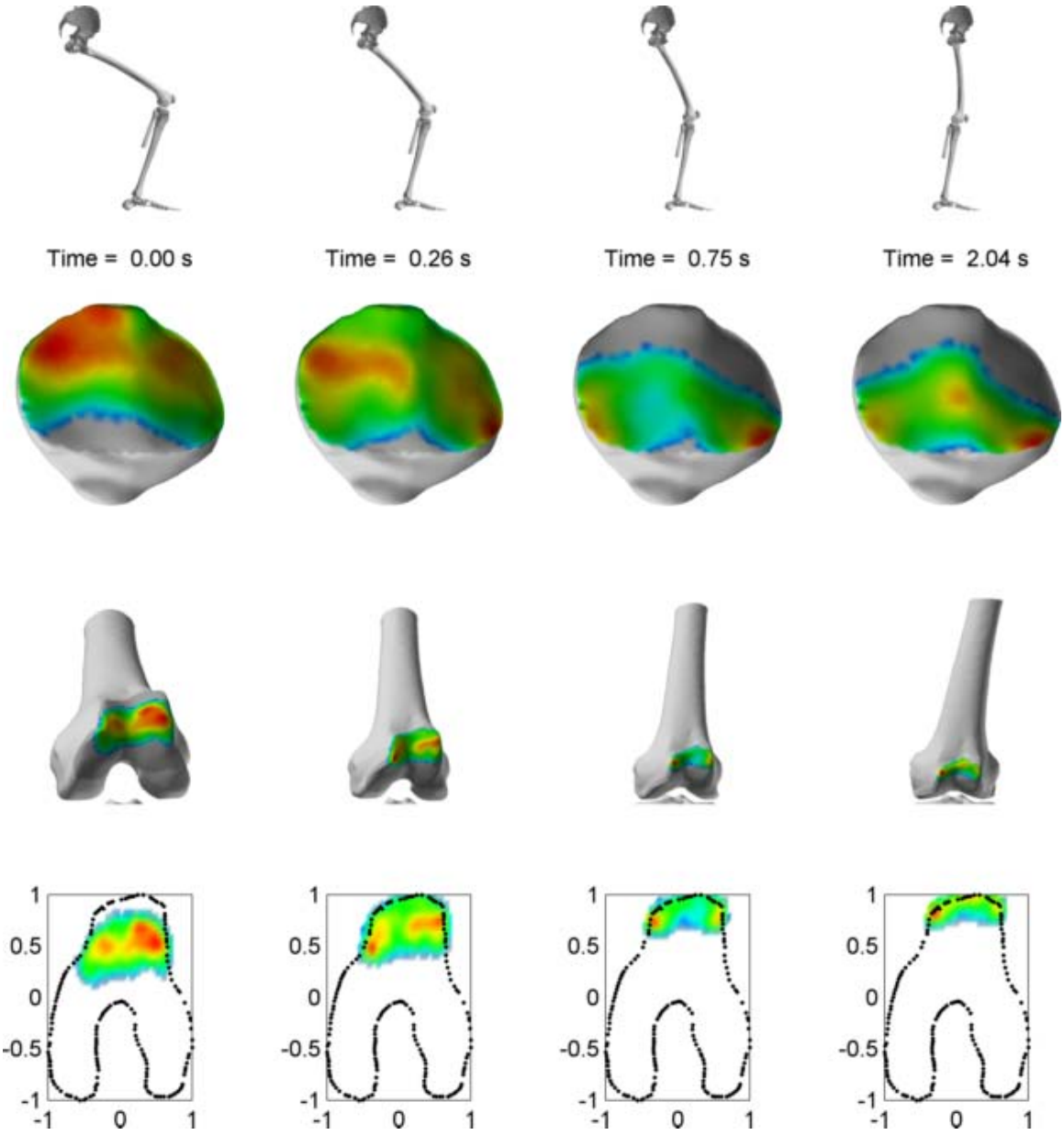


Figure A.113: Patient 19N dynamics model (top), patellofemoral contact location mapped on the patient's specific patella (2^{nd} from top) and femur (2^{nd} from bottom) bone models, as well as the normalized contact location mapped on the unfolded femoral trochlea surface (bottom).

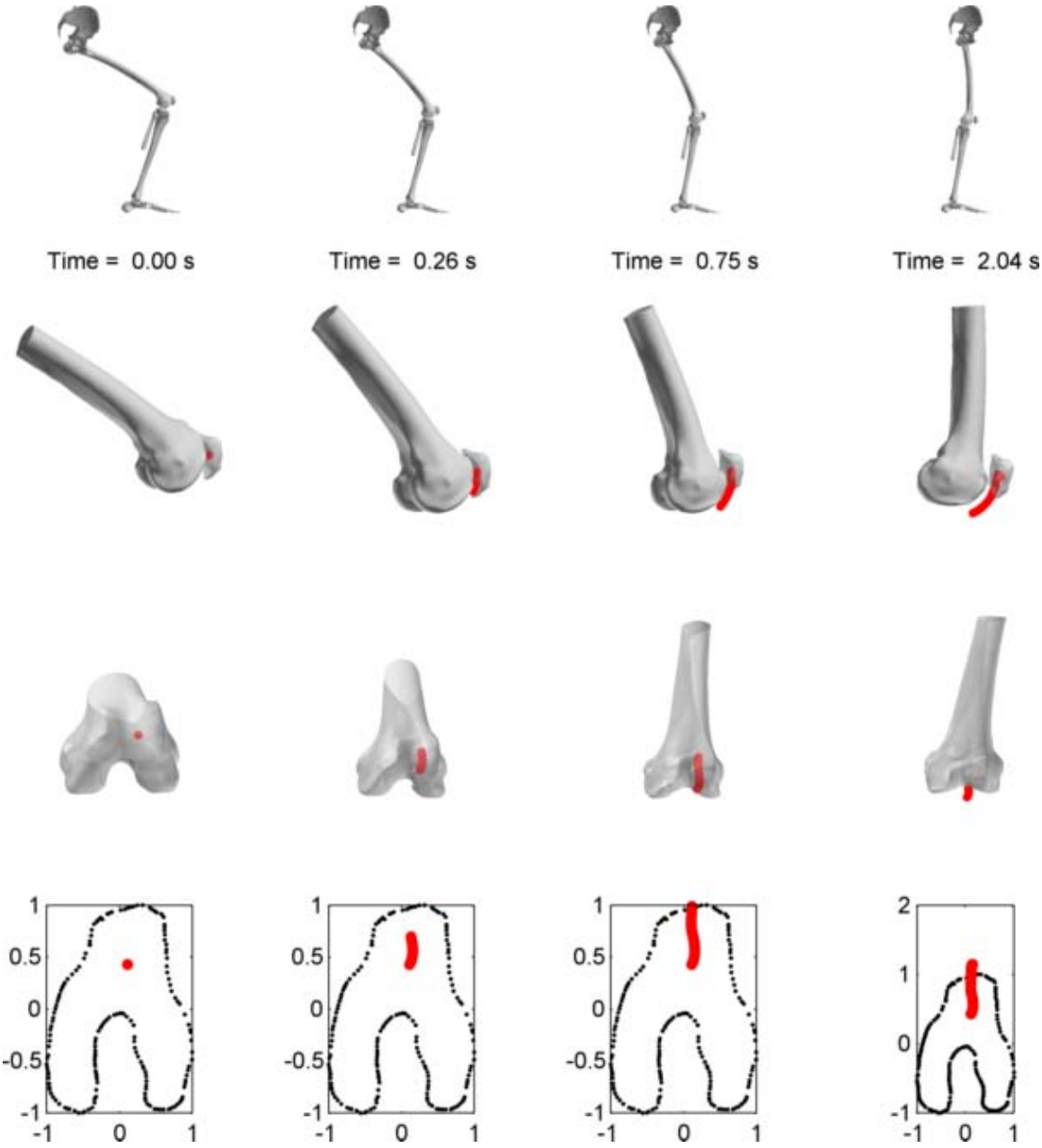


Figure A.114: Patient 19N dynamics model (top), patella center tracking in the sagittal (2^{nd} from top) and coronal (2^{nd} from bottom) planes, as well as the normalized patella tracking mapped on the unfolded femoral trochlea surface (bottom).

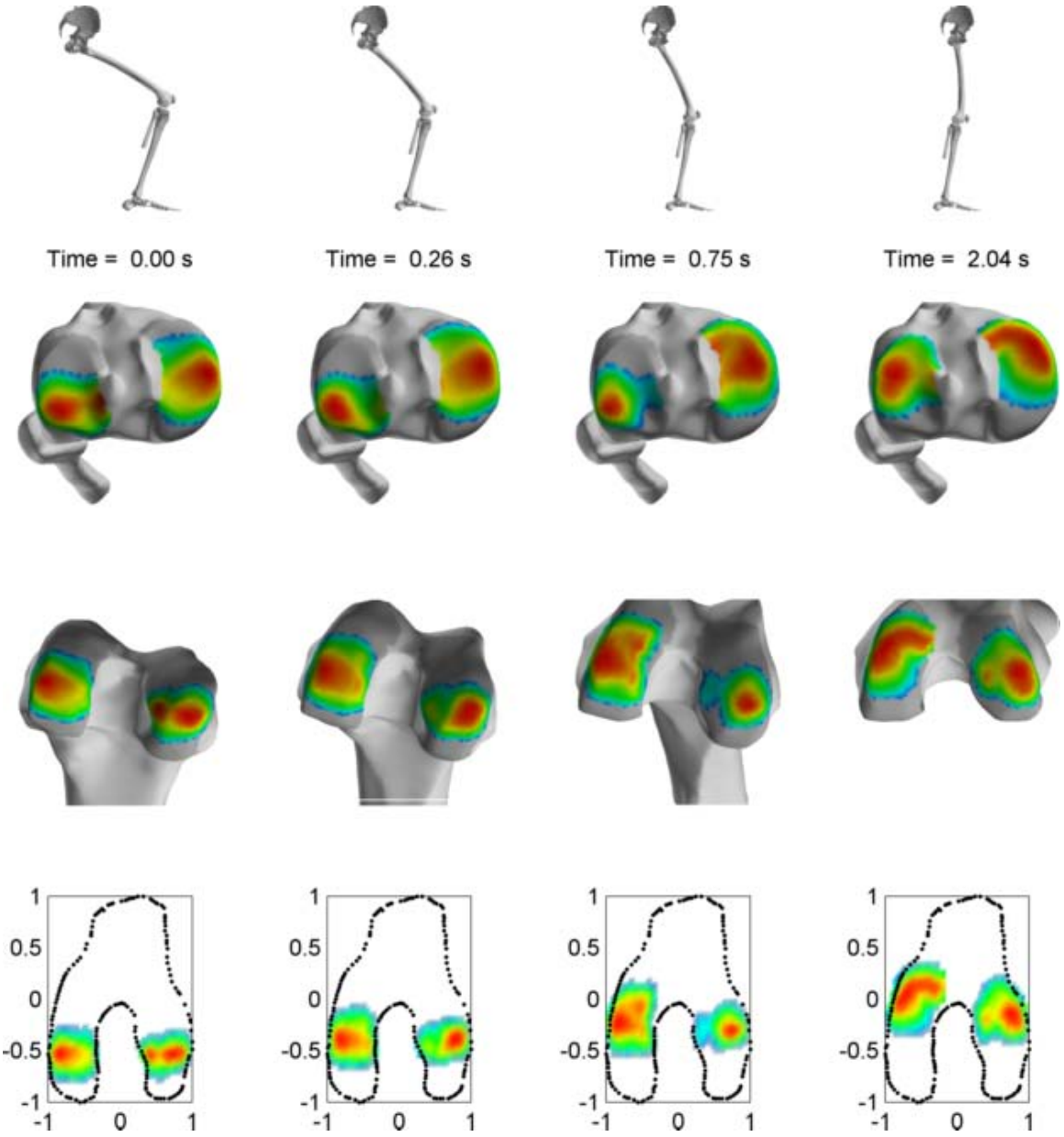


Figure A.115: Patient 19N dynamics model (top), tibiofemoral contact location mapped on the patient's specific patella (2^{nd} from top) and femur (2^{nd} from bottom) bone models, as well as the normalized contact location mapped on the unfolded femoral trochlea surface (bottom).

A.12.2 Electromyography and Inverse Dynamics analyses results

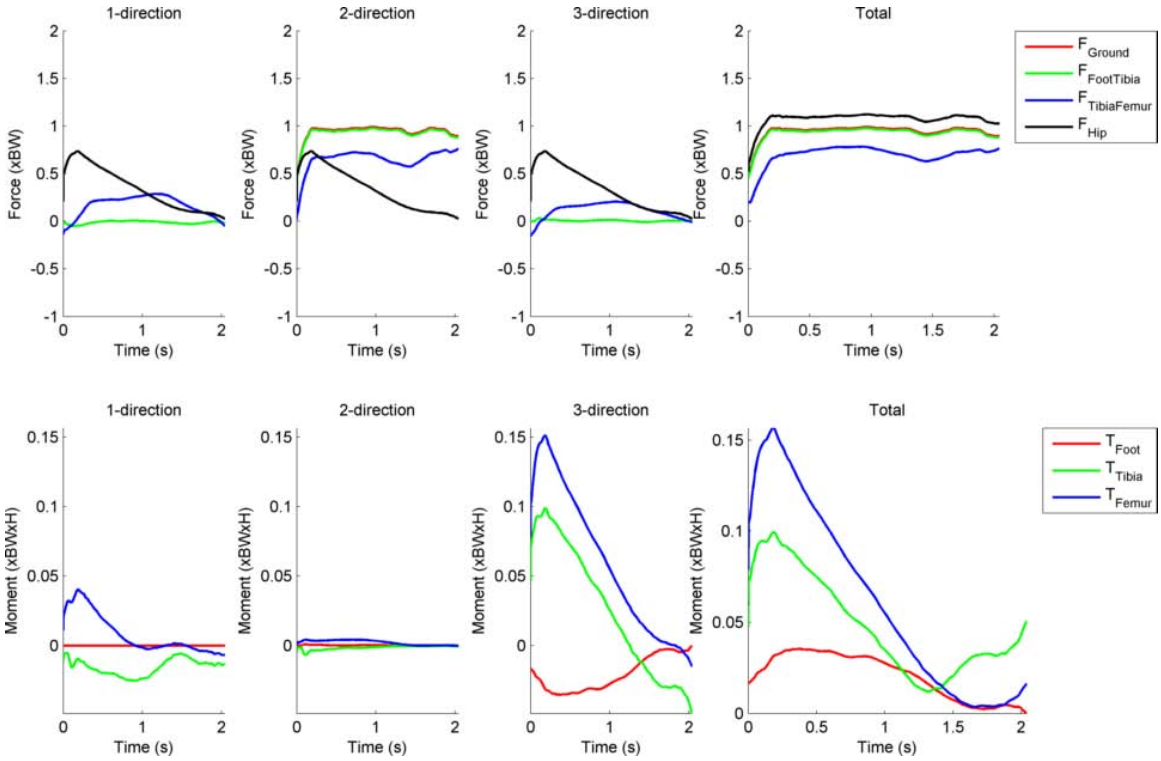


Figure A.116: Patient 19N knee joint reaction forces (top) and moments (bottom) normalized with respect to patient's body weight (BW). 1-direction = Anterior(+)/Posterior(-), 2-direction = Superior(+)/Inferior(-), 3-direction = Medial(+)/Lateral(-).

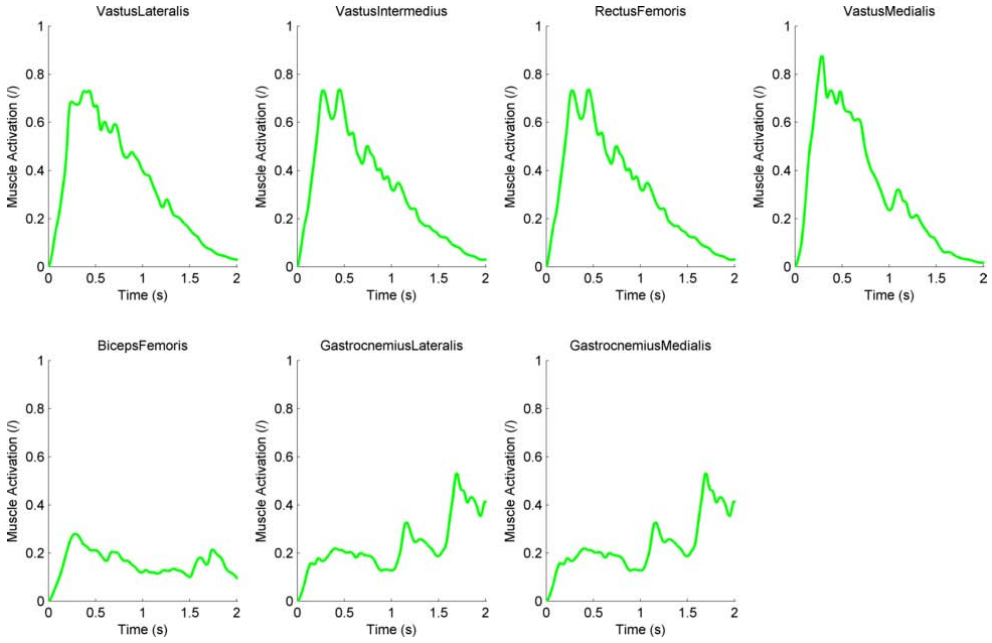


Figure A.117: Patient 19N muscle activation values obtained using the muscle activation dynamics[256].

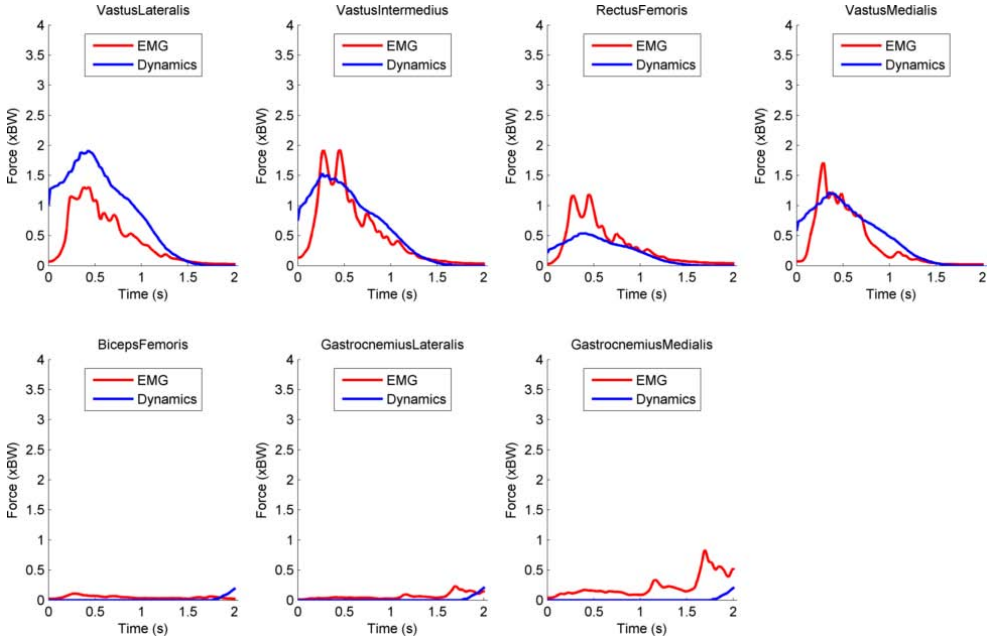


Figure A.118: Patient 19N muscle forces obtained using the EMG signal analysis (red) and pseudoinverse dynamics approach (green) normalized by patient's body weight (BW).

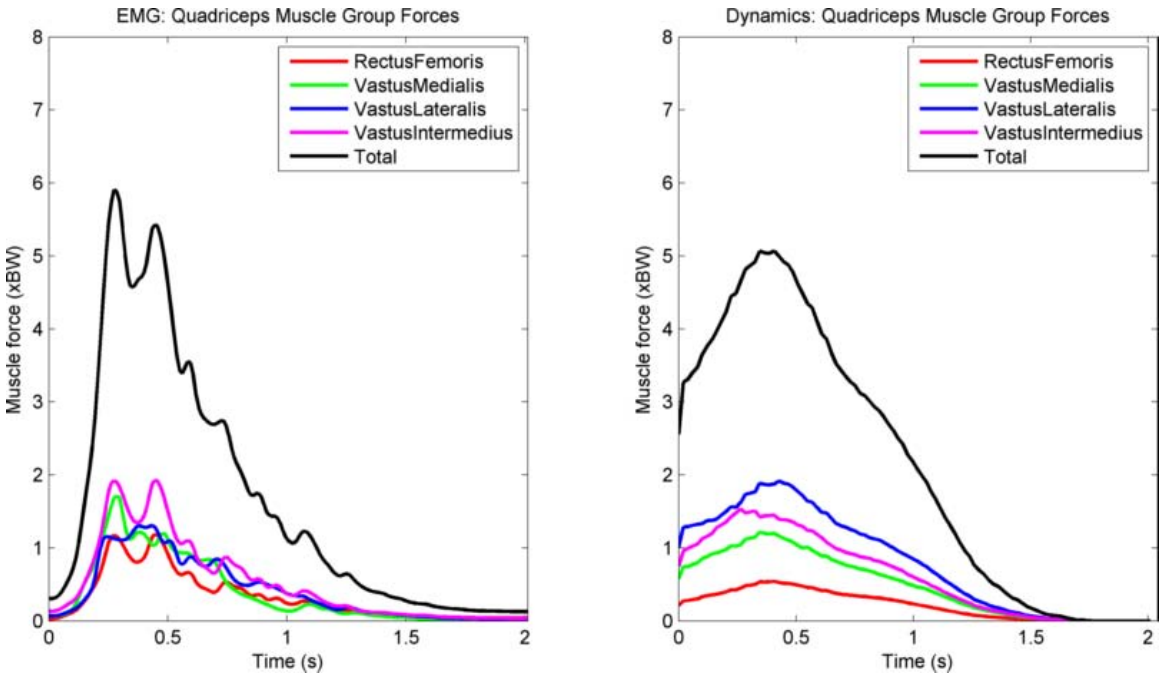


Figure A.119: Patient 19N quadriceps muscle group forces calculated from the EMG signals (left) and from the inverse dynamics (right) normalized by patient's body weight (BW).

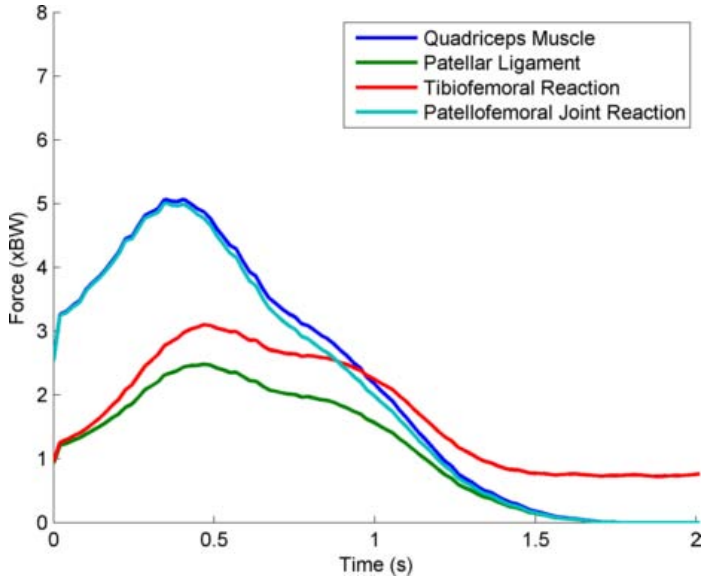


Figure A.120: Patient 19N total knee joint reaction forces incuding the action of the muscles, as well as the forces in the patellofemoral ligament, collateral and cruciate ligaments (if present) normalized by patient's body weight (BW).

A.13 Patient 22T

Patient demographic details:

ID# 22T

age: 75 yrs

height: 1.65 m

mass: 74 kg

leg side: Right

condition: TKA

A.13.1 Kinematics analysis results

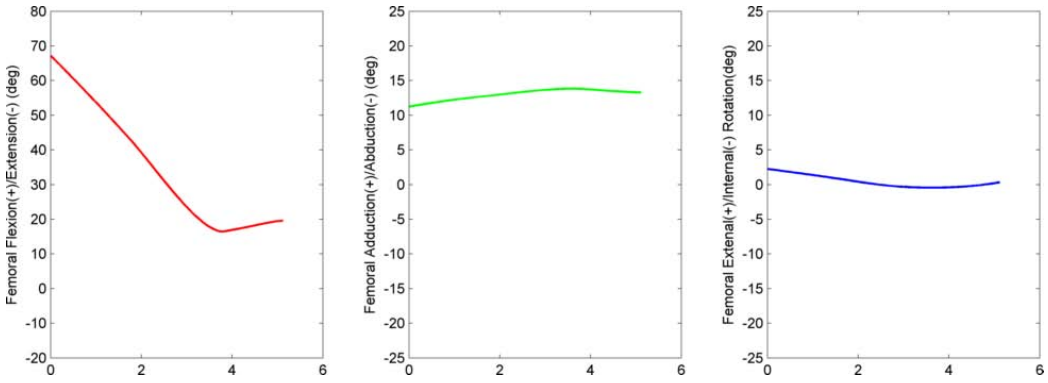


Figure A.121: Patient 22T patellofemoral joint kinematics.

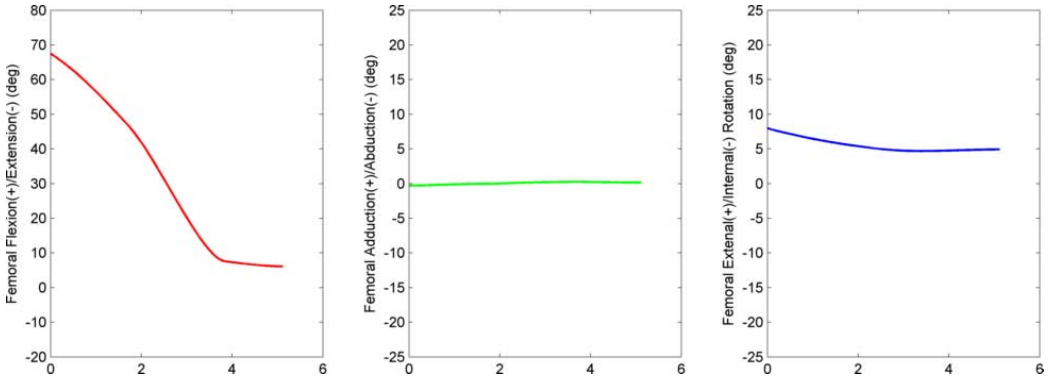


Figure A.122: Patient 22T tibiofemoral joint kinematics.

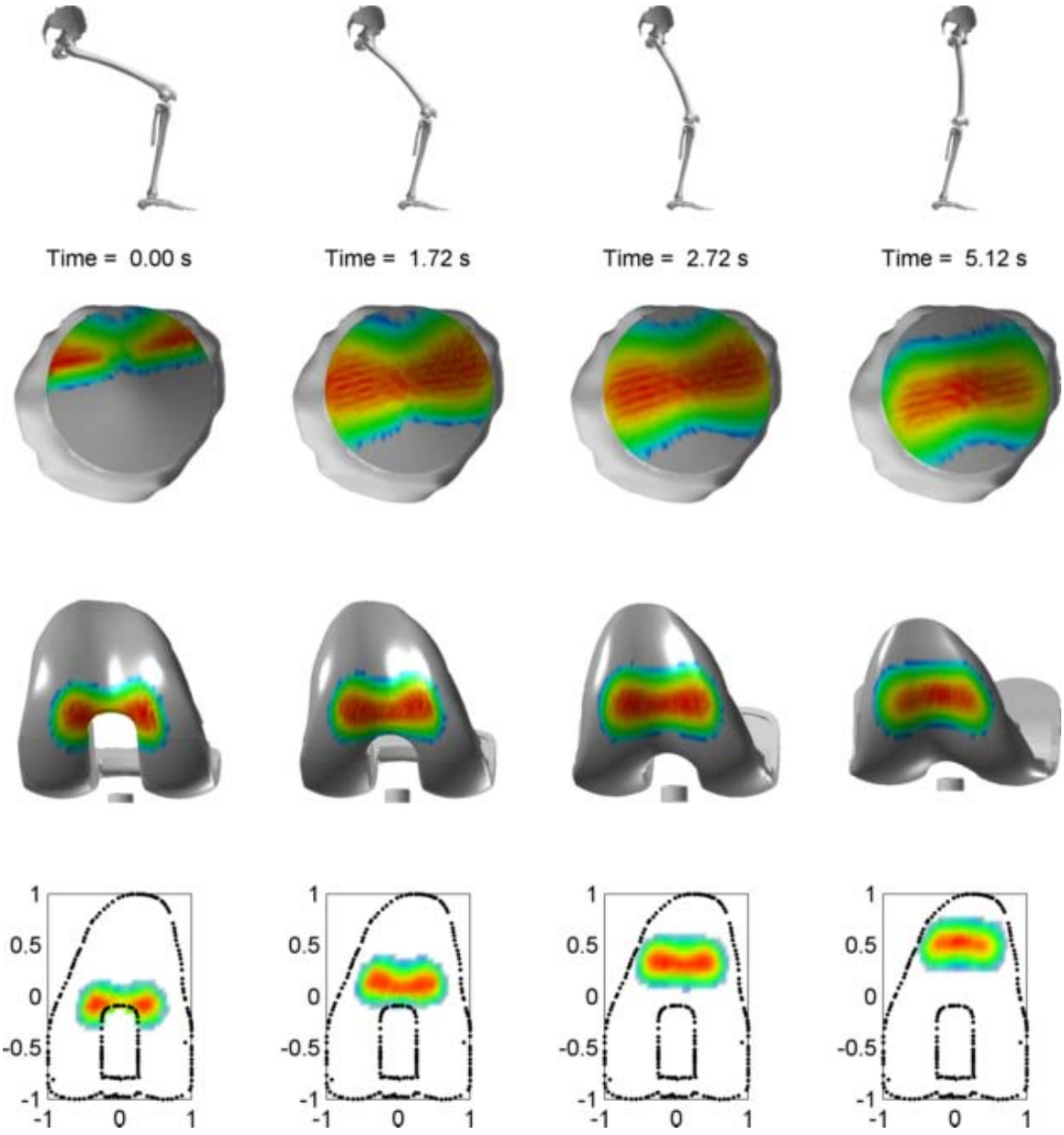


Figure A.123: Patient 22T dynamics model (top), patellofemoral contact location mapped on the patient's specific patella (2^{nd} from top) and femur (2^{nd} from bottom) bone models, as well as the normalized contact location mapped on the unfolded femoral trochlea surface (bottom).

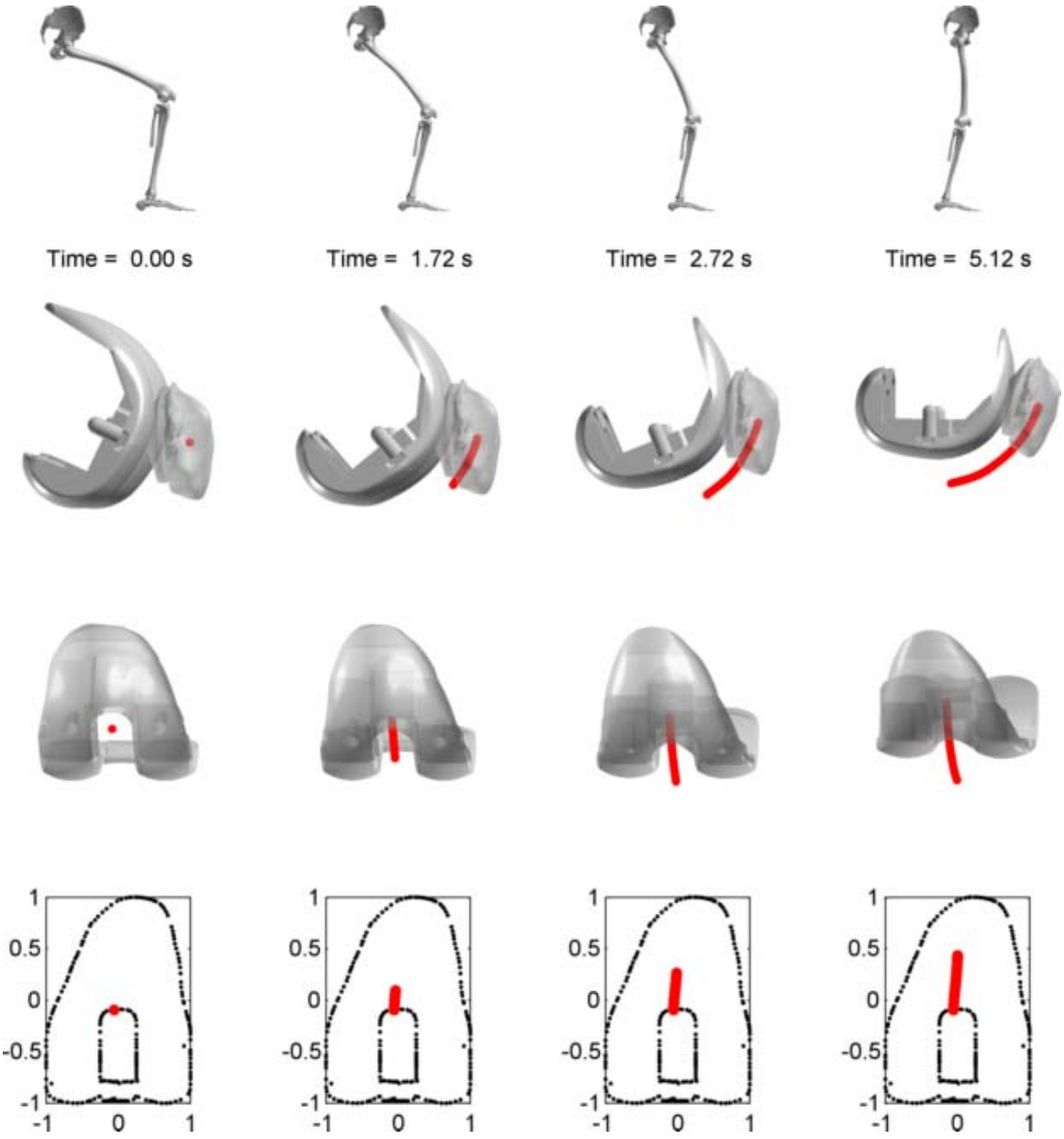


Figure A.124: Patient 22T dynamics model (top), patella center tracking in the sagittal (2^{nd} from top) and coronal (2^{nd} from bottom) planes, as well as the normalized patella tracking mapped on the unfolded femoral trochlea surface (bottom).

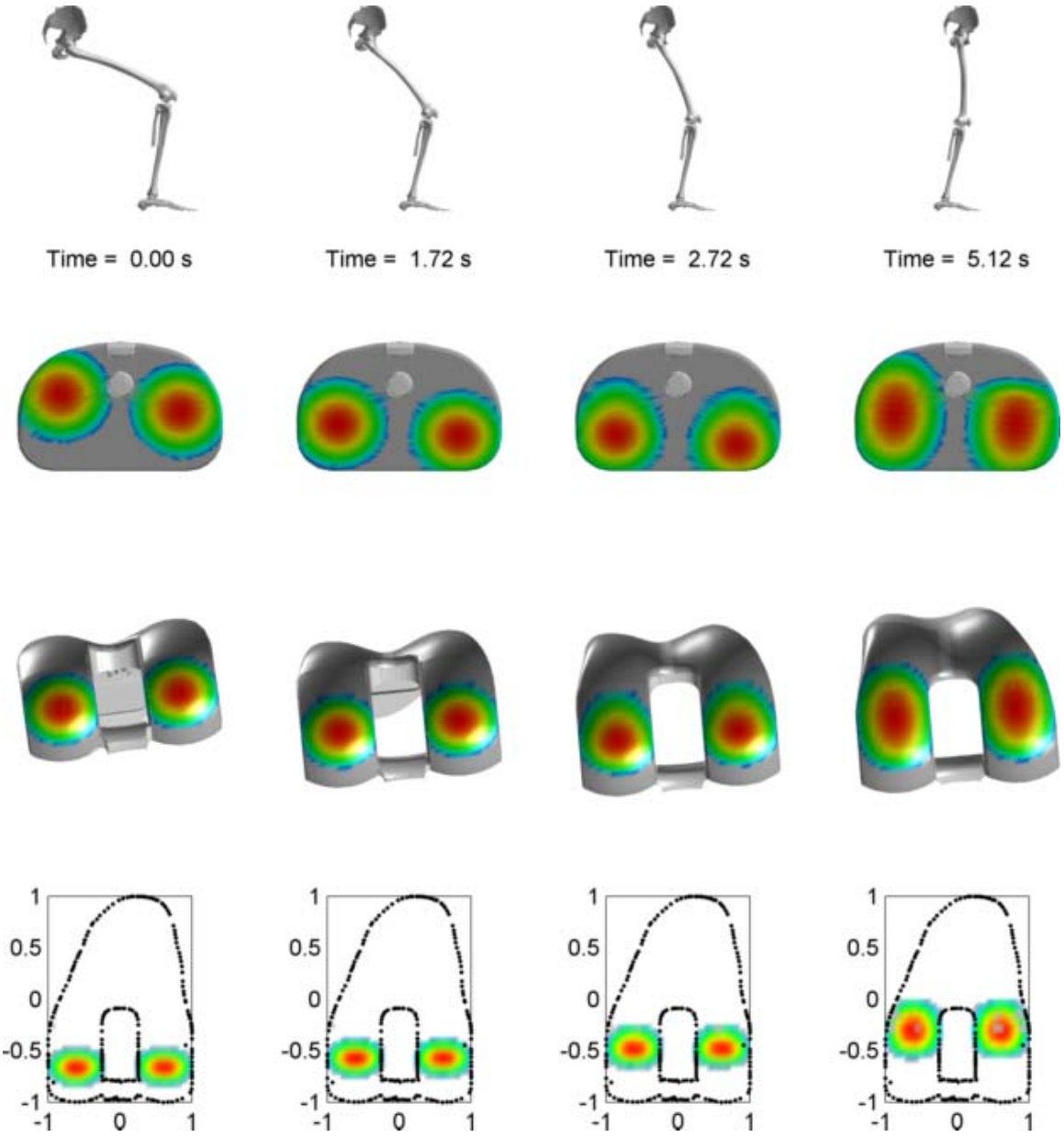


Figure A.125: Patient 22T dynamics model (top), tibiofemoral contact location mapped on the patient's specific patella (2^{nd} from top) and femur (2^{nd} from bottom) bone models, as well as the normalized contact location mapped on the unfolded femoral trochlea surface (bottom).

A.13.2 Electromyography and Inverse Dynamics analyses results

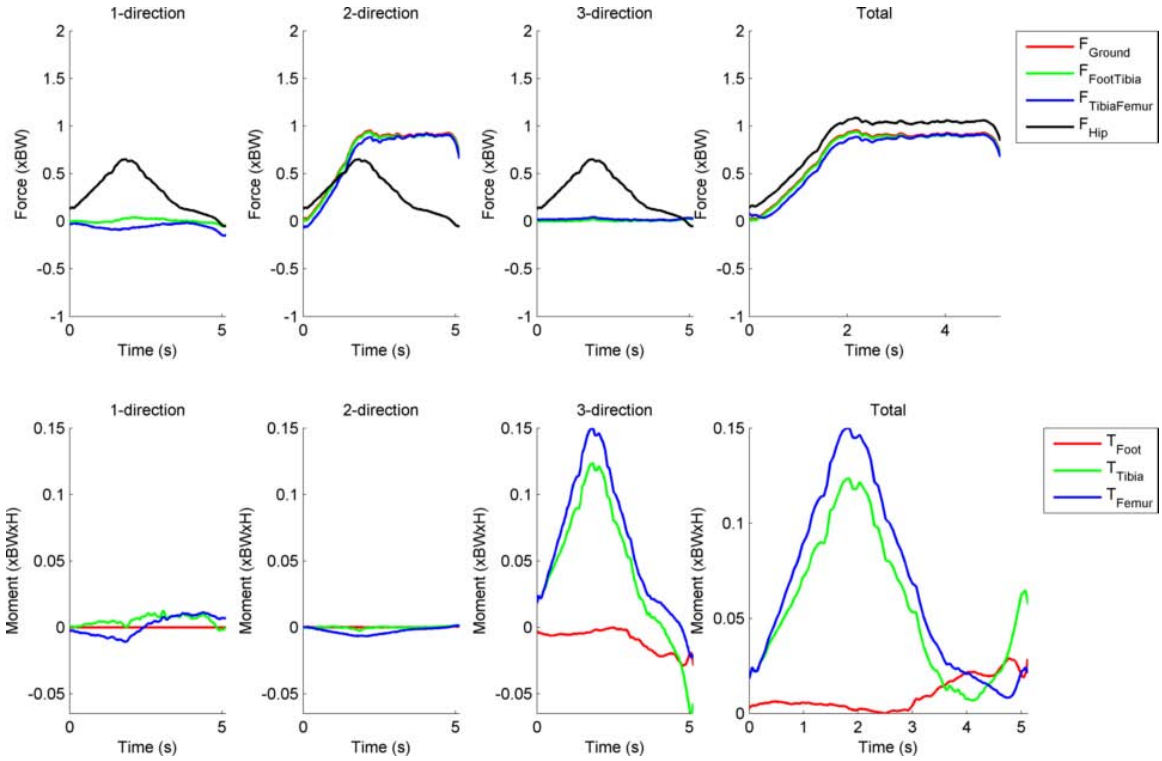


Figure A.126: Patient 22T knee joint reaction forces (top) and moments (bottom) normalized with respect to patient's body weight (BW). 1-direction = Anterior(+)/Posterior(-), 2-direction = Superior(+)/Inferior(-), 3-direction = Medial(+)/Lateral(-).

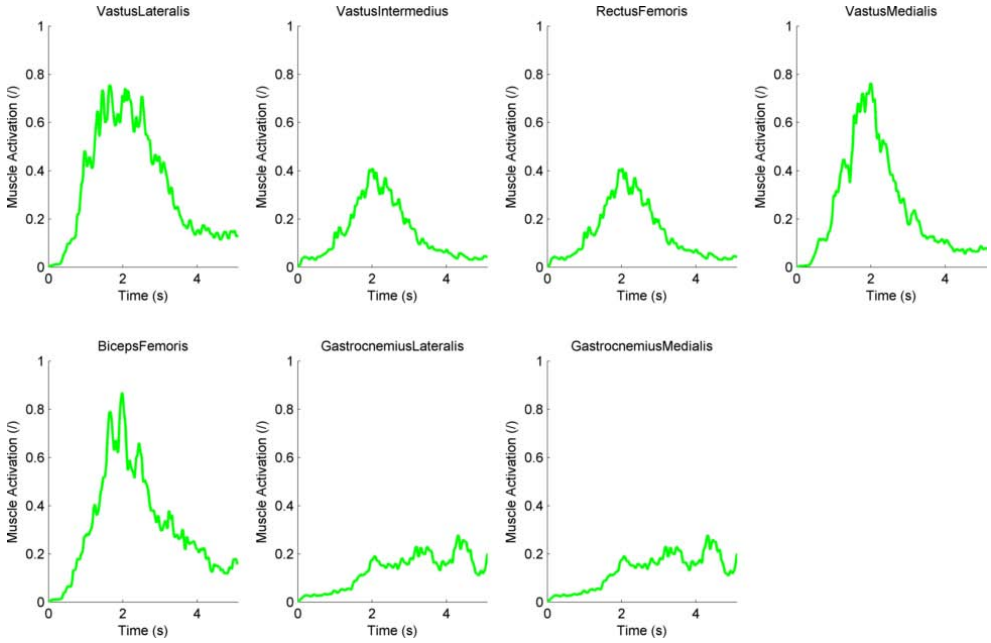


Figure A.127: Patient 22T muscle activation values obtained using the muscle activation dynamics[256].

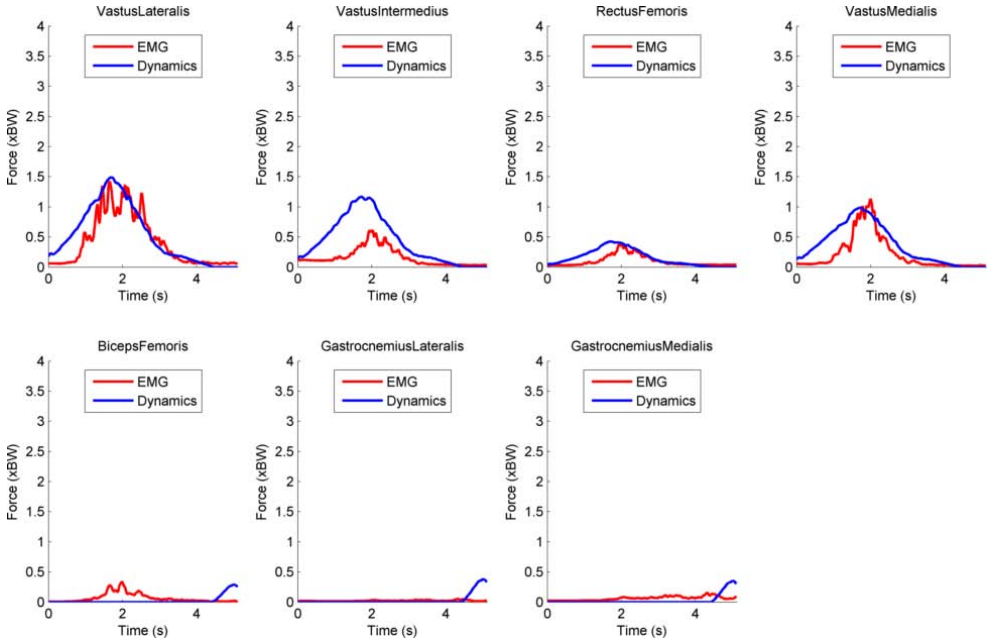


Figure A.128: Patient 22T muscle forces obtained using the EMG signal analysis (red) and pseudoinverse dynamics approach (green) normalized by patient's body weight (BW).

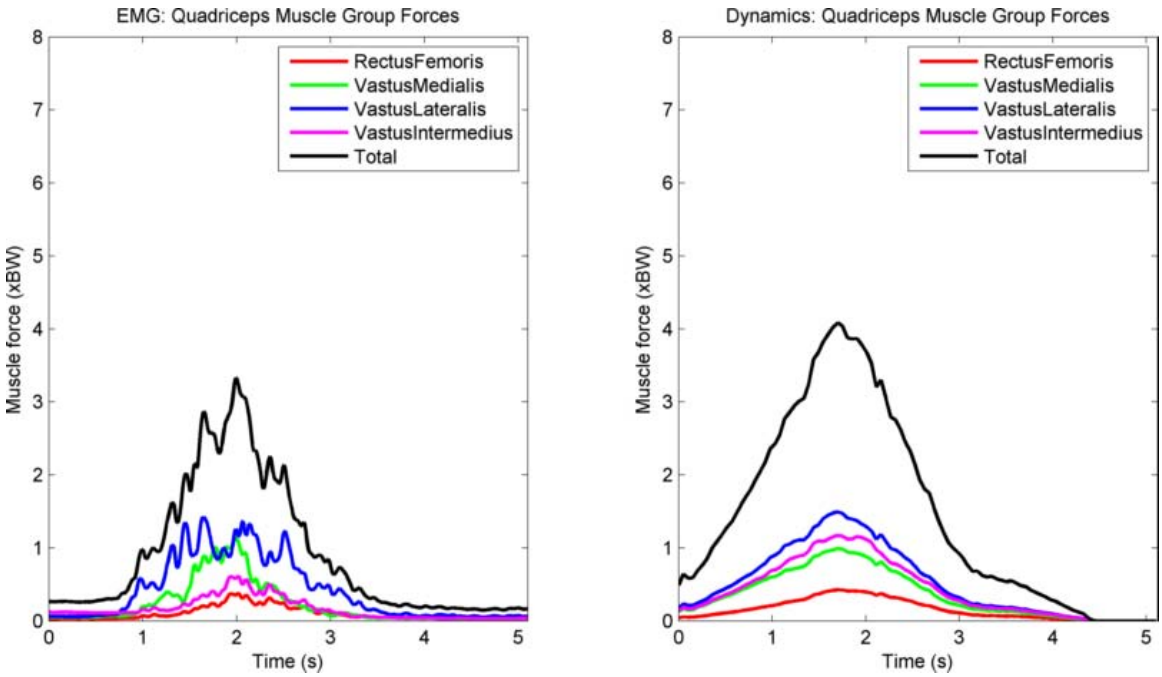


Figure A.129: Patient 22T quadriceps muscle group forces calculated from the EMG signals (left) and from the inverse dynamics (right) normalized by patient's body weight (BW).

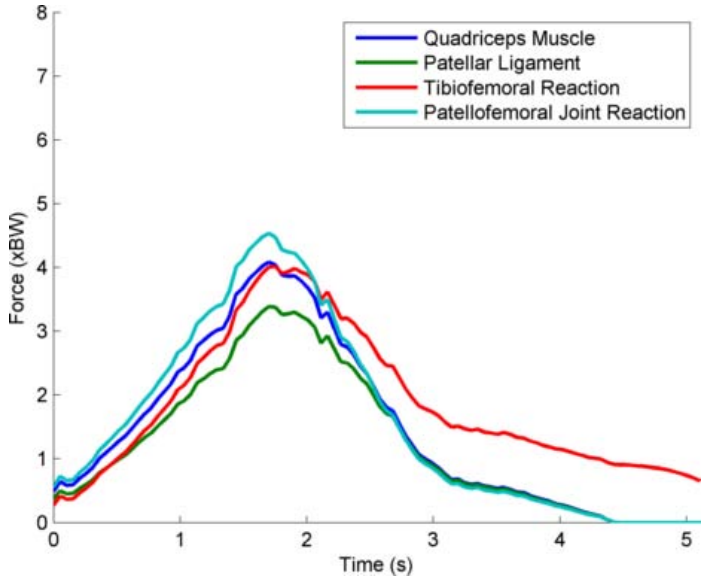


Figure A.130: Patient 22T total knee joint reaction forces incuding the action of the muscles, as well as the forces in the patellofemoral ligament, collateral and cruciate ligaments (if present) normalized by patient's body weight (BW).

A.14 Patient 22N

Patient demographic details:

ID# 22N

age: 75 yrs

height: 1.65 m

mass: 74 kg

leg side: Left

condition: Healthy

A.14.1 Kinematics analysis results

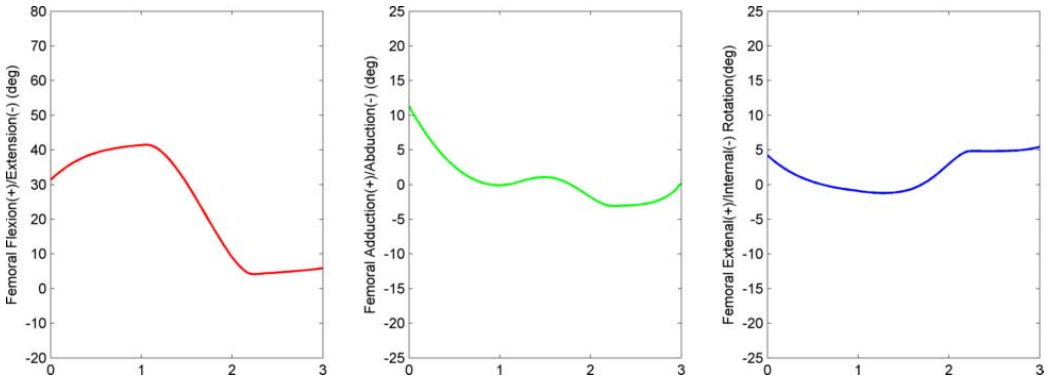


Figure A.131: Patient 22N patellofemoral joint kinematics.

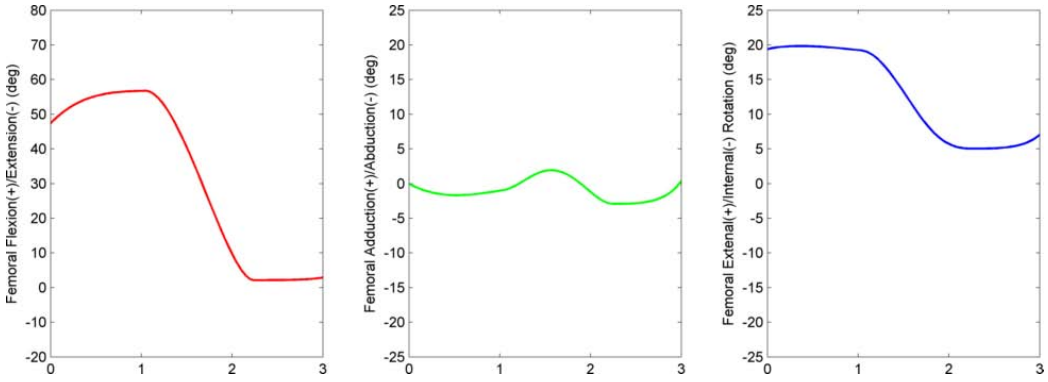


Figure A.132: Patient 22N tibiofemoral joint kinematics.

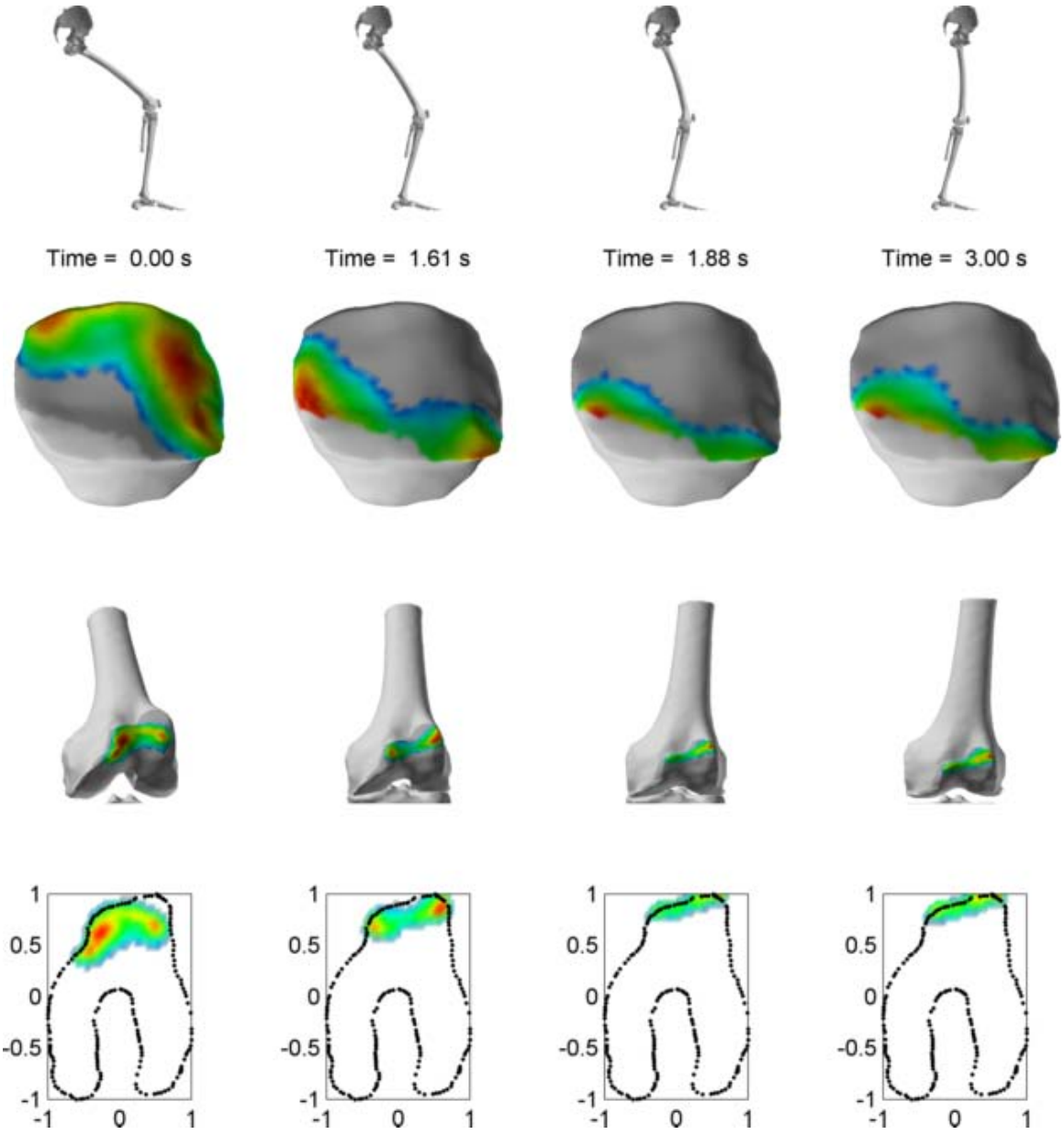


Figure A.133: Patient 22N dynamics model (top), patellofemoral contact location mapped on the patient's specific patella (2^{nd} from top) and femur (2^{nd} from bottom) bone models, as well as the normalized contact location mapped on the unfolded femoral trochlea surface (bottom).

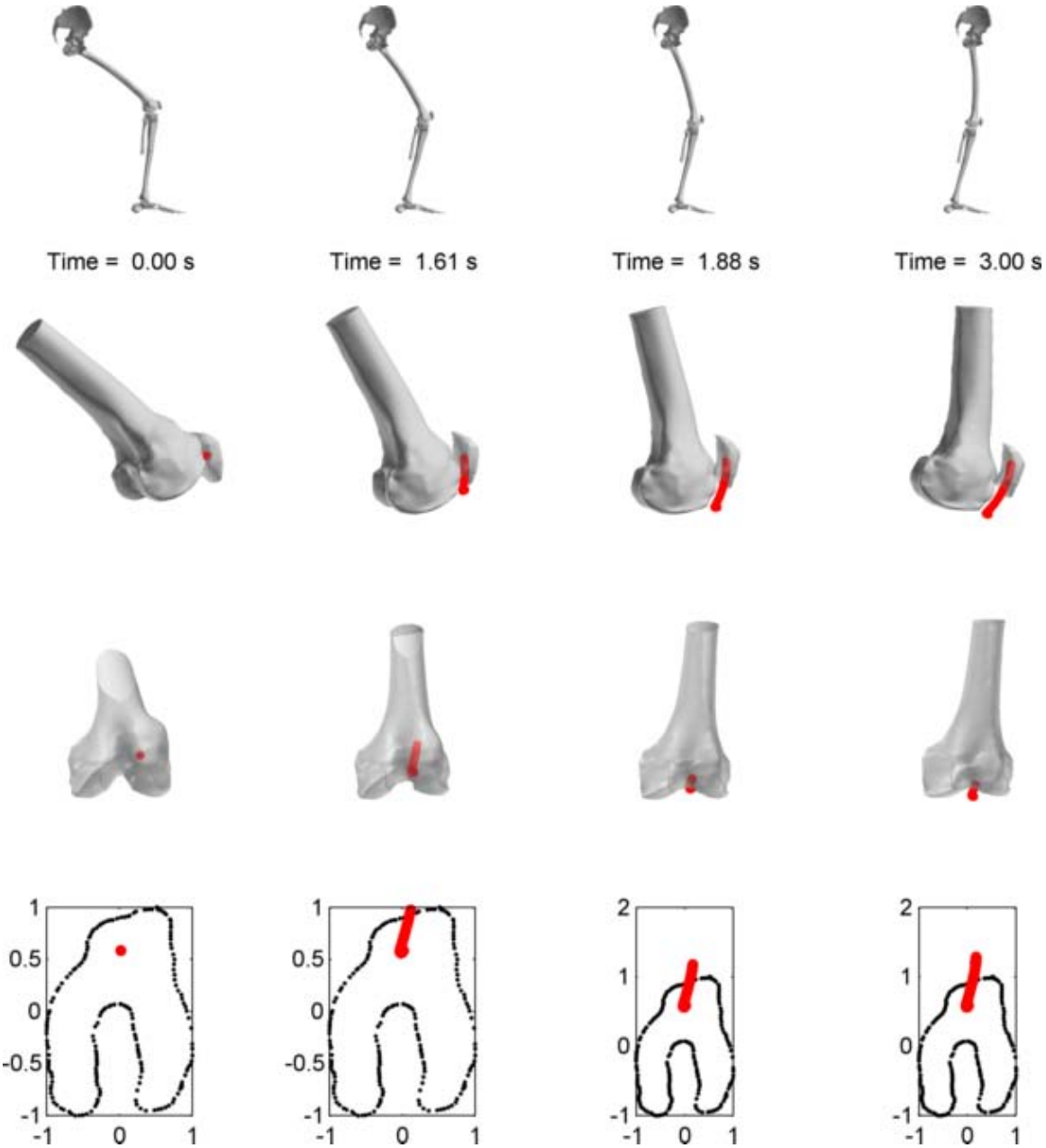


Figure A.134: Patient 22N dynamics model (top), patella center tracking in the sagittal (2^{nd} from top) and coronal (2^{nd} from bottom) planes, as well as the normalized patella tracking mapped on the unfolded femoral trochlea surface (bottom).

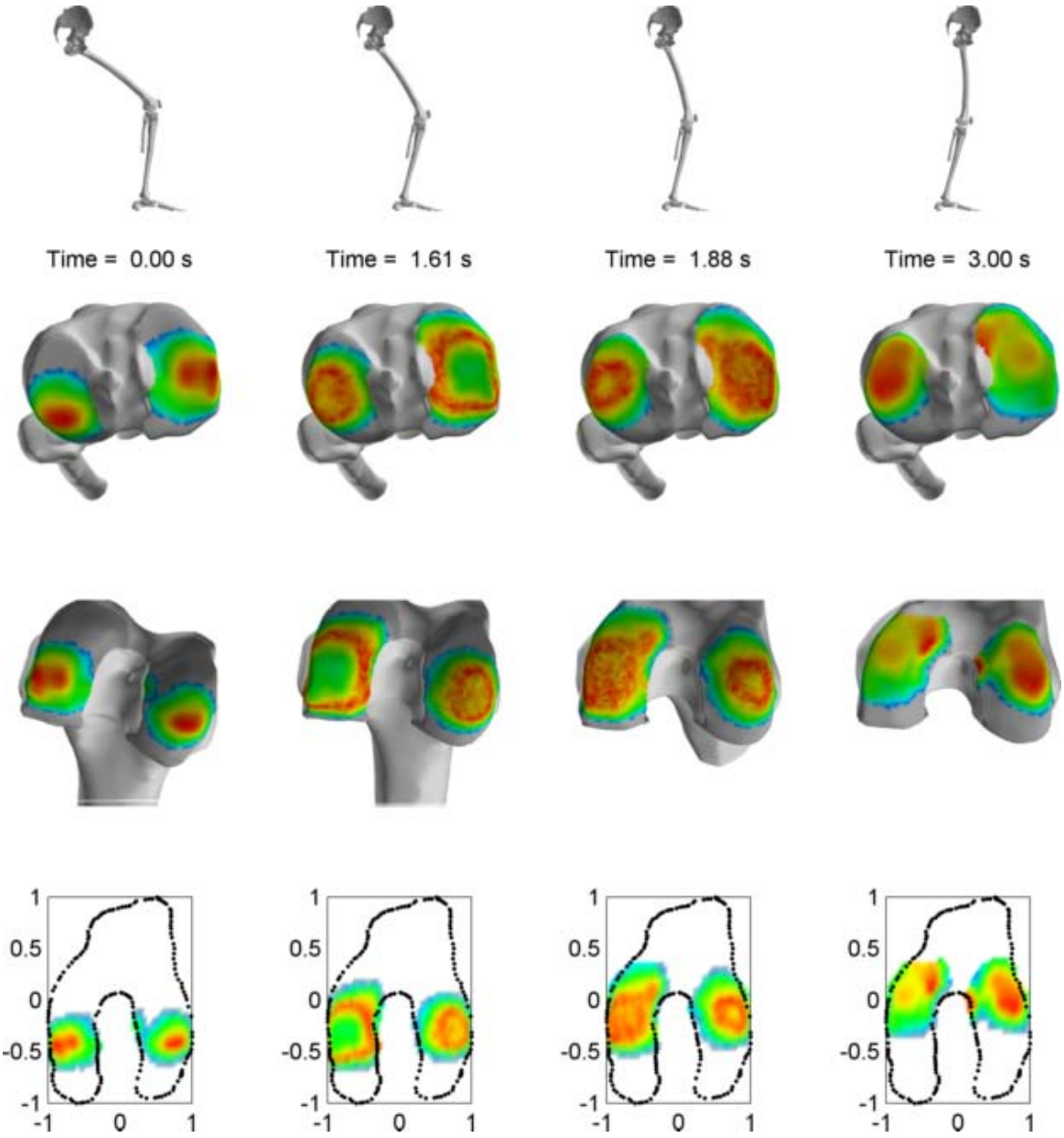


Figure A.135: Patient 22N dynamics model (top), tibiofemoral contact location mapped on the patient's specific patella (2^{nd} from top) and femur (2^{nd} from bottom) bone models, as well as the normalized contact location mapped on the unfolded femoral trochlea surface (bottom).

A.14.2 Electromyography and Inverse Dynamics analyses results

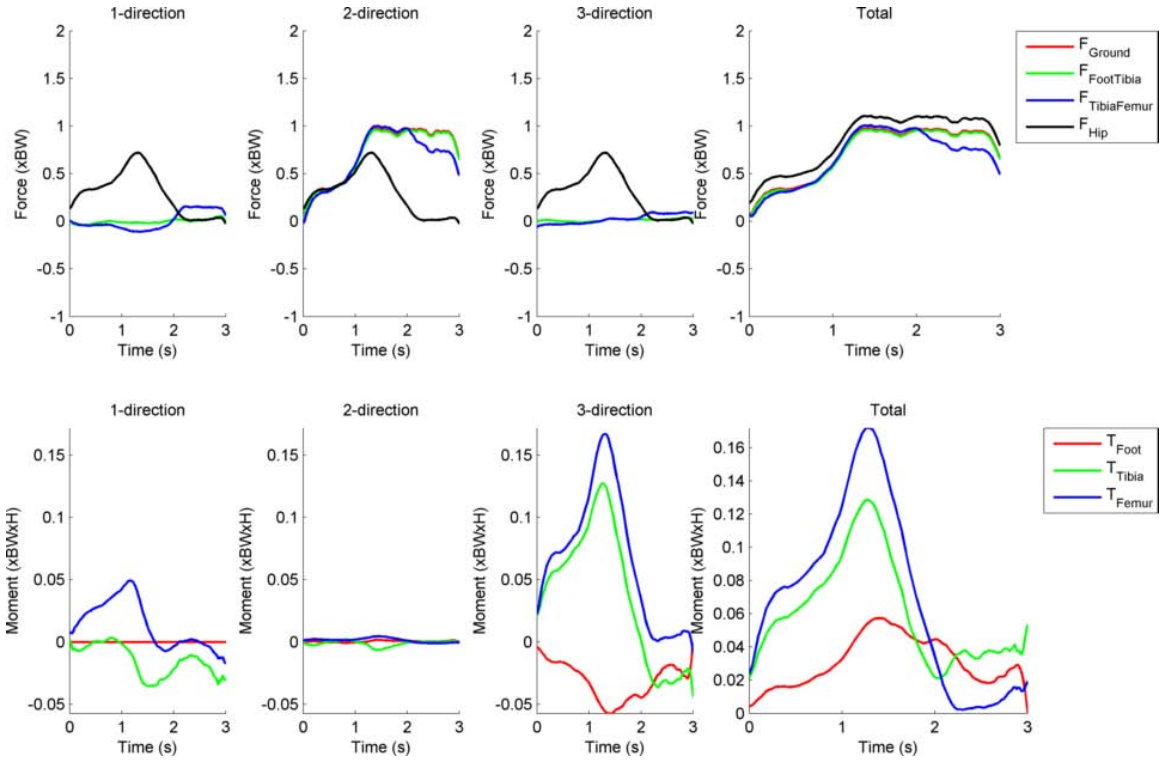


Figure A.136: Patient 22N knee joint reaction forces (top) and moments (bottom) normalized with respect to patient's body weight (BW). 1-direction = Anterior(+)/Posterior(-), 2-direction = Superior(+)/Inferior(-), 3-direction = Medial(+)/Lateral(-).

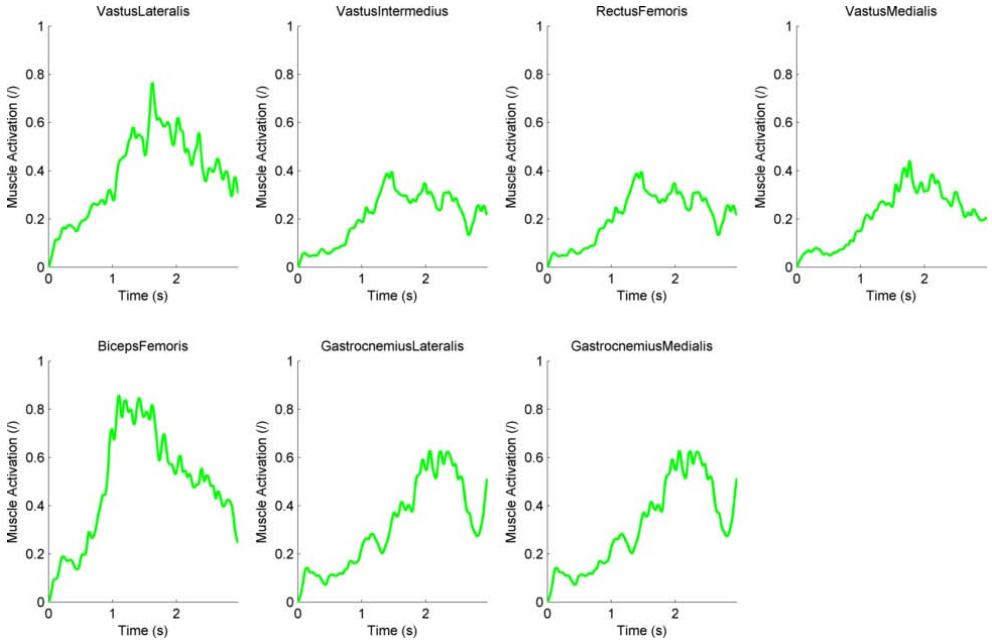


Figure A.137: Patient 22N muscle activation values obtained using the muscle activation dynamics[256].

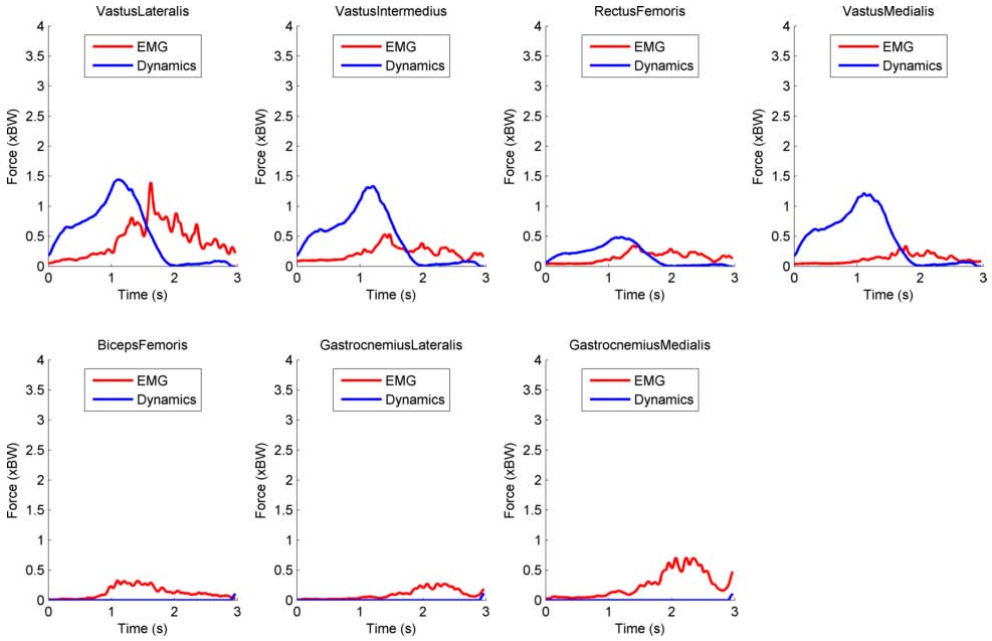


Figure A.138: Patient 22N muscle forces obtained using the EMG signal analysis (red) and pseudoinverse dynamics approach (green) normalized by patient's body weight (BW).

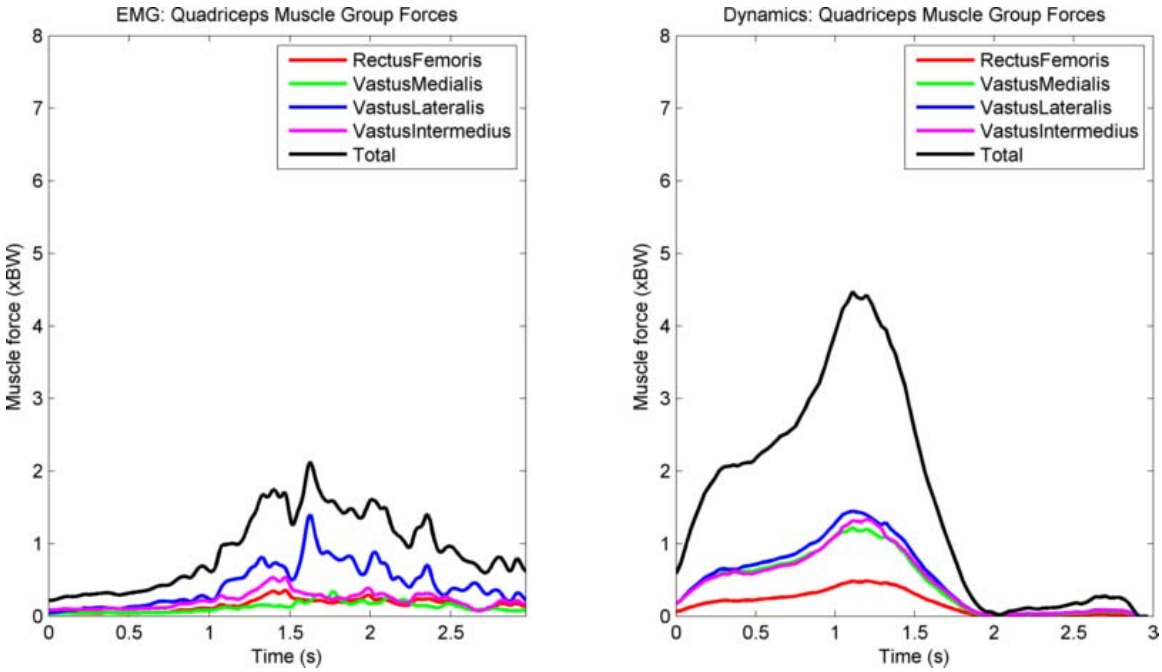


Figure A.139: Patient 22N quadriceps muscle group forces calculated from the EMG signals (left) and from the inverse dynamics (right) normalized by patient's body weight (BW).

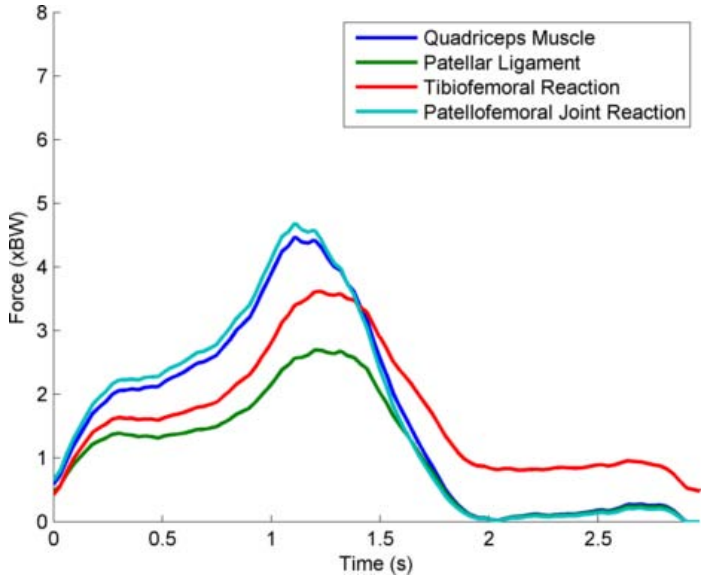


Figure A.140: Patient 22N total knee joint reaction forces incuding the action of the muscles, as well as the forces in the patellofemoral ligament, collateral and cruciate ligaments (if present) normalized by patient's body weight (BW).

A.15 Patient 23T

Patient demographic details:

ID# 23T

age: 70 yrs

height: 1.5 m

mass: 74 kg

leg side: Right

condition: TKA

A.15.1 Kinematics analysis results

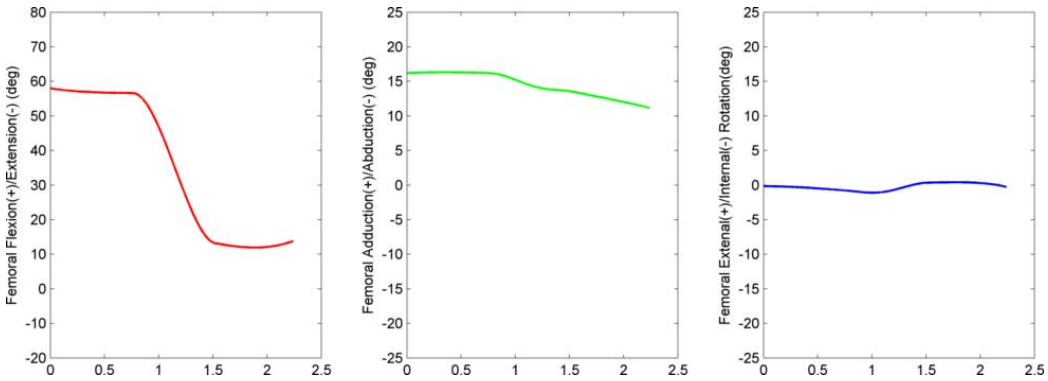


Figure A.141: Patient 23T patellofemoral joint kinematics.

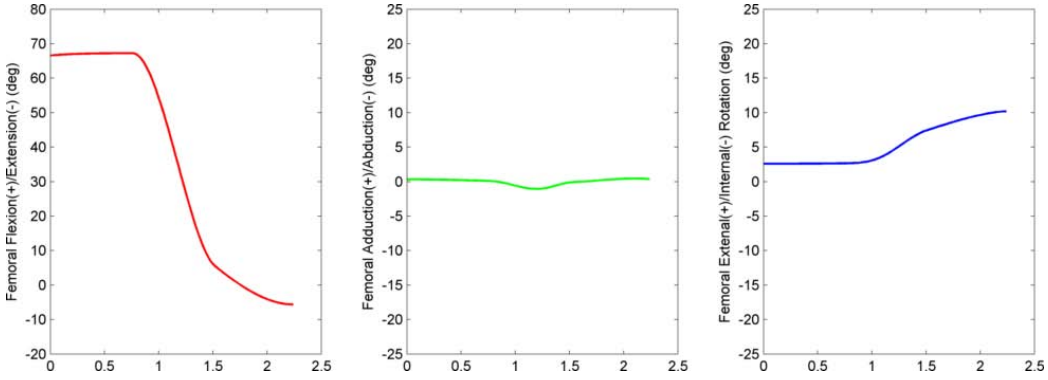


Figure A.142: Patient 23T tibiofemoral joint kinematics.

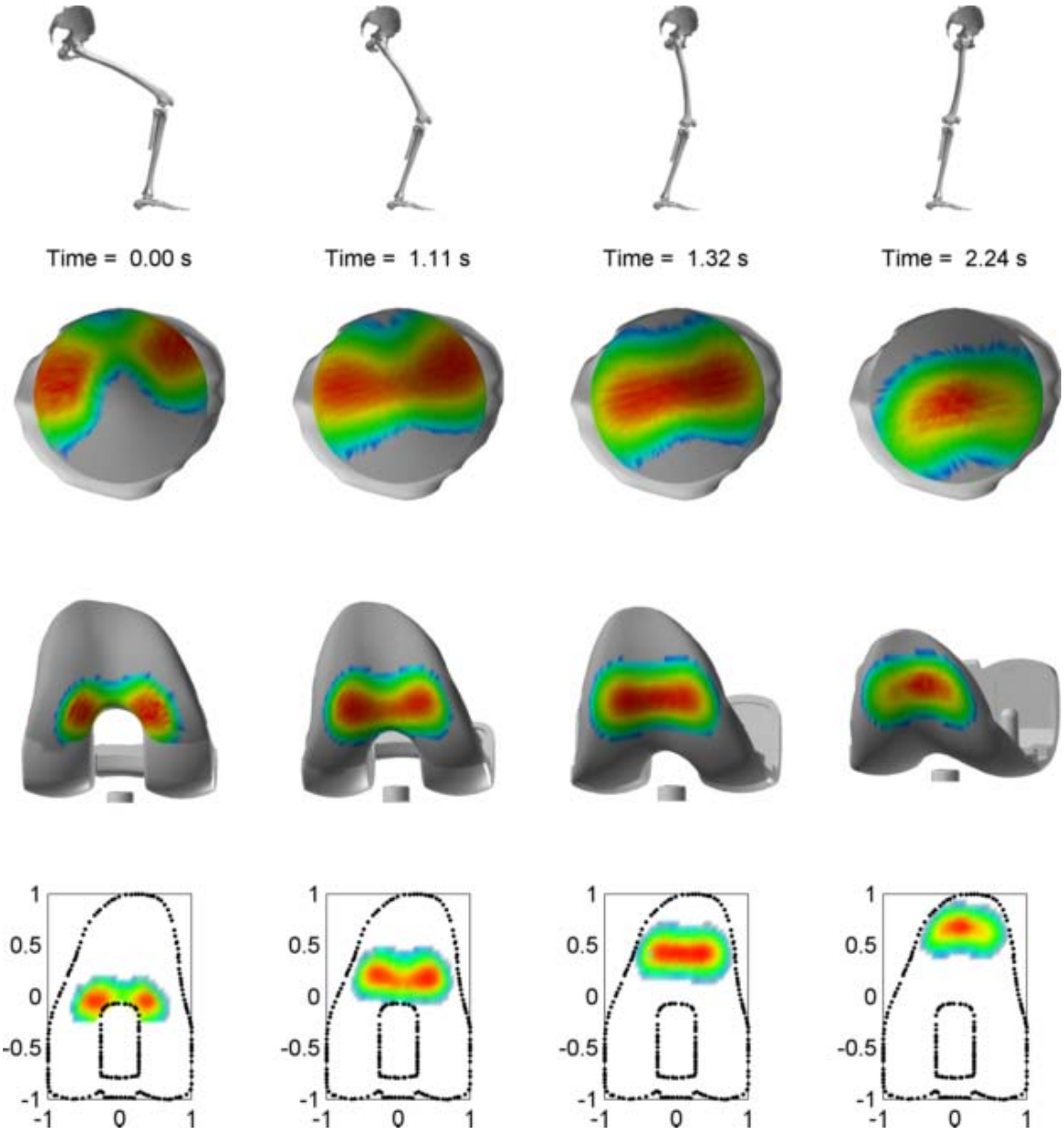


Figure A.143: Patient 23T dynamics model (top), patellofemoral contact location mapped on the patient's specific patella (2^{nd} from top) and femur (2^{nd} from bottom) bone models, as well as the normalized contact location mapped on the unfolded femoral trochlea surface (bottom).

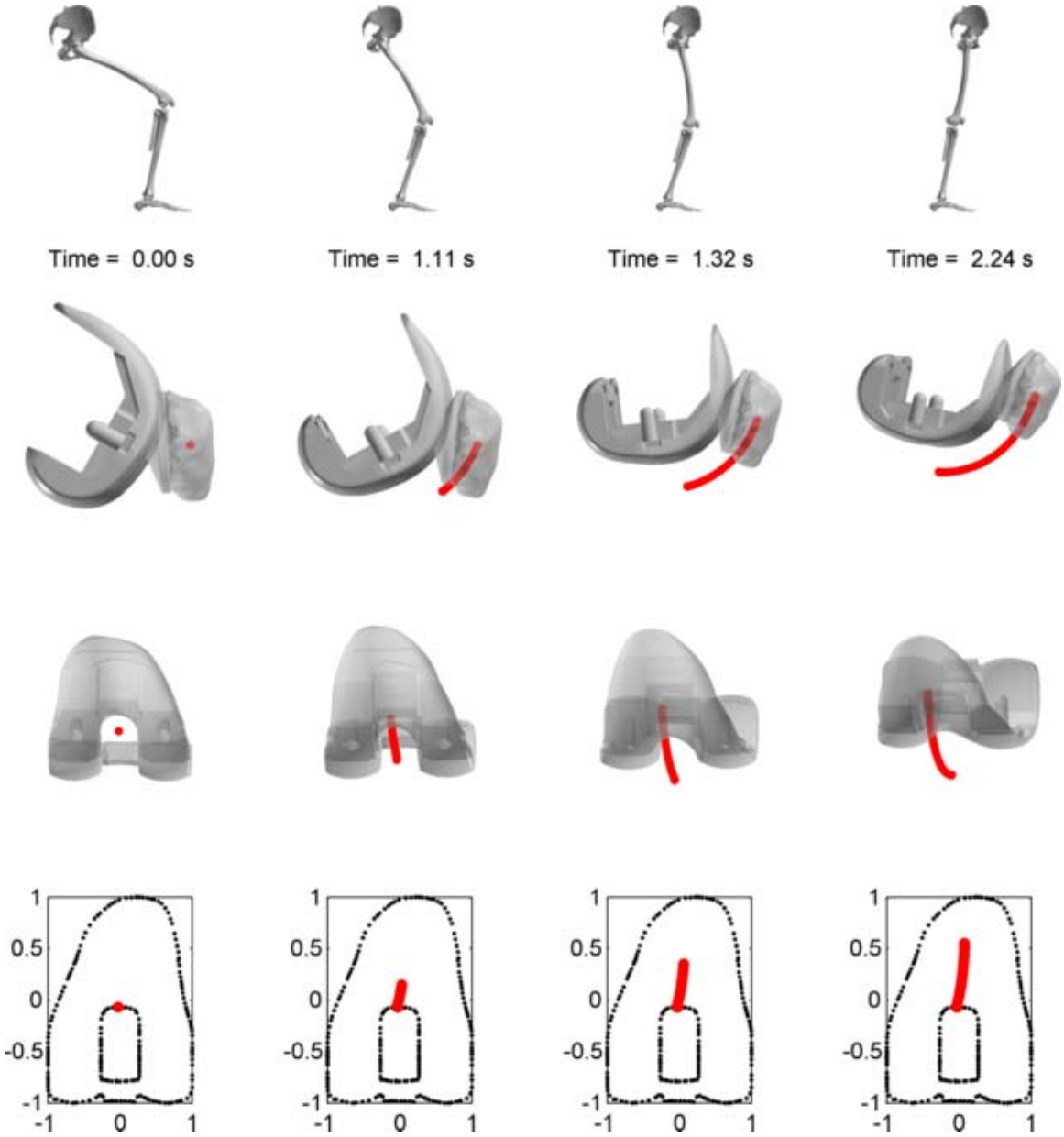


Figure A.144: Patient 23T dynamics model (top), patella center tracking in the sagittal (2^{nd} from top) and coronal (2^{nd} from bottom) planes, as well as the normalized patella tracking mapped on the unfolded femoral trochlea surface (bottom).

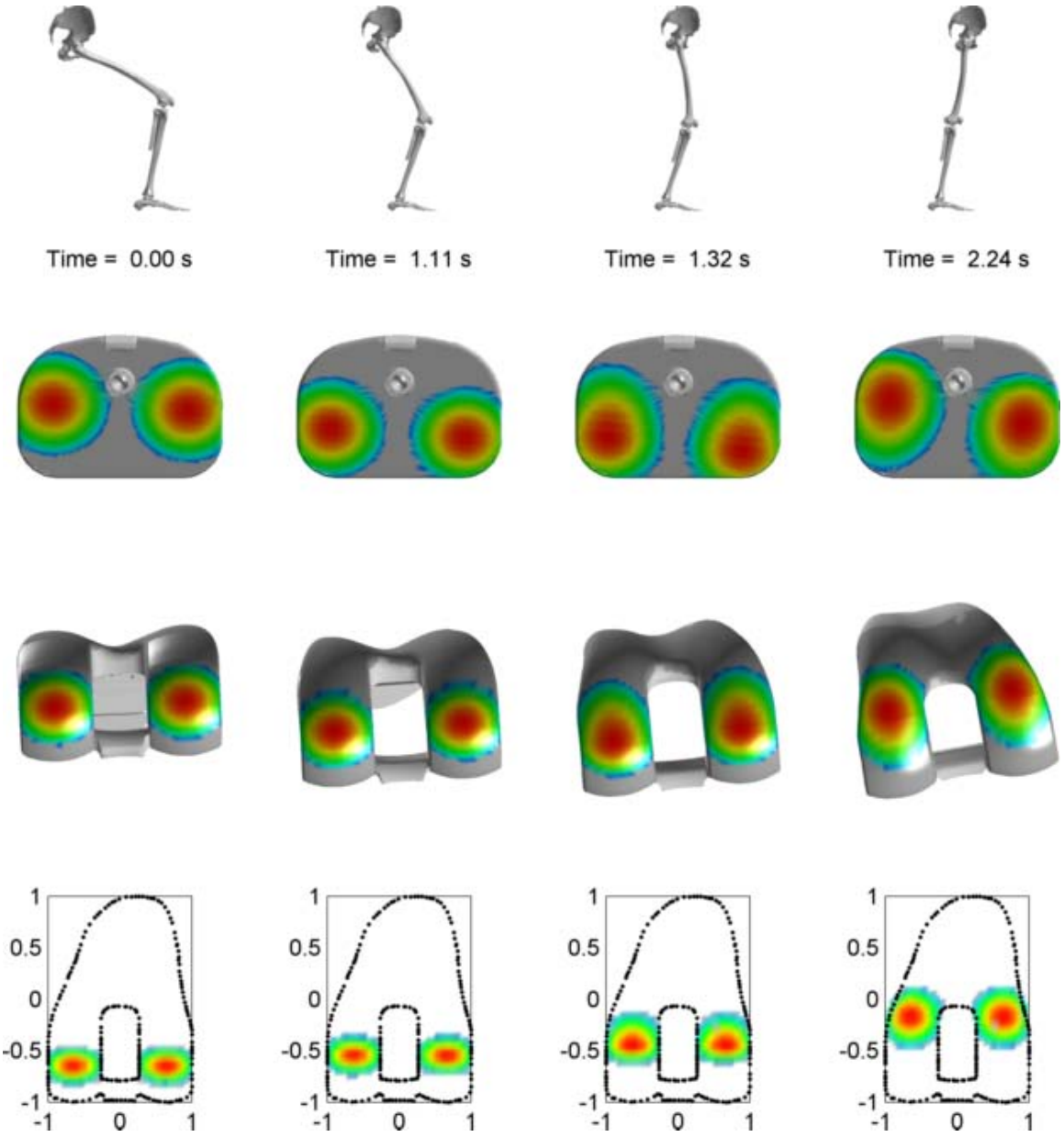


Figure A.145: Patient 23T dynamics model (top), tibiofemoral contact location mapped on the patient's specific patella (2^{nd} from top) and femur (2^{nd} from bottom) bone models, as well as the normalized contact location mapped on the unfolded femoral trochlea surface (bottom).

A.15.2 Electromyography and Inverse Dynamics analyses results

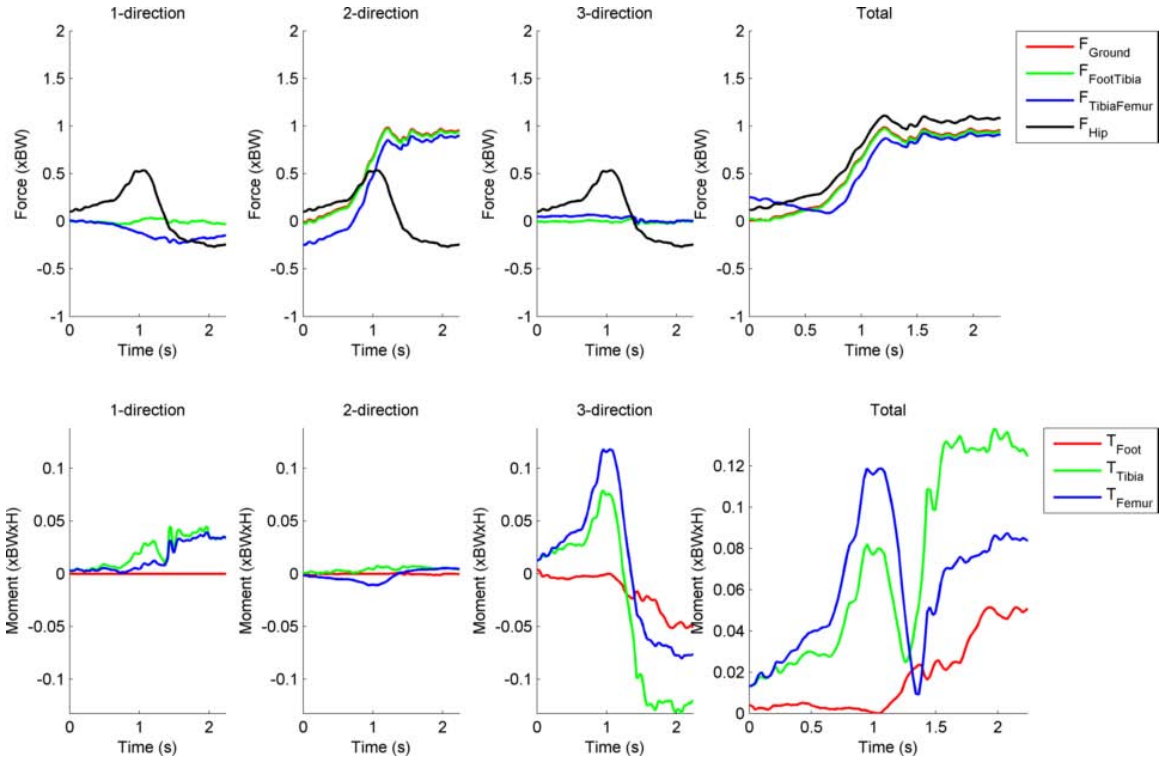


Figure A.146: Patient 23T knee joint reaction forces (top) and moments (bottom) normalized with respect to patient's body weight (BW). 1-direction = Anterior(+)/Posterior(-), 2-direction = Superior(+)/Inferior(-), 3-direction = Medial(+)/Lateral(-).

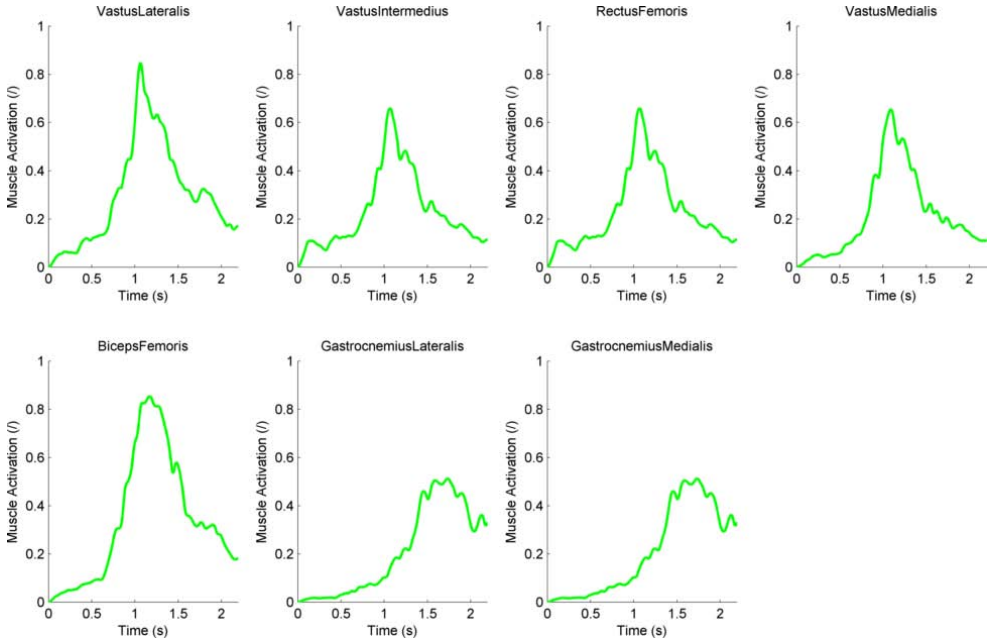


Figure A.147: Patient 23T muscle activation values obtained using the muscle activation dynamics[256].

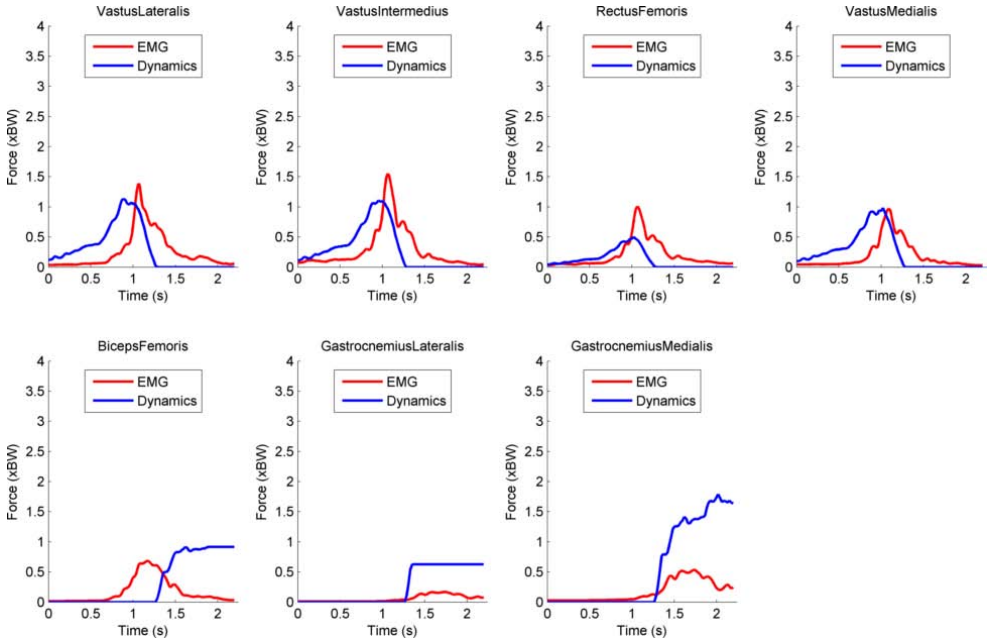


Figure A.148: Patient 23T muscle forces obtained using the EMG signal analysis (red) and pseudoinverse dynamics approach (green) normalized by patient's body weight (BW).

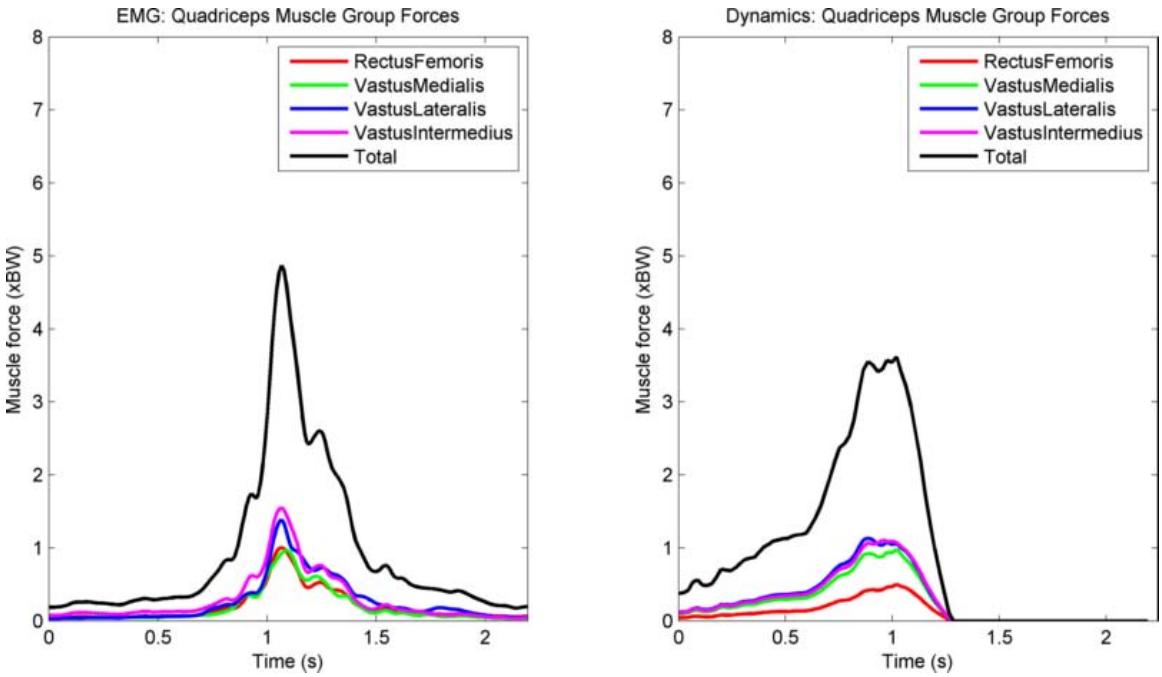


Figure A.149: Patient 23T quadriceps muscle group forces calculated from the EMG signals (left) and from the inverse dynamics (right) normalized by patient's body weight (BW).

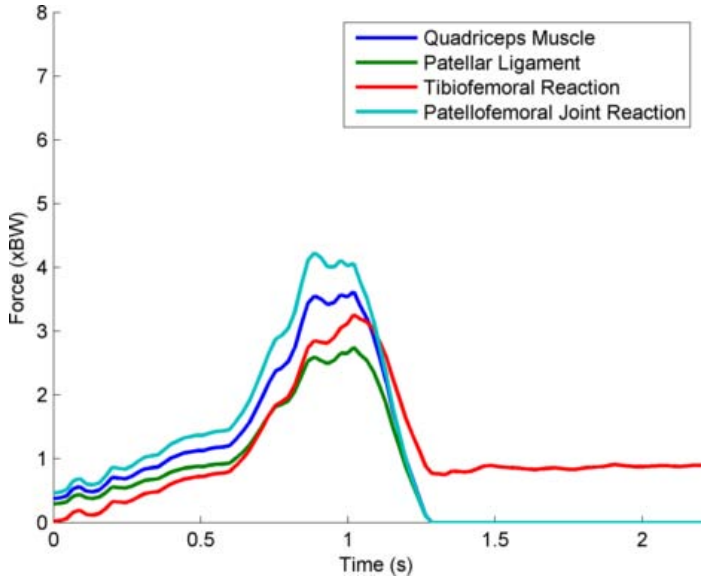


Figure A.150: Patient 23T total knee joint reaction forces incuding the action of the muscles, as well as the forces in the patellofemoral ligament, collateral and cruciate ligaments (if present) normalized by patient's body weight (BW).

A.16 Patient 23N

Patient demographic details:

ID# 23N

age: 70 yrs

height: 1.5 m

mass: 74 kg

leg side: Left

condition: Healthy

A.16.1 Kinematics analysis results

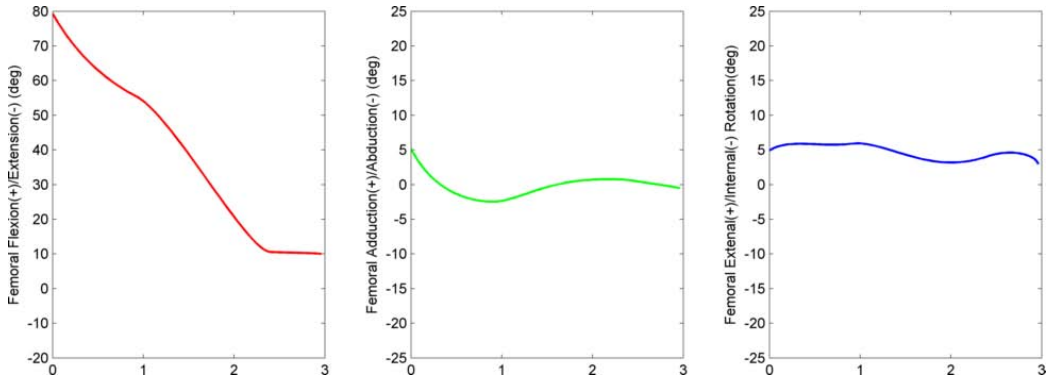


Figure A.151: Patient 23N patellofemoral joint kinematics.

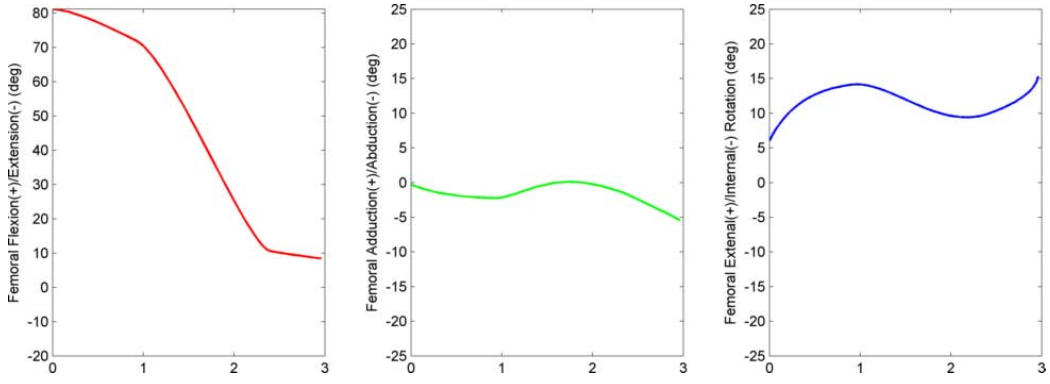


Figure A.152: Patient 23N tibiofemoral joint kinematics.

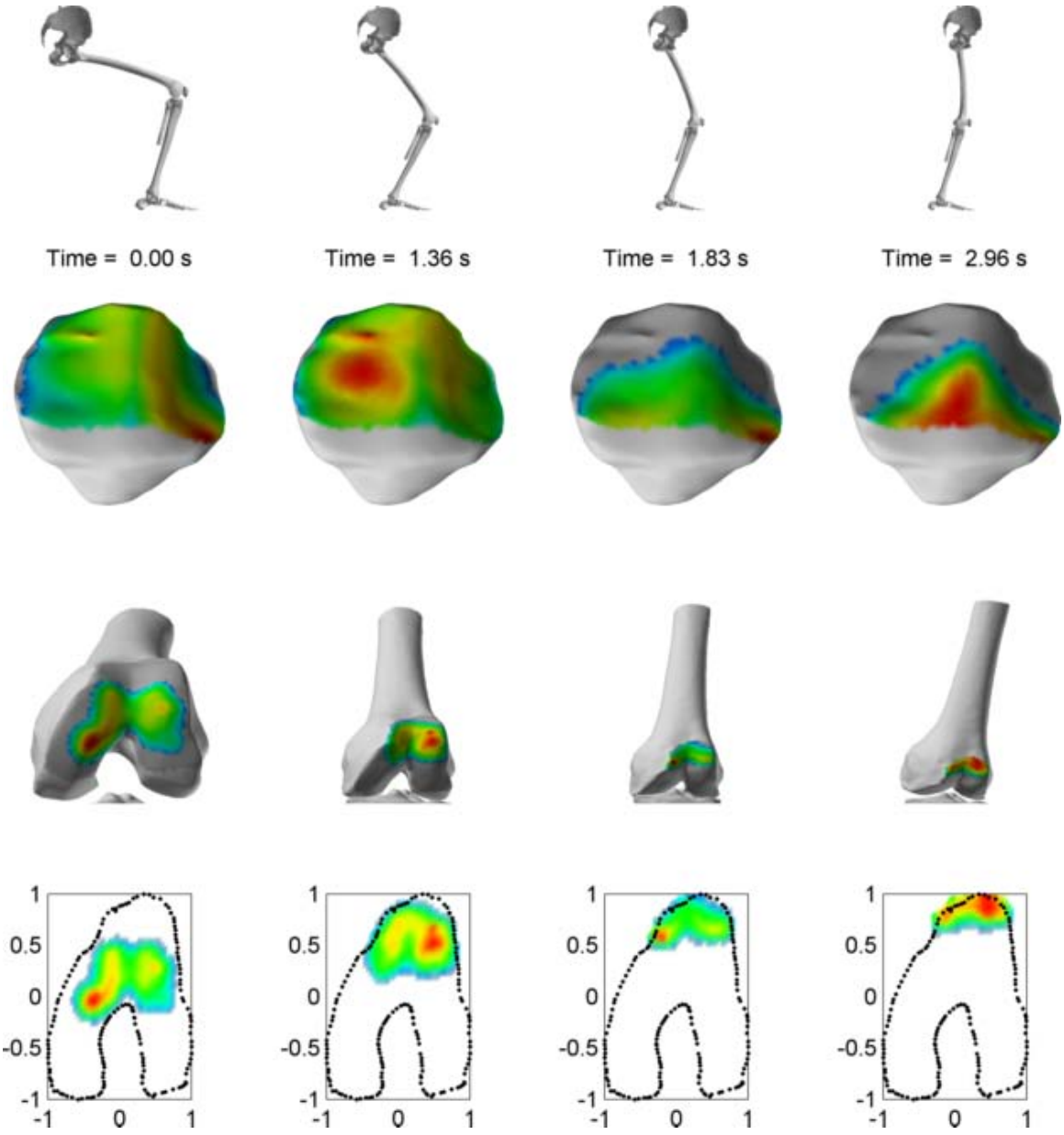


Figure A.153: Patient 23N dynamics model (top), patellofemoral contact location mapped on the patient's specific patella (2^{nd} from top) and femur (2^{nd} from bottom) bone models, as well as the normalized contact location mapped on the unfolded femoral trochlea surface (bottom).

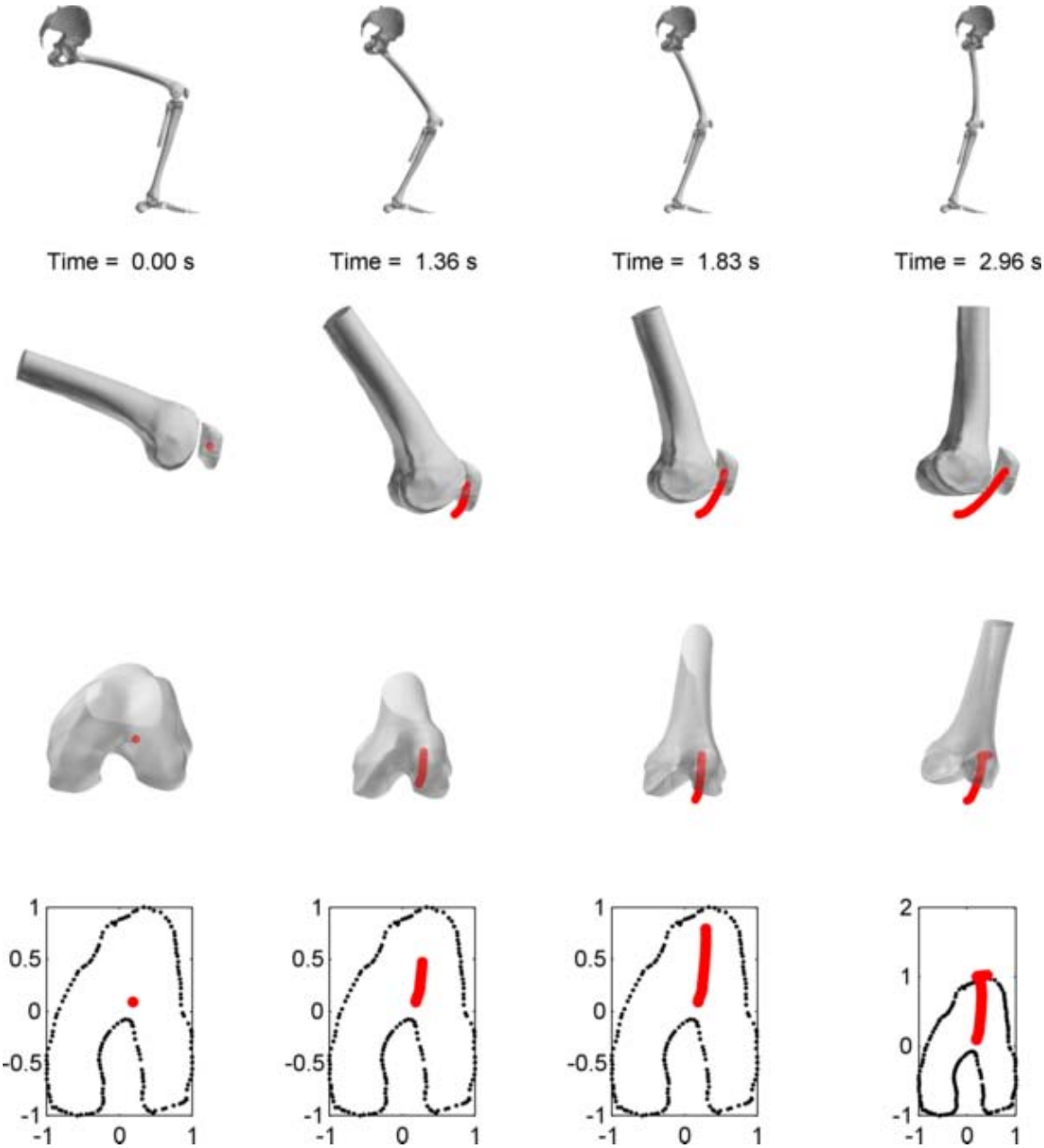


Figure A.154: Patient 23N dynamics model (top), patella center tracking in the sagittal (2^{nd} from top) and coronal (2^{nd} from bottom) planes, as well as the normalized patella tracking mapped on the unfolded femoral trochlea surface (bottom).

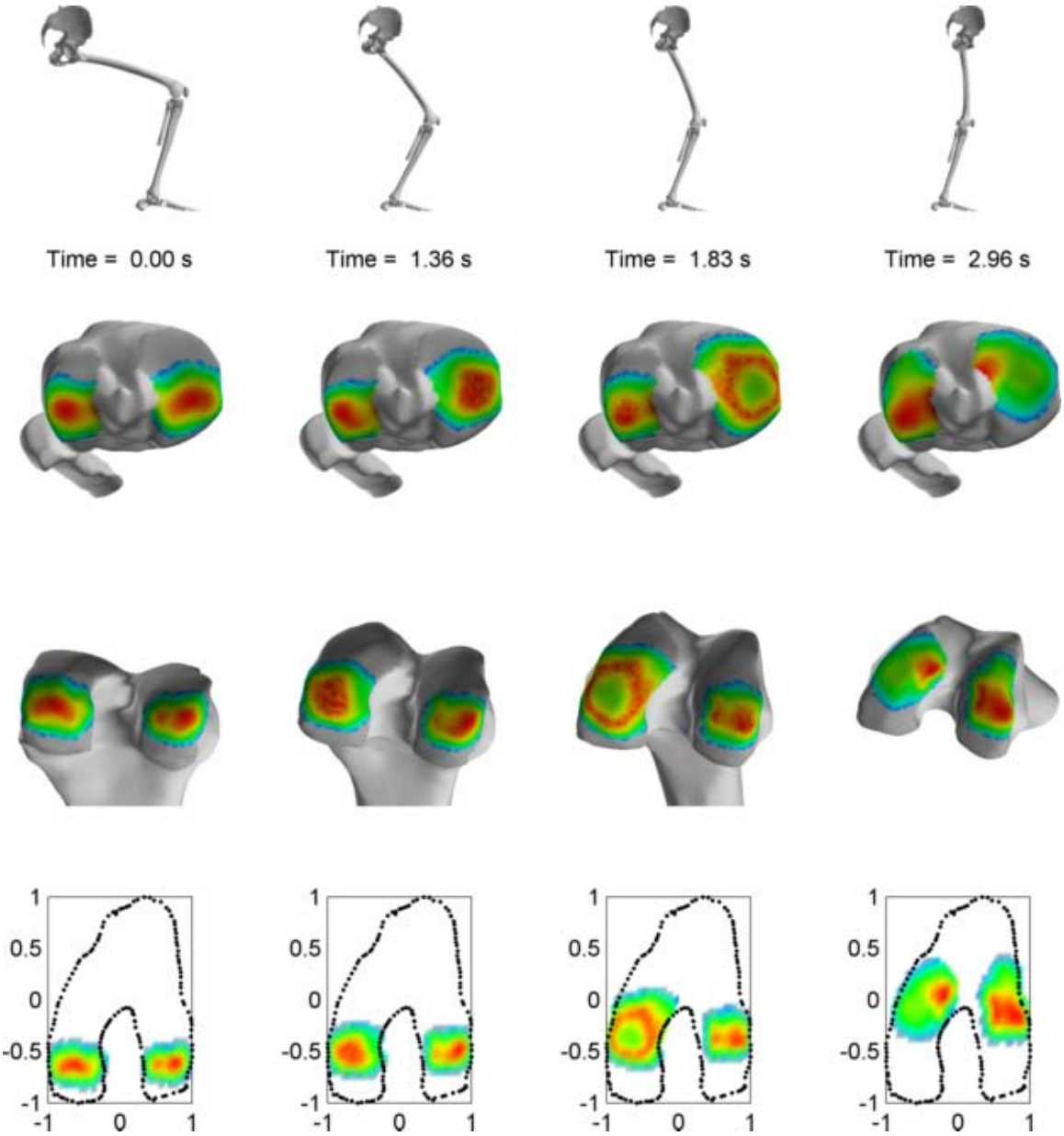


Figure A.155: Patient 23N dynamics model (top), tibiofemoral contact location mapped on the patient's specific patella (2^{nd} from top) and femur (2^{nd} from bottom) bone models, as well as the normalized contact location mapped on the unfolded femoral trochlea surface (bottom).

A.16.2 Electromyography and Inverse Dynamics analyses results

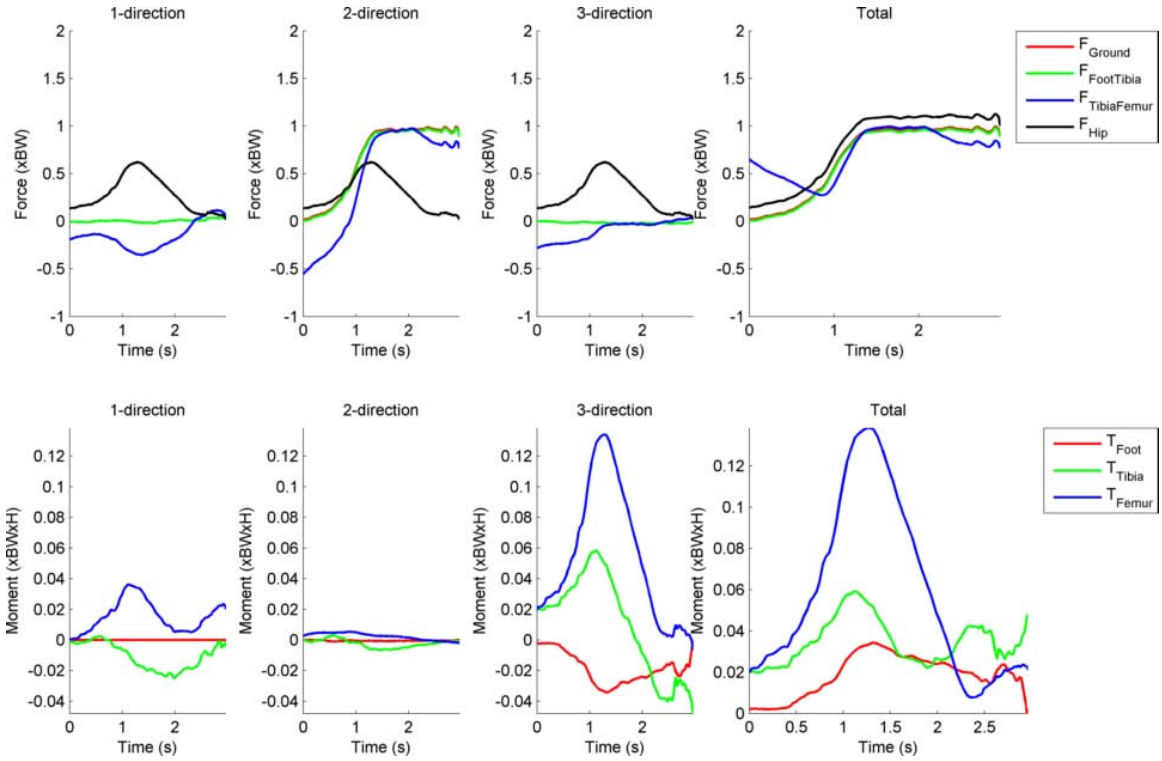


Figure A.156: Patient 23N knee joint reaction forces (top) and moments (bottom) normalized with respect to patient's body weight (BW). 1-direction = Anterior(+)/Posterior(-), 2-direction = Superior(+)/Inferior(-), 3-direction = Medial(+)/Lateral(-).

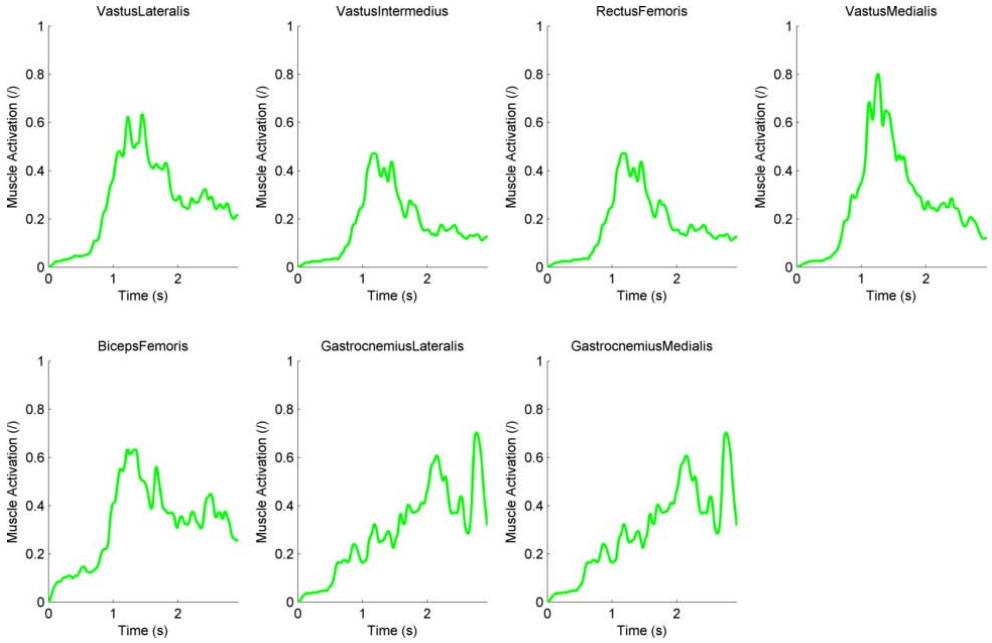


Figure A.157: Patient 23N muscle activation values obtained using the muscle activation dynamics[256].

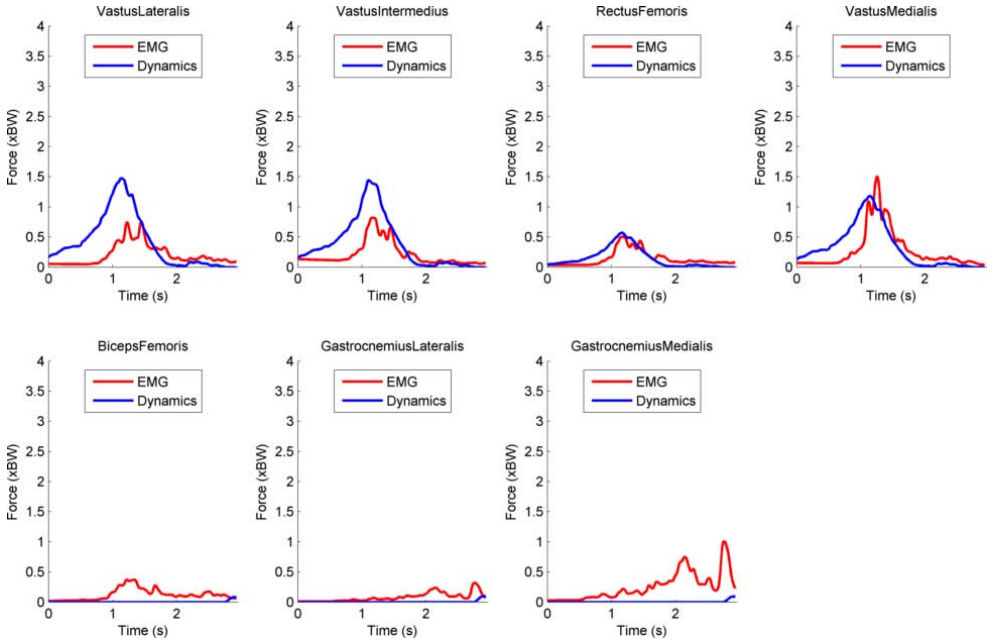


Figure A.158: Patient 23N muscle forces obtained using the EMG signal analysis (red) and pseudoinverse dynamics approach (green) normalized by patient's body weight (BW).

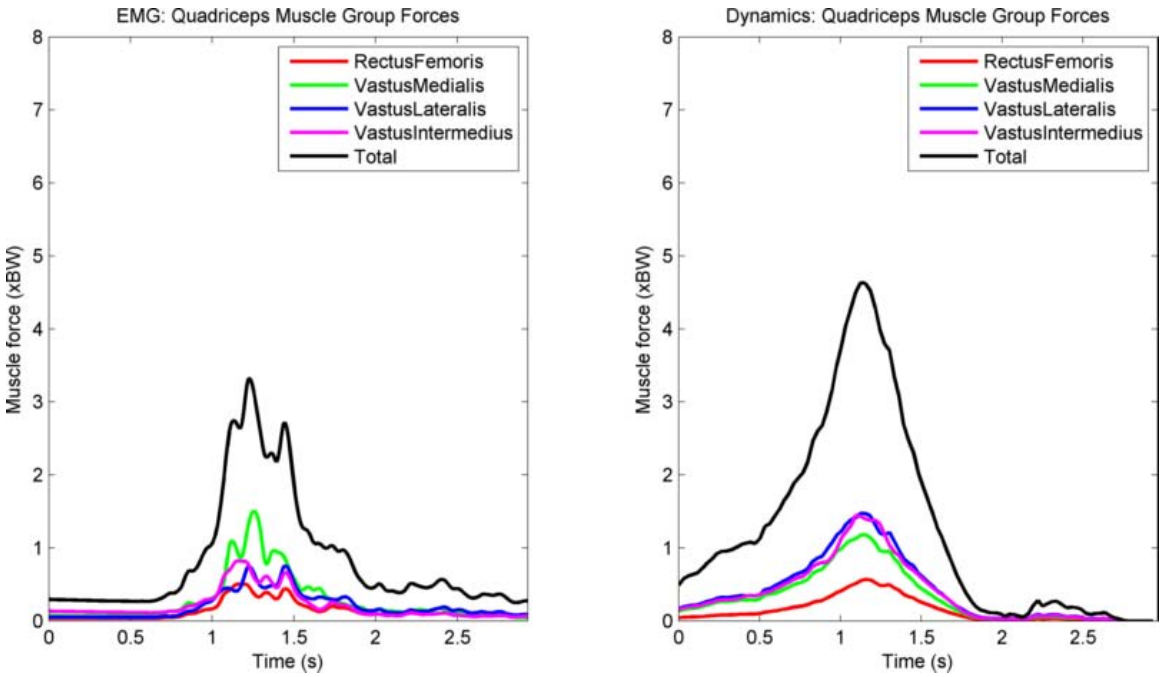


Figure A.159: Patient 23N quadriceps muscle group forces calculated from the EMG signals (left) and from the inverse dynamics (right) normalized by patient's body weight (BW).

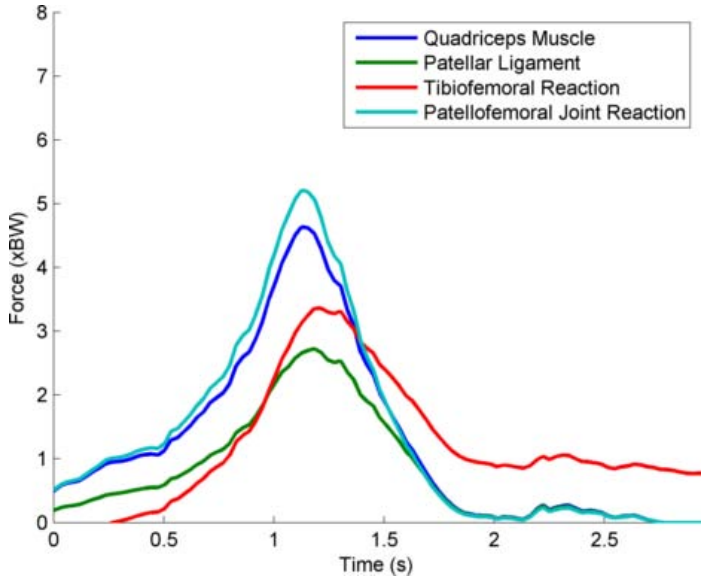


Figure A.160: Patient 23N total knee joint reaction forces incuding the action of the muscles, as well as the forces in the patellofemoral ligament, collateral and cruciate ligaments (if present) normalized by patient's body weight (BW).

A.17 Patient 6N

Patient demographic details:

ID# 6N

age: 30 yrs

height: 1.84 m

mass: 98 kg

leg side: Right

condition: Healthy

A.17.1 Kinematics analysis results

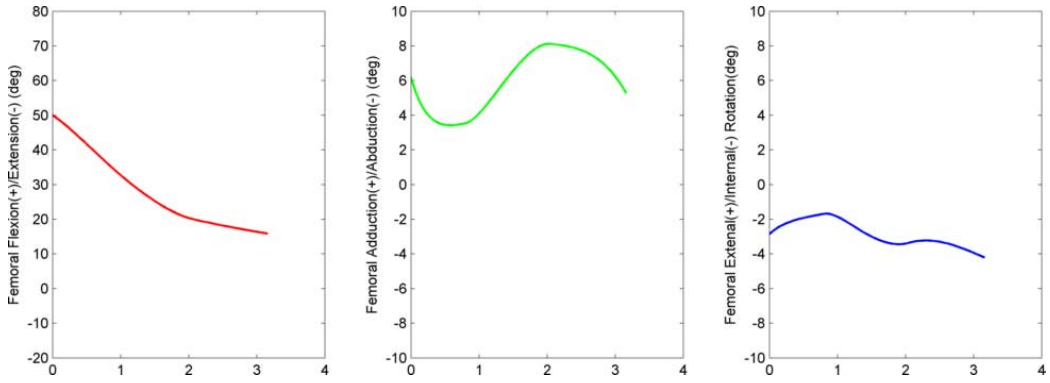


Figure A.161: Patient 6N patellofemoral joint kinematics.

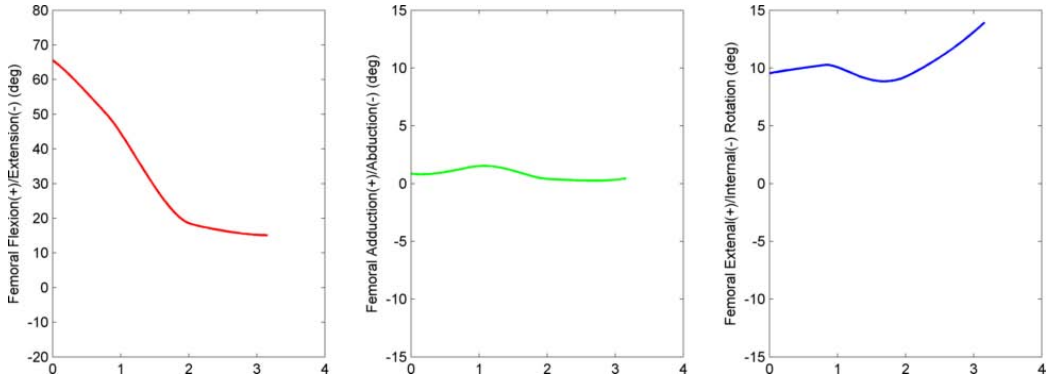


Figure A.162: Patient 6N tibiofemoral joint kinematics.

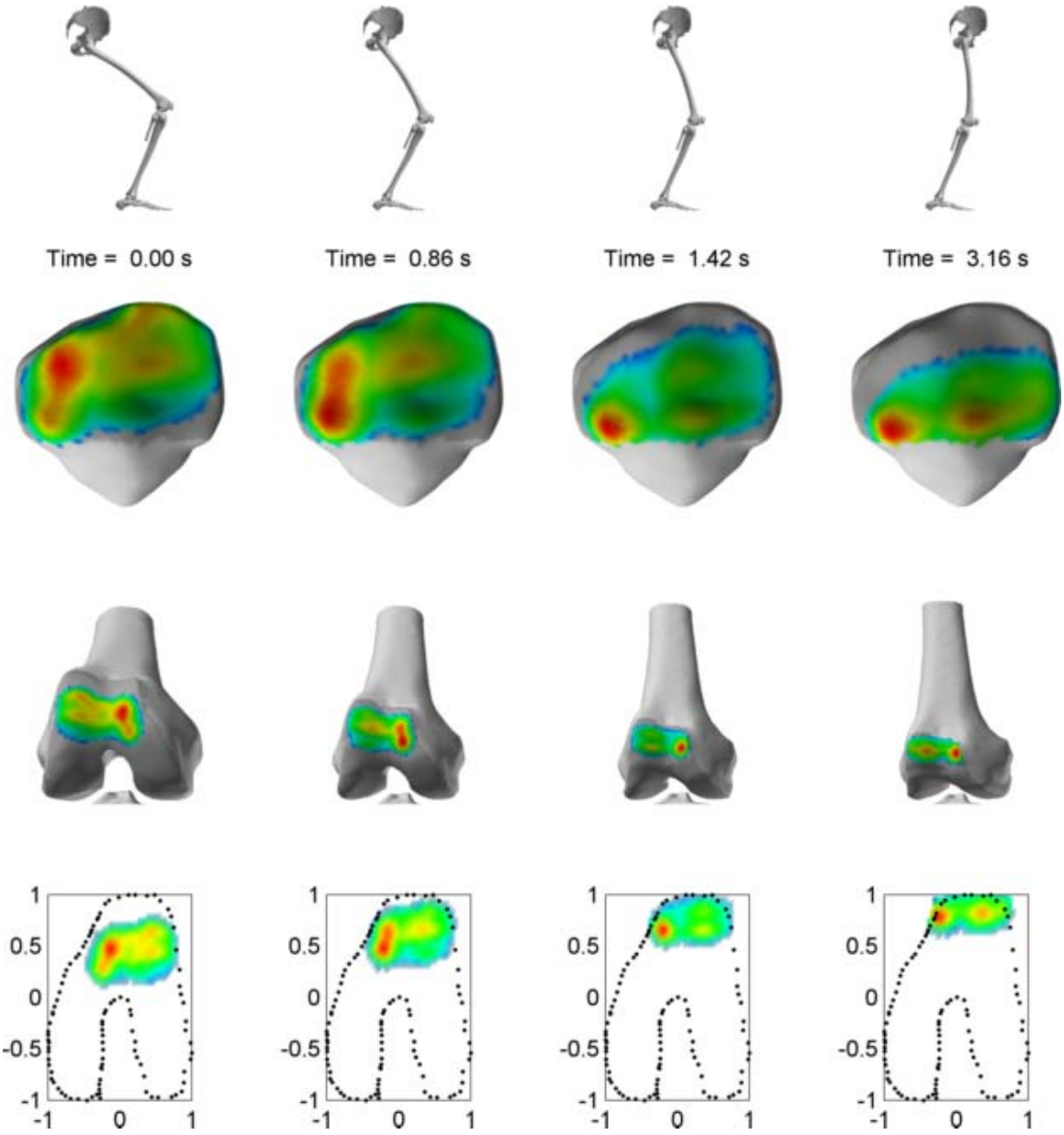


Figure A.163: Patient 6N dynamics model (top), patellofemoral contact location mapped on the patient's specific patella (2^{nd} from top) and femur (2^{nd} from bottom) bone models, as well as the normalized contact location mapped on the unfolded femoral trochlea surface (bottom).

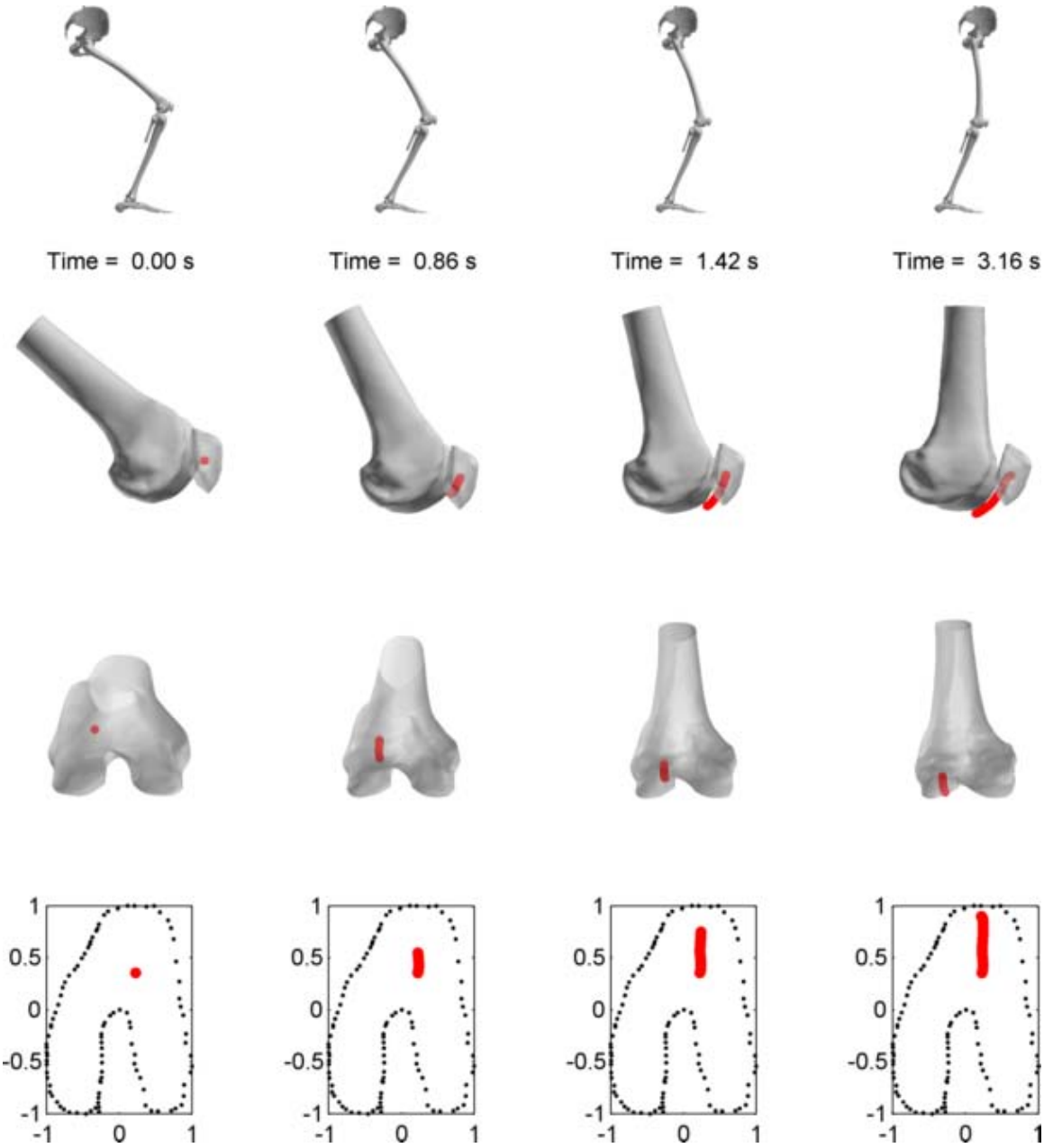


Figure A.164: Patient 6N dynamics model (top), patella center tracking in the sagittal (2^{nd} from top) and coronal (2^{nd} from bottom) planes, as well as the normalized patella tracking mapped on the unfolded femoral trochlea surface (bottom).

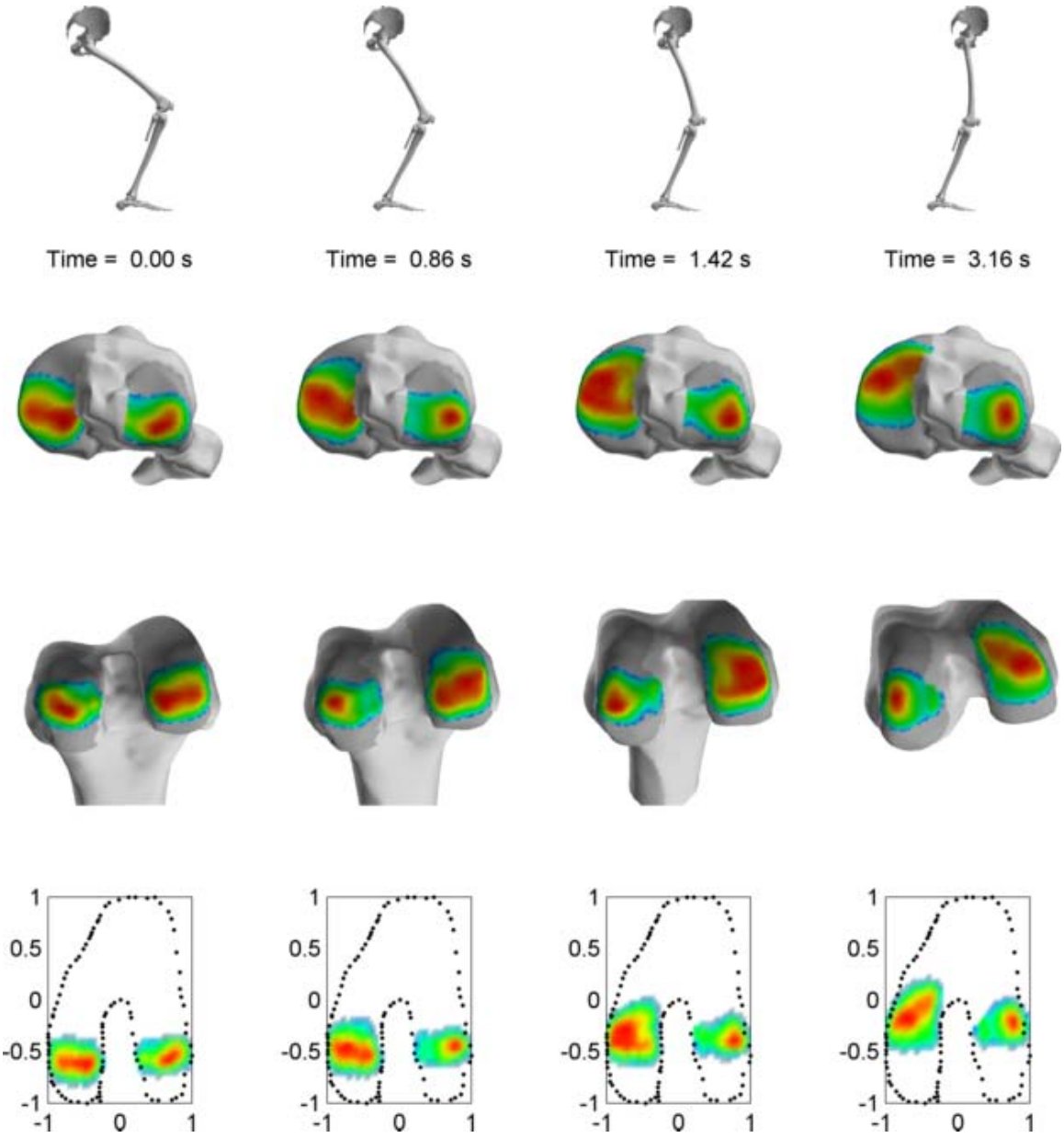


Figure A.165: Patient 6N dynamics model (top), tibiofemoral contact location mapped on the patient's specific patella (2^{nd} from top) and femur (2^{nd} from bottom) bone models, as well as the normalized contact location mapped on the unfolded femoral trochlea surface (bottom).

A.17.2 Electromyography and Inverse Dynamics analyses results

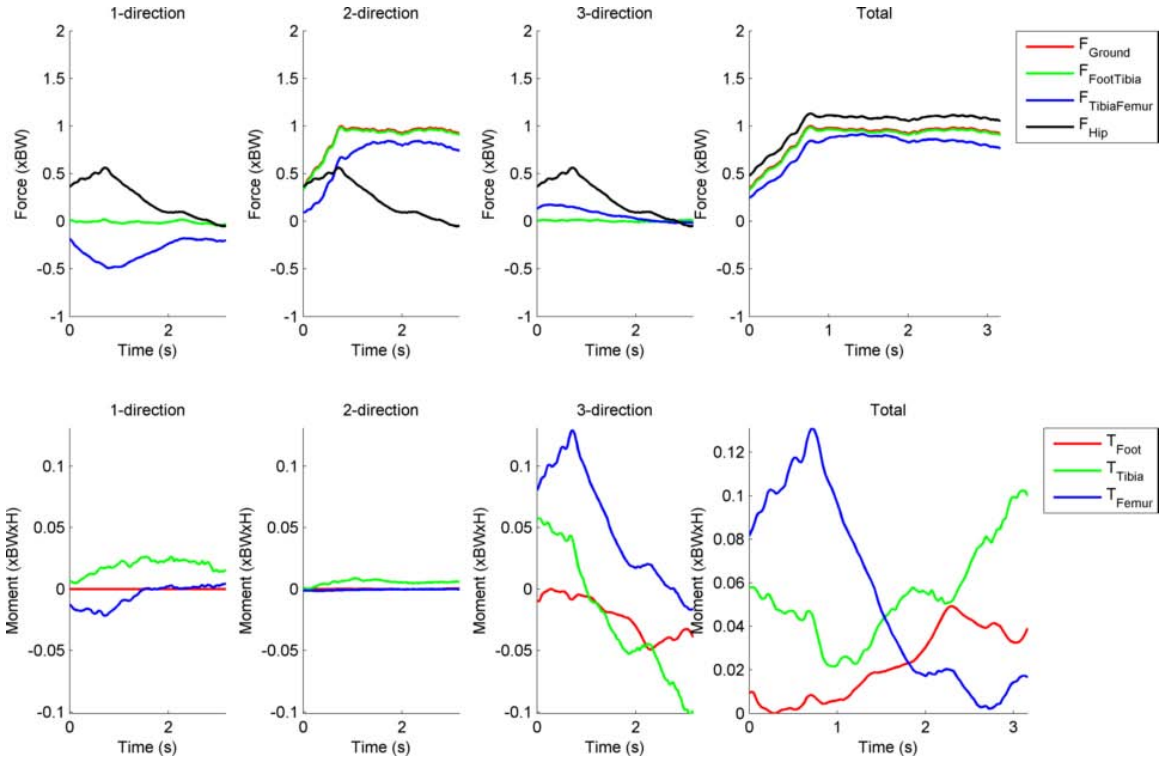


Figure A.166: Patient 6N knee joint reaction forces (top) and moments (bottom) normalized with respect to patient's body weight (BW). 1-direction = Anterior(+)/Posterior(-), 2-direction = Superior(+)/Inferior(-), 3-direction = Medial(+)/Lateral(-).

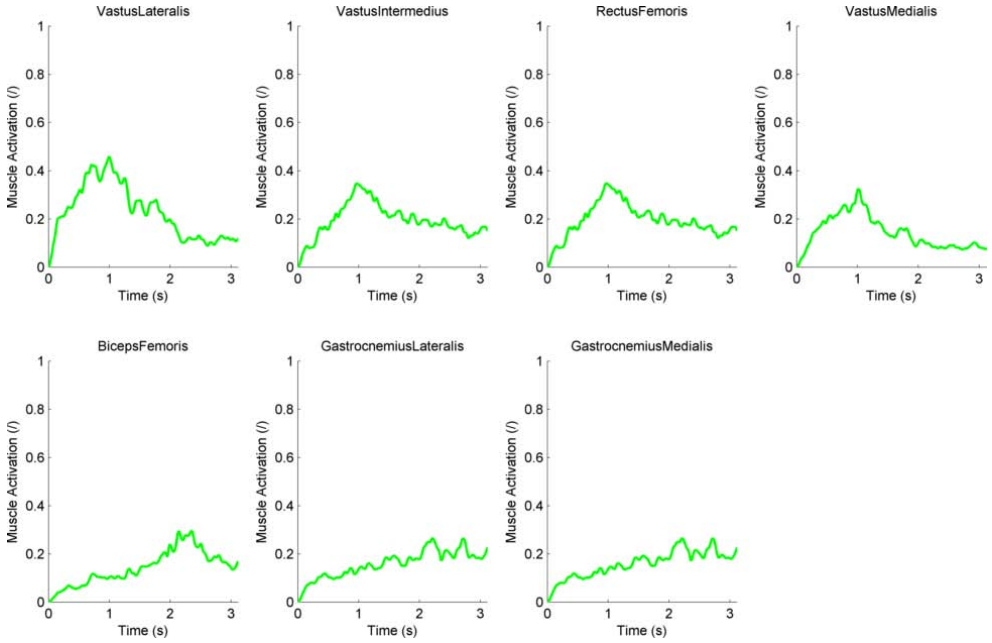


Figure A.167: Patient 6N muscle activation values obtained using the muscle activation dynamics[256].

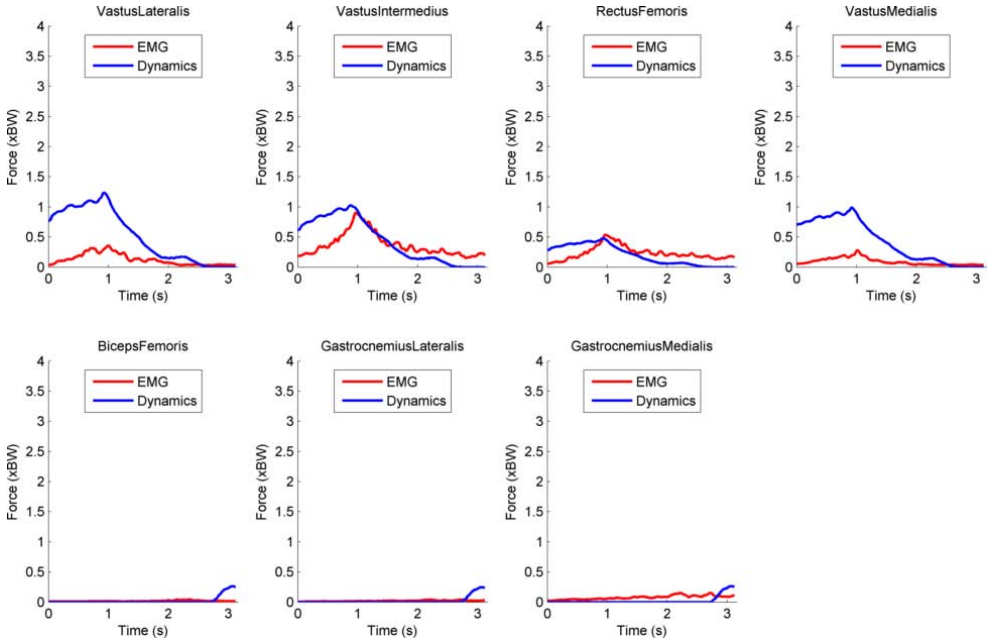


Figure A.168: Patient 6N muscle forces obtained using the EMG signal analysis (red) and pseudoinverse dynamics approach (green) normalized by patient's body weight (BW).

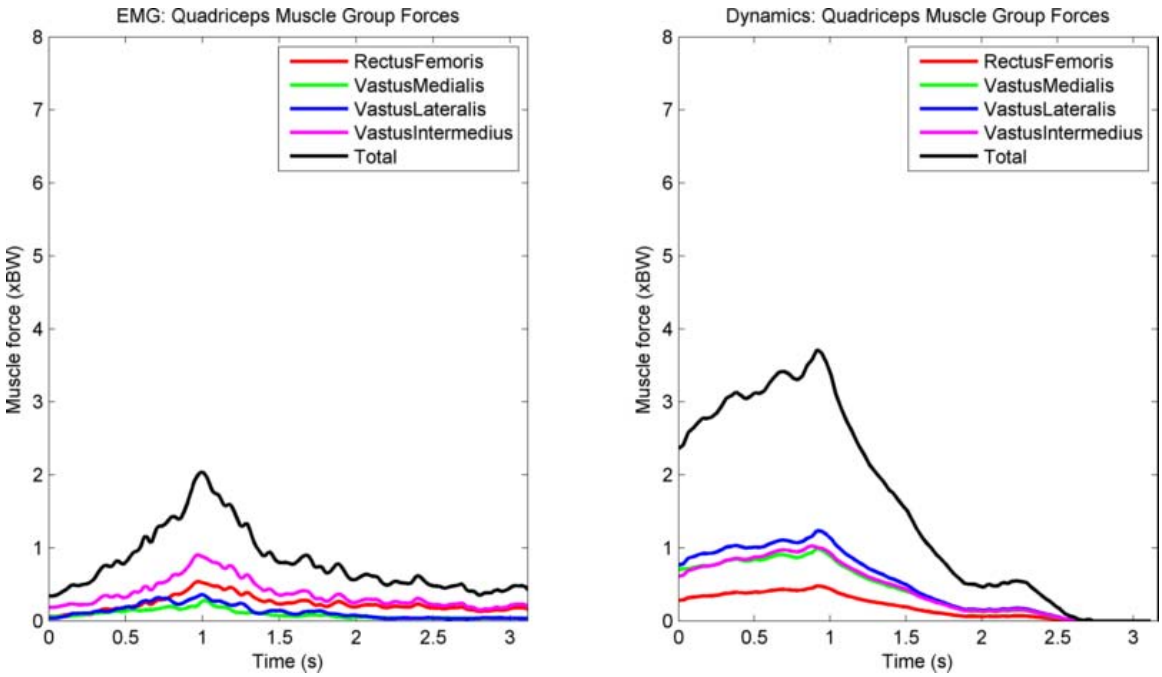


Figure A.169: Patient 6N quadriceps muscle group forces calculated from the EMG signals (left) and from the inverse dynamics (right) normalized by patient's body weight (BW).

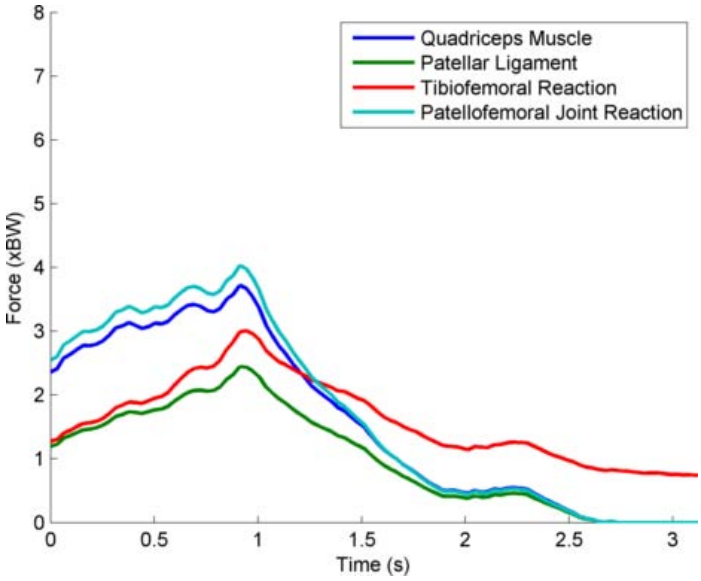


Figure A.170: Patient 6N total knee joint reaction forces incuding the action of the muscles, as well as the forces in the patellofemoral ligament, collateral and cruciate ligaments (if present) normalized by patient's body weight (BW).

A.18 Patient 7N

Patient demographic details:

ID# 7N

age: 30 yrs

height: 1.8 m

mass: 83 kg

leg side: Left

condition: Healthy

A.18.1 Kinematics analysis results

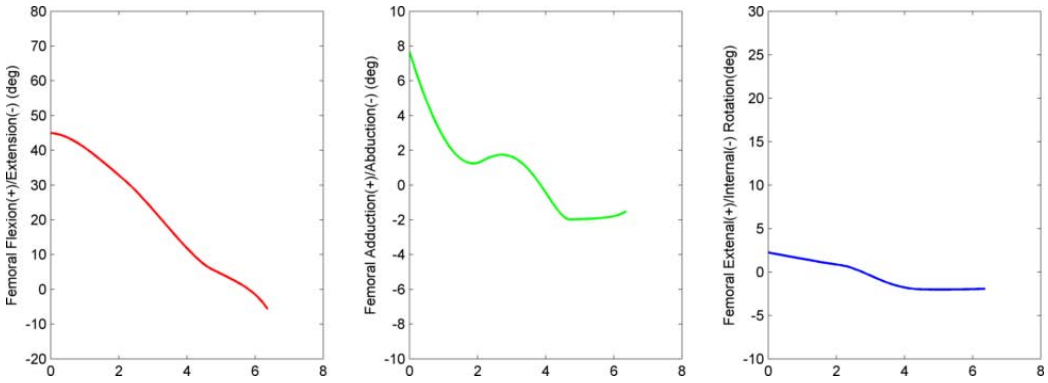


Figure A.171: Patient 7N patellofemoral joint kinematics.

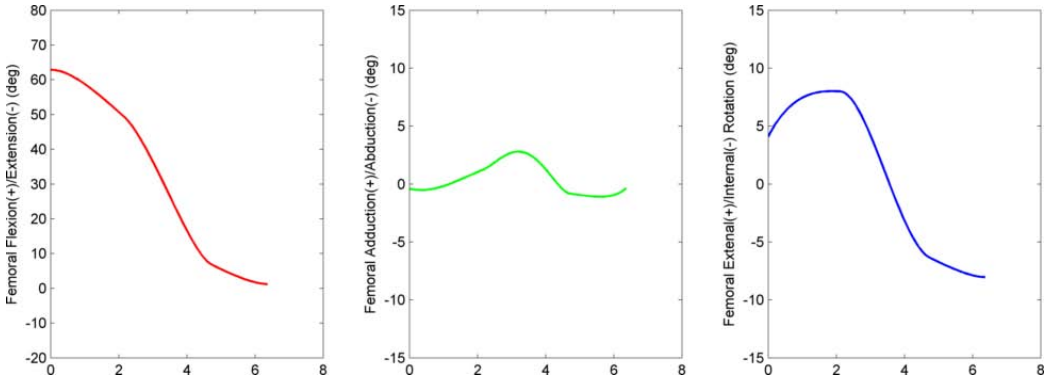


Figure A.172: Patient 7N tibiofemoral joint kinematics.

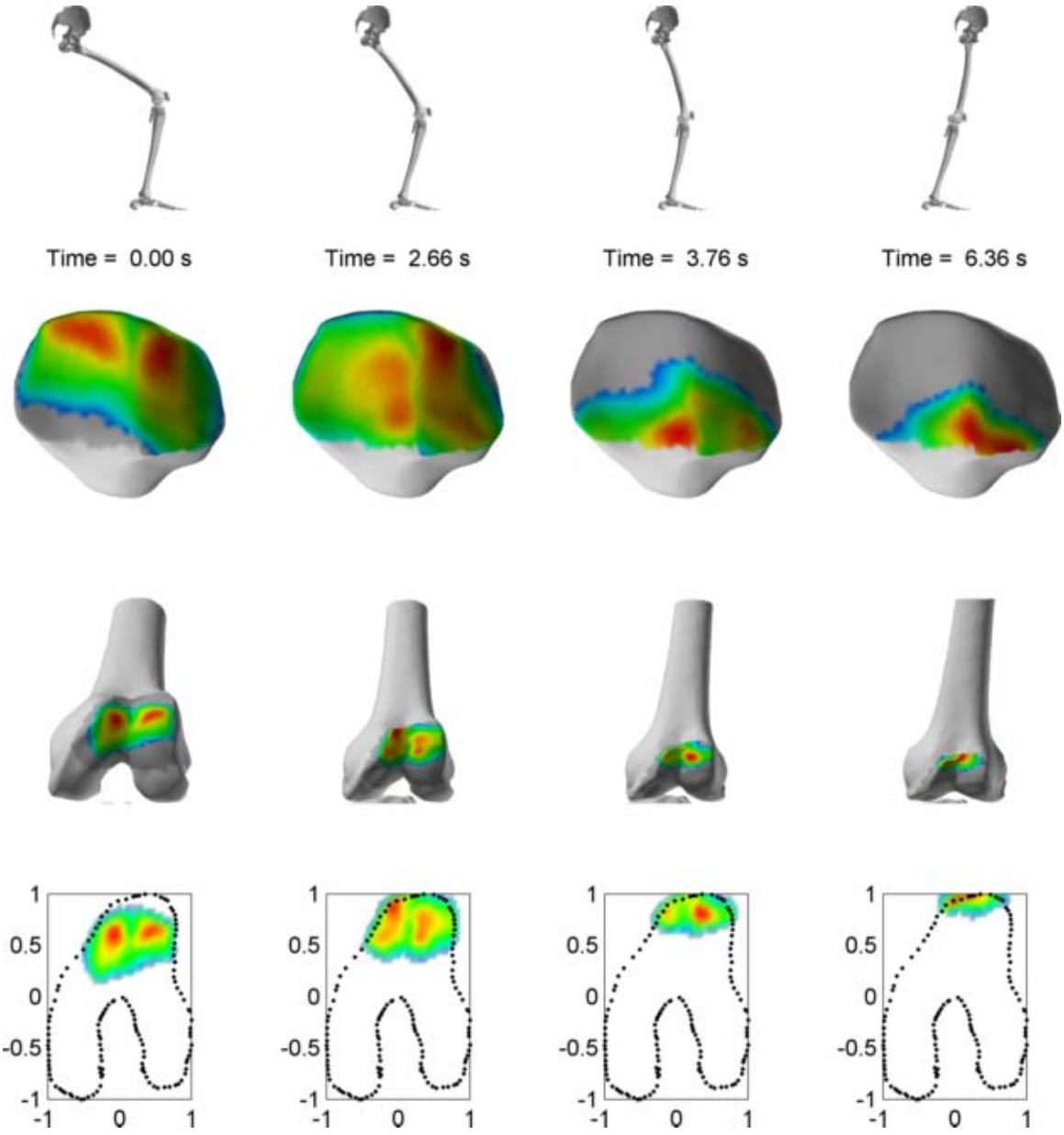


Figure A.173: Patient 7N dynamics model (top), patellofemoral contact location mapped on the patient's specific patella (2^{nd} from top) and femur (2^{nd} from bottom) bone models, as well as the normalized contact location mapped on the unfolded femoral trochlea surface (bottom).

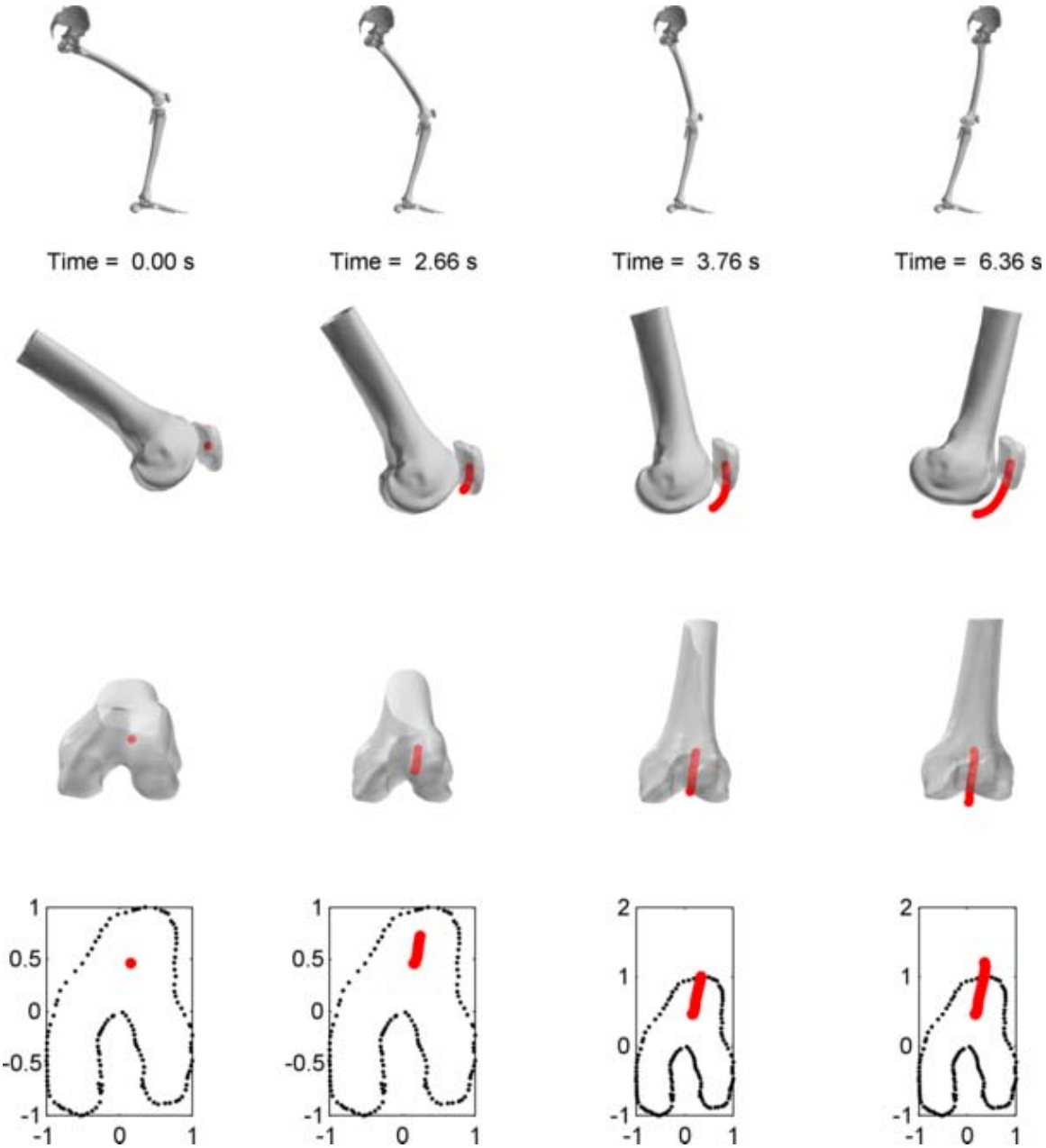


Figure A.174: Patient 7N dynamics model (top), patella center tracking in the sagittal (2^{nd} from top) and coronal (2^{nd} from bottom) planes, as well as the normalized patella tracking mapped on the unfolded femoral trochlea surface (bottom).

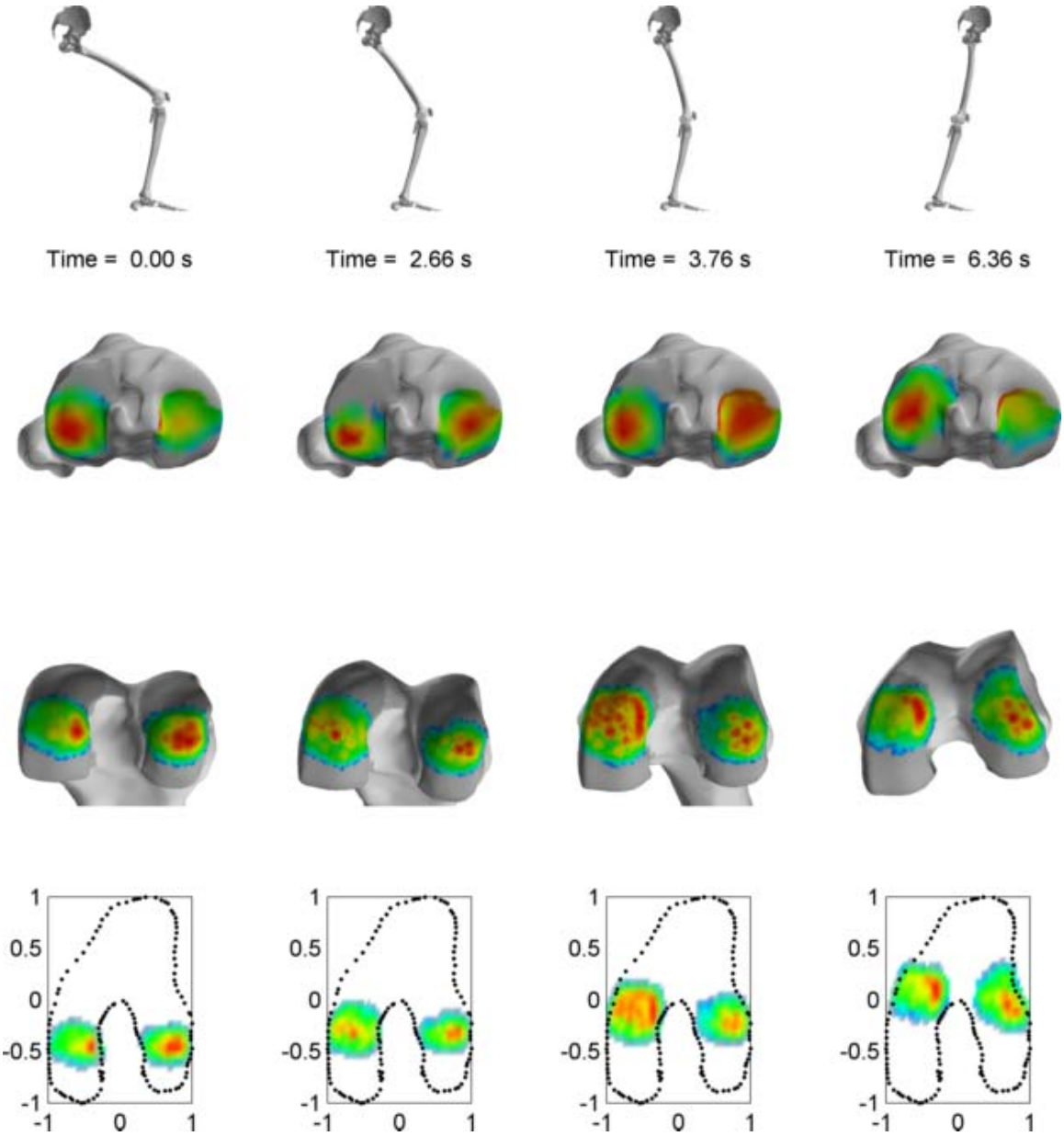


Figure A.175: Patient 7N dynamics model (top), tibiofemoral contact location mapped on the patient's specific patella (2^{nd} from top) and femur (2^{nd} from bottom) bone models, as well as the normalized contact location mapped on the unfolded femoral trochlea surface (bottom).

A.18.2 Electromyography and Inverse Dynamics analyses results

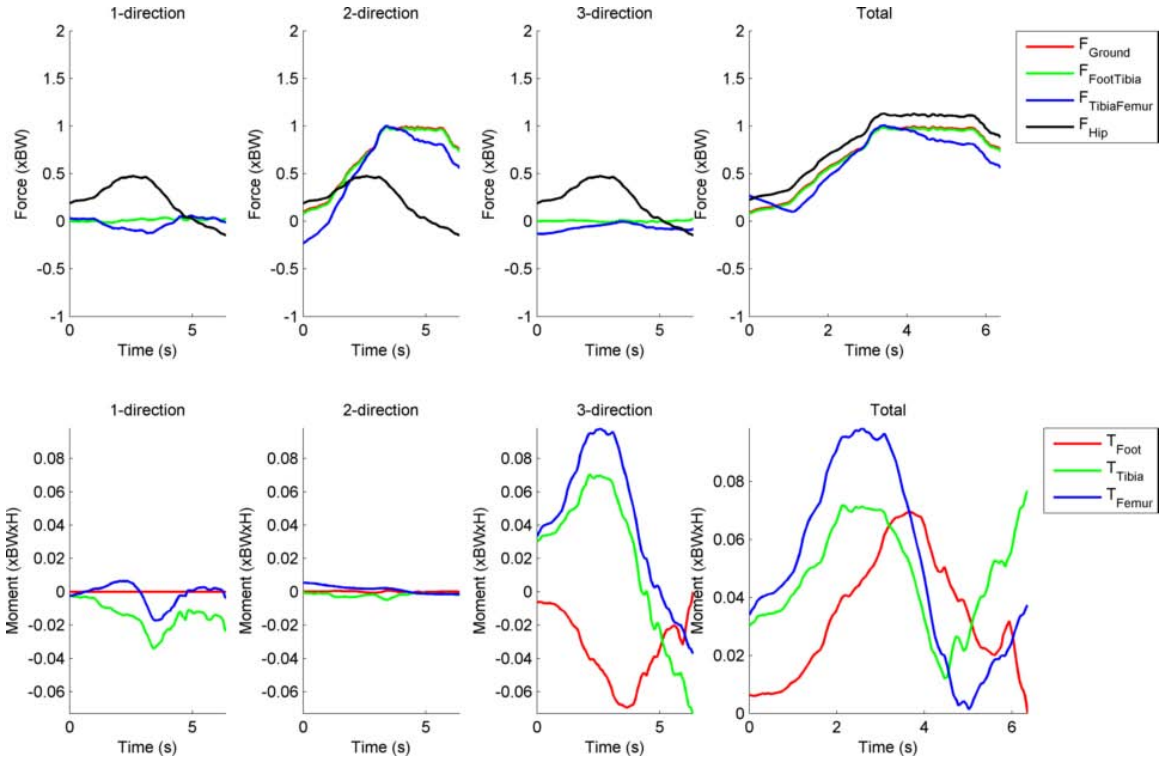


Figure A.176: Patient 7N knee joint reaction forces (top) and moments (bottom) normalized with respect to patient's body weight (BW). 1-direction = Anterior(+)/Posterior(-), 2-direction = Superior(+)/Inferior(-), 3-direction = Medial(+)/Lateral(-).

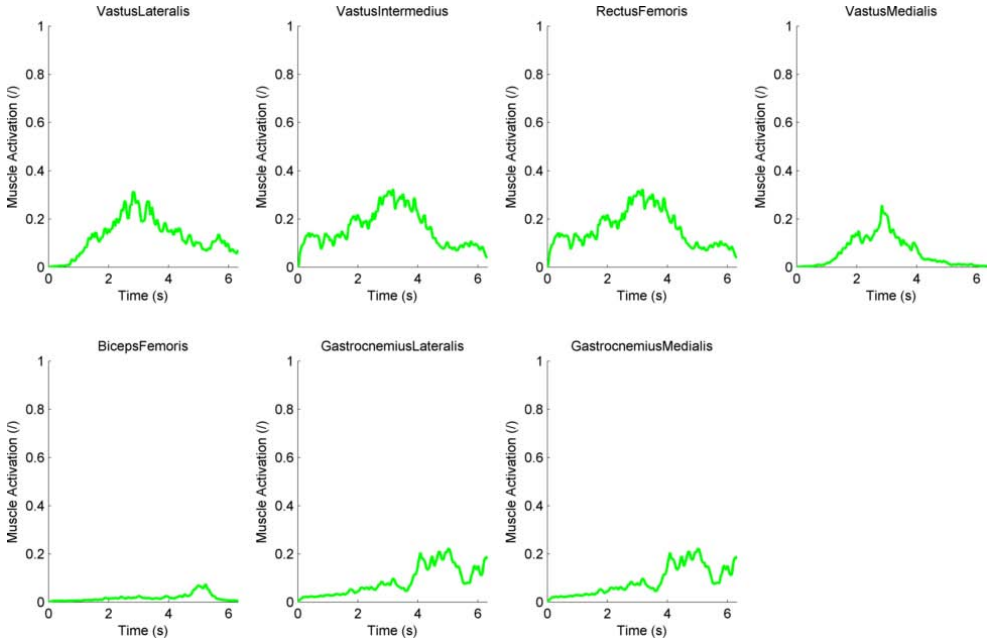


Figure A.177: Patient 7N muscle activation values obtained using the muscle activation dynamics[256].

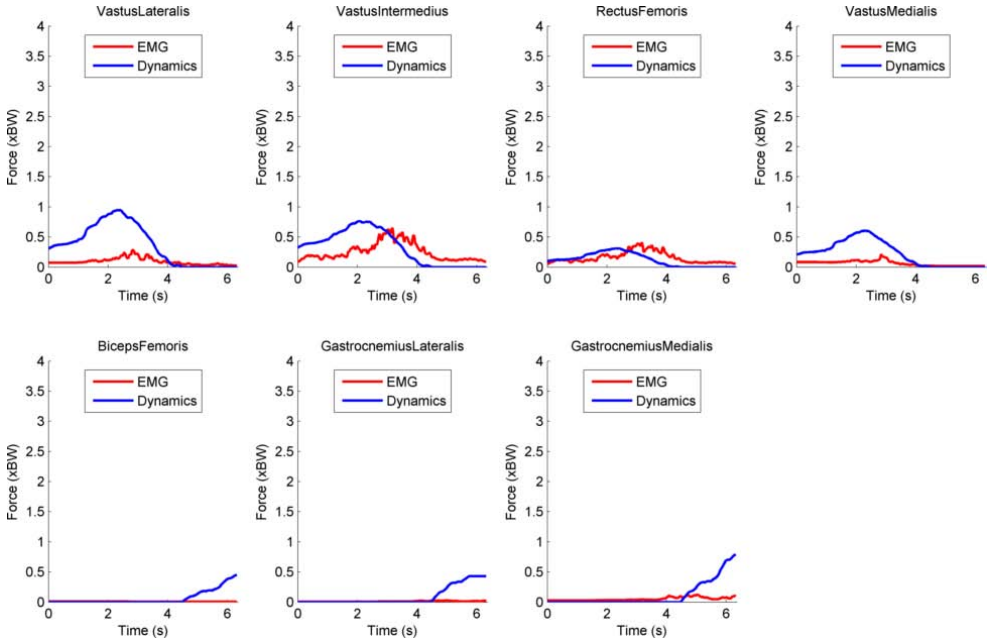


Figure A.178: Patient 7N muscle forces obtained using the EMG signal analysis (red) and pseudoinverse dynamics approach (green) normalized by patient's body weight (BW).

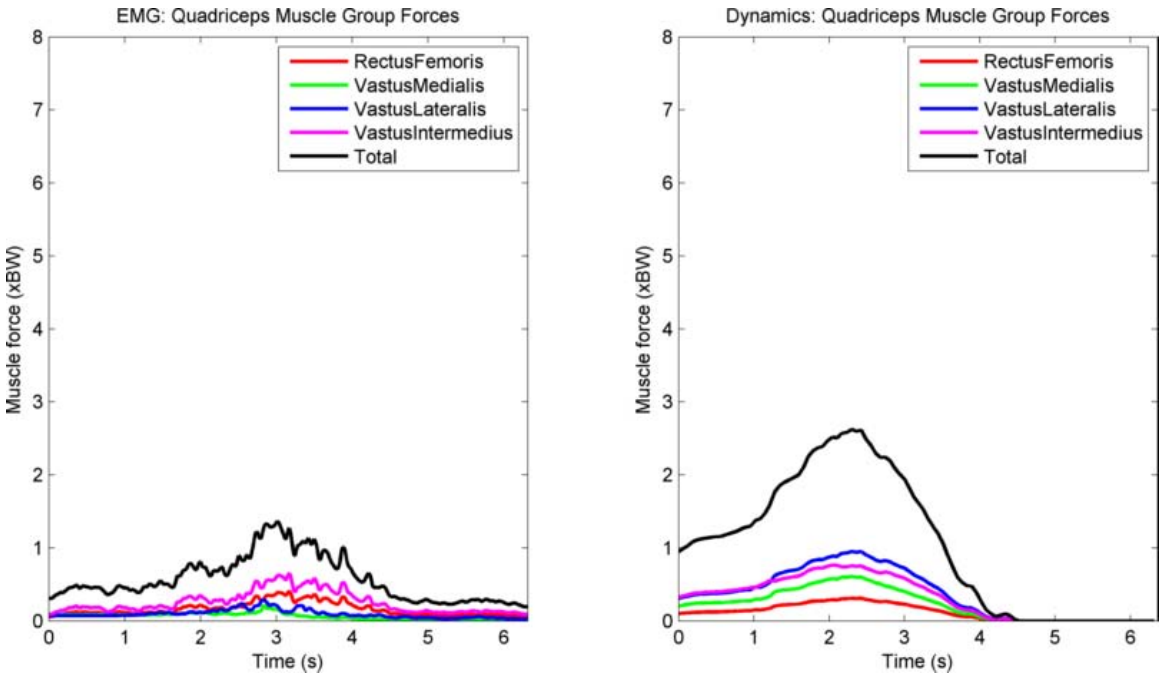


Figure A.179: Patient 7N quadriceps muscle group forces calculated from the EMG signals (left) and from the inverse dynamics (right) normalized by patient's body weight (BW).

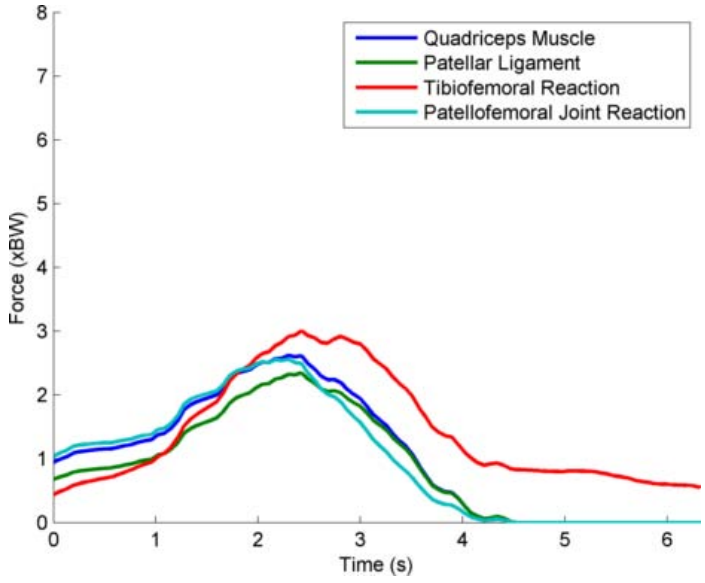


Figure A.180: Patient 7N total knee joint reaction forces incuding the action of the muscles, as well as the forces in the patellofemoral ligament, collateral and cruciate ligaments (if present) normalized by patient's body weight (BW).

A.19 Patient 15N

Patient demographic details:

ID# 15N

age: 35 yrs

height: 1.84 m

mass: 81.4 kg

leg side: Left

condition: Healthy

A.19.1 Kinematics analysis results

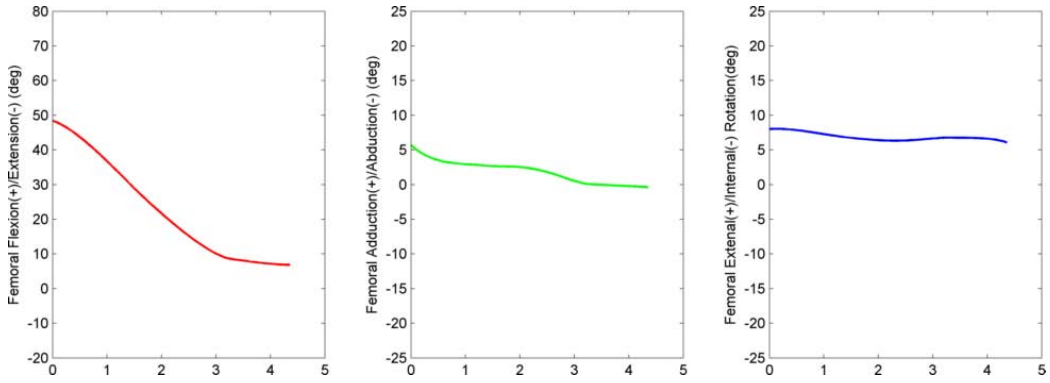


Figure A.181: Patient 15N patellofemoral joint kinematics.

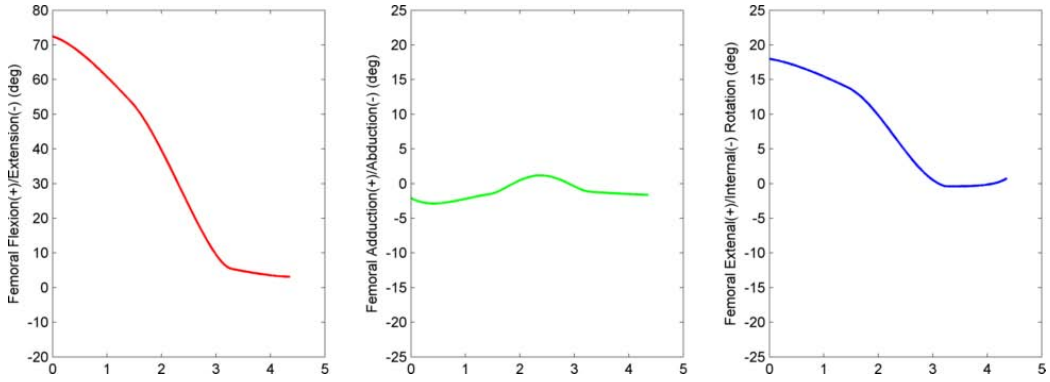


Figure A.182: Patient 15N tibiofemoral joint kinematics.

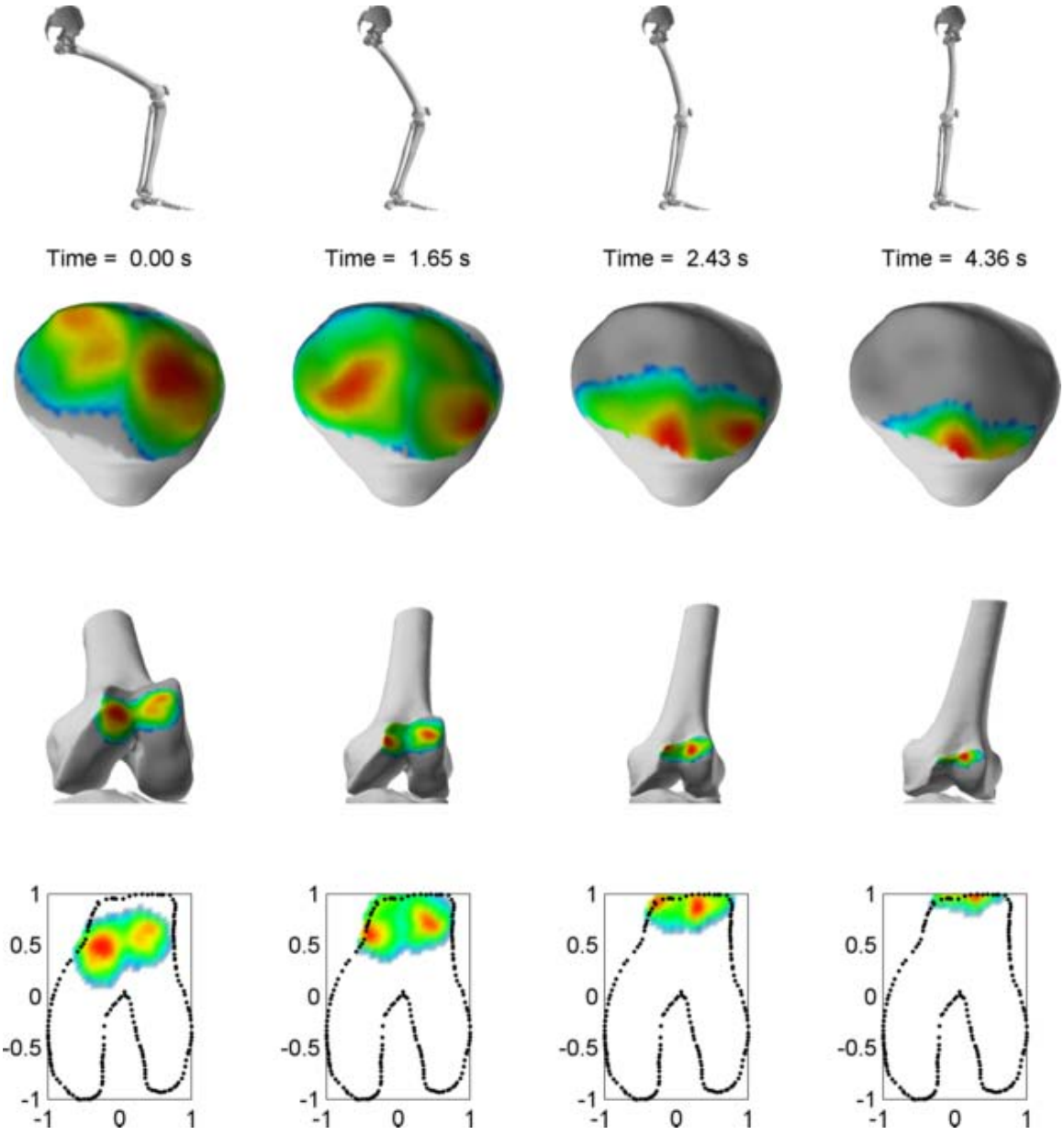


Figure A.183: Patient 15N dynamics model (top), patellofemoral contact location mapped on the patient's specific patella (2^{nd} from top) and femur (2^{nd} from bottom) bone models, as well as the normalized contact location mapped on the unfolded femoral trochlea surface (bottom).

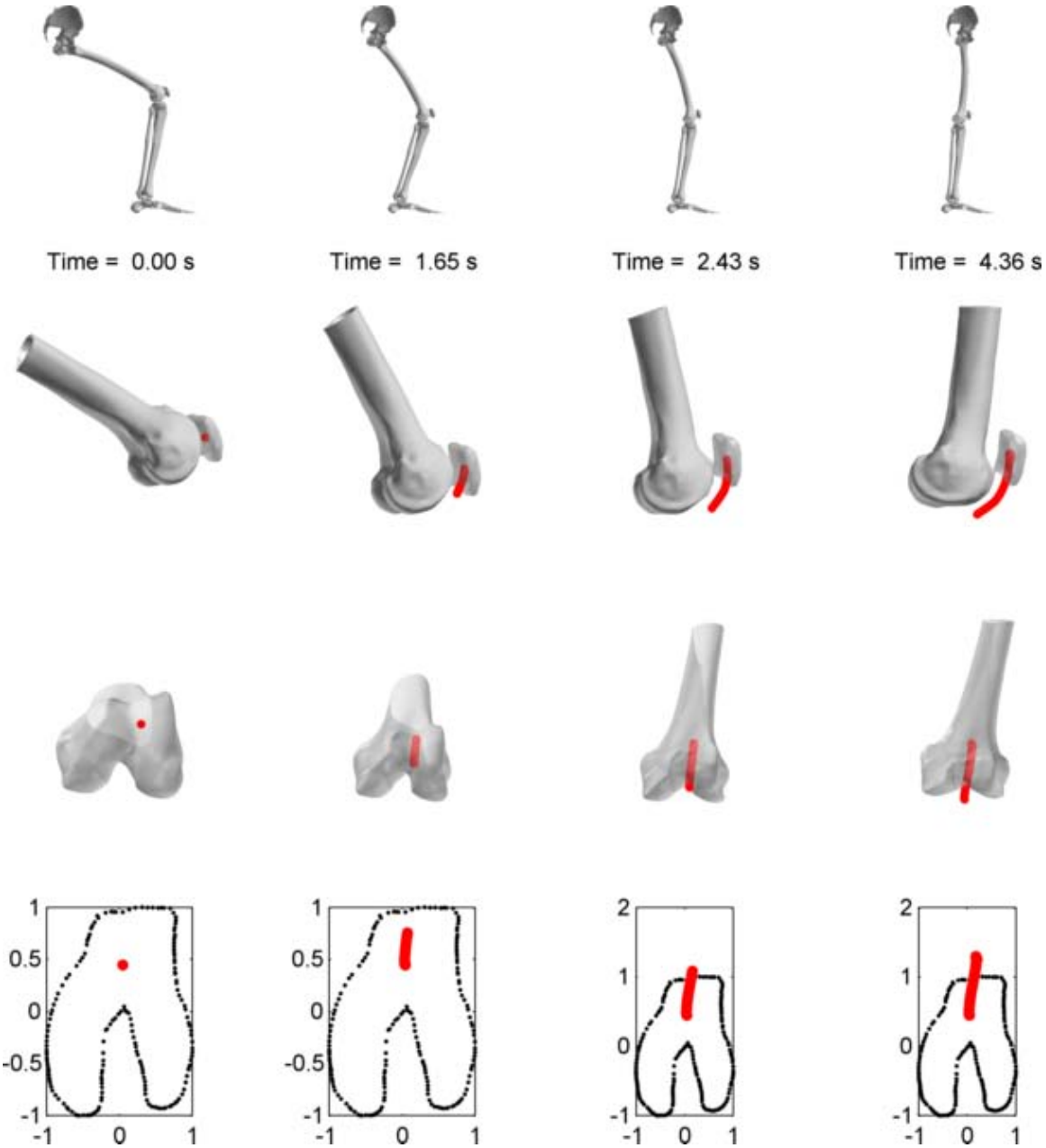


Figure A.184: Patient 15N dynamics model (top), patella center tracking in the sagittal (2^{nd} from top) and coronal (2^{nd} from bottom) planes, as well as the normalized patella tracking mapped on the unfolded femoral trochlea surface (bottom).

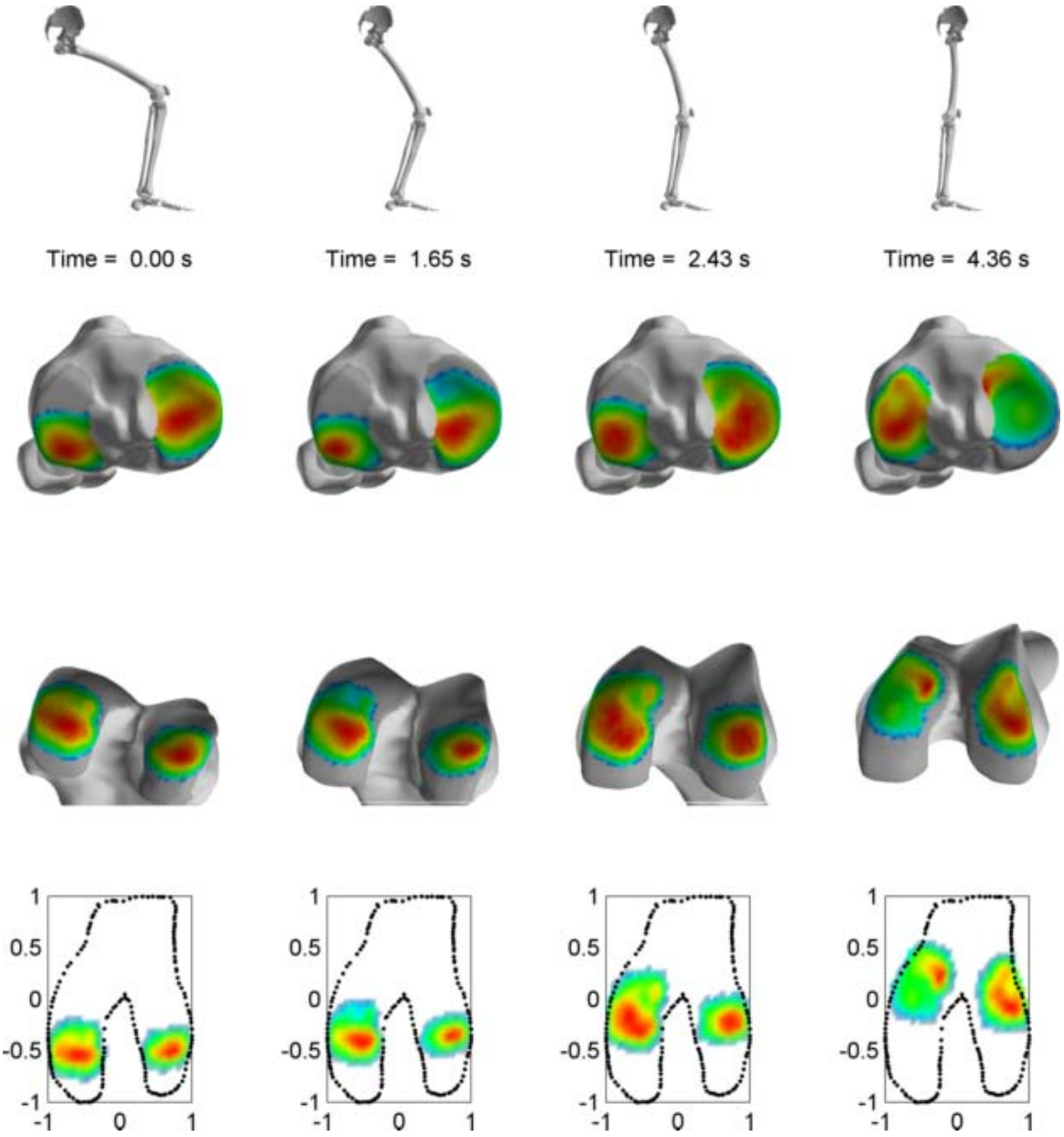


Figure A.185: Patient 15N dynamics model (top), tibiofemoral contact location mapped on the patient's specific patella (2^{nd} from top) and femur (2^{nd} from bottom) bone models, as well as the normalized contact location mapped on the unfolded femoral trochlea surface (bottom).

A.19.2 Electromyography and Inverse Dynamics analyses results

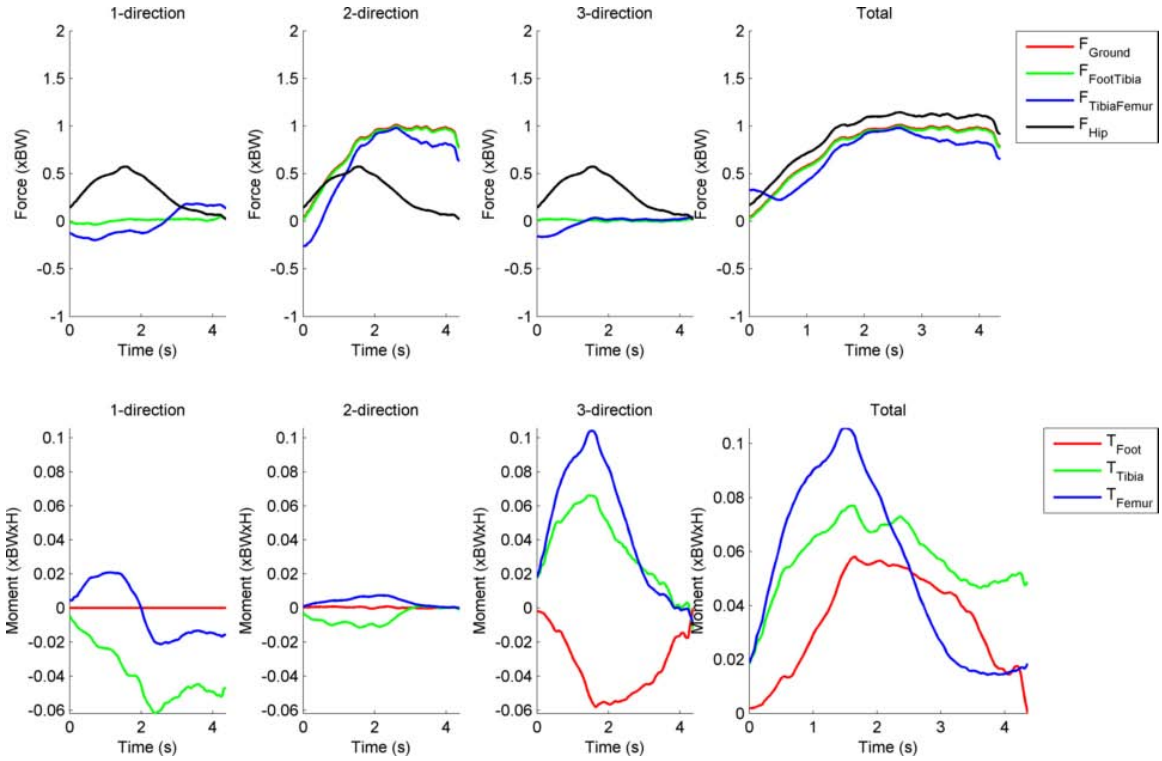


Figure A.186: Patient 15N knee joint reaction forces (top) and moments (bottom) normalized with respect to patient's body weight (BW). 1-direction = Anterior(+)/Posterior(-), 2-direction = Superior(+)/Inferior(-), 3-direction = Medial(+)/Lateral(-).

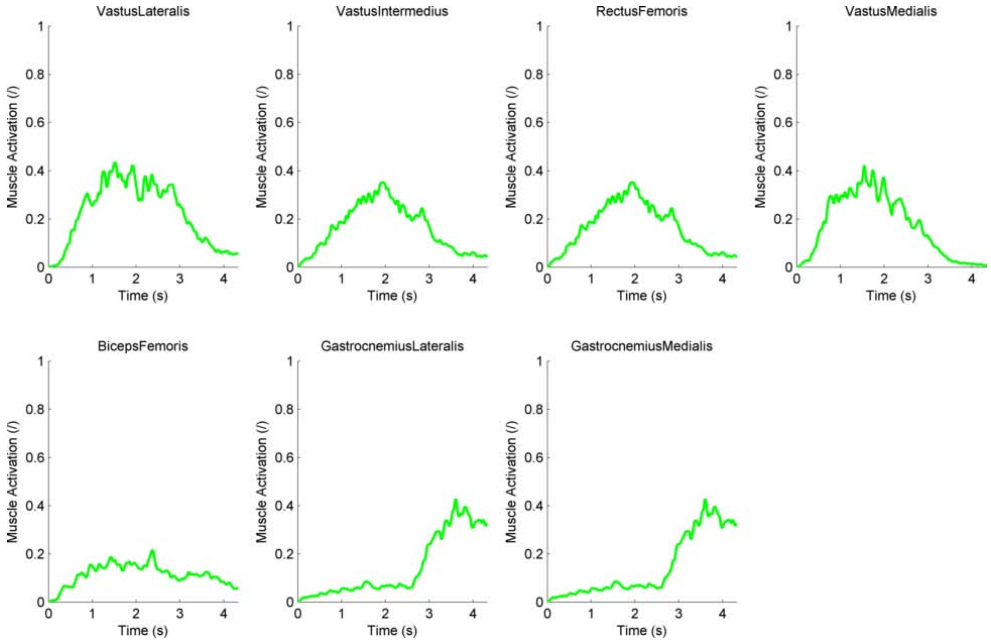


Figure A.187: Patient 15N muscle activation values obtained using the muscle activation dynamics[256].

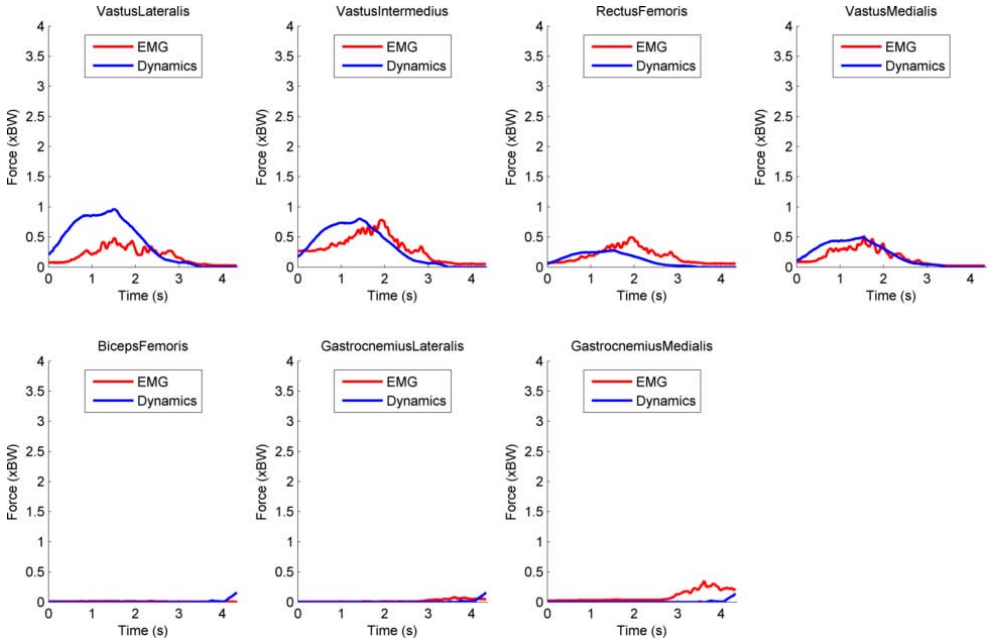


Figure A.188: Patient 15N muscle forces obtained using the EMG signal analysis (red) and pseudoinverse dynamics approach (green) normalized by patient's body weight (BW).

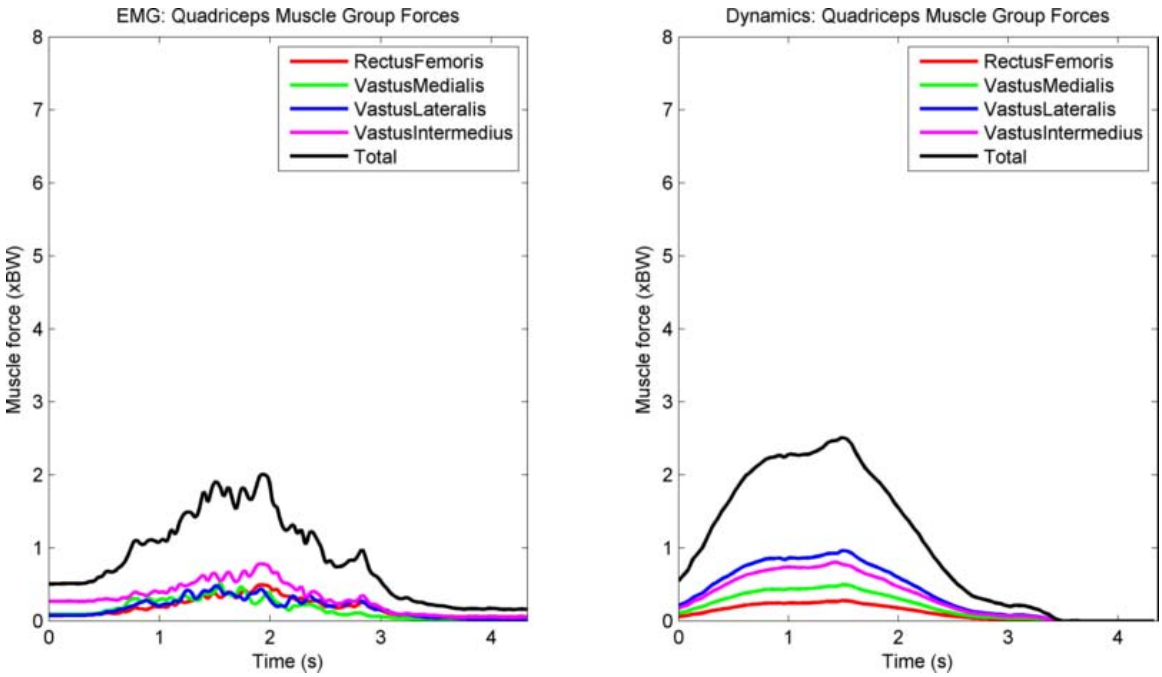


Figure A.189: Patient 15N quadriceps muscle group forces calculated from the EMG signals (left) and from the inverse dynamics (right) normalized by patient's body weight (BW).

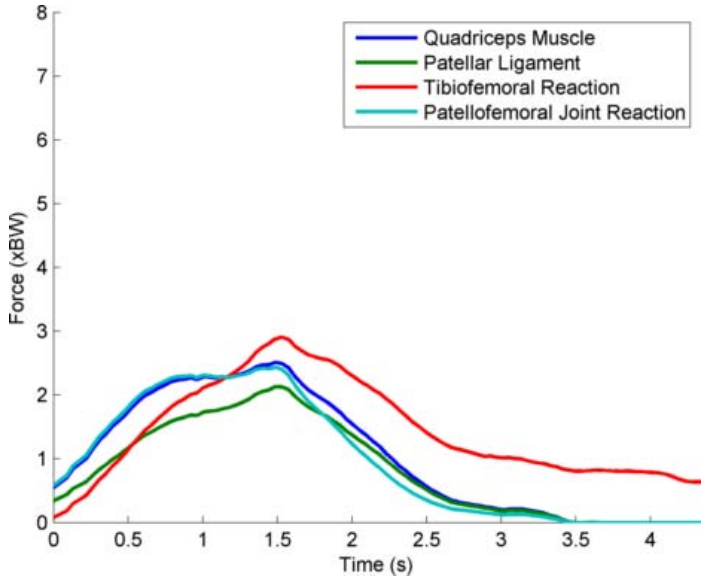


Figure A.190: Patient 15N total knee joint reaction forces incuding the action of the muscles, as well as the forces in the patellofemoral ligament, collateral and cruciate ligaments (if present) normalized by patient's body weight (BW).

A.20 Patient 16N

Patient demographic details:

ID# 16N

age: 28 yrs

height: 1.79 m

mass: 85.5 kg

leg side: Left

condition: Healthy

A.20.1 Kinematics analysis results

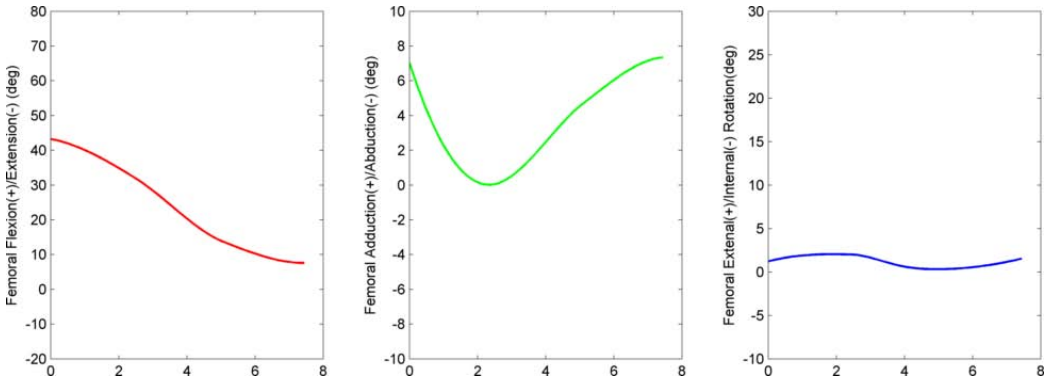


Figure A.191: Patient 16N patellofemoral joint kinematics.

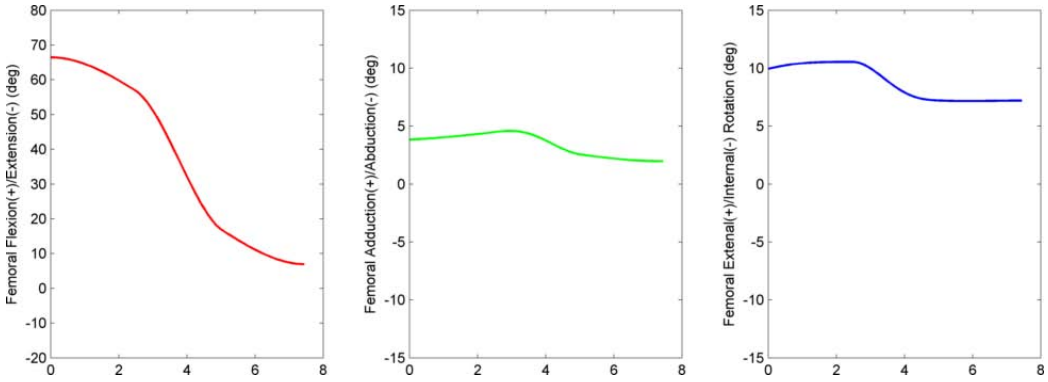


Figure A.192: Patient 16N tibiofemoral joint kinematics.

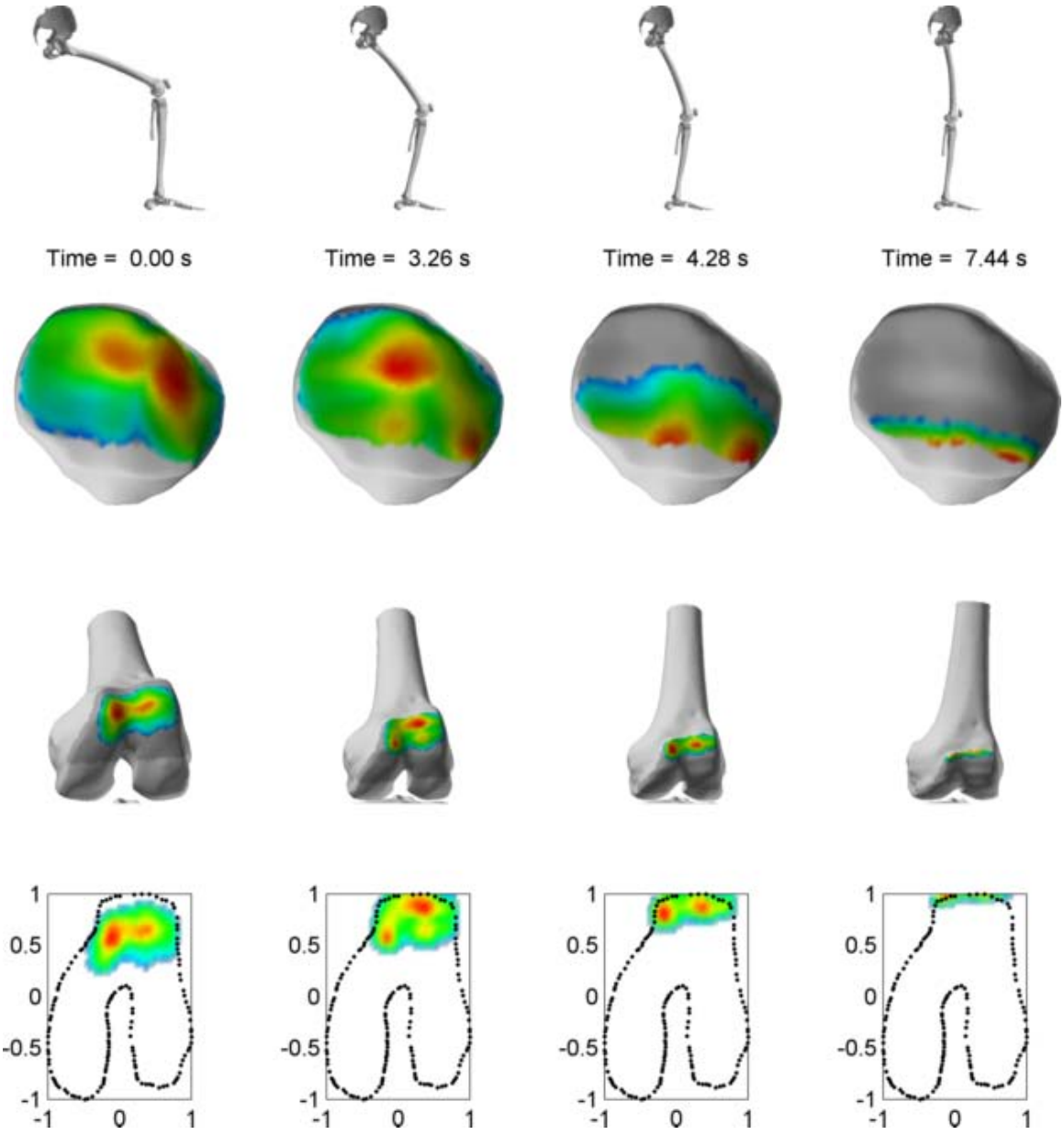


Figure A.193: Patient 16N dynamics model (top), patellofemoral contact location mapped on the patient's specific patella (2^{nd} from top) and femur (2^{nd} from bottom) bone models, as well as the normalized contact location mapped on the unfolded femoral trochlea surface (bottom).

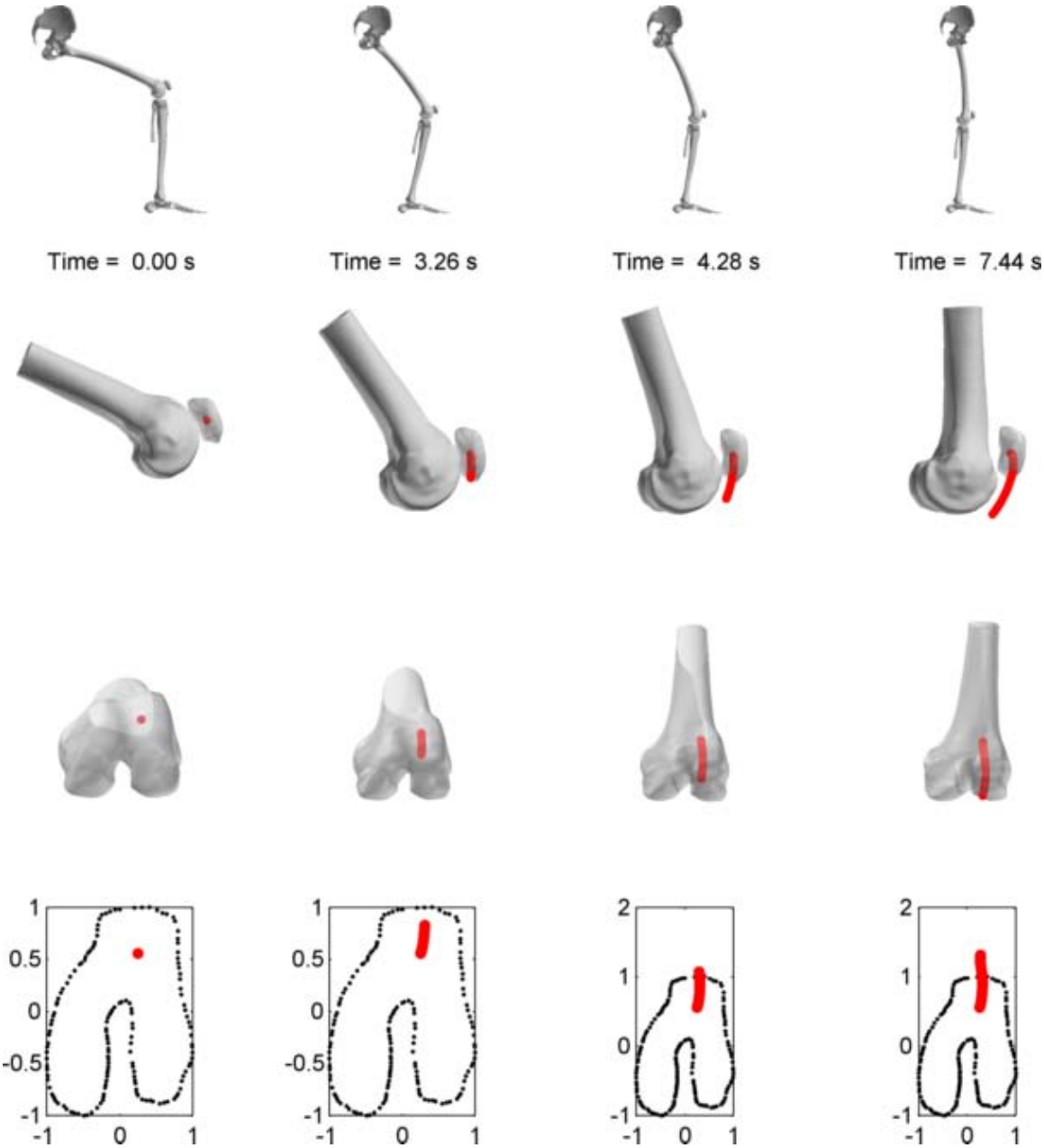


Figure A.194: Patient 16N dynamics model (top), patella center tracking in the sagittal (2^{nd} from top) and coronal (2^{nd} from bottom) planes, as well as the normalized patella tracking mapped on the unfolded femoral trochlea surface (bottom).

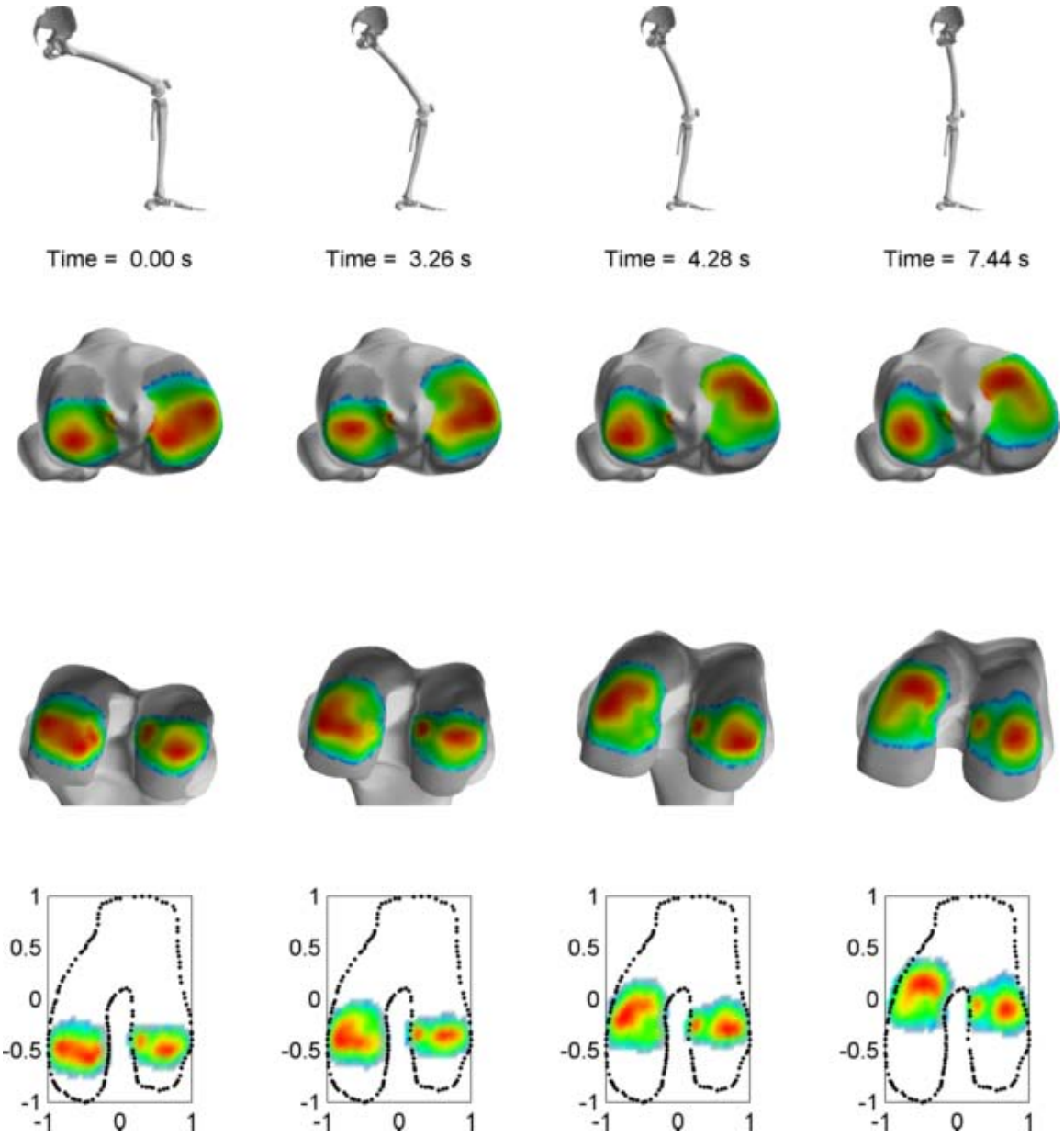


Figure A.195: Patient 16N dynamics model (top), tibiofemoral contact location mapped on the patient's specific patella (2^{nd} from top) and femur (2^{nd} from bottom) bone models, as well as the normalized contact location mapped on the unfolded femoral trochlea surface (bottom).

A.20.2 Electromyography and Inverse Dynamics analyses results

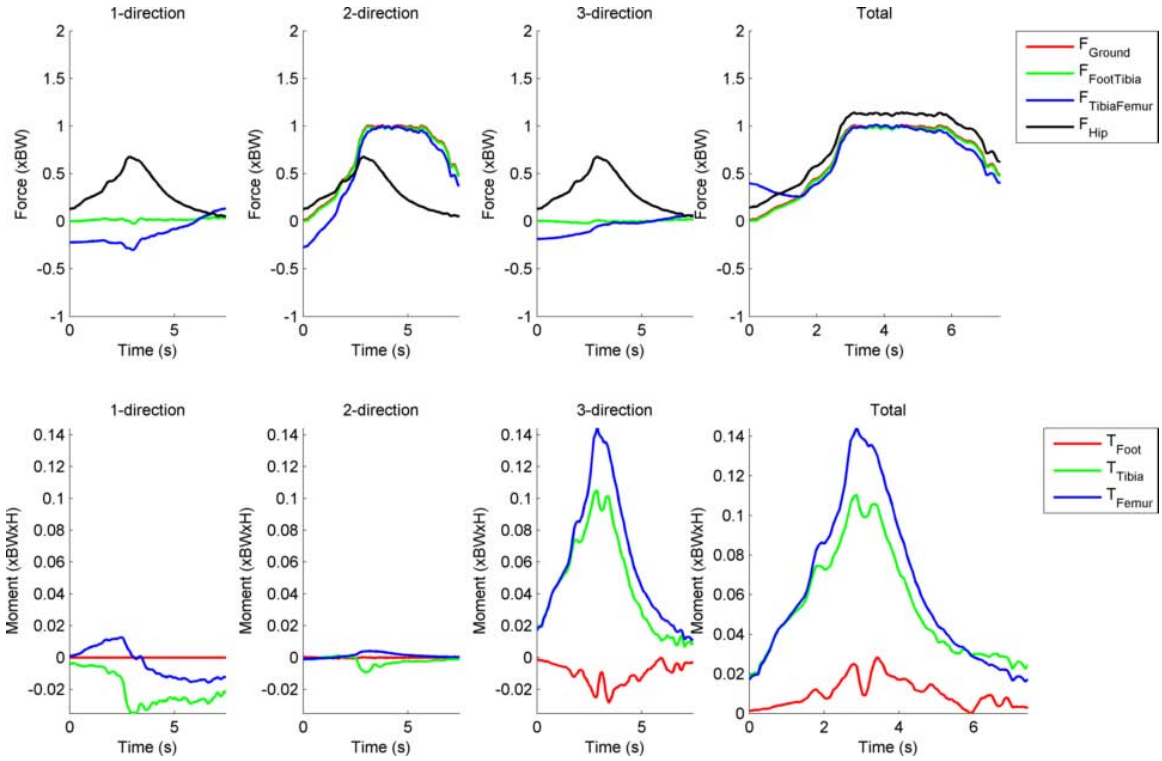


Figure A.196: Patient 16N knee joint reaction forces (top) and moments (bottom) normalized with respect to patient's body weight (BW). 1-direction = Anterior(+)/Posterior(-), 2-direction = Superior(+)/Inferior(-), 3-direction = Medial(+)/Lateral(-).

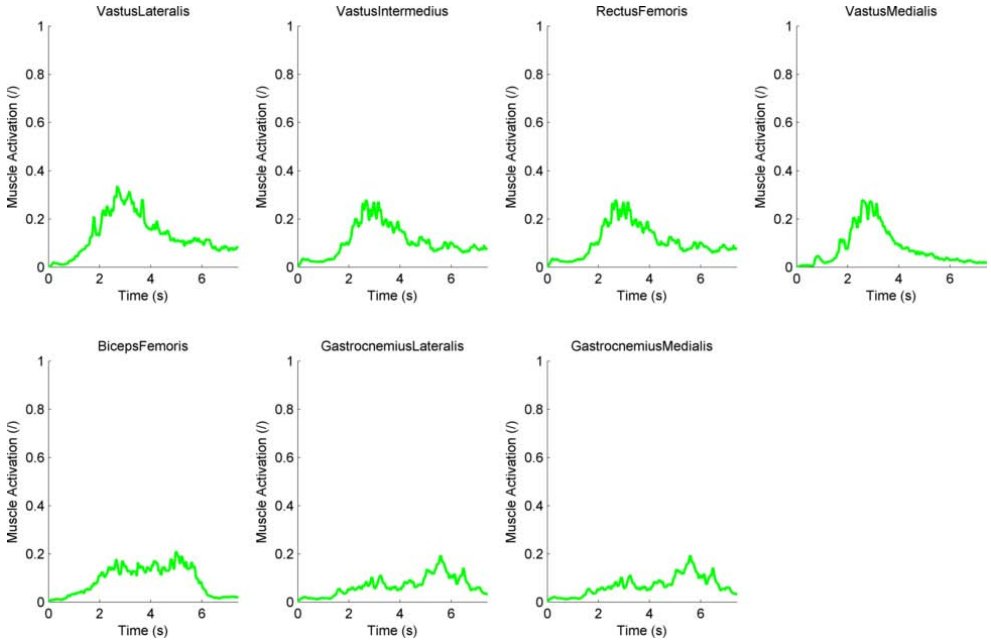


Figure A.197: Patient 16N muscle activation values obtained using the muscle activation dynamics[256].

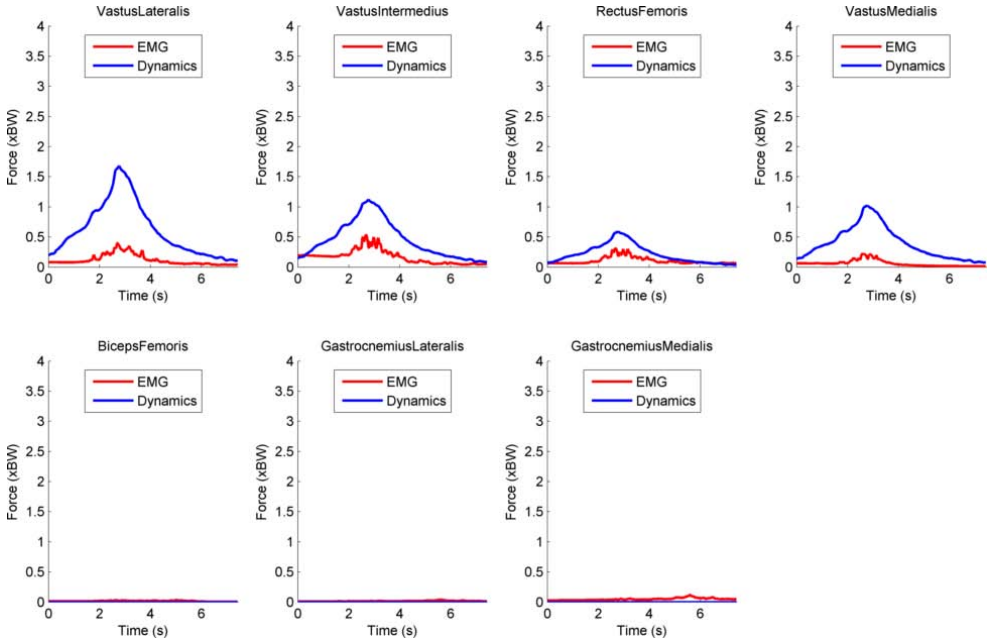


Figure A.198: Patient 16N muscle forces obtained using the EMG signal analysis (red) and pseudoinverse dynamics approach (green) normalized by patient's body weight (BW).

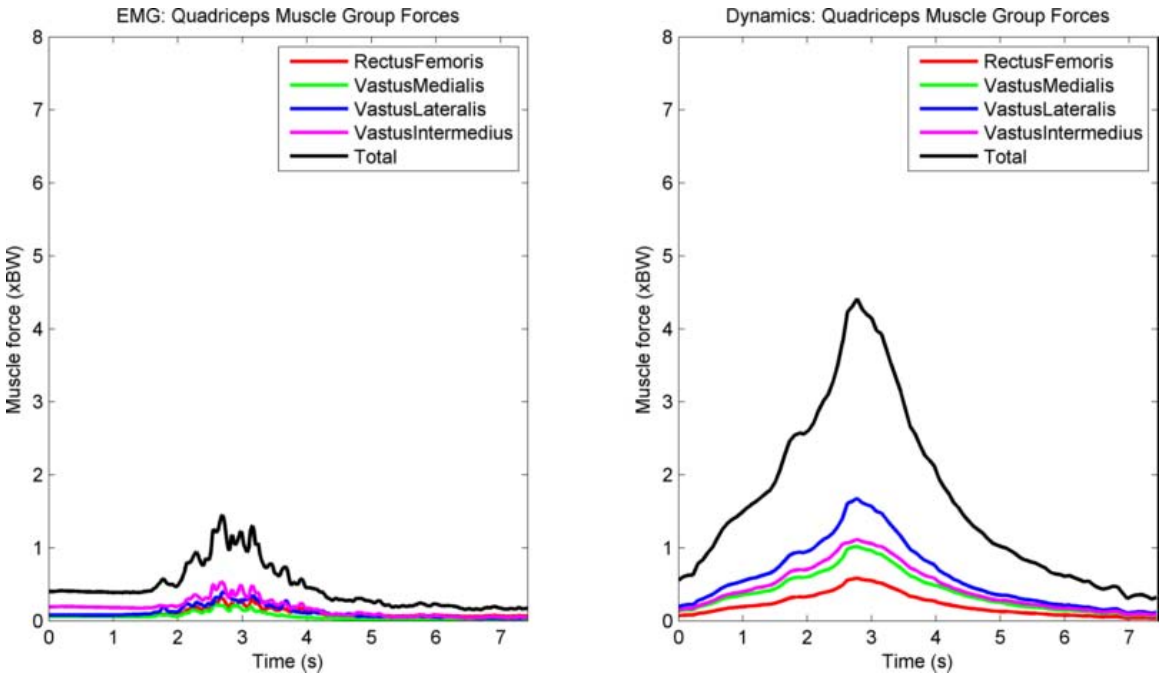


Figure A.199: Patient 16N quadriceps muscle group forces calculated from the EMG signals (left) and from the inverse dynamics (right) normalized by patient's body weight (BW).

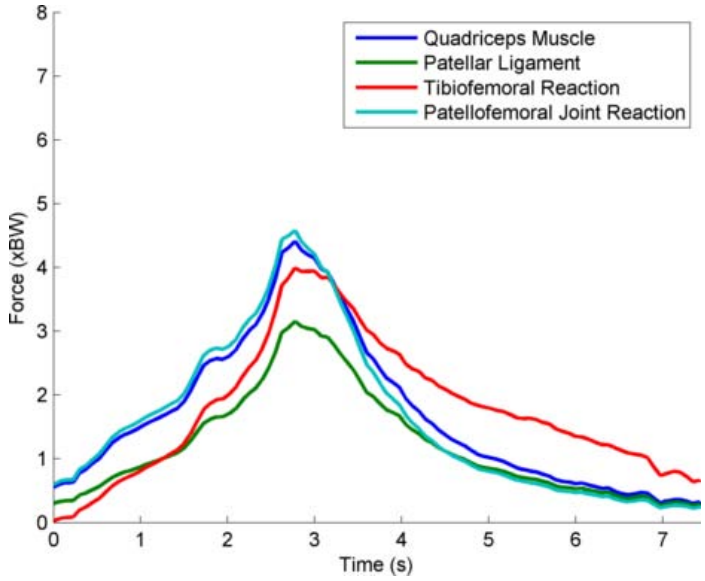


Figure A.200: Patient 16N total knee joint reaction forces incuding the action of the muscles, as well as the forces in the patellofemoral ligament, collateral and cruciate ligaments (if present) normalized by patient's body weight (BW).

Vita



Filip was born in Poland and received his BSc and MSc degrees in civil engineering from the Poznan University of Technology. He also studied at the Univeristy of Kaiserslautern in Germany, where he accomplished his Master's Thesis, for which he later received three major awards, including recognition from the Minister of Infrastructure.

During his studies, Filip became interested in applications of Finite Element Method in biomedical engineering. After his graduation he joined the Computer Aided Design Institute and focused on biomechanical analysis of the human knee joint.

Later, Filip received another opportunity to study abroad and came the United States to pursue a PhD degree in biomedical engineering at the University of Tennessee. He also accepted a position at the Center for Musculoskeletal Research Laboratory and worked on solving challenging problems related to joint replacement. At CMR, Filip accomplished a number of research projects for world-leading orthopeadic companies and collaborated with many renowned surgeons. The quality of Filip's research was recognized with a Student Biomechanics Award by the International Society for Technology in Arthroplasty. Filip was also invited to write a book chapter for the Insall & Scott "Surgery of the Knee", one of the most recognized knee surgery textbooks. He published his research in a number of journal articles and presented it at many international conferences.

Upon his graduation, Filip accepted an employment opportunity from one of the largest biomedical companies in the world and will continue his passion to develop products, which benefit patients suffering from musculoskeletal disorders.